UNIVERSITY OF LIVERPOOL

The role of the mitochondrial deubiquitylase USP30 in cellular fitness and death

Andreas Kallinos

Thesis submitted in accordance with the requirements of the University of Liverpool for the Degree Doctor in Philosophy

June 2021

The role of the mitochondrial deubiquitylase USP30 in cellular fitness and death

Andreas Kallinos

Abstract

Ubiquitylation is a protein post-translational modification that involves the covalent conjugation of ubiquitin onto protein substrates through the collective activities of E1, E2 and E3 ubiquitin ligases and is reversed by deubiquitylating enzymes (DUBs). Ubiquitylation serves a plethora of cellular functions, including modes of selective autophagy such as mitophagy as well as protein homeostasis by the proteasome. Defects in the different pathways that ubiquitylation is involved in are associated with a number of pathologies including neurodegeneration. Parkinson's disease (PD) is the second most common neurodegenerative disease, with approximately 10% of all cases having a genetic component to their aetiology. Mutations in PINK1 (*PARK6*) and Parkin (*PARK2*) are known causes of early onset juvenile parkinsonism. PINK1 and Parkin operate in unison in the mitochondrial quality control pathway of mitophagy, preventing accumulation of dysfunctional and potentially harmful mitochondria. PINK1 responds to instances of mitochondrial damage and phosphorylates ubiquitin (S65), which recruits and activates Parkin. Activated Parkin decorates outer mitochondrial membrane (OMM) proteins with more ubiquitin, which results in the recruitment of the autophagophore membrane through autophagy receptors. The mitochondrial DUB USP30 opposes the PINK1/Parkin pathway and USP30 depletion rescues PD-associated phenotypes caused by loss of PINK1 and Parkin in the fly. The above presented the very first evidence that USP30 silencing may be a valid therapeutic strategy in the treatment of PD. I contributed to a body of work from my host lab that showed that USP30 suppresses the PINK1-dependent component of basal mitophagy. This suggests USP30 inhibition may indeed have protective effects in the long-term by enhancing the basal rate of mitophagy. I have also shown that a pool of USP30 localises to peroxisomes independently of mitochondria.

Previous work from our lab has shown USP30 depletion enhanced the effect of BH3 mimetics in cells. I followed up on with this work and introduced other BH3 mimetic compounds, which are more selective in terms of which anti-apoptotic proteins they inhibit.

I utilised CRISPR/Cas9 technology to generate USP30KO in the HCT116 FlpIn TRex cell line. I characterised the metabolic parameters of these cells using Seahorse Technology, measured intracellular levels and sources of ATP, and assessed their proliferation and colony forming potential in different substrates. I also performed a transcriptome analysis and a small-scale proteome in the same cells to get an understanding of USP30 function in cells. I investigated the generation of pS65-Ub in cells that lacked detectable Parkin utilising a

global ubiquitylation inhibitor and in parallel investigated the role of USP30 in this process. Lastly, I assisted in the characterisation of a USP30 inhibitor in Parkin over-expressing cells as well as cells expressing endogenous Parkin. I have shown that USP30 inhibition phenocopied USP30KO in terms of enhanced TOMM20 ubiquitylation and enhanced pS65-Ub generation.
My work has led to the generation and characterisation of new tools that allow us to gain a deeper understanding of USP30 biology in PD and other pathologies.

Table of Contents

List of Figures

List of Tables

Abbreviations

A/O	Antimycin A/Oligomycin A
ACN	Acetonitrile
AMBRA1	Autophagy and Beclin Reguator 1
Amp	Ampicillin
APC/C	Anaphase Promoting Complex/Cyclosome
APF-1/2	ATP-dependent proteolysis factor 1/2
ARIH1	Ariadne Homolog 1
ATG	Autophagy related protein
ATP	Adenosine triphosphate
BAK	BCL-2 antagonist/killer
BAX	BCL-2 associated X
BCL-2	B-cell lymphoma 2
BECN1	Beclin 1
BH	BCL-2 homology domain
BNIP3	BCL-2 interacting protein 3
BNIP3L	BCL-2 interacting protein 3 like
CCCP	Carbonyl cyanide m-chlorophenyl hydrazone
CDK	Cyclin-dependent kinase
CDS	Coding sequence
CLR	Culling Ring Ligase
COPS5, 6	COP5 signalosome subunit 5, 6
CRISPR	Clustered regularly interspaced short palindromic repeat
CRL	Cullin Ring Ligase
CYLD	Cylindromatosis
dATP	Deoxy-ATP
DMEM	Dulbecco's Modified Eagle Medium
DMEM/F-12	Dulbecco's Modified Eagle Medium/Nutrient Mixture F-12
DMSO	Dimethyl sulfoxide
DNMT1	DNA methyl transferase 1
dNTPs	Deoxy Nucleotide Triphosphates
Dox	Doxycycline

DUB	Deubiquitylating enzyme
ER	Endoplasmic reticulum
ERAD	ER-associated degradation
ESCRT	Endosomal sorting complexes required for transport
EtBr	Ethidium Bromide
ETC	Electron transport chain
FACS	Fluorescence-activated cell sorting
FBS	Foetal bovine serum
FBXO7	F-box protein 7
FBXW7	F-box and WD repeat domain-containing 7
FCCP	Carbonyl cyanide-p-trifluoromethoxyphenyl hydrazone
FIP200	FAK family kinase-interacting protein 200
FKBP8	FKBP propyl isomerase 8
FUNDC1	FUN14 domain containing 1
GABARAP	GABA type A receptor-associated protein
GAP	GTPase activating protein
GEF	Guanine nucleotide exchange factor
GFP	Green fluorescent protein
H2A, 2B, 3, 4	Histone H2A, H2B, H3, H4
HECT	Homologous to the E6-AP carboxyl terminus
HGF	Hepatocyte growth factor
hTERT-RPE1	human telomerase reverse transcriptase immortalised retinal pigmented epithelial cells
HUWE1	HECT, UBA, WWE domain containing E3 ubiquitin protein ligase 1
IBR	In-between RING
IMS	Intermembrane space
JAMM	JAB1/MPN/MOV4 metalloenzyme
Kan	Kanamycin
LC-MS/MS	Liquid chromatography tandem mass spectrometry
LIR	LC3-interacting region
LUBAC	Linear ubiquitin chain assembly complex
MCL-1	Myeloid cell leukaemia 1

MFN1, 2	Mitofusin 1, 2
MIMP	Mitochondrial inner membrane permeabilization
MINDY	Motif-interacting with ubiquitin-containing novel DUB family
MJD	Machado-Joseph disease
MOMP	Mitochondrial outer membrane permeabilization
mTORC1	Mammalian target of rapamycin complex 1
MTS	Mitochondrial Targeting Sequence
MUL-1	Mitochondrial E3 ubiquitin ligase 1
MULE	MCL-1 ubiquitin ligase E3
MYC	V-Myc Avian Myelocytomatosis Viral Oncogene
NEDD8	Neuronal precursor cell expressed, developmentally downregulated 8
NOS	Nitric Oxide synthase
NT1	Non-targeting oligo 1
OMM	Outer mitochondrial membrane
OPTN	Optineurin
ORF	Open-reading frame
OTU	Ovarian tumour proteases
OxPhos	Oxidative Phosphorylation
PBS	Phosphate-buffered saline
PCNA	Proliferating cell nuclear antigen
PCR	Polymerase Chain Reaction
PD	Parkinson’s Disease
PEX	Peroxin/Peroxisomal biogenesis factor
PFA	Paraformaldehyde
PI	Propidium Iodide
PINK1	PTEN-inducible kinase 1
PLK-1	Polo-like kinase 1
PMP	Peroxisomal membrane protein
PNS	Post-nuclear supernatant
PRKN	Parkin
pS-65Ub	Phosphoserine 65 ubiquitin
PTEN	Phosphatase and Tensin Homologue

PTEN-L	PTEN-Long
PTM	Post-translational modification
RBR	RING-between-RING
RING	Really Interesting New Gene
RNA	Ribonucleic acid
ROS	Reactive Oxygen species
RT	Room temperature
SCF	SKP, Cullin, F-box containing protein
SD	Standard deviation
SDS-PAGE	Sodium dodecyl sulphate polyacrylamide gel electrophoresis
sgRNA	Small guide RNA
SILAC	Stable isotopic labelling of amino acids in culture
siRNA	Small interfering RNA
SUMO	Small ubiquitin-like modifier
SYNJ2BP	Synaptojanin 2 binding protein
TBS	Tris-buffered saline
TIMM	Translocase of the inner mitochondrial membrane
TOMM	Translocase of the outer mitochondrial membrane
UAE	Ubiquitin activating enzyme
Ub	Ubiquitin
UBC	Ubiquitin conjugating enzyme
UBD	Ubiquitin-binding domain
UBL	Ubiquitin-like domain
UCH	Ubiquitin C-terminal hydrolase
UPS	Ubiquitin-Proteasome System
USP	Ubiquitin specific peptidase
YFP	Yellow fluorescent protein
ZnF	Zinc Finger
ZUFSP	Zinc finger-containing ubiquitin peptidase

Acknowledgments

First and foremost, I would like to express my gratitude towards my supervisors Professors Sylvie Urbé and Michael Clague. I wish to thank them for allowing me to pursue my PhD alongside my research technician duties in their lab and be part of all the exciting research that takes place there. Special thanks go out to Professor Gerry Cohen and Dr. Shankar Varadarajan who advised us on aspects relating to apoptotic cell death and provided us with valuable reagents. I wish to extend my gratitude towards all collaborators who have generously shared reagents for this project: Dr. Jon Lane, Prof. Stephen Taylor, Dr. Louisa Nelson, Dr. Anthony Tighe, Prof. Jon Pines, Prof. David Komander, Dr. Malte Gersch, and Prof. Francis Barr.

I would also like to thank the other members of the USP30 team whom I have collaborated closely with over the course of my stay in the lab: Dr. Aitor Martinez-Zarate, Dr. Jane Jardine, Dr. Emma Rusilowicz-Jones and Dr. Elena Marcassa. I wish to extend my thanks to all members of the MCSUIP and JMC labs who made working on the 5th floor a fun and enjoyable experience. In no particular order I would like to thank: Dr. Erithelgi Bertsoulaki, Dr. Fiona Hood, Dr. Leah Wilson, Dr. Claire Heride, Dr. Lisa Mullee, Dr. Stephanie Mo, Dr. Alice Howard, Dr. Douglas Grimes, Dr. Yvonne Tang, Dr. Adam Linley, Dr. Francesca Querques, Dr Sarah Barnett, Dr. Andrew Fielding, Dr. Dorota Sabat-Pospiech, Dr. Leila Rochin, Francesca Frigenti, Svetlana Telnova, Yasmina Sahraoui, Hannah Elcocks, Hannah Warren, Hannah Glover, Liam Pollock, Francesco Barone, Katie McCarron, Vicky Smith and Anne Clancy.

Finally, I would like to thank my wonderful family for supporting me throughout this endeavour: my loving parents, Irene and Christakis, as well as my amazing brothers, Ilias and Alexandros. Their on-going support and unending love have been paramount in the completion of my PhD.

COVID19 Thesis Impact Statement

The onset of the COVID19 pandemic in the United Kingdom coincided with the last three months of my stay in the laboratory. The University of Liverpool enforced a shutdown of all activities in its premises on the 20th March 2020 without much notice prior. My initial plan was to finish experiments in the lab by May 2020 and therefore the shutdown did not pose a significant hurdle to my experiments.

I had already compiled much of my data and identified certain experiments that required refinement or more repetitions to ensure reproducibility that I was unable to perform due to the shutdown. Particularly experiments relating to apoptotic cell death in the context of USP30 knock-out (KO) where the initial efforts in establishing whether USP30KO cells were in fact more sensitive to BH3 mimetics were left incomplete. I would have used the time to perform more concise experiments aimed at addressing the above.

I believe not being able to use the lab during the writing up part of my thesis has impacted both the speed and efficiency of my write up. Having the opportunity to remain in the lab would have helped me maintain my focus at the task in hand. Certain instances specialised software was required for data processing and presentation that were not freely available but were available in the lab (e.g. Prism GraphPad and JMP). My supervisor made a substantial effort to provide licenses for my personal computer to facilitate the process as much as possible, which I am very thankful for. Furthermore, feedback and corrections of the different chapters were done over Zoom or Slack video calls and while these have always been smooth and thorough, I must recognise that having these sessions in person carry a different impact.

Chapter 1: Introduction

1.1 Homeostasis is central to the maintenance of life

Homeostasis in biology refers to all the bodily mechanisms living organisms utilise to maintain their internal environment constant and operating at optimal conditions of temperature, osmotic pressure, pH and ionic strength. Living things invest a great deal of their biological machinery, both in terms of genes and energy resources into homeostasis and that highlights the importance of the process for the maintenance of life. Protein homeostasis or proteostasis is the entire network of molecular and cellular machinery that spans protein synthesis, folding, trafficking and degradation (Powers et al., 2009).

1.1.1 Proteostasis operates at the cellular level

Cells are the basic unit of life and proteostasis is a major component of cellular homeostasis. Improperly folded or unfolded proteins can result in protein aggregates, which in turn may become toxic to the cell. Protein aggregation is a hallmark of many pathologies including a number of neurodegenerative diseases. Notable examples include the aggregation of α-synuclein in Lewy bodies in Parkinson's disease (PD) (Parkinson, 2002; Lewy, 1912), mutant Huntingtin in Huntingdon's disease (Andrew et al., 1993) and tau aggregation in Alzheimer disease (Goedert et al., 1988, 1989). The incidences of defective protein folding and aggregation in diseases highlight the importance of strict protein quality control and the need for a pathway to remove unwanted and potentially dangerous proteins or protein aggregates from cells.

Proteolysis, which is the degradation of proteins by proteolytic enzymes (proteases), is the set of pathways a cell uses to dispose of unwanted, superfluous or mutant proteins (Etlinger and Goldberg, 1977). Early experiments performed in reticulocytes showed that haemoglobin containing mutant globin chains or chains with non-proteogenic amino acids were rapidly degraded whereas wild-type haemoglobin molecules were spared (Rieder et al., 1975). At that time it has already been established that proteolysis had a

requirement for ATP, as compounds that inhibit energy production in the cells prevent the release of isotopically-labelled amino acids from rat liver proteins (Simpson, 1953). The ATP requirement suggested an active and highly regulated process for the destruction of such proteins.

1.2 The discovery of ubiquitin and the ubiquitin/proteasome system (UPS)

The Nobel Prize in Chemistry was awarded to Aaron Ciechanover, Avram Hershko and Irwin Rose who jointly shared the prize “for the discovery of ubiquitin-mediated protein degradation” in 2004. The first set of experiments that led to the discovery of the ubiquitin/proteasome system were aimed at purifying and identifying the factors responsible for ATP-dependent proteolysis (Ciechanover et al., 1978). The authors employed a DEAE-cellulose column to fractionate the lysate from rabbit reticulocytes into two fractions: The unabsorbed component (flow-through or Fraction I) did not display any proteolytic activity in the absence nor presence of ATP. The proteolytic activity of the absorbed fraction (fraction II) was stimulated in the presence of ATP but was unable to reach the levels of proteolysis of the starting material. When the two fractions were mixed in the presence of ATP, the proteolytic activities were restored to that of the total lysate. It was therefore determined that a factor in fraction I was drastically stimulating the proteolytic activity of fraction II in the presence of ATP, despite fraction I having no detectable proteolytic activity itself. The factor in fraction I responsible was determined to be a small, highly thermally-stable polypeptide that itself had no peptide bond cleaving activity and was named ATP-dependent proteolytic factor-1 (APF-1) (Ciechanover et al., 1978). The fraction II was analysed further and the high-molecular weight component responsible for proteolytic activity was identified as ATP-dependent proteolysis factor 2 (APF-2), thought to be the 26S proteasome (Hershko et al., 1979; Wilkinson, 2005).

Ubiquitin had already been discovered prior to the discovery of APF-1, in fact twice and independently. Goldstein *et al* (1975) isolated and characterised a new poly-peptide they named ubiquitous immunopoietic poly-peptide (UBIP) due to its ability to induce differentiation of T and B cells *in vitro*. UBIP expression was widespread in all of the tissues the authors tested and not confined to the thymus (Goldstein et al., 1975; Schlesinger et al., 1975). The

discovery of the ubiquitous expression and high sequence conservation across species and phyla ranging from fungi, animals and plants suggested that ubiquitin possessed integral cellular functions across all cell types and was not restricted to immune functions (Schlesinger et al., 1975).

Interestingly, a second study showed that the protein named “A24” was a modified version of histone H2A, with two amino termini but only one carboxy terminus (Goldknopf and Busch, 1977). Tryptic digestion of A24 generated a branched product that was the result of an iso-peptide bond between the ε-amino group of K119 of H2A and the carboxy terminus of another non-histone poly-peptide. It was only later discovered that APF-1, UBIP and the poly-peptide conjugated onto H2A were in fact the same.

1.2.1 The structure of ubiquitin

Ubiquitin is a small poly-peptide made up of 76 amino acids that is highly conserved across species and kingdoms (Zuin et al., 2014). In humans, ubiquitin is expressed as a product of four different genes; UBB, UBC, UBA52 and RPS27A (**Figure 1.1**).

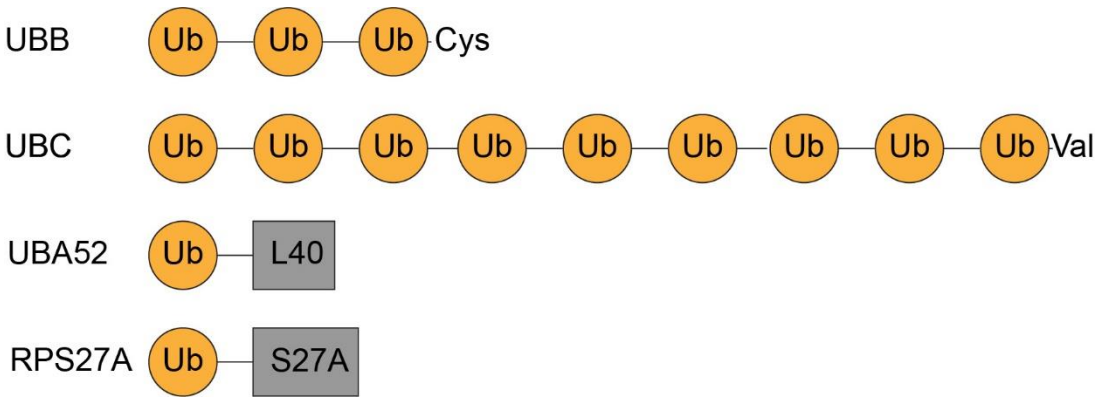

Figure 1.1: The architecture of the human ubiquitin genes
The four human genes and their gene products encoding for ubiquitin. UBB and UBC encode for linear poly-ubiquitin chains with 3 and 9 ubiquitin moieties respectively, and an additional terminal amino acid after the terminal ubiquitin moiety. UBA52 and RPS27A encode for a single ubiquitin fused to a ribosomal protein. Cys, cysteine; Val, Valine.

UBB and UBC produce linear poly-ubiquitin chains. The ubiquitin moieties are produced as a single uninterrupted gene product joined in a head-to-tail fashion that are subsequently processed into free ubiquitin (Özkaynak et al., 1984; Wiborg et al., 1985). In humans, UBB and UBC contain 3 and 9 ubiquitin repeats respectively (Uniprot entries: P0CG47 and P0CG48), however the number of ubiquitin repeats may differ across species (Baker and Board, 1987). The latter two genes, UBA52 and RPS27A, contain a single ubiquitin open-reading frame (ORF) fused to the 60S ribosomal protein L40 and the 40S ribosomal protein S27A respectively (Baker and Board, 1991).

Ubiquitin is famous for its thermal and chemical stability, and inherent resistance to proteases (Schlesinger et al., 1975; Lenkinski et al., 1977; Ciechanover et al., 1978, 1981). Ubiquitin exhibits such a remarkable stability across a range of temperatures and pH that it has been adopted as a protein standard for use in nuclear magnetic resonance studies.

The first crystal structure of human ubiquitin resolved at 2.8 Å revealed that ubiquitin is a globular and compact protein with a pronounced hydrophobic core, which is thought to be the reason for its observed thermal stability (Vijay-Kumar et al., 1985). An estimate of about 90% of its residues participate in extensive hydrogen bonding resulting in strong secondary structural elements. Overall, ubiquitin is a compact, mostly β-sheet protein with a single α-helical element. A second crystallographic study by the same lab at 1.8 Å resolution showed the accessibility of the lysine residues of ubiquitin, which is critical for the different linkage specific poly-ubiquitin chains that can be made. Three out of seven (K6, K33 and K63) lysine ε-amino groups are the most accessible on the surface of the molecule. The lysines at positions 11 and 27 are participating in ionic interactions whilst K29 and K48 participate in hydrogen bonding. Finally, lysines at position 27 and 29 are the least exposed in terms of chemical reactivity (Vijay-kumar et al., 1987).

1.2.2 Ubiquitylation: the covalent modification

The first evidence that ubiquitin was conjugated to protein substrates came from the observation that ^{125}I-labeled APF-1 was forming conjugates in the presence of ATP, a reaction termed ubiquitylation or ubiquitination (Ciechanover et al., 1980).

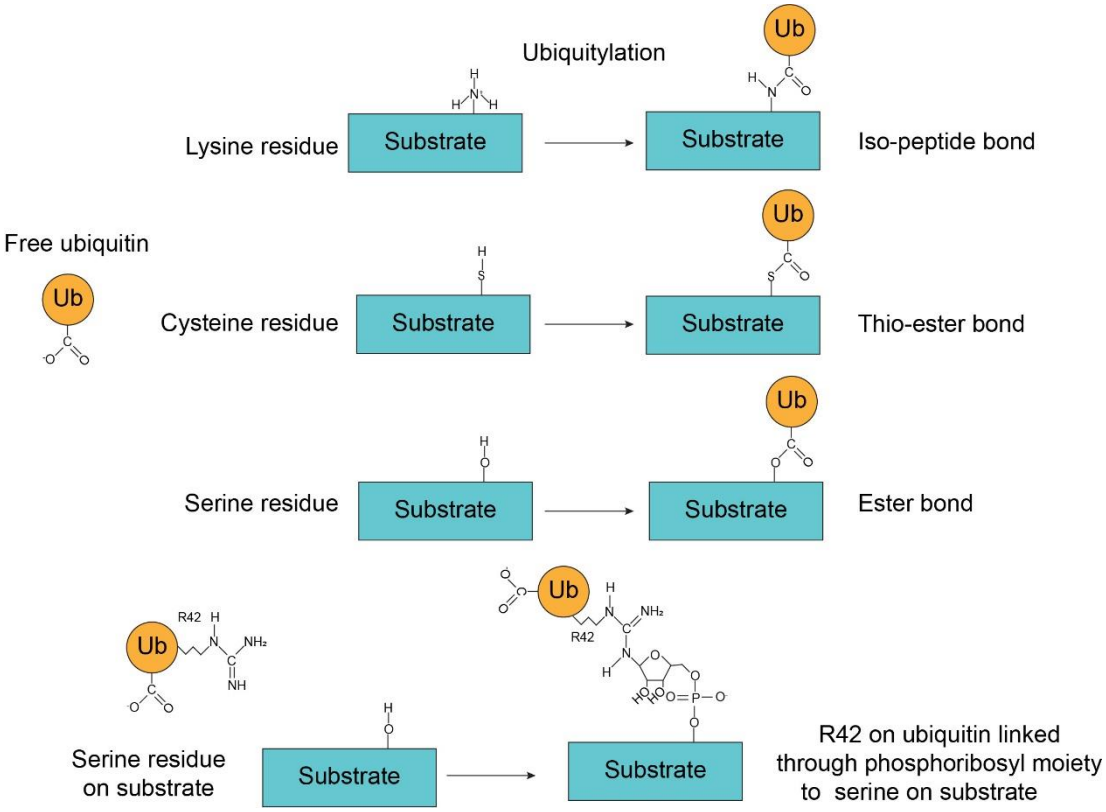

Figure 1.2: Chemistry of the ubiquitin-substrate covalent bond

Schematic diagram showing the structure of the bonds that ubiquitin may be conjugated onto target substrates based on the amino acid side-chain. Conjugation of ubiquitin on lysine, cysteine and serine residues results in the formation of iso-peptide, thio-ester and ester bonds respectively. Bottom diagram shows the atypical bond between the side chain of Arginine 42 (R42) on ubiquitin and a serine residue on the substrate linked with a phosphoribosyl moiety.

A subsequent study by the same lab showed that specific protein substrates could be conjugated with multiple molecules of APF-1, demonstrating that protein substates can be poly-ubiquitylated (Hershko et al., 1980). Ubiquitin and ubiquitylation as a post-translational modification (PTM) have a pivotal role to play in a number of ways in cell physiology as well as in human disease. Conjugation of ubiquitin on a protein substrate can have an impact on its activity, localisation and stability (Rape, 2018). Ubiquitin is attached to proteins through its carboxy terminus most commonly to the ε-amino group of lysine residues forming an iso-peptide (amide) bond (Goldknopf and Busch, 1977). Conjugation to cysteine or serine residue side

chains forming thioester and ester bonds respectively are known to occur but are far less common (Kelsall et al., 2019; De Cesare et al., 2021) (**Figure 1.2**.).

Recently a new type of ubiquitin linkage was discovered that is mediated by bacterial enzymes in *Legionella pneumophila*. This atypical ubiquitylation is performed by the bacterial enzyme SdeA and it involves the phosphoribosylation of the side chain of arginine 42 of ubiquitin and the conjugation onto a substrate protein through a serine side chain. The substrate and ubiquitin are not directly conjugated to each other. The bond is mediated through the phosphoribosyl moiety (Bhogaraju et al., 2016).

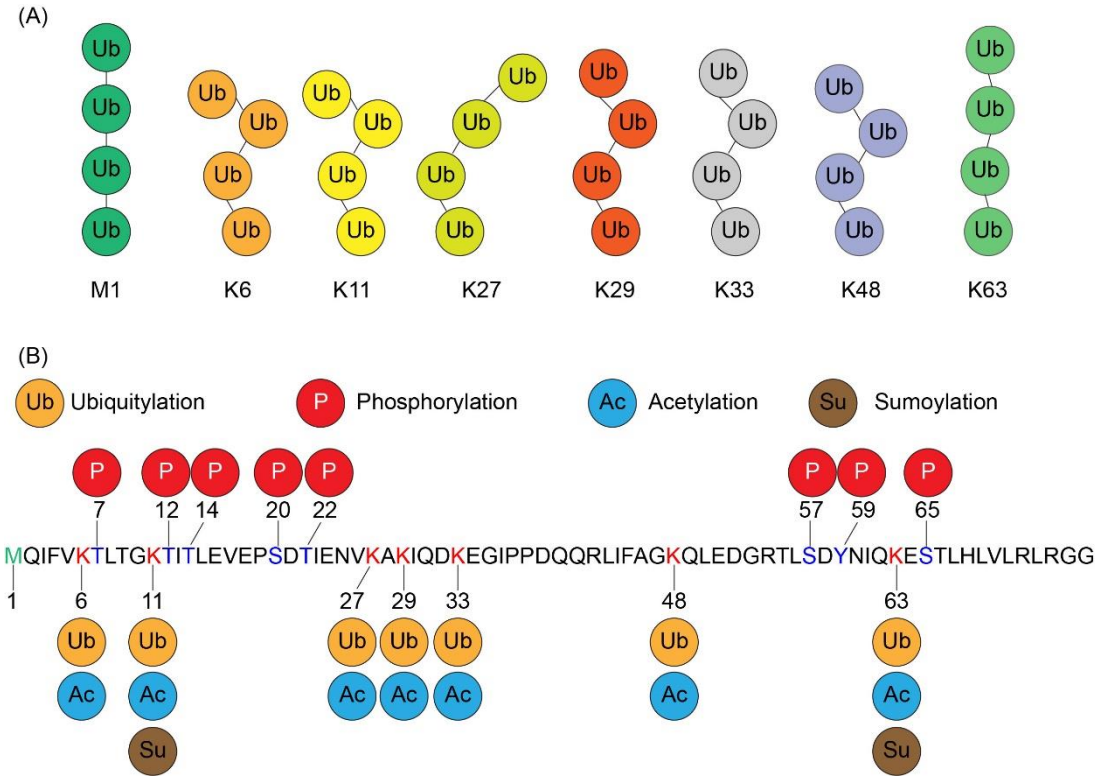

Figure 1.3: Ubiquitin chain linkages and post-translational modifications
(A) Overview of all the kinds of homotypic ubiquitin chains that may be generated. Diagram adapted from Lafont et al., (2018). (B) Diagram illustrating the major known post-translational modifications on ubiquitin. The initiator methionine is marked in green colour, all lysines are in red, and serines, threonines and tyrosine residues are shown in blue. Diagram adapted from information on PhosphoSitePlus® v6.5.9.3

Ubiquitin itself can be ubiquitylated to form poly-ubiquitin chains on substrate proteins. Ubiquitin has 7 lysine residues (6, 11, 27, 29, 33, 48 and 63) all of which have been shown to act as sites for ubiquitylation (**Figure 1.3**). Furthermore, ubiquitin may be conjugated to the amino terminus of another ubiquitin to form linear head-to-tail poly-ubiquitin chains termed M1 chains (Breitschopf, 1998). Ubiquitin can also undergo a number of other post-translational modifications (PTMs) other than ubiquitylation (**Figure 1.3**B). This includes serine/threonine/tyrosine phosphorylation (Lee et al., 2009; Malik et al., 2009; Moritz et al., 2010), lysine acetylation (Choudhary et al., 2009) and sumoylation, which is the conjugation of another small ubiquitin-like molecule, small ubiquitin modifier (SUMO) (Lamoliatte et al., 2013).

Ubiquitylation patterns on substrates can be highly variable and versatile due to the ability of ubiquitin to extend ubiquitin chains using its 7 lysine residues and its N-terminal methionine and further undergo other PTMs because ubiquitin is itself a protein (**Figure 1.4**). The multitude of ubiquitin modifications is often referred to as the “ubiquitin code” (Swatek and Komander, 2016).

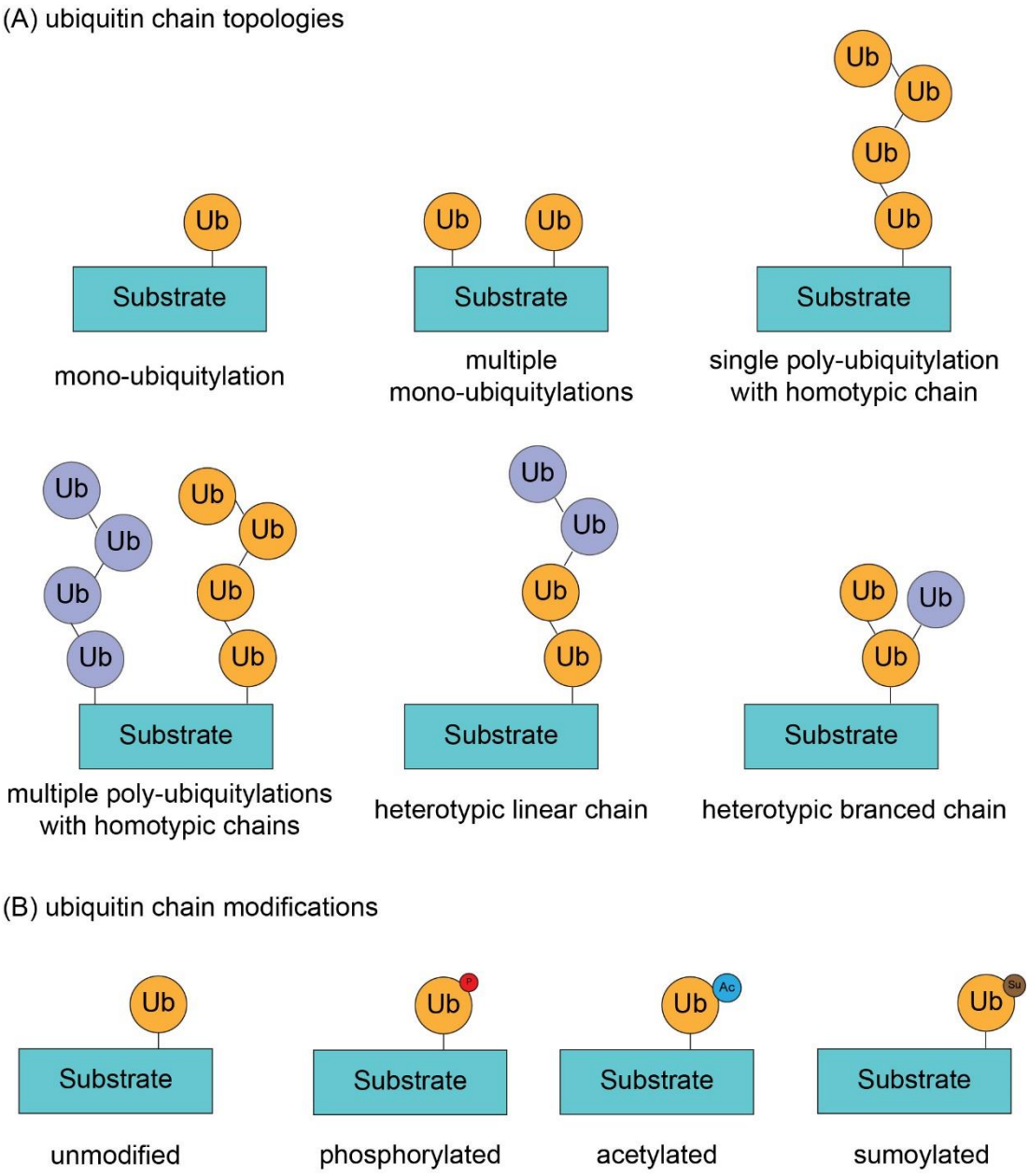

Figure 1.4: Expanding the ubiquitin code

Diagram of the different ways ubiquitin is used to generate different ubiquitin chain topologies by (A) being conjugated onto substrates as mono-ubiquitylation, multiple mono-ubiquitylations, single poly-ubiquitylation with homotypic chain, decorated with more than one poly-ubiquitin chain of different ubiquitin linkages, single poly-ubiquitin chain that includes more than one linkage, poly-ubiquitin of different ubiquitin linkage resulting in a branched chain and (B) post-translational modifications on ubiquitin itself including phosphorylation, acetylation and sumoylation. Collectively, the assembly of different types of ubiquitin chains and their modification therein expand upon the ubiquitin code. Ub, ubiquitin; P, phosphate; Ac, acetyl; Su, SUMO.

Information on the structure and conformation of poly-ubiquitin chains is derived from crystallographic studies or alternatively from nuclear magnetic resonance (NMR) experiments that also consider the dynamics of poly-ubiquitin in solution. Poly-ubiquitin chains of a particular linkage adopt either an “open” or “closed” conformation (Komander and Rape, 2012). An “open” conformation is characterised by an extended arrangement of the ubiquitin moieties where there are little or no interactions between the participating ubiquitin molecules apart from the iso-peptide bond. A “closed” conformation refers to a compact arrangement of the ubiquitin molecules where the ubiquitin moieties form intra-chain bonds between them.

Table 1.1: Summary of ubiquitin chain topology and conformation

Ubiquitin Chain	Conformation	Method	Reference
M1	Extended, linear	X-ray	Komander et al., 2009
K6	Compact, closed, asymmetric	X-ray	Virdee et al., 2010; Hospenthal et al., 2013
K11	Compact	Both	Bremm et al., 2010
K27	Open	NMR	Castañeda et al., 2016
K29	Open, extended	X-ray	Kristariyanto et al., 2015a; Michel et al., 2015
K33	di-Ub: Compact, symmetric tri-Ub: open, extended	X-ray	Kristariyanto et al., 2015b; Michel et al., 2015
K48	Closed, compact, symmetric	NMR, both, both	Varadan et al., 2002; Tenno et al., 2004; Eddins et al., 2007
K63	Extended, linear	both, NMR, X-ray	Tenno et al., 2004; Varadan et al., 2004; Komander et al., 2009

The table summarises the conformations of the 8 ubiquitin linkages and the methodology used in determining them

In both open and closed conformations, the poly-ubiquitin chains adopt a unique interface that becomes available for protein-protein interactions typically using a ubiquitin binding domain (UBD). **Table 1.1** summarises the conformations of the eight poly-ubiquitin chains as “open” or “closed” and the methodology used to determine them. Poly-ubiquitin chains linked with K6-, K11- and K48- links have been described as closed and compact. Yet, the poly-ubiquitin chains can exist in a number of conformations based on how the distal and proximal ubiquitin moieties interact with each other. K11- and K48-linked ubiquitin are known to exist in two compact conformations in solution and this switch between the two conformations may facilitate binding with other interactors (Komander and Rape, 2012). K27-linked ubiquitin chains remain the only poly-ubiquitin chain type for which there is no complete structure available. However, there is one NMR study showing that K27-linked di-Ub exists in an open conformation with no non-covalent contact between the participating ubiquitin moieties in the chain (Castañeda et al., 2016). K27 is the least accessible lysine out of the seven and it is known to participate in a number of interactions within the ubiquitin molecule. Formation of an iso-peptide bond at this position is thought to create changes in the residues surrounding K27 without affecting the overall structure of ubiquitin (Huang et al., 2014; Castañeda et al., 2016). These small changes may be sufficient to create a unique interface that is not shared with other poly-ubiquitin chains. K29-linked chains were shown to adopt open conformations and are often found as part of heterotypic ubiquitin chains, in particular K48-linked chains (Kristariyanto et al., 2015a). M1- and K63-linked chains are often described as “beads on a string” due to the open and extended conformation they adopt. The ubiquitin moieties in M1- and K63-linked chains are characterised by flexibility and conformational freedom from each other (Komander et al., 2009b).

Collectively, the above conformations offer a wide range of possible geometries that poly-ubiquitin chains may adopt, which in turn are used to distinguish between these molecular tags.

Ubiquitin chain-specific functions have traditionally been studied using ubiquitin K to R point mutants (e.g. K48R, K63R) or using lysine-free ubiquitin (Ub K0) both in yeast and mammalian systems (Spence et al., 1995; Huang et

al., 2014; Ordureau et al., 2015). The expression of these mutants prevents the assembly of specific ubiquitin chain types or all ubiquitin chains, except for M1-linked chains, in the case of Ub K0. For the detection of specific ubiquitin-chain linkages a number of specific antibodies, tandem ubiquitin-binding entities (TUBE) as well as affimers have been developed that allow the visualisation of ubiquitin linkage-specific chains in cell lysates and by immunofluorescence (Michel et al., 2017). In the absence of suitable reagents, an alternative methodology has been developed that utilised the ability of certain deubiquitylating enzymes to act very specifically against certain chain types, UbiCRest (Hospenthal et al., 2013, 2015). Lastly, ubiquitomics may be used to monitor the accumulation of linkage-specific ubiquitin chains in cells in an unbiased and holistic manner (Xu et al., 2010). This methodology utilizes the di-Gly remnant that is left on ubiquitin after poly-ubiquitin chains are treated with trypsin. The modification may be used to detect and quantitate the relative levels of the different linkage types based on which ubiquitin peptides accumulate with di-Gly “stumps”.

1.2.3 The functions of ubiquitylation

Ubiquitylation is performed by a cascade of an E1/E2/E3 ubiquitin conjugating and ligating enzymes and reversed by deubiquitylating enzymes (DUBs) (see sections 1.2.4 and 1.3). Ubiquitylation has been assigned a plethora of functions, including the proteasomal degradation of substates, the trafficking of cargo between endosomal compartments, regulation of transcription and genome maintenance, and selective autophagy (Komander and Rape, 2012; Rape, 2018).

Ubiquitylation of histones appears to be largely restricted to mono-ubiquitylation events (**Figure 1.5**). In fact, histone H2A was the first ever protein discovered to be ubiquitylated as protein A24 with two amino termini (Goldknopf and Busch, 1977). The earliest evidence of the role of histone ubiquitylation in cells suggested that ubiquitylated histone H2A in the context of nucleosomes correlated with transcriptionally active chromatin (Levinger and Varshavsky, 1982). On the other hand, ubiquitylated histones were mostly absent from the activated immunoglobulin κ chain gene locus (Huang et al., 1986). In this context, K119 ubiquitylation on H2A (uK119 H2A) was assigned

a transcriptionally repressive role as part of the polycomb repressive complex 2 (PRC2) and a marker of mechanical stability that hinders the passage of DNA and RNA polymerases (Wang et al., 2004; Xiao et al., 2020). Collectively, the data suggested that the functions of mono-ubiquitylated histones H2A and H2B were dependent on the cell type and the specific gene under investigation (Zhang, 2003; Meas and Mao, 2015). Histones H3 and H4 were shown to be ubiquitylated in response to UV-induced DNA damage and histone ubiquitylation in this context promoted the release of the histone from nucleosomes on the site of DNA damage (Wang et al., 2006). Furthermore, Histone H3 ubiquitylation on K18 and K23 was shown to mediate recruitment of DNMT1 to methylate DNA, which suppresses gene expression (Vann and Kutateladze, 2017).

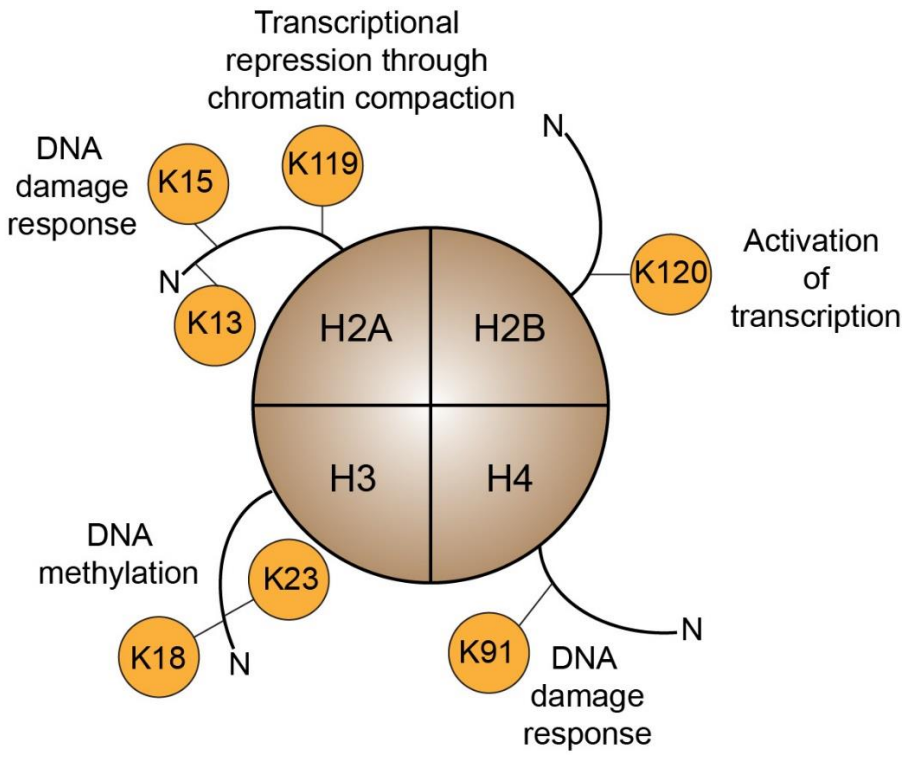

Figure 1.5: Functions of Histone mono-ubiquitylation

The diagram depicts the canonical nucleosome consisting of two copies of each histone protein H2A, H2B, H3 and H4, the residues that undergo ubiquitylation and their reported functions. The N-terminus is indicated as “N” and the C-termini are positioned in the centre of the nucleosome. The positioning of the residues on the histone tails is not to scale. Adapted from Oh et al., (2018).

Histone H1 sits on top of the canonical nucleosome and keeps the wrapped DNA in place. UV-induced DNA damage results in the ubiquitylation of H1, which triggers the RNF8/RNF168 signalling pathway for DNA repair (Thorslund et al., 2015; Mandemaker et al., 2017).

The most widely-known function of ubiquitylation is the targeting of proteins for proteasomal degradation. It was commonly thought that the tagging of a substrate with a poly-ubiquitin consisting of a minimum of four ubiquitin molecules is sufficient to target proteins to the proteasome (Hershko and Heller, 1985; Finley et al., 1994; Piotrowski et al., 1997). However, it has been shown that multiple mono-ubiquitylations on a single protein also suffice to target it to the proteasome (Boutet et al., 2007; Kravtsova-Ivantsiv et al., 2009; Dimova et al., 2012).

The first poly-ubiquitin chain to be assigned the function of targeting substrates for proteasomal degradation was K48-linked chains (Chau et al., 1989; Finley et al., 1994). Proteomic studies looking at the steady state levels of ubiquitylation have shown than K48-linked chains are one of the most abundant, and rapidly increase in response to proteasome inhibition, suggesting that a major role of K48-linked ubiquitin is proteasomal targeting (Peng et al., 2003; Komander and Rape, 2012). It is accepted however that most chain linkages may act as signals for proteasomal degradation to a variable extent, with K63-linked chains being a possible exception (Kim et al., 2011).

Upon proteasome inhibition, the di-Gly remnants corresponding to K6-linked ubiquitin peptides remained largely unchanged, suggesting the primary physiological roles of K6-linked ubiquitin chains were not proteasomal degradation (Kim et al., 2011). A study showed that K6- and K33-linked chains were enriched in cells that had undergone genotoxic stress due to UV-irradiation, placing K6-linked ubiquitin chains in the context of DNA damage (Elia et al., 2015). Another aspect of cellular physiology K6-linked chains play a role in is mitochondrial health and homeostasis. Overexpressing K6R and K63R mutant ubiquitin in cells caused a delayed response in mitophagy following mitochondrial damage, while other K to R ubiquitin mutants did not (Ordureau et al., 2015; Cunningham et al., 2015). The mitochondrial RING-between-RING E3 ubiquitin ligase Parkin (*PARK2*) was shown to specifically

generate K6-linked ubiquitin chains on depolarised mitochondria, while the deubiquitylase USP30 that opposes Parkin activity on mitochondria, is known to be specific against K6-linked chains (Ordureau et al., 2014; Cunningham et al., 2015; Gersch et al., 2017). Furthermore, K6- and K63-peptides were enriched during Parkin-dependent mitophagy as monitored by ubiquitin absolutely quantification (AQUA) proteomics (Kirkpatrick et al., 2005; Ordureau et al., 2015). Collectively, these data suggest a major role of K6-linked ubiquitin chains in mitochondrial health (Swatek and Komander, 2016).

K11-linked chains are generated by the anaphase promoting complex/cyclosome (APC/C) E3 complex in conjunction with the E2 ubiquitin conjugating enzyme UBE2S. The role of ubiquitylation by the APC/C is to ensure the timely degradation of mitotic substrates upon initiation of anaphase (Bremm and Komander, 2011; Wickliffe et al., 2011b). Interestingly, homotypic K11-linked poly-ubiquitin chains were shown to be poor substrates for proteasomal degradation. In contrast, heterotypic poly-ubiquitin chains comprising mostly of K11- and a minority K48-linked chains are much more efficiently targeted for proteasomal degradation (Grice et al., 2015).

K27-linked ubiquitin chains remain one of the least well-characterised in terms of function. DNA damage in the form of double strand breaks results in the generation of K27-linked ubiquitin chains on histones H2A and H2A.X that recruit DNA repair factors (Gatti et al., 2015, 168). Atypical K27- and K29-linked chains were shown to be attached to LRRK2, which leads to its aggregation (Nucifora et al., 2016). Furthermore, the autophagy adaptor Optineurin (OPTN) becomes decorated with K27-linked chains, which is thought to increase the autophagic flux mediated through OPTN (Liu et al., 2014). K29-linked chains were found to modulate proteasome activity itself. Ubiquitylation of the proteasome subunit RPN13 with K29-linked chains reduced the engagement of poly-ubiquitylated protein substrates to the proteasome without however affecting its proteolytic activity (Besche et al., 2014). The above mechanism is thought to act as a safeguard against overwhelming the proteasomes with substrates and assisting the protein loads to be degraded across different proteasome complexes. K33-linked ubiquitin chains were reported to be involved in retrograde membrane trafficking to the trans-Golgi network (Yuan et al., 2014).

Linear ubiquitin or M1-linked chains are generated by HOIL-1 interacting protein/RNF31 (HOIP), which is part of the linear ubiquitin chain assembly complex (LUBAC) in association with HOIL-1L (RBCK1) and Sharpin (Kirisako et al., 2006; Smit et al., 2012). The role of M1-linked chains in this context is in the regulation of gene expression and cell fate downstream the tumour necrosis factor (TNF) signalling pathway in infection and inflammation (Walczak, 2011). Complex I, that occurs in cells that express LUBAC components such as immune cells, induces the generation of M1-linked chains. M1-linked chains on complex I components lead to mitogenic signalling through the MAP kinase and NFκB signalling pathways resulting in proliferation, enhanced survival and activation of the cells (Haas et al., 2009). In the absence of LUBAC, complex II assembly occurs in response to TNF and that generates K63-linked chains and allows activation of the apoptotic pathway through activation of caspase 8 and necroptotic pathway through activation of RIPK1. M1- and K63-linked chains are characterised as linear chains with open conformations (**Table 1.1**). Despite their seemingly similar chain topology, they elicit functionally very different cellular responses to the same stimulus in the same signalling pathway.

K63-linked chains are also implicated in the DNA repair pathway (Chen and Sun, 2009). Proliferating cell nuclear antigen (PCNA) is a DNA clamp that is involved in DNA replication and DNA damage repair pathways. Mono-ubiquitylation of PCNA occurs as a result of DNA damage during DNA replication and recruits the translesion DNA polymerases to replace the high-fidelity and high processivity DNA polymerases used in DNA replication (Hoege et al., 2002). Despite offering error-prone DNA repair, the switch in DNA polymerases is essential to by-pass the site of DNA damage before progressive DNA replication proceeds further (Bienko, 2005). The less error-prone pathway of template-directed repair is activated instead when mono-ubiquitylation on PCNA is extended into K63-linked ubiquitin chains by RAD5.

1.2.4 The ubiquitylation cascade involves three enzymes

Ubiquitin is conjugated onto proteins through the ubiquitylation cascade that involves three enzymes: an E1 ubiquitin activating enzyme (UAE), an E2 ubiquitin conjugating enzyme and an E3 ubiquitin ligase enzyme (Swatek and

Komander, 2016). Ubiquitylation begins by the activation of free ubiquitin by the E1 UAE using ATP (Hershko et al., 1980; Haas et al., 1982). The carboxy terminus of ubiquitin is adenylated using ATP to form a ubiquityl-AMP conjugate and pyrophosphate (PPi) bound to the UAE (Haas et al., 1982). The first adenylation reaction is catalysed on the adenylation domain of the UAE and the high energy bond of ubiquityl-AMP is used to drive the conjugation on the thiol group of the catalytic cysteine of UAE and results in the release of AMP from the complex (**Figure 1.6**) (Haas et al., 1982; Hershko et al., 1983).

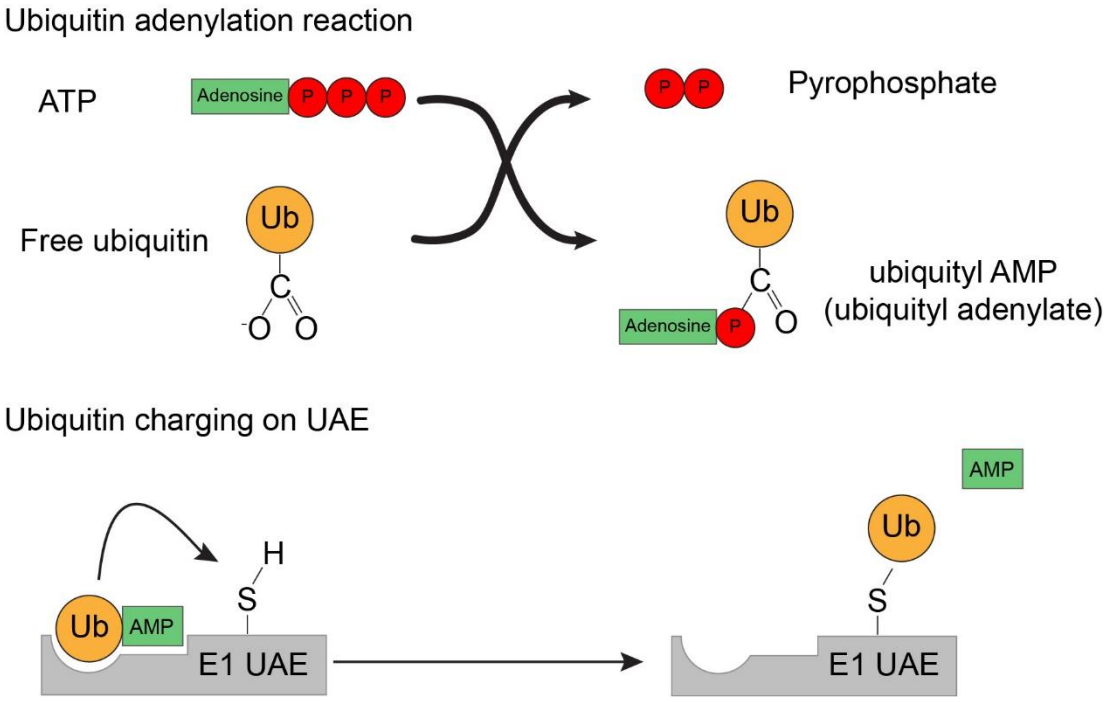

Figure 1.6: UAE uses ATP to charge itself with ubiquitin
Schematic representation of the two-step reaction the E1 UAE catalyses. The first reaction is the adenylation of the C-terminus of ubiquitin with ATP resulting in the generation of ubiquityl-AMP (ubiquityl adenylate) bound to UAE and the release of pyrophosphate (PPi). The second reaction is the covalent transfer of ubiquitin to the catalytic cysteine of UAE and the release of AMP. Ub, ubiquitin; ATP, adenosine triphosphate; AMP, adenosine monophosphate; P, inorganic phosphate group; E1 UAE, E1 ubiquitin activating enzyme.

Two E1 UAEs have been identified in mammals, UBA1 (McGrath et al., 1991, 1) and UBA6 (Jin et al., 2007). There are layers of regulation in ubiquitylation already at the level of the E1 UAE. E1 UAEs are largely specific to ubiquitin and do not typically act on other ubiquitin-like molecules such as SUMO, NEDD8 or ISG15, all of which have their own E1-type activating enzymes

(Schulman and Wade Harper, 2009). It is worthwhile mentioning that overexpression of NEDD8 results in the erroneous handling of NEDD8 by the ubiquitin cascade instead. The above resulted in NEDD8 conjugation onto ubiquitin substrates, suggesting overexpression is not an appropriate approach to study neddylation or similar conjugation cascades (Hjerpe et al., 2012a; b). Interestingly, one notable exception is that UBA6 was shown to activate FAT10, another ubiquitin-like protein, involved in inflammation and the immune response (Liu et al., 1999). Deletion of FAT10 in mice induces the loss of FAT10 conjugation without affecting viability of the animals, suggesting FAT10 function is not necessary for survival even though UBA6 itself was essential (Chiu et al., 2007). While the two UAEs activate ubiquitin with equal efficiency, they display differential expression profiles in tissues and sub-cellular localisation. UBA1 was shown to exhibit both cytoplasmic and nuclear localisations with its distribution and activity profile changing based on the cell cycle stage (Grenfell et al., 1994). UBA1 and UBA6 are ubiquitously expressed, however UBA1 is found to be about 10x more abundant than UBA6, suggesting the relative abundance of these two enzymes may reflect the amount of ubiquitylation that is channelled through each of them (Yang et al., 2013). Both enzymes share some but not all of the downstream E2 conjugating enzymes. USE1 for example, exclusively receives ubiquitin from UBA6 (Jin et al., 2007).

Next the ubiquitin is transferred from the catalytic cysteine of the E1 UAE to the catalytic cysteine of the E2 conjugating enzyme (Hershko et al., 1983). There are an estimated 38 E2 conjugating enzymes that are charged with ubiquitin before the engagement with the E3 ligases that mediate the ubiquitin transfer from the E2 to the specific substrate (Michelle et al., 2009; Ye and Rape, 2009). The handling of ubiquitin depends on the type of E3 ligase (Hershko et al., 1983). Three distinct classes of ubiquitin E3 ligases have been identified. Really Interesting New Gene (RING) E3 ligases are a family of about 600 proteins that share the RING domain in common (Freemont et al., 1991; Deshaies and Joazeiro, 2009). RING E3 ubiquitin ligases function by bridging ubiquitin-loaded E2 conjugating enzymes to specific substrates acting as both adaptors for substate recognition and the enzyme responsible for the ubiquityl transfer (**Figure 1.7**A).

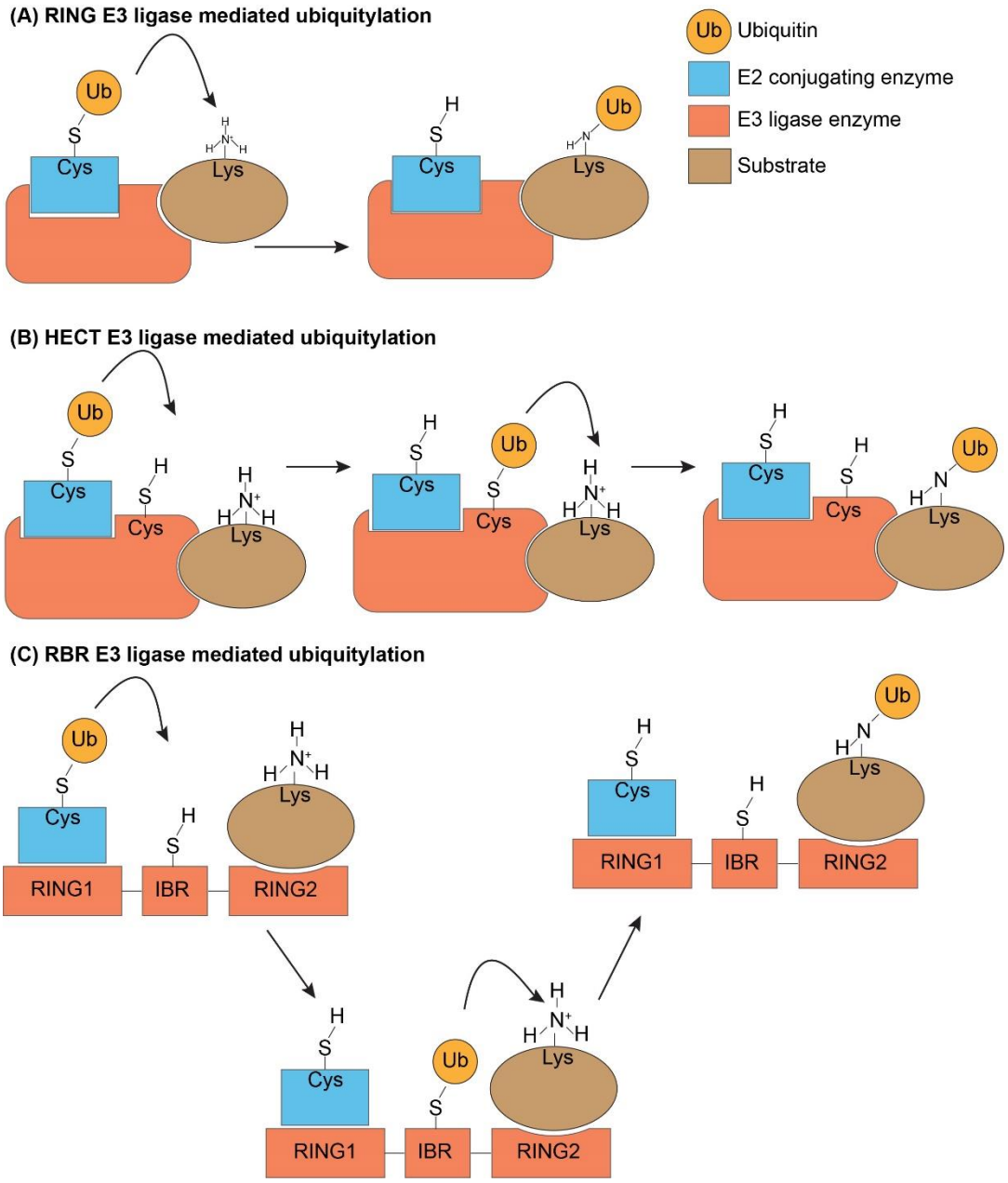

Figure 1.7: The mechanisms of ubiquitylation by E3 ubiquitin ligases

Schematic diagram depicting the mechanisms of ubiquitylation by showing how ubiquitin is transferred from the E2 conjugating enzyme to a substrate by (A) RING, (B) HECT and (C) RING-between-RING (RBR) E3 ubiquitin ligases. Ub, ubiquitin; Cys, cysteine; Lys, lysine; RING, really interesting new gene; HECT, Homologous to the E6AP carboxyl terminus; IBR, in-between-RING.

RING E3 ligases promote the transfer of ubiquitin by bringing the loaded E2 conjugating enzyme in a closed conformation towards the site of ubiquitin conjugation on the substrate (Plechanovová et al., 2012; Branigan et al., 2020). The association between E3 enzyme, ubiquitin-loaded E2 and substrate promotes the extension of the C-terminal tail of the donor ubiquitin in the E2 active site, facilitating the nucleophilic attack by the lysine on the substrate (Zheng and Shabek, 2017).

RING E3 ligases may function in complexes where the enzymatic component and the substrate recognition domains are found in different proteins such as is the case for the anaphase promoting complex/cyclosome (APC/C) (Chang and Barford, 2014) or the cullin-RING ligases (Sakata et al., 2007; Duda et al., 2008). Alternatively, the catalytic and substrate recognition domains may be found on the same poly-peptide such as for c-CBL (Joazeiro, 1999). The defining feature of RING E3 ligases is that they lack transfer of ubiquitin onto themselves during catalysis.

The HECT family of E3 ubiquitin ligases is characterised by the presence of the Homologous to the E6AP carboxyl terminus (HECT) domain and estimated to contain approximately 30 members (Huibregtse et al., 1995; Huang, 1999; Deshaies and Joazeiro, 2009). The distinguishing feature of HECT E3 ligases is the presence of a catalytically active cysteine, onto which ubiquitin becomes transferred first before being conjugated to the substrate (**Figure 1.7**B). In contrast to the closed conformation the ubiquitin-loaded E2 enzymes adopt when in complex with the RING E3 ligase, HECT E3 ligases promote the E2-Ub complexes to adopt an open conformation (Kamadurai et al., 2009; Zheng and Shabek, 2017). Once the transthiolation reaction has the ubiquitin transferred to the HECT E3 ligase active site, the ubiquitin tail adopts a fully extended conformation to facilitate transfer onto the substrate.

The RING-between-RING (RBR) E3 ligases constitute the smallest and the most recently discovered family of E3 ubiquitin ligases, (Morett and Bork, 1999; Qiu and Fay, 2006; Wenzel et al., 2011; Zheng and Shabek, 2017). RBR E3 ligases are considered a hybrid between RING and HECT E3 ligases due to having RING domains that interact with their partner E2 conjugating enzymes and transfer ubiquitin onto a catalytic cysteine prior to ubiquitin

transfer onto the substrate (Wenzel et al., 2011; Reiter and Klevit, 2018) (**Figure 1.7**C).

Rather than acting as a mere ubiquitin carrier intermediate between E1 and E3 enzymes, E2 conjugating enzymes play an active role in determining ubiquitin chain topology and length as well as the functional outcome of ubiquitylation (Ye and Rape, 2009; Komander and Rape, 2012). Such examples are UBE2W and UBE2D in conjunction with BRCA1-BARD1. BRCA1 is able to self-ubiquitylate using both UBE2W and UBE2D. However, the auto-ubiquitylation outcome of BRCA1 is different; BRCA1 in association with UBE2W results in mono-ubiquitylation whereas with UBE2K resulted in poly-ubiquitylation with K48-linked ubiquitin (Christensen et al., 2007). UBE2N utilises an E2-like subunit to position K63 on the acceptor ubiquitin towards the active site where the donor ubiquitin is bound, achieving K63-linked ubiquitin chains (Eddins et al., 2006). UBE2S orients K11 on the acceptor ubiquitin relative to the donor ubiquitin using acidic residues, achieving specificity towards K11-linked chains (Wickliffe et al., 2011a).

Cullin RING ligases (CRLs) are a class of RING E3 ubiquitin ligases that consist of a cullin subunit, an adaptor protein, an RBX RING subunit and a substrate receptor unit (Bulatov and Ciulli, 2015). CRLs are modular due to large number of different complexes that can be assembled. There are seven different cullin subunits (CUL1, 2, 3, 4A/B, 5, 7 and 9), each with its own adaptor protein and a plethora of substrate recruitment subunits (Fouad et al., 2019). It is estimated that up to 20% of all ubiquitin-mediated proteasomal degradation of proteins is driven by CRLs in certain cell types (Soucy et al., 2009). The defining feature of CRLs is the requirement of their cullin subunit to be neddylated, which refers to the conjugation of the small ubiquitin-like protein NEDD8 onto cullins for E3 ligase activity (Cardozo and Pagano, 2004). An example of the modular nature of CRLs are the SCF complexes (**Figure 1.8**).

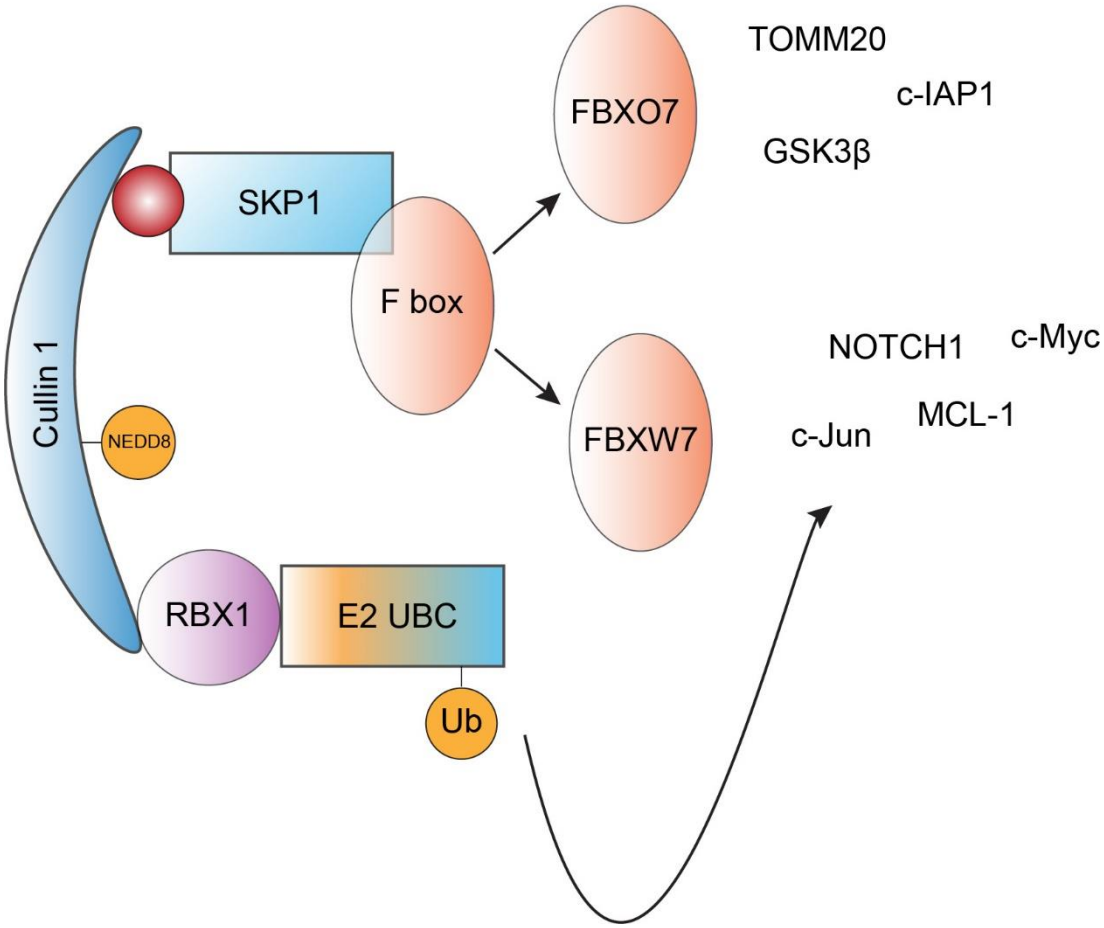

Figure 1.8: The SCF complex as Cullin RING E3 ubiquitin ligase

The SKP1/Cullin 1/F-box (SCF) complex as an example of a cullin RING ubiquitin ligase. The diagram depicts the SCF complex and shows two examples of F-box protein adaptors, FBXO7 and FBXW7 (FBW7), and their proposed substrates. SKP1, S-phase kinase-associated protein 1; RBX1, RING box protein 1; RING, Really Interesting New Gene finger domain; NEDD8, neuronal precursor cell-expressed developmentally downregulated protein 8; TOMM20, translocase of the outer mitochondrial membrane 20; GSK3β, glycogen synthase kinase 3β; c-IAP, cellular inhibitor of apoptosis protein 1; MCL-1, myeloid leukaemia protein 1; c-Myc, cellular myelocytomatosis; E2 UBC, E2 ubiquitin conjugating enzyme.

The SKP1/Cullin 1/F-box protein (SCF) consists of SKP1, Cullin 1, RBX1 as the RING subunit and one member of the F-box proteins that dictates substrate specific of the SCF. When FBXW7 (FBW7) is the F-box subunit of an SCF complex, the substrates need to be phosphorylated first prior to engaging with the SCF^{FBXW7} complex and then ubiquitylated (Welcker et al., 2004; Yada et al., 2004; Wertz et al., 2011; Inuzuka et al., 2011; Tong et al., 2017). If FBXO7 is included in the SCF complex (SCF^{FBXO7}) the E3 ligase activity of the complex was proposed to be directed against proteins such as TOMM20, GSK3β and c-IAP (Burchell et al., 2013; Teixeira et al., 2016). Loss of FBXO7 (*PARK15*) resulted in reduced proteasome activity and induced a parkinsonism-like disease in mice, suggesting FBXO7 targets distinct sets of substrates to other F-box proteins (Vingill et al., 2016). Overall, ubiquitylation of substrates by CRLs is dictated by the exact cullin RING complex and the substrate recruitment subunit. The complexity of ubiquitylation by CRLs is further expanded on by the discovery that ARIH1, a RBR E3 ligase, must first prime the substrate with mono-ubiquitylation before the CRL expands the ubiquitin chain length (**Figure 1.9**). ARIH1 was shown to function in conjunction with CRLs and physically engage in interactions in the ubiquitylation process (Scott et al., 2016; Hill et al., 2019). The above findings stipulate that all CRL activity requires prior priming ubiquitylation by ARIH1 and that the mono-ubiquitylation by ARIH1 is often the rate limiting step in the proteasomal degradation by CRLs.

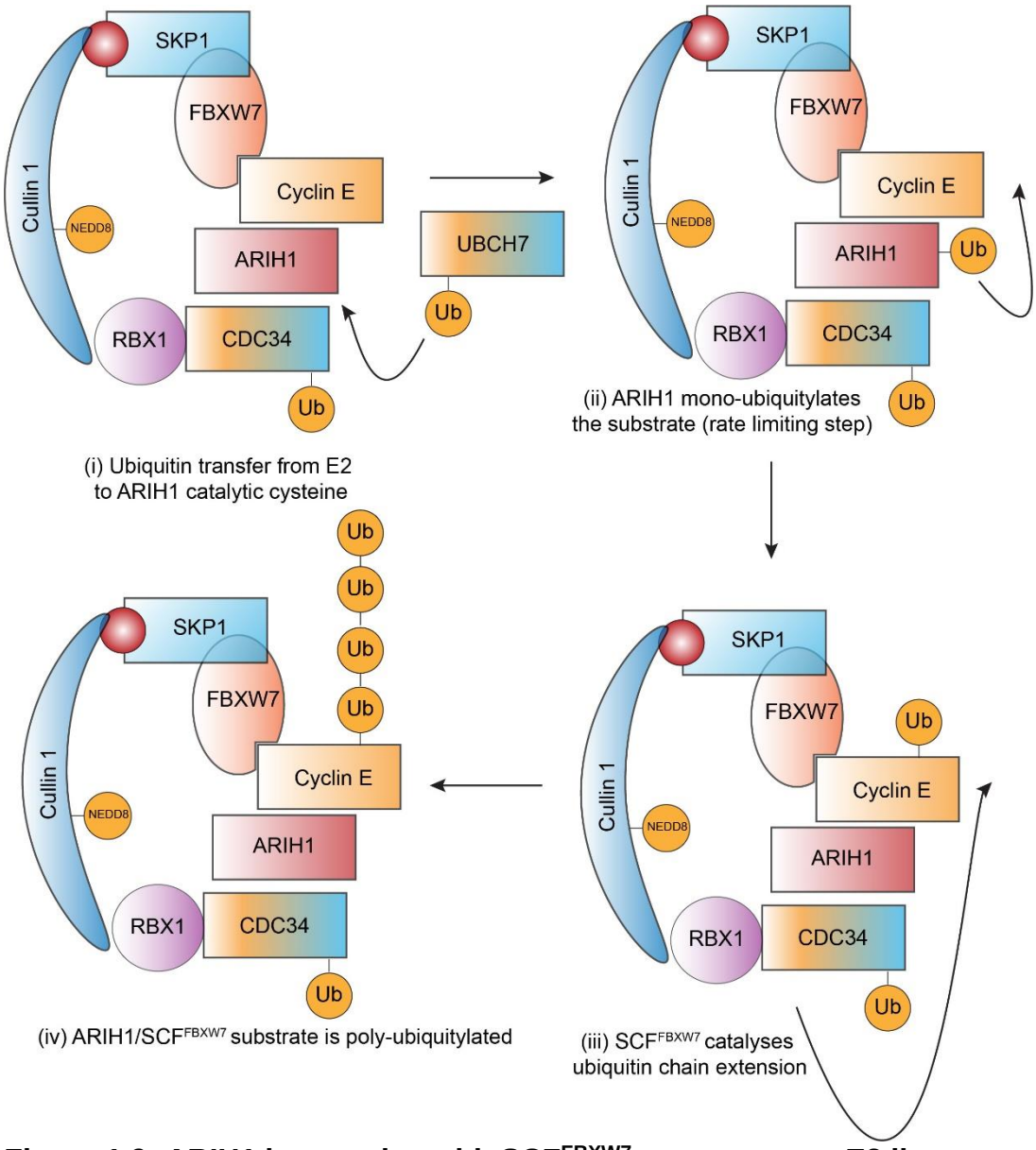

Figure 1.9: ARIH1 in complex with SCF^{FBXW7} co-operate as E3 ligases

Diagram depicts the sequential ubiquitylation of cyclin E by ARIH1 followed by SCF^{FBXW7}. Ubiquitin is transferred from (i) the E2 conjugating enzyme UBCH7 to the catalytic cysteine of ARIH1, which then (ii) mono-ubiquitylates cyclin E, and this ubiquitylation event is considered the rate limiting step of cyclin E ubiquitylation. Next (iii) the SCF^{FBXW7} extends the ubiquitin chain initiated by ARIH1 activity into a longer (iv) poly-ubiquitylated chain using CDC34 as the E2 conjugating enzyme. Diagram adapted from Scott et al., (2016).

1.3 The classification and catalytic mechanism of the Deubiquitylases

Ubiquitylation is a reversible protein post-translational modification; Once a protein substrate has been decorated with ubiquitin in one of the many ways outlined above (1.2.4), the ubiquitin modification may be altered or completely removed from substrates by the activity of deubiquitylases (DUBs). Deubiquitylases or deubiquitinases are a class of ubiquitin proteases whose collective function is the cleavage of ubiquitin from substrates, including free ubiquitin chain hydrolysis (Clague et al., 2019) (**Figure 1.10**).

DUBs display different modes of iso-peptidase activity against ubiquitylated substrates and poly-ubiquitin chains (Clague and Urbé, 2017). DUBs remove single ubiquitin moieties directly from substrates. Alternatively, in the instances of poly-ubiquitin chains, DUBs can remove the entire poly-ubiquitin chain from the substrate *en bloc* generating a free poly-ubiquitin chain and the unmodified substrate (Komander et al., 2009a). DUBs can act from the distal end of poly-ubiquitin chains removing one ubiquitin moiety at a time (exo-peptidase activity) or cleave within the poly-ubiquitin chains generating smaller free ubiquitin chains (endo-peptidase). Free poly-ubiquitin chains generated through endo-peptidase and *en bloc* cleavage are cleaved into single ubiquitin molecules through the activity of other DUBs such as USP5 (Clague et al., 2019).

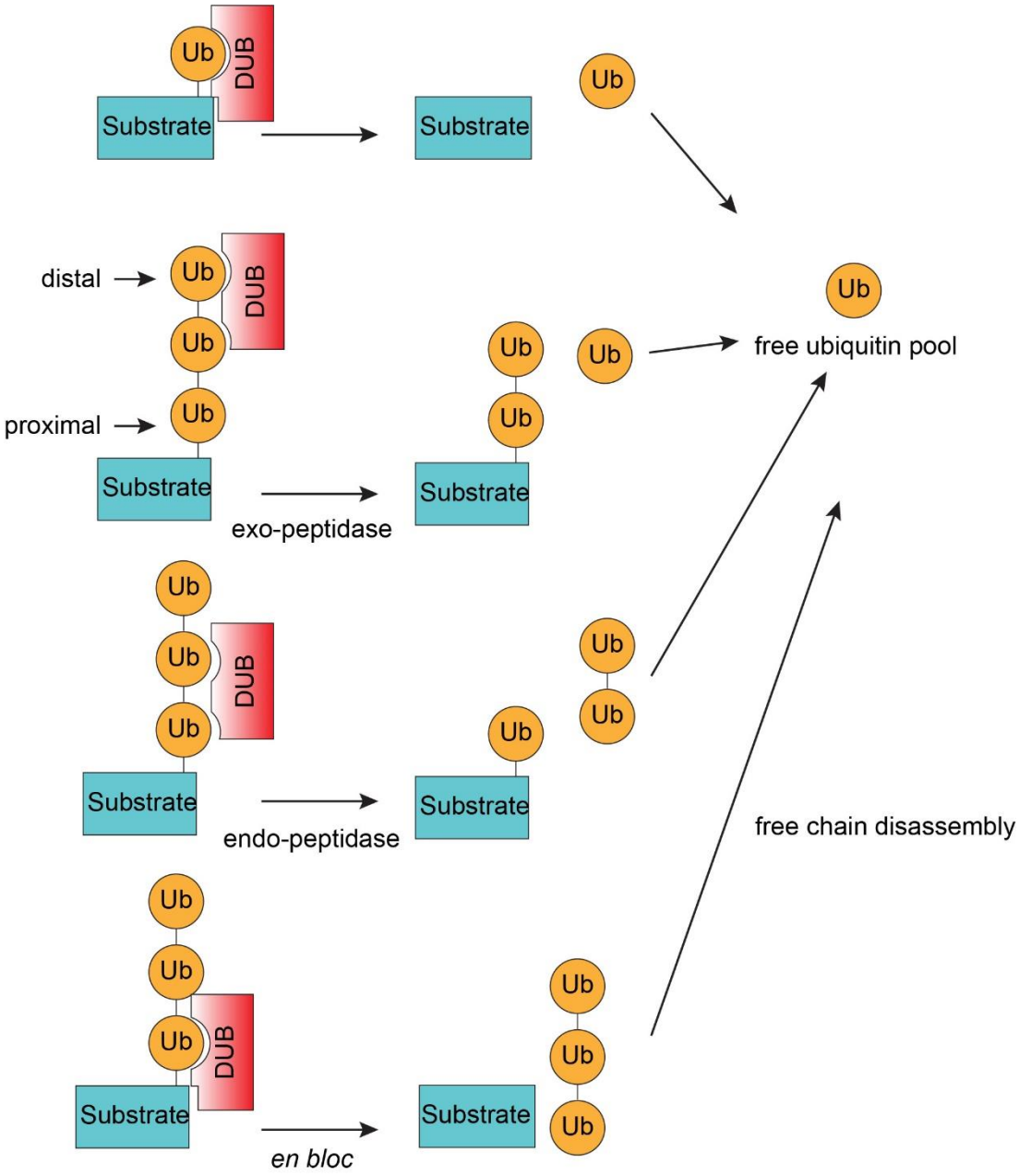

Figure 1.10: Deubiquitylating enzyme peptidase activity

The diagram depicts the different ways deubiquitylating enzymes (DUBs) cleave ubiquitin from substrates and disassembly of poly-ubiquitin chains. DUBs are able to remove ubiquitin from mono-ubiquitylated substrates, trim poly-ubiquitin chains from the distal end, cleave poly-ubiquitin chains through an endo-peptidase mode and remove the poly-ubiquitin chains *en bloc*. Ub, ubiquitin; DUB, deubiquitylating enzyme.

The discovery of DUBs dates back to the discovery of the ubiquitin conjugation cascade where an “amidase” was determined to be required for the recovery of free APF-1 from conjugated substrates (Hershko et al., 1980). There are seven families of DUBs identified in humans that consist of about 100 enzymes (Clague et al., 2019). The JAMM family is the only family that are metalloproteases and the remaining six families fall under the cysteine protease category (**Figure 1.11**).

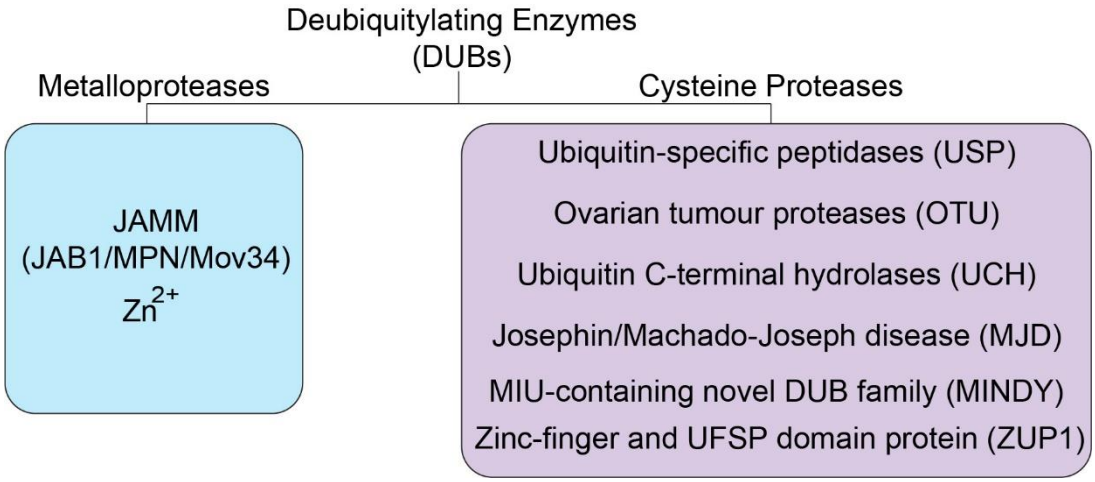

Figure 1.11: Overview of the human deubiquitylating enzyme families
Classification of human deubiquitylating enzymes into the JAMM family of metalloproteases and the cysteine proteases that includes Ubiquitin-specific peptidases (USP), Ovarian tumour proteases (OTU), Ubiquitin C-terminal hydrolases (UCH), Josephin/Machado-Joseph disease (MJD) family, Motif interacting with ubiquitin (MIU)-containing novel DUB family (MINDY) and Zinc-finger and UFSP domain protein (ZUP1).

The JAMM family of metalloprotease DUBs utilise the distinct JAMM domain that was originally discovered in bacteria (Cope, 2002). JAMM metalloproteases contain the consensus sequence of amino acids EX_nHS/THX_7SXXD, where X is any amino acid, that chelate a zinc (Zn^{2+}) ion (Maytal-Kivity et al., 2002; Ambroggio et al., 2003). The co-ordinated zinc is used to polarise a water molecule to perform a nucleophilic attack on the carbonyl carbon of the iso-peptide bond. A neighbouring glutamate accepts the proton from the water molecule, facilitating the reaction. This results in the formation of a tetrahedral intermediate, which collapses and releases ubiquitin

from the substrate (**Figure 1.12**A). DUBs of the JAMM family are highly selective in the poly-ubiquitin chains they hydrolyse, such as AMSH, AMSH-LP and BRCC36 all being highly selective against K63-linked poly-ubiquitin chains (McCullough et al., 2004; Nakamura et al., 2006; Zhu et al., 2015). An interesting fact of the JAMM family is that five of the twelve members are catalytically inactive as DUBs and yet perform vital functions as molecular scaffolds (Walden et al., 2018; Clague et al., 2019). JAB1/COPS5 is a JAMM metalloprotease and the catalytic component of the COP9 signalosome, responsible for the deneddylation of cullins (Cope, 2002; Maytal-Kivity et al., 2002). COPS6 is also a JAMM and forms part of COP9 signalosome even though it does not retain catalytic activity itself, a property that is confined to COPS5 alone. Cullin deneddyllation is required for the CRL complex to exchange F-box protein subunits and a major regulatory step in CRL activity (Liu et al., 2018b).

Cysteine proteases have a conserved catalytic triad that consists of a cysteine, histidine and aspartate or asparagine and the reaction proceeds via a covalent intermediate between the ubiquitin to be cleaved and the DUB itself (**Figure 1.12**B). The histidine residue assists in the deprotonation of the thiol group of the cysteine residue, which is facilitated by the electrostatic interaction that is subsequently formed between the protonated form of the histidine and the aspartate. The deprotonated thiol of the cysteine performs a nucleophilic attack on the carbonyl of the iso-peptide bond, forming a tetrahedral intermediate. The tetrahedral intermediate then collapses and the substrate is released. At this stage ubiquitin and the DUB are covalently bonded. A water molecule is then activated to perform a nucleophilic attack on the acetylated thiol. The subsequent tetrahedral intermediate collapses and releases ubiquitin, and the thiol group of the cysteine is regenerated.

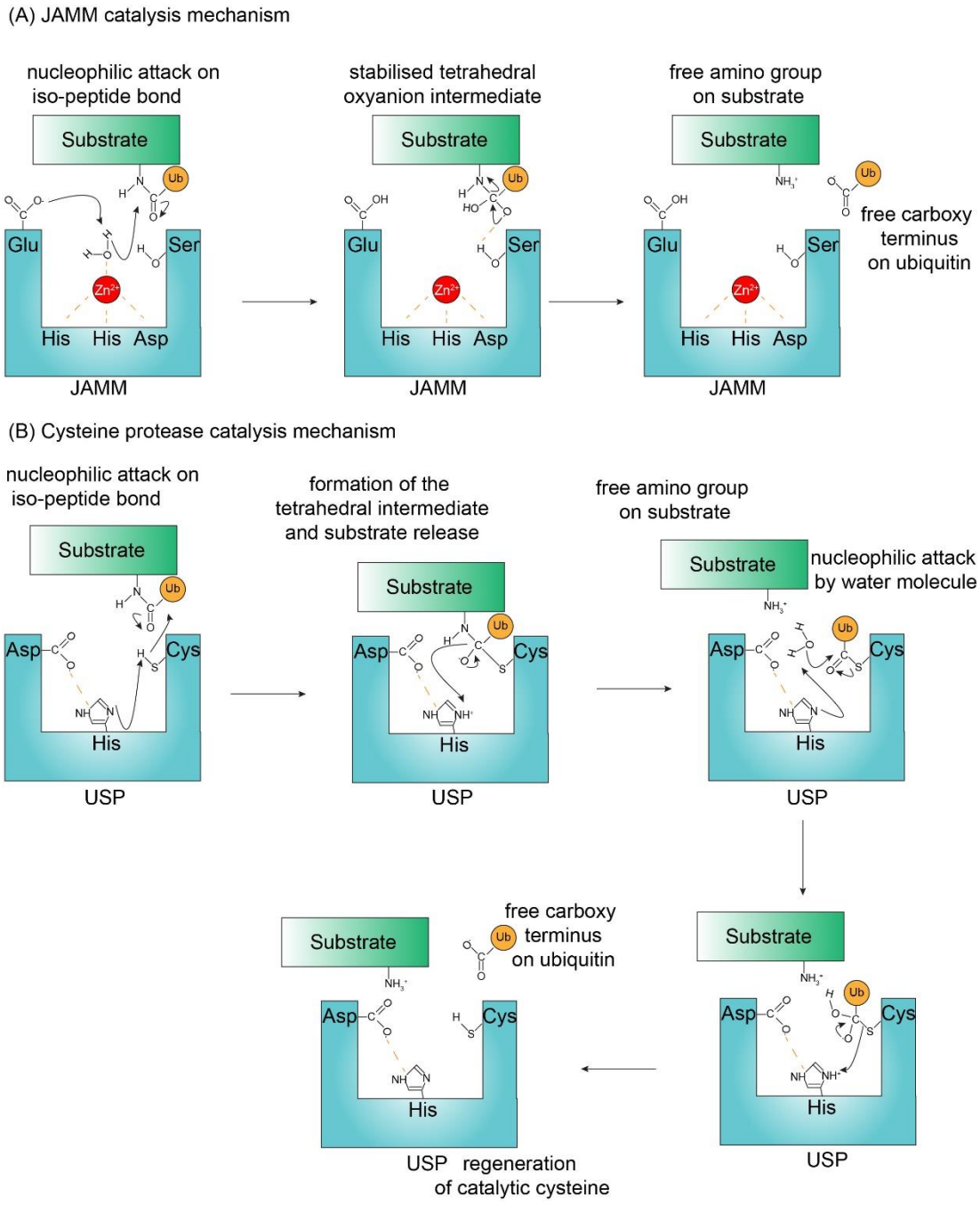

Figure 1.12: Reaction mechanisms of the DUBs

Diagram depicts the reaction mechanisms that operate during the catalytic cycle of a typical (A) JAMM domain deubiquitylase and (B) cysteine protease of the USP domain family. The substrate may be ubiquitin if the DUB is acting on poly-ubiquitin chains or it may be another protein in the instance of mono-ubiquitylation. JAMM, JAB1/MPN/MOV34; USP, ubiquitin specific peptidase; Asp, aspartate; Cys, cysteine; His, histidine; Glu, glutamate; Zn^{2+}, zinc ion. Diagram is adapted from Clague et al., (2013).

1.3.1 Ubiquitin C-terminal hydrolases (UCH) family

The family of Ubiquitin C-terminal hydrolases (UCH) were the first family of DUBs to be identified (Rose and Warms, 1983). There are four members to the UCH family: UCHL1, UCHL3, UCHL5 and BAP1. The UCH DUBs show poor processivity of most di-ubiquitin chain linkages and in contrast show excellent activity towards ubiquitin C-terminal fusions to other moieties (Bett et al., 2015). There is evidence to suggest that UCH family members are involved in the recycling of ubiquitin and maintaining a free ubiquitin pool in the cells for ubiquitylation to proceed. The C-terminus of ubiquitin may become modified by cellular nucleophiles such as glutathione or poly-amines and the purpose of UCHL1 and UCHL3 enzymes is thought to be to clear these conjugates from ubiquitin moieties (Larsen et al., 1996, 1998; Nijman et al., 2005). UCHL1 was shown to be highly expressed in neuronal tissues, making up an estimated 1-2% of the total protein in neuronal cells and certain mutations in UCHL1 are associated with hereditary forms of Parkinson's Disease (Wilkinson et al., 1989; Liu et al., 2002). UCHL3 is highly expressed in haematopoietic cells where it is thought to perform similar functions to UCHL1. UCHL5 is widely expressed in all tissues due to its association with the 26S proteasome (Patel et al., 2018). Interestingly, UCHL5 is only able to process longer ubiquitin chains when in association with the proteasome subunit RPN13 (Maiti et al., 2011; VanderLinden et al., 2015). In its free form, UCHL5 is thought to exist as an auto-inhibited dimer and associating with RNP13 relieves auto-inhibition by freeing the ubiquitin binding site (Jiao et al., 2014; Sahtoe et al., 2015).

BRCA1-associated protein 1 (BAP1) is involved in the regulation of transcription by promoting the deubiquitylation of histone H2A (Daou et al., 2015; Sahtoe et al., 2016; Campagne et al., 2019). BAP1 was found to be mutated in about 85% of uveal melanoma metastases, while germ-line mutations in BAP1 were shown to predispose to melanoma and mesothelioma (Jensen et al., 1998; Harbour et al., 2010; Wiesner et al., 2011; Testa et al., 2011). Collectively, it appears the UCH family of DUBs serves a protective role in cells, both in the contexts of cancer and neurodegeneration.

1.3.2 Ubiquitin specific peptidases (USP) family

The ubiquitin specific peptidases (USP) family is the largest family of DUBs numbering 56 members, making up over 50% of all identified DUBs in humans (Komander et al., 2009a; Clague et al., 2013, 2019). Members of the USP family share the USP catalytic domain as well as additional domains that may affect activity and sub-cellular localisation. USP19 and USP30 have short trans-membrane domains that allow them to anchor to the membranes of the endoplasmic reticulum and the outer mitochondrial membrane respectively, with their catalytic domains facing towards the cytosol (Hassink et al., 2009; Nakamura and Hirose, 2008). Certain USPs contain one or multiple ubiquitin-like domains (UBL) such as USP4, USP7 and USP15 (Clague et al., 2013). For some USPs, the UBL domain appears to promote the activity of the catalytic domain as shown for USP4 and USP7 (Clerici et al., 2014; Kim et al., 2016). An intrinsically unstructured region in USP21 is responsible for the DUB associating with microtubules and the centrosome, where USP21 regulates microtubule growth after cold-induced de-polymerisation (Urbé et al., 2012). The same study sought to systematically investigate the sub-cellular localisation of DUBs. The data showed that certain USPs are exclusively nuclear such as USP1, exclusively cytoplasmic such as USP18 or those that shared compartments such as USP5.

DUBs of the USP family are thought to be generally non-specific in terms of the types of ubiquitin chains they can process. Certain USPs have a preference towards a specific chain linkage but are still able to process other chain types as well. A known example is USP30 that processes K6-linked ubiquitin chains with very high efficiency but is still able to process K11 and K48 chains albeit at lower rates (Gersch et al., 2017). Other USPs such as USP2 and USP21 appear to be entirely non-selective and process all ubiquitin chains with similar efficiencies (Ye et al., 2011; Hospenthal et al., 2015). Cylindromatosis (CYLD) is perhaps the only known exception, aside from USP30, of a USP that displays high specificity towards M1- and K63-linked ubiquitin chains (Komander et al., 2008; Sato et al., 2015). Interestingly, USP18 is highly specific against ISG15-decorated proteins, a ubiquitin-like modifier involved in inflammation and infection (Malakhov et al., 2002).

1.3.3 Ovarian tumour protease (OTU) family

The OTU family of cysteine proteases were first identified as homologues to the *Drosophila melanogaster* otu gene that was implicated in RNA localisation during the development of the fly oocyte (Steinhauer et al., 1989; Makarova et al., 2000; Goodrich, 2004).

Members of the OTU family tend to be more selective in terms of the ubiquitin chains that they hydrolyse (Mevissen et al., 2013; Clague et al., 2019). For instance, OTULIN is highly specific towards linear M1-linked chains (Keusekotten et al., 2013). On the other hand, Cezanne and A20 have a strong preference towards K11- and K48-linked ubiquitin chains respectively (Bremm et al., 2010; Kulathu et al., 2013). Interestingly, A20 gains significant activity towards K63-linked poly-ubiquitin chains upon phosphorylation (Mevissen et al., 2013; Wertz et al., 2015; Draber et al., 2015).

1.3.4 Josephin/Machado-Joseph disease (MJD) family

The Josephin family or Machado-Joseph disease (MJD) family consists of four members that share the Josephin domain; Josephins 1 and 2 (JOS1 and JOS2), Ataxin-3 and Ataxin-3-like (ATXN3 and ATXN3L) (Tzvetkov and Breuer, 2007; Komander et al., 2009a). Mutations in the *ATXN3* gene result in the generation of a poly-glutamine stretch in Ataxin-3, causing aggregation of the protein (Takiyama et al., 1993). The mutations are inherited in an autosomal dominant manner and result in the patient developing spinocerebellar ataxia type 3 or Machado-Joseph disease, which led to the identification of the first member of the family (Sequeiros and Coutinho, 1993).

In terms of ubiquitin chain processivity, K48-linked poly-ubiquitin chains are readily hydrolysed by ATX3 and ATXN3L while Josephins 1 and 2 show very little activity (Weeks et al., 2011). The same study determined that out of the Josephin/MJD family, Josephin 2 and ATXN3L showed the highest activity against K63-linked poly-ubiquitin chains while ATX3 and Josephin 1 showed the least. ATX3 may in fact prefer editing longer poly-ubiquitin chains such as poly-K48-linked chains mixed with K63-linkages, preferentially cleaving at the K63-linked moieties (Winborn et al., 2008).

1.3.5 Motif interacting with ubiquitin (MIU)-containing novel DUB family (MINDY) family

The MINDY family is one of the most recently discovered family of DUBs, consisting of five members, MINDY1, -2, -3, -4 and -4B. They are characterised by the presence of a ubiquitin binding domain (UBD) referred to as motif interacting with ubiquitin (MIU) that binds mono-ubiquitin (Abdul Rehman et al., 2016). MINDY family members were shown to be highly selective against K48-linked poly-ubiquitin chains and they act as exo-peptidases, trimming poly-ubiquitin chains from the distal end in a processive manner (Abdul Rehman et al., 2016; Kristariyanto et al., 2017). Due to their high specificity towards K48-linked ubiquitin chains, DUBs of the MINDY family are considered important for the rescue of proteins destined for proteasomal degradation.

1.3.6 Zinc-finger and UFSP domain protein (ZUP1) family

The Zinc-finger and UFSP domain protein (ZUP1) is the newest family of DUBs discovered and it is named after the first, and currently, only member ZUP1 (Kwasna et al., 2018). ZUP1 appears to be highly selective against K63-linked ubiquitin chains in the context of genome maintenance and stability, following DNA damage (Kwasna et al., 2018; Hermanns et al., 2018; Haahr et al., 2018). Interestingly, the fission yeast homologue Mug105 is a highly active deubiquitylase against K48-linked but not K63-linked chains (Hermanns et al., 2018).

1.4 The structure and function of the proteasome

The proteasome is a large, multi-subunit, protein complex that recognises ubiquitylated proteins, unfolds them in an ATP-dependent manner, recycles the ubiquitin chain tags and proteolytically degrades the protein substrate (Tanaka, 2009). The proteasome is the major site of protein degradation in eukaryotic cells and there are proteasomes that are associated with certain cellular compartments, including the nucleus, cytoskeleton, endoplasmic reticulum and mitochondria (Hilt and Wolf, 1995; Rivett et al., 1997).

The proteasome consists of a cylindrical 20S core particle and two 19S regulatory particles on either end of the core particle that make up the 26S proteasome (Coux et al., 1996; Schweitzer et al., 2016). The 20S core particle consists of two homo-heptamers of β subunits, sandwiched between two homo-heptamers of α subunits. The β-ring core confers the proteasome with proteolytic activity of caspase-like, trypsin-like and chemotrypsin-like threonine proteases that cleave proteins after acidic, basic and hydrophobic residues respectively (Tanaka, 2009). The 19S regulatory particle is divided into two distinct sections, the base that interacts directly with the 20S core particle and the lid that faces towards the outside of the proteasome. The lid contains the proteasome-associated DUBs RPN11, USP14 and UCHL5 and it functions in recognising poly-ubiquitylated protein substrates destined for proteasomal degradation. The lid compartment facilitates substrate recognition and entry into the proteasome through interactions with other proteasome subunits. The accessory subunits RPN10, RPN1 and RPN13 recognise ubiquitylated substates partnered with RNP11, USP14 and UCHL5 respectively (Marshall and Vierstra, 2019). Furthermore, the ubiquitin receptor subunit activates the deubiquitylating activates of their partner proteasome-associated DUB (Hamazaki et al., 2006; Yao et al., 2006; Jiao et al., 2014; Shi et al., 2016). The function of the lid is to then remove ubiquitin from substrates before proceeding farther, thus preventing the unnecessary degradation of ubiquitin by the proteasome.

Next in the sequence are the six ATPase subunits RPT1-6, which are the chaperones that induce the unfolding of the substrate driven by ATP hydrolysis (Wawrzynow et al., 1995; Liu et al., 2006). The unfolded substrate enters the core particle and it is proteolytically cleaved into oligopeptides of varying lengths, typically between three and fifteen amino acids long. The smaller peptides are subsequently hydrolysed by cytosolic endopeptidases and amino-carboxy peptidases to yield free amino acids.

1.4.1 The proteasome-associated DUBs

The three DUBs that associate with the lid subcomplex of the proteasome belong to distinct families of DUBs. RPN11 belonging to the JAMM family is inactive in isolation and gains activity only as a part of the complete 26S

proteasome (Yao and Cohen, 2002; Pathare et al., 2014). RPN11 predominantly removes poly-ubiquitin chains *en bloc* and promotes the translocation of the substrate towards the 20S core particle via the ATPases (Tanaka, 2009; Worden et al., 2017).

USP14 is a ubiquitin specific peptidase that physically associates with the 26S proteasome (Borodovsky et al., 2001; Hu et al., 2005). Interestingly, the UBL domain of USP14 was shown to promote RPN11 DUB activity in removing poly-ubiquitin chains from substrates as well as promoting overall 26S proteasome proteolytic activity (Kim and Goldberg, 2018). USP14 trims ubiquitin chains from the distal end in a seemingly chain-type non-specific manner (Homma et al., 2015). However, it has also been shown that USP14 is able to remove the last poly-ubiquitin chain *en bloc* as long as that was the last chain on the substrate prior to its degradation (Lee et al., 2016). USP14 cleaves supernumenary ubiquitin chains from proteasome-bound substrates, reducing the time the proteasome is engaged by any one substrate (Lee et al., 2016).

UCHL5 (or Uch37 in yeast) is the third DUB to associate with the proteasome and belongs to the UCH family. UCHL5, similarly to USP14 and RPN11, is inactive in isolation and only gains significant activity in association with the proteasome (Maiti et al., 2011). RPN11 and UCHL5 stably associate with the proteasome while USP14 was shown to associate in a dynamic manner (Koulich et al., 2008; Chadchankar et al., 2019).

The collective function of the proteasome-associated DUBs is to co-ordinate entry of poly-ubiquitylated proteins into the proteasome for degradation. The removal of ubiquitin chains from substrates serves several functions. The ubiquitin itself is spared from degradation and additionally the ubiquitin-binding sites on the proteasomes become accessible for the next poly-ubiquitylated substrate to bind on. Furthermore, the removal of ubiquitin chains also prevents clogging up the proteasome during degradation of proteins. Finally, the activity of the proteasome-associated DUBs returns ubiquitin back to the free ubiquitin pool of the cell, ensuring the ubiquitin “economy” is not disrupted.

1.5 Autophagy is an alternative mechanism for protein degradation

The term “autophagy” is derived from the Greek words “auto” and “phagy” meaning self and eating respectively and it was observed as early as in the 1960s. The cells were observed enclosing their own components within a lysosome membrane for destruction (Deter and de Duve, 1967; Takeshige et al., 1992). Autophagy is a fundamental cellular mechanism that serves a plethora of metabolic, homeostatic and cytoprotective purposes (Dikic and Elazar, 2018). While the proteasome is primarily concerned with the degradation of individual proteins in the cytosol, the lysosomal pathway degrades macromolecules on a larger scale. This may include cytosolic proteins, protein aggregates, damaged organelles and vesicles following endocytosis that may contain internalised plasma membrane receptors and their ligands. Three types of autophagy have been identified so far : macroautophagy, microautophagy and chaperone-mediated autophagy (Mizushima et al., 2008). There are also different modes of autophagy including selective and non-selective autophagy, induced by different types of cellular stresses.

1.5.1 The cellular mechanism of autophagy

The autophagy related genes (ATG) were initially identified in budding yeast as autophagy-deficient strains (Tsukada and Ohsumi, 1993). These strains accumulated cargo in their vacuoles that was not being degraded and they displayed reduced viability in conditions of nitrogen starvation. Autophagy requires the formation of a membrane, called a phagophore, that eventually encapsulates the cargo for destruction. The components of autophagy are divided into four functionally distinct groups. The ULK1/2 (ATG1 in yeast) protein kinase complex, ATG9 in association with ATG9 vesicles, the BECN1/VPS34 lipid kinase complex and two ubiquitin-like conjugation cascades for the association of ATG8 homologues with membranes (**Figure 1.13**).

Autophagy is actively suppressed in conditions where the cell is “fed” and enjoying an abundance of nutrients such as amino acids (Axe et al., 2008). Abundance of amino acids maintains the mammalian target of rapamycin complex 1 (mTORC1) in an activated state (Avruch et al., 2009). Activated

mTORC1 hyperphosphorylates ATG13 and ULK1/2, which reduces ATG13 affinity towards ULK1/2 and the kinase activities of ULK1/2 (Ganley et al., 2009; Jung et al., 2009). In the absence of amino acids, mTORC1 remains inactive, resulting in the dephosphorylation of ULK1/2 and ATG13. ATG13 stimulates ULK1/2 to phosphorylate the scaffold protein FIP200 (functionally similar to ATG17 in yeast) (Hara et al., 2008). ULK1/2 in association with ATG13, ATG101 and phosphorylated FIP200 phosphorylate AMBRA1 (Maria Fimia et al., 2007; Hosokawa et al., 2009). AMBRA1 then interacts with the lipid kinase complex, VPS34 in association with BECLIN-1 (BECN1) and ATG14, to phosphorylate phosphatidyl inositol (PI) to produce phosphatidyl inositol 3-phosphate (Ptdins3*P* thereafter referred to as PI3P) (Auger et al., 1989; Herman and Emr, 1990; Schu et al., 1993; Volinia et al., 1995; Kihara et al., 2001). ATG14 is required for the interaction of the PI3P-generating complex I on autophagic isolation membranes (Itakura et al., 2008; Ohashi et al., 2020). Interestingly, BECN1/VPS34 in association with UVRAG result in generation of PI3P on endosomal compartments instead, where other PI3P-binding proteins, such as HRS and EEA1, are recruited (Christoforidis et al., 1999; Gaullier et al., 1999; Xu et al., 2001; Murray et al., 2002). In fact, VPS34 was first identified in yeast as component required for vacuolar protein sorting before the discovery for its role in autophagy (Robinson et al., 1988; Rothman et al., 1989; Schu et al., 1993).

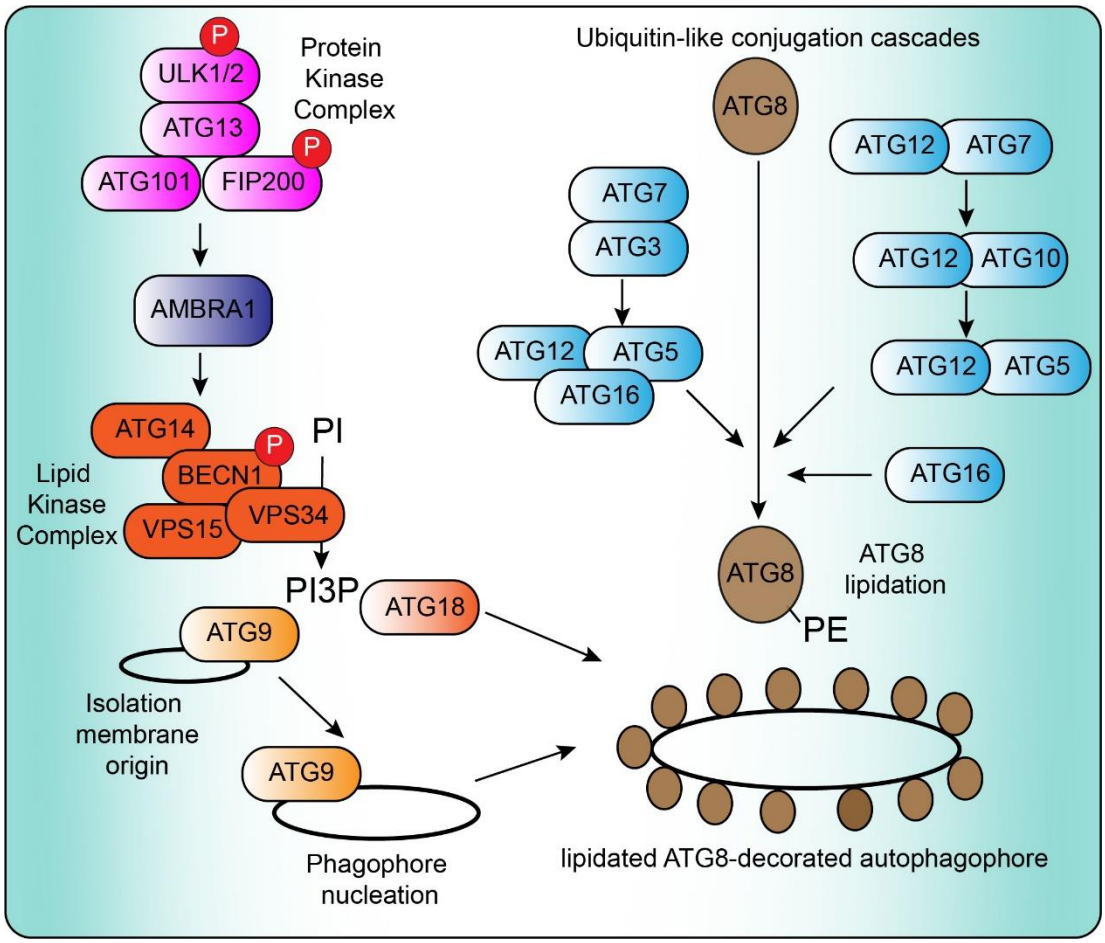

Figure 1.13: Initiation of autophagy

Autophagy is initiated by the sequential activity of a protein kinase complex and a lipid kinase complex. The activity of VPS34 generates phosphatidyl inositol 3-phosphate (PI3P) from phosphatidyl inositol (PI). PI3P mediates the formation of a phagophore membrane by activating and recruiting ATG18 (WIPI2 in mammals). The next step is the lipidation of ATG8 by phosphatidyl ethanolamine (PE) that is mediated by the ubiquitin-like conjugation cascade involving the E1, E2 and E3-like enzymes ATG7, ATG3, ATG5, ATG12 and ATG16. ATG18 is then responsible for recruiting the ATG12, ATG5, ATG16 complex that mediated lapidated ATG8 recruitment to the membrane.

Generation of PI3P mediates initiation of phagophore formation or nucleation (Axe et al., 2008). The exact origin of the phagophore initiation remains controversial in mammals but there is evidence to suggest it is derived from the endoplasmic reticulum (ER) and/or Golgi complex (Axe et al., 2008; Simonsen and Tooze, 2009). A recent study using recombinantly-expressed yeast components showed that ATG9 vesicles are a site of recruitment of the

PI3P-generating complex that in turn promotes lipid influx from the ER to promote expansion of the isolation membrane into the eventual autophagophore (Sawa-Makarska et al., 2020). The next step is the ubiquitin-like conjugation of ATG8 homologs onto the lipid phosphatidyl ethanolamine (PE). The reaction is often described as ubiquitin-like conjugation because like ubiquitin, ATG8 and its mammalian homologs LC3 (A, B and C), GABARAP, GABARAPL1,2 and 3, undergo a sequential transfer through an E1, E2 and E3-like conjugation cascade (Lee and Lee, 2016). The final acceptor of ATG8 is a lipid instead of a protein (Mizushima et al., 1998; Ichimura et al., 2000). The lipidated ATG8 species is now able to interact directly with the phagophore membrane through its lipid moiety. PI3P that is generated by VPS34 recruits and activates WIPI2 (ATG18 homologue) to the membrane, which in turn recruits ATG16L in complex with ATG5 and ATG12, that mediate ATG8 lipidation (Polson et al., 2010; Dooley et al., 2015). The ATG8-decorated autophagophore is recruited through autophagy receptors to cargo sequestered for degradation, which may include cytosolic proteins and organelles. The autophagophore membrane fuses to form a double membrane compartment that carries the cargo, mediated by ESCRT-III complex components CHMP2A and VPS4 (**Figure 1.14**) (Takahashi et al., 2018; Zhou et al., 2019). The last step is the fusion of the outer membrane of the autophagophore with a lysosome to form an autophagolysosome, mediated by SNAREs/Syntaxins (Gutierrez et al., 2004; Jäger et al., 2004; Itakura et al., 2012; Saleeb et al., 2019). The contents are degraded by the acidified hydrolytic enzymes derived from the lysosome and the building blocks of the degraded macromolecules are assimilated by the cell.

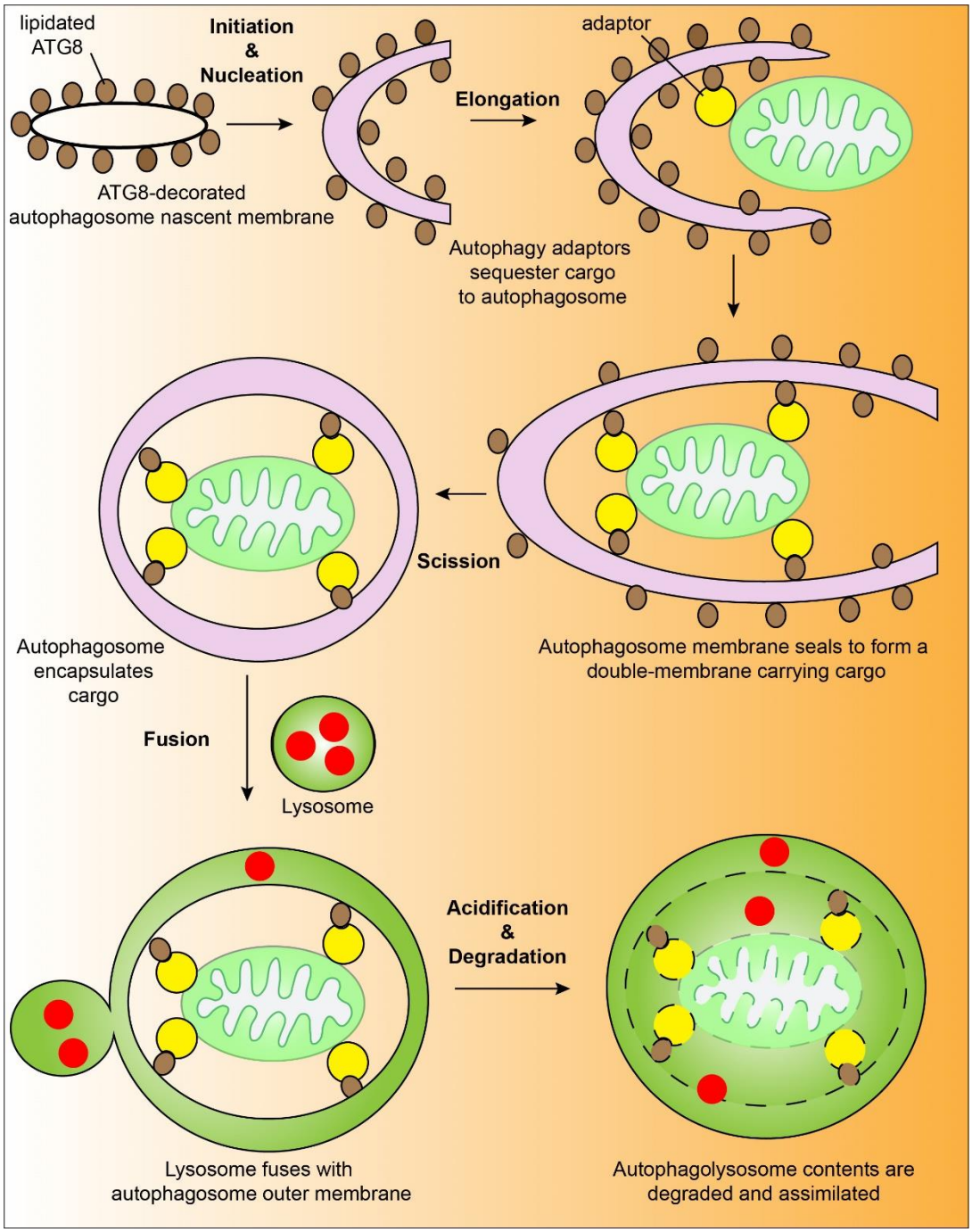

Figure 1.14: Overview of autophagy

Diagram depicts the steps in autophagy starting from initiation, to cargo sequestration, autophagolysosome formation and content degradation. The ATG8-decorated autophagophore nascent membrane is recruited to the cargo destined for degradation through autophagy receptors (initiation and nucleation). The autophagophore membrane encapsulates the cargo (elongation) and it fuses to form a double membrane compartment that carries the cargo (autophagosome closure or scission). The lysosome fuses with the outer membrane of the autophagosome to form an autophagolysosome (fusion). The contents of the autophagolysosome are degraded by the hydrolases of the lysosome.

1.5.2 Autophagy serves vital roles in cell physiology

Autophagy mediates the degradation of cellular components for the production of nutrients such as amino acids and lipids for the cell to drive its metabolism when nutrient supply is scarce (Mizushima and Komatsu, 2011). Furthermore, autophagy serves a number of protective functions, including the degradation of invading pathogens and antigen presentation in the context of immunity (Jiang et al., 2019). The destruction of malfunctioning and potentially dangerous organelles such as damaged mitochondria, peroxisomes and fragments of the ER, as well as abnormal protein aggregates is also mediated through autophagy (Singh and Cuervo, 2011).

Autophagy is an essential cellular and developmental process. Autophagy-deficient mice die during gestation or soon after birth at different stages of development, depending which gene is deleted, and show a number of developmental and morphological abnormalities (Kuma et al., 2017). It is accepted that all cells undergo autophagy at the basal level under otherwise optimal conditions, even in the absence of cellular stress. Autophagy-deficient cells show elevated levels of protein aggregates in the form of inclusions bodies that are often decorated with ubiquitin. The presence of these aggregates suggests constitutive autophagy is required for their proper clearance (Hara et al., 2006; Ebato et al., 2008). The inability to clear abnormal protein aggregates and dysfunctional organelles is linked to a number of neurodegenerative diseases and malignancies, which highlights the importance of autophagy and the lysosomal pathway in proper cell homeostasis (Stamatakou et al., 2020).

1.5.3 The roles of autophagy in cancer

The role of autophagy in neurodegenerative diseases is rather straight-forward. Autophagy appears to protect against neurodegenerative diseases by promoting the clearance of protein aggregates and damaged organelles that may lead to inflammation and eventual cell death, contributing to neurodegeneration (Sarkar et al., 2009). The relationship between autophagy and cancer is more complex as autophagy may prevent cancer incidence on one hand but may also promote cancer progression or reduce the

effectiveness of cancer treatments on the other (Rosenfeldt and Ryan, 2011; Jiang et al., 2019).

In the classical model of cancer development and progression, certain oncogenes such as KRAS, AKT and mTOR are well-established autophagy suppressors. Therefore, gain of function mutations or overexpression of these oncogenes in cancers inadvertently suppresses autophagy in the affected cells. Furthermore, members of the anti-apoptotic family of proteins such as BCL-2 are known to interact with and inhibit BECN1, preventing autophagy initiation (Decuypere et al., 2012). The interplay between autophagy and apoptotic cell death will be discussed more extensively in subsequent sections.

Core autophagy genes have been assigned tumour suppressive roles in certain contexts. Loss of BECN1 leads to a reduction in autophagic flux and also correlates with increased cell proliferation suggesting BECN1 may act as a tumour suppressor (Qu et al., 2003; Yue et al., 2003). Furthermore, BECN1 expression is reduced in certain breast cancers and oesophageal squamous cell carcinomas, and high levels of BECN1 expression correlate with a positive prognosis (Liang et al., 1999; Chen et al., 2009). Deletion of ATG5 or ATG7 predisposes mice to liver cancers, suggesting that ATG5/7 are acting as tumour suppressors (Takamura et al., 2011). The inability to clear damaged or defective mitochondria through autophagy may promote production of elevated levels of ROS. In turn, ROS induce DNA damage and promote genomic instability and tissue inflammation, drivers in both cancer initiation and progression (Li et al., 2018). Autophagy may be required for antigen cross-presentation during cancer treatment for successful elimination of the tumours (Li et al., 2012; Michaud et al., 2014; Pietrocola et al., 2016). Taken together, these pieces of evidence suggest that autophagy plays a tumour protective role.

Cancer cells that proliferate at high rates also have high bioenergetic requirements and some cancer cells require autophagy to provide additional fuel to maintain this elevated metabolism (Yang et al., 2011). Proper ER function is required for the assembly, folding and trafficking of proteins (Scriven et al., 2009; Wang et al., 2010). The increased rates of proliferation of cancer cells, combined with production of mutated proteins can lead to increased levels of misfolded proteins in the ER making cancer cells particularly sensitive

to proteotoxic and ER stress (Guang et al., 2019). Unfolded protein response (UPR) regulation needs to be kept in check in tumour cells, since insufficient use of the UPR can be toxic to the tumour whereas excessive or sustained activation of the UPR may commit the cells to apoptosis (Madden et al., 2019). Tumour cells are selected for activated UPR by suppressing pro-apoptotic components and upregulating anti-apoptotic whilst others maintain the right levels of ER stress and UPR that do not cross the threshold to commit to an apoptotic pathway. One such cytoprotective mechanism is through the use of autophagy, which otherwise would result in cell death (Hart et al., 2012).

This is also evident from the observation that cancer cells may utilise autophagy as a whole to survive treatments with cytotoxic agents and even develop mechanisms of resistance through autophagy (Scriven et al., 2009; Han et al., 2011; Santana-Codina et al., 2017). The tumour micro-environment may become inherently inhospitable to tumour cells with abnormal and disorganised vasculature, hypoxic conditions, chronic inflammation and nutrient deprivation. In these situations, cancer cells may utilise autophagy to survive and, in the process, become autophagy dependent. Autophagy-dependent tumours present an opportunity to employ synthetic lethality for treatment with autophagy inhibitors and anti-neoplastic drugs (Sotelo et al., 2006; Briceño et al., 2007; Liang et al., 2012; Mulcahy Levy and Thorburn, 2020).

1.5.4 Mitophagy is the autophagic engulfment of mitochondria

Specialised forms of autophagy have been described over the years in relation to the type of cargo the core autophagy machinery handles. Different cellular components and compartments are selectively sequestered for degradation: for instance ribophagy, reticulophagy and nucleophagy refer to the selective degradation of ribosomes, ER and nuclei respectively (Cebollero et al., 2012; Nakatogawa and Mochida, 2015). Mitophagy refers to the sequestration for engulfment and subsequent lysosomal degradation of mitochondria (Ding and Yin, 2012). Mitophagy targets damaged or dysfunctional mitochondria as a safety mechanism to ensure the proper functioning of the mitochondrial network as a whole. Mitochondria are critical organelles that are an integral part of the cell’s metabolism that manufacture a

variety of cellular metabolites on top of performing catabolic processes and generate ATP through oxidative phosphorylation (Osellame et al., 2012). They are also integral for the regulation and execution of apoptotic cell death, calcium buffering in the cell and part of the cell's anti-viral response (Eisner et al., 2018). Mitophagy remains the most extensively studied branch of selective autophagy due to its association with a number of major diseases (Wang et al., 2019). Failure to execute mitophagy as a mitochondrial quality control mechanism to eliminate damaged or malfunctioning mitochondria may lead to the generation of ROS. High levels of ROS can introduce mutations leading to malignancies, and induce aberrant cell death leading to neurodegeneration (Wang et al., 2019). Mitophagy is also important as a developmental process in the context of erythrocyte maturation, heart muscle mitochondrial network remodelling during heart development and adipocyte differentiation (Mizushima and Levine, 2010). Mitochondrial quality control is therefore critical for the maintenance of proper mitochondrial function in cells.

1.5.5 PINK1 and Parkin pathway of mitophagy

One of the most extensively studied pathways in mitophagy is the one driven by the PTEN-induced putative kinase 1 (PINK1) and the RING-between-RING E3 ubiquitin ligase Parkin. The discovery that loss-of-function mutations in *PARK2* and *PARK6*, the genes that encode for Parkin and PINK1 respectively, are found in hereditary forms of early onset autosomal recessive juvenile Parkinsonism, sparked the interest in the study of this pathway (Kitada et al., 1998; Valente et al., 2004; Park et al., 2006; Klein and Westenberger, 2012).

PINK1 is a ubiquitously expressed protein kinase that consists of an N-terminal mitochondrial targeting sequence, a short trans-membrane domain, a serine/threonine kinase domain and a C-terminal domain (Schubert et al., 2017) (**Figure 1.15**A). PINK1 is constantly synthesized in cells and targeted to mitochondria where it is imported through the TOMM and TIMM translocases. The import of PINK1 into mitochondria is mediated by its mitochondrial targeting sequence and driven by the mitochondrial membrane potential ($\Delta\Psi$). In healthy mitochondria with intact membrane potential, PINK1 is imported through the outer and inner mitochondrial membranes (**Figure 1.15**B).

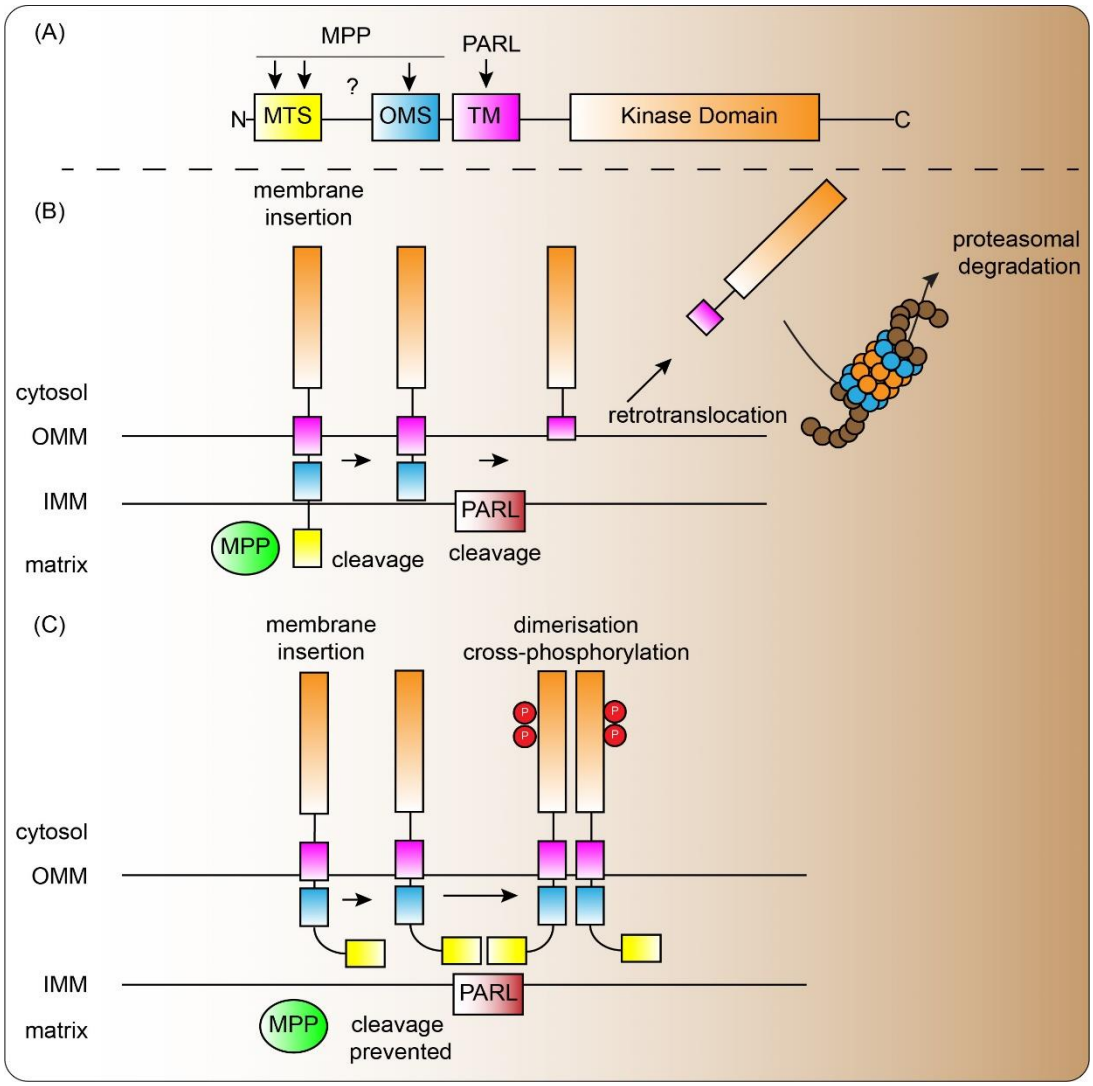

Figure 1.15: PINK1 import and stabilisation mechanism

(A) Diagram illustrating the domain architecture of PINK1 protein. The mitochondrial targeting sequence (MTS) is on the N-terminus, followed by the outer mitochondrial membrane signal (OMS), the transmembrane domain (TM) and the kinase domain. The arrows show where the cleavage sites between the MTS and OMS for matrix protease (MPP) and the cleavage site at the TM domain for Presenilin-associated rhomboid-like protease (PARL). The question marks (?) indicate that the exact cleavage site for PINK1 by MPP is unknown. (B) The model illustrates how full length PINK1 behaves when inserted through the outer and inner mitochondrial membranes when mitochondria are healthy. Once the MTS is exposed to the matrix side of the inner membrane, it is cleaved off by MPP. PARL then proceeds to cleave the TM domain between residues A103 and F104. The cleaved fragment retro-translocates back to the cytosol where it is targeted for proteasomal degradation. (C) In the presence of mitochondrial damage, the cleavage events mediated by MPP and PARL are prevented due to insufficient import of PINK1 through the inner mitochondrial membrane (IMM). The OMS allows PINK1 to remain localised to the outer mitochondrial membrane (OMM) where it dimerises and cross-phosphorylates to become the fully active kinase. Diagram adapted from Sekine, 2019.

Upon its emergence on the matrix side, the MTS is cleaved by matrix protease MPP (Sim et al., 2012) and subsequently by PARL at the transmembrane (TM) domain (Deas et al., 2011).The cleavage by PARL generates a novel N-terminus for the protein and PINK1 is released into the cytoplasm (retro-translocation) where it is recognised by the UBR1, 2 and 3 family of E3 ubiquitin ligases that target it for proteasomal degradation (Tasaki et al., 2005; Takatori et al., 2008).

In the absence of a mitochondrial membrane potential, PINK1 import through the TIMM complex is impeded. MPP and PARL are unable to cleave PINK1, which accumulates on the outer mitochondrial membrane using the outer mitochondrial membrane signal (OMS) (Okatsu et al., 2015). The OMS is a short sequence between the MTS and TMD of PINK1 and has been shown to be required for PINK1 accumulation in response to mitochondrial damage (Okatsu et al., 2015; Sekine et al., 2019). The OMS domain is thought to interact with the TOMM7 subunit of the TOMM complex to achieve arrest of PINK1 import. PINK1 is then able to dimerise and cross-phosphorylate its kinase domain, which leads to its activation (Zhou et al., 2008; Okatsu et al., 2012, 2013; Zhuang et al., 2016). Activated PINK1 phosphorylates ubiquitin moieties on S65 to generate phosphoS65-ubiquitin (pS65-Ub) (Koyano et al., 2014; Kane et al., 2014; Kazlauskaite et al., 2014). The generation of pS65-Ub on the sites of mitochondrial damage recruits and activates the cytosolic E3 ubiquitin ligase Parkin. PINK1 phosphorylates Parkin on an analogous position on S65 on its ubiquitin-like domain (UBL), which leads to full Parkin activation (Kim et al., 2008b; Shiba-Fukushima et al., 2012, 2014). Activated Parkin ubiquitylates a number of outer mitochondrial membrane proteins. The ubiquitylated proteins can serve as additional PINK1 substrates for phosphorylation, which in turn leads to further recruitment and activation of Parkin. Once ubiquitylated, certain proteins such as Mitofusins 1 and 2, MIRO and TOMM20 are extracted and targeted for proteasomal degradation (Ziviani et al., 2010; Tanaka et al., 2010; Liang et al., 2015a). The ubiquitylated proteins also signal autophagy receptors to be recruited to the ubiquitin-decorated mitochondria (Chan et al., 2011; Sarraf et al., 2013). Autophagy receptors, such as OPTN and NDP52 contain UBD and LC3-interacting

regions (LIR) (Birgisdottir et al., 2013; Lazarou et al., 2015). They therefore allow the LC3-decorated autophagosome membrane to sequester the ubiquitin-coated mitochondrial membrane as cargo for the autophagy machinery, promoting the degradation of the damaged mitochondria.

The activity of Parkin on depolarised mitochondria is counteracted by DUBs USP15 and USP30. USP15 overexpression prevents Parkin-mediated mitophagy in HeLa Parkin-overexpressing cells (Cornelissen et al., 2014). Furthermore, USP15 depletion enhances Parkin translocation and depletion of mitochondrial marker TOMM20 in HeLa cells, SH-SY5Y cells and human fibroblasts overexpressing Parkin. USP30 depletion enhances the ubiquitylation levels and rate of degradation of TOMM20 in cells overexpressing Parkin in response to depolarisation agents (Bingol et al., 2014; Cunningham et al., 2015; Liang et al., 2015a). Depletion of either USP15 or USP30 rescues Parkinson's disease-associated phenotypes in the fly that were caused by loss of Parkin function (Cornelissen et al., 2014, 15; Bingol et al., 2014).

Basal mitophagy appeared to be independent of PINK1 *in vivo* in Drosophila and the mouse. Mice expressing the mito-QC probe that allows for real time measurements of mitophagy in living cells, demonstrated that basal mitophagy proceeds normally even in the absence of PINK1 (McWilliams et al., 2018b). Similarly, depletion of PINK1 in the fly did not affect the basal mitophagy measurements in the fly expressing mito-QC or mito-mKeima mitophagy reporters (Lee et al., 2018). The above observations suggested that PINK1 was dispensable for basal mitophagy *in vivo* or that the contribution of PINK1-dependent mitophagy was too low to detect in this setting. However, USP30 depletion or deletion enhanced the rate of basal mitophagy in a PINK1-dependent manner in cells expressing no detectable Parkin i.e. depletion of PINK1 in USP30-depleted cells restored basal mitophagy levels back to baseline (Marcassa et al., 2018). The above suggested that there is a PINK1-dependent component in basal mitophagy, which is normally suppressed by USP30. This PINK1-dependent component only becomes detectable in the absence of USP30, which explains why depletion of PINK1 alone does not show a decrease in basal mitophagy. Interestingly, the activity of USP8 was shown to be required for Parkin translocation on mitochondrial, suggesting that

USP8 is a DUB that promotes Parkin-mediated mitophagy (Durcan et al., 2014). USP8 has been proposed to restrict the generation of inhibitory K6-linked ubiquitin chains generated on Parkin through auto-ubiquitylation, thus enabling Parkin activity on mitochondria. USP8 downregulation or inhibition resulted in the restoration of MFN protein levels back to baseline, reduction in the loss of dopaminergic neurons and reduction in locomotor defects in PINK1-deficient flies (von Stockum et al., 2019). The above suggests a role for USP8 in opposing the PINK1/Parkin pathway and therefore a context-specific response, which may arise from the other known functions of USP8 in the regulation of sorting of endosomal compartments and promoting autophagy in the fly (Jacomin et al., 2015).

Overexpressing USP35 delayed Parkin-mediated mitophagy without affecting Parkin recruitment to mitochondria in response to depolarisation whilst USP30 overexpression delayed both Parkin recruitment and mitophagy (Wang et al., 2015). USP30 is the only known DUB to permanently associate with mitochondria whilst USP35 was shown to dissociate from mitochondria during mitochondrial depolarisation. Most pieces of evidence point that USP30 is the major DUB that regulates the PINK1/Parkin pathway. The data on the role of USP30 on mitochondria and in opposing PINK1/Parkin-mediated mitophagy has been corroborated across a number of different labs over multiple studies (Bingol et al., 2014; Liang et al., 2015a; Cunningham et al., 2015; Marcassa et al., 2018; Ordureau et al., 2020; Rusilowicz-Jones et al., 2020).

The PINK1/Parkin pathway of mitophagy offers an example of a very well-orchestrated quality control mechanism. The ability of the sensor PINK1 to initiate mitophagy is tightly linked to mitochondrial health through its degradation in a ΔΨ-dependent manner. PINK1 stabilisation may also be brought about by accumulation of misfolded mitochondrial proteins or inability of mitochondria to import cytosolic proteins (Jin and Youle, 2013; Fiesel et al., 2017).

1.5.6 Other pathways of mitophagy

Mitophagy is also mediated by other pathways, independent of PINK1 or Parkin in the contexts of development and in response to stress (Wang et al.,

2019). Some forms of mitophagy are independent of Parkin but still dependent on ubiquitin, in which case some of the same mitophagy adaptors that contain UBDs are still relevant. Alternative E3 ligases that mediate mitophagy include MUL-1, a mitochondrially-localised E3 ubiquitin ligase. MUL-1 mediates selenite-induced mitophagy, a treatment that induces ROS in cells (Li et al., 2015). Loss of MUL-1 aggravated the phenotypes associated with loss of PINK1 and Parkin in the fly, whilst MUL-1 overexpression offered some protection (Yun et al., 2014). The above suggested that MUL-1 operated in parallel to the PINK1/Parkin pathway and could in some cases compensate for loss of PINK1/Parkin. The ER-associated E3 ligase GP78 has been implicated in mitophagy through ubiquitylation of Mitofusins, MFN1 in particular, and mediated degradation of mitochondria proximal to ER-resident GP78 (Fu et al., 2013). A Parkin-independent but PINK1-dependent mitophagy pathway shows the involvement of synphilin-1 in recruiting the E3 ligase SIAH-1 (Szargel et al., 2016). SIAH-1 ubiquitylates OMM proteins and mediates clearance of mitochondria in cells that lacked Parkin.

In instances where mitophagy is ubiquitin-independent is mediated through alternative receptors that lack UBDs and are recruited at the OMM, which are then responsible for recruiting the autophagophore membrane using their LIR domains.

OMM proteins BNIP3 and BNIP3L (NIX) are related to the BH3-only proteins that are involved in the regulation of apoptosis. BNIP3/BNIP3L contain TM domains anchoring them to the OMM and LIR domains that allow them to recruit the LC3-decorated autophagosome membrane to the OMM and sequester mitochondria as cargo (Zhang and Ney, 2009). BNIP3/BNIP3L mediate mitophagy involved in the maturation of reticulocytes (Novak et al., 2010; Zhu et al., 2013). FKBP8 contains a TM domain and an N-terminal LIR domain, which allow it to anchor to the OMM and recruit LC3A-decorated autophagophores to mitochondria (Bhujabal et al., 2017, 8; Lim and Lim, 2017, 8). Interestingly, FKBP8 itself is able to escape autophagic engulfment and degradation during mitophagy.

FUNDC1 is another mitophagy adaptor protein that is anchored to the OMM through three TM domains. FUNDC1 mediates induction of mitophagy in response to hypoxia (Liu et al., 2012). Dephosphorylation of FUNDC1, which

is achieved by the concomitant activation of the PGAM5 phosphatase and inactivation of c-SRC and CK2 kinases. This enhances the interactions between the LIR domain of FUNDC1 and LC3 and triggers mitophagy under hypoxic conditions (Chen et al., 2014). FUNDC1 levels at mitochondria are further regulated by the activity of the mitochondrial E3 ligase MARCH5/MITOL (Chen et al., 2017).

AMBRA1 was also shown to act as a mitophagy adaptor through its LIR domain and mediate mitophagy in a Parkin-independent manner (Strappazzon et al., 2015). It has however been shown that AMBRA1 collaborates with Parkin in inducing mitophagy as well (Van Humbeeck et al., 2011). It is therefore evident that AMBRA1 activity is essential for acting upstream of phagophore initiation and nucleation as well as acting downstream as a mitophagy adaptor.

1.5.7 The links between metabolism and mitophagy

Metabolism and mitophagy are intrinsically linked due to the integral role of mitochondria in cellular metabolism. Conditions of hypoxia that disfavour aerobic metabolism using the mitochondrial electron transport chain, promote mitophagy in a FUNDC1-dependent manner (Wu et al., 2014; Zhang et al., 2016). Hypoxia-induced mitophagy is part of the metabolic reprogramming of the cell away from aerobic metabolism and towards a more glycolytic metabolism. In doing so, the cell is protected from unnecessary ROS production and in the process recycles redundant mitochondrial components (Daskalaki et al., 2018).

Hexokinases are a class of metabolic enzymes that catalyse the phosphorylation of glucose to glucose-6-phosphate, which is the first reaction of glycolysis. A pool of hexokinases is cytosolic while a smaller portion (iso-enzymes I and II only) is associated with the outer mitochondrial membrane through interactions with the VDACs (Pastorino and Hoek, 2008). The physical association of Hexokinases I and II on mitochondria through VDACs coincides with a functional association as well. Mitochondrially-bound hexokinases utilise mitochondrially-generated ATP instead of cytosolic, directly coupling hexokinase activity to mitochondrial function (Robey and Hay, 2006). Hexokinases have been shown to interact with and become ubiquitylated by

Parkin in response to depolarisation (Sarraf et al., 2013). More importantly, hexokinases are required for Parkin translocation to depolarised mitochondria and appear to be an indispensable part of the PINK1/Parkin pathway (McCoy et al., 2014). The link between hexokinases and mitophagy may in part be that hexokinase activity on the outer mitochondrial membrane is associated with increased glycolytic capacity, which would allow for mitophagy to proceed. When cells are made dependent on their mitochondria for energy by culturing them in galactose, depolarisation results in Parkin translocation, however mitophagic engulfment of mitochondria is prevented (MacVicar and Lane, 2014). The above suggests that there is a metabolic block for clearing mitochondria from cells that are dependent on them for ATP generation. During retinal ganglion cell differentiation and macrophage M1 polarisation, NIX-dependent mitophagy is required for the metabolic switch to occur (Esteban-Martínez et al., 2017). When general autophagy or specifically mitophagy were blocked, both the metabolic switch and the differentiation programme were halted. The above places mitophagy upstream of the metabolic switch, whereas the inability of galactose-cultured YFP-Parkin overexpressing hTERT-RPE1 cells to undergo mitophagy in response to depolarisation, places mitophagy downstream of the metabolic switch. The differences of where mitophagy and the metabolic switch lays may differ on whether mitophagy is developmentally-induced or stressed induced (mitochondrial damage in response to depolarisation). Alternatively, it may depend on the specific pathway that mediates mitophagy i.e. NIX dependent or PINK1/Parkin dependent. Cells that arrest during mitosis are susceptible to undergoing apoptosis, termed mitotic cell death (MCD). Autophagy that also mediates mitophagy acts as a pro-survival mechanism to prevent MCD in these cells. It has been proposed that AMPK mediates a metabolic switch during mitophagy in mitotic cells (Doménech et al., 2015). Activation of AMPK mediates activation the PFKFB3 phosphatase that dephosphorylates PFK and allows flux through the glycolytic pathway. General autophagy and mitophagy inhibitors prevented the upregulation of genes associated with glycolysis in response to cell cycle arrest. Furthermore, AMPK inhibitors prevented the glycolytic switch in mitotically-arrested cells whilst glycolysis inhibitors sensitized the cells to taxol. The above suggested that mitotically-arrested

cells underwent a mitophagy-induced metabolic switch mediated through AMPK/PFKFB3 as a pro-survival mechanism to prevent MCD.

During neuronal differentiation of induced neuronal progenitor cells (iNPCs) a metabolic switch occurs from the stem cells being heavily reliant on glycolysis to the differentiated dopaminergic (DA) neurons being heavily reliant on oxidative phosphorylation (Schwartzentruber et al., 2020). Furthermore, the differentiated DA displayed higher levels of mitophagy compared to their undifferentiated iNPC counterparts. iNPCs derived from PD patients harbouring *PARK2* mutations underwent the same metabolic switch whilst suffering greater extent of cell death during differentiation. Interestingly, *PARK2* mutant cells exhibited higher levels of depolarisation-induced mitophagy than the control iNPCs, even though the response did not sustain for as long, prior to differentiation. The *PARK2* mutant cells displayed reduced levels of both basal and depolarisation-induced mitophagy, higher levels of ROS, elevated levels of cell death, and altered mitochondrial mass and morphology after differentiation into dopaminergic neurons. The above data suggest that Parkin-mediated mitophagy protects the differentiated neurons, which are OxPhos-dependent from aberrant cell death resulting from ROS and damaged mitochondria.

1.5.8 The roles of PINK1 and Parkin in cancer

Cancer and neurodegeneration are often regarded as opposites in their manifestation as diseases, despite having a number of risk factors in common including aging, exposure to dangerous chemicals and lifestyle factors such as diet, smoking and obesity. Epidemiological evidence exists to support that patients who are suffering with neurodegenerative diseases display lower cancer incidence, suggesting an inverse correlation between cancer and neurodegeneration (Tabarés-Seisdedos and Rubenstein, 2013). This inverse co-morbidity is especially notable in patients suffering from PD whose cancer incidence for most cancers is reduced, except for melanoma that is in fact elevated (Rugbjerg et al., 2012; Garcia-Ratés and Greenfield, 2017).

PTEN induced putative kinase 1 (PINK1) was named after its functional association with the major tumour suppressor PTEN, linking PINK1 expression to the context of cancer (Unoki and Nakamura, 2001). Ectopic expression of

PTEN induced the transcriptional expression of PINK1 mRNA in cells. PINK1 appears to perform both pro- anti-tumourigenic functions. Expression profiles from the Oncomine database show that PINK1 expression is reduced in liver, ovarian and renal cancers while it is elevated in endometrial and haematopoietic malignancies (O'Flanagan and O'Neill, 2014). The *PARK6* gene is located on chromosome 1 in a region that is often deleted in a number of tumours and it is thought to contain tumour suppressor genes (Valente et al., 2001; O'Flanagan and O'Neill, 2014). Loss of the *PARK6* locus may contribute to tumourigenesis through loss of PINK1 and the other neighbouring tumour suppressor genes. Alternatively, loss of *PARK6* is a passenger mutation owing to the loss of other tumour suppressors whose loss is driving the disease (Bagchi and Mills, 2008). As discussed above, loss of PINK1 hinders the proper clearance of damaged mitochondria through mitophagy and promotes the accumulation of dysfunctional mitochondria that produce higher levels of ROS in the cells. ROS may induce DNA damage to the nuclear DNA of cells that gives rise to cancer-inducing mutations. Furthermore, damage to mitochondrial DNA specifically may create a more tumour permissive environment for the cancer cell (Weir et al., 2013; Pereira et al., 2012).

Mouse cancer cell lines with high levels of PINK1 expression displayed higher metastatic potential (Nakajima et al., 2003). PINK1 was shown to activate AKT through activation of mTORC2, which promotes proliferation, glycolytic metabolism of cancer cells and anti-apoptotic mechanisms (Miyamoto et al., 2008; Murata et al., 2011; Lee et al., 2013). Furthermore, loss of PINK1 is known to reduce the survival of neuroblastoma cells subjected to proteasomal inhibition with MG132 whilst PINK1 overexpression improved survival, suggesting PINK1 serves a protective role against apoptosis induced by proteotoxic stress (Muqit et al., 2006; Klinkenberg et al., 2010). PINK1-dependent but Parkin-independent mitophagy may be used by cancer cells to survive attack by chemotherapeutic drugs, as long as another E3 ligase takes up the role of acting in lieu of Parkin downstream of PINK1 (Villa et al., 2017). In this context PINK1 displays cytoprotective functions that are beneficial for the survival and proliferation of cancer cells. The same cytoprotective mechanisms that give PINK1 its pivotal role in protecting against

neurodegeneration may potentially be exploited by cancer cells to survive the enhanced levels of cellular stress they may have.

Parkin is a more well-established tumour suppressor than PINK1 and is thought to be deleted or mutated in many different cancers (Veeriah et al., 2010; Bernardini et al., 2017). Parkin expression is in fact very low or absent in many established colorectal cancer cell lines while *PARK2* deletion is frequent in colorectal cancer and accelerates the development of adenomas in mice (Poulogiannis et al., 2010). Furthermore, sporadic loss-of-function mutations in Parkin that specifically affect its E3 ubiquitin ligase activity were reported in glioblastomas and other cancers (Veeriah et al., 2010). Parkin appears to prevent loss of PTEN and cooperates with PTEN in suppressing the PI3K/AKT pathway (Gupta et al., 2017a). The above is achieved by Parkin maintaining cellular levels of ATP produced by mitochondria and suppressing nitric oxide production by eNOS, which can result in the S-nitrosylation of PTEN that targets it for proteasomal degradation, effectively reducing the levels of PTEN in the cell (Gupta et al., 2017b). Parkin is also implicated in the regulation of the cell cycle by directly controlling the levels of cyclins D and E in the cell in association with the SCF^{FBW7} complex. Loss of Parkin promotes accumulation of cyclin E in the cell while Parkin overexpression prevents it (Staropoli et al., 2003). Deletions in *PARK2* appear to anti-correlate with amplifications of the genes for CDK4 and cyclins D and E, suggesting that either *PARK2* deletion or oncogene amplification is sufficient to provide the tumour with a growth advantage i.e. they are mutually exclusive (Gong et al., 2014). Further in the context of mitotic progression, Parkin loss was shown to induce chromosome misalignment and missegregation (Lee et al., 2015). Specifically, Parkin was shown to be phosphorylated and subsequently activated by Polo-like kinase 1 (PLK1) that allows it to associate with CDC20 and CDH1, both of which are subunits of the anaphase promoting complex/cyclosome (APC/C). Parkin in association with CDC20 or CDH1 recognises and ubiquitylates some of the same substrates of the APC/C in association with the same respective subunits. In doing so, Parkin has been proposed to facilitate proper mitotic progression through ubiquitylation of APC/C substrates. In summary, Parkin activity has been proposed to promote proper mitotic progression and prevent chromosome missegregation and

genomic instability, which is a hallmark of Cancer (Hanahan et al., 2000; Hanahan and Weinberg, 2011).

Parkin is also thought to promote apoptotic cell death during mitochondrial stress by targeting the anti-apoptotic protein MCL-1 for degradation (Carroll et al., 2014). Finally, loss of PINK1 or Parkin was shown to accelerate the progression of pancreatic ductal adenocarcinoma (PDAC) in mice. Specifically, loss of either PINK1 or Parkin in this context reduced the lifespan of the mice by preventing the loss of Mitoferrins-1 and -2, causing iron accumulation in the mitochondria, promoting ROS-mediated genomic instability, local inflammation and expression of the immunosuppressive molecule PD-L1 (Li et al., 2018).

1.6 Apoptosis is a form of programmed cell death

Apoptosis is a fundamental cellular mechanism of programmed cell death. It is a developmentally essential process by which cell death is executed in a deliberate manner by a distinct set of cellular machinery in response to stress stimuli or developmental bodily cues (Campbell and Tait, 2018). Apoptosis was first described to take place in two morphologically distinct phases. First, the genomic DNA and the cytosolic compartments condense and membrane-bound inclusions of the cell contents are formed (apoptotic bodies) (Kerr et al., 1972). Second the apoptotic bodies are released into the environment and are taken up by other cells by phagocytosis. Apoptosis was described to be a genetically encoded process in the nematode worm *C. elegans* (Ellis, 1986; Hengartner et al., 1992). The first genes identified were ced-3 (executioner caspase orthologue) and ced-4 (APAF-1 orthologue) whose mutation resulted in the survival of cells that normally underwent apoptosis during development. Mutations in ced-9 (BCL-2-like homologue), whose function is to prevent apoptosis, resulted in embryonic lethality demonstrating that apoptosis is a tightly controlled process.

Apoptosis is a developmentally important process as part of tissue development, morphogenesis and maintaining the total number of cells in the body constant. Apoptosis is also critical for normal immune and nervous system development and function (Singh et al., 2019). Apoptosis also serves protective functions in the body by eliminating damaged or potentially

dangerous cells, such as virally infected cells and cancer cells. Deregulated apoptosis is implicated in instances of human pathology, including tissue atrophy, neurodegeneration and failure of organ transplants (Graft vs host disease) (Renehan, 2001; Singh et al., 2019).

1.6.1 The mechanism of apoptosis

Apoptosis is typically brought about by the proteolytic activity of caspases, a class of cysteine proteases that cleave after an aspartate residue. Caspases are divided into inflammatory, initiator and executioner caspases with the latter two playing a key role in apoptosis (Elmore, 2007). Initiator caspases are activated by intrinsic (caspase 9) or extrinsic pathways (caspase 8) and in turn cleave and activate the executioner caspases (caspases 3, 6 and 7) (Cohen, 1997). Cleavage by executioner caspases results in the destruction of certain substrates and the enzymatic activation of others (Bortner et al., 1995): Cleavage of poly (ADP-ribose) polymerase (PARP) involved in DNA repair results in its destruction. Cytoskeletal and other structural components of the cell, such as nuclear lamins are cleaved and the actin cytoskeleton is disassembled by actin depolymerases that are activated by caspase cleavage. Furthermore, cell cycle regulatory components such as cyclin-dependent kinase inhibitors and WEE1 kinase are cleaved and inactivated by caspases during apoptosis, resulting in elevated CDK activity in the cell (Zhou et al., 1998). On the other hand, processing of endonucleases such as DNA fragmentation factor (DFF) by caspases results in their activation (Chang and Yang, 2000). Collectively, the activity of caspases on their apoptotic substrates brings about the ordered disassembly of the cell from the inside: inactivation of housekeeping proteins, dismantlement of the structural elements of the cell, degradation of gDNA and proteins involved in DNA/RNA metabolism (**Figure 1.16**) (D'Arcy, 2019).

Caspase activation from the extrinsic pathways

Activation of caspases can either be achieved in an intrinsic manner in the cell or triggered by the extrinsic pathways. The common theme in both pathways is the activation of initiator caspases that then activate executioner caspases. The intrinsic pathway in mammals is activated at mitochondria and

it ultimately results in mitochondrial outer membrane permeabilization (MOMP). The release of pro-apoptotic factors from the mitochondrial intermembrane space causes or triggers in the activation of caspases 9 and then 3.

The intrinsic or mitochondrial pathway of apoptosis is primarily governed by the activity of the BCL-2 or BH3 family of proteins and is initiated by a number of cellular stresses including DNA damage, cytotoxic agents and hypoxia (Singh et al., 2019). The extrinsic pathways of apoptosis are typically mediated by immune cells including macrophages, $CD8^+$ cytotoxic T-cells and natural killer cells. Engagement of cell death receptors by secreted factors such as tumour necrosis factor (TNF) or the transmembrane FAS Ligand (FAS-L) on the extracellular site induces recruitment and activation of caspase 8 on the cytoplasmic side, which then activates caspases 3 and 7 (D'Arcy, 2019). Once activated, caspase 8 can also process the BH3-only protein BID into truncated BID (tBID), which allows it to feed into the intrinsic pathway of apoptosis. Immune cells also secrete granzymes and perforin. Perforin oligomerises and inserts into the target cell's membrane and allows granzymes to enter the cytoplasm from the extracellular side. Granzyme B is an active zymogen that is able to activate caspases without the need of upstream signalling cascades. Granzyme A on the other hand is able to directly cleave caspase substrates inducing caspase-independent apoptosis instead (Elmore, 2007).

The FAS/FAS-L pathway is primarily used in the elimination of auto-reactive T cells and it is a critical regulatory component involved in the mechanisms of central and peripheral tolerance (Volpe et al., 2016). TNF secretion is used by pro-inflammatory macrophages and natural killer cells (NK cells) (Brunner, 2003; Josephs et al., 2018).

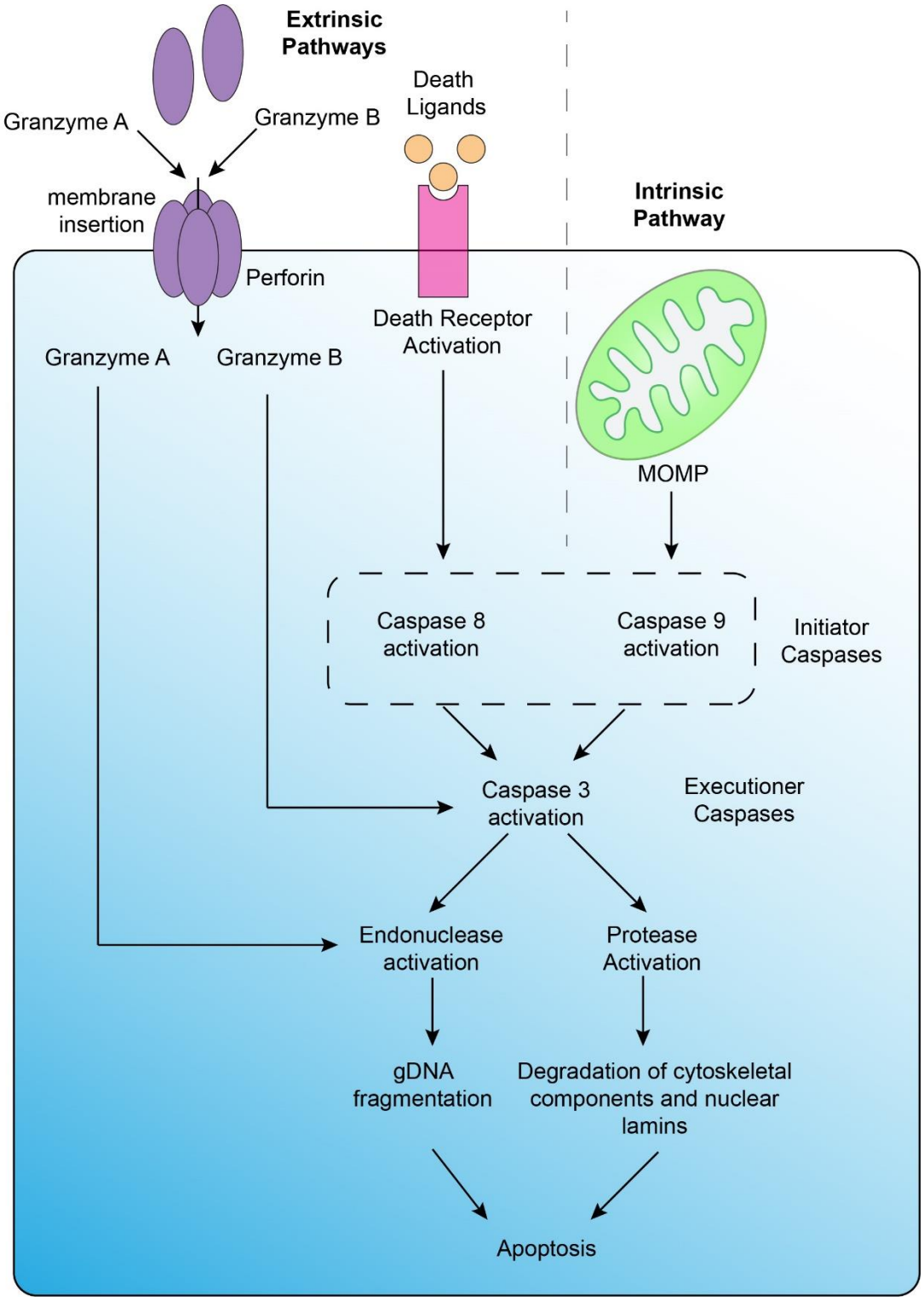

Figure 1.16: Overview of cellular apoptotic pathways

The figure shows how the intrinsic and extrinsic pathways of apoptosis converge on caspase activation and how caspase activity brings about apoptosis in a cell. The intrinsic or mitochondrial pathway is initiated when a stress stimulus brings about mitochondrial outer membrane permeabilization (MOMP) and induces caspase 9 activation. The extrinsic pathway is initiated when death ligands engage with cell membrane death receptors, which recruit and activate caspase 8. Granzymes A and B along with perforin are secreted

by immune cells and enter the target cell through perforin oligomers that insert in the cell's surface membrane. Granzyme B induces caspase activation while Granzyme A induces caspase-independent apoptosis by acting downstream.

1.6.2 The BCL-2 family of proteins are the master regulators of MOMP

The intrinsic pathway of apoptosis is also referred to as the mitochondrial pathway of apoptosis in higher animals because the pro- and anti-apoptotic signals converge on mitochondria. The fate of the cell is governed by the activities of the BCL-2 or BH3 family of proteins at the OMM (Kale et al., 2018; Bock and Tait, 2020).

The first member, BCL-2, was identified in 1984 and also provided the name to the whole family. B-cell lymphoma 2 (BCL-2) was discovered in patients with B-cell lymphomas that had undergone chromosome translocations bringing the BCL-2 gene under the control of the immunoglobulin promoter resulting in BCL-2 overexpression (Tsujimoto et al., 1984). It was only later that BCL-2 was assigned an anti-apoptotic function and several other members of this family were identified to contain BCL-2 homology (BH) domains (Vaux et al., 1988). BCL-2 family proteins are classified in three distinct subfamilies based on their function in apoptosis (**Figure 1.17**) (Pentimalli, 2018).

The first class encompasses the multi-domain pro-apoptotic effectors BAK and BAX. BAK and BAX have pro-apoptotic activity and are responsible for forming pores in the OMM and MOMP. BAK and BAX are largely functionally redundant in the context of apoptosis and typically cells only require one of the two to induce the intrinsic pathway of apoptosis (Dewson, 2001). BOK is the third member of the pro-apoptotic family with high homology to BAK and BAX. BOK primarily acts to induce MOMP in response to ER stress (Carpio et al., 2015; Llambi et al., 2016). BOK was recently shown to be required for ER-mitochondrial contact sites (Carpio et al., 2021). BOK was shown to enhance ER-mitochondrial contact sites and required for Calcium transfer from the ER to the mitochondria through these contact sites during apoptosis induced by ER-stress or use of proteasome inhibitors.

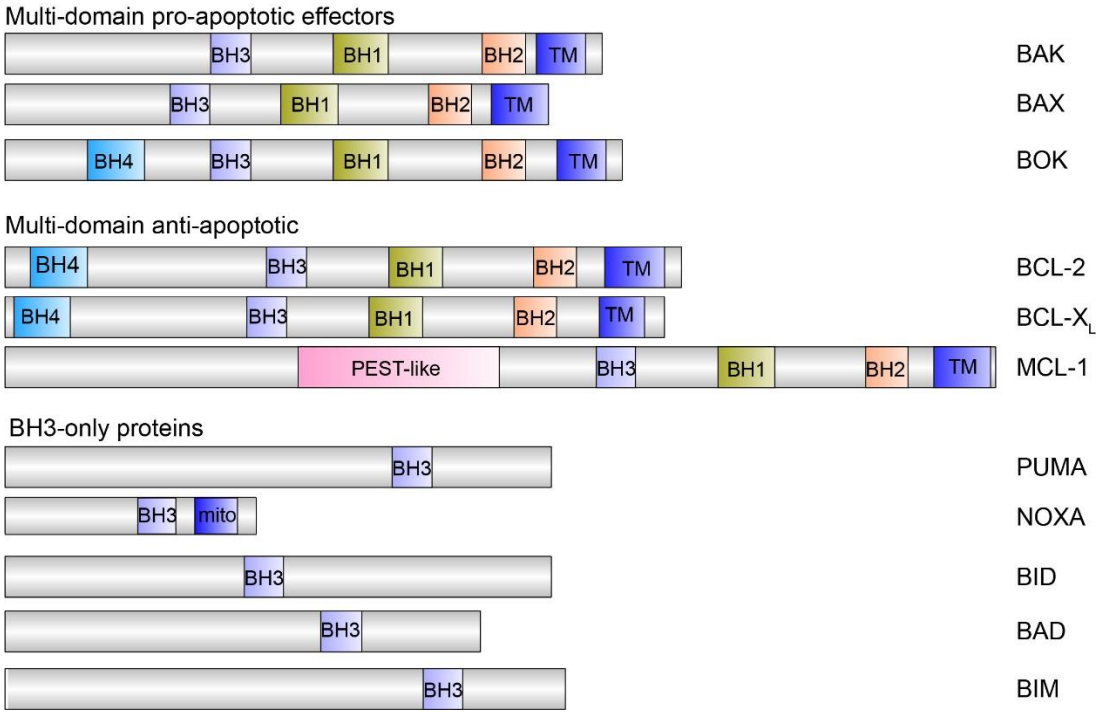

Figure 1.17: The BCL-2 family is divided into three functionally distinct classes

Overview of the three functionally distinct classes of BCL-2 family: The multi-domain pro-apoptotic effectors, the multi-domain anti-apoptotic and the BH3-only proteins. Domain architecture is shown with particular focus on the BCL-2 homology domains (BH) and the transmembrane (TM) domains.

The second class is the anti-apoptotic family that includes notable members such as BCL-2, BCL-X_L and MCL-1, and whose collective function is to prevent the activation of the MOMP effectors, BAK and BAX (Kale et al., 2018). An odd case is BCL-rambo (*BCL2L13*) that has similar architecture to BCL-2 but whose overexpression induces caspase-dependent apoptosis (Kataoka et al., 2001). BCL2L13 is rather atypical since its pro-apoptotic functions are attributed to its C-terminal domain and not the BH3-domain. BCL2L13 was also independently shown to act as a mitophagy receptor in a ubiquitin-independent manner. BCL2L13 may be functionally homologous to the yeast ATG32 mitophagy receptor (Murakawa et al., 2015). In fact, several BCL-2 family proteins have been described to serve functions in both apoptosis and mitophagy, such as NIX and BNIP3 (1.5.6).

The third class of BCL-2 proteins are referred to as BH3-only proteins since most of these members lack other BCL-2 homology domains apart from BH3 (Bock and Tait, 2020). Their function is to promote apoptosis by

preventing the anti-apoptotic proteins from inhibiting BAK and BAX whilst certain members may also act as activators for BAK/BAX as well (**Figure 1.18**). BH3-only proteins are typically maintained at low levels in the cells or kept in an inactivated state through post-translational modifications. For instance, the PI3K/AKT and MAP kinase pathways are known to promote cell proliferation and cell survival by phosphorylating the BH3-only protein BAD (Datta et al., 1997; Fang et al., 1999). In its phosphorylated state, BAD is not able to induce apoptosis at mitochondria and there is some evidence that suggests it is actively sequestered in the nucleus instead (Kizilboga et al., 2019). BID requires proteolytic cleavage by activated caspases to exert its pro-apoptotic activity (Schug et al., 2011). Stress caused by DNA damage, cytotoxic agents, hypoxia or sustained oncogenic signalling promotes transcriptional activation and expression of BH3-only proteins (Villunger et al., 2003; Lomonosova and Chinnadurai, 2008). The elevated levels of BH3-only proteins prevent the anti-apoptotic family from inhibiting the activation of BAK and BAX. Certain activator BH3-only proteins are present in the cell and are prevented from activating BAK/BAX through direct interaction by the anti-apoptotic family. One such example is BIM being kept in check by interacting with MCL-1 (Singh et al., 2019). Induction of DNA damage or viral infection results in the upregulation of sensitizer BH3-only protein NOXA. NOXA displaces BIM from MCL-1 and BIM is liberated to activate BAK/BAX (Sun and Leaman, 2005; Han et al., 2007).

1.6.3 Mitochondrial outer membrane permeabilization (MOMP) and beyond

BAK is resident on the OMM while BAX operates at equilibrium from the cytosol and shuttles to mitochondria where it is kept at low levels (Wolter et al., 1997). BAX is actively retro-translocated to the cytosol by the activity of anti-apoptotic proteins such as BCL-2 and BCL-X_L (Billen et al., 2008; Edlich et al., 2011; Lauterwasser et al., 2016). In fact, efficient BAX retro-translocation is required to prevent commitment towards apoptosis as the default cell fate. One study suggested that a small cytosolic pool of BAK exists and similarly to BAX, BAK retro-translocates from mitochondria to the cytosol at much lower rates (Todt et al., 2015). Therefore, the majority of BAK is on mitochondria at steady state.

Once activated, the BH3 domains of BAK and BAX are exposed, which allows them to homo-dimerise on the OMM (Dewson et al., 2008). BAK and BAX homo-dimers are able to form higher order oligomers and produce channels that span the OMM. This allows pro-apoptotic factors such as cytochrome c and DIABLO/SMAC/OMI to enter the cytosol (Yang, 1997; Ott et al., 2002).

In the presence of deoxy-ATP or ATP, cytochrome c and APAF-1 assemble into the heptameric complex called the apoptosome (Zou et al., 1997; Chinnaiyan, 1999). The apoptosome serves as an activation platform for pro-caspase 9 dimerisation and cleavage into the active form and then leads to caspase 3 activation (Seshagiri and Miller, 1997; Acehan et al., 2002). Caspase activation is opposed by cytosolic anti-apoptotic factors such as XIAPs, which prevent against caspase activation in conditions of limited MOMP or accidental leakage from the OMM. These antagonists in turn are neutralised by the other molecules released into the cytosol from the mitochondrial intermembrane space such as SMAC and DIABLO (Verhagen et al., 2000).

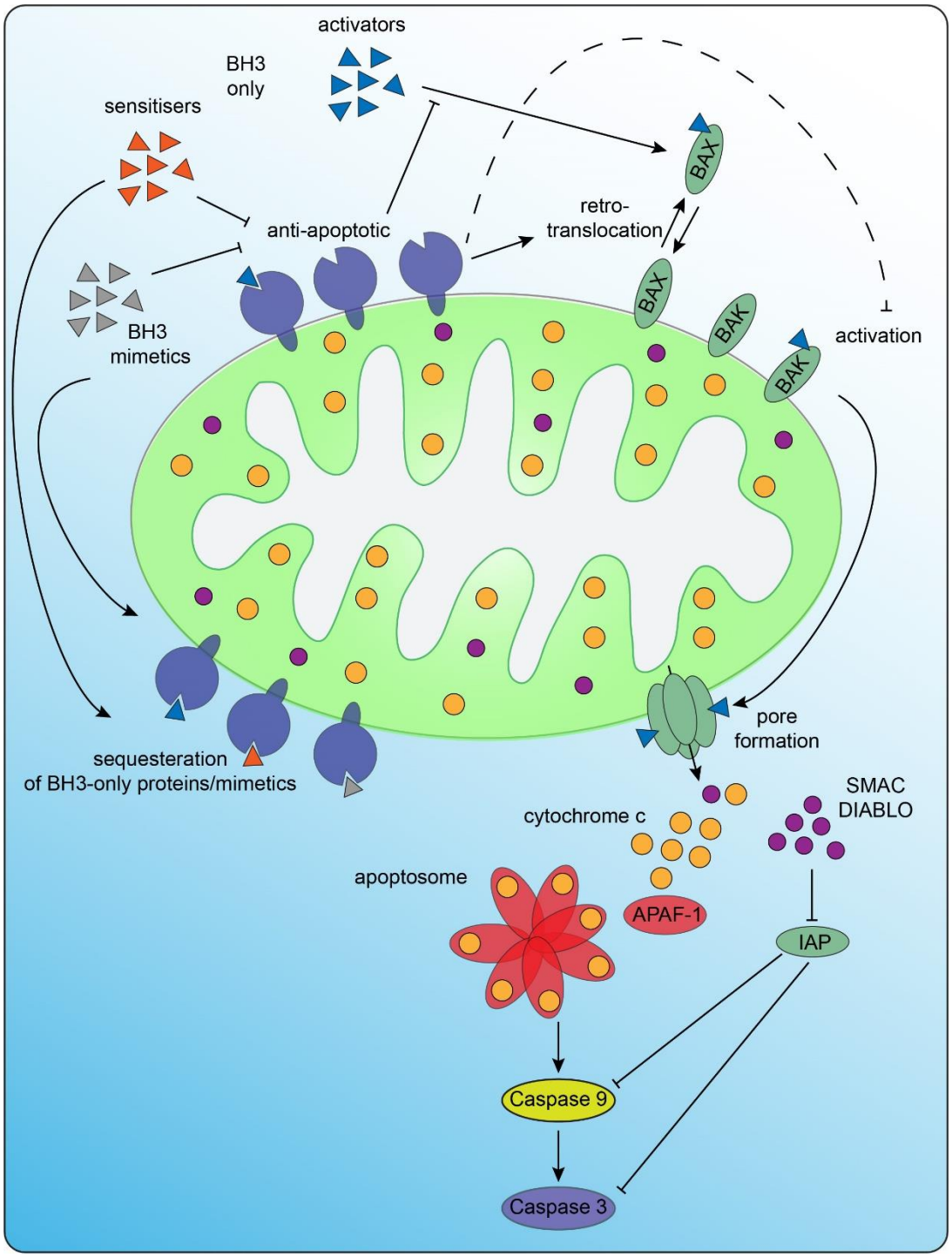

Figure 1.18: BCL-2 proteins control mitochondrial outer membrane permeabilization

Overview of the mechanisms by which the different classes of BCL-2 proteins interact with each other to promote or hinder mitochondrial outer membrane permeabilization (MOMP). Anti-apoptotic proteins promote retro-translocation of BAX to the cytosol and prevent activation of BAK and BAX. Furthermore, anti-apoptotic proteins prevent activation and homo-oligomerisation of BAK and BAX already in the outer mitochondrial membrane. BH3-only protein that act as activators are able to directly activate BAX recruitment to the membrane and promote BAK/BAX activation to form pores. BH3-only proteins acting as sensitizers prevent anti-apoptotic protein from inhibiting their targets, which

consist of pro-apoptotic proteins BAK and BAX as well as BH3-only proteins acting as activators. BH3 mimetics copy the activity of BH3-only proteins acting as sensitizers. BH3-only proteins and BH3 mimetics sequester anti-apoptotic proteins, releasing BAK/BAX and BH3-only proteins acting as activators. Adapted from Singh et al., (2019).

1.6.4 BH3 mimetics are therapeutic tools that target BCL-2 proteins

Evasion of, or resistance to, apoptosis is described as a hallmark of cancer (Hanahan et al., 2000; Hanahan and Weinberg, 2011). Many tumours are described as oncogene addicted since they require certain oncogenes to survive, which may include members of the anti-apoptotic BCL-2 family such as BCL-2 and MCL-1. Many solid or liquid tumours exhibit upregulation or genomic amplification of anti-apoptotic proteins resulting in enhanced survival and reduced cell death in response to therapy. The above dependency in many instances presents an Achilles heel for therapeutic intervention. Neutralisation of anti-apoptotic proteins may be achieved by the use of chemical inhibitors termed BH3 mimetics (Delbridge and Strasser, 2015). BH3 mimetics as their name implies, mimic the activity of sensitizer BH3-only proteins by inhibiting anti-apoptotic proteins and causing them to disengage from BAK/BAX and activator BH3-only proteins. BH3 mimetics were developed as tools to directly interfere with the dependence of tumours on anti-apoptotic BCL-2 proteins and resensitize tumour cells to apoptotic cell death. ABT-737 was the first BH3-mimetic to be developed and it was rationally designed using the BH3 domain of the BH3-only protein BAD (Oltersdorf et al., 2005). Administration of ABT-737 enhances cell death in cells treated with chemotherapeutic agents whilst also being effective as a single agent in small cell lung cancer mouse models. BH3 mimetics can be very specific in terms of which members of the anti-apoptotic family they are able to inhibit. ABT-737 is able to inhibit BCL-2, BCL-X_L, BCL-w but not BCL-B or MCL-1, which mirrors the anti-apoptotic proteins BAD interacts with.

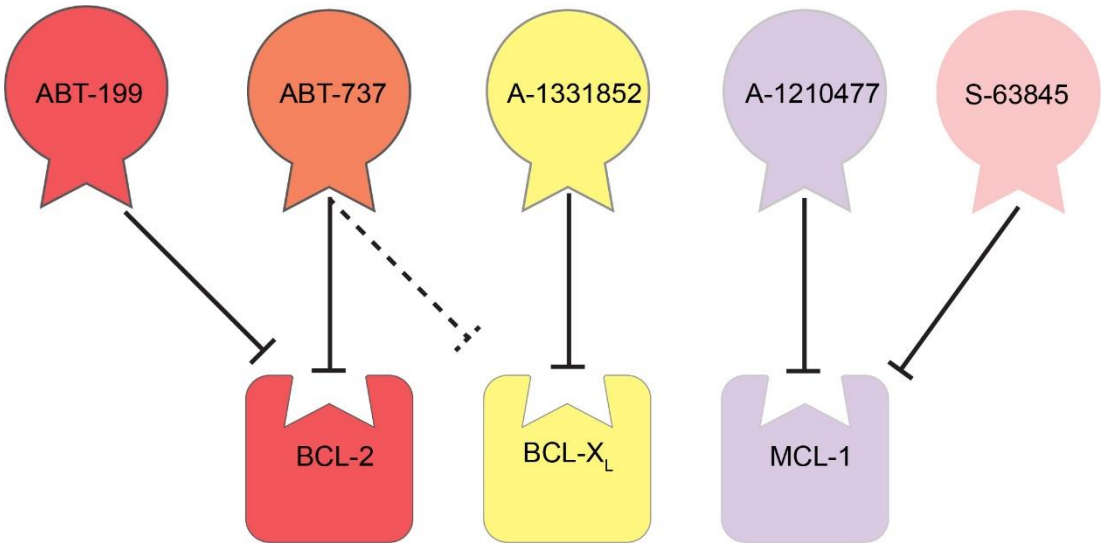

Figure 1.19: Selectivity of BH3-mimetics used in the present thesis
Overview of the specificity of BH3-mimetics used in the present thesis against members of the anti-apoptotic family. Solid lines suggest strong inhibition while dotted lines suggest weaker inhibition.

Eventually ABT-737 led to the development of the clinical analogue ABT-263 with improved oral bioavailability (Tse et al., 2008). ABT-263 was used in the treatment of chronic lymphocytic leukaemia (Kipps et al., 2015). However, administration of ABT-263 was accompanied by severe thrombocytopaenia caused by the simultaneous inhibition of BCL-X_L as well as BCL-2 (Shoemaker et al., 2006; Davids and Letai, 2013). ABT-199 was specifically developed to be a more potent and specific compound against BCL-2, that does not target BCL-X_L and is better tolerated (Debrincat et al., 2015). ABT-199 administration demonstrated that BCL-2 inhibition is an efficacious strategy in patients with chronic lymphocytic leukaemia (CLL), without the side effects of thrombocytopaenia (Seymour et al., 2014). The use of ABT-199 is limited to the treatment of CLL due to the dependence of the disease to BCL-2 and is not effective against solid tumours that are typically dependent on MCL-1 and BCL-X_L. Incidences of resistance to ABT-199 are also common as the disease became dependent on MCL-1 and BFL-1 for survival (Yecies et al., 2010).

Over the last two decades several other compounds have been developed that are more selective and specific against different members of the anti-apoptotic family (**Figure 1.19**). Compounds against MCL-1 were also developed as it is often upregulated in cancer. Compounds such as A-1210477

and S-63845 are specific to MCL-1 *in vitro* and effective against tumours. Furthermore, MCL-1 inhibitors re-sensitize cells to ABT-737 or other chemotherapeutic agents, alleviating some of the resistance mechanisms (Mathieu et al., 2014; Kotschy et al., 2016; Lian et al., 2018). A-1331852 is an orally bio-available inhibitor against BCL-X_L (Wang et al., 2020). A-1331852 administration induced dissociation of BCL-X_L:BIM complexes while synergizing with chemotherapeutic agents such as docetaxel to inhibit tumour growth *in vivo* (Leverson et al., 2015a). The newer compounds present an opportunity to expand the clinical tools against the BCL-2 family and fulfil an unmet clinical need in the treatment of cancer (Xiang et al., 2018).

1.6.5 Proposed models of BCL-2 family interactions

The first model wherein BH3-only proteins directly activate BAK and BAX is referred to as the direct activation model. In this model, certain BH3-only proteins such as tBID and BIM are able to directly interact with BAK and BAX and promote their conformational change towards their activated conformation (Wang et al., 1996; Desagher et al., 1999; Wei et al., 2000; Marani et al., 2002). Anti-apoptotic proteins prevent the activation of BAK/BAX by sequestering the activator BH3-only proteins, which in turn maintains BAK/BAX in their inactive conformation. Expression of sensitizer BH3-only proteins or addition of BH3 mimetic compounds causes the release of activator BH3-only proteins from the anti-apoptotic, which are in turn sequestered themselves (Letai et al., 2002). BH3-only proteins acting as activators are then free to activate BAK/BAX (Bock and Tait, 2020).

In the second model, BAK and BAX are thought to always be in an activated conformation and it is necessary they are always held in an inhibited state by the anti-apoptotic family (Willis et al., 2005). This model wherein BH3-only proteins relieve inhibition against BAK/BAX by inhibiting anti-apoptotic proteins is referred to as the indirect activation model (or displacement model) (Giam et al., 2008). This model stipulates that BAK/BAX activation is achieved by inhibiting their inhibitors and not by direct activation.

A study that utilised a mutant BIM variant that could not directly activate BAK/BAX but could still be sequestered by anti-apoptotic proteins, showed that apoptosis was still taking place albeit not as potently (Mérino et al., 2009). The

above highlighted that relieve of inhibition against anti-apoptotic proteins (indirect model) was the primary mechanism of apoptosis induction in this context but the direct activation mechanism still had a part to play. Furthermore, HCT116 cells that lack the eight key BH3-only proteins (8KO cells) were equally responsive to MCL-1 and BCL-X_L inhibition using BH3 mimetics as long as both anti-apoptotic proteins were inhibited (O'Neill et al., 2016; Greaves et al., 2019). The above observation directly challenges the direct activation model, since activation of BAK/BAX was possible without activator BH3-only proteins. The cells were however more resistant to other apoptotic stimuli, suggesting that direct activation still plays a part in some contexts. It does not exclude the possibility however that other proteins may act as activator BH3 proteins that are in operation in this context. It should be noted that both models are probably in operation simultaneously and which model is more prevalent may depend which BH3-only proteins are expressed in the cells under conditions of stress. BH3-only proteins that are described as activators like BIM are typically considered to be weak sensitizers compared to BH3-only proteins that are considered solely as sensitizers.

The "embedded together" model incorporates aspects of both the direct and the indirect models (Leber et al., 2007). In the "embedded together" model, anti-apoptotic proteins are continuously inhibiting active BAK/BAX and BH3-only proteins. For induction of apoptosis, sensitizer BH3-only proteins sequester anti-apoptotic proteins and in doing so release both activator BH3-only proteins and BAK/BAX. The activator BH3-only proteins are then free to activate previously-inactive BAK/BAX. The BAK/BAX molecules that were previously bound to anti-apoptotic proteins are already in an activated conformation and do not require activation. Activated BAK/BAX are then able to induce MOMP.

The unified model builds and expands upon the "embedded together" model (Llambi et al., 2011). In the unified model, the anti-apoptotic family inhibits activator BH3-only proteins (mode 1) and activated BAK/BAX (mode 2) but do not interact with inactive BAK/BAX molecules. The inhibitory effect of the anti-apoptotic proteins in these two modes is not equal, with mode 2 being a stronger inhibitory interaction than mode 1. The above stipulates that mode 1 is more readily derepressed by sensitizer BH3-only proteins or BH3 mimetics

than mode 2. Another consequence of the unified model is that anti-apoptotic proteins preferentially associate with activated BAK/BAX rather than activator BH3-only, which may allow for a small fraction of activator BH3-only proteins to remain unbound even in the presence of unengaged anti-apoptotic proteins. The unbound activator BH3-only proteins can activate a small pool of BAK/BAX that is kept in check by the anti-apoptotic proteins.

The functional redundancy between members of the BH3-only protein family makes it difficult to dissect the exact mode of action of each member, that is whether they function as direct BAK/BAX activators or sensitizers. Cells lacking all eight BH3-only proteins (8KO), anti-apoptotic proteins BCL-2, BCL-X_L, MCL-1, BCL-w and A1, and BNIP3 and BNIP3L (NIX) and BAK/BAX termed “BCL-2allKO” were generated (O’Neill et al., 2016). Reintroducing BAK and BAX in these cells, even at moderate levels of expression, was sufficient to induce MOMP and apoptosis. This spontaneous activation of BAK/BAX does not require BH3-only proteins. Furthermore, removing helix 9 from BAK/BAX that contains their TM domain is sufficient to prevent MOMP in these cells even in the absence of anti-apoptotic proteins. The above evidence suggests that BAK/BAX activation is primarily mediated by association with the OMM, giving rise to the lipid-mediated spontaneous activation model (O’Neill et al., 2016; Luo et al., 2020). The anti-apoptotic proteins normally keep BAK/BAX from activating and diffusing freely on the OMM. The BH3-only proteins neutralise the anti-apoptotic proteins, which allows BAX to associate with the OMM and BAK/BAX to diffuse through the lipid bilayer freely, which leads to their activation and oligomerisation. In this model, BH3-only proteins are considered purely as sensitizers or derepressors of the anti-apoptotic family and do not act as BAK/BAX activators. The lipid activation rationalises the spontaneous activation of BAK/BAX, that is not in fact spontaneous but mediated by the lipid bilayer through their TM domain.

1.6.6 The interplay between apoptosis and autophagy

Autophagy and apoptosis are cellular responses to stress. These two processes however result in two different outcomes, the former promoting survival and the latter a form of cell death. In the context of cancer, apoptosis

is a purely tumour suppressive pathway while autophagy was shown to have both tumour protective and tumour promoting capabilities (1.5.3).

The cross-talk between autophagy and apoptosis is extensive (Su et al., 2013). First of all, BECN1 has a BH3 domain that allows it to interact with other BH3 domain-containing proteins (Sinha and Levine, 2008). BECN1 was in fact first isolated as a BCL-2 interacting protein (Liang et al., 1998). The interaction between BECN1 and BCL-2/BCL-X_L was shown to inhibit autophagy. Mutations in the BH3 domain of BECN1 prevents the interaction with BCL-2 and promote autophagy and cell death that were dependent on ATG5 (Pattingre et al., 2005; Pattingre and Levine, 2006).

Mechanisms that modulate BCL-2 activity also affect BCL-2 function in autophagy. The interaction between BECN1 and BCL-2/BCL-X_L is inhibited by the BH3 mimetic ABT-737 that targets BCL-2/BCL-X_L and results in elevated levels of autophagy (Maiuri et al., 2007). However, ABT-737 was unable to induce autophagy in cells that lacked BAK/BAX (Lindqvist et al., 2014). It was therefore concluded that the effect of ABT-737 in stimulating autophagy was thought to be a result BAK/BAX activation and induction of apoptosis instead of disrupting the interactions between BCL-2 and BECN1 (Lindqvist and Vaux, 2014). It was therefore proposed that the interactions reported between anti-apoptotic BCL-2 proteins and BECN1 are not as significant as initially thought.

The interaction of BCL-2/BECN1 is also regulated through BCL-2 phosphorylation by JNK1 (Wei et al., 2008a). Phosphorylated BCL-2 also has reduced ability to bind BAX or BIM and promotes cell death (Bassik et al., 2004). Under conditions of starvation JNK1 phosphorylates BCL-2 causing it to dissociate from and alleviate its inhibition against BECN1, allowing autophagy to proceed. If starvation is sustained and the autophagy triggered is not able to provide sufficient nutrients, then phosphorylated BCL-2 accumulates in the cell further. The inhibition against BAK/BAX is relieved and the cell undergoes apoptosis instead (Wei et al., 2008b).

UVRAG, which is part of the BECN1/VPS34 complex that functions in autophagosome initiation, was shown to bind and inhibit BAX (Yin et al., 2011b). More specifically, UVRAG overexpression prevents BAX activation and translocation to mitochondria during UV irradiation (Yin et al., 2011a).

Another core component of the autophagy machinery, ATG12 that participates in the ubiquitin-like conjugation of ATG8 homologues (LC3) to PE, was also shown to have a BH3-like domain which allows it to interact with MCL-1 and to a lesser extend BCL-2 (Rubinstein et al., 2011). ATG12 depletion protects cells from apoptotic cell death treated with chemotherapeutic agents.

The activity of proteases also modulates the activity of apoptotic and autophagic components. Calpains are a class of non-caspase proteases that are activated by influx of calcium ions in the cytosol during apoptosis (Momeni, 2011). ATG5 is a calpain substrate during apoptosis and the proteolytic cleavage of ATG5 removes its autophagic functions and directs it towards mitochondria instead (Yousefi et al., 2006). Cleaved ATG5 antagonises the activity of BCL-2 and BCL-X_L at mitochondria and indirectly promotes BAK/BAX activation. BECN1 was shown to be cleaved by caspases during apoptosis. The cleavage of BECN1 hinders autophagy while at the same time facilitating the release of more pro-apoptotic factors from mitochondria committing the cell to apoptosis (Wirawan et al., 2010).

1.6.7 The roles of p53 in apoptosis and autophagy

The tumour suppressor protein p53 is thought to be the most commonly mutated gene in human cancers and is referred to as the “guardian of the genome” due to its central role in DNA damage response and repair (Matlashewski et al., 1986; Hafner et al., 2019). DNA damage induces p53 stabilisation, which in turn transcriptionally activates the expression of a number of pro-apoptotic proteins including BAX, PUMA, NOXA and APAF-1 (Toshiyuki and Reed, 1995; Nakano and Vousden, 2001; Fortin et al., 2001; Shibue et al., 2003). Furthermore, the cytosolic pool of p53 directly interacts with and activates BAX (Chipuk, 2004). Cytoplasmic p53 also promotes activation of JNK1, which activates autophagy through BCL-2 phosphorylation and inhibition, as discussed above (Thomas et al., 2000; Wei et al., 2008a; b). Interestingly, p53 was also shown to interact with BCL-2/BCL-X_L at the OMM, inhibiting them and in the process promoting apoptosis (Mihara et al., 2003). Nuclear p53 transcriptionally upregulates expression of the lysosomal Damage-regulated autophagy modulator (DRAM) that promotes autophagosome formation and at the same time is required for p53-dependent

apoptosis (Crighton et al., 2006, 2007). Collectively, both cytoplasmic and nuclear functions of p53 appear to promote apoptosis and autophagy.

1.6.8 Interplay between apoptosis and inflammation in neurodegeneration

Neurodegeneration arises from aberrant cell death of post-mitotic neurons combined with their inability to proliferate, resulting in a reduction in the number of functioning neurons. For PD specifically, it is the inability of dopaminergic neurons in the *substantia nigra* of the midbrain to produce and secrete sufficient amounts of dopamine, as a result of damage or cell death (Poewe et al., 2017). The role of inflammation in the pathogenesis and manifestation of PD is becoming increasingly recognised. Evidence of inflammation is detected in the brains and bodily fluids of PD patients, including activated pro-inflammatory macrophages and microglia (Moehle and West, 2015; George and Brundin, 2015). There is also evidence of α-synuclein aggregates inducing innate and adaptive immune responses against dopaminergic neurons, implicating auto-immunity as part of the mechanism of PD pathophysiology (Gao et al., 2008). Patients with inflammatory bowel disease appear to have double the incidence of PD compared to the general population in a Danish nationwide cohort study that spanned over a thirty-year period (Villumsen et al., 2019). Furthermore, there is evidence that α-synuclein aggregates in the gut promote inflammation locally before inflammation in the brain manifests (Challis et al., 2020). Lastly, bacterial infections in the gut of PINK1KO mice appear to promote PD-like symptoms (Matheoud et al., 2019). It seems that inflammation and auto-immunity have a major role to play in PD progression, especially in association with the gut.

Defective or damaged mitochondria may result in improper execution of apoptosis, which may lead to MOMP and mitochondrial inner membrane permeabilization (MIMP) and the release of mtDNA into the cytosol. The presence of mtDNA in the cytosol activates the cGAS/STING pathway, a component of the type I interferon response (Chen et al., 2016; Riley et al., 2018). Initiation of apoptosis using BH3 mimetics in the presence of caspase inhibitors, can result in MOMP and eventually MIMP, extending the survival of cells in the short-term (Riley et al., 2018). Under those conditions or conditions of incomplete or minority MOMP, mtDNA is released into the cytosol following

MIMP (Bock and Tait, 2020; Riley and Tait, 2020). Activation of the cGAS/STING pathway results in the production and secretion of pro-inflammatory molecules Interleukin-1 (IL-1) and interferon (IFN) (Decout et al., 2021). IL-1β specifically, produced by the cGAS/STING pathway may act in an autocrine and paracrine manner by inducing release of mtDNA in neighbouring cells, further activating the cGAS/STING pathway and enhancing the inflammatory response (Aarreberg et al., 2019).

Elevated levels of pro-inflammatory cytokines were found in the sera of mice and humans harbouring either PINK1 or Parkin mutations (Sliter et al., 2018). The same study also found elevated levels of circulating mtDNA and determined that the mechanism of inflammation induced by mtDNA was through the cGAS/STING pathway, as concomitant loss of STING prevented inflammation and neurodegeneration in Parkin and PINK1 KO mice. This was taken to suggest that PINK1 and Parkin have a protective role in preventing mitochondrial damage that may induce shedding of mtDNA into the cytosol and eventually extracellularly, and subsequent activation of the cGAS/STING pathway. The resulting inflammation may contribute towards PD pathogenesis (Riley and Tait, 2020).

1.6.9 E3 ubiquitin ligases and DUBs involved in cell death

A number of E3 ubiquitin ligases and DUBs have been implicated in the regulation of apoptosis and other cell death pathways and this section is concerned with discussing some of the most important discoveries.

TNF signalling elicits distinct outputs and cellular responses depending on the tissue involved and reversible ubiquitylation by E3 ligases and DUBs plays a pivotal role in the regulation of this pathway (Kupka et al., 2016).

Binding of TNF ligand to the extracellular side of the TNF receptor (TNFR) results in trimerization and assembly of TNFR signalling complex 1 (TNFR-SC1) (Yang et al., 2018). Downstream effectors that are recruited to the complex are TNFR associated via death domain (TRADD) and receptor interacting serine/threonine kinase 1 (RIPK1). TRADD recruits TRAF2, which results in the recruitment of cellular inhibitors of apoptosis proteins (cIAP) 1, 2 and 3 (Bertrand et al., 2008; Varfolomeev et al., 2008). TRAF2 and cIAPs are E3 ubiquitin ligases that decorate TRADD, RIPK1 and other complex

components with K11-, K48- and K63-linked poly-ubiquitin chains (Rothe et al., 1995; Shu et al., 1996; Park et al., 2004; Dynek et al., 2010; Dittmar and Winklhofer, 2020). The K63-linked ubiquitin chains recruit the LUBAC E3 ligase complex (Kirisako et al., 2006). LUBAC generates linear (M1-linked) ubiquitin chains on the existing K63-linked ubiquitin chains on RIPK1 (Gerlach et al., 2011; Emmerich et al., 2013). The K63-linked and the M1-linked poly-ubiquitin chains recruit TAK1 and IKK as well as NEMO respectively (Kanayama et al., 2004; Rahighi et al., 2009). IKK phosphorylates IkB, which creates a phosphodegron recognised by the $SCF^{\beta TRCP}$ (Chen et al., 1995). $SCF^{\beta TRCP}$ decorates IkB with K48-linked ubiquitin chains and targets it for proteasomal degradation (Winston et al., 1999; Orian et al., 2000). NFκB is then released and translocates into the nucleus where it enhances transcription of target genes involved in promoting survival, proliferation and induction of inflammation. Assembly of TNFR-SC1 simultaneously promotes the assembly of the cytosolic complex TNFR-SC2, which consists of RIPK1, TRADD, TRAF2 and caspase 8. TNFR-SC2 activity is suppressed by ubiquitylation of its components by cFLIP, one of the downstream targets of LUBAC transcriptional activation. Suppression of TNFR-SC2 activity hinders activation of caspase 8 and RIPK1 and thereby prevents downstream activation of apoptosis and necroptosis respectively (Griewahn et al., 2019). Therefore, LUBAC activity in generating M1-linked chains promotes cell survival by stabilising formation of TNFR-SC1. The cell fate is further reinforced by cFLIP, which supresses activation of TNFR-SC2. LUBAC-mediated ubiquitylation is reversed by the activity of the DUBs CYLD and OTULIN (Elliott et al., 2014, 2016). CYLD hydrolyses M1- and K63-linked ubiquitin chains whereas OTULIN only hydrolyses M1-linked chains (Komander et al., 2008; Keusekotten et al., 2013; Sato et al., 2015; Elliott and Komander, 2016). Furthermore, phosphorylated OTUD4 is converted to a K63-linked DUB and with A20 that binds M1-linked chains, suppress LUBAC-mediated downstream signalling by hydrolysing K63-linked ubiquitin chains and preventing binding of other downstream effectors (Verhelst et al., 2012; Tokunaga et al., 2012; Zhao et al., 2018, 4). The collective activity of these four DUBs suppresses LUBAC-mediated downstream signalling and promotes activity of TNFR-SC2.

The pro-apoptotic effectors BAK and BAX are also regulated through ubiquitylation. The E3 ligase IBRDC2 specifically targets activated BAX for proteasomal degradation at mitochondria, in association with BCL-X_L (Benard et al., 2010). An apoptotic stimulus triggers the translocation of IBRDC2 to mitochondria concomitantly with BAX and was shown to bind and ubiquitylate BAX with the 6A7 epitope exposed. The envelope protein E6 from human papilloma virus (HPV) associates with BAK and the HECT E3 ligase E6-AP, targeting BAK for proteasomal degradation during viral infection (Thomas and Banks, 1998, 1999). The proteasomal degradation of BAK hinders proper execution of apoptosis allowing for the survival of the infected cell, playing an important role in the cellular transformation caused by HPV.

The BH3-only protein BIM becomes ubiquitylated and is targeted for proteasomal degradation by the $SCF^{\beta TRCP}$ following phosphorylation by ERK (Dehan et al., 2009). BIM ubiquitylation is reversed by USP27x, which stabilises BIM levels in the cell and activates apoptosis (Weber et al., 2016).

Regulation of MCL-1 stability is of great interest due to the frequency of MCL-1-dependent tumours. Its short half-life makes MCL-1 a prime target in the clinical setting by modulating the activity of enzymes that regulate MCL-1 stability. MCL-1 has been described to be ubiquitylated and targeted for proteasomal degradation by several E3 ubiquitin ligases including HUWE1 (MULE), TRIM17, SCF^{FBXW7}, $SCF^{\beta TRCP}$ and APC/C CDC20 (Ding et al., 2007; Inuzuka et al., 2011; Gupta et al., 2018). HUWE1 was shown to regulate the stability of MCL-1 through interactions mediated by its BH3 domain (Zhong et al., 2005). It has also been proposed that the BH3 domain of HUWE1 resembles the BH3 domain of BAK, an MCL-1 interactor and therefore HUWE1 may act as a BH3-only protein freeing MCL-1/BAK dimers (Zhong et al., 2005). USP9x was shown to deubiquitylate MCL-1, rescuing it from proteasomal degradation (Schwickart et al., 2010). Furthermore, USP9x depletion reduced MCL-1 levels and rendered cancer cell lines more responsive to ABT-737-induced apoptosis. Interestingly, NOXA overexpression promotes the interaction between HUWE1 and MCL-1 thus promoting MCL-1 degradation (Czabotar et al., 2007; Gomez-Bougie et al., 2011). At the same time the interaction between MCL-1 and USP9x is suppressed when NOXA is overexpressed. The role of USP9x in the regulation of MCL-1 remains

controversial. USP24, a USP9x paralogue, has been proposed to regulate MCL-1 instead (Peterson et al., 2015). USP24 depletion and inhibition, and not USP9x, were shown to induce apoptosis in Jurkat cells (Luo et al., 2019). More recently, USP13 was shown to interact with MCL-1 and correlate in expression and gene amplification to MCL-1 in a variety of cancers (Zhang et al., 2018). USP13 inhibition and CRISPR-mediated KO caused a reduction in the levels of MCL-1 and sensitized to treatment with ABT-263, suggesting a synergistic effect between USP13 inhibition and BH3 mimetics.

Parkin has been assigned both pro- and anti-apoptotic roles in relation to ubiquitylating and targeting BCL-2 family proteins for degradation. BAX undergoes a number of major conformational changes as part of its activation from the cytosol to the mitochondrial outer membrane (Todt et al., 2015; Lauterwasser et al., 2016). These intermediate conformational states of BAX shape the intrinsic predisposition of a cell to undergo apoptosis in response to stress. In the context of post-mitotic neurons this increased sensitivity to apoptotic stimuli may result in aberrant cell death, which contributes to neurodegeneration (Cakir et al., 2017). Parkin was found to selectively target activated BAX molecules for degradation and helps prevent against apoptosis in this context. However, Parkin has also been proposed to mediate degradation of MCL-1 following mitochondrial depolarisation, sensitizing to depolarisation-induced apoptosis in a PINK1-dependent manner (Carroll et al., 2014; Zhang et al., 2014).

Depolarisation-induced apoptosis in a Parkin overexpressing cell line is PINK1-dependent and involves cytochrome c release into the cytosol and caspase activation but is BAK/BAX independent (Carroll et al., 2014; Liang et al., 2015a). Inhibition of the proteasome delayed but did not rescue against activation of caspases, suggesting proteasomal degradation of ubiquitin-decorated OMM proteins were part of the mechanism. The above effect is thought to be mediated by the non-specific rupture of the OMM during parkin-mediated ubiquitylation and extraction of OMM proteins.

Interestingly, activation of caspases in parkin-overexpressing cells in response to depolarisation was exacerbated when USP30 was depleted (Liang et al., 2015a). The sensitisation to depolarisation-induced cell death by USP30 depletion is also PINK1 and Parkin dependent but importantly BAK and

BAX independent in this context. USP30 is proposed to enable Parkin to ubiquitylate certain OMM proteins to a higher extent and enhance their proteasomal degradation, which damages the OMM further. However, USP30 depletion was also shown to enhance the effect of BH3 mimetic ABT-737 in inducing apoptosis (Liang et al., 2015a). The sensitisation to ABT-737 was more reliant on BAX than BAK, and co-depletion of both was necessary to completely lose the effect, as with the baseline response. The above pieces of evidence suggested that USP30 is normally suppressing BAK/BAX activation that results in MOMP or USP30 restricts cytochrome c release. USP30 is of particular interest in this context because it is the only DUB known to permanently associate with the OMM via a transmembrane domain (Nakamura and Hirose, 2008). The position of USP30 at the OMM places it in a prime position to regulate events relating to apoptotic cell death as well as mitophagy.

1.7 Aims of this thesis

My project was initially conceived as a continuation of the work of a previous PhD student in the lab, Amos Liang. He showed USP30 was limiting BH3 mimetic-induced apoptotic cell death, implicating USP30 in the regulation of apoptosis (Liang et al., 2015a). In my thesis I wish to take this further by:

1. expanding the repertoire of BH3 mimetics to more potent and selective compounds that target other members of the anti-apoptotic BCL-2 family and in the context of other cell lines.
2. generating USP30KO cells to study apoptotic cell death.
3. investigating novel aspects of USP30 biology relating to cellular fitness and survival.
4. generating and characterising new tools around USP30 to expand the arsenal of reagents in the broader scientific community.
5. Investigate the “druggability” of USP30 by comparing USP30KO and inhibitor-treated cells with the ultimate aim of understanding whether USP30 is a druggable DUB in the context of cancer and neurodegeneration.

Chapter 2: Materials and Methods

2.1 Cell Biology

2.1.1 Cell lines and reagents

The HCT116 cells and HCT116 FlpIn TRex cells were a gift from Bert Vogelstein (Johns Hopkins, Baltimore), and Louisa Nelson, Anthony Tighe and Stephen Taylor (University of Manchester, UK) respectively. The human telomerase reverse transcriptase immortalised retinal pigmented epithelial (hTERT-RPE1) cells were a gift from Francis Barr (University of Oxford, UK) and hTERT-RPE1 cells overexpressing YFP-Parkin were a gift from Jon Lane (University of Bristol) (MacVicar and Lane, 2014). The hTERT-RPE1 FlpIn TRex cells were a gift from Jon Pines (ICR, London). SH-SY5Y cells (94030304) were purchased from ECACC (Sigma-Aldrich). Finally, the HCT116 BAKKO cells were a gift from Dr. Shankar Varadarajan (University of Liverpool, UK) (Wang and Youle, 2012).

Tissue culture media Dulbecco's Modified Eagle's Medium GlutaMAX (DMEM) (31966-021), DMEM no glucose, no pyruvate, with L-glutamine (11966025) and DMEM/F-12 (1:1) GlutaMAX (31331-028) were purchased from Gibco (ThermoFisher). Foetal bovine serum (FBS) (10270106) was purchased from Gibco (ThermoFisher) and it was heat-inactivated by heating to 56°C in a water bath for 20 min. Trypsin-EDTA (15400-054) was purchased from Invitrogen (ThermoFisher) and aseptically diluted to 1x working concentration using phosphate buffered saline (PBS). All transfection reagents Lipofectamine 2000 (11668019), Lipofectamine LTX (15338030), Oligofectamine (12252011), Lipofectamine RNAiMax (13778150) and reduced serum media Opti-MEM GlutaMAX (51985-026) were purchased from Invitrogen (ThermoFisher). Genejuice (70967) was purchased from EMD Millipore. Hygromycin B (10687010), Blastidicin S (R21001) and Zeocin (R25005) were purchased from Invitrogen (ThermoFisher), G-418 (4727878001) was purchased from Roche, and doxycycline hyclate (D9891) was purchased from Sigma-Aldrich. TAK-243 (CT-M7243) and MLN4924 (CT-M4924) were purchased from Chemietek (IN, USA). ABT-737 (S1002), ABT-

199 (S8048), A-1210477 (S7790) and A-1331852 (S7801) were purchased from Selleckchem while S-63845 (A8737) was purchased from ApexBio (Boston, MA, USA). Oligomycin A (75351), antimycin A (A8674), rotenone (R8875), trifluoromethoxy carbonylcyanide phenylhydrazone (FCCP: C2920), carbonyl cyanide 3-chlorophenylhydrazone (CCCP: C2759), Propidium Iodide (PI: P3566), Poly-L-Lysine (P4832), crystal violet (C6158), 2-deoxyglucose (D8375) were purchased from Sigma-Aldrich. Epoxomicin (324800) was purchased from Calbiochem (Sigma-Aldrich). Seahorse DMEM base medium (103334) was purchased from Agilent Technologies (UK). FT3967385 (hereafter FT385) was synthesized and provided by our colleagues in Forma Therapeutics (Boston, MA, USA) (Rusilowicz-Jones et al., 2020). Annexin V-FITC and Tetramethylrhodamine, ethyl ester (TMRE: 87917 Sigma Aldrich) were gifts from from Dr. Shankar Varadarajan (University of Liverpool, UK) (Vogler et al., 2008; Varadarajan et al., 2013).

All tissue culture dishes, plates, flasks, centrifugation tubes, serological and aspiration pipettes were purchased from Corning or Starlabs.

2.1.2 Mammalian Tissue Culture

HCT116, HCT116 BAKKO and HCT116 FlpIn TRex cells were maintained in 10% FBS DMEM GlutaMAX while hTERT-RPE1, YFP-Parkin hTERT-RPE1 FlpIn TRex and SH-SY5Y cells were cultured in 10% FBS DMEM/F-12 GlutaMAX. All cells were maintained in a humidified 5% CO_2 incubator at 37°C. Cells were passaged at frequent time intervals in 10 cm dishes or T75 flasks as required.

2.1.3 DNA transfections

HCT116 and HCT116 FlpIn TRex cells were transfected using Lipofectamine LTX with PLUS reagent while hTERT-RPE1 cells were transfected using Genejuice according to manufacturers' instructions. Both cell lines were typically seeded in 6-well plates the day prior transfection with 500, 000 cells in antibiotic-free media for a 24-hour transfection. For experiments involving immunofluorescence microscopy, cells were seeded directly onto sterile coverslips at a lower density. For transfections in HCT116 cells 1 µg of plasmid DNA was diluted in 200 µl Opti-Mem GlutaMAX supplemented with 2

µl PLUS reagent and 4 µl Lipofectamine LTX diluted in 200 µl Opti-Mem GlutaMAX and incubated separately for 5 min at room temperature. The two solutions were then mixed and incubated a further 20 min at room temperature before being added to the cells in a dropwise manner. For transfections in hTERT-RPE1 cells, 4 µl Genejuice were diluted in 100 µl Opti-Mem GlutaMAX and incubated for 5 min at room temperature before adding 1 µg of plasmid DNA and incubating the mixture for a further 20 min at room temperature. The mixture was then added to the cells in a dropwise manner. Cells were either fixed on coverslips or lysed in lysis buffer 24 hours post transfection, unless otherwise specified. For larger scale transfections such as those performed in 10 cm dishes, the quantities of cells and reagents used were adjusted based on the increase in surface area of the cell growth area.

2.1.4 siRNA knockdown transfections

All siRNA oligonucleotides were purchased from Dharmacon/Horizon with the exception of USP30 Q6 that was purchased from Qiagen. All oligonucleotides were resuspended in 1x siRNA resuspension buffer (Dharmacon, ThermoFisher: NC1338268) to a stock concentration of 20 µM and stored at -20°C. All the details and sequences of all oligonucleotides used in the thesis are shown in **Table 2.1**.

All siRNA-mediated knockdown transfections were performed using a forward protocol except for those in section 4.3, where a reverse transfection protocol was performed in parallel as indicated in the respective figure legend. Cells were seeded in 6-well plates the day prior the transfection in their standard growth medium without any antibiotics. HCT116 and HCT116 FlpIn TRex cells were seeded at 250,000 cells per conditions and hTERT-RPE1, hTERT-RPE1 YFP-Parkin and hTERT-RPE1 FlpIn TRex cells were seeded at 150,000 cells per condition. SH-SY5Y were seeded at 600,000 cells per condition. Media were replaced on the day of transfection for 730 µl per well of the same base medium without serum. 2 µl RNAiMax diluted into 83 µl Opti-Mem GlutaMAX and 2 µl 20 µM siRNA oligonucleotides in 83 µl Opti-Mem GlutaMAX were incubated separately for 5 min at room temperature. The two solutions were mixed and incubated a further 20 min at room temperature and added to the cells in a dropwise manner to a final concentration of 40 nM

siRNA. The media were replaced with complete media 24 hours for SH-SY5Y cells and 6 hours for all other cells post transfection.

Table 2.1: siRNA oligonucleotide sequences

Target	Name	Catalogue Number	Sequence
-	Non-targeting control (NT1)	D-001810-01-50	UGGUUUACAUGUCGACUAA
USP30	USP30 D1 siGenome	Custom	CAAAUUACCUGCCGCACAAUU
	USP30 D3 siGenome	D-021294-03	ACAGGAUGCUCACGAAUUA
	USP30 Q6 (Qiagen)	S104286044	CUCCGAUGACACUGUCCGCAA
PINK1	PINK1 SmartPool	L-004030-00	GCAAAUGUGCUUCAUCUAA, GCUUUCGGCUGGAGGAGUA, GGACGUUGUUCCUCGUUAU, GGAGACCAUCUGCCCGAGUA
BAK	BAK SmartPool	L-003305	CGACAUGAACCGACGCUAU, UAUGAGUACUUCACCCCGA, GACGGCAGCUCGCCAUCAU, AAUCAUGACUCCCAAGGGU
BAX	BAX SmartPool	L-003308	AAGUGGAGCUGACAUGUUU, UGCCGGAACUGAUCAGAAC, GCAAACUGGUGCUCAAGGC, CAUCAUGGGCUGGACAUUG

The total duration of the siRNA knockdown was 72 hours unless otherwise stated. The cells were either lysed in the indicated lysis buffer or treated before being lysed as indicated in the figure legends. For immunofluorescence experiments, cells were split 1:3 at the day prior to harvesting and fixation. One part was seeded onto coverslips in 6-well plates and the remaining 3 parts in fresh 6-well plates for lysis and immunoblot analysis.

2.1.5 Generation of USP30KO cells in the HCT116 FlpIn TRex cell line

The HCT116 FlpIn TRex were seeded at a density of $2.5x10^6$ cells in 10 cm dishes the day prior to the transfection, preparing one 10 cm per sgRNA-carrying plasmid. Transfections were performed using 24 µl Lipofectamine LTX diluted in 750 µl Opti-Mem GlutaMAX and 6 µg of the pX458 sgUSP30-1 or sgUSP30-2 and 4 µl PLUS reagent were diluted in 750 µl Opti-Mem GlutaMAX according to manufacturer's instructions. The two mixtures were incubated separately for 5 min at room temperature before being mixed and incubated a further 20 min at room temperature. The media were exchanged to 10 ml 10% FBS DMEM before the transfection mixture was added in a dropwise manner.

The fluorescence activated cell sorting (FACS) took place 24 hours post transfection. Conditioned media was prepared using 10% FBS DMEM media from exponentially growing HCT116 FlpIn TRex cells. The media were diluted 1:3 with fresh 10% FBS DMEM media and supplemented with 10 mM HEPES pH 7.4 (ThermoFisher), before being filtered through a 0.22 µm filter (Corning). Flow-sort solution (10% FBS in PBS supplemented with 10 µg/ml DNAse (Qiagen)) was prepared fresh on the day. Cells were washed once with sterile PBS and trypsinised for 1 min at 37°C. Cells were resuspended in 7 ml flow-sort solution to stop the reaction and centrifuged for 5 min at 200 g. The supernatant was aspirated, and cells were resuspended in 13 ml flow-sort solution. The cells were counted and passed through a 100 µm cell strainer (Corning). Cell density was adjusted to $1x10^6$ cells/ml using flow-sort solution and cells were aliquoted into flow sort FACS tubes (2 ml/tube). Recipient flow sort tubes were prepared using 1 ml/tube of conditioned media. The cells were then transported to the cell sorting facilities on ice. GFP^+ population sort was performed using a FACSAria III cell sorter instrument (BD Biosciences) operated by Dr. Ka Sin Christopher Law (Magnetic Resonance & Image

Analysis research Centre MARIARC, University of Liverpool). Following the sorting, cells were centrifuged for 5 min at 200g, the supernatant was aspirated and gently resuspended in 5 ml 10% FBS conditioned media and cultured in 6 cm dishes. The cells were allowed to recover for 48 hours before any further manipulation and all subsequent culturing was performed using fresh 10% FBS DMEM media. The cells were single-cell diluted in 96-well plates in order to pick individual clones. The media were exchanged, and the cells were regularly inspected under a microscope until the colonies were large enough to transfer into 24-well plates and eventually into 12-well and 6-well plates. At the 6-well plate stage, duplicate plates were seeded, and cells were lysed in NP-40 lysis buffer to perform an immunoblot and screen for USP30 expression.

2.1.6 Generation of USP30-GFP stably-expressing cells in the HCT116 FlpIn TRex cell line

HCT116 FlpIn TRex cells were grown in 10% DMEM supplemented with of Zeocin (10 µg/ml) and Blasticidin S (4 µg/ml) for a period of a week prior to transfection. HCT116 FlpIn TRex cells were seeded at a density of 500,000 cells/well in 6-well plates the day before the transfection. The cells were transfected with 900 ng pOG44 (Invitrogen) and 100 ng pcDNA5FRT/TO USP30siRNAres1-GFP WT or C77S construct. The plasmids diluted in 200 µl Opti-Mem GlutaMAX with 2 µl PLUS reagent and 4 µl Lipofectamine LTX diluted in 200 µl Opti-Mem GlutaMAX were incubated separately for 5 min then and incubated a further 20 min at room temperature before being added to the cells in a dropwise manner. 24 hours post-transfection cells were transferred to 10 cm dishes and antibiotic selection of Blasticidin S (4 µg/ml) and Hygromycin B (50 µg/ml) was introduced. The cells were inspected on a daily basis under a microscope and the media were exchanged on a regular basis until individual colonies comprising >50 cells could be identified. The clones were transferred using a 20 µl pipette tip first to 24-, then 12- and finally to 6-well plates. Once at the 6-well plate stage, duplicate 6-well plates were setup for expression testing and the clones at the same time transferred into T25 flasks for further maintenance. The clones were induced by addition of doxycycline (1 µg/ml) for 24 hours prior to lysis. Successful integration of

USP30-GFP construct into the FlpIn site was determined by immunoblot against USP30 and GFP.

2.1.7 Apoptosis assay using TMRE

Floating cells and adhered cells were trypsinised and pooled into the same tubes. The cells were centrifuged at 1000 g for 2 min and washed once in PBS. Cells were stained in 50 nM TMRE in their standard medium for 5 min at 37°C protected from light. Cells were analysed on an Attune NxT flow cytometer (ThermoFischer) using the BL-2 filter to collect data. The BL-2 intensity of the population was plotted as a histogram to determine TMRE uptake by active mitochondria. All analyses were performed in the Attune NxT software (ThermoFisher) or Flowjo (BD Biosciences).

2.1.8 Apoptosis assay using Annexin V and PI

Floating cells and adhered cells were trypsinised and pooled into the same tubes. The cells were centrifuged at 1000 g for 2 min and washed once in PBS. Cells were stained in Annexin V-binding buffer (10 mM HEPES NaOH pH 7.4, 150 mM NaCl, 1 mM $MgCl_2$, 5 mM KCl, 1.8 mM $CaCl_2$) with 1:20,000 Annexin V-FITC and PI (5 ng/ml) for 5 min at room temperature. Cells were analysed on an Attune NxT flow cytometer (ThermoFischer) using the BL-1 and BL-3 filters. Intensity of Annexin V-FITC (BL-1) was plotted against intensity of PI (BL-3) to produce scatter plots. Phosphatidyl-serine positive cells were those that were positive for Annexin V-FITC staining. All analyses were performed in the Attune NxT software (ThermoFisher) or Flowjo (BD Biosciences).

2.1.9 Seahorse Mito Stress Assay

At least 16 hours prior to the assay the calibration plate was filled with 200 µl of calibration solution/well and placed in a 37°C non-CO_2 incubator until use. For the HCT116 FlpIn TRex cells, the Seahorse 96-well plates were pre-treated with 20 µl of filtered 0.01% Poly-L-Lysine per well for 30 min at RT. For the hTERT-RPE1 FlpIn TRex cells, the Seahorse 96-well plates were pre-treated with 78 µl autoclaved 1% (w/v) pig skin gelatin for 30 min at room temperature. The wells were washed using 100 µl PBS before plating a

minimum of 6 technical replicates 35,000 cells/well for each clone. Wells were supplemented with their respective 10% FBS-supplemented medium to a total volume of 100 µl and incubated in a 5% CO_2 incubator at 37°C. On the day of the assay, 50 ml of Seahorse assay media were prepared fresh: 50 ml Seahorse DMEM base medium supplemented with D-glucose (4.5 mg/ml), sodium pyruvate (1 mM), L-glutamine (2 mM) and filter sterilised through a 0.22 µm filter. Assay media was incubated at 37°C to equilibrate and pH was adjusted to pH 7.4 ± 0.05 using 0.1 M NaOH. For the HCT116 FlpIn TRex cells port A of the calibration plate was loaded with 25 µl oligomycin A (8 µM), port B with 25 µl FCCP (4.5 µM) and port C with 25 µl antimycin A (10 µM) and rotenone (10 µM). For the hTERT-RPE1 FlpIn TREx cells, port A was loaded with 25 µl oligomycin A (12 µM), port B with 25 µl FCCP (22.5 µM) and port C with 25 µl antimycin A (10 µM) and rotenone (10 µM). All drug dilutions were in assay media starting from 2.5 mM stocks in DMSO and the concentration of the compounds in the different ports includes the dilution factor introduced by each injection (Port A 1:8, Port B 1:9 and Port C 1:10). The calibration plate was inserted into the Seahorse XFe96 analyser instrument (Agilent Technologies) to initiate the process. The cells were washed twice by aspirating the media and replacing it with 200 µl of assay media using a multi-channel pipette. The final assay volume used was 175 µl of assay media. The cell plate was placed in an incubator at 37°C (no CO_2) until ready to use. The instrument recorded both oxygen consumption rate (OCR) and extra-cellular acidification rate (ECAR) taking three reading before and after every injection. The data were analysed using the Agilent Wave software.

2.1.10 Colony Formation Assay (CFA)

500 HCT116 FlpIn TRex cells and 250 hTERT-RPE1 FlpIn TRex cells were seeded in triplicate in 1 ml 10% FBS DMEM no glucose, no pyruvate, with L-glutamine supplemented with sodium pyruvate (1 mM) and glucose (25 mM) or galactose (25 mM) and allowed to grow for 10 days. Media were replaced 5 days after seeding and 10 days after seeding cells were washed once in 1 ml ice-cold PBS and fixed with 1 ml pre-chilled methanol for 10 min at -20°C and stained with 0.1% (w/v) crystal violet, 20% (v/v) methanol for 30 min at RT. Colonies were washed once with ddH_2O and allowed to dry

overnight at room temperature. HCT116 FlpIn TRex colonies were imaged using a colony counter kindly provided by Dr. Jason Parsons, North West Cancer Research Centre (Liverpool, UK). hTERT-RPE1 FlpIn cells did not form colonies and were instead imaged using a Li-Cor Odyssey CLx instrument.

2.1.11 ATP measurements

The day prior to the assay, HCT116 FlpIn TRex and hTERT-RPE1 FlpIn cells were seeded at 25,000 and 35,000 cells per well respectively in 100 µl of their respective 10% FBS-supplemented media in black-wall 96-well plates (Corning: 3603). Some wells had only media in them to serve as controls for background luminescence. For the HCT116 FlpIn TRex cells, the plates were pre-treated with 20 µl Poly-L-Lysine per well for 30 min at RT prior to seeding the cells. On the day of the assay cells were treated with 100 µl of 10% FBS-supplemented media with either Oligomycin A (1 µM) for the HCT116 FlpIn TRex cells and Oligomycin A (1.5 µM) for the hTERT-RPE1 cells, or 50 mM 2-deoxyglucose or both treatments, or left untreated for 30 min in a humidified 5% CO_2 incubator at 37°C. Cell TiterGlo™ (100 µl) reagent was added to the cells. The plate was first shaken for 2 min at RT on a circular-moving shaker at 250 rpm to induce cell lysis while covered with foil then incubated at RT for a further 10 min before luminescence was read on a Promega GloMax® Multi-Detection system. Background luminescence was corrected by subtracting the luminescence from the wells without any cells for each treatment before calculating luminescence for each condition.

2.2 Molecular Biology

2.2.1 Reagents

All restriction endonucleases, Quick Ligase (M2200) and their respective reaction buffers, purple loading dye (B7025) and DNA ladders (N3231 and N3232) were purchased from New England Biolabs (Hitchin, UK). All primers were ordered through Eurofins Genomics MWG Operon (Ebersberg, Germany) and are listed in **Table 2.2**. Pfu Ultra DNA polymerase (600670) and their respective buffers, deoxynucleotide mix (200415-1) and XL1 blue

competent cells (200249) were purchased from Agilent Technologies (Cheshire, UK). Nuclease Free water and ethidium bromide (E1510) were purchased from Sigma-Aldrich. Chemically competent DH5α (18265017) and One shot™ TOP10 (C404010), S.O.C medium (S1797), SYBR™ Safe DNA gel stain (S33102), Zero Blunt™ TOPO™ PCR cloning kit (450031), and pcDNA™5/FRT/TO vector kit (V652020) were purchased from Invitrogen (ThermoFisher). The Miniprep kit (27106), Hispeed Midiprep (126430), HiSpeed Maxiprep (12633), Gel extraction kit (28704), RNeasy Plus mini kit (74106), QIAshredder (79656) and RNase-free DNase (79254) were purchased from Qiagen (Crawley, UK). TAE buffer (EC-872) was purchased from National Diagnostics (Hull, UK). The pSpCas9(BB)-2A-GFP (pX458) was a gift from Feng Zhang (Addgene: 48138) (Ran et al., 2013). The GFP-BAK plasmid was a gift from Richard Youle (Addgene: 32564) (Nechushtan et al., 2001). Vector backbone pEGFP-N3 (6080-1) and pBluescript SKII (212205) were purchased from Clontech and Stratagene respectively. The pHis-myc-ubiquitin plasmid was a gift from Oliver Rocks (Max-Delbrück-Center for Molecular Medicine, Germany) (Eccles et al., 2016). All other plasmids pGFP-USP30, pUSP30-GFP, pUSP30ΔTM-GFP, pUSP30-C77S-GFP, pUSP30-GFP siRNAres1 and pUSP30-C77S-GFP siRNAres1 were provided by Richard Buus (University of Liverpool, UK). The pCR4Topo GW USP30 plasmid was from Sebastian Hayes (University of Liverpool, UK).

Table 2.2: Primer List

Primer Name	Used for	Sequence
AK_sgUSP30_1_BbsI_R	sgRNA	CACCGAGTTCACCTCCCAGTACTCC
AK_sgUSP30_1_BbsI_R	sgRNA	AAACGGAGTACTGGGAGGTGAACTC
AK_sgUSP30_2_BbsI__F	sgRNA	CACCGTGAAAGCAGGACAGGCAGAC
AK_sgUSP30_2_BbsI_R	sgRNA	AAACGTCTGCCTGTCCTGCTTTCAC
AK_BAK_K113R_1F	SDM	ATGAGTACTTCACCAGGATTGCCA CCAGCCTGTTTG
AK_BAK_K113R_1R	SDM	CAAACAGGCTGGTGGCAATCTCGGTGAAGTACTCAT

AK-BamHI-USP30-F1	Cloning	TGGGGATCCACCATGCTGAGCTCCCGGGCCGAGG
AK-XhoI-USP30-W53-R1	Cloning	GTGCTCGAGCCAAATAACATATATTCCTGCTGCAAGAGCAGCAGCG
AK-XhoI-USP30-P68-R1	Cloning	GTGCTCGAGAGGCACAAGCCCTTTTCTACGCTTC
AK-EMA-U30-KRmut1_F1	SDM	ACCGGGGCGGCCGTCACATATAACGTCATGAACAACTGG
AK-EMA-U30-KRmut1_R1	SDM	TATAACTCCCCAGTTGTTCATGACGTTATATGTGACGGCCGCCCCGGT
AK_EMA_U30_KRmut2_F1	SDM	GGGGTCCCATTACAGAAAACAACGCTAGCAACAACGGGCTTGTGCCTGGC
AK_EMA_U30_KRmut2_R1	SDM	GCCAGGCACAAGCCCGTTGTTGCTAGCGTTGTTTTCTGTAATGGGACCCC
AK_BamHI_USP30v2_F1	Cloning	TGGGGATCCACCATGAAGAACTGGGGAGTTATAGGTGGAAT
AK_XhoI_USP30v2_R1	Cloning	GTGCTCGAGTTCTTCAGACTTGCACTCCTGGCTCTGGTGC
EMA-USP30-KO-1-PCRUP-FW	PCR UP	GTGCCTGGCCTTGTTAATTTAG
EMA-USP30-KO-1-PCRUP-RV	PCR UP	CAGGCATGAGCCACTGCAC

The names, purpose and sequence of the primers used are listed above. sgRNA reflects that the primer was purchased for use in a CRISPR-compatible plasmid as a small guide RNA template. Side directed mutagenesis (SDM) reflects that the primer was used in mutating one on more nucleotides on the template. In a “PCR up” the primer was used in a simple PCR with the intention of amplifying a region of the template. Cloning suggests the primer was used to amplify a region of interest on the template and includes restriction enzymes sites to facilitate downstream cloning strategies.

2.2.2 DNA agarose gel electrophoresis

Agarose gels were prepared by adding 0.8 g of electrophoresis grade agarose to 100 ml 1x TAE buffer (40 mM Tris-acetate, 1 mM Na_2-EDTA) and melted by heating in the microwave ensuring the mixture was homogenous and the agarose fully dissolved. The molten agarose was supplemented with ethidium bromide (0.5 µg/ml) or SYBR safe (1:10,000) before being poured into a gel cast with a comb of appropriate well volume to solidify. The samples were loaded alongside DNA ladder and run in the presence of 1x TAE buffer in a horizontal midi electrophoresis tank (Fisher Scientific, Loughborough, UK)

at 90 V between 10 min to 1 hour as required for sufficient band resolution. Gels were visualised on a UV-dock and bands were extracted using a clean scalpel. DNA was purified using the Gel extraction kit (Qiagen) as per manufacturer's instructions.

2.2.3 Polymerase Chain Reaction (PCR)

Polymerase Chain Reactions (PCR) were performed as described in the following sections for each construct, in a standard thermal cycler with the lid heated to 110°C at all times.

2.2.4 TOPO blunt cloning

The pCR4Topo blunt reaction kit was used to insert blunt-ended PCR products in the pCR4Topo backbone, according to the manufacturer's instructions. Briefly, a reaction was set up on ice as shown in **Table 2.3**:

Table 2.3 pCR4Topo blunt reaction set up

Component	Volume (µl)
PCR product	0.5-4
6x salt solution	1
pCR4Topo vector	1
ddH_2O	Up to a total of 3.5
Total	6

The reaction was allowed to proceed for 5 min at room temperature and 2 µl were used to transform into chemically competent DH5α or TOP10 cells as described below (2.2.5).

2.2.5 Plasmid Transformation

Bacterial transformations were performed using 50 µl DH5α (plasmids or TOPO reactions) or XL1 blue cells (ligations or SDM) or TOP10 bacteria cells (PCR product for FlpIn compatible plasmids). For plasmid transformations 50 ng of plasmid DNA were used or 2 µl of a ligation reaction or PCR product were used. Briefly, the bacterial cells were thawed on ice and the DNA was added and incubated for 20 min on ice. The bacteria were then heat shocked

for 1 min in a 42°C water bath, followed by a further incubation for 2 min on ice. 200 µl of SOC medium was added to the bacteria and incubated at 225 rpm for 1 hour at 37°C. The culture was divided 1:4 and spread onto ampicillin (100 mg/ml) or kanamycin (10 mg/ml) LB agar plates overnight at 37°C.

2.2.6 Plasmid Preparation

4-6 colonies per transformation were picked and inoculated in 5 ml LB broth with the appropriate antibiotic at the concentrations stated above and were grown as minipreps at 225 rpm for 14-18 hours at 37°C. Plasmid DNA was extracted using the Qiagen miniprep kit according to manufacturer's instructions. Correct transformations were identified by restriction digest followed by gel electrophoresis, and where appropriate DNA sequencing (Dundee DNA services, University of Dundee, UK). Overnight cultures were used to inoculate a larger culture of 150 ml (Midiprep) or 250 ml (Maxiprep) and grown at 225 rpm for 14-18 hours at 37°C. Plasmid DNA was extracted using the Qiagen Midiprep or Maxiprep kit according to manufacturer's instructions.

2.2.7 Restriction Digest protocol

A diagnostic restriction digest was set up using 250 ng plasmid and 0.5 µl restriction enzyme in the appropriate buffer in a total reaction volume of 20 µl, following manufacturer's instructions. If multiple restriction enzymes were used, the rection buffer that yielded the highest activity amongst all enzymes was selected. All diagnostic restriction digests were performed for 1 h at 37C. For the purposes of cloning 4 µg plasmid were used instead. All restriction digests set up were performed in a thermal cycler for a minimum of 1 h at 37°C with a heated lid at 110°C.

2.2.8 Quick Ligation protocol

The vector backbone and source of insert were digested with the appropriate restriction enzymes. Successful digestion was verified by DNA agarose gel electrophoresis. Vector and insert bands were cut out and gel extracted using the Qiagen gel extraction kit following manufacturer's instructions. The concentrations of vector and insert solutions were measured

using a Nanodrop (ThermoFisher). The following ligation reactions were set up using the Quick Ligation kit (NEB):

Table 2.4: Quick Ligation reaction set up

Component	Quantities			
	Vector self-ligation control (0:1)	1:1	3:1	Insert only control
Vector	100 ng			-
Insert	-	X µl		
ddH_2O	X µl			
2x Quick buffer	10 µl			
Quick ligase	1 µl			
Total	20 µl			

The molar ratios of insert to vector backbone were calculated based on the size of the insert and the size of the digested vector in order to accomplish 1:1 and 3:1 (insert: backbone) reactions for 100 ng of vector. Self-ligation and insert only control reactions were also set up to determine background and efficiency of ligation. The ligation mixtures were incubated for 5 min at room temperature and 2 µl of each reaction were used to immediately transform DH5α or XL1 blue cells as described (2.2.5). Correct transformants were verified using restriction digest.

2.2.9 RNA extraction

RNA extraction was performed as part of the RNA-seq experiments conducted in the HCT116 FlpIn TRex USP30KO cells. The RNA was extracted from two polled confluent 10 cm dishes using the RNA RNeasy Plus mini kit after using the QIAshredder kit, following the manufacturer's instructions. RNA concentrations were determined using a Nanodrop (ThermoFisher) and samples stored at -80°C. The samples were then shipped on dry ice to Forma Therapeutics (Watertown, Boston, MA, USA) for further processing for RNA-seq.

2.2.10 Site Directed Mutagenesis (SDM)

For the generation of pGFP-BAK K113R the pGFP-BAK was used as a template for Quickchange mutagenesis PCR with primers AK_BAK_K113R_1F and AK_BAK_K113R_1R as follows:

Table 2.5: PCR reaction set up

Component	Quantity (µl)
Template (10 ng/µl)	5.0
10x Pfu turbo buffer	5.0
25 mM dNTPs	1.0
10 µM Primer F	1.25
10 µM Primer R	1.25
ddH_2O	35.5
PFU Turbo DNA polymerase	1.0
Total	50

Table 2.6: PCR cycling parameters

Segment	Cycles	Temperature (°C)	Time (mm:ss)
1	1	95	2:00
2	18	95	00:30
		55	1:00
		68	5:30
3	1	4	hold

The PCR product was then treated with 1 µl DpnI for 1 hour at 37°C to digest the template and 2 µl were then used to transform chemically competent DH5α cells as described (2.2.5). Correct transformants were screened by restriction digest and sequencing.

For the generation of the USP30 point mutants KRmut1 and KRmut2 I employed a similar strategy as previously demonstrated (Nakamura and Hirose, 2008). USP30KRmut1 was generated using primers AK-EMA-USP30KRmut1-F1 and AK-EMA-USP30KRmut1-R1 and USP30KRmut2 was generated using USP30KRmut2-F1 and AK-EMA-USP30KRmut2-R1 using

pCR4Topo GW USP30 as template in both cases as described in **Table 2.5** and **Table 2.6** and extending the DNA polymerase extension step to 6:00 min. The PCR products were treated with 1 µl DpnI for 1 hour at 37°C to digest the template and 2 µl were used to transform chemically competent XL1 blue cells as described (2.2.5). Correct transformants were screened by restriction digest using NheI for USP30KRmut2 and sequencing for both constructs. The inserts of USP30KRmut1 and 2 were digested with BamHI and XhoI while the backbone of pEGFP-N3 was digested with BglII and SalI. The backbone and inserts were quick ligated as described (2.2.8). Correct transformants were identified by restriction digest and DNA sequencing.

2.2.11 Generation of USP30 truncation and USP30 isoform 2 constructs

The USP30 (1-53) and USP30 (1-68) constructs were generated using AK-BamHI-USP30-F1 and AK-XhoI-USP30-W53-R1 and AK-BamHI-USP30-F1 and AK-XhoI-USP30-P68-R1 respectively using pCR4Topo GW USP30 as a template. The reaction was set up as described in **Table 2.5** and **Table 2.6** with the DNA polymerase extension time set to 0:30 min. The PCR products were resolved on a 0.8% agarose/TAE gel and the bands of correct size were cut out and gel extracted using the Qiagen gel extraction kit. The pCR4topo reaction was performed on 1 µl of the gel extracted products as described (2.2.4). Successful transformants were screened by restriction digestion using EcoRI and DNA sequencing. The pCR4TOPO USP30 (1-53) and USP30 (1-68) constructs were digested with BamHI and XhoI while the backbone of pEGFP-N3 was digested with BglII and SalI. The backbone and inserts were quick ligated as described (2.2.8). Correct transformants were identified by restriction digest and DNA sequencing.

USP30 isoform 2 was generated using primers AK_BamHI_USP30v2_F1 and AK_XhoI_USP30v2_R1 on pCR4Topo GW USP30 as template as described in **Table 2.5** and **Table 2.6** and extending the DNA polymerase extension step to 2:00 min. The PCR product was processed and subcloning performed as discussed above for the truncation constructs.

2.2.12 Subcloning USP30 sgRNAs into pX458

Suitable small guide (sg)RNA sequences against USP30 were suggested by Jin-Rui Liang (Institute for Molecular Biosciences, Zurich, Switzerland). sgUSP30-1 (5'-AGTTCACCTCCCAGTACTCC-3') and sgUSP30-2 (5'-TGAAAGCAGGACAGGCAGAC-3') and their respective reverse complements were ordered as single-stranded oligonucleotides (AK_sgUSP30_1_BbsI_R and AK_sgUSP30_1_BbsI_R, AK_sgUSP30_2_BbsI__F and AK_sgUSP30_2_BbsI_R). The oligonucleotides were re-suspended in nuclease-free water (Sigma) at 100 µM and 1 µl (100 pmol) of each pair were mixed with 10x T4 ligation buffer and T4 polynucleotide kinase. Phosphorylation and annealing of the primers to form duplexes was achieved by incubation in a thermal cycler first at 37°C for 30 min, then at by 95° C for 5 min followed by a gradual decrease to 25° C at the rate of 5° C/min. Of the annealed products 1 µl (10 pmol) were cloned into 50 ng of digested pX458 (hSpCas9(BB)-2A-GFP) using BbsI. Correct insertion was verified by restriction digest using BbsI and DNA sequencing.

2.2.13 Genomic DNA (gDNA) extraction from mammalian cells

Cells were seeded in a 6-well plate and allowed to grow to confluency before harvesting. Media were aspirated and cells were washed on ice three times with ice-cold PBS. Cells were dislodged using a cell scraper in 500 µl ice-cold PBS and were centrifuged at 1000 g for 5 min at 4°C. The supernatant was aspirated, and cell pellets stored at -20°C until gDNA extraction. gDNA was extracted using the Quick DNA™ Universal kit (ZymoResearch) according to manufacturer's instructions. PCR was performed using 100 ng of gDNA from each clone with primers EMA-USP30-KO-1-PCRUP-FW and EMA-USP30-KO-1-PCRUP-RV and Pfu Ultra HotStart (HS) DNA polymerase. The reactions were then run on a 0.8% agarose/TAE and the 383 bp PCR products at were cut out using a clean scalpel. The PCR products were gel extracted and a TOPO reaction was performed as described above (2.2.4). Five colonies were picked and grown in 5 ml LB Kanamycin overnight at 37°C. Plasmid DNA was prepared using the Qiagen miniprep kit according to manufacturer's instructions. A restriction digest using EcoRI-HF was performed to confirm the

presence of an insert before being sent for sequencing using the M13F and M13R sequencing primers.

2.2.14 Generation of FlpIn system compatible USP30-GFP plasmids

The pUSP30 siRNAres1-EGFP and pUSP30 C77S siRNAres1-EGFP were used as templates with primers AK_FRTTO_USP30sires1_F1 and AK_FRTTO_CtermEGFP_R1 to generate pcDNA5FRT/TO USP30 siRNAres1-EGFP and pcDNA5FRT/TO USP30 C77S siRNAres1-EGFP as described in **Table 2.5** and **Table 2.6**.

The PCR reaction was incubated with 1 µl Taq polymerase (Bioline) for a further 10 min at 72 °C. The product was resolved on a 0.8% agarose/TAE gel and the band of correct size was cut out and gel extracted using the Qiagen gel extraction kit. The gel eluted product was used to perform a TA-ligation reaction with linearized pcDNA5FRT/TO vector:

Table 2.7: pcDNA5FRT/TO TA ligation set up

Component	Volume (µl)
PCR product	2
salt solution	1
pcDNA5FRT/TO vector	1
ddH_2O	2
Total	6

The reaction was incubated for 5 min at room temperature and 2 µl of the reaction were used to transforms 50 µl of chemically competent TOP10 cells following the standard transformation protocol (2.2.5).A minimum of six colonies were picked per construct to inoculate minipreps as described (2.2.6). Restriction digest was used to confirm correct transformants and HindIII to verify the presence of C77S in the mutant plasmid. Correct orientation and sequence integrity of the USP30-GFP open reading frame were confirmed by DNA sequencing.

2.3 Imaging

2.3.1 Reagents

Methanol-free 16% formaldehyde ampoules (28908), Triton™ X-100 (10102913), 4',6'-diamidino-2-phenylindole (DAPI, D1306), Annexin V-Alexa Fluor™ 350 conjugate (A23202), DRAQ7™ dye (D15106), glass square coverslips (12363138) and Frosted microscope slides (15545650) were purchased from Invitrogen/ThermoFisher (Paisley, UK). Mowiol-488 (475904) was purchased from Merck Millipore (UK). All other reagents were purchased from Sigma-Aldrich. The primary antibodies and secondary antibodies used in imaging are listed in **Table 2.8**

Table 2.8: Antibodies used in immunofluorescence microscopy

Target	Manufacturer/Supplier	Product Code	Dilution
Primary Antibodies			
TOMM20	Sigma-Aldirch	HPA011562	1:500
TOMM20	BD Transduction	612278	1:500
pS65-Ub	Millipore	ABS1513-I-AF488	1:500
pS65-Ub	Cell Signalling Technologies	62802	1:500
CALN	ABR	PA3-900	1:250
PMP70	Sigma-Aldirch	SAB4200181	1:500
Secondary Antibodies			
Donkey anti-rabbit AF350	Invitrogen	A10039	1:500
Donkey anti-mouse AF350		A10035	
Donkey anti-rabbit AF488		A21206	
Donkey anti-mouse AF488		A21202	
Donkey anti-rabbit AF594		A21207	
Donkey anti-mouse AF594		A21203	

2.3.2 Live cell microscopy

Cells were seeded in 6-well plates and allowed to adhere at least a day before the imaging. Media were exchanged to media supplemented with Annexin V-AF350 conjugate (1:200) according to manufacturer's instructions, 0.1 µM DRAQ7 and 2.5 mM calcium chloride ($CaCl_2$). Drug treatments and vehicle controls were introduced at the indicated concentrations as described in the appropriate figure legends. Live cell imaging was carried out on a Nikon Ti-Eclipse equipped with a CFI Plan Apo 20x objective and a digital camera CoolSNAP EZ Turbo 1394 (Photometrics) for the indicated duration as specified in the figure legend.

2.3.3 Immunofluorescence microscopy

Cells were seeded on coverslips in 6-well plates in their standard media. The media were aspirated, cells were washed twice and fixed in 4% paraformaldehyde (PFA) in PBS for 15 min at room temperature. The reaction was quenched by addition of 50 mM ammonium chloride (NH_4Cl) in PBS for 5 min at room temperature. For experiments where the integrity of the ER was critical, all reagents were pre-warmed to 37°C for the duration of the washes and fixation. The cells were permeabilised in 0.2% TritonX-100/PBS for 2 min at room temperature and washed once with filtered PBS. The coverslips were blocked in 3% BSA/PBS for 1 hour at room temperature. The primary antibody incubations were performed in 3% BSA/PBS at the indicated concentrations (**Table 2.8**) by inverting the coverslips on a drop of the solution in a humid chamber covered in foil for 1 hour at room temperature. The coverslips were washed twice in filtered PBS for 5 min at room temperature. The secondary antibodies were diluted in 3% BSA/PBS at the indicated concentrations (**Table 2.8**) in the same manner as above for 45 min at room temperature. The coverslips were washed twice in filtered PBS for 5 min at room temperature. The coverslips were washed once in PBS and once in ddH_2O before being mounted onto microscope slides using mowiol/DAPI (10% (w/v) mowiol, 25% (w/v) glycerol, 0.1% (w/v) DAPI in 100 mM Tris-HCl pH 8.5). Mowiol without DAPI was used instead in experiments where AF350 conjugated secondary antibodies were used. The slides were left to dry overnight in a dark

compartment protected from light at room temperature and stored at 4°C until imaging.

Images were acquired on a Marianas spinning disk confocal microscope (3i, Intelligent Imaging Innovations, Germany) equipped with a 63x NA 1.4 oil immersion objective and a Hamamatsu Flash 4 sCMOS camera or a Zeiss LSM800 with Airyscan confocal microscope equipped with 63x NA 1.4 oil immersion objective, as indicated in the respective figure legends.

2.4 Biochemistry

2.4.1 Reagents

NuPAGE BisTris (BT) 4-12% gradient gels (NP0321PK2, NP0303BOX, and W61402A), MOPS buffer (NP0001-02), MES buffer (NP0002-02), NuPAGE antioxidant (NP0005), Amersham Protran 0.45 µm nitrocellulose membrane (10600002), Amersham Protran 0.22 µm nitrocellulose membrane (45004004), Amersham ECL full range rainbow marker (RPN800E) and Pierce BCA reagent kit (PI23223 and PI23224) were purchased from ThermoFisher. Tris base (T60040) and glycine free base (G36050) were purchased from Melford (UK). Ponceau S (P7170), mammalian protease inhibitor cocktail (MPI, P8340), bovine IgG (I5506), β-mercaptoethanol (M6250), Proteinase K (P2308), phenylmethanesulfonyl fluoride (PMSF, 78830) and gelatin from cold water fish skin (FSG: G7765) were purchased from Sigma-Aldrich. PhosSTOP phosphatase inhibitor tablets (4906845001) were purchased from Roche. Unstained broad range molecular weight markers (P7702, P7704 and P7717) were purchased from New England Biolabs (Hitchin, UK). Fatty acid-free bovine serum albumin (BSA) was purchased from First Link LTD (UK). Marvel skimmed milk powder was purchased from Premier Brands (UK). Purified recombinant USP30 was a gift from Dr. Malte Gersch and Prof. David Komander (Cambridge, UK) (Gersch et al., 2017).

2.4.2 Cell lysis

The media were aspirated from cells, which were then washed twice using ice-cold PBS. Cells were directly lysed in nonidet P-40 lysis buffer (NP-40; 0.5% (w/v) NP-40, 25 mM Tris pH 7.5, 100 mM NaCl, 50 mM NaF) or RIPA

lysis buffer (10 mM Tris pH 7.5, 150 mM NaCl, 1% (w/v) Triton-X 100, 0.1% (w/v) SDS, 1% sodium deoxycholate) rocking on ice for 15 min. The lysis buffers were supplemented with one PhosSTOP tablet per 10 ml lysis buffer and MPIs (1:250) as per manufacturer's instructions, as indicated in the figure legends. The lysates were collected and clarified by centrifugation at top speed (21,000 g) in a refrigerated countertop centrifuge for 10 min at 4°C. The clarified lysates were transferred into fresh tubes and kept on ice until sample preparation or stored at -80°C if not prepared immediately.

The cells were alternatively lysed in SDS lysis buffer (hot lysis buffer: 2% (w/v) SDS, 1 mM EDTA, 50 mM NaF). The hot lysis buffer was pre-warmed to 110°C in screw-top tubes (Corning) and the cells were briefly rinsed at room temperature with PBS, then harvested using a cell scraper in the hot lysis buffer while on a hot plate at 110°C. The lysates were collected in the screw-top tubes and boiled for at least 10 min at 110°C, vortexing harshly every 2 min.

2.4.3 Protein concentration determination and sample preparation

Sample protein concentration was determined using the Pierce BCA assay kit in a 96-well plate. A standard curve was generated using bovine IgG as standards from duplicate wells. Samples were added in triplicate on the same plate and 200 µl of the reconstituted BCA reagent was added to each well. The plate was incubated for 30 min at 37°C and the absorbance at 562 nm was read using a Multiskan spectrum plate reader (Thermo Labsystems, ThermoScientific). The standard curve was then used to calculate the protein concentration of the samples by linear interpolation. The protein concentration of all samples was adjusted to the sample with the lowest protein concentration using lysis buffer and 5x sample buffer (312.5 mM Tris-HCl, pH 6.8, 15% (w/v) SDS, 50% (w/v) glycerol, 16% (w/v) 2-Mercaptoethanol, 0.05% w/v Bromophenol Blue) was added. When hot lysis buffer was used, an alternative sample buffer was used (312.5 mM Tris-HCl, pH 6.8, 9% (w/v) SDS, 50% (w/v) glycerol, 16% (w/v) 2-Mercaptoethanol, 0.05% w/v Bromophenol Blue). The prepared samples were then boiled for 5 min at 95°C and stored at -20°C.

2.4.4 SDS-PAGE and immunoblot analysis

Protein samples were loaded on 4-12% polyacrylamide Bis Tris gels in the NuPAGE running systems by Invitrogen (ThermoFisher, UK). For small proteins <25 kDa MES buffer was used and for all other proteins MOPS buffer was used instead. The gels were run at 150 V constant voltage until the loading dye reached the foot of the gel.

The proteins were transferred onto nitrocellulose membrane using the Genie blotter (Idea Scientific, MN, USA) in the presence of transfer buffer (0.303% (w/v) unbuffered tris base, 1.44% (w/v) glycine, 20% (v/v) methanol) at 25 V constant current not exceeding 1.0 for 1 hour at room temperature. Transfer of proteins onto the membrane was verified by staining with Ponceau S. The Ponceau S stain was completely removed by washing the membrane in TBST (10 mM Tris HCl pH 7.5, 150 mM NaCl, 0.1% (v/v) Tween-20). The membranes were blocked in 5% (w/v) skimmed milk/TBST or 5% (w/v) BSA/TBST or 0.1% (v/v) FSG/TBST as indicated in on a rocker for 1 hour at room temperature. Primary antibodies listed in **Table 2.9** were incubated in the same blocking buffer overnight on a rocker at 4 C. The membranes were washed three times in TBST on a rocker for 5 min at room temperature. The secondary antibodies listed in **Table 2.10** were incubated at 1:10000 dilution in the same blocking buffer for 45 min to 1 hour at room temperature. The membranes were washed three times in TBST on a rocker for 5 min at room temperature before being scanned on a Licor Odyssey imaging system (Licor, USA). The images were visualised, quantitated and exported using the Image Studio Software (Licor, USA) or using the FIJI software. Figures with immunoblots were assembled using Adobe Photoshop and Adobe Illustrator software.

Table 2.9: Primary antibodies for immunoblot

Target	Product/Source	Buffer	Dilution
USP30	HPA016952 (Sigma-Atlas)	milk	1:500
USP30	PA5-53523 (ThermoFisher)	milk	1:1000
USP30	sc-515235 (SantaCruz)	milk	1:1000
BAK	B5897 (Sigma)	milk	1:1000
BAK	sc-832 (SantaCruz)	milk	1:1000
BAK	sc-517390 (SantaCruz)	milk	1:1000
BAX	610982 (BD Transduction)	milk	1:1000
MCL-1	sc-819 (SantaCruz)	milk	1:1000
BCL-2	ab692 (Abcam)	milk	1:1000
BCL-X_L	2764 (Cell Signalling)	milk	1:1000
Caspase 3	9668 (Cell Signalling)	milk	1:1000
p85 PARP	9546 (Cell Signalling)	BSA	1:2000
PINK1	6946 (Cell Signalling)	milk	1:1000
PINK1	BC100-494 (Novus Biologicals)	milk	1:1000
TOMM20	HPA011562 (Sigma)	milk	1:1000
TOMM20	612278 (BD Transduction)	milk	1:1000
TOMM22	sc-58308 (SantaCruz)	milk	1:1000
PRKN (*PARK2*)	sc-32282 (SantaCruz)	milk	1:250
pS65-Ub	ABS1513-I (Millipore)	BSA	1:1000
pS65-Ub	62802 (Cell Signalling)	BSA	1:1000
Ubiquitin (VU1)	VU101 (LifeSensor)	FSG	1:2000
HSP60	sc-1052 (SantaCruz)	milk	1:1000
PMP70	SAB4200181 (Sigma)	milk	1:1000
Catalase	ab1877 (Abcam)	milk	1:1000
ACOX1	ab184032 (Abcam)	milk	1:1000
GFP	Gift from Prof. Ian Prior (Liverpool, UK)	milk	1:5000
Myc tag	05-724 (Millipore)	milk	1:1000
MFN2	ab56889 (Abcam)	milk	1:1000
FIS1	10956-1-AP (Proteintech)	milk	1:1000
CUL5	A302-173A (Bethyl)	milk	1:2000
β-actin	ab6276 (Abcam)	milk	1:10000

β-actin	A2266 (Sigma)	milk	1:10000
β-actin	66009-1-Ig (Proteintech)	milk	1:10000
β-actin	20536-1-AP (Proteintech)	milk	1:10000

Table 2.10: Secondary antibodies for immunoblot

Secondary Antibodies	Product Number/Source	Source
Donkey anti-mouse IRDye 800CW	926-32212	Licor
Donkey anti-mouse IRDye 680CW	926-32222	
Donkey anti-rabbit IRDye 800CW	926-32213	
Donkey anti-rabbit IRDye 680CW	926-32223	
Donkey anti-sheep IRDye 800CW	926-32214	
Donkey anti-sheep IRDye 680CW	926-32224	

2.4.5 Total and free ubiquitin SDS-PAGE immunoblots

Immunoblots to visualise free and total ubiquitylated proteins were conducted as previously described (Swerdlow et al., 1986). Equal amounts of cell lysate were resolved on a 4-12% NuPAGE gel in MES buffer as above taking extra care not to lose the 10 kDa rainbow molecular weight marker. The transfer was performed on a 0.22 µm nitrocellulose membrane as described above for 45 min at room temperature. Immediately after the Ponceau S staining the membrane was sandwiched between two glass plates and boiled in ddH_2O in a beaker on a Bunser burner for 30 min. The membrane was blocked in 0.1% FSG/TBST as described above and the VU1 antibody was used to probe for ubiquitylated proteins and free ubiquitin. The remaining procedure was the standard immunoblot protocol described in 2.4.4.

2.4.6 USP30 membrane topology experiment

This experiment was performed to determine the membrane topology of USP30 on peroxisomes as previously described (Nakamura and Hirose, 2008; Marcassa et al., 2018). Two 15 cm dishes of hTERT-RPE1 YFP-Parkin cells were seeded for the untreated condition and three 15 cm dishes of hTERT-RPE1 YFP-Parkin cells were seeded for the treatement with 1 µM antimycin A/oligomycin A (A/O) for 24 hours. On the day of the experiment the dishes

were fully confluent. The media were discarded, and the cells washed gently with ice-cold PBS. The cells were scraped in 5 ml ice-cold PBS using a silicone cell scraper and collected in 15 ml centrifuge tubes. Cells were centrifuged at 1000 g for 2 min at 4°C and the cell pellet resuspended in 10 ml sice-cold homogenisation buffer (HIMM: 200 mM D-mannitol, 70 mM sucrose, 1 mM EGTA, 10 mM HEPES-NaOH pH 7.5) for a second wash and centrifuged at 1000 g for 2 min at 4°C. The cells were resuspended in 1 ml HIMM buffer supplemented with MPIs (1:250) and homogenised by pipetting six times up and down with a P1000 Gilson and passing four times through a 23 gauge needle. A sample was retrieved and inspected under a microscope in the presence of trypan blue (Invitrogen) to verify homogenisation. Post nuclear supernatant (PNS) was obtained by centrifuging the samples at 600 g for 10 min at 4°C. A BCA assay was performed to determine the protein concentration of the two samples and the PNS of the two samples were adjusted to the same final concentration using HIMM buffer. 50 µl were retained of each sample and the remaining was split into three equal parts and subjected to ultracentrifugation at 100,000 g for 40 min at 4°C in a TLA120.2 rotor in a Beckmann ultracentrifuge. The supernatant (S) from this centrifugation step was retained and prepared in 5x sample buffer. The first pellet (P) for each PNS were re-suspended in 100 µl HIMM buffer and prepared in 5x sample buffer. The second pellet for each PNS were resuspended in ice-cold 100 µl alkaline carbonate buffer (100 mM Na_2CO_3,10 mM Tris-HCl pH 11.5) supplemented with MPIs (1:250) for 30 min on ice. The third pellet for each PNS were resuspended in ice-cold 100 µl detergent buffer (2% Triton X-100, 1 M NaCl) supplemented with MPIs (1:250) for 30 min on ice. The re-suspended pellets were centrifuged again for 40 min at 4°C in a TLA120.2 rotor in an ultracentrifuge. The resulting supernatants were collected and prepared in 5x sample buffer (S Na_2CO_3 and S Tx-100 for the alkaline carbonate buffer and the detergent buffer respectively.) The resulting pellets were re-suspended in 100 µl of the respective buffers and prepared in 5x sample buffer (P Na_2CO_3 and P Tx-100 for the alkaline carbonate buffer and the detergent buffer respectively). Equal amounts of the above were analysed by SDS-PAGE and immunoblot.

2.4.7 USP30 Protease protection assay

The protease protection assay was used to determine the orientation of USP30 on peroxisomes (Marcassa et al., 2018). Two 15 cm dishes of hTERT-RPE1 YFP-Parkin cells were seeded for the untreated condition and three 15 cm dishes of hTERT-RPE1 YFP-Parkin cells were seeded for the treatement with 1 µM A/O for 24 hours. On the day of the experiment the dishes were fully confluent. The media were discarded, and the cells washed gently with ice-cold PBS. The cells were scraped in 5 ml ice-cold PBS using a silicone cell scraper and collected in 15 ml centrifuge tubes. Cells were centrifuged at 1000 g for 2 min at 4°C and the cell pellet resuspended in 10 ml ice-cold homogenisation buffer (HIMM: 200 mM D-mannitol, 70 mM sucrose, 1 mM EGTA, 10 mM HEPES-NaOH pH 7.5) for a second wash and centrifuged at 1000 g for 2 min at 4°C. The cells were resuspended in 1 ml HIMM buffer supplemented without any protease inhibitors and homogenised by pipetting six times up and down with a P1000 Gilson and passing four times through a 23 gauge needle. A sample was retrieved and inspected under a microscope in the presence of trypan blue (Invitrogen) to verify homogenisation. Post nuclear supernatant (PNS) was obtained by centrifuging the samples at 600 g for 10 min at 4°C. A BCA assay was performed to determine the protein concentration of the two samples and the PNS of the two samples were adjusted to the same final concentration using HIMM buffer. The PNS was split in six parts and treated with Proteinase K (100 µg/ml) in 50 mM Tris-Cl pH 7.4, 10 mM $CaCl_2$ for 30 min on ice in the presence or absence of 1% (w/v) TritonX-100 in HIMM buffer or treated only with equal volumes of the buffers. The reactions were stopped by adding PMSF (2 mM) in ethanol to all samples and incubated for a further 5 min on ice. The samples were prepared with 5x sample buffer and equal amounts were analysed by SDS-PAGE and immunoblot.

2.4.8 SILAC reagents

L-Lysine-free and L-Arginine-free DMEM SILAC-compatible media (D633) was purchased from Dundee Cell Products (University of Dundee, UK). All SILAC amino acids (**Table 2.11**), ammonium bicarbonate (AmBic; 09830) and iodoacetamide (IAA; T6125) were purchased from Sigma-Aldrich (Dorset,

UK). Dithiothreitol (DTT; MB1015) were purchased from Melford (Suffolk, UK). Lobind Eppendorf centrifuge tubes (022431081) were purchased from Eppendorf (Hamburg, Germany).

Table 2.11: SILAC amino acids

Amino Acid	Label	Isotope abbreviation	Product Number
L-Proline	light	P0	P5607
L-Lysine		K0	L8662
L-Arginine		R0	A8094
L-Lysine	medium	K4	616192
L-Arginine		R6	643440
L-Lysine	heavy	K8	608041
L-Arginine		R10	609033

HPLC-grade water (23595328), HPLC-grade formic acid (20318.297) and HPLC-grade acetonitrile (ACN; 20060320) were purchased from VWR (Leicestershire, UK). Mass spectrometry-grade trypsin Gold (V5280) was purchased from Promega (WI, USA). Dialysed FBS (FB-1001D/500) was purchased from Biosera (France).

2.4.9 Tissue culture for SILAC-labelling

The HCT116 FlpIn TRex USP30KO and WT cells were cultured in 10% FBS SILAC DMEM supplemented with 146 mg/ml K0, 84 mg/l R0 and 200 mg/l P0 for light media or 146 mg/l K4, 84 mg/l R6 and 200 mg/l P0 for medium media or 146 mg/l K8, 84 mg/l R10 and 200 mg/l P0 for heavy media. The three types of media were reconstituted to the above stated concentrations of the isotopically-labelled amino acids, supplemented to 10% dialysed FBS and filtered through a 0.2 µm vacuum-assisted filter bottle prior to use. The cells were cultured for a minimum of 2 weeks and passaged every 2-3 days to ensure incorporation of the labelled amino acids before proceeding further.

2.4.10 Sample preparation for SILAC-based proteomics

Samples were lysed in NP-40 lysis buffer supplemented with MPIs (1:250) as described in 2.4.2. The samples were resolved on a 4-12%

NuPAGE gel as described in 2.4.4. For the purposes of assessing efficient label incorporation into the proteome (label test) the samples were run individually. For the purposes of the small-scale USP30 proteome, the three isotopically-labelled samples were combined 1:1:1 and run as a triplex in the same well of the gel.

From this point onwards all solutions used were made up in HPLC-grade water and all reagents and plastics were of high quality, non-autoclaved or undergone UV irradiation in order to prevent compromise of the polymers and carry over into the sample. The gel was placed in HPLC-grade water and then fixed in 42% (v/v) methanol, 6% (v/v) acetic acid rocking for 1 hour at room temperature. The gel was washed into HPLC-grade water and the gel was cut into individual gel pieces using a clean scalpel and placed into LoBind Eppendorf tubes. For the label test 4 gel pieces were cut for each sample. For the small-scale proteome the entire gel lane was cut into approximately 15 pieces of equal size. The gel pieces were washed once using 50 mM ammonium bicarbonate (AmBic)/50% (v/v) acetonitrile (ACN) for 10 min at 37°C. The gel pieces were then dehydrated by incubating in 100% ACN for 5 min at 37°C. The supernatant was discarded using gel loading tips and the gel pieces were dried by placing into a speed vacuum for 5 min at 37°C. The proteins in the gel pieces were fully reduced using 100 mM DTT in 100 mM AmBic for 1 hour at 56°C. The reducing solution was removed and replaced with 50 mM IAA in 100 mM AmBic for 30 min at room temperature.

2.4.11 In-gel digestion and peptide extraction

The gel pieces were washed once in 100 mM AmBic for 15 min at room temperature. The gel pieces were then dehydrated by incubating in 100% CAN for 5 min at 37°C. The supernatant was discarded using gel loading tips and the gel pieces were dried by placing into a speed vacuum for 5 min at 37°C. The gel pieces were then treated with trypsin gold diluted in 40 mM AmBic, 9% (v/v) ACN overnight at 37°C. The total amount of protein loaded onto the gel was divided by the number of gel pieces generated. The amount of trypsin gold used per gel piece was calculated as protein in gel: trypsin ratio of 50:1. The reaction volume used per gel piece was kept to a minimum, just enough to cover the gel piece. Upon completion of the reaction an equal volume of 100%

ACN was added to each tube and incubated for 30 min at 30°C. The supernatant was transferred into a fresh LoBind Eppendorf tube. The gel pieces were incubated with 50 µl 1% (v/v) formic acid for 20 min at room temperature. The supernatant was transferred to the same LoBind tubes. The step was repeated with 100 µl 1% (v/v) formic acid. The step was repeated with 100 µl ACN for each gel piece for 10 min at 37°C. The tubes containing the extracted peptides were speed vacuum dried at 45°C until there was no liquid. Extracted peptides were stored at -20°C.

2.4.12 Mass-spectrometry, peptide identification and quantitation

The peptides were resuspended in 25 µl 1% (v/v) formic acid vortexing hard and centrifuging at 14,000 rpm for 15 min at 4°C. Peptides were separated using a nanoACQUITY UPLC system (Waters) coupled to a Proxeon nanoelectrospray source and LTQ-Orbitrap XL mass spectrometer (ThermoFisher). Samples were loaded onto a 180 µm x 20 mm, 5 µm C18 symmetry trapping column (Waters) in 1% (v/v) Acetonitrile, 0.1% (v/v) formic acid at a flow rate of 10 µl/min for 5 min. Peptides were resolved on a 25 cm x 75 µm BEH-C18 column (Waters) using a 50 min gradient of 7-35% acetonitrile and a 300 nl/min flow rate. The mass spectrometer acquired full MS survey scans in the Orbitrap (R = 30 000; m/z range 350–2000) and performed MSMS on the top six multiple charged ions in the linear quadrupole ion trap (LTQ) after fragmentation using collision-induced dissociation (30 ms at 35% energy). MS spectra were analysed using MaxQuant (version 1.5.3.8) using default settings with re-quantification.

Chapter 3: Fundamental biology of USP30

3.1 Introduction

USP30 is a protein that has been extensively studied in the field of PINK1/Parkin-dependent mitophagy and remains one of the strongest candidates for the development of drugs in the treatment and management of Parkinson's disease (Miller and Muqit, 2019). Over the last years several small molecule inhibitors against USP30 have been developed with the aim of improving the mitochondrial function in people with Parkinson's disease (Yue et al., 2014; Kluge et al., 2018). The Michael J. Fox Foundation (MJFF), a major charitable funder of Parkinson's disease research, has supported the development of USP30 inhibitors in collaboration with several Biotech companies including Mission Therapeutics (Cambridge, UK) and Forma Therapeutics (Watertown, MA, USA).

Despite the strong interest in designing strategies to inhibit or silence USP30, our understanding of the potential roles of USP30, outside the scopes of mitophagy and mitochondria quality control, are limited. Discovering alternative roles of USP30 may help to assess the risks for potential unwanted side-effects of strategies that involve USP30 inhibition. I therefore sought to understand USP30 function in the greater context of cellular physiology and validate USP30 as a targetable DUB. The present chapter compiles what is known about USP30 and explores new aspects of its biology with a focus on the following questions:

1. What subcellular compartments does USP30 localise to?
2. How does it reach its destination?

3.2 USP30 domain architecture and sequence conservation

3.2.1 USP30 isoforms and domain structure

USP30 belongs to the Ubiquitin Specific Peptidases (USP) family of cysteine proteases. In humans, USP30 is encoded on the 38.p13 region of chromosome 12 and is known to produce two mature mRNA transcripts from alternative splicing (**Figure 3.1**).

Gene ID	Isoform	Transcript Name	Transcript ID	Protein size	Uniprot
84749	1	USP30-201	ENST00000257548.10	517 aa/ 58503 Da	Q70CQ3
84749	2	USP30-203	ENST00000392784.6	486 aa/ 55109 Da	B3KUS5

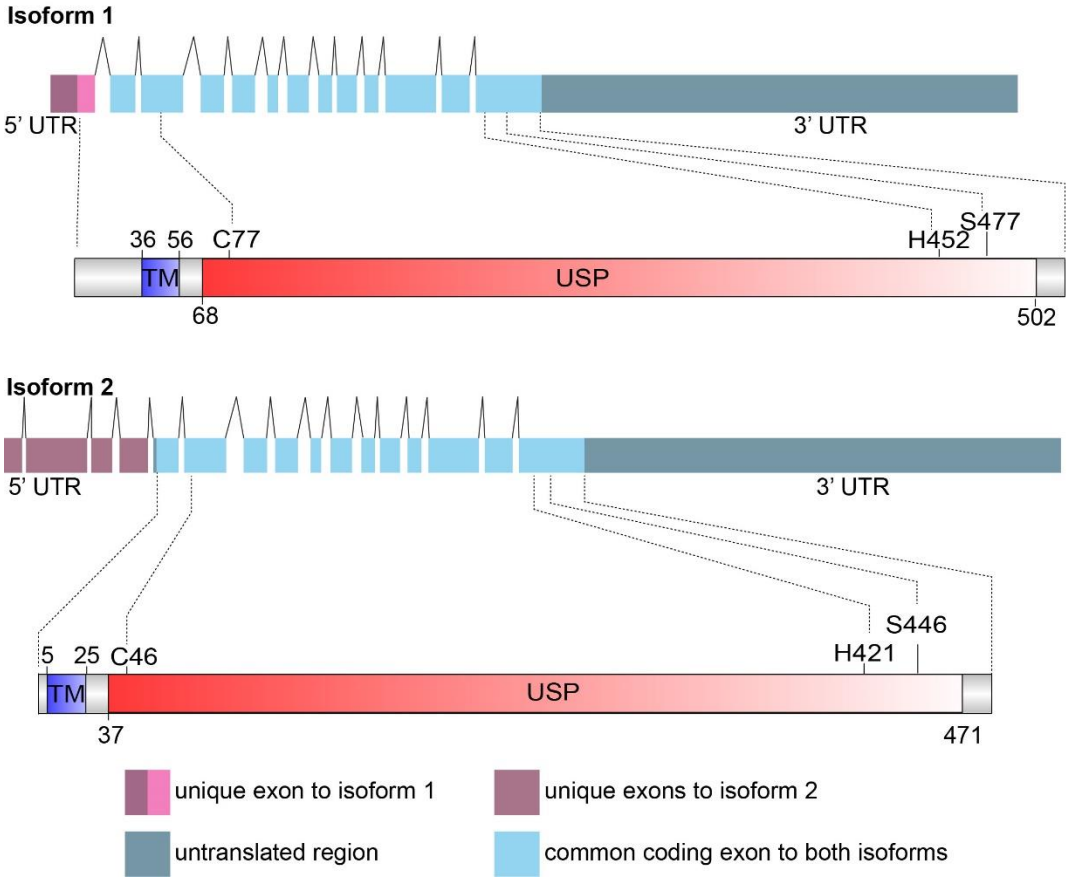

Figure 3.1: The USP30 gene codes two isoforms

The table summarises the two USP30 transcripts with the associated information extracted from Ensembl (https://www.ensembl.org/) Transcript ID, protein size in amino acids (aa), molecular weight (Da) and UniProt entries (https://www.uniprot.org/). Schematic representation of the USP30 gene and two transcript variants coding for isoforms 1 and 2. Domain boundaries are indicated and mapped onto exons. The catalytic triad residues C77, H452 and S477 for isoform 1 and C46, H421 and S446 for isoform 2 are indicated. 5' UTR, 5' untranslated region; 3' UTR, 3' untranslated region; TM, transmembrane domain; USP, Ubiquitin Specific Peptidase domain.

Isoform 2 encodes a 482 amino acid protein of 55 kDa that lacks the first 35 amino acids of isoform 1. Isoform 2 retains the full USP domain and it is therefore expected to be catalytically active. This truncated USP30 may be a testis-specific isoform where it is expressed alongside isoform 1, whilst it appears absent in 9 other tissues tested: thymus, brain, lung, liver, spleen, kidney, muscles and ovaries (Nakamura and Hirose, 2008). From this point onward when mentioning USP30 I am referring to isoform 1, unless otherwise specified. USP30 has a catalytic triad consisting of a Cysteine at position 77,

a Histidine at position 452 and an atypical Serine at position 477. All other USPs, apart from USP30 and USP45, have an Aspartate or Asparagine as the third critical residue (Quesada et al., 2004). USP30 was shown to cleave K48-linked and, to a lesser extent, K63-linked tetra-ubiquitin chains (Nakamura and Hirose, 2008). More recently, USP30 has been shown to display strong selectivity towards processing K6-linked ubiquitin chains over K11, K48 and K27 in decreasing order, with only limited activity towards K63-linked di- and tetra-ubiquitin (Cunningham et al., 2015; Gersch et al., 2017).

3.2.2 USP30 is highly conserved in animals

The primary sequence of proteins dictates their function and the essentiality of a cellular function is often accompanied by high sequence homology. I therefore sought to examine the sequence similarities of USP30 homologues across different species. I retrieved the primary sequences of human USP30 (Q70CQ3) and the other known USP30 orthologues in other organisms that included the nematode worm (*C.elegans*: Q9BKQ6), fruit fly (*D.melanogaster*: Q9W462), zebrafish (*D.rerio:* A2BGT0) and the domestic mouse (*M.musculus*: Q3UN04) from UniProt. I then used the domain boundaries for the USP domain from those entries to perform a multiple sequence alignment on the EMBL-EBI website, using the Clustal Omega function (Madeira et al., 2019). The resultant phylogenetic tree and multiple sequence alignment are shown in **Figure 3.2**.

The USP30 orthologue for *C.elegans* was identified as CELE_Y67D2.2 based on sequence similarity. It was interesting to note that the catalytic domain of the *C.elegans* USP30 was phylogenetically closer to the vertebrate animals than that of *D.melanogaster*. The conservation was naturally higher between murine and human USP30 compared to evolutionarily earlier organisms. Overall, the catalytic domain of USP30 is highly conserved across species.

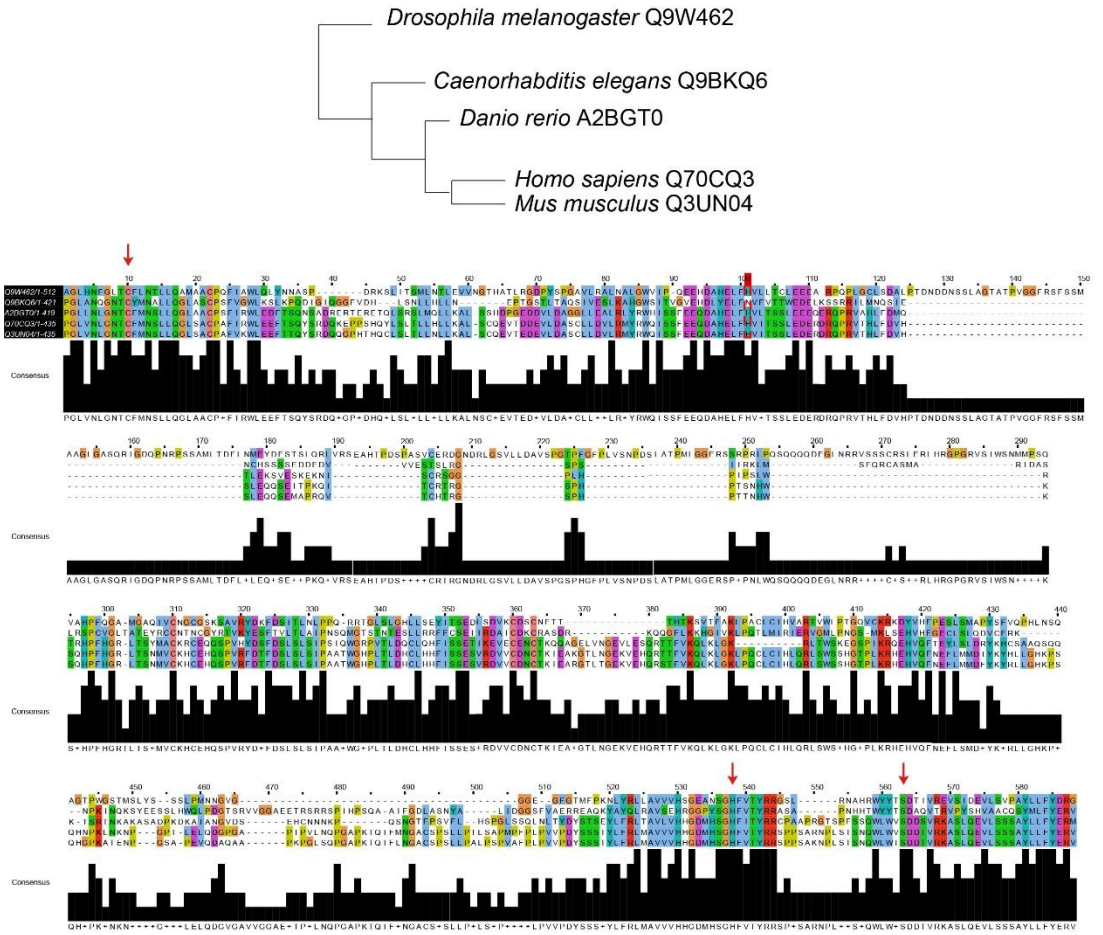

Figure 3.2: USP domain multiple sequence alignments across species

The sequences of USP30 orthologues for *H.sapiens* (Q70CQ3), *M.musculus* (Q3UN04), *D.rerio* (A2BGT0), *D.melanogaster* (Q9W462) and *C.elegans* (Q9BKQ6) and USP domain boundaries were extracted from UniProt. The USP domain sequences from the different species were aligned using the Clustal W2 Omega function on the EMBL-EBI website: https://www.ebi.ac.uk/Tools/msa/clustalw2/ to generate (top) phylogenetic tree analysis and (bottom) multiple sequence alignments at the single amino acid level. The multiple sequence alignment was exported using Jalview 2.11.1.3 (Waterhouse et al., 2009). Red arrows show the catalytic triad.

S.cerevisiae and *S.pombe* have their own mitochondrially localised DUBs called Ubp16 and ubp16 respectively. The *S.cerevisiae* UBP16 does not bear any sequence homology to USP30 and remains functionally uncharacterised (Kinner and Kölling, 2003; Huseinovic et al., 2018). UBP16 overexpression or deletion did not induce any differences in mitochondria morphology nor differences in growth on non-fermentable carbon sources. The authors concluded that Ubp16 is not important for the regulation of mitochondrial function in yeast. Interestingly, loss of Ubp16 was identified to confer a slight growth advantage in a large-scale screen employing a

fluorescent-based high-throughput assay of deletion and wildtype strains growing in the same well of a 384-well plate over multiple generations (Breslow et al., 2008).

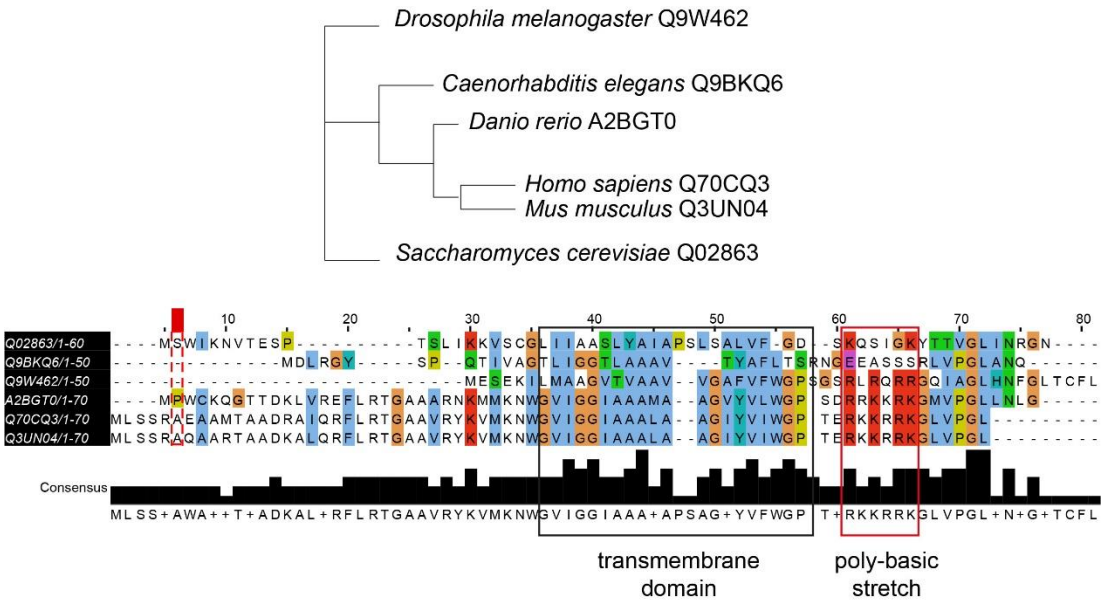

Figure 3.3: Transmembrane domain and poly-basic stretch comparison between species

The sequences of USP30 orthologues for *H.sapiens* (Q70CQ3), *M.musculus* (Q3UN04), *D.rerio* (A2BGT0), *D.melanogaster* (Q9W462), *C.elegans* (Q9BKQ6) and *S. cerevisiae* (Q0286) were extracted from UniProt. The N-terminal domain sequences before the USP domains from the different species were aligned using the Clustal W2 Omega function on the EMBL-EBI website: https://www.ebi.ac.uk/Tools/msa/clustalw2/ to generate (top) phylogenetic tree analysis and (bottom) multiple sequence alignments at the single amino acid level. The multiple sequence alignment was exported using Jalview 2.11.1.3 (Waterhouse et al., 2009). The black and red boxes highlight the locations of the transmembrane domains and poly-basic stretch according to the human USP30.

Ubp16 contains a short stretch of hydrophobic amino acids near its N-terminus described as an “Alanine-rich” region that is thought to act as a transmembrane domain (**Figure 3.3**). USP30 also has a short transmembrane (TM) domain near its N-terminus and a positive stretch of amino acids downstream of the TM domain, both of which are necessary for mitochondrial localisation (Nakamura and Hirose, 2008). No such stretch of positively-charged amino acids has been identified for UBP16 and it may be that the presence of the TM domain alone is sufficient to localise it to the OMM (Kinner and Kölling, 2003).

It is interesting that the Alanine-rich TM domain of USP30 is conserved across all the species that I selected to analyze, while the poly-basic stretch appears to be a more evolutionarily recent development. More specifically, the number of positive residues in the stretch increases with more evolutionarily recent species, starting from 4 in the fruit fly and increasing to 6 in humans and mice.

3.3 USP30 localises to mitochondria as well as to peroxisomes

3.3.1 USP30 localises to peroxisomes

During her experiments using transiently transfected USP30-GFP in hTERT-RPE1 cells, my colleague Elena Marcassa noticed that there was a pool of USP30-GFP that was not co-localising with the mitochondrial marker TOMM20. We wondered whether these structures could be peroxisomes as these organelles share a great deal of functions with mitochondria, such as lipid metabolism and have proteins in common such as FIS-1, MUL-1 and DRP-1. Elena tested this hypothesis by transiently expressing USP30-GFP in hTERT-RPE1 cells and performing immunofluorescence staining against peroxisomal marker proteins PMP70 and catalase. PMP70 and catalase stain co-localised with a small pool of USP30-GFP. Importantly, my colleague Jane Jardine was able to show the peroxisomal localisation of endogenous USP30 in SH-SY5Y cells by immunofluorescence microscopy (Marcassa et al., 2018). Furthermore, our collaborator Markus Islinger (University of Mannheim, Germany) demonstrated that USP30 co-fractionates with both mitochondrial and peroxisomal protein markers in density gradient centrifugation experiments performed in HepG2 cells (Marcassa et al., 2018).

The newly discovered sub-cellular localisation raised the following fundamental questions about USP30 and peroxisomes:

1. What is the topology of USP30 on peroxisomes?
2. How does USP30 reach peroxisomes?
3. What is the function of USP30 on peroxisomes?

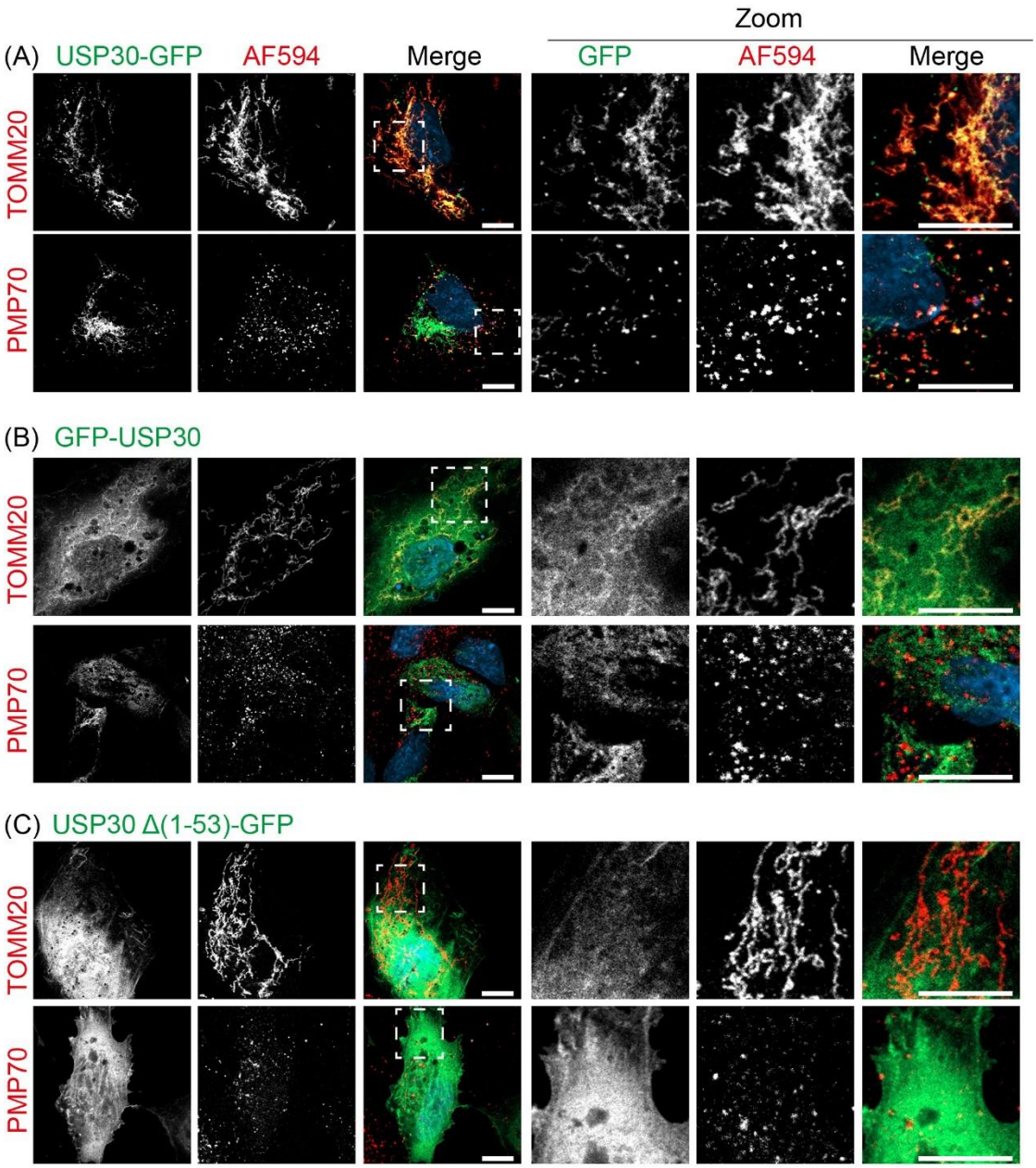

Figure 3.4: USP30-GFP localises to mitochondria and peroxisomes

hTERT-RPE1 cells were transfected with (A) USP30-GFP, (B) GFP-USP30 and (C) with USP30 Δ(1-53)-GFP for 24 hours. Cells were fixed with 4% PFA/PBS, stained with anti-TOMM20 or anti-PMP70 and the appropriate secondary antibodies conjugated to AF594. Representative images were taken on an LSM800 confocal microscope using a 63x oil immersion objective. Scale bars represent 10 µm.

Together with Jane Jardine, I performed a set of immunofluorescence experiments using GFP-tagged USP30 constructs and stained the transfected cells with either the mitochondrial marker TOMM20 or the peroxisomal marker PMP70 (**Figure 3.4**A). In addition to the co-localization of the bulk of the USP30-GFP signal with TOMM20, I also saw a clear overlap between the USP30-GFP punctate structures and PMP70.

The earliest study from Nakamura and Hirose (2008) determined that the TM domain of USP30 was close to its N-terminus and used a C-terminally tagged FLAG construct of USP30 for their imaging experiments. I wondered whether the position of the fluorescent tag would interfere with either localisations and tested this by transfecting GFP-USP30 into hTERT-RPE1 cells (**Figure 3.4**B). GFP-USP30 adopted a diffused staining that was largely cytosolic and was excluded from the nucleus. Furthermore, a portion of GFP-USP30 formed a reticular pattern, which co-localised with TOMM20. There was no clear co-localisation of GFP-USP30 with PMP70. The above indicates that the presence of the GFP tag on the N-terminus hinders translocation with membranes.

The TM domain of USP30 has been shown to be necessary for mitochondrial localisation (Nakamura and Hirose, 2008). I wanted to test whether the same was true for peroxisomes. I transfected USP30 Δ(1-53)-GFP that lacked the TM domain but retained the USP domain in full. I saw that the construct was cytosolic and unable to co-localise with either TOMM20 or PMP70 (**Figure 3.4**C). The above experiment suggests that the amino terminus that includes the TM domain is required for both mitochondrial and peroxisomal localisations.

3.3.2 Peroxisomal USP30 is an integral membrane protein with its catalytic domain facing the cytosol

Nakamura and Hirose used alkaline carbonate extraction and protease protection assays to determine that the mitochondrial pool of USP30 is an integral membrane protein on the OMM with the catalytic domain facing towards the cytosol (Nakamura and Hirose, 2008). I wanted to determine the membrane topology and orientation of USP30 on peroxisomes by performing the analogous experiments.

Alkaline carbonate extraction is a well-established method to investigate whether membrane proteins are directly integrated into membranes or peripherally-associated through interactions with other membrane proteins (Kim et al., 2015). The methodology involves generating cell homogenates and a post-nuclear supernatant (PNS) followed by a series of ultra-centrifugation steps to separate membrane fractions from soluble material in different buffers (**Figure 3.5**). The PNS is split into three equal volumes and ultra-centrifuged to enrich for the membrane fraction by separating the membranes from the cytosolic compartments. The three pellets are then resuspended in the three different buffers. Treating the membrane fraction with a basic solution of sodium carbonate (Na_2CO_3) causes membrane vesicles to convert into membrane sheets, which disrupts protein-protein interactions, releasing peripheral membrane proteins in solution (Kim et al., 2015). However, integral membrane proteins are not affected as they remain inserted into the lipid bilayer. As a control a buffer containing Triton X-100 is used, which solubilises all membrane proteins into the soluble fraction. The third pellet is resuspended in homogenisation buffer (HIM) as a control that retains all membrane proteins in the membrane fraction.

One of the difficulties in conducting these experiments is that most cells do not have a lot of peroxisomes but have a lot of mitochondria. Since USP30 occupies both compartments, even a small contamination of the peroxisomal fraction with mitochondrial membranes would make interpretation of the results impossible. My colleague, Emma Rusilowicz-Jones and I sought to circumvent this issue by removing mitochondria from the equation. We achieved this by making use of the YFP-Parkin overexpressing hTERT-RPE1 cells (MacVicar and Lane, 2014).

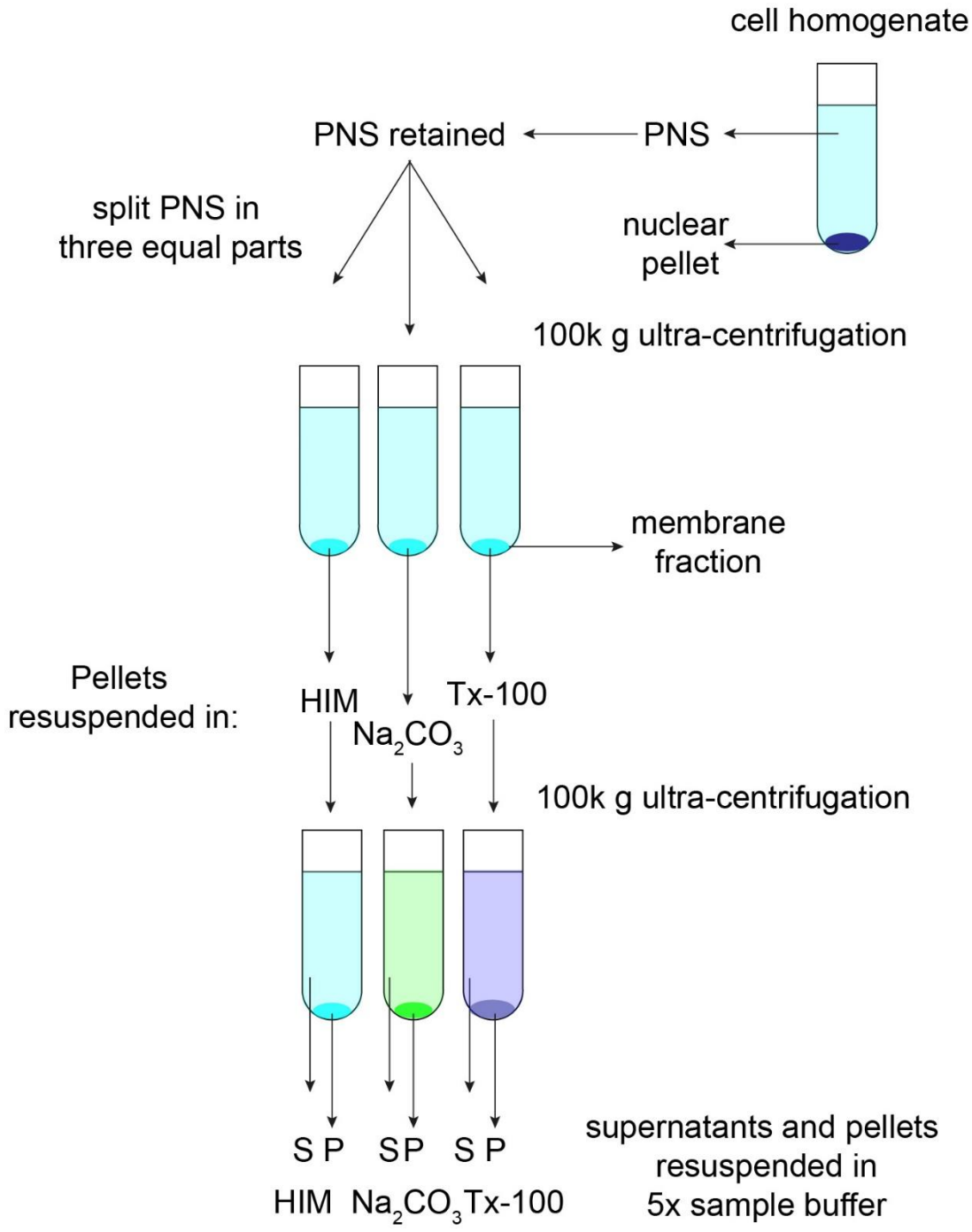

Figure 3.5: Outline of membrane topology experiment

Schematic representation of the alkaline carbonate extraction experiment to determine the membrane topology of membrane proteins. PNS, post-nuclear supernatant; HIM, homogenisation buffer, Na_2CO_3; alkaline carbonate buffer, Tx-100, detergent buffer with TritonX-100; P, pellet; S, supernatant.

Upon depolarisation with antimycin A and oligomycin A (A/O) for 24 hours, these cells lose the majority of their mitochondria through Parkin-dependent mitophagy. I therefore performed an alkaline carbonate extraction and a protease protection assay on the homogenates derived from mitochondria-depleted cells as well as from control cells.

In the untreated cells, USP30 was retained in the pellet after alkaline carbonate extraction and only partitioned into the supernatant in the presence of detergent, suggesting USP30 is an integral membrane protein (

Figure 3.6). The same pattern was observed for other integral membrane proteins such as TOMM20 (mitochondrial marker) and PMP70 (peroxisomal marker). Non-integral membrane proteins that are enveloped in membrane-bound compartments such as catalase and ACOX1, behaved differently. Following homogenisation catalase and ACOX1 were membrane associated. Alkaline carbonate buffer caused the two markers to appear in both soluble and membrane associated fractions possibly due to incomplete membrane rupture of peroxisomes. Finally, the detergent buffer fully solubilised all proteins tested, except for PMP70 where a fraction of it remained membrane associated, which may suggest the protein is prone to forming insoluble aggregates.

As expected, mitochondrial marker TOMM20 was strongly reduced in the PNS of cells treated with A/O for 24 hours, indicative of the loss of mitochondria while the peroxisomal markers PMP70 and ACOX1 were unaffected. In the A/O-treated cells, USP30 behaved in the same way as in the untreated cells in terms of how it partitioned in the different buffers. The above suggests that USP30 is an integral membrane protein also on peroxisomes.

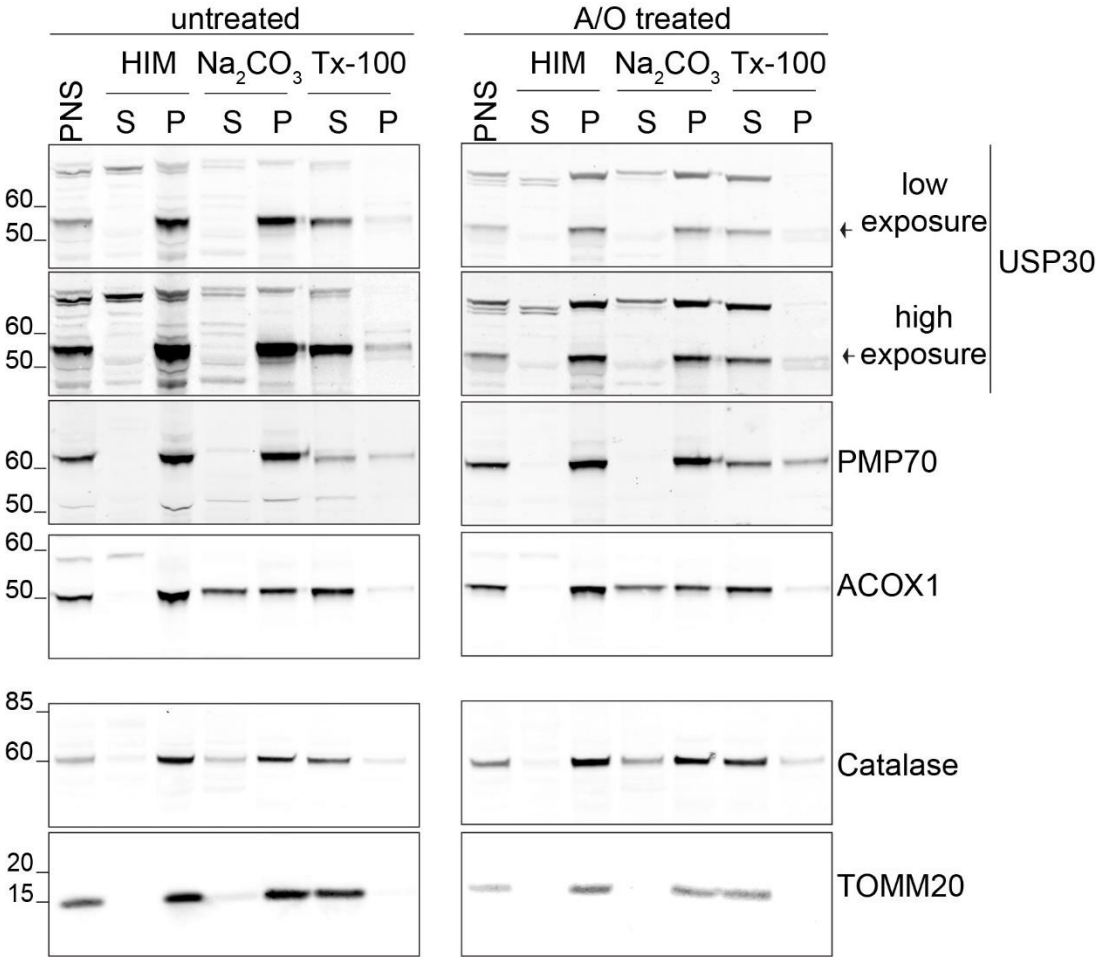

Figure 3.6: USP30 is an integral membrane protein

hTERT-RPE1 YFP-Parkin cells were treated with 1 µM antimycin A and 1 µM oligomycin A (A/O) or left untreated for 24 hours. Cells were homogenised in HIM buffer and a post-nuclear supernatant (PNS) was generated. PNS was split in three parts and ultracentrifugated at 100000 g for 40 min. The supernatant (S) was collected and the three pellets (P) were resuspended in HIM buffer or alkaline buffer (Na_2CO_3) or detergent buffer (Tx-100) before re-ultracentrifugated at 100000 g. Pellets and supernatants were prepared in sample buffer and equal fractions were resolved on SDS-NuPAGE gels. The arrow shows the specific band for USP30. The blots are from a representative experiment from two independent experiments (n=2).

3.3.3 The catalytic domain of peroxisomal USP30 is facing to the cytosol

I next wanted to investigate the orientation of USP30 on peroxisomes using a protease protection assay (**Figure 3.7** upper). A similar approach had been previously used to determine the orientation of USP30 on mitochondria (Nakamura and Hirose, 2008). The protease protection assay involves treating the cell homogenate with Proteinase K, a broad-spectrum serine protease. Proteins enclosed in intact membrane compartments such as mitochondria or peroxisomes and the transmembrane domains of integral membrane proteins remain intact. Any cytosolic proteins, peripheral membrane proteins and any cytosolic-facing domains of membrane proteins are digested. Protected proteins only become susceptible to proteolysis once membranes are solubilised by a detergent such as Triton X-100. In the case of USP30 on peroxisomes, if the USP30 domain is facing towards the cytosol then most of the USP30 would be digested and the antibody that recognises the USP domain of the protein would no longer react with it. If peroxisomal USP30 had the USP domain on the luminal side then only the small N-terminal portion would be digested and that would result in a small downshift in molecular weight on the gel.

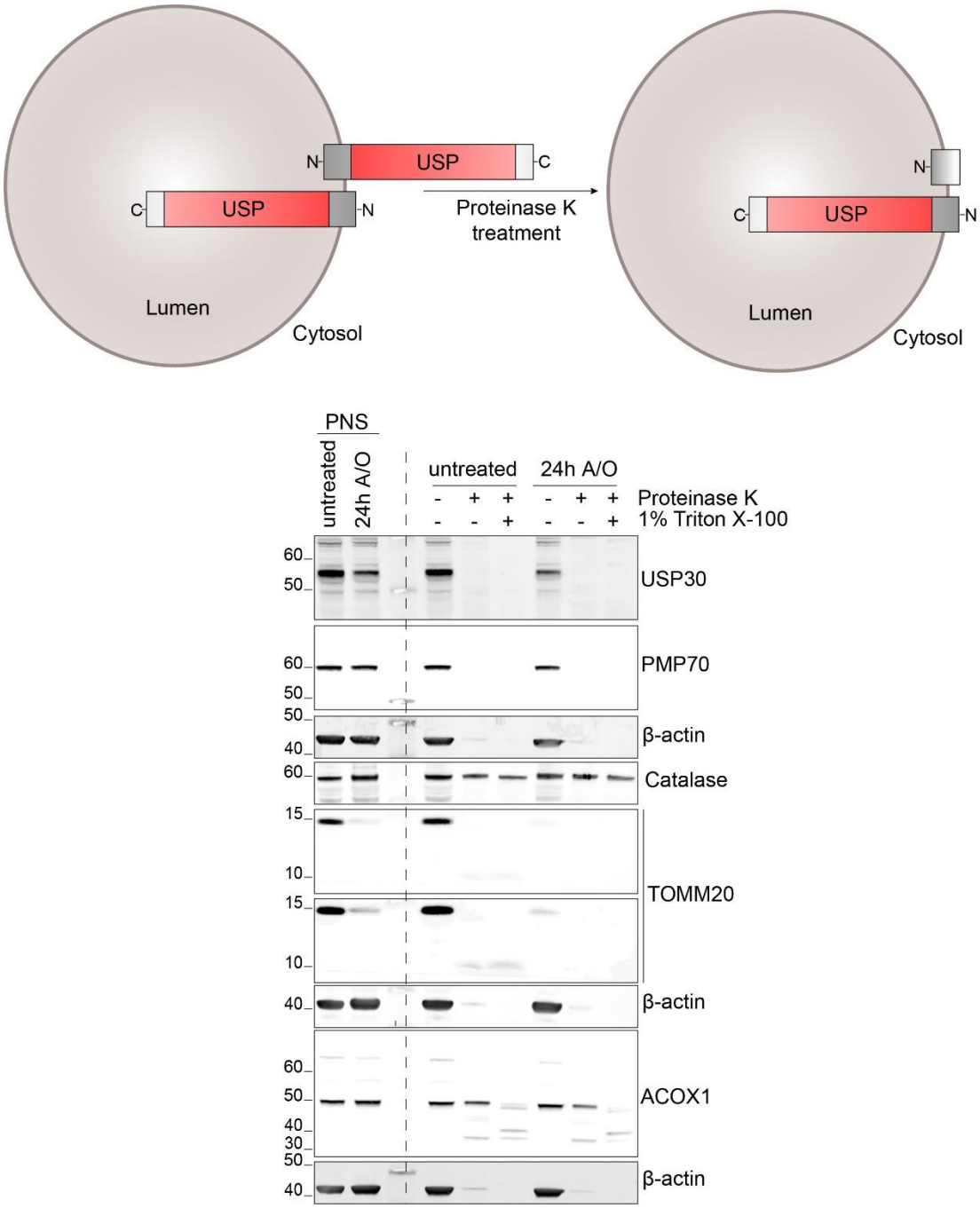

Figure 3.7: Protease protection assay on the peroxisomal pool of USP30

Schematic diagram outlining the two possible orientations of USP30 on peroxisomes and how a protease protection assay is used to distinguish between the two. The red domain represents the catalytic domain. hTERT-RPE1 YFP-Parkin cells were treated with 1 µM antimycin A and 1 µM oligomycin A (A/O) or left untreated for 24 hours. Cells were homogenised in HIM buffer and post-nuclear supernatant (PNS) was generated. The PNS was split in three parts and aliquots were treated with Proteinase K in the absence or presence of Triton X-100 or left untreated. N-, N-terminus; C-, C-terminus; USP, ubiquitin specific peptidase domain. The blots are from a representative experiment from two independent experiments (n=2).

First, we induced mitophagy in the hTERT-RPE1 YFP-Parkin cells using 1 μM A/O for 24 hours in order to deplete cells of mitochondria. These cells were homogenised in HIM buffer in the absence of protease inhibitors. The PNS derived from cells with and without mitophagy induction were adjusted to the same final protein concentration and split into three equal parts. One part was left untreated, the second was treated with Proteinase K to digest all proteins that were exposed and the third had Triton X-100 added to the Proteinase K digestion in order to expose all proteins previously protected by membranes. After a 30 min incubation on ice, the reactions were stopped by adding PMSF for 5 min on ice before being prepared in sample buffer.

In the A/O treated condition, TOMM20 was strongly reduced in the PNS, indicating the removal of mitochondria, while peroxisomal markers PMP70 and ACOX1 remained constant. USP30 levels were also reduced in the PNS, suggesting a pool of USP30 was lost in response to A/O treatment. In the control cells, USP30, PMP70 and TOMM20 are all digested by Proteinase K, suggesting that the domains recognised by the antibodies are accessible to Proteinase K without the need to disrupt membranes with Triton X-100 (**Figure 3.7** lower). TOMM20 exposure to Proteinase K yielded a low molecular weight fragment, suggesting incomplete digestion. On the contrary, ACOX1 is protected and only accessible in the presence of Triton X-100. Peroxisomal USP30 was also sensitive to Proteinase K digestion, suggesting that USP30 is orientated as such on peroxisomes that the catalytic domain is facing into the cytosol. Catalase remained resistant to Proteinase K digestion, even in the presence of Triton X-100. The other peroxisomal protein, ACOX1, that shares the same localisation as catalase was not protected in the presence of Triton X-100, suggesting that catalase may be intrinsically resistant to proteases in this context (Francisco et al., 2013; Schrader, 2017).

3.4 Investigating the targeting sequences of USP30 for mitochondrial and peroxisomal localisations

OMM proteins such as TOMM20 and TOMM70 have characteristic stretches of positively-charged amino acids flanking their TM domains that have been shown to be required for correct localisation (Kanaji et al., 2000; Edmonson et al., 2002; Iwashita et al., 2010). The first study describing USP30 as a mitochondrial DUB hypothesised that USP30 is an N-terminally anchored membrane protein similar to TOMM20 and TOMM70 (Nakamura and Hirose, 2008). The authors identified two stretches of basic amino acids flanking the TM domain, one preceding and one following it (**Figure 3.8**). Neutralising the positive charge on the one preceding the TM domain (KRmut1) did not affect mitochondrial localisation, while mutating the one following the TM domain (KRmut2) was sufficient to mis-localise USP30 to the endoplasmic reticulum (ER) instead of mitochondria (**Figure 3.8**).

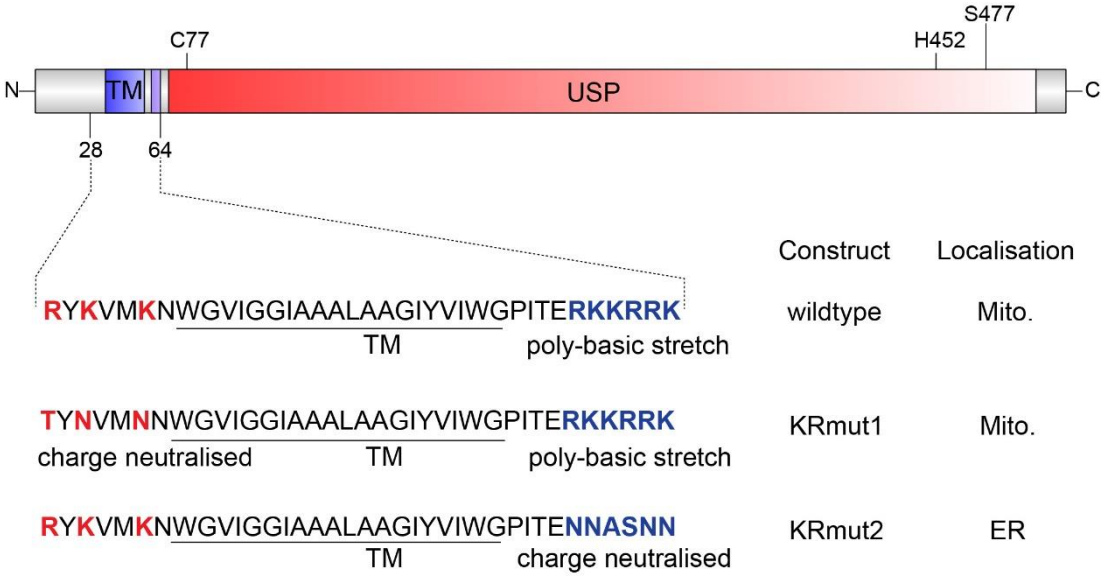

Figure 3.8: USP30KR mutants used by Nakamura and Hirose (2008)
Schematic diagram of USP30 protein showing the positions of the two stretches of basic amino acids flanking the trans-membrane (TM) domain identified by Nakamura and Hirose. The basic residues are shown in red and blue for the stretch preceding and following the TM domain respectively. TM; trans-membrane domain, USP; ubiquitin-specific peptidase domain, ER; endoplasmic reticulum. Mito, mitochondria.

I investigated whether the same two basic stretches were relevant for the peroxisomal localisation of USP30 and I generated the same mutations, KRmut1 and KRmut2, as GFP-tagged constructs (Nakamura and Hirose, 2008). I first transfected the two mutants alongside wild-type USP30-GFP and assessed their ability to co-localise with TOMM20, CALN (calreticulin) and PMP70 as markers for mitochondria, endoplasmic reticulum and peroxisomes respectively (**Figure 3.9**).

USP30-GFP adopted a reticular pattern and co-localised strongly with TOMM20. USP30-GFP also decorated distinct punctate structures a portion of which co-stained with PMP70. USP30-GFP did not co-localise with the ER marker CALN.

USP30 KRmut1-GFP equally co-localised with TOMM20, suggesting the construct localised on mitochondria. USP30 KRmut1-GFP however did not appear to decorate the same distinct punctate structures and did not co-localise with PMP70. The reticular pattern of USP30 KRmut1-GFP was distinct from that of CALN.

USP30 KRmut2-GFP appeared to adopt a reticular pattern in the cell and was excluded from the nucleus. The construct however did not co-localise with CALN, contrary to the previous report (Nakamura and Hirose, 2008). The CALN stain may had been unsuccessful in this experiment given that the staining pattern did not resemble ER. Furthermore, the staining adopted by USP30 KRmut2-GFP was not completely diffused, suggesting the construct was not cytoplasmic and looked reticular, suggesting this was in fact ER-localised. USP30 KRmut2-GFP failed to co-localise with TOMM20, which is consistent with what was published for the relevance of the poly-basic stretch being required for mitochondrial localisation. Lastly, USP30 KRmut2-GFP did not co-localise with PMP70 puncta.

The above IF experiment showed that the three positive amino acids before the TM domain (in KRmut1) may be important for the localisation to peroxisomes but not to mitochondria. In contrast, I was able to confirm that the poly-basic stretch after the TM domain was shown to be important for mitochondrial localisation.

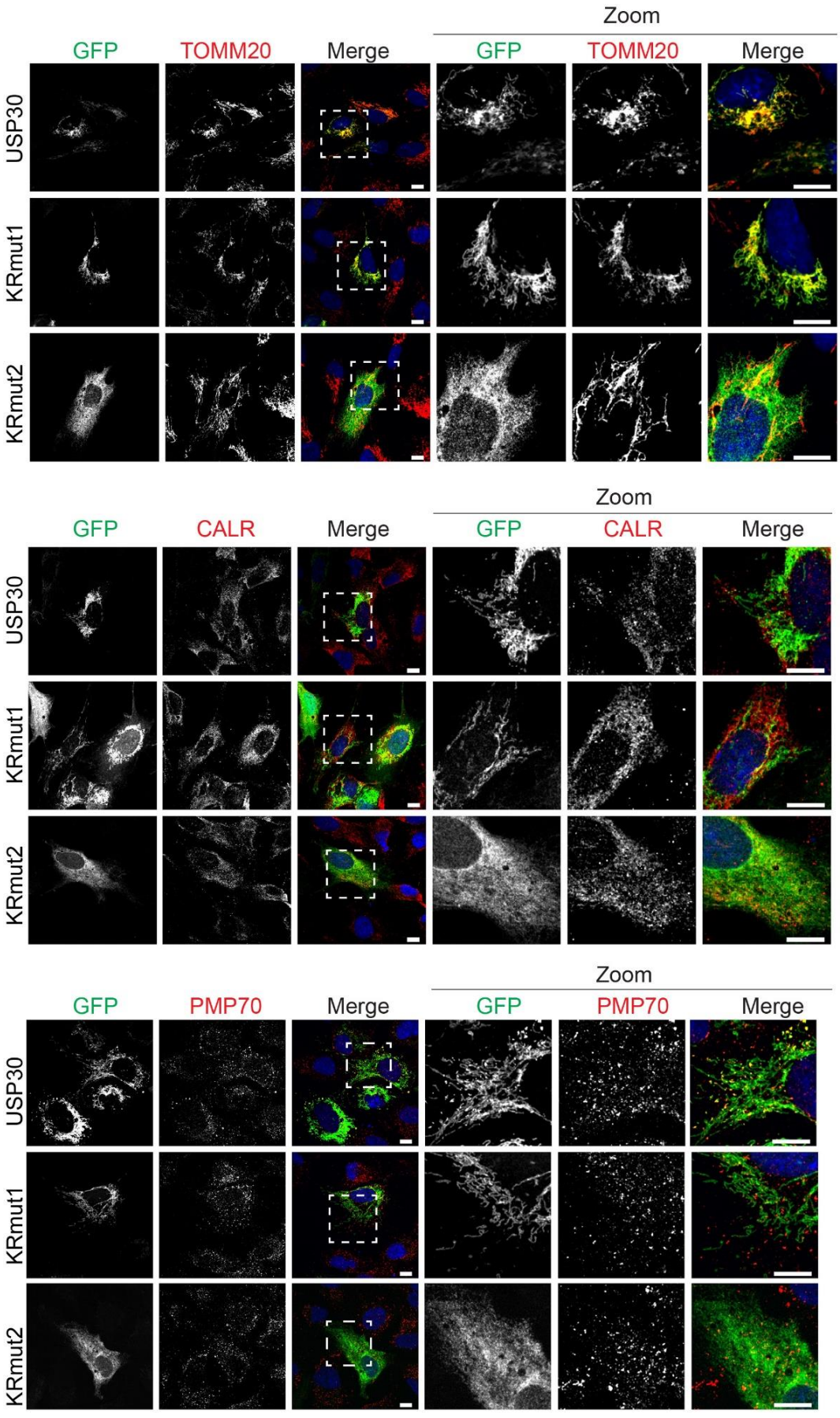
Zoom
GFP
TOMM20
Merge
GFP
TOMM20
Merge
USP30
KRmut1
KRmut2
Zoom
GFP
CALR
Merge
GFP
CALR
Merge
USP30
KRmut1
KRmut2
Zoom
GFP
PMP70
Merge
GFP
PMP70
Merge
USP30
KRmut1
KRmut2

Figure 3.9: USP30 KR mutants localisation on mitochondria, ER and peroxisomes

hTERT-RPE1 cells were transfected with USP30-GFP or USP30 KRmut1-GFP or USP30KR mut2-GFP for 24 hours. Cells were fixed with 4% PFA/PBS and stained with anti-TOMM20 or anti-CALR or anti-PMP70 antibodies and the appropriate secondary antibodies conjugated to AF594 and mounted onto microscope slides using mowiol/DAPI. Representative images were taken on a Zeiss 3i confocal spinning disk microscope using a 63x oil immersion objective. Scale bars represent 10 µm.

I next set out to identify the minimum sequence of USP30 that was required to reach mitochondria and peroxisomes. I generated two additional truncations of USP30. Firstly, I constructed USP30 (1-53) that includes the entire amino-terminus up to and including the TM domain but lacks the adjacent poly-basic stretch that I confirmed to be required for mitochondrial localisation (**Figure 3.8**). I generated a further N-terminal fragment USP30 (1-68) that includes the poly-basic stretch. My colleague, Elena Marcassa, transfected these truncations into hTERT-RPE1 cells and determined that USP30 (1-68) was able to reach both peroxisomes and mitochondria while the (1-53) construct only reached peroxisomes (Marcassa et al., 2018). In conclusion, the first 53 amino acids of USP30 that include the TM domain were sufficient to target it to peroxisomes, while including amino acids 54-68 was required for targeting USP30 to mitochondria (**Figure 3.10**). Based on the above results, it appeared likely that the three positive residues preceding the TM domain might be relevant for peroxisomal localisation but dispensable for mitochondrial targeting of USP30. Interestingly USP30 isoform 2 (**Figure 3.1**) is identical in sequence to a 35 amino acid N-terminal truncation of isoform 1, which means it is missing two out of the three critical residues preceding the TM domain.

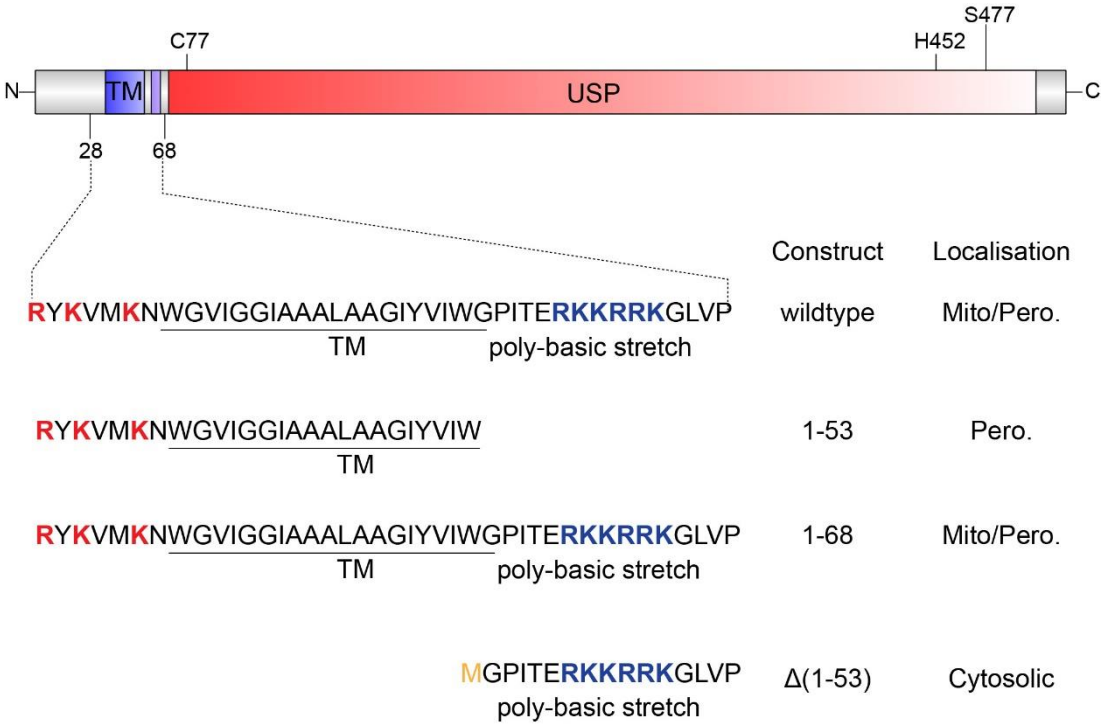

Figure 3.10: USP30 truncations used in Marcassa *et al* (2018)
Schematic diagram of USP30 protein showing the positions of the two stretches of basic amino acids flanking the trans-membrane (TM) domain identified by Nakamura and Hirose. The basic residues are shown in red for the amino acids preceding the TM domain and in blue for the stretch following the TM. The M residue shown in yellow is the initiator methionine residue introduced to generate the Δ(1-53) truncation. TM; trans-membrane domain, USP; ubiquitin-specific peptidase domain, Pero; peroxisomes.

I hypothesized that isoform 2 only localises on mitochondria and not peroxisomes. The above point may also shed some light onto the physiological role of isoform 2 of USP30 in the testis that is the only tissue it has been shown to be expressed in this far (Nakamura and Hirose, 2008).

I generated USP30 isoform 2, subcloned it into the same GFP expression vector as isoform 1 and asked whether USP30-GFP isoforms 1 and 2 localised to mitochondria and peroxisomes in hTERT-RPE1 cells (**Figure 3.11**). As expected, both USP30-GFP isoforms co-localised with TOMM20 suggesting that isoform 2 was still able to reach mitochondria (**Figure 3.11**, upper panel).

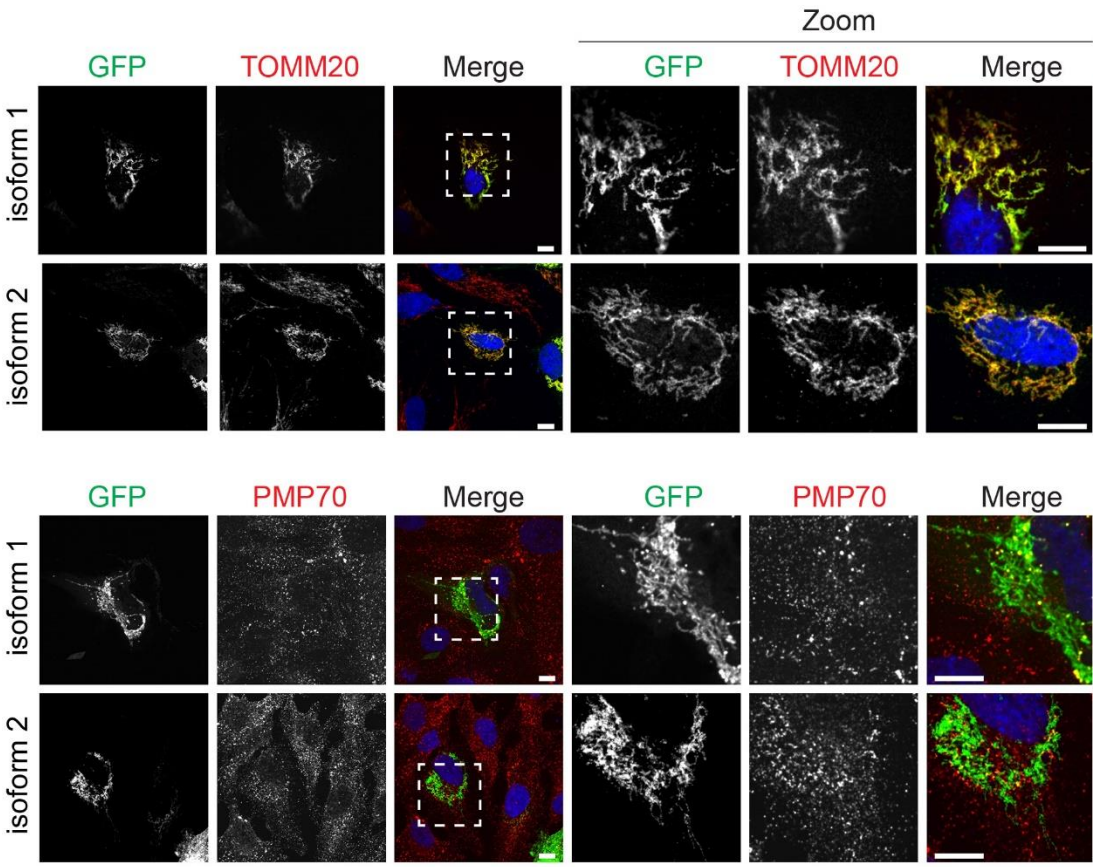

Figure 3.11: USP30 isoform 2 localisation on mitochondria and peroxisomes

hTERT-RPE1 cells were transfected with USP30-GFP isoform1 or 2 for 24 hours. Cells were fixed with 4% PFA/PBS and stained with anti-TOMM20 or anti-PMP70 antibodies and the appropriate secondary antibodies conjugated to AF594 and mounted onto microscope slides using mowiol/DAPI. Representatives images were taken using a 63x oil immersion objective on a Zeiss 3i confocal spinning disk microscope. Scale bars represent 10 µm.

USP30-GFP isoform 1 displayed a clear co-localisation with PMP70 positive puncta that were distinct from the filamentous mitochondrial network. In contrary, USP30-GFP isoform 2 had a primarily filamentous appearance with a much less prominent co-localisation with PMP70. The above suggested that USP30 isoform 2, similarly to USP30KRmut1, is perhaps less efficiently targeted to peroxisomes compared to isoform 1.

3.5 Quantification of USP30 copy number across model cell lines

Macromolecules are the fundamental building blocks of cells. A lot of the biology that is described as part of a protein's function often fails to capture the concept of numbers in the cell. In order to fully and fundamentally understand the role of a protein in cellular physiology, one needs to consider how much protein exists in the cell at any one time or in other words the copy number of protein molecules per cell.

Using quantitative mass-spectrometry, the number of USP30 molecules was determined at 4915 copies per HeLa cell (Kulak et al., 2014) and 233 copies per NIH3T3 cell (Schwanhäusser et al., 2011). In the same studies, the number for TOMM20 was determined to be 1449697 and 148155 respectively. The above means that there would approximately be 300 TOMM20 molecules per USP30 molecule in HeLa cells and 600 TOMM20 per USP30 molecule in NIH3T3 cells. This observation suggests that not all TOMM20 molecules would have a USP30 partner but also the stoichiometry between TOMM20 and USP30 can vary quite significantly between cell lines. Needless to say, the above ratio is probably an underestimate since it does not take into account the peroxisomal pool of USP30 that does not interact with TOMM20. Understanding the relative number of USP30 molecules in the cell will inform our thinking regarding its function in cellular physiology.

I wanted to estimate the number of USP30 molecules in the four cell lines that our team has been using to study USP30 function: HCT116, hTERT-RPE1, U2OS and SH-SY5Y. I performed these experiments in collaboration with my colleague, Jane Jardine. Jane and I seeded the cells in duplicate 10 cm dishes. Once they were confluent, we used one dish to count the number of cells and used the duplicate dish to perform RIPA lysis using 500 µl of lysis buffer. This way we were able to know how much protein was corresponding to what number of cells. Malte Gersch, a post-doctoral fellow in the lab of our collaborator David Komander at the MRC laboratory of Molecular Biology in Cambridge (UK) was so kind to supply us with some purified recombinant USP30 ($USP30_{64-502}$) of known concentration.

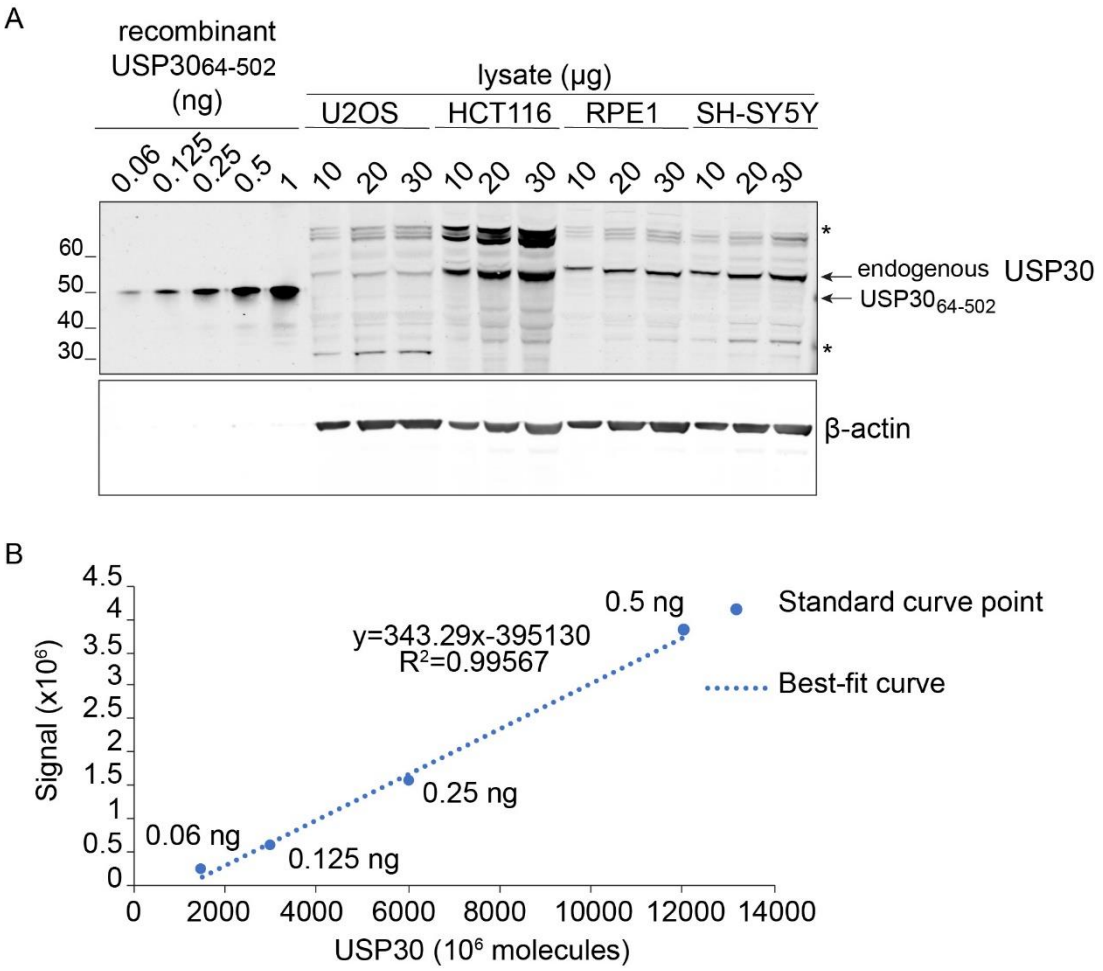

Figure 3.12: USP30 copy number in different cell lines

(A) Increasing amounts of purified recombinant USP30 (64-502) and 10, 20 and 30 µg of U2OS, HCT116, hTERT-RPE1 (RPE1) and SH-SY5Y lysates were loaded on the same gel. (B) The amount of recombinant USP30 was converted to number of molecules and plotted against the signal intensity of the bands. The equation describes the linear relationship between the x-axis (number of USP30 molecules) and y-axis (USP30 band intensity). R^2 is the linear regression term that describes the linearity of the relationship. * correspond to non-specific bands.

The purified USP30 was used to generate a standard curve with known absolute amounts of USP30, which I used to compare with known total protein loaded from our cell lines. I loaded 10, 20 and 30 µg of RIPA lysates from all the cell lines in order select the data points that fit best to the linear range of the standard curve (**Figure 3.12**).

The intensity corresponding to 1 ng of USP30 was a lot higher compared to the highest intensity band of USP30 in the cell lines, which was the 30 µg for the HCT116 cell line. By excluding the 1 ng data point I was ensuring that

the standard curve was generated from datapoints that are most relevant to the datapoints I was trying to use.

The U2OS cell lysate contained the least USP30, followed by SH-SY5Y, hTERT-RPE1 and lastly the HCT116 cells contained the highest. The above observation held true in terms of total cell lysate loaded, however it did not consider the number of cells that were lysed.

I next overlaid the standard curves with the datapoints from the cell lines (**Figure 3.13**). For the U2OS cell line, I only used the 20 and 30 µg datapoints that lay within the linear range of the standard curve (**Figure 3.13**A).

I used the equation to convert from USP30 band intensity to number of USP30 molecules, which I then normalised to the volume of lysate loaded. I then used the three different values from 10, 20 and 30 µg of lysate volume to generate a mean number of USP30 molecules per µl of lysate, except for the U2OS cells for which I only used the 20 and 30 µg datapoints. I then worked backwards converting the total number of cells lysed on the dish to cells lysed per volume of lysis buffer (500 µl). This allowed me to convert number of USP30 molecules/volume of lysate into number of USP30 molecules/cell (**Table 3.1**).

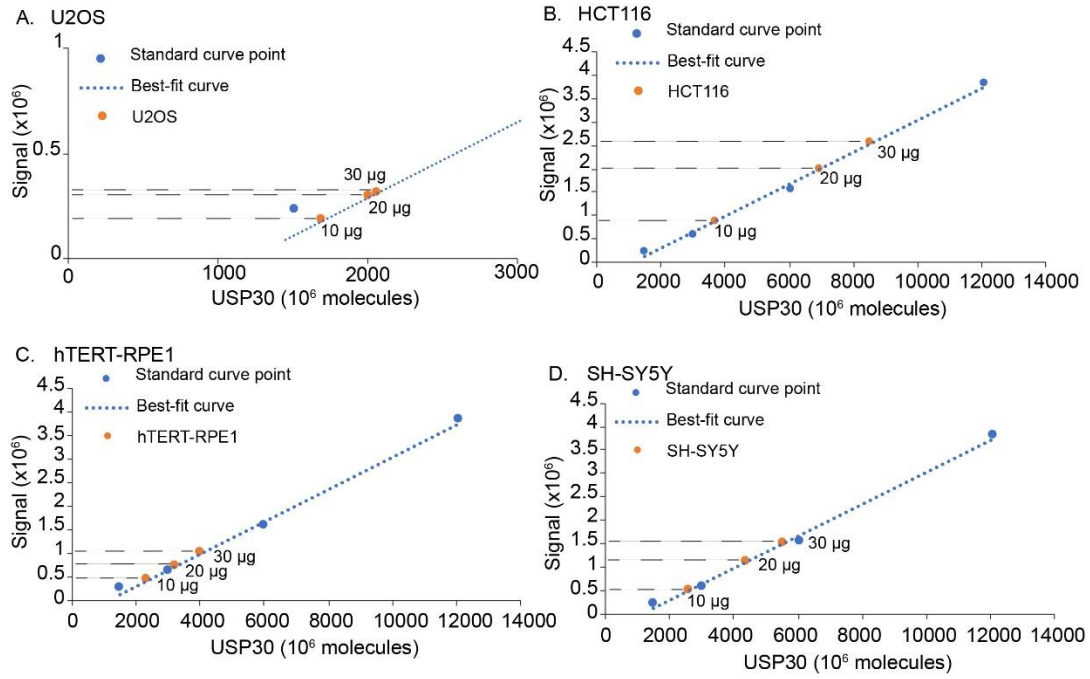

Figure 3.13: Quantification of USP30 copy number in model cell lines

Standard curves as Figure 3.12 plotted with the USP30 band intensity corresponding from 10, 20 and 30 µg of (A) U2OS, (B) HCT116, (C) hTERT-RPE1 and (D) SH-SY5Y cells.

Table 3.1: USP30 copy number in model cell lines

Cell Line	Number of cells lysed (x10^6)	Lysis buffer (µl)	Number of cells in lysate (cells/µl)	Number of USP30 (copies /µl)	Number of USP30 copies/cell
U2OS	4.68	500	9360	84808034.0	9060
HCT116	21.72		43400	769858132.2	17722
RPE1	2.55		5100	290384924.1	56938
SH-SY5Y	6.3		12600	327673900.2	26005

Table that summarises the calculations performed to determine the copy number of USP30 molecules in the four cell lines.

3.6 Conclusions

3.6.1 USP30 is an integral membrane protein of the OMM and peroxisomes

USP30 is an integral membrane protein on the OMM with its catalytic domain facing into the cytosol (Nakamura and Hirose, 2008). I have shown here that transfected USP30 also localises on peroxisomes (**Figure 3.4**) as our team has also shown for endogenous protein (Marcassa et al., 2018). I have shown that USP30 is an integral membrane protein on peroxisomes (

Figure 3.6) that is orientated with its catalytic domain facing into the cytosol just as in the mitochondria (**Figure 3.7**). As a team, we have shown that USP30 suppresses basal pexophagy as it suppresses basal mitophagy (Marcassa et al., 2018). My experiments show that USP30 behaves similarly to integral membrane proteins on mitochondria such as TOMM20 and integral membrane proteins on peroxisome membranes such as PMP70 (**Figure 3.14**). This indicates that the USP30 substrates relevant for peroxisomes and pexophagy are found on the cytosolic face and this has important implications for the biology of peroxisomes. A recent study confirmed our findings regarding the peroxisomal localisation and involvement of USP30 in pexophagy (Riccio et al., 2019a)

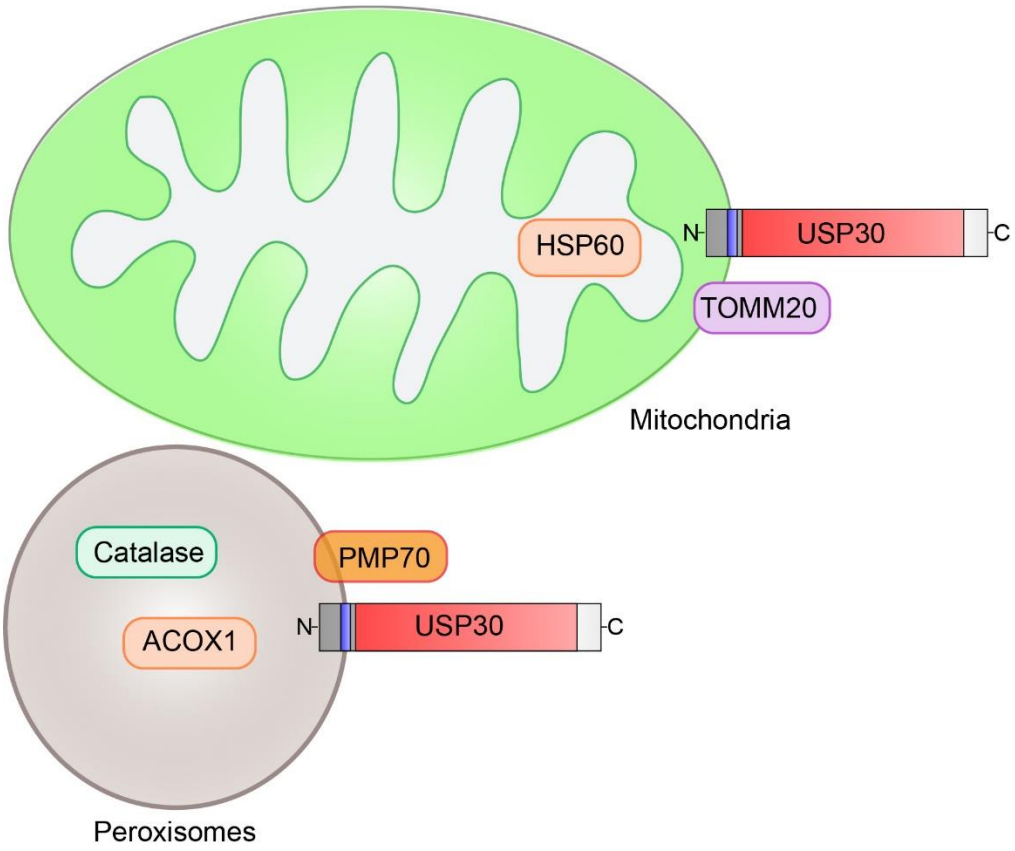

Figure 3.14: USP30 topology and orientation on mitochondria and peroxisomes

Graphical representation of USP30 membrane topology and orientation on mitochondria and peroxisomes in relation to other known organelle markers.

3.6.2 Identifying the sequence responsible for the peroxisomal localisation of USP30

Discovering a new subcellular localisation for a protein beckons the question how it reaches the compartments. I wanted to examine the sequences responsible for targeting to both mitochondria and peroxisomes (**Figure 3.15**). I validated the previously-identified poly-basic stretch after the TM domain and confirmed it was necessary for mitochondrial localisation. Interestingly, I found that neither KRmut1 nor 2 were able to reach peroxisomes. USP30 has a short TM domain of moderate hydrophobicity followed by a stretch of positive amino acids. In this regard, USP30 is similar to other mitochondrial localised proteins such as TOMM20 (Kanaji et al., 2000) and TOMM70 (Suzuki et al., 2002).

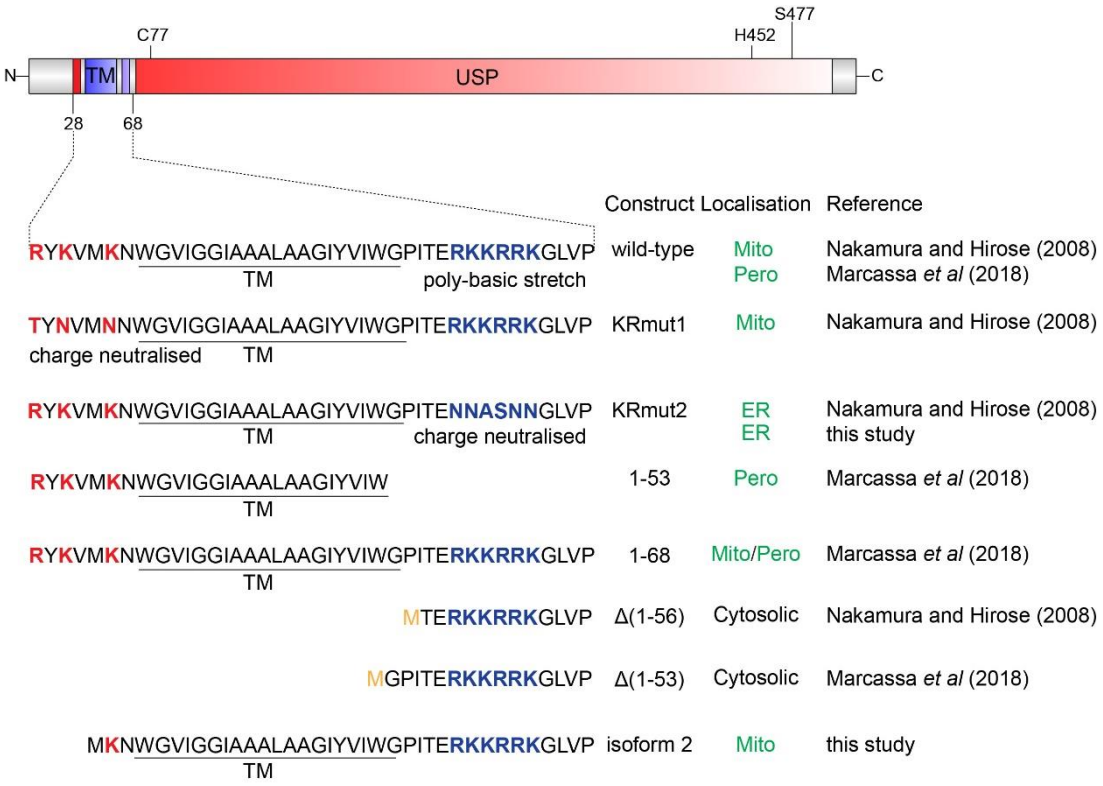

Figure 3.15: USP30 constructs and their localisations

Schematic diagram of USP30 protein showing the positions of the two stretches of basic amino acids flanking the trans-membrane (TM) domain identified by Nakamura and Hirose. The basic residues are shown in red for the amino acids preceding the TM domain and in blue for the stretch following the TM. The M residue shown in yellow is the initiator methionine residue introduced to generate the Δ(1-53) and Δ(1-56) truncations and is not part of the canonical USP30 sequence. The reported localisation of each construct and the reference therein is included. TM; trans-membrane domain, USP; ubiquitin-specific peptidase domain, Pero; peroxisomes.

The N-terminal fragment 1-53, encompassing the TM domain was sufficient to target USP30 to peroxisomes. Furthermore, mutating the three basic residues N-terminal to the TM domain showed a reduction in peroxisomal localisation. Lastly, USP30 isoform 2 that lacks two out of three basic residues N-terminal to the TM domain did not co-localise with PMP70 as well as isoform 1. The above piece of evidence suggests that the three basic residues N-terminus to the TM domain may be important for peroxisomes. A moderately hydrophobic TM domain flanked by positive charges was a common feature for Tail-anchored (TA) proteins, that localise to peroxisomes (Costello et al., 2017). In fact, the presence of a strong positive charge flanking the TM domain appeared to be the determining feature for peroxisomal

localisation. USP30 is atypical since it is not a tail-anchored protein. However it shares similarities with other known dually-targeted peroxisomal and mitochondrial tail-anchored proteins such as FIS-1 and MIRO-1,2 (Costello et al., 2017; Covill-Cooke et al., 2020).

Fluorescence microscopy using fluorescently-tagged proteins is a common procedure to establish the endogenous sub-cellular localisation of proteins as I have done above for the different constructs of USP30. In these sets of experiment I should have employed quantitative co-localisation analysis of the images acquired to score the degree of overlap of each construct to the sub-cellular compartment of interest such as Pearson's coefficient or Manders (Zinchuk et al., 2007).

Aitor Martinez-Zarate depleted mitochondria using A/O in YFP-Parkin hTERT-RPE1 cells, and then transfected USP30-mRFP into cells. Aitor's work showed that USP30-mRFP was still co-localising with peroxisomal markers, suggesting that mitochondria were not required for USP30 to reach peroxisomes (Marcassa et al., 2018). Many Peroxisomal Membrane Proteins (PMPs) traffic from the ER to peroxisomes through PEX16 (Hua et al., 2015) or through PEX19-mediated insertion into peroxisomal membranes (Kashiwayama et al., 2005). A recent study from the lab of Peter Kim demonstrated that co-expressing sa-PEX16a (PEX16 construct with an ER-stop anchor-sequence) and USP30-FLAG resulted in USP30-FLAG localising to the ER, without affecting its localisation to mitochondria. The above suggested that a portion of USP30 may traffic from the ER to peroxisomes through PEX16, a feature that is not shared with the mitochondrial pool (Riccio et al., 2019a). The above further supports our model that USP30 can be targeted to mitochondria and peroxisomes independently of each other and through distinct targeting sequences (Marcassa et al., 2018). The data thus far cannot exclude the possibility of additional mechanisms of targeting USP30 to peroxisomes that have yet to be discovered.

3.6.3 USP30 copy number varies greatly between cell lines

The calculation revealed that U2OS cells had the fewest USP30 molecules per cells at 9060, which was quite similar to the HeLa estimate

(Kulak et al., 2014). Surprisingly, the HCT116 cell line had the second lowest USP30 copies per cell at 17772 copies/cells despite showing the highest levels in the immunoblot (**Figure 3.12**). The neuroblastoma cell line SH-SY5Y came 2nd with 26000 copies/cell and the hTERT-RPE1 cells had the highest number of USP30 copies/cell with 56900 copies per cell (**Table 3.1**). It would have been very useful to determine the copy number of TOMM20 using the same methodology in our model cell lines, since that would allow me to calculate the ratio of TOMM20 to USP30 per cell and make comparisons to the existing datasets (Schwanhäusser et al., 2011; Kulak et al., 2014). Having the ratio of TOMM20 to USP30 in these cells would have been beneficial in understanding USP30 function. The above parameter has become increasingly significant since the recent discovery that USP30 deubiquitylates matrix proteins during their import through the TOMM complexes (Phu et al., 2020; Ordureau et al., 2020). The data suggests that USP30 promotes import of matrix proteins as they pass though the TOMM complexes and having an estimate of TOMM20 to USP30 ratio may facilitate to improve on our understanding of this model.

Chapter 4: The role of USP30 in the regulation of apoptosis

4.1 Introduction

USP30 has been extensively studied in the context of mitophagy, primarily on the PINK1/Parkin mitophagy axis and has emerged as a major target for therapeutic intervention in the treatment of Parkinson's disease (Bingol et al., 2014; Cunningham et al., 2015; Liang et al., 2015a; Marcassa et al., 2018; Harrigan et al., 2018). USP30 remains however somewhat understudied in the field of oncology. Two studies from our lab have identified USP30 as an interesting regulator of processes relating to cancer. Firstly, USP30 was shown to be required for HGF-dependent cell scattering of A549 cells, a characteristic of a metastatic phenotype and invasive behaviour of many tumours (Stella, 1999; Grotegut et al., 2006; Buus et al., 2009). The second study demonstrated that USP30 depletion enhanced the cellular response to BH3 mimetics, suggesting USP30 was opposing the mitochondrial pathway of apoptosis (Liang et al., 2015a).

The main objective of this chapter is to address the function of USP30 in the regulation of apoptosis. I will introduce new and more selective BH3 mimetic compounds as well as generate and characterise stably expressing USP30-GFP FlpIn cell lines for rescue experiments.

4.2 The HCT116 cell line

The hTERT-RPE1 YFP-Parkin cells were the primary cell line that was used to study apoptosis in the past in the lab (Liang et al., 2015a). I selected the HCT116 cells as my primary model cell line to study apoptotic cell death in the context of USP30 while in parallel keeping the hTERT-RPE1 without Parkin overexpression as a reference cell line.

The HCT116 cells are an established human colorectal cancer cell line of epithelial origin. HCT116 cells are wild-type for p53 and were shown to elicit p53-dependent responses under conditions of DNA damage (Liu and Bodmer, 2006). It is therefore an appropriate cell line to study p53-dependent cell death should that become relevant. Interestingly, HCT116 cells are one of the few colorectal cancer cell lines to retain Parkin expression (Poulogiannis et al.,

2010). This was of importance to my study as USP30 opposes PINK1/Parkin-mediated mitophagy and may also oppose other, for example known tumour suppressive, functions of Parkin (Liu et al., 2018a). Furthermore, our lab has acquired the HCT116 lacZeo TO FlpIn TRex from Stephen Taylor (University of Manchester, UK), a cell line that allows for the generation of stable cell lines, expressing transgenes from a unique locus, under the control of a tetracycline repressor.

4.3 Optimisation of siRNA-mediated knockdown in HCT116 FlpIn TRex cells

There are many products marketed to allow for efficient uptake of short interfering (si)RNA oligos in cells, most of which are liposome-based. Two reagents routinely used in the lab for siRNA oligos are Oligofectamine (Invitrogen) and Lipofectamine RNAiMax (Invitrogen) hereafter referred to as RNAiMax.

I performed a small number of experiments in order to determine which of the two was the most appropriate for use with the HCT116 FlpIn TRex cell line using two oligos against USP30 (D1 and D3) and the non-targeting oligo (NT1). I compared the two reagents in parallel by performing a 72-hour knockdown with 40 nM siRNA in HCT116 FlpIn TRex cells using a forward and a reverse knockdown protocol. In the reverse protocol the seeding and the knockdown are performed on the same day whereas in the forward protocol the knockdown is performed the day after seeding.

Depletion of USP30 by either of the two oligos (D1 and D3) was overall more efficient when RNAiMax was used compared to Oligofectamine (**Figure 4.1**). Interestingly, I observed a reduction in the levels of MCL-1 with oligo D3 using the RNAiMax protocol but not with Oligofectamine, which was also less efficient, particularly in the reverse protocol setting, at reducing USP30 levels. The reduction in the levels of MCL-1 by oligo D3 was previously shown to reflect a decrease in the levels of MCL-1 mRNA in YFP-Parkin hTERT-RPE1, U2OS and MCF7 cells, and since it was only seen by a single oligo against USP30 (D3) it was considered a non-specific effect (Liang et al., 2015a).

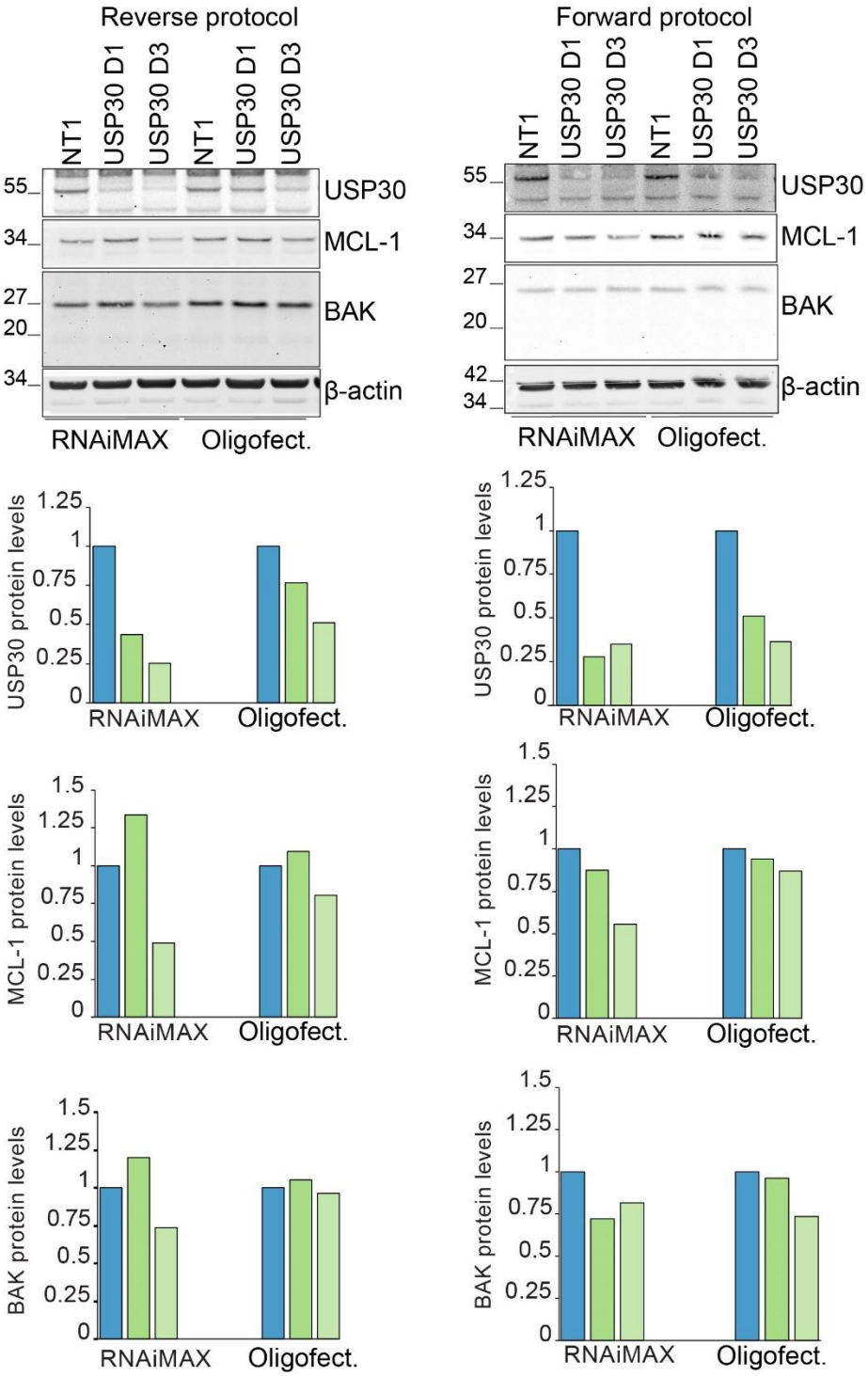

Figure 4.1: RNAiMax outperformed Oligofectamine in depleting USP30 in HCT116 FlpIn TRex cells

HCT116 FlpIn TRex cells were transfected with 40 nM siRNA oligos against USP30 (D1 and D3) or non-targeting oligo (NT1) using RNAiMax and Oligofectamine (Oligofect.) following a reverse (left) or a forward (right) transfection protocol for a total of 72 hours. Cells were subsequently lysed in RIPA buffer supplemented with MPIs (1:250) and 20 µg protein were resolved on a NuPAGE gel and probed for USP30, MCL-1, BAK and β-actin. The normalised quantitation for each protein relative to NT1 is shown in the bar charts. Data is from a single independent experiment (n=1).

There was a small increase in the levels of BAK in the cells treated with the D1 siRNA using the reverse transfection protocol. The increase in BAK had previously been seen consistently using both siRNA oligos against USP30 in the three aforementioned cell lines (Liang et al., 2015a). I have selected to use RNAiMax as the standard reagent for siRNA depletion experiments in HCT116 FlpIn TRex cells, since the reagent is overall more efficient in depleting USP30 in my cell line and allows me to use either the forward or the reverse protocol for more versatility in experiments.

4.4 USP30 depletion and apoptotic cell death

The first experiments were aimed at testing whether USP30 depletion enhances the response to ABT-737 in my model cell line, as previously had been shown in hTERT-RPE1 YFP-Parkin cells, MCF7 and U2OS (Liang et al., 2015a). I investigated this using live cell imaging since that would allow me to see the kinetics of the process. I depleted USP30 using two siRNAs (D1 and D3) and then prepared the cells for live-cell imaging by incubating the cells with fresh media supplemented with Annexin V conjugated to AF350, 0.1 µM DRAQ7 and 2.5 mM $CaCl_2$. The Annexin V conjugate allowed me to visualise cells that have externalised phosphatidyl-serine (PS), which is a hallmark of apoptotic cell death. Supplementing media with Calcium Chloride ($CaCl_2$) allows Annexin V to bind PS more efficiently. DRAQ7 is a cell-impermeable dye that functions very similarly to propidium iodide used in flow cytometry experiments, whereby it only stains the nuclei of cells with breached cell surface membranes. I induced apoptosis with 20 µM ABT-737, a concentration previously shown to induce apoptosis in these cells (Okumura et al., 2008), and took images every hour for a total of 15 hours of treatment. I then selected four time points from the movies to quantitate the number of apoptotic cells based on PS externalisation (Annexin V-binding on cell membrane) and DRAQ7 uptake (**Figure 4.2**). I observed substantial levels of cell death over the course of the experiment, reflected by the number of Annexin V and DRAQ7 positive cells that were increasing with time in all conditions even in the absence of an apoptotic stimulus. This made visualising the effect of treating the cells with ABT-737 difficult.

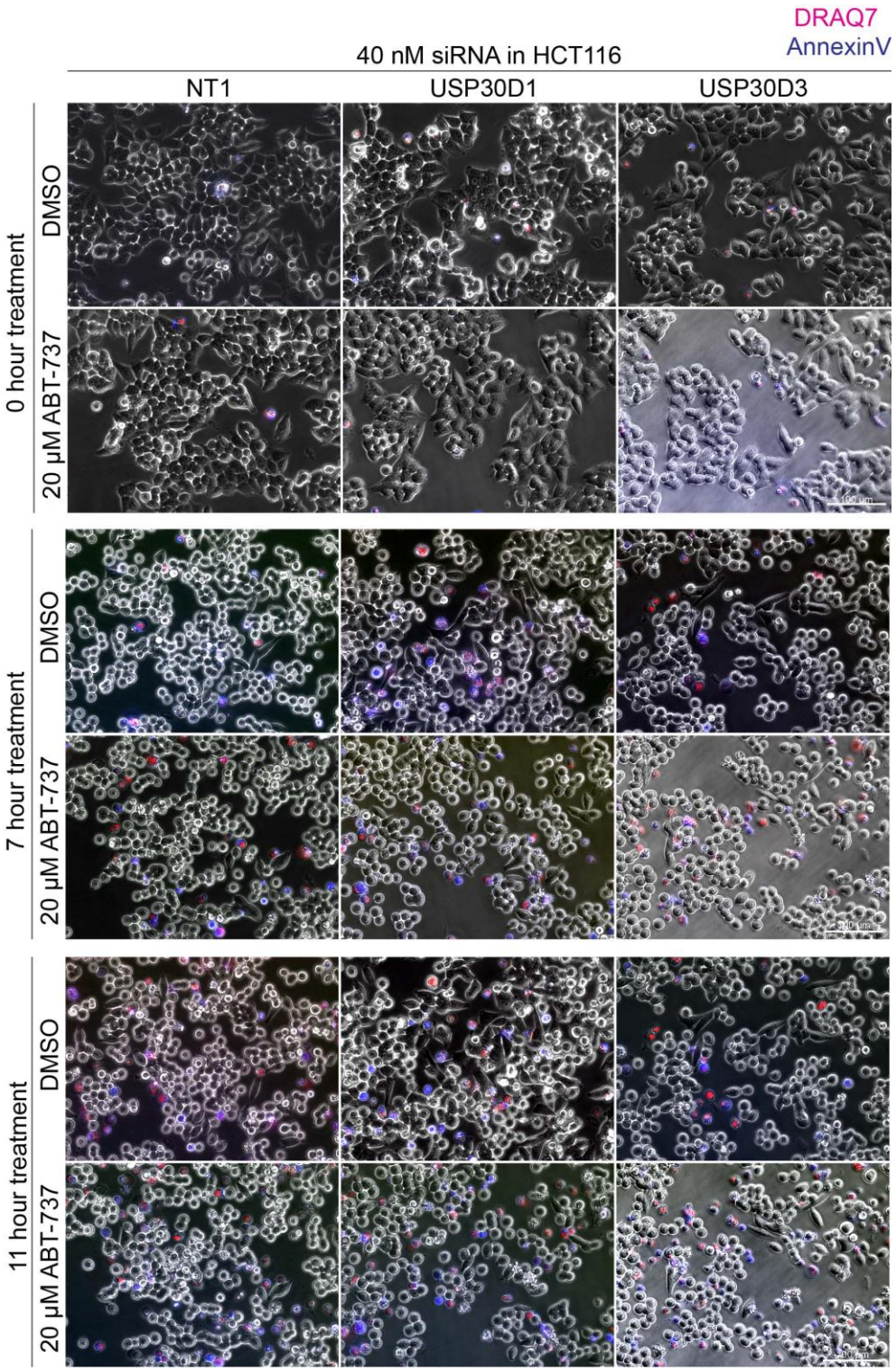

Figure 4.2: Monitoring apoptosis with live-cell imaging

HCT116 cells were transfected with two oligos against USP30 (D1 and D3) or non-targeting (NT1) for 60 hours. Cells were treated with DMSO or 20 μM ABT-737 for a further 15 hours. The cells were imaged in the presence of Annexin V-AlexaFluor 350 (blue) and membrane impermeable dye DRAQ7 (magenta) every hour under a 20x objective on a Nikon TiEclipse microscope. Representative fluorescent images of each condition at 0, 7 and 11 hours are shown in the panel as still images. Scale bar represents 100 μm and the time indicates duration of the drug treatment.

The data suggested that USP30 depletion induced basal cell death (0^{th} time point). At all other time-points, the normalised levels of cell death were elevated in the USP30 depleted cells compared to the control oligo (**Figure 4.3**). The effect was more pronounced with oligo D3 presumably due to the afore-mentioned effect on reducing levels of MCL-1. The differential was most prominent at the 3^{rd} hour time point where the levels of cell death in the USP30-depleted cells were double than the control. From that point onwards the cell populations displayed similar levels of cell death, suggesting the experiment may have reached saturation in terms of signal. The data suggested that USP30-depleted cells were undergoing apoptosis with accelerated kinetics compared to the control.

This experiment was also technically difficult to quantitate as the cells are quite small and therefore hard to segment. Imaging may not be the best suited methodology to study HCT116 cells, and it is better suited for cell lines that are flatter. Furthermore, the repeated exposure to a light source may have exacerbated the high levels of basal cell death observed.

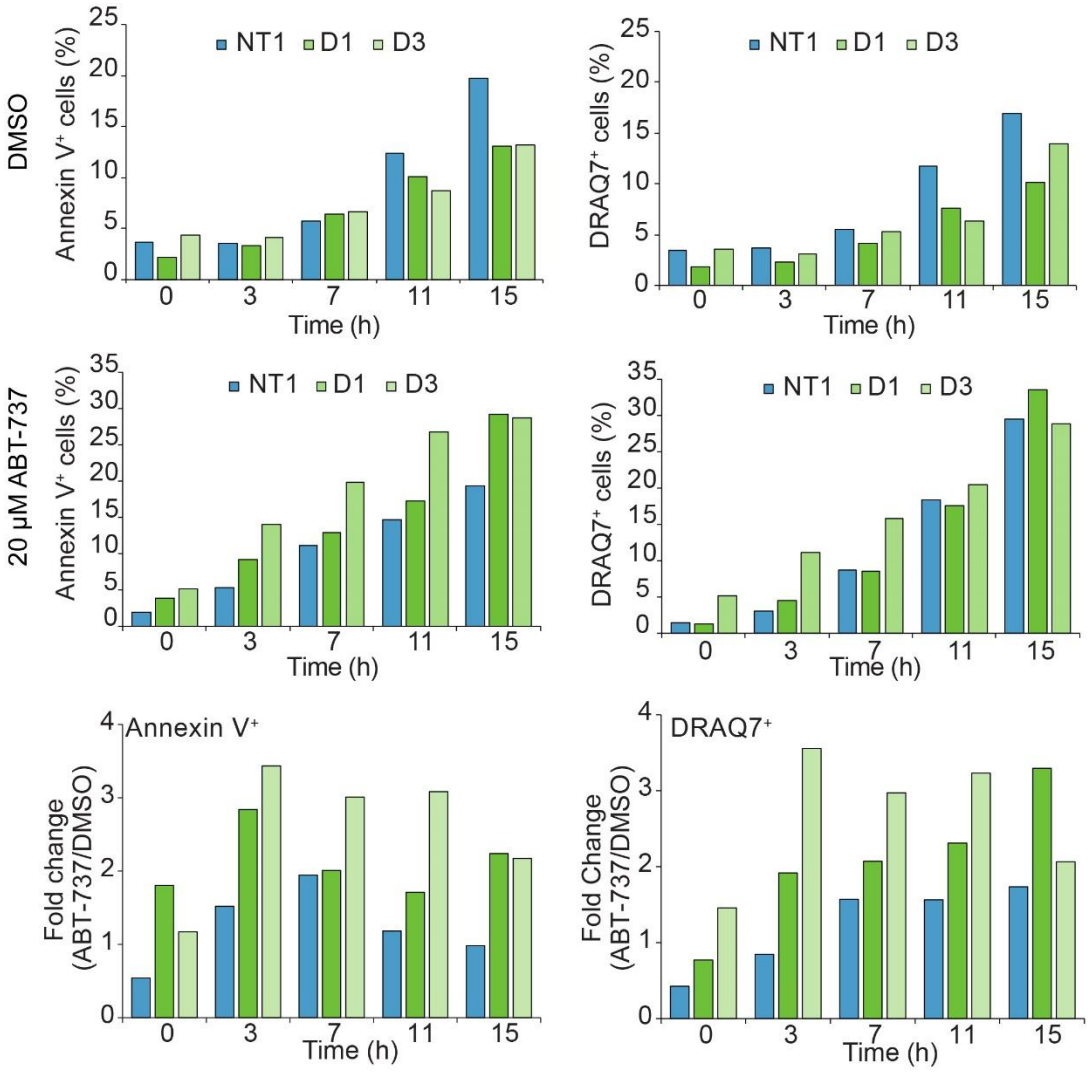

Figure 4.3: Quantitation of cell death in USP30-depleted HCT116 cells by live-cell imaging

The bar charts show the percentage (%) of Annexin V$^+$, DRAQ7$^+$ cells and the normalised percentages of the ABT-737 treatment to the DMSO (vehicle) control at 0, 3, 7, 11 and 15 hours from the live-cell imaging experiment in **Figure 4.2**.

In a separate set of experiments I set out to assess apoptosis biochemically by monitoring PARP cleavage after 15 hours of treatment with ABT-737. My colleague, Elena Marcassa, had prepared the analogous experiment in hTERT-RPE1 cells, which I also lysed and analyzed (**Figure 4.4**). I probed for USP30 to assess the efficiency of the knockdown as well as a number of protein markers relating to apoptotic cell death. The USP30-depleted HCT116 displayed clearly higher levels of cleaved PARP (p85 fragment) compared to the control oligo NT1, suggesting sensitisation to ABT-737.

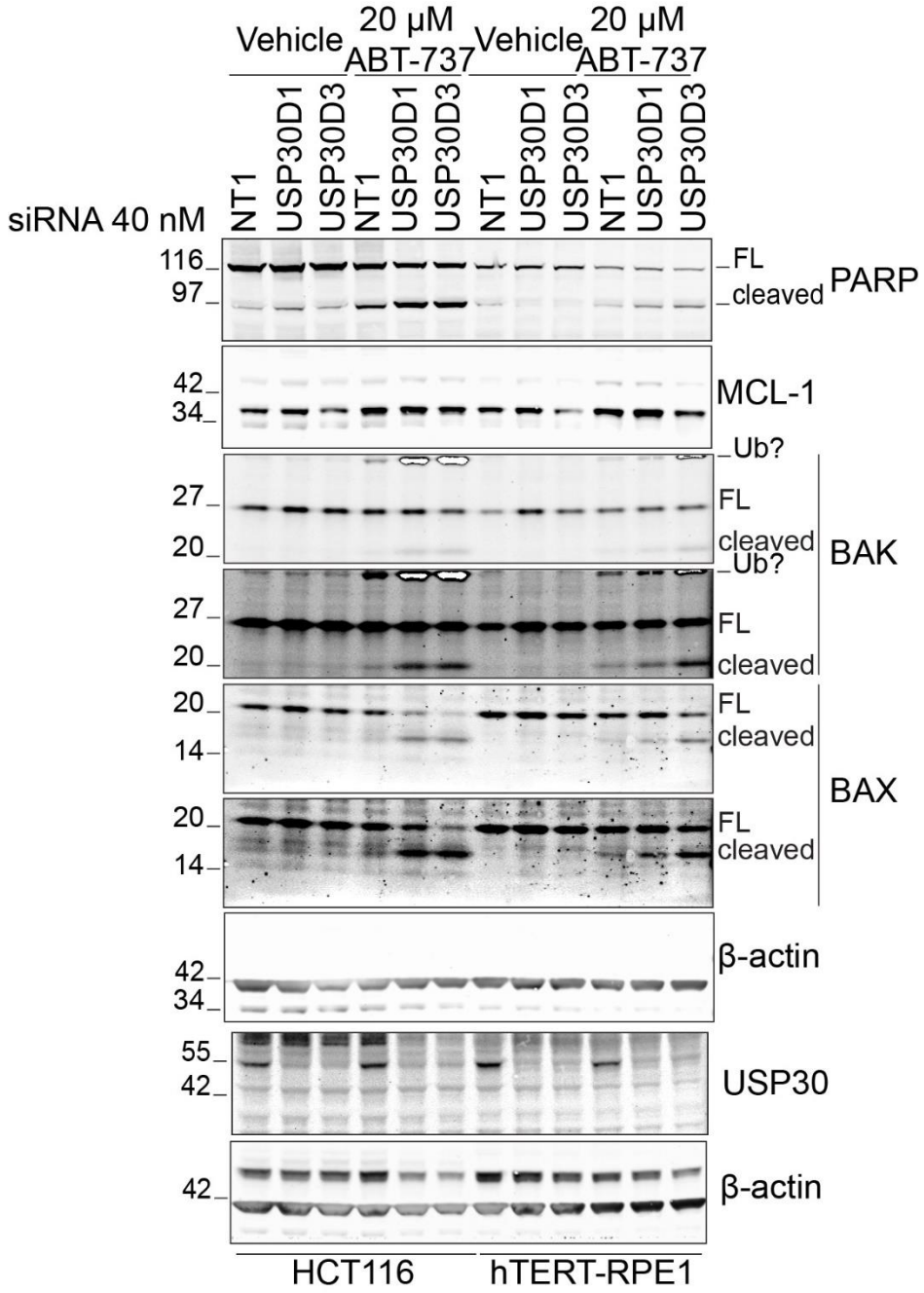

Figure 4.4: **USP30 depletion sensitizes HCT116 and hTERT-RPE1 cells to ABT-737**

HCT116 and hTERT-RPE1 cells were transfected with two siRNA oligos against USP30 (D1 and D3) or non-targeting oligo (NT1) for 60 hours before being treated with 20 μM ABT-737 for 15 hours. Cells were lysed in RIPA buffer and analysed by Western blotting. F, full length; Ub?, potential ubiquitylated species. White bands are saturated.

A similar behaviour was seen for the hTERT-RPE1 cells. Overall, sensitization to ABT-737 was observed in both cell lines when USP30 was depleted. However, I also made a number of additional interesting observations in this experiment. I observed lower molecular weight bands of BAX and BAK, most likely corresponding to cleavage products, which were more evident in the USP30-depleted cells. Cleavage of BAX during strong induction of apoptosis has been previously described as a calpain-dependent response generating an 18 kDa fragment that promotes apoptotic cell death (Wood et al., 1998; Cao et al., 2003). The pattern of BAX cleavage directly correlated with the cleavage pattern for PARP.

The most interesting observation was the appearance of higher molecular weight species in the BAK blot labelled as “Ub-BAK” that appeared to be equally enhanced in USP30-depleted cells (**Figure 4.4**). The molecular weight of this previously uncharacterised species was around 32 kDa, which is about 8 kDa higher than the molecular weight of unmodified BAK (23.4 kDa). Since the blot (**Figure 4.4**) was very tightly cropped and the bands in question oversaturated in the exposure I re-ran the same samples again without cutting the membrane horizontally in order to get a better picture. There were no additional bands in the higher molecular weight range and the shift in molecular weight was consistent with the addition of a single ubiquitin moiety onto BAK, suggesting this might be a mono-ubiquitylation event (**Figure 4.5**).

The intensity of the band correlated with the degree of PARP cleavage and it therefore seemed to correlate with strong induction of apoptosis. If this band was indeed corresponding to a ubiquitylated species, then its increased abundance in the USP30-depleted cells may indicate that BAK is a direct substrate of USP30. The above would open the possibility that USP30 depletion enhances apoptosis by modulating BAK, especially since it has been shown that ubiquitylation of BAK by Parkin regulates BAK activity during apoptosis (Bernardini et al., 2019).

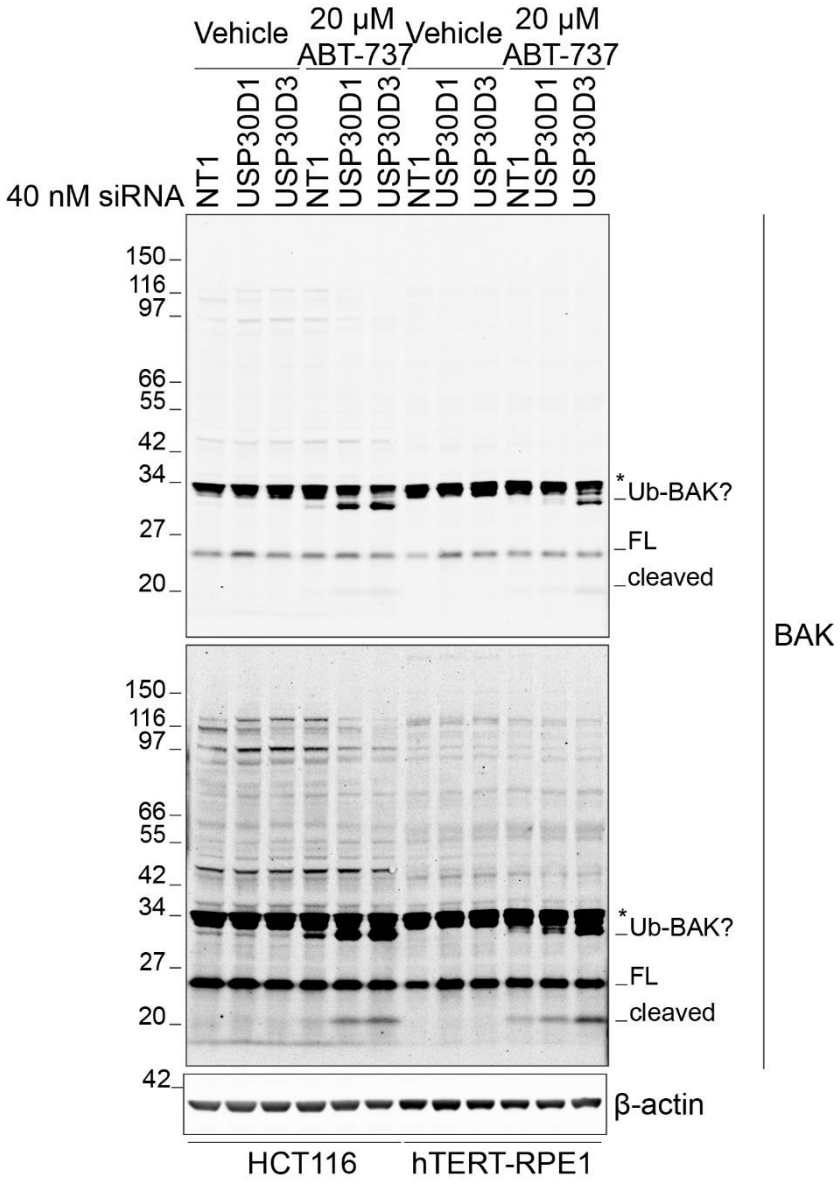

Figure 4.5: Only a single species of ubiquitylated BAK is visible

HCT116 and hTERT-RPE1 cells were transfected with two siRNA oligos against USP30 (D1 and D3) or non-targeting oligo (NT1) for 60 hours before being treated with 20 μM ABT-737 for 15 hours. Cells were lysed in RIPA buffer and analysed by Western blotting. The samples are the same as in **Figure 4.4**. FL, full length; Ub?, potential ubiquitylated species; *, non-specific band.

4.5 Does BAK become ubiquitylated during apoptosis?

I decided to further explore the appearance of the suspected “Ub-BAK” band before revisiting the sensitisation phenotype.

I wanted to specifically address whether the band:

1. was truly a ubiquitylated species and specific to BAK,
2. dependent on USP30,
3. contributed to induction or was the result of stronger apoptosis

4.5.1 BAK is ubiquitylated on K113

BAK has been shown to be targeted for proteasomal degradation in Human Papilloma Virus (HPV)-infected cells by the viral onco-protein E6 (Thomas and Banks, 1998). Viral E6 is able to recruit the E3 ubiquitin ligases E6AP and HERC1 to ubiquitylate BAK and target it for proteasomal degradation (Thomas and Banks, 1998; Holloway et al., 2015).

BAK and USP30 share similar membrane topologies. Both proteins have trans-membrane (TM) domains that anchor them to the OMM while their functional domains are facing the cytosolic face. Only a small fragment is exposed in the inter mitochondrial membrane space (IMS). BAK has two lysines (K113 and K210) and only K113 is exposed on the cytosolic face and thus the only likely lysine residue that can be targeted by the UPS (**Figure 4.6**). Indeed, K113R mutant BAK has previously been shown to be rescued from proteasomal degradation by HPV E6/HERC1, demonstrating that K113 was the relevant residue in this context (Holloway et al., 2015). Ubiquitylated K113 is also the only position that could theoretically be targeted by USP30 during apoptosis. Interestingly, data from PhosphositePlus (v6.5.9.3) revealed that K113 is conserved between human, mouse and rat, however, the residue has not been identified as a ubiquitylation site in any of the three species. Instead, K118 was identified as a ubiquitylation site in the mouse but the residue does not correspond to a lysine residue in human BAK.

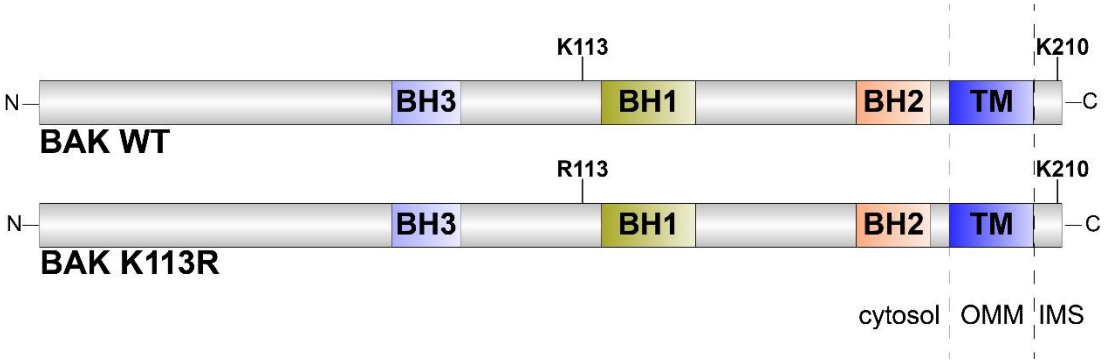

Figure 4.6 The topology of BAK on mitochondria

Diagram depicting the topologies of BAK WT and BAK mutant K113R and. Lysines 113 and 210, and mutated residue K113R are shown. The N- and C-termini, domains and trans-membrane (TM) domains are indicated. Topologies are indicated as cytosolic (cytosol), outer mitochondrial membrane (OMM) and inter mitochondrial membrane space (IMS).

I was concerned that the putative Ub-BAK band I had observed reflected non-specific cross-reactivity of the BAK antibody I was using. I therefore made use of a GFP-tagged BAK construct in order to circumvent the limitation of using a BAK antibody. Simultaneously, it allowed me to introduce the K113R mutation and determine whether this was the relevant putative ubiquitylation site. I used the epitope-tagged version of the wild-type and K113R BAK to assess whether a higher molecular weight species for this transgene can be visualised and whether this is dependent on K113.

4.5.2 GFP-BAK is not modified during apoptosis

I co-transfected GFP-BAK and GFP-BAK K113R with a plasmid carrying His-myc-Ubiquitin as co-transfection of cells with ubiquitin plasmids promotes ubiquitylation and that would make visualising ubiquitylated species easier. I then induced cell death using 20 μM ABT-737. GFP-BAK wt and K113R were successfully transfected at very similar levels to each other. “Ub-BAK” was visible at the endogenous level and was not affected by the transfection of the GFP-tagged nor the His-myc-ubiquitin constructs (**Figure 4.7**).

However, there were no corresponding high molecular weight bands for “ubiquitylated” GFP-tagged BAK visible neither with the BAK or the GFP antibody (**Figure 4.7**). This experiment suggested that GFP-BAK was not ubiquitylated or the band that I was observing was not BAK to begin with.

In order to address the above question, I returned to endogenous BAK and obtained two additional independent antibodies. The BAK antibody I was originally using and had seen the “Ub-BAK” with, was the rabbit polyclonal BAK G-23 (sc-832) from Santa Cruz (SC) Biotechnologies. I selected two additional BAK antibodies whose reported immunogens mapped to a distinct part of the BAK protein (**Figure 4.8**). I chose the mouse monoclonal anti-BAK AT38E2 (sc-517390) from SC, hereafter referred to as mouse SC and the rabbit polyclonal anti-BAK from Sigma-Aldrich (B5897).

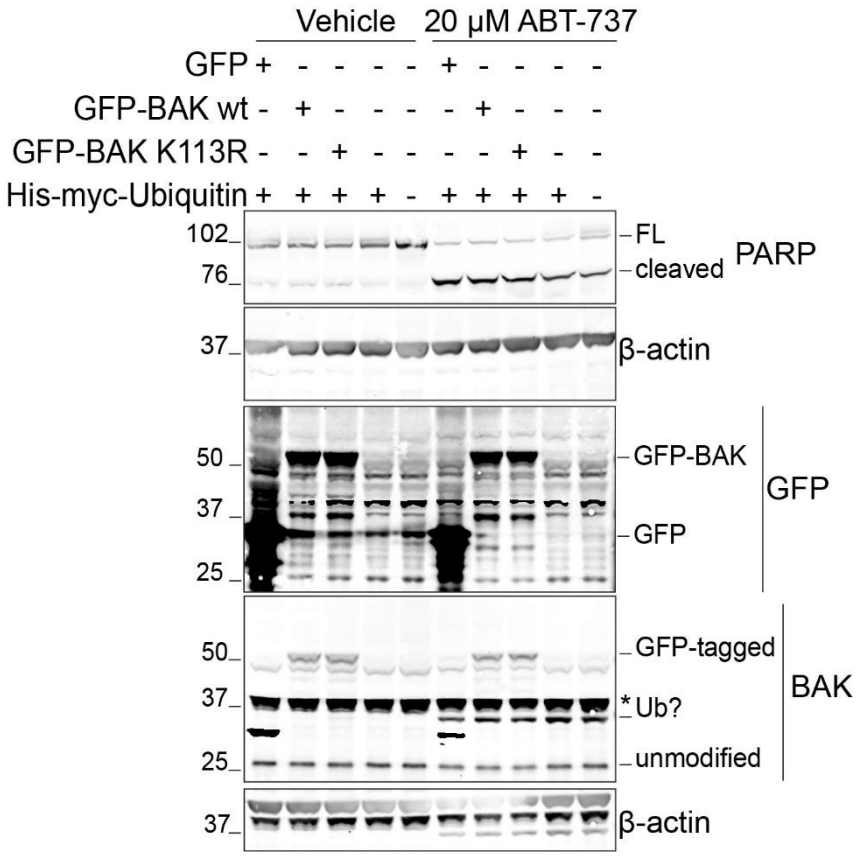

Figure 4.7: GFP-tagged BAK is not modified during apoptosis

HCT116 cells were co-transfected with His-myc-Ubiquitin and GFP (empty vector) or GFP-BAK wt or GFP-BAK K113R for 24 hours. Cells were subsequently treated with 20 μM ABT-737 for 15 hours, lysed in RIPA and analysed by Western blotting. FL, full length; Ub?, Ubiquitylated species?; *, non-specific band.

4.5.3 Only one anti-BAK antibody reacts with “Ub-BAK”

I tested whether any of the two new anti-BAK antibodies were able to detect “Ub-BAK” in addition to the one I was already using and in parallel assessed their specificity towards unmodified BAK itself. I depleted BAK using siRNA in HCT116 and hTERT-RPE1 cells and performed an immunoblot using these antibodies. In parallel, I depleted USP30 in HCT116 FlpIn TRex cells, which I treated with 20 μM ABT-737 for 15 hours. All antibodies used were specific for detecting full length unmodified BAK (**Figure 4.8**A). However, only the rabbit anti-BAK G-23 SC was able to detect “Ub-BAK” in the experiment when cell death was induced (**Figure 4.8**A). I checked where the immunogens used in the generation of the antibodies mapped on the BAK protein. The rabbit anti-BAK G-23 epitope lies between residues 75-125 and covers the potential

ubiquitylation site K113 (**Figure 4.8**B). The addition of a single ubiquitin moiety on K113 could in principle block access of the antibody to the epitope however that does not seem to be case, since the BAK G-23 antibody is the only one that reacts with this band. The rabbit anti-BAK from Sigma-Aldrich recognises an epitope near the N-terminus of BAK and addition of ubiquitin at K113 should not block it (**Figure 4.8**B). The immunogen of the mouse monoclonal anti-BAK from SC provided covers a very large part of BAK, residues 29-187 and the exact epitope of the monoclonal antibody is unknown as it is proprietary information. The data so far was shedding some serious doubts on whether the putative BAK band was BAK to begin with. I therefore used a more direct approach to address this question using siRNA-mediated depletion of BAK.

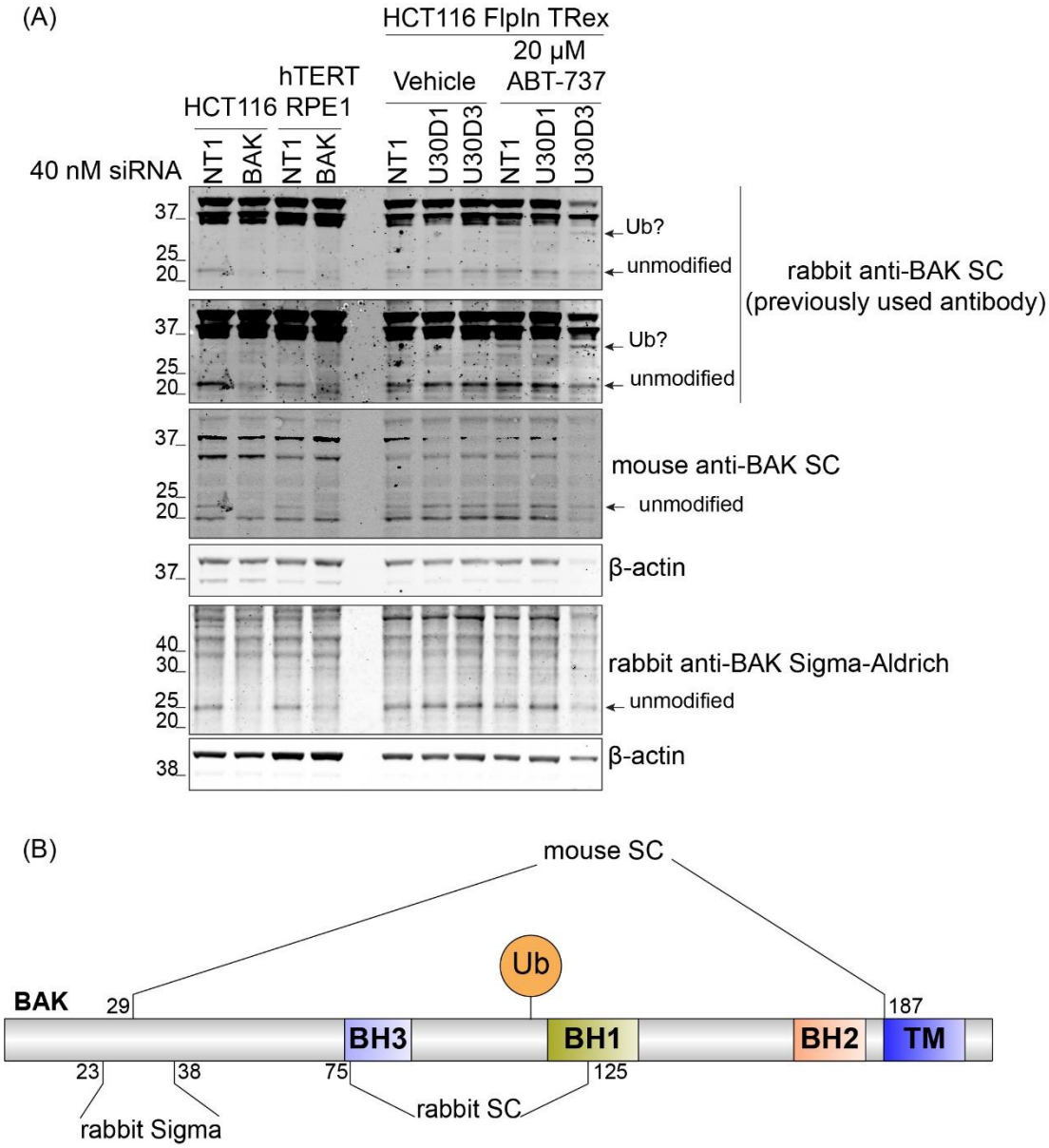

Figure 4.8: Reactivity of BAK antibodies against unmodified and "Ub-BAK"

(A) HCT116 and hTERT-RPE1 cells were transfected with 40 nM siRNA oligos against BAK or non-targeting oligo (NT1) for 72 hours. HCT116 FlpIn TRex cells were transfected with 40 nM nucleotides against USP30 (D1 and D3) or non-targeting oligo (NT1) for 60 hours before being treated with 20 μM ABT-737 for 15 hours. Ub?, suspected ubiquitylated species.
(B) Schematic diagram mapping the epitopes of the three anti-BAK antibodies used in (A) above.

4.5.4 BAK depletion does not abolish putative “Ub-BAK”

In this experiment I depleted BAK, BAX and BAK/BAX together in hTERT-RPE1 cells and induced cell death using A-1210477 and A-1331852, which target MCL-1 and BCL-X_L respectively (4.6) that I knew induced a strong response. BAK depletion only marginally prevented apoptotic cell death as seen by PARP cleavage, whereas BAX depletion alone was sufficient to ablate cell death altogether, bringing it to the same levels as the combined depletion of BAK and BAX (**Figure 4.9**).

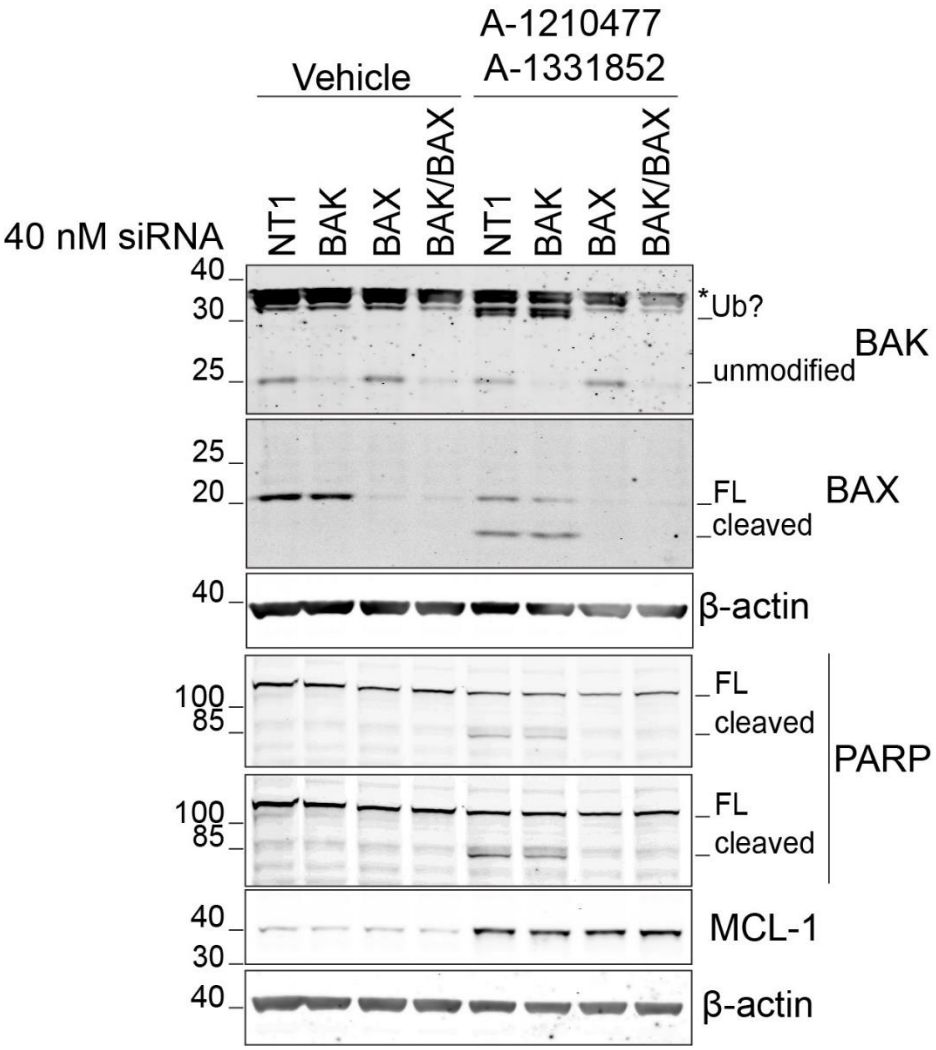

Figure 4.9: "Ub-BAK" is not dependent on BAK in hTERT-RPE1 cells
hTERT-RPE1 cells were transfected with 40 nM siRNA oligos against BAK, BAX, both BAK/BAX and non-targeting oligo (NT1) for 60 hours before being treated with 10 µM A-1210477 and 100 nM A-1331852 for an additional 17 hours. Cells were lysed in RIPA supplemented with PhosSTOP and MPIs (1:250). Ub, suspected ubiquitylated species; FL, full length; *, non-specific bands.

The appearance of the suspected ubiquitylated species again correlated closely with the levels of cleaved PARP (**Figure 4.9**). However, depletion of BAK did not prevent cell death nor the appearance of the “Ub” band suggesting this band was not BAK.

4.5.5 Putative Ub-BAK band is also seen in BAK KO cells

I wanted to confirm the above finding by using a BAK KO cell line. I induced cell death in wild-type and BAK KO HCT116 cells and monitored whether the band was still appearing in response to BH3 mimetics. The experiment demonstrated that even in BAK KO cells the “Ub-BAK” was still observed (**Figure 4.10**), demonstrating that the band does not correspond to BAK.

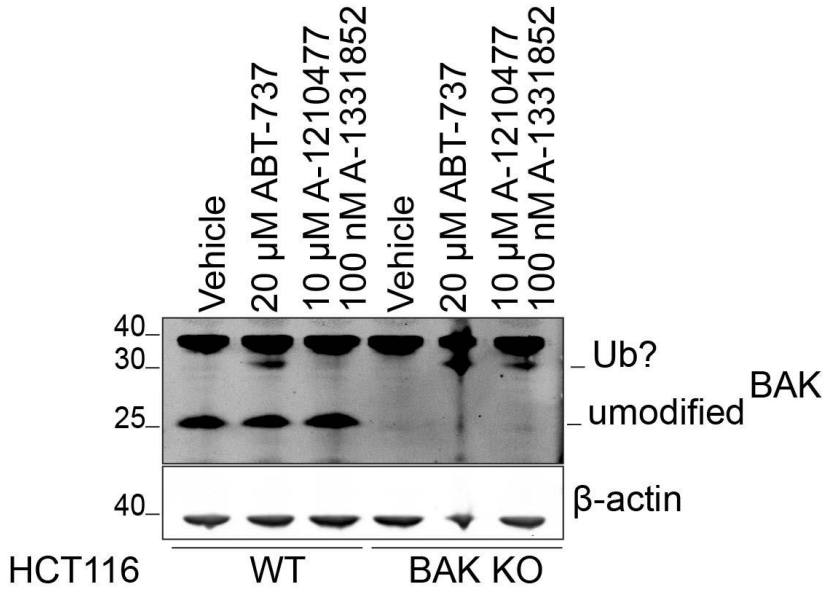

Figure 4.10: "Ub-BAK" is not dependent on BAK in HCT116 BAK KO cells
HCT116 wt and BAK KO cells were treated with 20 µM ABT-737 or 10 µM 1210477 and 100 nM A-1331852 for 17 hours. Cells were lysed in RIPA supplemented with PhosSTOP and MPIs (1:250). Ub, suspected ubiquitylated species.

4.6 Investigating the baseline response of HCT116 FlpIn TRex and hTERT-RPE1 FlpIn cells to different BH3 mimetics.

The previously published work on USP30 and apoptotic cell death demonstrated that USP30 depletion enhanced the cellular response to ABT-737 in YFP-Parkin hTERT-RPE1, MCF7 and U2OS cells (Liang et al., 2015a). I wanted to revisit and expand this further in the HCT116 cells, and in parallel use the hTERT-RPE1 cells, without the Parkin overexpression as a comparison. First, I established the basal sensitivities of these cells to an array of different BH3 mimetics in order to determine their dependence for survival on specific members of the anti-apoptotic BCL-2 family such as BLC-2, BCL-X_L, MCL-1 and BCL-w. I used ABT-737 that targets BCL-2, BCL-w and BCL-X_L, but not MCL-1, and introduced other BH3 mimetic compounds that target individual members of the anti-apoptotic BCL-2 family such as ABT-199 targeting BCL-2, A-1210477 targeting MCL-1 and A-1331852 targeting BCL-X_L only (**Figure 1.19**). I treated HCT116 FlpIn TRex and hTERT-RPE1 FlpIn TRex cells with the indicated BH3 mimetics and probed for p85 PARP to assess the effectiveness of the compounds in inducing apoptosis (**Figure 4.11**). Treatment of HCT116 with 10 μM ABT-737 for 4 hours led to very low levels of cleaved PARP while treatment with ABT-199 or A-1210477 did not induce a response. Treatment with A-1331852 yielded higher levels of cleaved PARP than ABT-737 and the highest response was seen when cells were treated with both A-1210477 and A-1331852. The hTERT-RPE1 FlpIn TRex cells were showing a very weak response to ABT-737 and no response to any of the other single agents. The cells however displayed a very strong response to simultaneous treatment of A-1210477 and A-1331852, suggesting a strong co-dependence on MCL-1 and BCL-X_L (**Figure 4.11**). These sets of experiments in HCT116 FlpIn TRex and hTERT-RPE1 FlpIn TRex allowed me to establish the baseline responses of these cell lines to the different BH3 mimetics and understand which anti-apoptotic BCL-2 family members are critical for their survival.

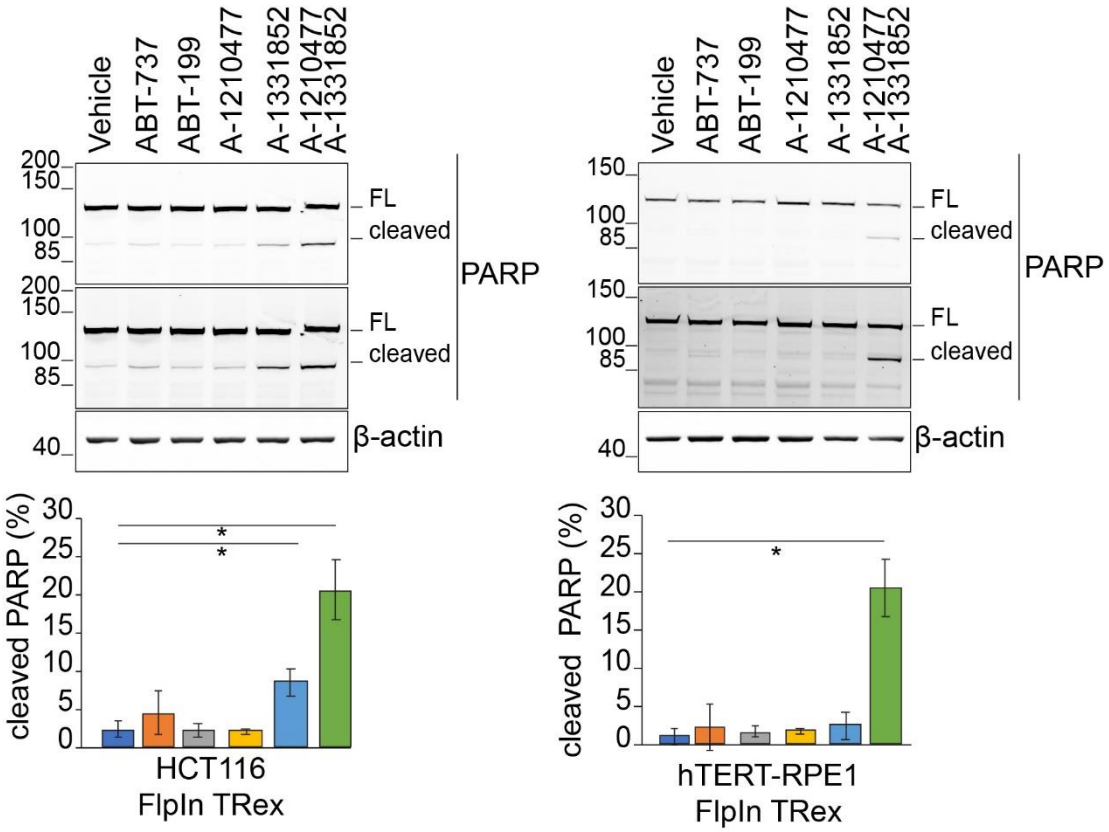

Figure 4.11: HCT116 FlpIn TRex and hTERT-RPE1 FlpIn TRex cells are dependent on BCL-X_L and MCL-1 for survival

HCT116 FlpIn TRex and hTERT-RPE1 FlpIn TRex cells were treated with 10 µM ABT-737 or 100 nM ABT-199 or 10 µM A-1210477 or 100 nM A-1331852 or a combination of 10 µM A-1210477 and 100 nM A-1331852 or DMSO (vehicle) for 4 hours. Cells were lysed in RIPA supplemented with PhosSTOP and MPIs (1:250) and cell lysates were probed as indicated. Quantitation of percentage of cleaved PARP to total PARP (cleaved fragment + FL) for each condition are shown as the mean percentage ± S.D. of three independent experiments (n=3). One-way ANOVA with Dunnett correction. *, P< 0.05; FL, full length PARP; cleaved, cleaved PARP fragment.

4.7 USP30 depletion sensitizes HCT116 cells to BH3 mimetics

All the previous work on apoptotic cell death in the context of USP30 depletion was performed using ABT-737 and the related compound ABT-263 (Liang et al., 2015a). I have also reproduced these findings using ABT-737 in HCT116 and hTERT-RPE1 cells (**Figure 4.4**). As an additional step I wanted to investigate what the effect of USP30 depletion was on the response of cells to the wider range of BH3 mimetics introduced above.

I depleted USP30 in HCT116 cells using two independent oligos (D1 and D3) and then induced cell death using a variety of BH3 mimetics. As previously demonstrated, USP30-depleted HCT116 cells showed elevated levels of cleaved PARP when treated with ABT-737 (**Figure 4.12**). Similarly, treatment with the BCL-X_L inhibitor (A-1331852) alone or in combination with the MCL-1 inhibitor (A-1210477) affected USP30-depleted HCT116 cells to a greater extent than control cells (**Figure 4.12**). The response to the dual inhibition of MCL-1 and BCL-X_L was more robust over the two experiments, compared to the inhibition of BCL-X_L alone. The cells did not respond at all to the individual treatments with ABT-199 or A-1210477 suggesting that BCL-2 and MCL-1 inhibition alone was not sufficient to induce apoptosis, even in USP30-depleted cells. Another interesting observation in this experiment was the stabilisation of MCL-1 in the presence of its BH3 mimetic, A-1210477. Since A-1210477 inhibits MCL-1 by binding to its BH3 domain, it could also prevent MCL-1 from interacting with E3 ubiquitin ligases (Leverson et al., 2015b).

One such E3 ubiquitin ligase that is known to target MCL-1 and also contains a BH3 domain is HUWE1, also known as **M**CL-1 **U**biquitin **L**igase **E**3 (MULE) (Zhong et al., 2005). It is possible that treatment with A-1210477 prevents interactions between MCL-1 and HUWE1 by blocking the BH3 domain of MCL-1, thus preventing HUWE1 from targeting MCL-1 for poly-ubiquitylation and degradation, resulting in stabilisation of the protein (Czabotar et al., 2007; Leverson et al., 2015a; Mallick et al., 2019).

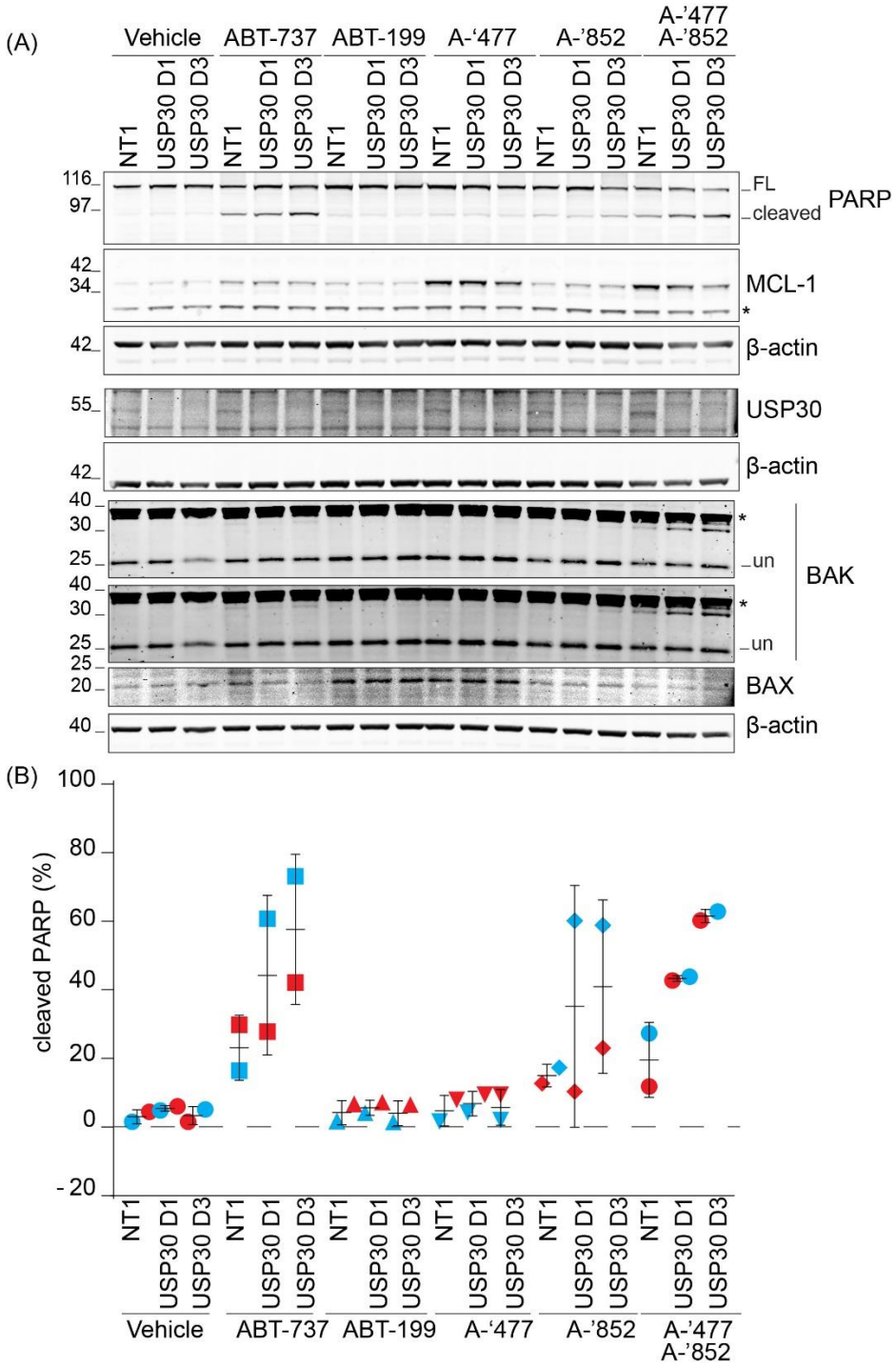

Figure 4.12: USP30 depletion sensitizes HCT116 cells to a number of BH3 mimetics

HCT116 cells were transfected with two oligos against USP30 (D1 and D3) for 72 hours. Cells were then treated with 10 µM ABT-737 or 100 nM ABT-199 or 10 µM A-1210477 (A-‘477) or 100 nM A-1331852 (A-‘852) or the combination of A-1210477 and A-1331852 for 15 hours. Cells were lysed in RIPA supplemented with PhosSTOP and MPIs (1:250). (A) Western blot analysis showing the effect of BH3 mimetics in USP30 depleted HCT116 cells. FL; full length, * non-specific band; un, unmodified. (B) The chart shows the percentage (%) of cleaved PARP to total PARP (cleaved fragment + FL) indicated as red and blue for the two independent experiments (n=2).

The next step was to attempt a rescue experiment in relation to cell death by re-introducing USP30 into USP30-depleted cells. However, the transfection efficiency was not high enough to provide protection in all the cell population, which would make experiments by immunoblot impossible. I wanted to overcome this issue by generating stable USP30-GFP expressing FlpIn cells as discussed below (4.8). Prior to generating stable cells, I sought to recapitulate the sensitisation in the parental line of HCT116 FlpIn TRex and furthermore optimise the time needed for the induction of apoptosis in USP30-depleted and control cells. I conducted an experiment where I depleted USP30 using only the D1 oligo, avoiding the complications associated with the D3 oligo that depletes MCL-1 as well (**Figure 4.1**). I only used the BCL-X_L inhibitor, A-1331852, in order to simplify the experiment, since BCL-X_L inhibition alone was sufficient to induce apoptosis in these cells (**Figure 4.11**) and used shorter time-points hoping to capture the optimal time window for the biggest difference in response between USP30-depleted cells and control cells.

USP30-depleted cells exhibited higher levels of cleaved PARP in response to treatment with A-1331852 across all time-points. However, there were already significantly elevated levels of cleaved PARP in the USP30-depleted cells at the 0^{th} time-point, which makes the experiment difficult to interpret (**Figure 4.13**A). I repeated the experiment twice more and found that the overall response of the cells, both the USP30-depleted and control cells, was lesser in terms of cleaved PARP compared to the first (**Figure 4.13**C and D). The above may indicate that there was inefficient induction of apoptosis in the latter two experiments, except for the final 4-hour time-point. Only at the final time-point there was evidence of sensitisation in one experiment. However, the response was not robust between experiments in order to draw meaningful conclusions.

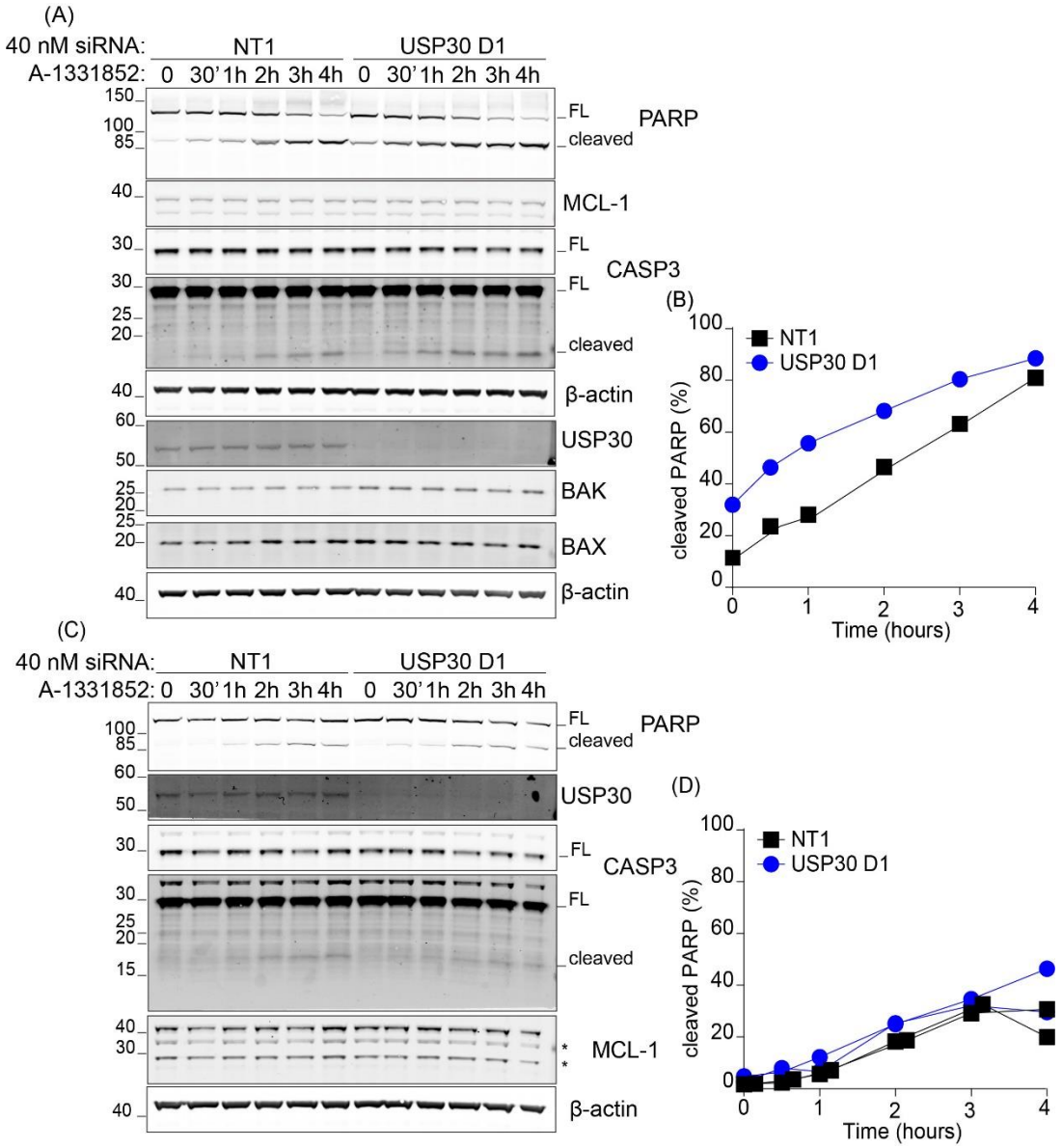

Figure 4.13: The response of USP30-depleted HCT116 FlpIn TRex cells to BCL-X_L inhibition

HCT116 FlpIn TRex cells were transfected with 40 nM siRNA oligos against USP30 (D1) and non-targeting oligo (NT1) for 72 hours. Cells were then treated with 100 nM A-1331852 for the indicated time points and lysed in RIPA supplemented with PhosSTOP and MPIs (1:250). (A) Immunoblot showing levels of cleaved PARP and cleaved caspase 3 (CASP3) as an indicator of apoptosis. (B) Quantitation of cleaved PARP as a percentage (%) of total PARP (cleaved+FL) for the immunoblot in (A). (C) Repetition of the experiment in (A). Quantitation of cleaved PARP as a percentage (%) of total PARP (cleaved+FL) for the immunoblot in (C) and a third independent experiment. FL, full length.

4.8 The lacZeo FlpIn TRex system

The lacZeo FlpIn TRex system, developed by Invitrogen, offers a range of advantages over the more commonly used random integration of plasmids in the genomes of cell lines or transient plasmid overexpression experiments. The lacZeo FlpIn system allows for:

1. The integration of a single copy of the gene of interest per cell and only at the engineered FlpIn recombinase (FRT) site. This feature prevents disruption of existing gene loci and or integration of the plasmid carrying the gene of interest in heterochromatic regions resulting in low expression.
2. Control over the expression of the introduced gene by means of the tetracycline repressor (TetR) protein (Hillen et al., 1984). This feature is particularly useful when the protein expressed is suspected or known to have toxic effects on the cells.
3. Near-endogenous levels of expression, when combined with controlled induction (see 2 above) preventing artefacts due to overexpression.
4. The generation of a more homogenous population of cells, all of which carry the gene of interest and express at similar levels within that population. Additionally, it allows for direct comparison of isogenic cell lines expressing wildtype and mutant proteins. This increases the versatility of experiments that can be performed such as proteomic-based experiments and rescue experiments following siRNA-mediated depletion or inhibition using drugs (Turnbull et al., 2017).

4.8.1 Generation of USP30-GFP FlpIn TRex compatible plasmids

A series of rescue experiments had been performed by Jin-Rui Amos Liang with limited success, using transient transfection of USP30 plasmid in hTERT-RPE1 YFP-Parkin cells (Jin-Rui Liang, 2014). One caveat was that only a small number of cells were successfully transfected and the degree of rescue was limited. I sought to circumvent the above limitation of plasmid transfections by generating FlpIn stable cell clones in the HCT116 cell line. Stable expression of equal amounts of USP30 wt or C77S (catalytically inactive) would allow me to address whether re-introducing wt USP30 rescued the sensitisation to BH3 mimetics and whether this was dependent on USP30 catalytic activity.

I used the USP30-GFP and USP30 C77S-GFP plasmids that had been mutated to be insensitive to USP30 D1 siRNA depletion, and had previously been successfully used for transient transfection rescue experiments (Marcassa et al., 2018). Having constructs that are insensitive to a particular oligo allows for depletion of the endogenous protein without affecting the re-introduced construct. Thus, I amplified siUSP30 D1-resistant USP30-GFP wt and C77S from the existing pEGFP-N3 vectors (**Figure 4.14**A).

I then incubated the PCR product with Taq polymerase that adds single Adenosine overhangs on the 3' end of the PCR product (**Figure 4.14**A). The addition of 3' Adenosine to generate overhangs allows for a TA-based cloning reaction further down the line. The pcDNA5 FRT/TO is available as an activated linearized vector that has two molecules of Topoisomerase covalently attached to the entry sites. The TOPO reaction takes advantage of the Thymidine (T) 5' overhangs on the vector and the Adenosine (A) 3' overhangs on the PCR product to bring the vector and the insert together. The topoisomerase then catalyses the ligation and produces a circularised vector with the insert in the correct position (**Figure 4.14**B). I screened several clones for successful insertions and correct orientations using restriction digests. I then fully sequenced the plasmids to ensure no other mutations were introduced during the procedure.

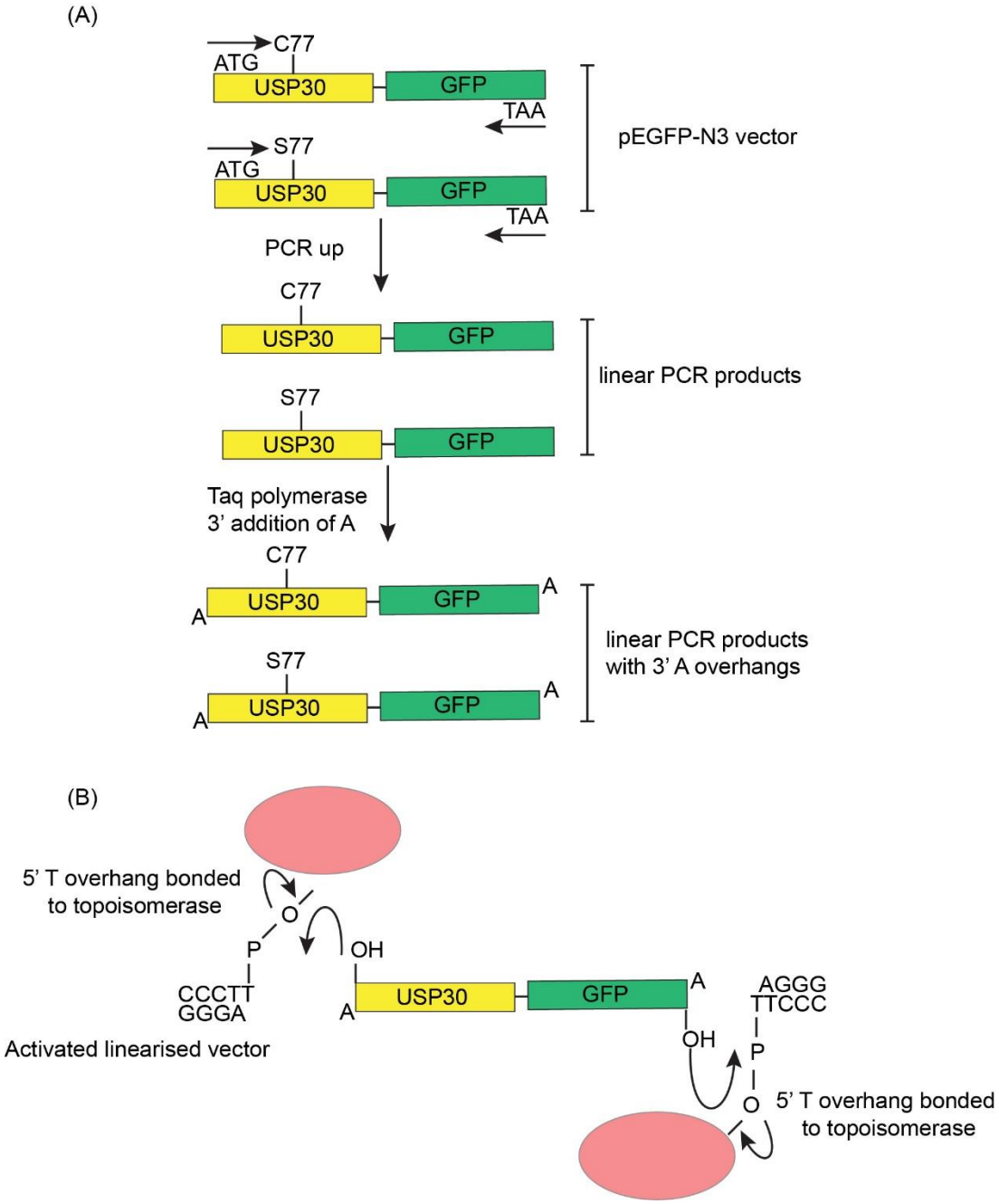

Figure 4.14: PCR up of USP30-GFP and TOPO reaction

(A) USP30-GFP wt (C77) and catalytically inactive (S77) in the pEGF-N3 were amplified in a PCR reaction. The reactions were then incubated with Taq polymerase to add Adenosine (A) to the 3'-end of the PCR products to produce overhangs. ATG and TAA represent the initiator and stop codons respectively.

(B) Overview of the pcDNA5/FRT/TO TOPO reaction between the activated vector backbone and the PCR product**.** Diagram was adapted from the pcDNA5/FRT/TO TOPO TA expression kit manual, Life Technologies (Invitrogen).

4.8.2 Plasmid transfections and screening of clones

My colleague, Elena Marcassa, performed the transfection and I took over screening the clones at a later stage. I expanded the clones that survived the selection and treated one set with 1 μg/ml doxycycline (a tetracycline derivative) for 24 hours and lysed them in order to perform a western blot to screen for USP30-GFP expression (**Figure 4.15**).

The screening resulted in two positive clones (4 and 5) both carrying USP30-GFP wild-type and displaying high levels of expression of USP30-GFP in response to doxycycline. USP30-GFP expression was detected by both the USP30 and the GFP antibody and appeared to be “leaky” since it was present even in the absence of doxycycline. The high levels of expression over the 24-hour period of induction were generating degradation or cleavage products, which is not uncommon. All the catalytically inactive clones (USP30 C77S-GFP) that I tested were negative for USP30-GFP expression as was clone 7 transfected with pEF5-GFP that carried GFP. The above meant that I was currently lacking a “vector” only control and I could not investigate whether the effects of re-introducing USP30 in the rescue experiments were a result of catalytic activity.

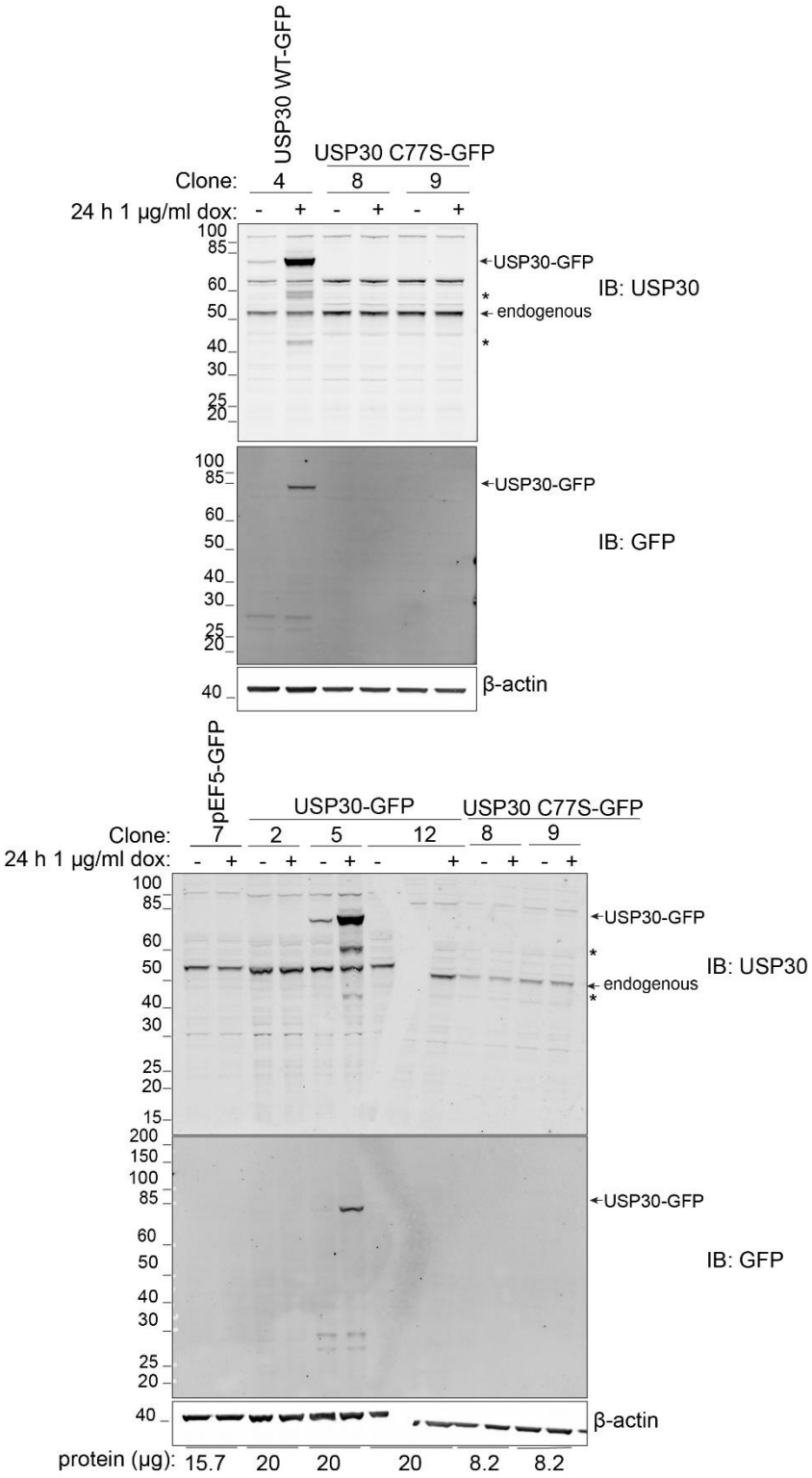

Figure 4.15: Screening of HCT116 USP30-GFP stable clones

HCT116 FlpIn TRex USP30-GFP WT and C77S mutant stable clones were treated with 1 µg/ml for 24 hours before being lysed in RIPA buffer supplemented with MPIs (1:250). Immunoblot analysis against USP30 and GFP to detect endogenous and GFP-tagged USP30 respectively. Dox, doxycycline. Protein (µg) denotes the amount of protein loaded in the wells of the lower gel since they were not equal. Dox, doxycycline; * degradation products; IB, immunoblot.

I performed a time-course induction with the two positive clones in which I assessed the percentage of GFP positive (GFP^+) cells by fluorescence microscopy and in parallel conducted an immunoblot to assess the relative levels of expression between USP30-GFP and endogenous protein (**Figure 4.16**). I performed this experiment using tetracycline free FBS (tet-free) in an attempt to eliminate the "leaky" expression I had seen in the screening process (**Figure 4.15**). Despite these precautions, both clones expressed a small amount of USP30-GFP constitutively that was increased by the addition of doxycycline. Interestingly, the levels of basal USP30-GFP expression were very similar to the endogenous (**Figure 4.16**A and B). Clone 4 was expressing USP30-GFP in a more homogenous manner since nearly all cells were GFP^+ (**Figure 4.16**C). Clone 5 displayed about 80% GFP^+ population, which increased upon treatment with doxycycline. Lastly, I took a few higher magnification images of clone 5 at 4-hour induction with doxycycline and saw that USP30-GFP signal, albeit too weak to show a distinct mitochondrial staining, was clearly cytoplasmic (**Figure 4.16**D).

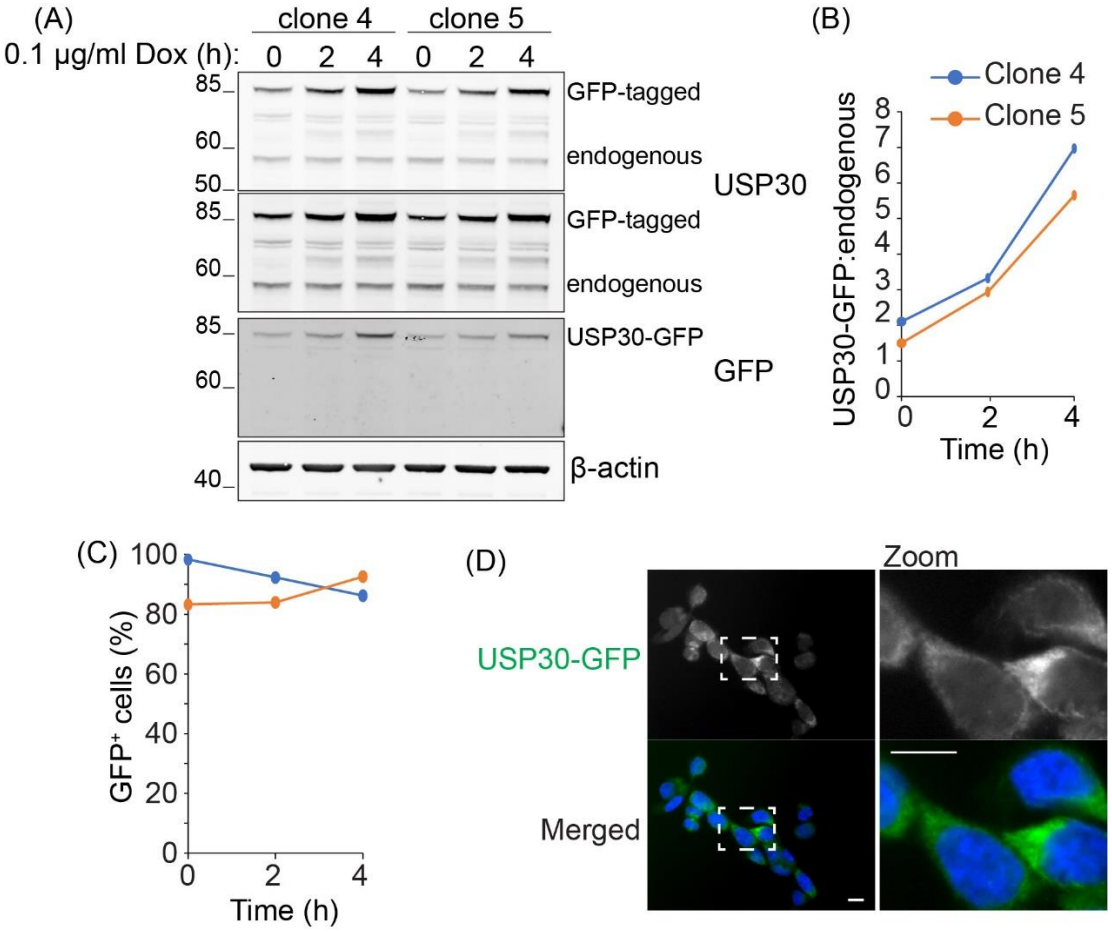

Figure 4.16: Time-course induction of HCT116 USP30-GFP clones with doxycycline

HCT116 FlpIn USP30-GFP clones 4 and 5 were treated with 0.1 µg/ml doxycycline for 0, 2 and 4 hours. (A) Cells were lysed in RIPA buffer supplemented with PhosSTOP and MPIs (1:250). Immunoblot analysis against USP30 and GFP. (B) Quantitation of the relative levels of expression of USP30-GFP normalised to the endogenous. (C) Cells were fixed in 4% PFA/PBS onto coverslips and mounted onto microscope slides using mowiol/DAPI. Coverslips were imaged using a 20x objective on a Nikon TiEclipse microscope and the percentages of GFP^+ cells were determined by counting a minimum of 100 cells per condition. (D) Representative image of HCT116 USP30-GFP clone 5 at the 4-hour timepoint imaged on a 60x oil-immersion objective on a Nikon TiEclipse microscope. Scale bars are 10 µm.

4.8.3 Cell death rescue experiment in HCT116 USP30-GFP stable cells

I next performed a rescue experiment using HCT116 FlpIn TRex USP30-GFP clone 4. I chose not to induce expression of USP30-GFP using doxycycline since the basal expression was already comparable to the endogenous. I depleted USP30 in these cells using two siRNA oligos: oligo D1, which was able to deplete the endogenous USP30 and should leave USP30-GFP unaffected and Q6 (Qiagen), which should target both endogenous and the tagged protein (**Figure 4.17**).

USP30 D1 reduced the levels of endogenous USP30 to about 20%, however this depletion was not as efficient as I had previously observed in the parental line (**Figure 4.12**). More importantly, USP30 D1 also reduced the levels of USP30-GFP to nearly 50% even though the construct should be resistant against this siRNA. Finally, the USP30 Q6 oligo was less efficient at reducing endogenous USP30 than USP30 D1. In addition, USP30 Q6 was not able to reduce the levels of USP30-GFP and the endogenous protein to significantly low levels to execute a complete USP30 depletion. Collectively these caveats made this experiment difficult to interpret.

The USP30-depleted cells using the Q6 siRNA exhibited higher levels of cleaved PARP compared to the control siRNA and the USP30 D1-depleted cells. The levels of cleaved PARP were very similar between USP30 D1 and NT1, suggesting the cells were responding very similarly to BCL-X_L inhibition and only the Q6 siRNA was showing an enhanced response, despite in fact having higher levels of USP30 expression than the D1-treated cells.

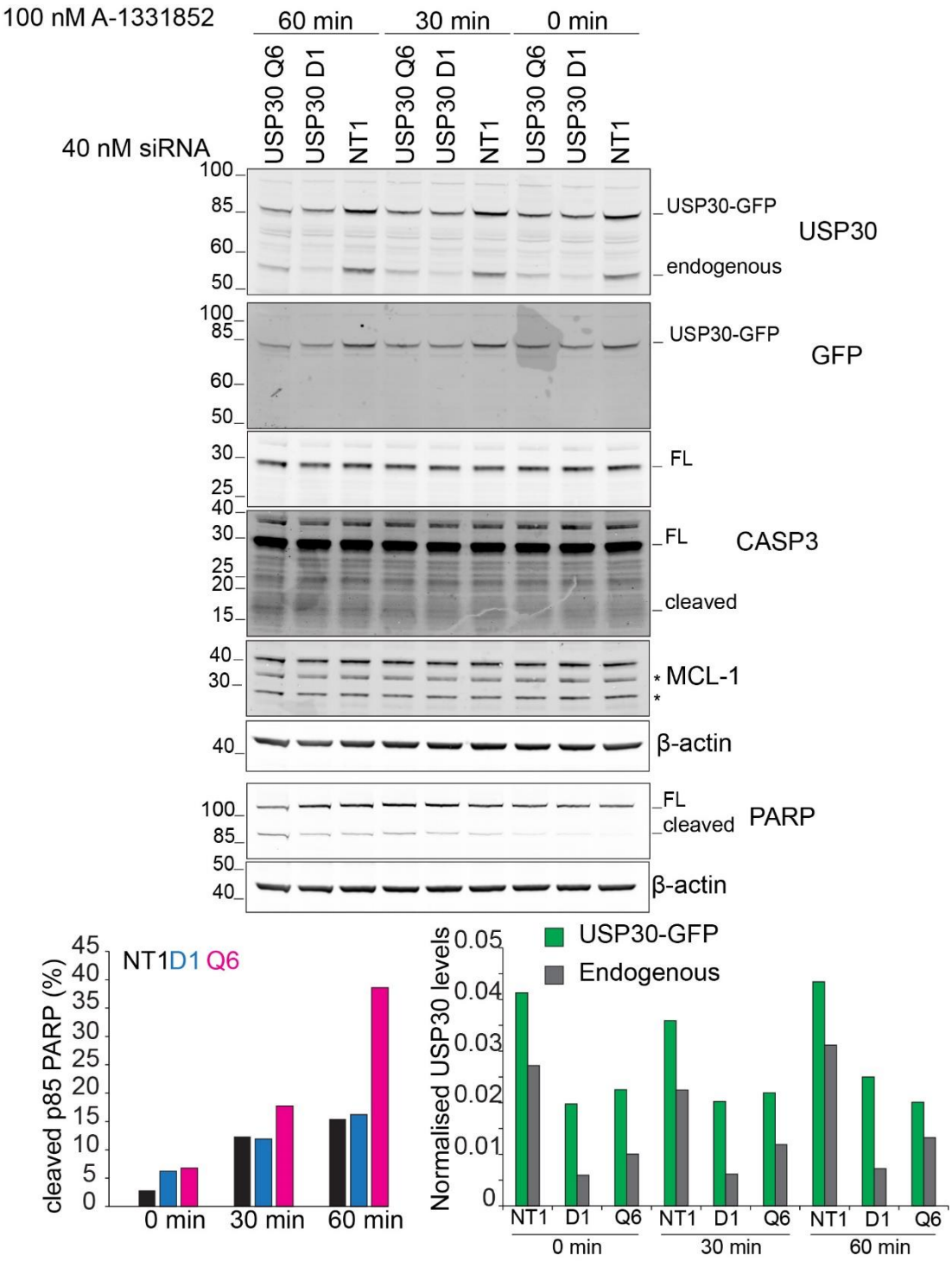

Figure 4.17: Cell death rescue experiment in HCT116 FlpIn TRex USP30-GFP cells

HCT116 FlpIn TRex USP30-GFP (clone 4) cells were transfected with 40 nM siRNA oligos against USP30 (D1 and Q6) for 72 hours. Cells were then treated with 100 nM A-1331852 for 0, 30 and 60 minutes as indicated. Cells were lysed in RIPA buffer supplemented with PhosSTOP and MPIs (1:250). FL, full length. The charts show the percentage of cleaved PARP (left) and the normalised levels of USP30-GFP and endogenous protein normalised to the control oligo for the same time-point (right) for the immunoblot in the upper panel.

I performed two additional experiments with the above set-up and then ran the two experiments on the same gel (**Figure 4.18**). The depletions achieved by USP30 D1 and Q6 siRNAs were very similar as the experiment above. The levels of cleaved PARP were consistently higher in the Q6 siRNA-depleted cells compared to the control oligo. The D1 siRNA-depleted cells displayed similar or slightly higher levels of cleaved PARP compared to NT1, however they were consistently lower than the respective Q6 oligo for the same time-point.

I plotted the total levels of USP30 (USP30-GFP and endogenous USP30) against the percentage of cleaved PARP in order to determine whether there was a correlation between USP30 expression and induction of apoptosis. The control siRNA NT1 was coloured as black while the USP30 oligos D1 and Q6 were coloured as blue and magenta respectively. The total amount of USP30 was higher in NT1 than D1 or Q6. The total levels of USP30 in D1 and Q6 appeared to be segregating together, suggesting they were in fact similar. There was a trend of the Q6 siRNA being more evenly spread than the D1 siRNA, which was segregating more towards the right, suggesting that the D1 may on average have slightly higher levels of USP30.

In terms of cleaved PARP, on average the Q6 siRNA displayed higher levels while D1 and NT1 were displaying lower levels of cleaved PARP. The levels of D1 and NT1 were more closely clustering together in terms of cleaved PARP.

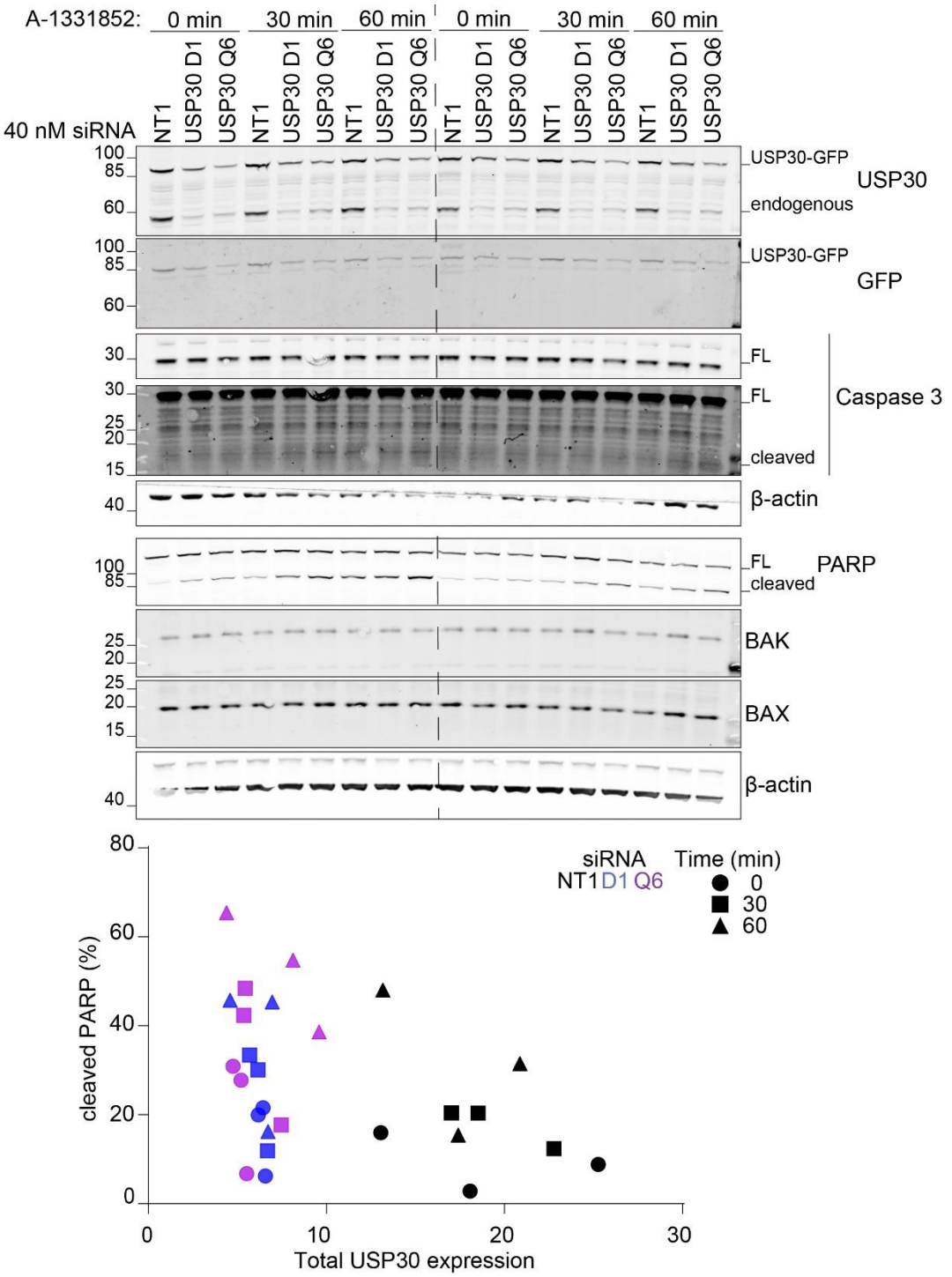

Figure 4.18: Cell death rescue experiment in HCT116 FlpIn TRex USP30-GFP cells

HCT116 FlpIn TRex USP30-GFP (clone 4) cells were transfected with 40 nM siRNA oligos against USP30 (D1 and Q6) for 72 hours. Cells were then treated with 100 nM A-1331852 for 0, 30 and 60 minutes as indicated. Cells were lysed in RIPA buffer supplemented with PhosSTOP and MPIs (1:250). Exp 2 and 3 indicate two independent experiments. The chart shows the quantitation of cleaved PARP as a percentage (%) of total PARP (cleaved+FL) over three independent experiments (n=3) plotted against the total USP30 expression in the sample (USP30-GFP + endogenous). FL, full length.

In the absence of sufficient depletion of both endogenous and GFP-tagged USP30 by the Q6 siRNA, it was necessary to find another suitable control. I used the parental cell line that alongside the stable USP30-GFP expressing clone (clone 4) to revisit the rescue experiment. I depleted USP30 using the D1 siRNA in both cell lines and treated the cells with the BCL-X_L inhibitor (A-1331852) and the newer generation MCL-1 inhibitor, S-63845, both at 100 nM for 1 or 2 hours (**Figure 4.19**).

The depletion of endogenous USP30 by the D1 siRNA was incomplete and was similar to the previous rescue experiments. Similarly, there was a small reduction in the levels of USP30-GFP in clone 4 by D1 siRNA in this experiment as well. The quantitation of total USP30 (USP30-GFP + endogenous) showed that the USP30 D1-depleted USP30-GFP expressing cells had very similar levels of USP30 as the parental control cells.

The USP30-depleted cells in the parental cell line showed elevated levels of cleaved PARP. The pattern of caspase 3 was 9.4% in D1 vs 4.5% in NT1 at the 1-hour time point and 11.6% in D1 vs 7.7% in NT1 at the 2-hour time-point. The above was indicating accelerated kinetics in the USP30-depleted cells in the cleavage of caspase 3, suggesting accelerated induction of apoptosis. The levels of p85 PARP and cleaved caspase 3 were very similar between USP30 D1-depleted and control cells in the USP30-GFP expressing clone. In fact, the USP30-GFP expressing clone behaved more similarly to the USP30-depleted parental cell line, exhibiting elevated levels of cleaved PARP and caspase 3. The above was perhaps suggesting that the induction of apoptosis by BH3 mimetics may be sensitive to both USP30 depletion and overexpression. The above is contradicted by the observation that D1-depleted cells in the USP30-GFP expressing clone were similarly sensitive as the control cells in the same cell line. Alternatively, and the most likely explanation would be that the USP30-GFP expressing clone was intrinsically more sensitive to BH3 mimetics than the parental cell line due to being a clonal population of cells with additional mutations and idiosyncrasies.

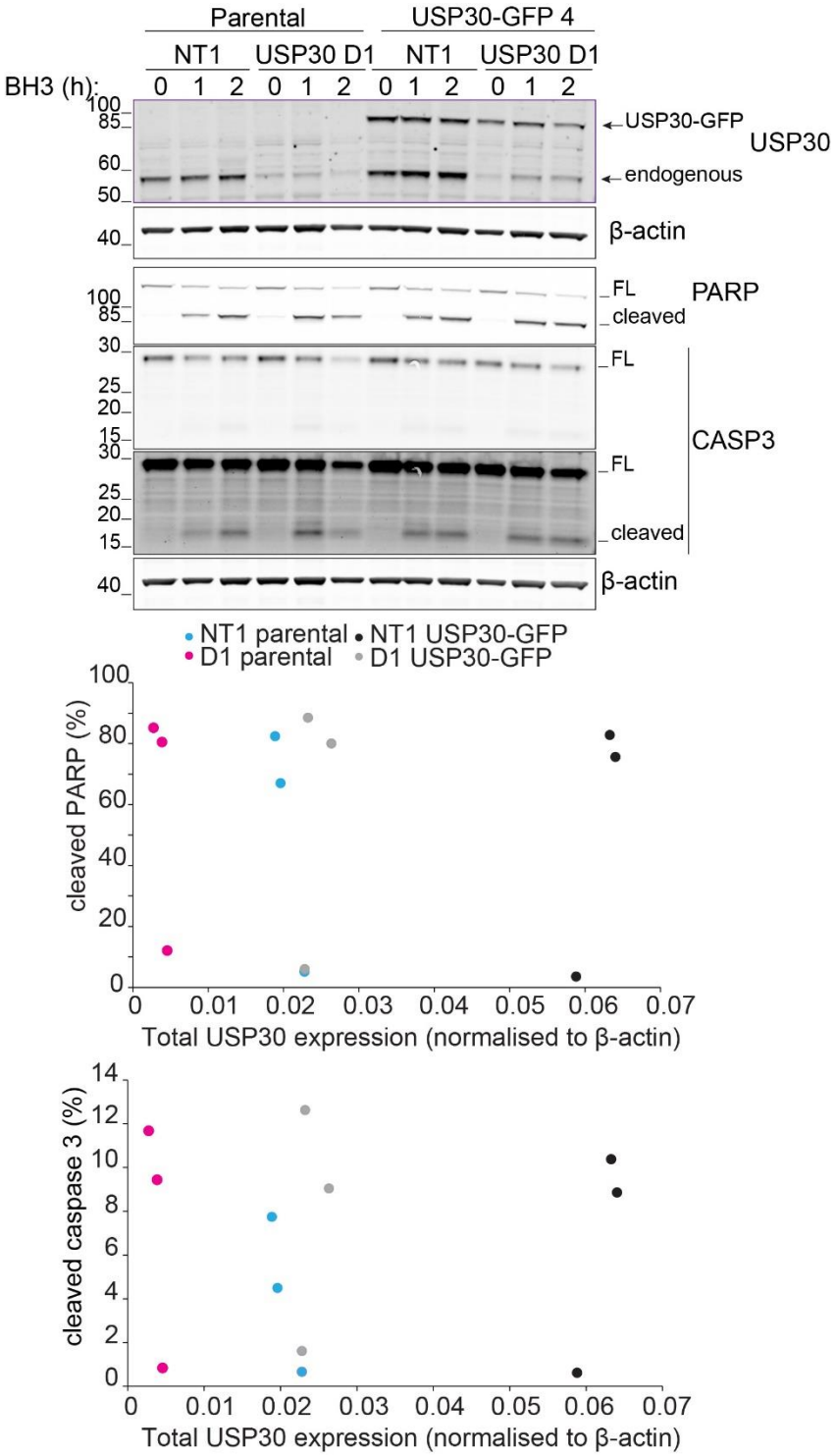

Figure 4.19: Cell death rescue experiment in HCT116 FlpIn TRex parental and USP30-GFP clone 4

HCT116 FlpIn TRex USP30-GFP (clone 4) and the parental cells were transfected with 40 nM siRNA oligos against USP30 (D1) on non-targeting oligo for 72 hours. Cells were then treated with 100 nM A-1331852 and 100 nM S-63845 for 1 or 2 hours as indicated. Cells were lysed in RIPA buffer supplemented with PhosSTOP and MPIs (1:250). The charts show the quantitation of cleaved PARP as a percentage (%) of total PARP (cleaved+FL) and the percentage of cleaved caspase 3 (%) plotted against the total USP30 expression in the sample (USP30-GFP + endogenous).

4.9 Discussion

4.9.1 The HCT116 cell line is dependent on MCL-1 and BCL-X_L for survival

I have determined that the HCT116 and the HCT116 FlpIn TRex are a suitable cell line model to study USP30 function in cells. Interestingly, inhibition of BCL-X_L alone by A-1331852 was sufficient to generate a response as was ABT-737 suggesting that as long as BCL-X_L is available to inhibit BAK/BAX from initiating apoptosis, the other two major anti-apoptotic proteins BCL-2 and MCL-1 are dispensable (**Figure 4.11** and **Figure 4.12**). This observation is supported by the lack of response to A-1210477 (MCL-1 inhibitor) and ABT-199 (BCL-2 inhibitor) as single treatments. The enhanced effect of combining A-1331852 and A-1210477 suggests that MCL-1 becomes important only when BCL-X_L was inhibited in this cell line.

I also determined that live-cell microscopy is an unsuitable methodology to employ with the HCT116 FlpIn TRex cells due to possible concerns of photo-toxicity during imaging and the round nature of these cells.

In the hTERT-RPE1 FlpIn TRex cells, the combination of MCL-1 and BCL-X_L inhibition is required for a strong response which seems to suggest that MCL-1 and BCL-X_L can fully compensate for the loss of one another. Overall, my data were in line with previous reports that solid tumour cell lines were dependent on MCL-1 and BCL-X_L, but not BCL-2 for survival (Lee et al., 2019).

4.9.2 USP30 depletion enhances the effect of BH3 mimetics in cells

USP30 depletion enhanced the effect of ABT-737 in inducing apoptosis in HCT116 cells and hTERT-RPE1 cells without Parkin overexpression (**Figure 4.4**). My work extended the above paradigm established by Jin-Rui Amos Liang to include two additional cell lines (Liang et al., 2015a). Furthermore, I demonstrated that the sensitisation occurs also when different and more specific BH3 mimetic compounds other than ABT-737 are used (**Figure 4.12**).

Most importantly, I have shown that USP30 depletion did not cause cells to respond to BH3 mimetics that they were not previously responding to.

USP30 depletion only enhanced existing apoptotic responses to the compounds.

The observation that USP30-depleted cells were sensitized to MCL-1 inhibition, as long as BCL-X_L was also inhibited at the same time, suggested that the sensitisation did not occur through MCL-1 (**Figure 4.12**). In fact, dual inhibition of MCL-1 and BCL-X_L were required for a more robust sensitized response compared to BCL-X_L inhibition alone (**Figure 4.12** and **Figure 4.13**). USP30 depleted cells exhibited enhanced levels of cleaved PARP and cleaved caspase 3, which were detectable at earlier time-points, which in turn may indicate accelerated kinetics. Taken together, the data suggests that USP30 may be acting downstream of the anti-apoptotic BCL-2 family in the apoptotic cascade, at the level of BAK/BAX activation or at the level of cytochrome c release.

4.9.3 BAK modifications during apoptosis

The levels of BAK were shown to increase in USP30-depleted cells, which may in part explain the sensitized responses to BH3 mimetics (Liang et al., 2015a). However, co-depletion of BAK and USP30 alleviated the sensitized response to a very small degree, which was not statistically significant compared to the single USP30 depletion. The above suggests that while the increased levels of BAK in the USP30-depleted cells are contributing towards a more sensitized response to BH3 mimetics, they do not account for the majority of the sensitized response. In fact, BAX was shown to be required more than BAK for both the sensitized and baseline responses to BH3 mimetics (Liang et al., 2015a). In my own experiments I also observed a small increase in BAK in USP30-depleted cells, particularly with the D1 siRNA (**Figure 4.1**, **Figure 4.4**, **Figure 4.12** and **Figure 4.13**).

During the experiments with long treatments with BH3 mimetics where the extent of apoptotic cell death was strong, I saw an additional band appearing in the BAK blot, about 8 kDa higher than the unmodified protein. The appearance of the band correlated with USP30 depletion in the presence of BH3 mimetics, even though it appeared to be of higher intensity in the D3-treated cells. Furthermore, the band also appeared in control cells, in the absence of USP30 depletion, where it was typically of lower intensity under

these conditions. I therefore hypothesized that this band correlated with the extend of apoptosis in the cell population and may be mono-ubiquitylated BAK.

I addressed the nature of this band by transfecting GFP-tagged BAK plasmids into cells, testing different BAK antibodies in their ability to detect this species and by performing experiments in BAK-depleted and BAK KO cells. With all the above experiments, I can conclusively say that the aforementioned species is not mono-ubiquitylated BAK. The nature of this band and its possible role in apoptosis remains unknown.

In some of the same experiments above there were also instances where lower molecular weight species of BAK and BAX were observed. A cleavage product of BAX (18 kDa), under conditions of strong apoptosis has previously been reported (Wood et al., 1998). The p18 fragment of BAX is a product of calpain cleavage that makes it refractory to BCL-X_L inhibition and enhancing its cell death function (Wood and Newcomb, 2000). The cleavage product of BAK is less characterised and is similarly thought to be a product of calpain activity (Dadakhujaev et al., 2009). Expression of high levels of the TrkA receptor resulted in phosphorylation of ERK and activation of caspase 7, which induced apoptosis, autophagic cell death and activation of calpains, resulting in the cleavage of BAK and BAX (Jung and Kim, 2008; Dadakhujaev et al., 2009). The properties of cleaved BAK however in the contexts of cell death have yet to be investigated. It is first necessary to address whether this cleaved product is indeed BAK by depleting endogenous BAK in conditions where this cleavage occurs. The next step is to locate the cleavage site and perform mutagenesis to demonstrate whether it can be prevented. Lastly, the importance and function of this cleavage product should be investigated and particularly whether the cleavage is only a by-product of cell death or also contributes to it.

4.9.4 Cell death rescue experiments by re-introducing USP30-GFP

The efficiency by which the oligos against USP30 were depleting the endogenous and GFP-tagged proteins was a concern during these experiments. The D1 siRNA was affecting the levels of USP30-GFP when the construct should have been insensitive to the siRNA. Furthermore, the Q6 siRNA was unable to deplete the endogenous nor the USP30-GFP to a

satisfactory level. Overall, the above complications made interpretation of these experiments impossible.

I attempted to circumvent the complication of using the Q6 siRNA by using the D1 siRNA alone in the USP30-GFP expressing clone and the parental line. However, the partial depletion of USP30-GFP by D1 persisted, which meant that the rescue experiment could not be performed. Depletion of endogenous USP30 by the D1 siRNA in the USP30-GFP expressing stable clone resulted in similar levels of total USP30 expression as the parental line. The above suggests that the USP30-GFP expressing clones are an appropriate model to perform rescue experiments, since the objective was to demonstrate that by having near-endogenous levels of USP30 restored the sensitivity of cells to BH3 mimetics back to baseline. The above was not successful since the USP30-GFP expressing clone showed enhanced response to BH3 mimetics compared to the parental cell line. Depleting endogenous USP30 in the USP30-GFP stably expressing clone did not restore the response to baseline. Nevertheless, the experiment did present the opportunity to see whether USP30 overexpression could protect against the effect of BH3 mimetics in cells. These preliminary results suggest that USP30 overexpression did not restrict the ability of BH3 mimetics in inducing apoptotic cell death.

The rescue experiments need to be revisited using other siRNA oligos against USP30. An alternative for this type of experiment would be to use siRNA oligos that target the 3'UTR of endogenous USP30. Additionally, an siRNA against GFP could be used in conjunction to allow a simultaneous siRNA-depletion of both endogenous and GFP-tagged USP30. The above experiment may provide more confidence in the result. Furthermore, it is important to generate the catalytically inactive counterpart of the HCT116 FlpIn TRex USP30-GFP cell line to determine whether USP30 catalytic activity is required for the rescue.

One caveat of using PARP cleavage to monitor sensitisation to apoptosis is that the methodology reflects the pooled effect in a cell population rather than the effect on individual cells and therefore does not constitute a direct quantitation measure of apoptotic cell death.

Chapter 5: Generation and characterisation of USP30KO cells in the HCT116 FlpIn TRex cell line

5.1 Introduction

This far I was able to extend the observation that USP30 depletion enhanced the effect of BH3 mimetic compounds to the HCT116 cell line. Furthermore, I was able to recapitulate the sensitisation using other BH3 mimetic compounds that are more selective and that target different members of the BCL-2 anti-apoptotic family. However, a lot remain unanswered and most importantly of all is to understand the molecular and cellular mechanism by which USP30 depletion enhances the effect of BH3 mimetics.

In order to take the project farther and further understand the role of USP30 in apoptosis and other processes, we sought to generate USP30 stable knock-out (KO) cells in the HCT116 FlpIn TRex cells. The stable KO cells will help simplify the experiments in terms of design by removing the need for siRNA depletion that takes times and removes the caveat of incomplete USP30 depletion. The above will also allow us to employ unbiased approaches to discover novel USP30 substrates and USP30-dependent processes.

5.1.1 CRISPR/Cas9 technology as a gene editing tool

Clustered Regularly Interspaced Short Palindromic Repeats (CRISPR) is a system of an adaptive immune response initially discovered in archaea (Ishino et al., 1987) and bacteria (Mojica et al., 1993) against invading bacteriophages (Pourcel et al., 2005). CRISPR has successfully been adapted to edit genes in human cells (Liang et al., 2015b) and it is widely used in a variety of gene-editing applications.

Briefly, CRISPR genome editing involves the use of the nuclease CRISPR-associated protein 9 (Cas9) (Garneau et al., 2010) that cleaves double-stranded DNA (Marraffini and Sontheimer, 2008) at specific DNA sequences determined by the protospacer adjacent motif (PAM) (Bolotin et al., 2005) sequence and CRISPR RNAs (crRNAs) (Brouns et al., 2008), which are complimentary to the target DNA sequence. The double-stranded nick introduced in the DNA is perceived as DNA damage by the cell and activates

the DNA damage response (DDR) to repair the damaged locus. The two main DNA damage pathways activated are the non-homologous ends joining (NHEJ) and Homology-Directed repair (HDR). The choice of pathway activated depends on the cell line and the cell cycle stage. This is a critical choice since the type of repair pathway activated can result in differential outcome in terms of mutations introduced at the cleaved DNA locus by Cas9.

NHEJ is primarily used by cells in G1 since it is rather simply the re-ligation of two exposed DNA strands. Very often however the DNA repair machinery will either trim down or add some nucleotides prior to ligation. The insertion or deletion of nucleotides, termed indels, may interrupt protein open reading frames (ORFs) by introducing frame shifts and premature stop codons. The resulting protein is therefore incomplete, non-functional and in many cases unstable and targeted for degradation. This method allows for the generation of knock-out (KO) cells provided both alleles suffer inactivating indel mutations.

The HDR pathway involves the repair of a damaged DNA strand using an intact strand as a template that carries flanking sequences homologous to the damaged strand. Cells undergoing DNA replication (S-phase) and in mitosis (G2/M-phase) predominantly use this pathway to repair DNA damage as this is less error-prone compared to NHEJ. This system can be exploited in order to introduce specific mutations in genes by providing the cell with a template carrying the desired mutations to use in HDR. The above approach is termed knock-in and is less efficient than the KO approach by NHEJ since it requires successful targeting of the gene locus by Cas9 but also successful repair of the damage using the provided template. HDR or NHEJ may preferentially be induced in cells depending on the desired outcome, typically by manipulating the stage of the cell cycle the cells are in (Lin et al., 2014). In my case, the desired outcome is to produce KO cells and therefore NHEJ is the preferred pathway.

5.2 Generation of USP30KO clones

Two small guide (sg)RNA sequences were used to target the USP30 locus, kindly suggested by Jin-Rui Amos Liang. The two sgRNAs (sgUSP30-1 and sgUSP30-2) both target exon 3 of isoform 1 of USP30 (**Figure 5.1**)

proximal to the catalytic Cysteine (C77). The two sgRNA satisfy the following important requirements:

Both sgRNAs target exon 3 that comprises part of the USP domain of USP30 (**Figure 5.1**). Indel mutations within structured and undoubtedly vital domains of proteins are more likely to render the protein non-functional (He et al., 2019). Misfolded domains in proteins are detected by the cell's protein quality control mechanism and are targeted for degradation. Non-sense indel mutations will produce non-functional truncations of USP30 with most of the USP domain missing and thus will have no catalytic activity, even if the truncated protein was allowed to persist in the cell.

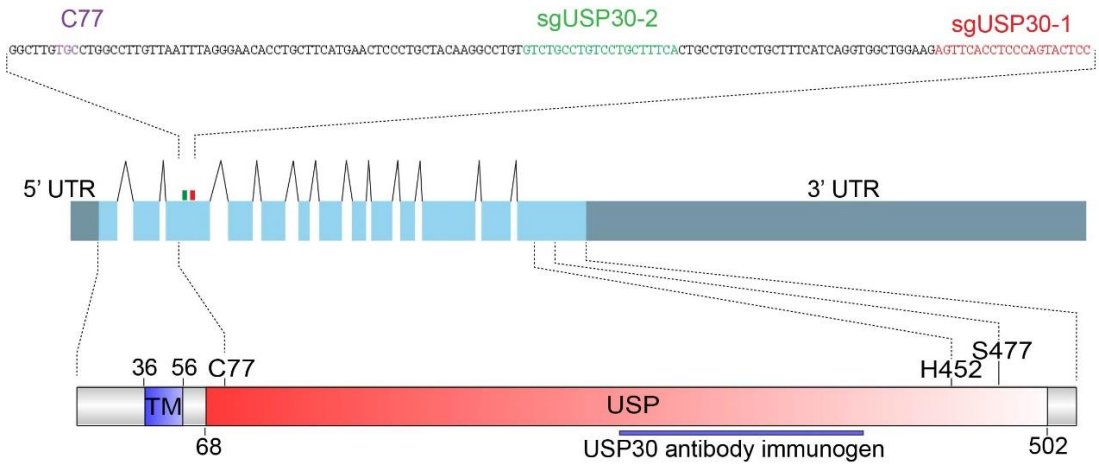

Figure 5.1: Two sgRNAs targeting USP30 near the catalytic cysteine
Schematic diagram showing the exons mapping on the USP30 protein. The two sgRNAs, sgUSP30-1 and sgUSP30-2 are shown in red and green respectively. The catalytic cysteine (C77) is highlighted in purple. The immunogen of the USP30 antibody (Sigma-Atlas: HPA016952) used to screen for USP30KO cells is mapped on the protein, between residues 290-433. TM; trans-membrane domain, USP; ubiquitin specific peptidase domain, 5' and 3' UTR; untranslated region. H452 and S477 form part of the catalytic triad.

Always a concern with CRISPR/Cas9 gene-editing is the use of downstream initiation codons to still make protein. The two sgRNAs described here make such a possibility much less likely, since any protein product being made from a downstream initiation codon will be missing two vital parts of

USP30. The trans-membrane (TM), required for membrane anchoring of USP30 into the OMM and peroxisomal membranes, would be missing and so would the catalytic Cysteine (C77), rendering the putative truncated protein mis-localised and catalytically inactive.

Both sgRNAs target proximal to the catalytic Cysteine (C77) and are therefore suitable candidates for performing CRISPR knock-in to introduce different mutations that might be worth exploring in the future. One mutation could be C77S or C77A, both rendering USP30 catalytically inactive but still present in the cell as full-length protein, allowing us to distinguish between enzymatic and non-enzymatically dependent cellular functions of USP30.

The two sgRNAs were cloned into the pX458 (pSpCas9(BB)-2A-GFP) vector using the BbsI cloning sites. The subcloned vectors pX458 sgUSP30-1 and pX458 sgUSP30-2 drive expression of GFP-tagged Cas9 and the desired sgRNA under the control of a CMV and a U6 promoters respectively. The HCT116 FlpIn TRex cells were transfected with 6 µg of the plasmids per 10 cm dish using Lipofectamine LTX (4:1 ratio of Lipofectamine LTX to DNA) and PLUS reagent. Twenty four hours post-transfection, the cells were trypsinized and suspended in flow sort solution (10% FBS/PBS) with their density adjusted to approximately $1x10^6$ cells/ml. The GFP^+ cells were sorted into tubes using Fluorescence Activated cell sorting (FACS) on a FACSAria III cell sorter instrument operated by Dr. Ka Sin Christopher Law (Magnetic Resonance & Image Analysis research Centre MARIARC, University of Liverpool). The GFP^+ cells were allowed to recover after the sorting for 48 hours in 6 cm dishes in conditioned media. Subsequently, I performed single cell dilutions to 96-well plates. I prepared three 96-well plates calculating 0.5, 1 and 2 cells/well in order to account for errors in cell counting and pipetting. Following the single-cell dilution, I inspected the 96-well plates under the microscope to identify wells with single cells and excluded wells with no or more than one cells. Wells with only one cell had their medium exchanged every 3-5 days, as required. Once the surface area of the well was nearly covered by cells, the colony was transferred to a 24-well plate, maintaining the original number of the well and the 96-well plate as a name for the clone. Gradually, the clones were transferred to a 12-well and eventually a 6-well plate. Once in the 6-well plate stage, duplicate 6-well plates were set up and one replicated was lysed in NP-

40 lysis buffer and an immunoblot was performed to check for USP30 expression (**Figure 5.2**).

Four clones out of the ten tested were identified as USP30KO (**Figure 5.2**). Three were generated using sgUSP30-1 (B10-0.5, F5-2 and C6-1) and one using sgUSP30-2 (B8). Clone B8-0.5 generated with sgUSP30-1, exhibited reduced levels of USP30 compared to the parental and wild-type clones and it was excluded as it might be a heterozygous or mixed clone.

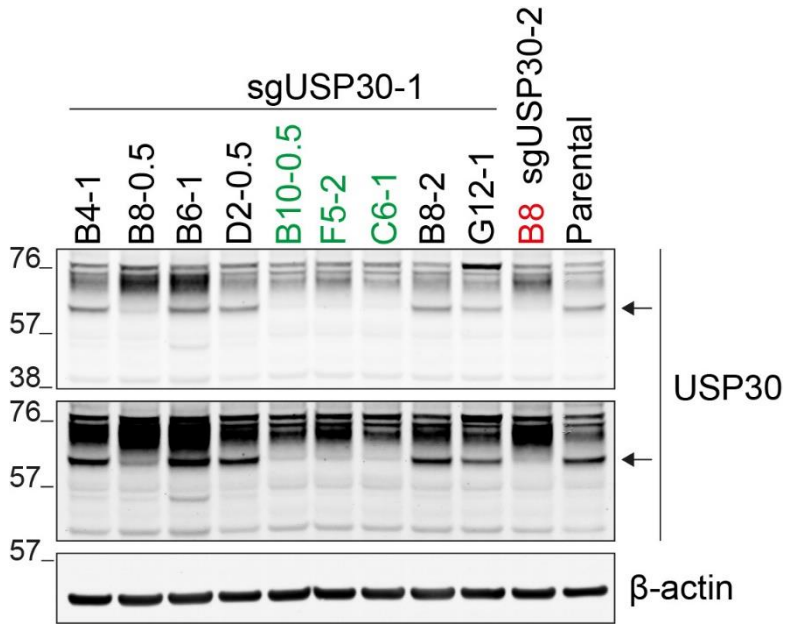

Figure 5.2: Screening of USP30KO HCT116 FlpIn TRex cells by immunoblot

Candidate USP30KO clones and the parental cells were lysed in NP40 lysis buffer supplemented with MPIs and analysed by immunoblot to screen for USP30 expression. The numbers on the top were used to trace back the plate the clones originated in and the sgRNA used to generate is shown. USP30KO clones generated by sgUSP30-1 and sgUSP30-2 are coloured in green and red respectively. The arrow shows the band corresponding to USP30.

The HCT116 cell line is described as having 45 chromosomes (-Y) and to be chromosomally stable, with a very low levels of polyploidy (Zasadil et al., 2013). It was important to verify that the USP30KO clones were truly knock-out for USP30 on both alleles and furthermore establish these were clonal populations and not mixed as this might affect their behaviour. To address this, I sequenced the genomic locus to identify the exact mutation that occurred to result in USP30KO. Primers were designed spanning exon 3 of USP30 where

the two sgRNAs bind to. Genomic DNA (gDNA) was extracted from the clones and used in a polymerase chain reaction (PCR) to amplify the region. The PCR product was run on an agarose gel and extracted. The purified product was sub-cloned into the pCR4Topo cloning vector and transformed into competent bacteria. Six positive colonies were grown under selection and had plasmid DNA extracted. I verified successful transformants using the two EcoRI sites that flank the insert and sent the plasmids for DNA sequencing in an attempt to identify the mutations suffered on both USP30 alleles and identify the presence of any potential contaminating clones. The sequencing results were compared against the expected sequence of a wild-type locus using the same set of primers. This presented a good opportunity to assign the clones new names for simple annotation.

Table 5.1: Sequencing results of the HCT116 FlpIn TRex USP30KO clones

Original Name	sgUSP30	New Name	Mutation suffered	Protein (aa)	Frequency
B10-0.5	1	KO1	Δ221-248 STOP at 282	108	5/5
F5-2	1	KO2	Δ221-248 STOP at 282	108	1/3
			Insertion of T at 203 STOP at 213	71	2/3
C6-1	1	KO3	Δ221-248 STOP at 282	114	2/4
			Δ221-273 STOP at 309	108	1/4
			Insertion of C at 310 STOP at 402	133	1/4
B8	2	KO4	Δ221-248 STOP at 282	108	1/7
			Δ221-269 STOP at 391	130	6/7

The table summarises the results of sequencing the mutations suffered by the USP30KO clones during the CRISPR process. The clones are assigned an original name, the sgRNA used to generate them (sgUSP30-1 or -2), the exact mutation suffered at the nucleotide level and the pre-mature STOP codon introduced, the length of the putative truncated protein that would be generated instead and finally, the frequency at which these mutations were encountered during the sequencing process. The numbering begins from the initiator codon for the mature mRNA of USP30 (isoform 1), Δ; deletion, STOP; stop codon.

Table 5.1 summarises the outcome of this endeavour. Each clone is described by its original name, sgRNA used to generate it, its newly assigned name, the mutation suffered identified by the sequencing result at the nucleotide level with the numbering starting from the initiation codon, the expected length of the USP30 remnant being translated and lastly the frequency at which the same sequencing result was found. The mutation Δ221-248 indicates a deletion of nucleotides 221 to 248, which results at the introduction of a stop codon at position 282. The potential protein product resulting from such a mutation is 108 amino acids long. This mutation was the most commonly occurring and it was seen across all the KO clones. KO3 yielded three different sequencing results and three different mutations. This suggests there are at least two clonal cell populations in KO3. For this reason, I decided not to use KO3 for further experiments.

I assigned new names for all of the clones initially screened were assigned different names that would be easier to work with (**Table 5.2**). Furthermore, I included two wild-type clones (WT1 and WT3) as additional controls clones to be used alongside or instead of the parental cell line. These clones underwent the same procedure as the KOs but have retained USP30 expression.

Table 5.2: New assigned names of USP30KO and WT clones

Original Name	sgUSP30 used	USP30 band	Notes	New Name
B4-1	1	+	To be used as wt	WT3
B8-0.5	1	±	Ambiguous	WT4
B6-1	1	+		WT5
D2-0.5	1	+	To be used as wt	WT1
B10-0.5	1	-		KO1
F5-2	1	-		KO2
C6-1	1	-		KO3
B8-2	1	+		WT2
G12-1	1	+		WT6
B8	2	-		KO4

The table describes the status of the USP30KO and USP30WT clones as well as their newly assigned names.

5.2.1 Monitoring the major BCL-2 family proteins in HCT116 FlpIn TRex USP30KO cells

Before performing cell death experiments in the USP30KO cells, I wanted to characterise the basal expression levels of the major players of the apoptotic process, the BCL-2 family proteins. This was necessary in case the KO of USP30 induced any changes to the basal levels of these proteins. I prepared RIPA lysates from all the WT and KO clones and compared them to the parental cell line. I blotted for the multi-domain pro-apoptotic effectors BAK and BAX and the major anti-apoptotic proteins MCL-1, BCL-X_L and BCL-2, and quantitated their relative levels across all the cell lines, normalised to the actin loading control and then normalised to the parental of each experiment to show the fold change in the levels of expression (**Figure 5.3**). Overall, there were no major nor consistent changes in the levels of expression of the major BCL-2 family members across the USP30KO and their wild-type counterparts compared to the parental cells. Any differences were most likely due to technical aspects such as uneven transfer of the proteins during blotting or misloading of the samples.

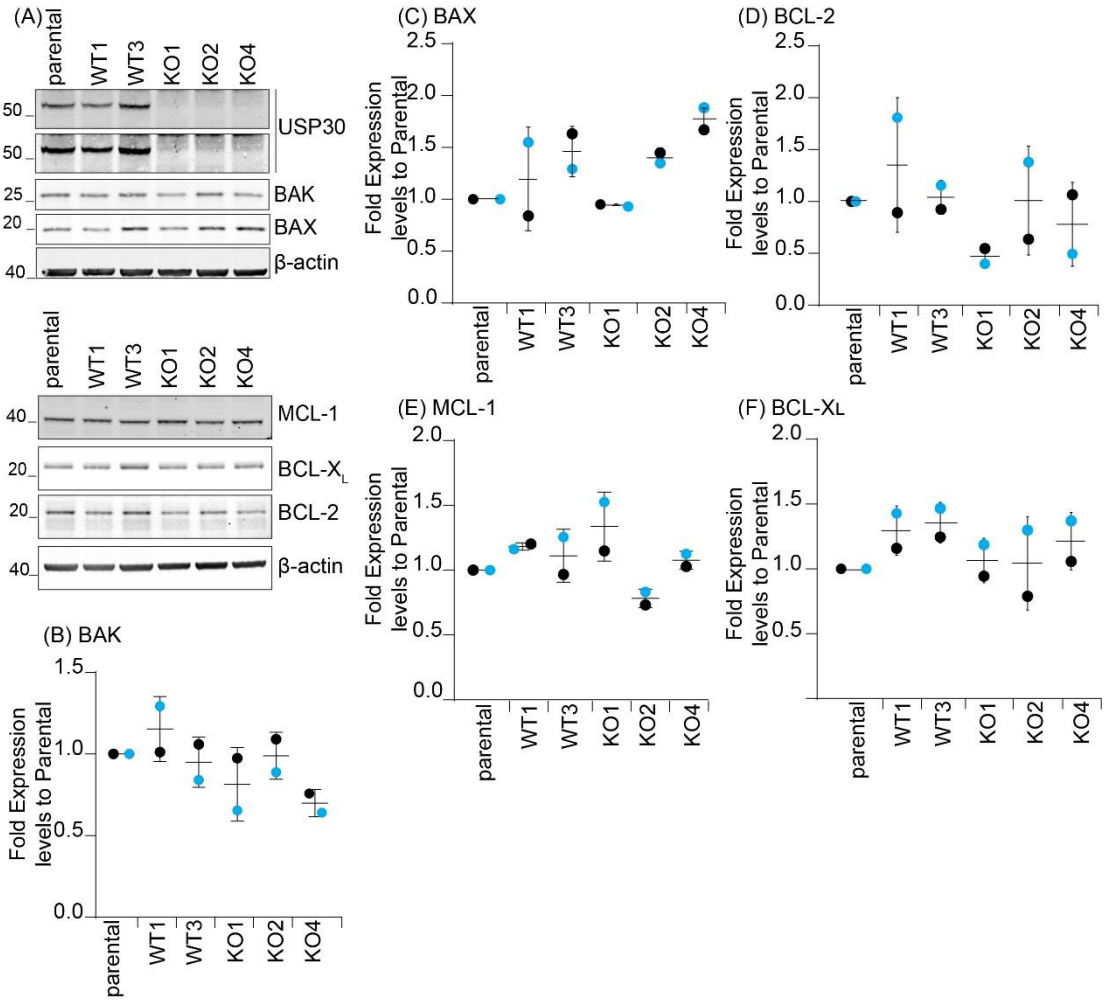

Figure 5.3: Levels of BCL-2 family proteins in HCT116 FlpIn TRex USP30KO cells

HCT116 FlpIn TRex cells USP30 WT1, WT3, KO1, KO2, KO4 and the parental cell line were lysed in RIPA buffer supplemented with MPIs (1:250). Blots show the protein levels of USP30, BAK, BAX, MCL-1, BCL-X_L and BCL-2 (A). The levels of protein were quantitated across cell lines, normalised to the β-actin loading control and then to the parental cell line within the experiment. Data is from two independent experiments (n=2) and are shown for (B) BAK, (C) BAX, (D) BCL-2, (E), MCL-1 and (F) BCL-X_L. The individual data points are shown as black for the immunoblots show in (B) and (C) and the cyan data points are from the second experiment.

5.2.2 Response of HCT116 FlpIn TRex USP30KO cells to BH3 mimetics

I assessed the effect of ABT-737 in the USP30KO cells I generated by treating the cells with 20 μM ABT-737 for 8 and 24 hours and analysed the samples by immunoblot analysis (**Figure 5.4**). At the 8-hour time-point USP30KO clones 1 and 4 displayed enhanced levels of cleaved PARP compared to the parental, while USP30KO2 showed similar levels of cleaved PARP to the parental. One of the USP30WT clones (clone 1) showed

enhanced levels of cleaved PARP while the other USP30WT clone (clone 3) was very similar to the parental. At the 24-hour time point all clones, both USP30KOs and USP30WTs showed enhanced levels of cleaved PARP compared to the parental.

Apoptosis can be monitored using additional biochemical and morphological markers. Phosphatidyl-serine (PS) is a phospholipid that becomes exposed on the outer leaflet of the plasma membrane of apoptotic cells and can be detected using Annexin V conjugated to fluorophores. The cell membrane of apoptotic cells becomes breached to the extra-cellular medium and this event can be monitored using cell-impermeable dyes such as propidium iodide (PI). A cell with breached plasma membrane takes up PI, which intercalates in the DNA and allows PI to become fluorescent and detectable. The population of PS^+ cells indicates cells undergoing apoptosis while the addition of the PI indicates cells that are further down the apoptotic pathway (late apoptotic cells) as an additional piece of information.

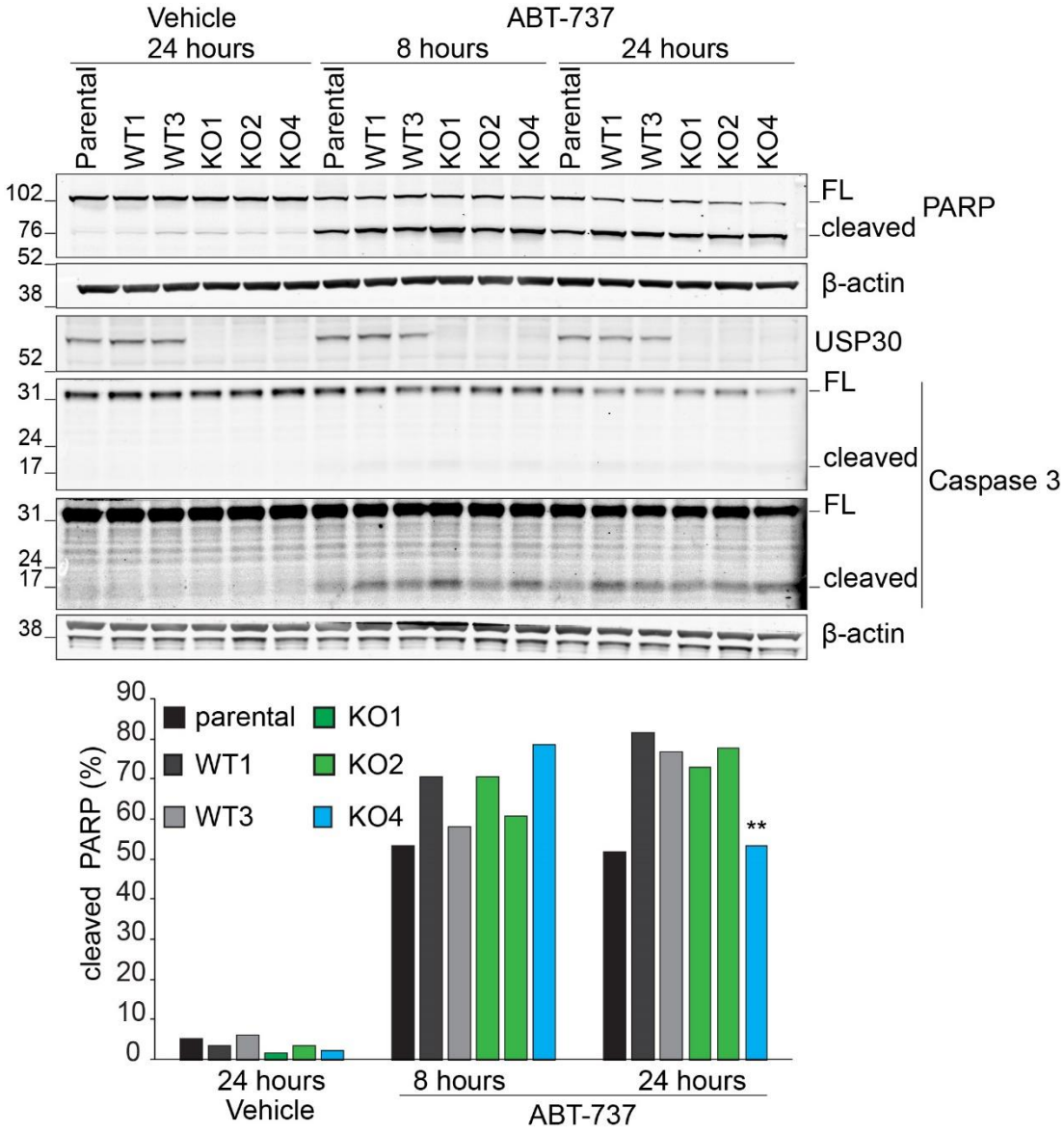

Figure 5.4: Immunoblot of HCT116 FlpIn TRex cells in response to ABT-737

HCT116 FlpIn TRex cells USP30 WT1, WT3, KO1, KO2, KO4 and the parental cell line were treated with 20 μM ABT-737 for 8 or 24 hours or DMSO (vehicle) for 24 hours. Cells were lysed in RIPA supplemented with MPIs (1:250) and probed with the indicated antibodies (upper panel). Quantitation of percentage of cleaved PARP (lower panel) across conditions. ** indicate error in quantitation of band intensity due to presence of saturated pixels on the band of interest.

I also prepared a duplicate set of plates of the above experiment to analyse the effects of ABT-737 on HCT116 FlpIn TRex USP30KO cells by PS externalisation using Annexin V-FITC and PI in a flow cytometer (**Figure 5.5**).

By 8 hours, 14% of the parental cells were PS^+ whereas all three USP30KO clones displayed nearly twice as high levels of PS^+ cells. USP30WT3 showed similarly high levels of PS^+ as the USP30KO clones and USP30WT1 was at very similar levels as the parental cells. By 24 hours, all the USP30KO and USP30WT clones displayed similarly high levels of PS^+ cells of over 70%, while the parental cells were at 50%.

While all three of the USP30KO clones consistently displayed higher levels of PS externalization than the parental, so did one of the USP30WT clones. By the 24 hour time-point, all clones, regardless of USP30 status were behaving very similarly. Overall, it appeared that the clones were more responsive to ABT-737 than the non-clonal parental population. Altogether, this experiment did not provide evidence for a role for USP30 in the response to ABT-737 in the HCT116 FlpIn TRex cell line.

I performed a similar experiment and introduced the MCL-1 and BCL-X_L inhibitors in parallel to ABT-737, focusing on the 8-hour time-point only. In this experiment I wanted to look at an earlier event as well, the loss of mitochondrial membrane potential induced by MOMP. MOMP induces release of cytochrome c into the cytosol, which interrupts electron transport by the mitochondrial respiratory chain and causes loss of the mitochondrial membrane potential. Tetramethylrhodamine, Ethyl Ester (TMRE) is a cell-permeable cationic dye that is sequestered by active mitochondria using their membrane potential. Depolarised mitochondria are unable to uptake TMRE and the above can be minitored by flow cytometry.

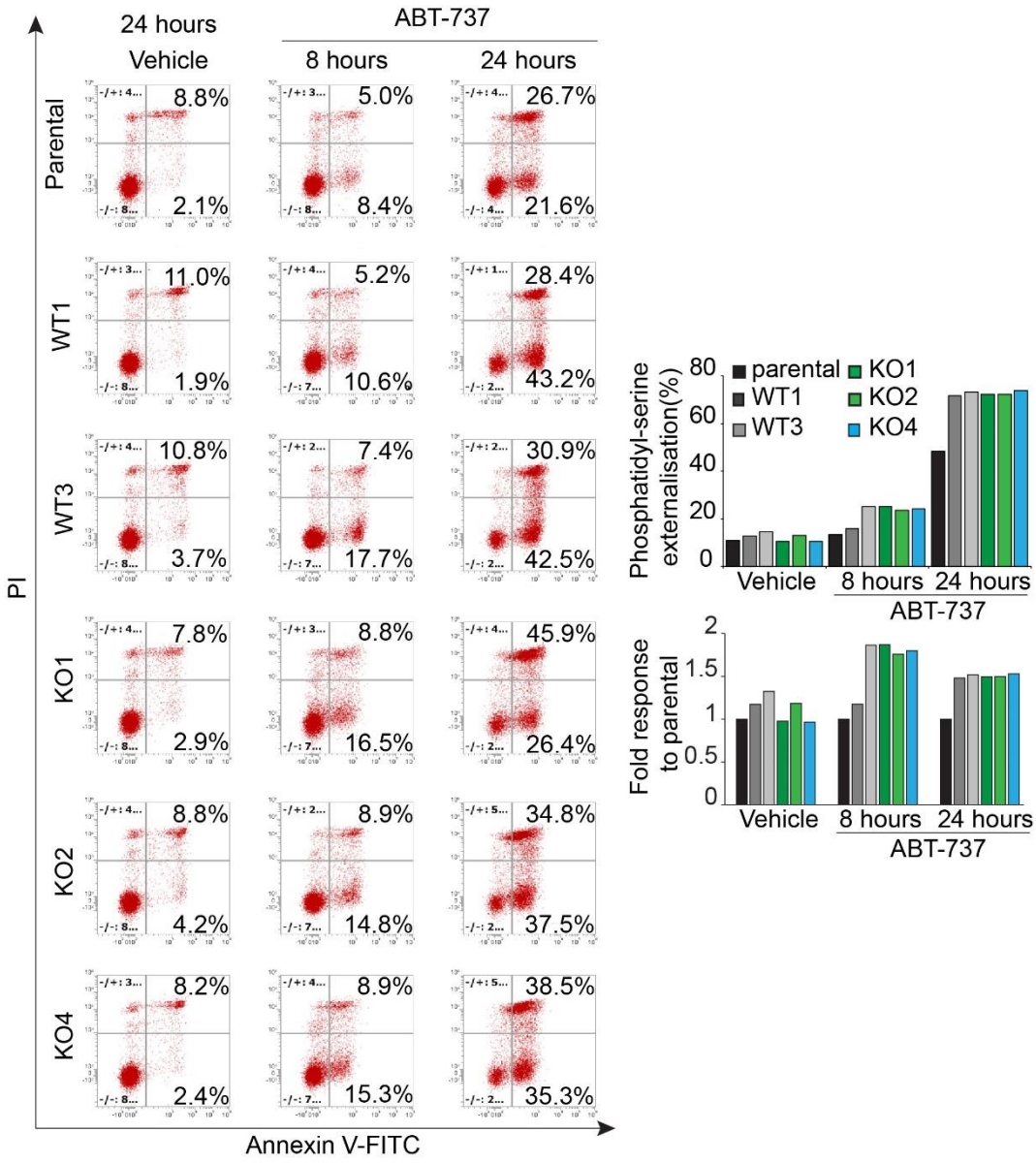

Figure 5.5: Phosphatidyl-serine externalisation in HCT116 FlpIn TRex cells to ABT-737

HCT116 FlpIn TRex cells USP30 WT1, WT3, KO1, KO2, KO4 and the parental cell line were treated with 20 μM ABT-737 for 8 or 24 hours or DMSO (vehicle) for 24 hours. Cells were stained with Annexin V-FITC and Propidium Iodide (PI) and analysed on an Attune NxT acoustic flow cytometer. Scatter plots show the cell populations stained with Annexin V/PI for each condition. The bar charts show the percentage (%) of phosphatidyl-serine externalised cells (Annexin V^+) and the same data normalised to the parental cell line as fold change.

I treated the cells with 20 μM ABT-737 or 10 μM A-1210477 and 100 nM A-1881852 for 8 hours and then split the cells into two part, one stained with AnnexinV/PI as previously (**Figure 5.6**) and the second part was stained with TMRE (**Figure 5.7**). In the presence of ABT-737, USP30KO4 showed elevated levels of PS externalization compared to the parental while USP30KO1 and KO2 were at very similar levels (**Figure 5.6**). Using the combination of MCL-1 and BCL-X_L inhibitors (A-1210477 and A-1331852), USP30KO2 and KO4 displayed elevated levels of PS externsaliztion while USP30KO1 was very similar to the parental cells.

In the TMRE uptake assay, there were very few vehicle-treated cells with depolarised mitochondria whilst the combination of A-1210447 and A-1331852, but not ABT-737, induced the appearance of a clear peak of cells with depolarised mitochondria (**Figure 5.7**). The combination of A-1210447 and A-1331852 resuled in higher levels of cells with collapsed mitochondrial membrane potential in USP30KO2 and USP30KO4, whilst USP30KO1 had similar levels to the parental cells. The extent of apoptosis was marginally higher in some clones (USP30KO2 and 4) whilst KO1 behaved in a similar fashion to the WT clones and parental line.

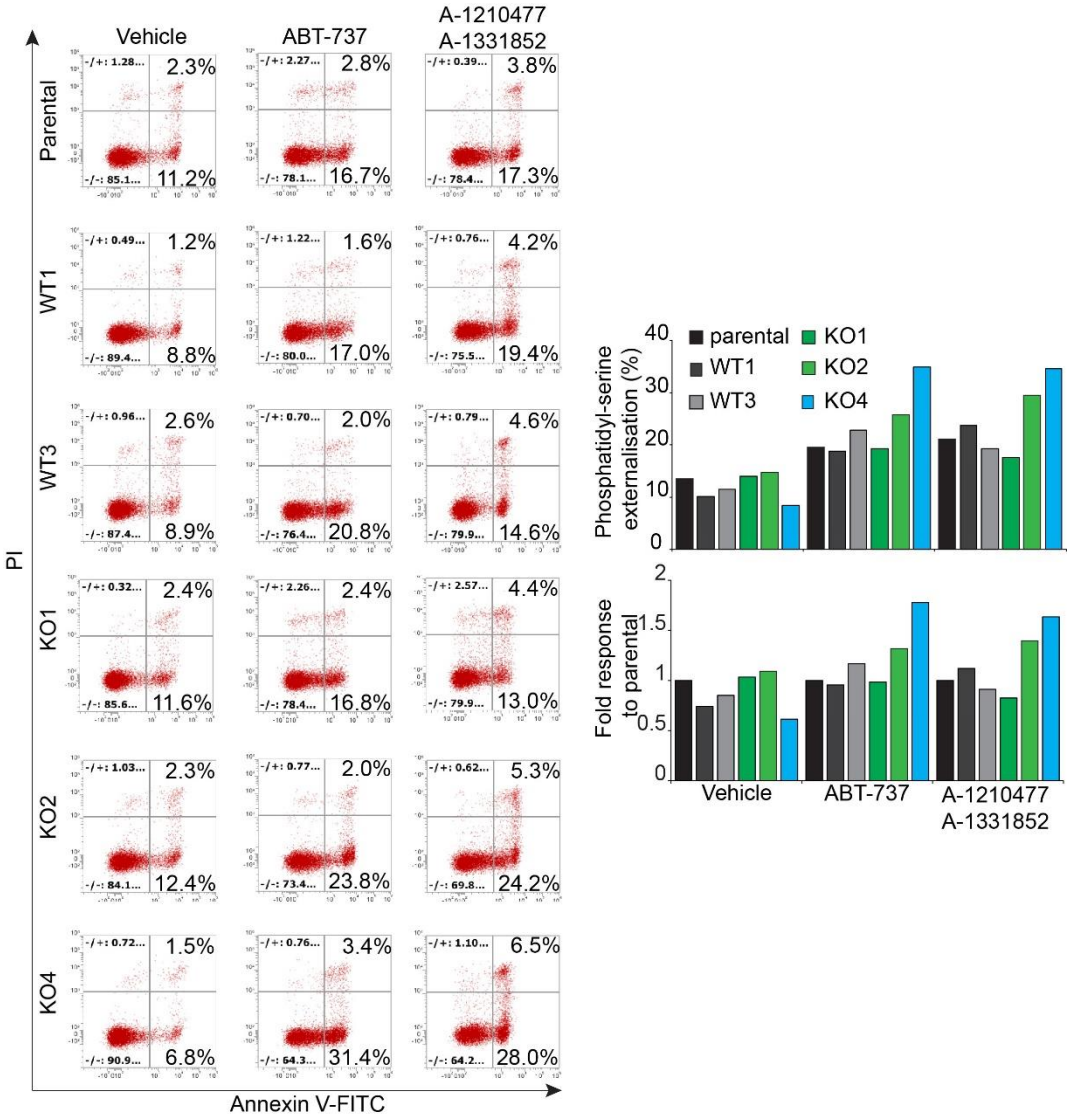

Figure 5.6: Phosphatidyl-serine externalisation of HCT116 FlpIn TRex USP30KO cells to different BH3 mimetics

HCT116 FlpIn TRex cells USP30 WT1, WT3, KO1, KO2, KO4 and the parental cell line were treated with 20 μM ABT-737 or 10 μM A-1210477 and 100 nM A-1331852 or DMSO (vehicle) for 8 hours. Cells were stained with Annexin V-FITC and Propidium Iodide (PI) and analysed on an Attune NxT acoustic flow cytometer. Scatter plots show the cell populations stained with Annexin V/PI for each condition. The bar charts show the percentage (%) of phosphatidyl-serine externalised cells (Annexin V^+) and the same data normalised to the parental cell line.

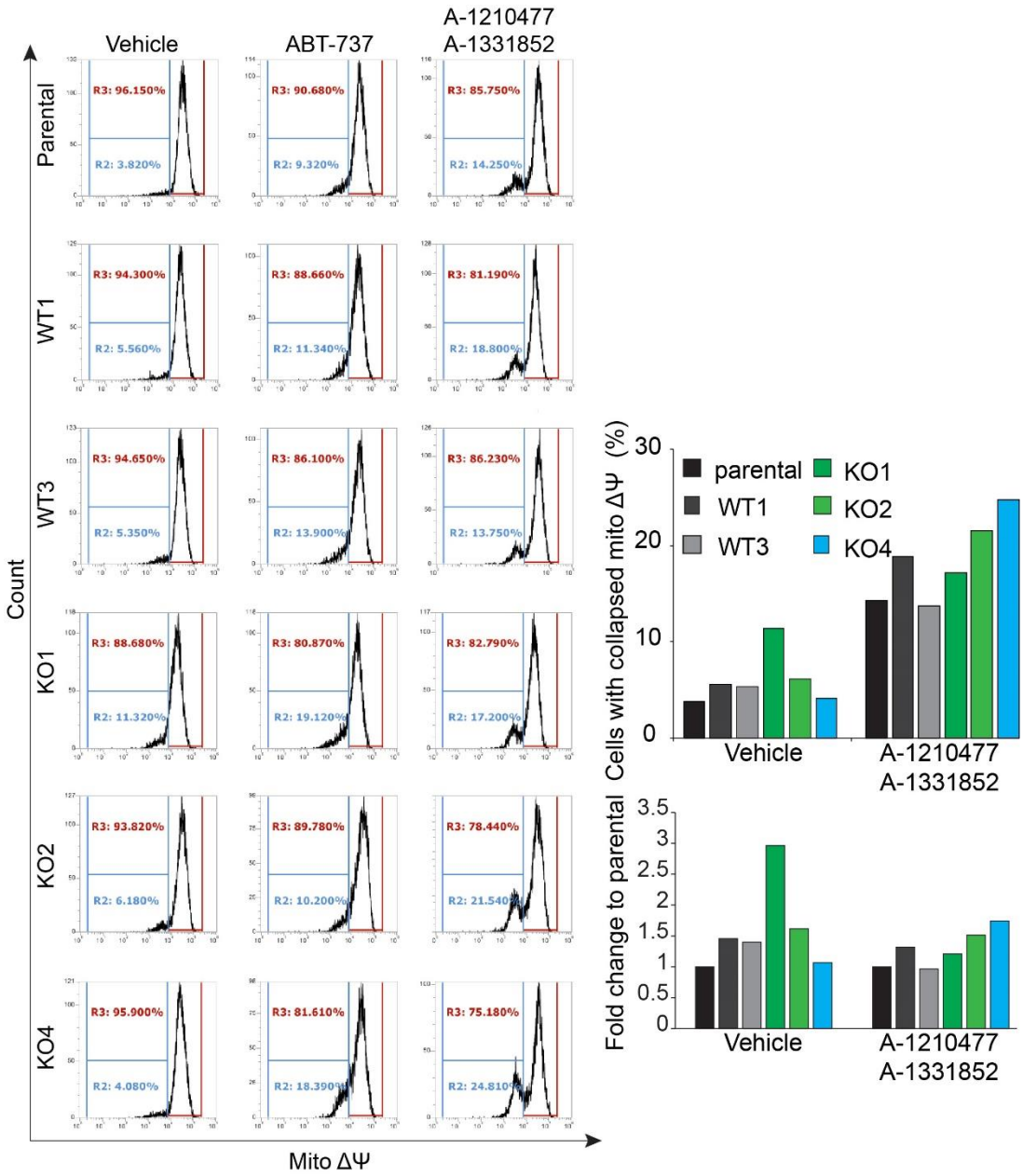

Figure 5.7: TMRE uptake in HCT116 FlpIn TRex USP30KO cells

HCT116 FlpIn TRex cells USP30 WT1, WT3, KO1, KO2, KO4 and the parental cell line were treated with 20 μM ABT-737 or 10 μM A-1210477 and 100 nM A-1331852 or DMSO (vehicle) for 8 hours. Cells were stained in media containing TMRE and the mitochondrial membrane potential (ΔΨ) was measured on an Attune NxT flow cytometer.

I compiled the PS externalisation data from the two experiments with ABT-737 for the 8-hour time point (**Figure 5.8**). There was a clustering of WT1 and the parental cell line near 15% PS externalisation and the KOs (1, 2 and 4) were ranging between 22%-28%. USP30KO2 and KO4 appeared to be the most consistent in displaying a sensitized response to ABT-737. WT3 showed elevated levels of PS externalisation compared to the parental, very similar to the levels of the KOs. It seemed that over two independent experiments there was a separation in the response of USP30KO clones compared to one WT clone and the parental cell line, suggesting a trend of a more sensitized albeit weak response (**Figure 5.8**).

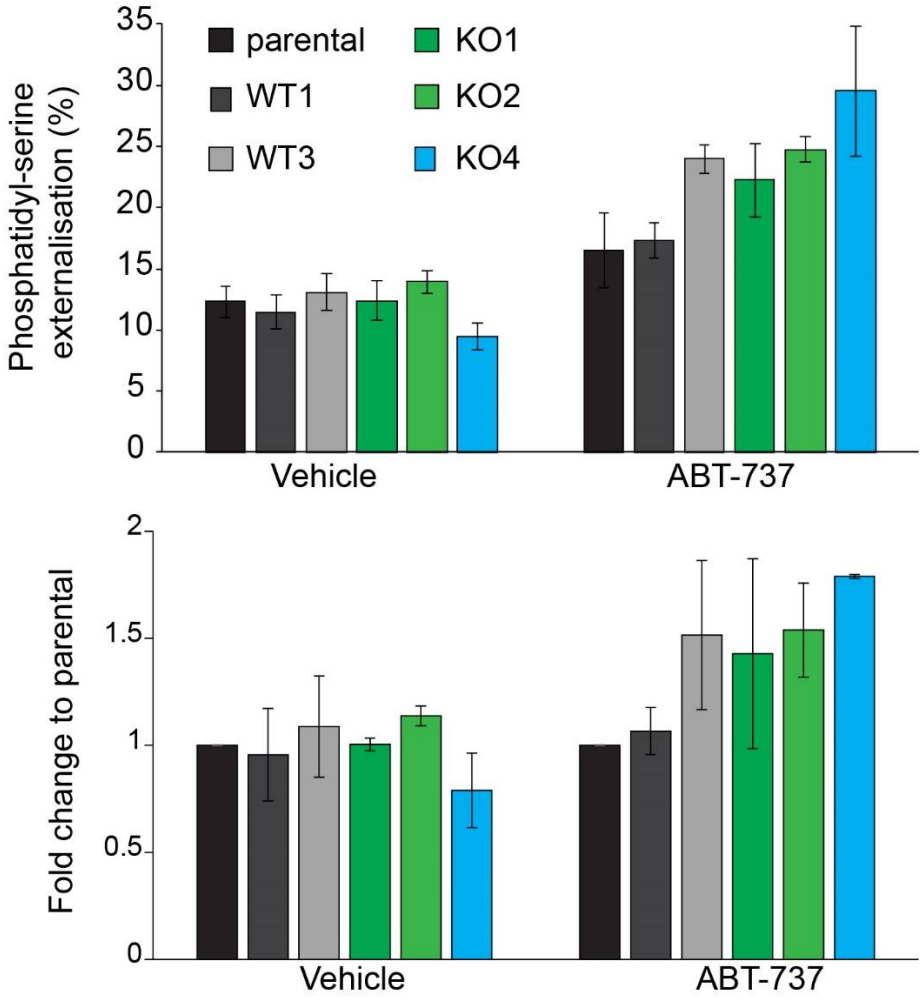

Figure 5.8: Quantitation of PS externalisation in the HCT116 FlpIn TRex USP30KO cells

Quantitation of PS externalisation assay in HCT116 FlpIn TRex USP30KO cells in response to 8 hours treatment with 20 μM ABT-737 or vehicle (DMSO). Bar chart is the mean and the error bars are the range between two independent experiments (n=2). Data are from **Figure 5.5** and **Figure 5.6**.

I next investigated whether sensitisation could be captured better by looking at earlier time points. I treated the HCT116 FlpIn TRex parental, USP30WT and USP30KO cells with 100 nM S-63845 and 100 nM A-1331852 for 0.5, 1, 2 and 4 hours (**Figure 5.9**). S-63845 is a newer generation of MCL-1 inhibitor that displays a 20-fold higher affinity for MCL-1 than the more well-established compound A-1210477 (Leverson et al., 2015b; Kotschy et al., 2016). A-1210477 has the additional disadvantage of binding serum albumin, reducing its effective concentration the cells are experiencing (Leverson et al., 2015b). I also included a pre-treatment with zVAD.fmk for 30 min prior to treating with the BH3 mimetics as a control for caspase-independent cleavage of PARP and caspase 3. The samples needed to be separated into two gels but the blots were scanned together with the same dynamic range making the two blots as directly comparable to each other as technically possible.

The USP30 blot showed that USP30KO4 may have a contaminating population of USP30WT cells and therefore that needs to be taken into account when trying to interpret the results. The pre-treatment with zVAD.fmk rescued the cleavage of PARP, albeit not completely, across all clones. It also produced a cleavage product of caspase 3 near 20 kDa instead of the typical cleavage product of 17 kDa. Pro-caspase 3 is found in the cytosol as inactive dimers and gets cleaved by activated caspase 9 at the interdomain linker into a large p20 subunit and a smaller p10 fragment. The p20 subunit undergoes a conformational change that exposes its own active site. The activated p20 subunit then removes its pro-domain and generates the fully-active p17 subunit (Ponder and Boise, 2019). This suggested that zVAD.fmk was preventing the efficient self-cleavage of the p20 subunit of caspase 3 into its mature form.

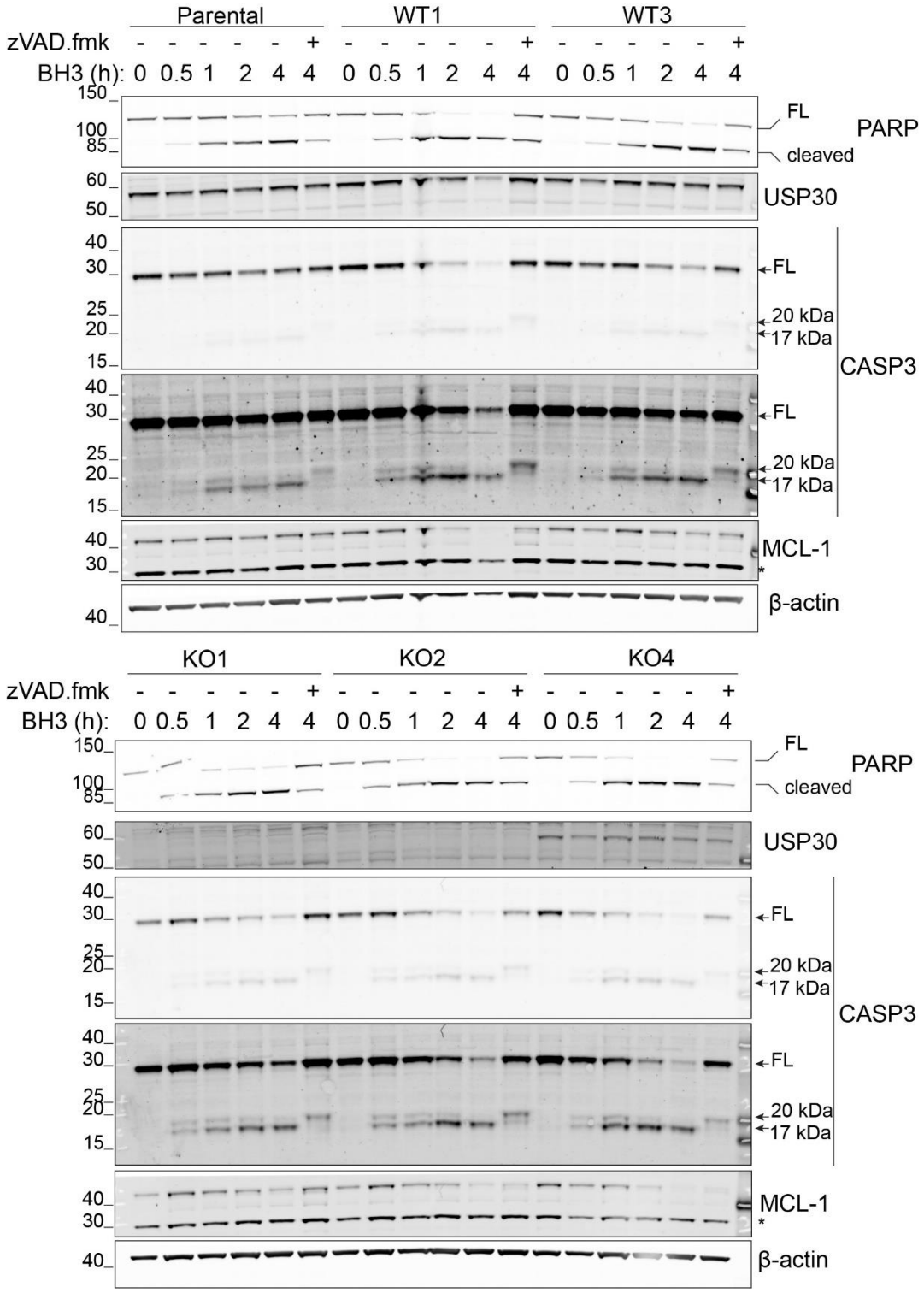

Figure 5.9: HCT116 FlpIn TRex time-course with BH3 mimetics

HCT116 FlpIn TREx USP30KO cells were treated with 100 nM S-63845 and 100 nM A-1331852 (BH3 mimetics) for the indicated time points (0.5, 1, 2 and 4 hours). A pre-treatment of 30 min with 30 μM zVAD.fmk was included in one of the 4-hour time-points. Cells were lysed in RIPA supplemented with PhosSTOP and MPIs (1:250). FL, full length; *, non-specific bands.

The levels of cleaved caspase 3 accumulated with faster kinetics in all three USP30KO clones compared to the parental cells in response to BH3 mimetics (**Figure 5.10**, upper graph). The enhancement was also evident from the loss of the full length (32 kDa fragment) of caspase 3 that was more pronounced in the USP30KO clones. Both USP30WT clones (WT1 and WT3) appeared to be display accelerated kinetics in the cleavage of caspase 3 compared to the parental, whilst not matching the kinetics of the USP30KO clones.

PARP cleavage was very similar in the USP30 clones, regardless of their USP30 status, and overall exhibited accelerated kinetics compared to the parental cells (**Figure 5.10**, lower graph). Both PARP and caspase 3 cleavage are direct readouts for apoptotic cell death. However, it appeared that PARP cleavage was reaching saturation earlier.

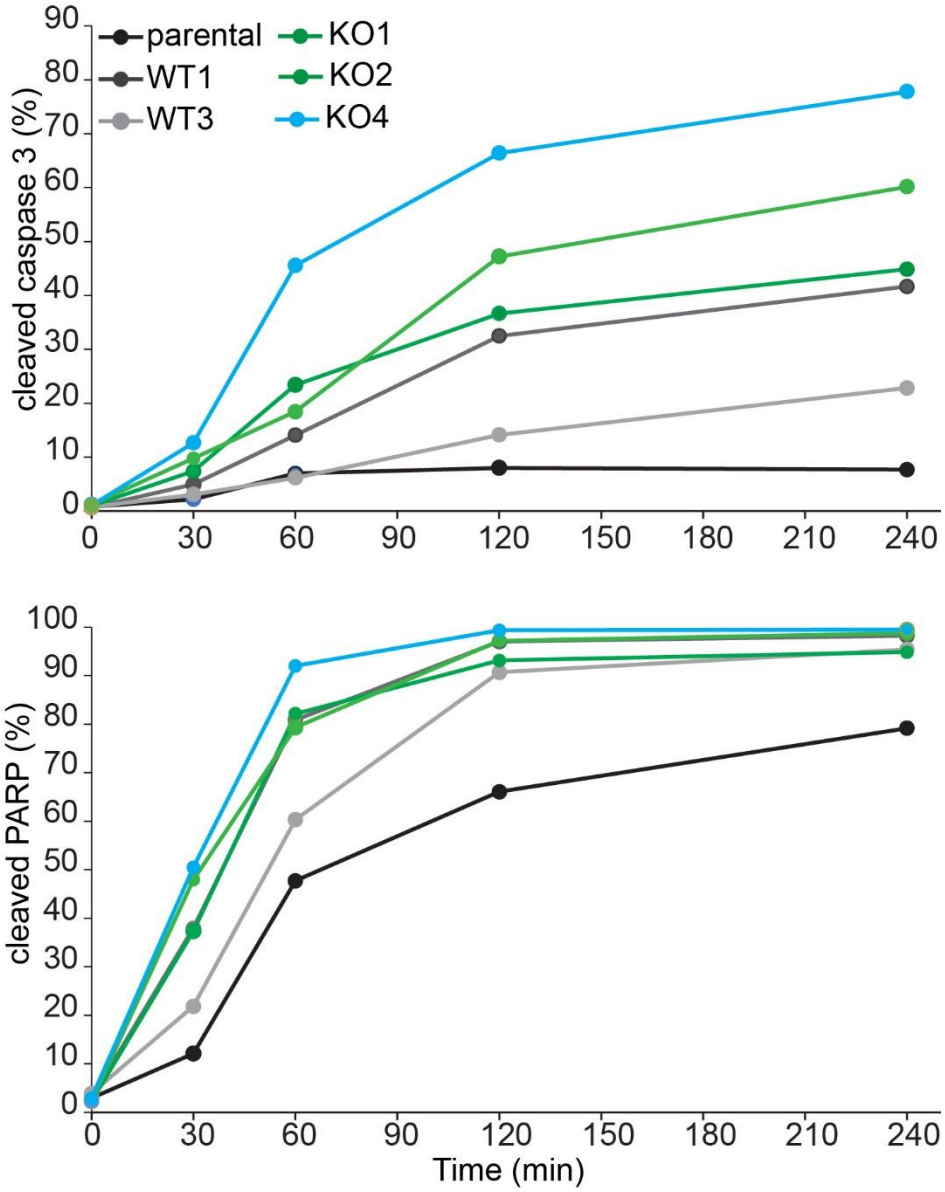

Figure 5.10: Quantitation of the response of HCT116 FlpIn TRex USP30KO to BH3 mimetics

The graphs show the quantitation of the percentages (%) of cleaved caspase 3 (12 + 20 kDa fragments as a percentage of total caspase 3 signal) and PARP (cleaved fragment as a percentage of total PARP signal) from the immunoblots in **Figure 5.9**.

the USP30KO clones exhibited significant levels of p85 PARP cleavage already from the 0.5 hour time-point whereas the WT clones and the parental line it required at least 1 hour (**Figure 5.9**). A similar pattern was observed for cleaved caspase 3, the USP30KO clones were showing detectable levels of cleaved caspase 3 from 0.5 hour and the WT clones needed the full hour to do so. Most importantly, this experiment appeared to be showing some evidence that the apoptotic cascade began earlier in USP30KO cells, as shown by the presence of cleaved caspase 3 and p85 PARP already at the half-hour time point.

I refined the above experiment to include only the earliest time-points since by 2 and 4 hours saturation was reached. Based on both PARP and caspase 3 cleavage, USP30KO2 and KO4 showed accelerated kinetics in their response to BH3 mimetics, as did USP30WT3. On the other hand USP30KO1 and USP30WT1 clones behaved very simiarly to the parental cells (**Figure 5.11**). The responses of the clones were inconsistent between USP30 positive and negative clones as well as between experiments.

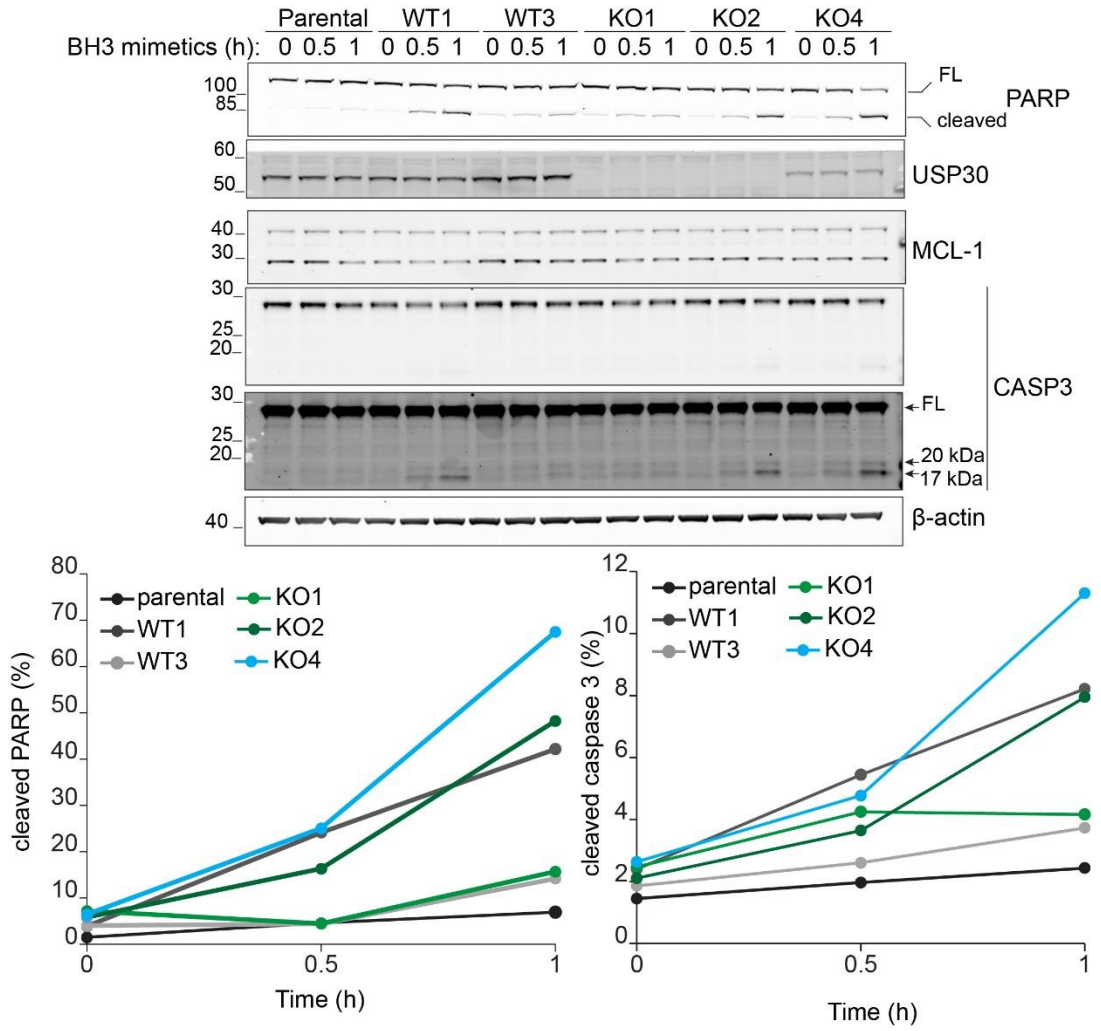

Figure 5.11: BH3 mimetic time course in HCT116 FlpIn TRex USP30KO cells

HCT116 FlpIn TREx USP30KO cells were treated with 100 nM S-63845 and 100 nM A-1331852 (BH3 mimetics) for the indicated time points (0.5, 1, and 2 hours). Cells were lysed in RIPA supplemented with PhosSTOP and MPIs (1:250). The graphs show the percentage of cleaved PARP and cleaved caspase 3 for each of the conditions.

5.2.3 The response of hTERT-RPE1 FlpIn TRex USP30KO cells to BH3 mimetics

I wanted to investigate the response of another USP30KO cell line that was available in the lab, the hTERT-RPE1 FlpIn TRex cells made by Elena Marcassa using the same procedure that I made use of (5.2). In chapter 4, I had determined that hTERT-RPE1 FlpIn TRex cells responded strongly to dual inhibition of MCL-1 and BCL-X_L and I chose to focus on using these inhibitors. I made use of A-1210477 and S-63845 as MCL-1 inhibitors and A-1331852 as the BCL-X_L inhibitor. I treated three USP30KO clones (KO1, KO2 and KO6), two WT clones (WT1 and WT3) and the parental cell line with 10 μM A-1210477 and 100 nM A-1331852 or 100 nM S-63845 and 100 nM A-1331852 for 6 hours. I assessed the effect of the BH3 mimetics using TMRE uptake by flow cytometry (**Figure 5.12**) and lysed a duplicate plate for immunoblot analysis (**Figure 5.13**).

The combination of A-1210477 and A-1331852 induced a substantial loss of mitochondrial membrane potential across the clones, whereas S-63845 and A-1331852 barely produced a response (**Figure 5.12**). This may suggest that S-63845 either has gone off or the treatment did not work despite the same inhibitor having worked in the previous experiments (**Figure 5.9** and **Figure 5.11**). More importantly, all clones showed higher percentage of cells with depolarised mitochondria than the parental cells, with no apparent differences between USP30 positive and negative clones (**Figure 5.12**).

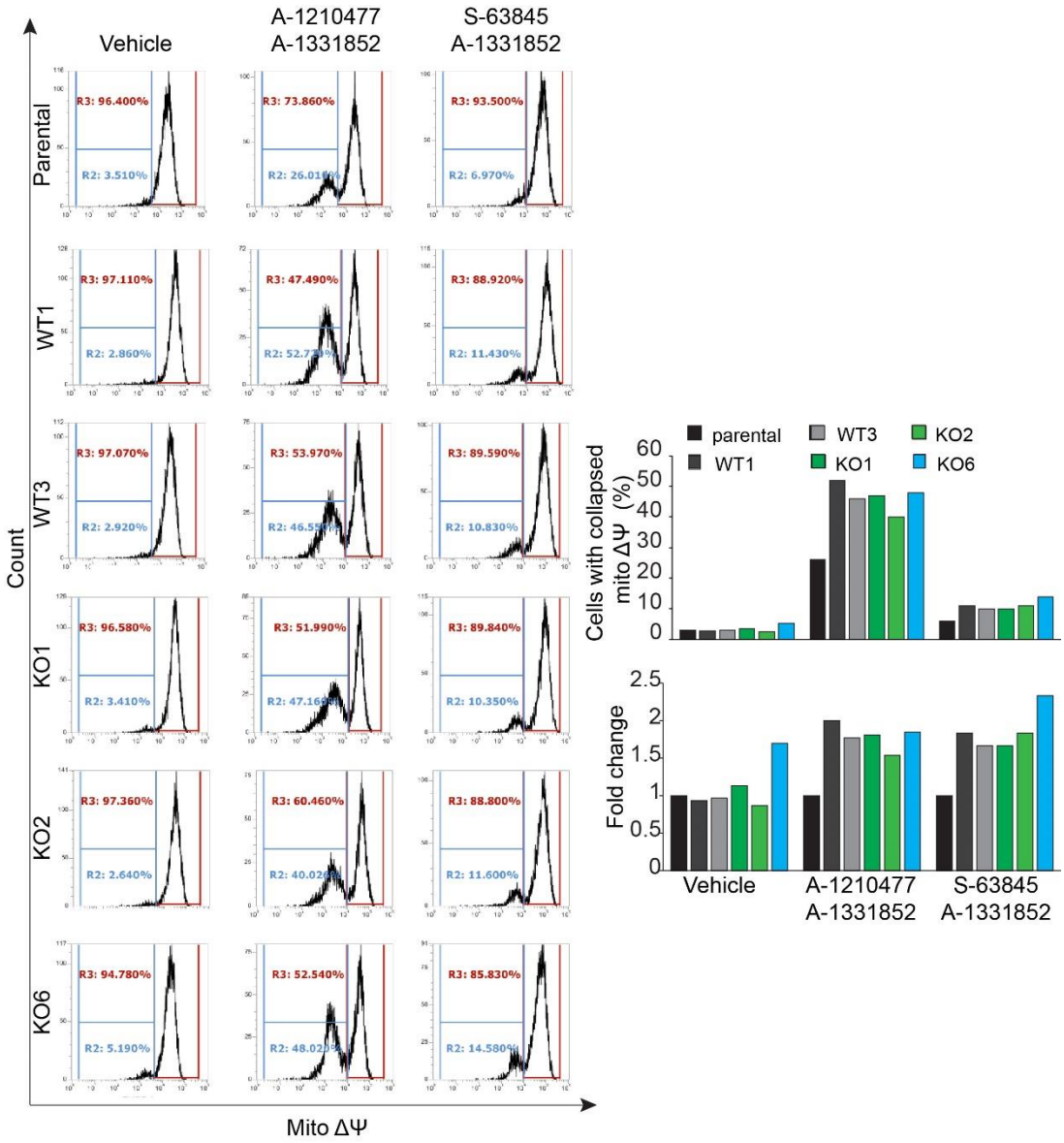

Figure 5.12: TMRE uptake in hTERT-RPE1 FlpIn TRex USP30KO cells in response to BH3 mimetics

hTERT-RPE1 FlpIn TRex cells USP30 WT1, WT3, KO1, KO2, KO6 and the parental cell line were treated 10 μM A-1210477 and 100 nM A-1331852 or 100 nM S-63845 and 100 nM A-1331852 or DMSO (vehicle) for 6 hours. Cells were stained in media containing TMRE and mitochondrial membrane potential (ΔΨ) was measured on an Attune NxT flow cytometer. The graphs show the percentage (%) of cells with collapsed mitochondrial membrane potential (ΔΨ) and the fold change to the parental for the same data.

Out of the USP30KO clones only KO6 displayed enhanced levels of cleaved PARP in the presence of A-1210477/A-1331852. All other clones showed very similar levels of cleaved PARP to the parental cell line. Interestingly, there were also substantial levels of cleaved BAK and BAX in the USP30KO clones and USP30WT1 compared to the parental, which is another hallmark of enhanced apoptosis (**Figure 5.13**).

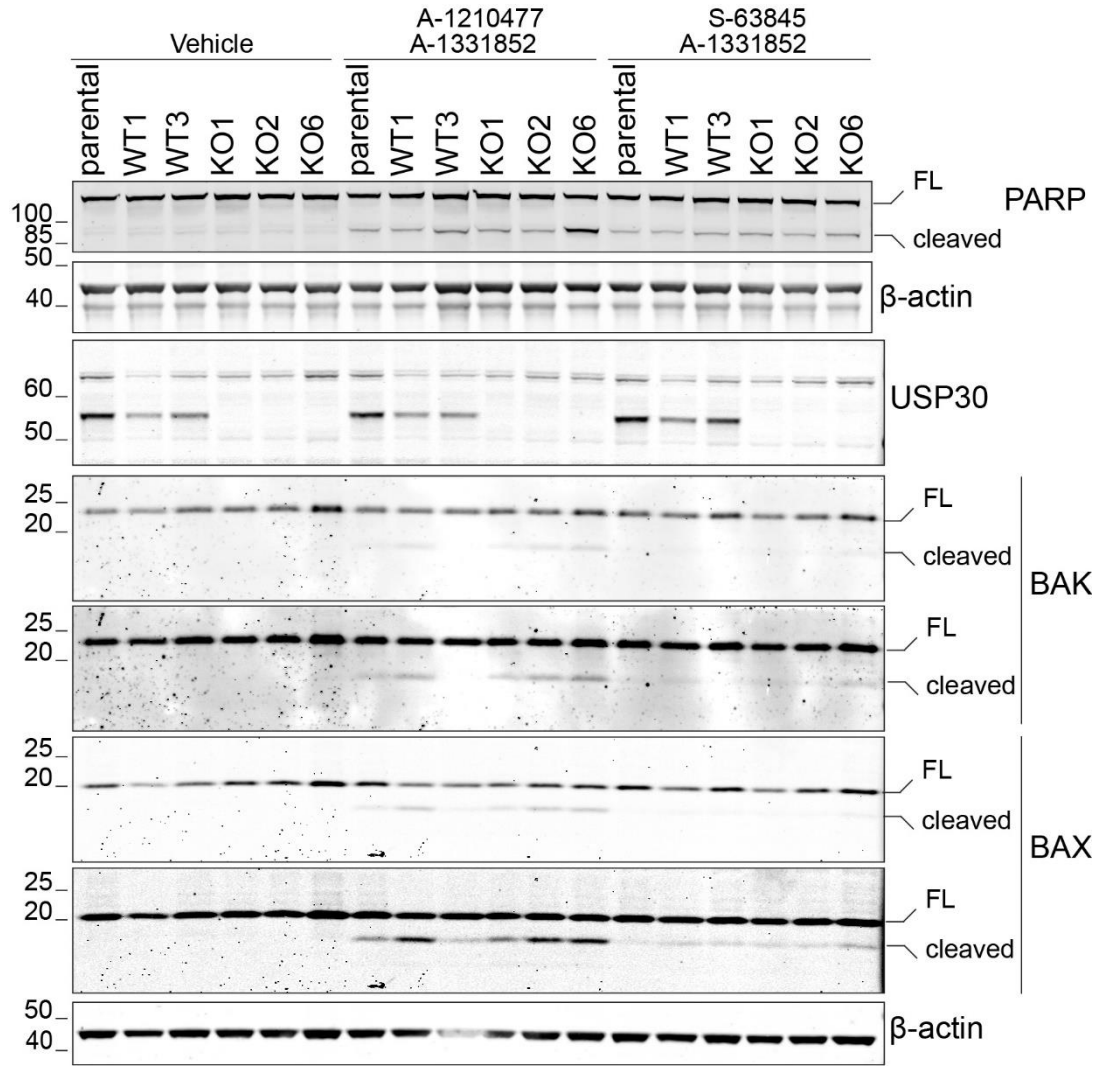

Figure 5.13: Response of hTERT-RPE1 FlpIn TRex USP30KO cells to BH3 mimetics

hTERT-RPE1 FlpIn TRex cells USP30 WT1, WT3, KO1, KO2, KO6 and the parental cell line were treated 10 µM A-1210477 and 100 nM A-1331852 or 100 nM S-63845 and 100 nM A-1331852 or DMSO (vehicle) for 6 hours. Cells were lysed in RIPA supplemented with PhosSTOP and MPIs (1:250).

The immunoblot recapitulated what the TMRE uptake was showing, which was that the S-63845/A-1331852 treatment did not seem to as efficient in inducing apoptosis. Overall, only USP30KO6 was showing evidence of sensitisation.

It remains that the USP30KO cells that I generated in the HCT116 FlpIn TRex cell line as well as the USP30KO cells in other cell lines generated by my colleagues in the lab, are an invaluable set of tools to study USP30 function in a variety of contexts.

The remaining sections of this chapter are focused on the role of USP30 in contexts outside that of apoptotic cell death. Such aspects are those concerned with the ability of cells to survive and proliferate under different conditions. Furthermore, I have sought to expand USP30 biology as a whole be performing RNA sequencing (RNA-seq) experiments and a small-scale proteomic experiment using these cells in an attempt to discover novel USP30 substrates or USP30-regulated processes.

5.3 Mitochondrial proteins expression in HCT116 FlpIn TRex USP30KO cells

I had previously assessed the levels of pro-apoptotic and anti-apoptotic BCL-2 proteins across the USP30KO clones that I generated in the HCT116 FlpIn TRex cells and there were no significant consistent changes in the levels of those proteins across the USP30KO cells (**Figure 5.3**). I also assessed the expression levels of OMM proteins including TOMM20 and TOMM22 that had previously been shown to be substrates of USP30 in Parkin-overexpressing cells (Liang et al., 2015a).

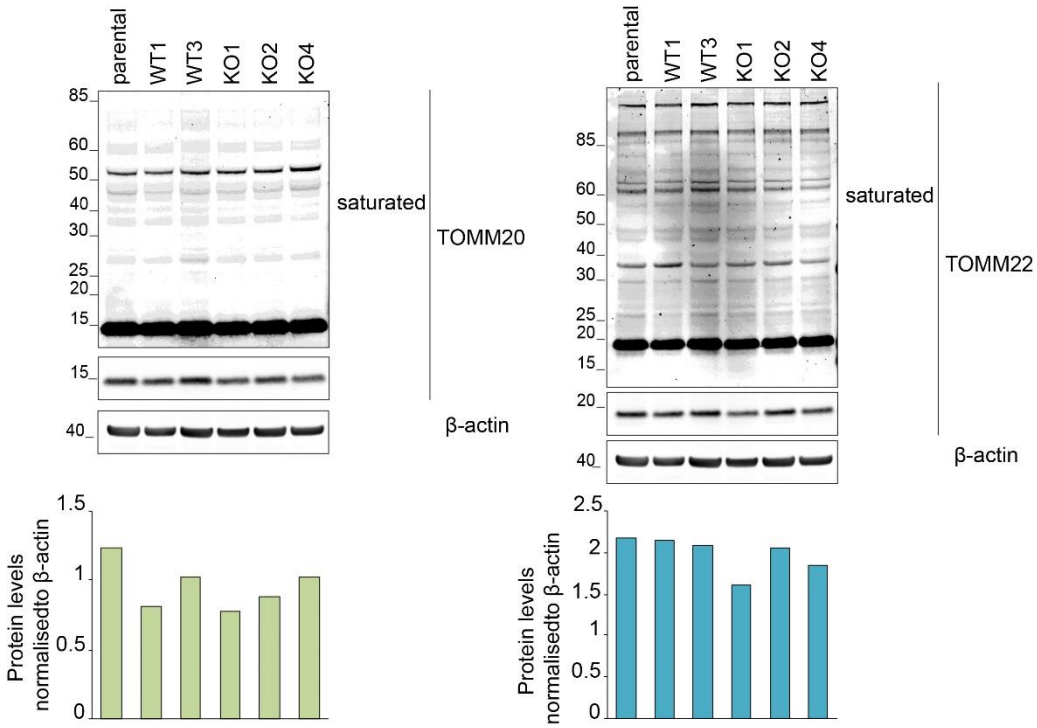

Figure 5.14: TOMM20 and TOMM22 protein levels in HCT116 FlpIn TRex USP30KO cells

HCT116 FlpIn TRex cells USP30 WT1, WT3, KO1, KO2, KO4 and the parental cell line were lysed in RIPA buffer supplemented with MPIs (1:250). The levels of protein were quantitated across cell lines and normalised to the β-actin loading control and are shown for TOMM20 and TOMM22.

There appeared to be no changes in the levels of neither TOMM20 nor TOMM22 when USP30 was knocked out, nor did I observe higher molecular weight species of these proteins that could be indicative of increased ubiquitylation (**Figure 5.14**).

I hypothesized that TOMM20 ubiquitylation may become detectable only if a mitophagy trigger was applied to the USP30KO cells. I treated the cells with 1 μM antimycin A/oligomycin A in the presence or absence of the proteasomal inhibitor epoxomicin for 6 hours (**Figure 5.15**). The proteasome inhibitor treatment was included in case the ubiquitylated species were not captured in the experiment due to rapid degradation. There were no changes in the levels of unmodified TOMM20 in response to any of the treatments. Furthermore, no consistent changes in high molecular weight bands corresponding to ubiquitylation of TOMM20 were visible.

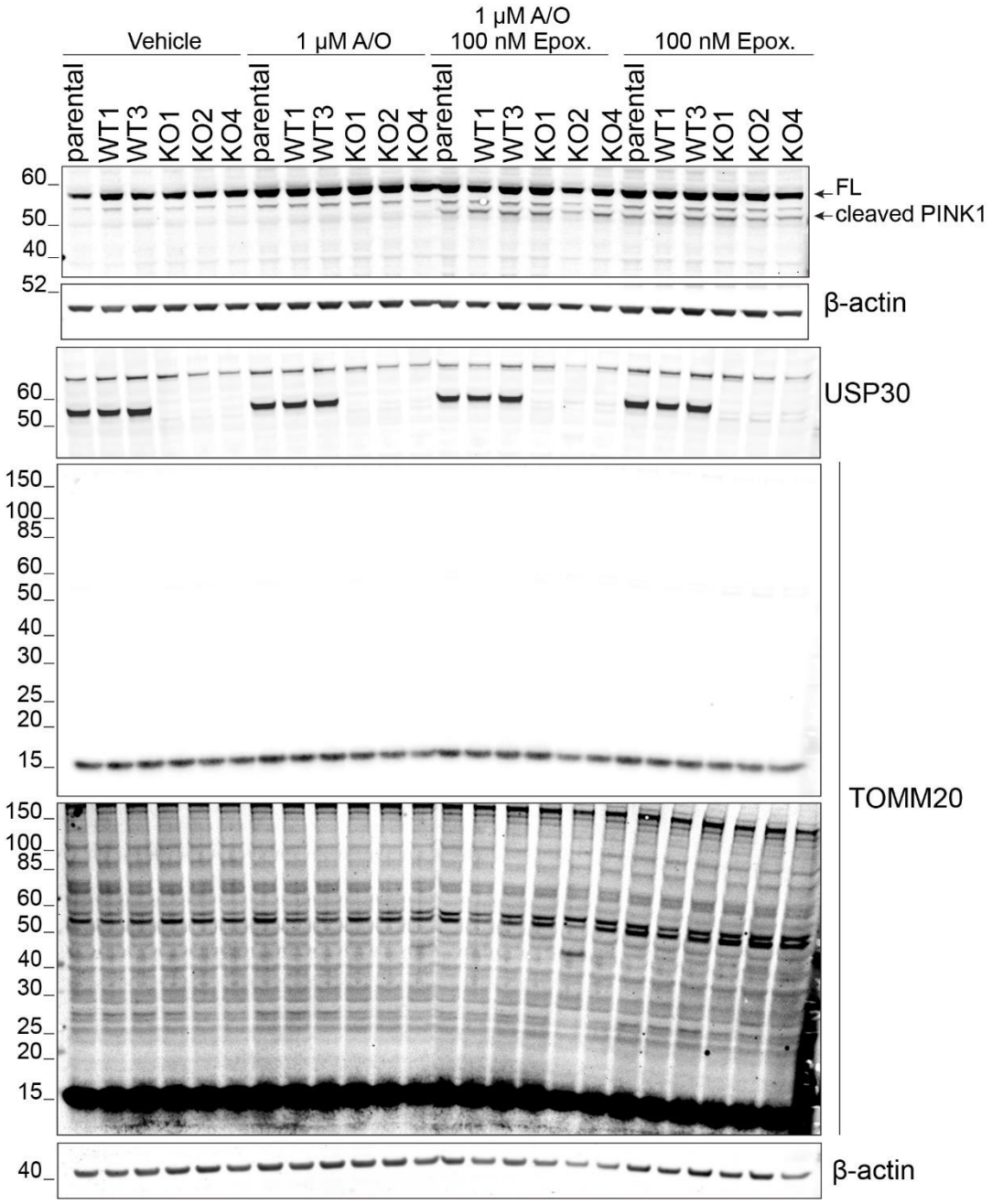

Figure 5.15: Mitophagy trigger in HCT116 FlpIn TRex USP30KO cells

HCT116 FlpIn TRex USP30KO clones (1, 2 and 4), USP30WT clones (1 and 3) and the parental cell line were treated with 1 µM antimycin A and 1 µM oligomycin A (A/O) or 100 nM Epoximicin (Epox.) or 1 µM A/O in the presence of 100 nM Epoxomicin or vehicle (DMSO) for 6 hours. Cells were lysed in NP-40 lysis buffer supplemented with PhosSTOP and MPIs (1:250). FL, full length.

The result was not unexpected given what is known about USP30 and TOMM20 ubiquitylation. The levels of TOMM20 ubiquitylation may be too low to detect in a straightforward immunoblot without having Parkin overexpression or a form of enrichment such as a pulldown or mitochondrial fractionation. The HCT116 cell line has detectable levels of endogenous Parkin, however they are probably too low to induce a detectable effect even in the absence of USP30.

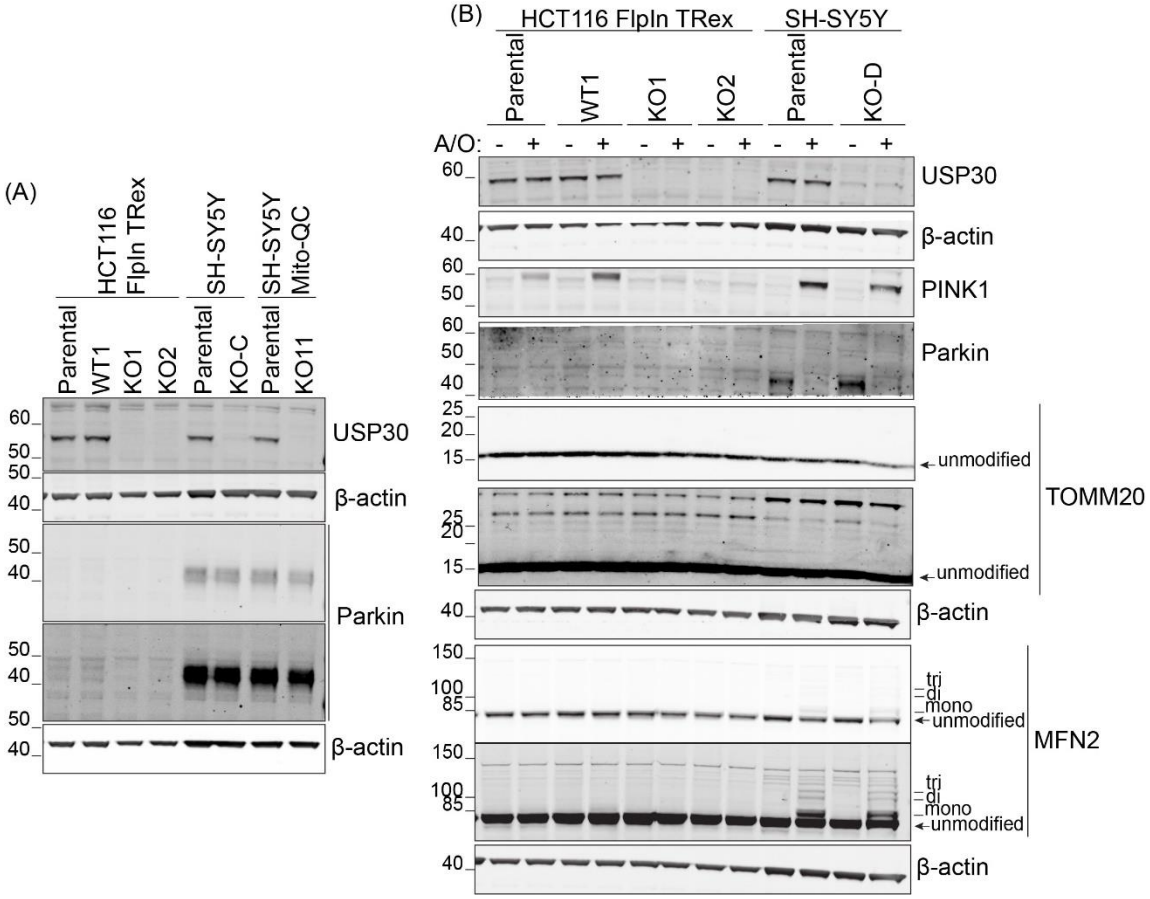

Figure 5.16: The effect of Parkin expression between HCT116 FlpIn TRex and SH-SY5Y cells

(A) Cell lysates from HCT116 FlpIn TRex parental, USP30WT1, USP30KO1 and KO2, SH-SY5Y parental and USP30KO-C and SH-SY5Y Mito-QC parental and USP30KO11 in RIPA supplemented with PhosSTOP and MPIs (1:250)

(B) HCT116 FlpIn TRex parental, USP30WT1, USP30KO1 and KO2, and SH-SY5Y parental and USP30KO-D were treated with 1 μM antimycin A and 1 μM oligomycin A (A/O) for 24 hours. Cells were lysed in RIPA supplemented with PhosSTOP and MPIs (1:250).

I selected two of the USP30KO clones, USP30WT1 and the parental HCT116 FlpIn TRex cells and compared the Parkin levels of expression to the neuroblastoma cells, SH-SY5Y and SH-SY5Y Mito-QC as well as their respective USP30KO clones that my colleague, Jane Jardine generated (**Figure 5.16**A). The SH-SY5Y cells express significantly higher levels of Parkin compared to the HCT116 FlpIn TRex, irrespective of USP30 status. Parkin expression is in fact barely detectable by immunoblot analysis in the HCT116 FlpIn TRex cells, which is typical for many established cell lines that often have very low or no detectable levels of Parkin.

I induced mitochondrial depolarisation using A/O for 24 hours in the USP30KO clones in the HCT116 FlpIn TRex and SH-SY5Y cells and analyzed the response of the cells by immunoblot (**Figure 5.16**B). In this particular experiment, TOMM20 was not differentially affected between USP30KO and WT cells in either of the two cell lines. The HCT116 FlpIn TRex USP30KO clones appeared to produce lower levels of PINK1 in response to A/O. I made a similar observation for PINK1 in KO-D in the SH-SY5Y cells even though the reduction was less pronounced. One plausible explanation for the reduced levels of PINK1 in the USP30KO clones is the enhanced levels of mitophagy USP30KO cells undergo and therefore there is a loss of the full length PINK1 species that accumulates on sites of mitochondrial damage through mitophagy. The same can be seen in the SH-SY5Y cells for Parkin, irrespective of USP30 status: Parkin is greatly reduced in the SH-SY5Y cells treated with A/O for 24 hours. The most striking difference was seen in the Mitofusin 2 (MFN2) blot where MFN2 mono-, di- and tri-ubiquitylated species were clearly visible on the blot only in the SH-SY5Y cells, suggesting that the levels of Parkin expression had a significant effect in the behaviour of cells in response to mitochondrial damage. The above effect was independent of USP30.

5.4 Phenotypic characterisation of USP30KO cells

5.4.1 Metabolic parameters assessed using SeaHorse Technology

Given its sub-cellular localisation, USP30 might also be implicated in the regulation of metabolic pathways operating in mitochondria, including the

tricarboxylic acid cycle (TCA cycle) or Kreb's cycle and the electron transport chain (ETC). Mitochondria produce ATP through the process of oxidative phosphorylation (OxPhos) using the ETC (Hill et al., 2012). The respiratory complexes of the ETC are large multi-subunit protein complexes that are embedded into the inner mitochondrial membrane. The function of the respiratory complexes is to transfer high energy electrons from substrates such as reduced Nicotinamide Adenine nucleotide (NADH) and succinate to the final electron acceptor, molecular oxygen (O_2), to create water. The overall process is thermodynamically driven by the high affinity of oxygen for electrons (Berry et al., 2018). The components of the ETC harvest the energy of electrons as they pass through this molecular wire and use it for the pumping of protons (H^+) from the matrix to the intermembrane space (IMS) across the inner mitochondrial membrane. This accumulation of protons in the IMS creates the proton-motive force (Δp), which consists of a chemical component (ΔpH) and a charge component ($\Delta\Psi_m$), involving all charged species (Mitchell, 1961). The energy stored in the proton-motive force is then used by the F_1F_0 ATPase or ATP synthase (sometimes referred to as Complex V of the ETC) to synthesize ATP. The processes of electron transfer, the pumping of protons and ATP synthesis are very tightly coupled to one another. When one of the three changes then the other two must follow by the same factor. The coupling of the three processes allows us to monitor their rate by measuring oxygen consumption since the ETC operates on oxygen.

Seahorse technology employs an oxygen electrode that allows oxygen consumption measurements by cells. The Mitochondrial Stress test that can be performed on the Seahorse instrument can be used to assess the operational capacity of mitochondria in the USP30KO clones (**Figure 5.17**). The mito stress test uses a number of mitochondrial poisons to sequentially perturb the ETC and enzymes involved in mitochondrial ATP production to extract metabolic parameters based on changes in oxygen consumption rate (OCR). The assay begins by measuring the basal levels of oxygen consumption by the cells termed **basal rate of respiration**. The first drug used is the F_1F_0 ATPase inhibitor, Oligomycin A. Oligomycin A stops the production of ATP by the ATPase causing OCR to decrease. The decrease in OCR corresponds to the oxygen previously consumed by the ETC to produce **ATP**.

Carbonyl cyanide-4-(trifluoromethoxy)phenylhydrazone (FCCP) is added, a proton ionophore that is able to pass membranes in either its protonated or deprotonated form. It continuously shuttles protons from the IMS to the matrix, resulting in the collapse of the proton-motive force.

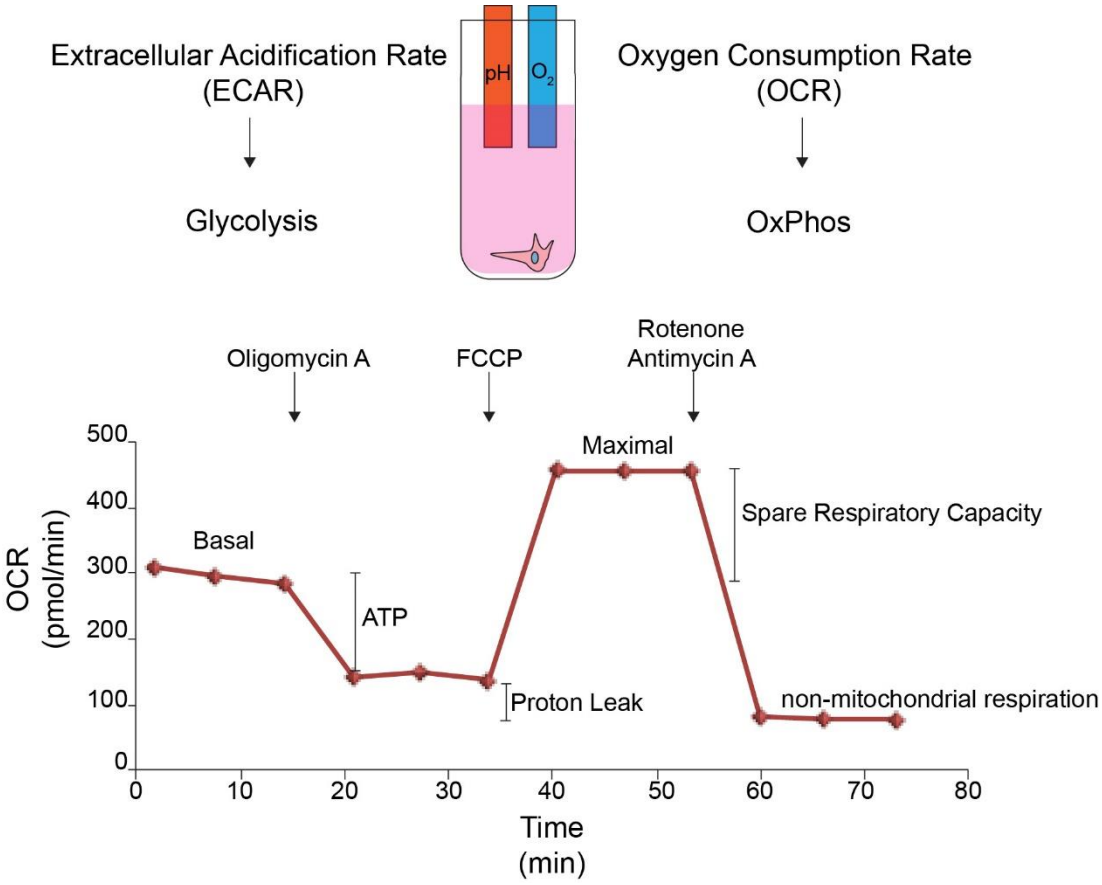

Figure 5.17: Measuring OCR using Seahorse Technology

Schematic representation of how a Seahorse instrument measures Extracellular Acidification Rate (ECAR) and Oxygen Consumption Rate (OCR) using a pH and an oxygen (O_2) electrode. A typical mito stress test trace measured as OCR (pmol of oxygen per min) is shown. The trace is first allowed to stabilise to establish the basal rate of respiration, before sequential addition of oligomycin A, FCCP and antimycin A/rotenone. The metabolic parameters of ATP production, proton leak, maximal respiration, spare respiratory capacity and non-mitochondrial respiration are indicated on the diagram. ATP, adenosine triphosphate; FCCP, Carbonyl cyanide-4-(trifluoromethoxy)phenylhydrazone.

With the proton-motive force collapsed, the ETC can operate at its **maximum capacity**, consuming oxygen at the highest possible rate. At this uncoupled state the instrument measures the maximal rate of respiration that is the maximal rate that the ETC is able to theoretically operate at. The difference between basal and maximal rates of respiration is termed **spare respiratory capacity** and it is a measure of how much the electron transport chain can be upregulated by should the cell require additional ATP. The final injection in the assay simultaneously introduces rotenone and antimycin A, which inhibit Complexes I and III respectively. With complexes I and III inhibited, the ETC does not operate and oxygen consumption by the mitochondrial ETC ceases. Therefore, any further oxygen consumption by the cells is termed **non-mitochondrial respiration** or **non-mitochondrial oxygen consumption**. The difference between non-mitochondrial oxygen consumption and the consumption after the addition of oligomycin A is termed **proton leak**, since it corresponds to oxygen consumption while ATP production is inhibited whilst ETC is still operational. Proton leakage is a measure of how well coupled the production of ATP is to oxygen consumption. Proton leak can be used as an indirect measure of mitochondrial fitness to produce ATP. The proton leak can be further subdivided into two components: true proton leak and electron leak. Electron leak refers to pre-mature escaping of electrons to oxygen prior to Complex IV. This translates into the energy of those electrons not being fully harnessed by the ETC to generate proton-motive force and produce ATP. Electron leak could be a result of damaged electron transport complexes allowing rogue electrons from escaping the wire pre-maturely. True proton leak refers to protons shuttling back to the matrix from the IMS by means other than through the F_1F_0 ATPase, which might be the result of damaged components in the inner mitochondrial membrane or expression of uncoupling proteins (Busiello et al., 2015; Berry et al., 2018). Proton leakage through these mechanisms does not result in ATP production.

I seeded 35,000 cells per well in a 96-well Seahorse cell culture microplate the day prior, in order to produce an evenly distributed monolayer on the day of the assay.

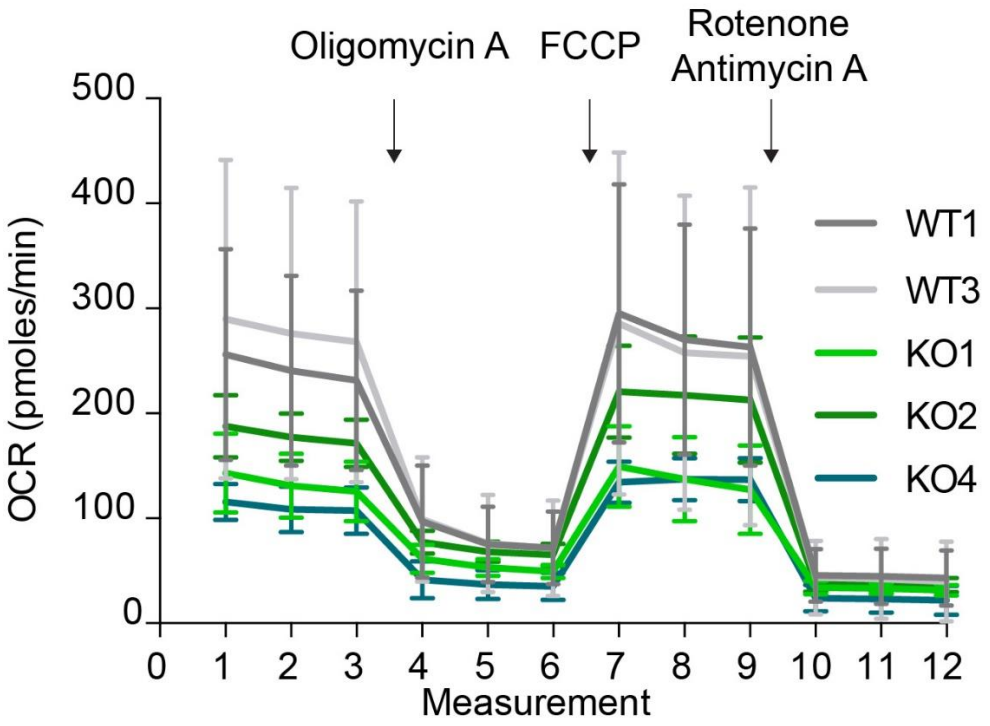

Figure 5.18: Mito Stress test in HCT116 FlpIn TRex USP30KO cells
HCT116 FlpIn TRex USP30KO clones (1, 2 and 4) and USP30WT clones (1 and 3) were seeded in a 96-well Seahorse cell culture microplates. Cells were treated with 1 µM oligomycin A, 0.5 µM FCCP and 1 µM antimycin A/rotenone after the indicated measurements. Oxygen Consumption Rate (OCR) was measured using a Seahorse XFe96 analyser instrument. The graph shows the mean values for each clone at each time point of measurement with standard deviation around the mean: WT1 (n=4), WT3 (n=3), KO1 (n=3), KO2 (n=4) and KO4 (n=3).

The Mito stress assay produced some interesting findings. First of all, I observed that the traces for the two wild-type and the three USP30KO clones clearly segregated from each other (**Figure 5.18**). All three USP30KO clones appeared to have lower rates of basal respiration compared to wild-type clones (**Figure 5.19**A). The oligomycin A injection lowered the OCR of all clones to the same baseline (**Figure 5.19**B). This result suggested that USP30KO clones might utilise the ETC to a lesser extent to meet their bioenergetics requirements in ATP. In other words, it is possible that USP30 null cells shift their metabolism towards a more glycolytic metabolism and utilise their mitochondria less.

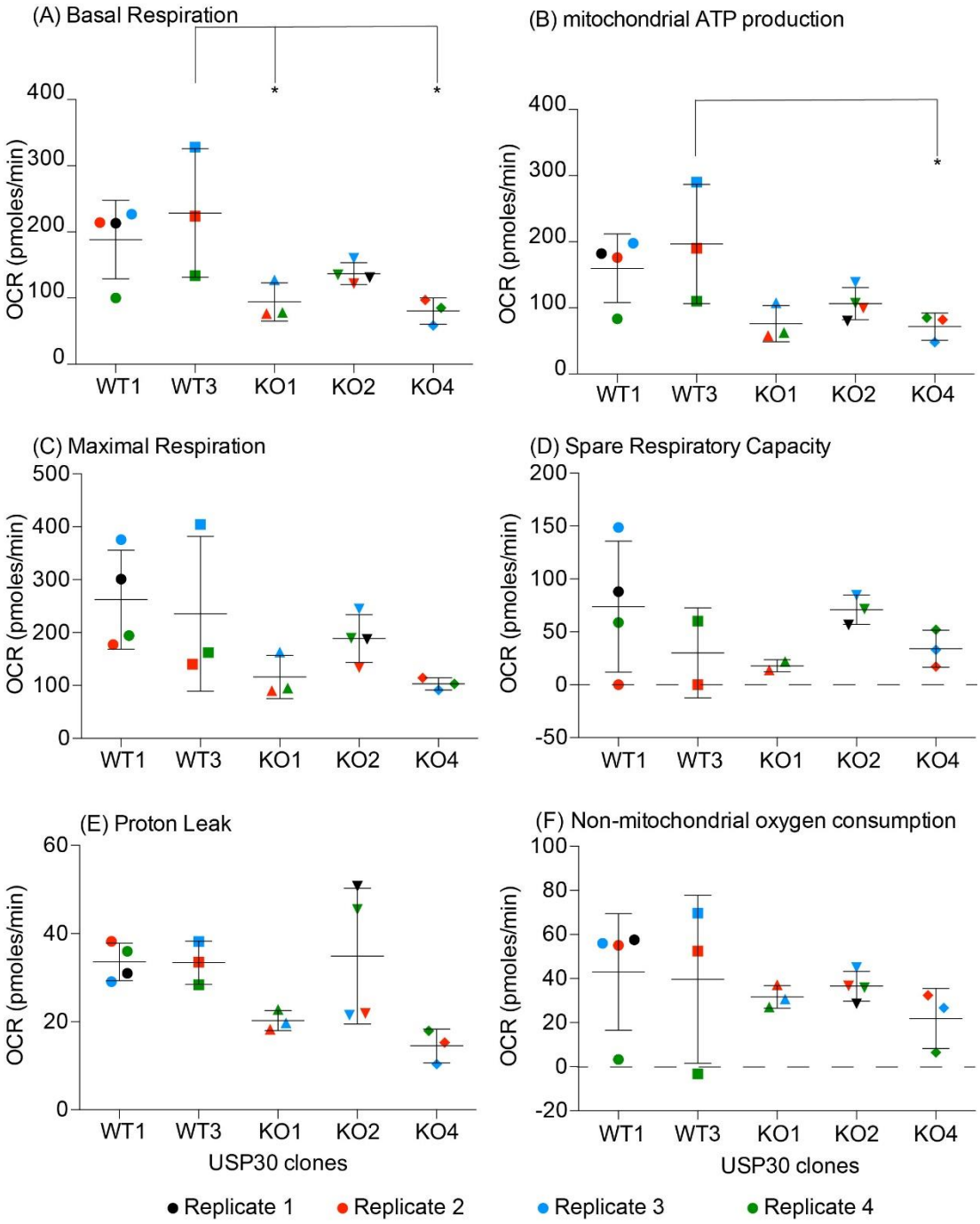

Figure 5.19: Specific metabolic parameters from Seahorse Mito Stress test in HCT116 FlpIn TRex USP30KO cells

Data from **Figure 5.18** for (A) Basal respiration, (B) Mitochondrial ATP production, (C) Maximal Respiration, (D) Spare Respiratory Capacity, (E) Proton Leak and (F) non-mitochondrial oxygen consumption. Data is coloured to show the spread of data amongst independent experiments. One-way ANOVA with Sidak multiple comparisons correction. *; p> 0.05.

Injection of FCCP depolarised mitochondria across all clones (**Figure 5.18**). Overall, there were no significant differences in the maximal respiration between USP30 positive and USP30 null cells, suggesting that the theoretical maximal rate of respiration was in fact very similar (**Figure 5.19**C). The data for basal respiration and maximal respiration may be indicative that whilst USP30KO cells may have the same maximal capabilities for respiration as their WT counterparts, they operate the ETC to a lesser extent under basal conditions.

Finally, the injection of Rotenone and Antimycin A suggested that the non-mitochondrial oxygen consumption of USP30KO clones was very similar to the wild-type clones, even though there was a trend that non-mitochondrial oxygen consumption was lower in USP30KO clones (**Figure 5.18**). The difference observed through was rather small and did not appear to be significant (**Figure 5.19**F). The proton leak calculated for this dataset was lower in the USP30KO compared to wild-type (**Figure 5.19**E). Again, the differences were small and did not prove to be statistically significant.

Extracellular acidification rate (ECAR) was simultaneously measured for the mito stress assays that I performed. ECAR is a measure of glycolytic function. Glycolysis produces lactate as a by-product and contributes to the acidification of the medium, which is then measured by the pH electrode in the instrument (**Figure 5.17**). Basal ECAR reflects the basal rate of glycolysis and maximal ECAR is after the injection of oligomycin A, which disables mitochondrial ATP production. Cells without mitochondrial ATP production can often upregulate glycolytic function to compensate for the loss of mitochondria and that is reflected as an increase in ECAR measurements. In my experiments there were no significant differences in basal nor maximal ECAR measurements between USP30KO and USP30WT cells, suggesting glycolytic function was unaffected (**Figure 5.20**, upper).

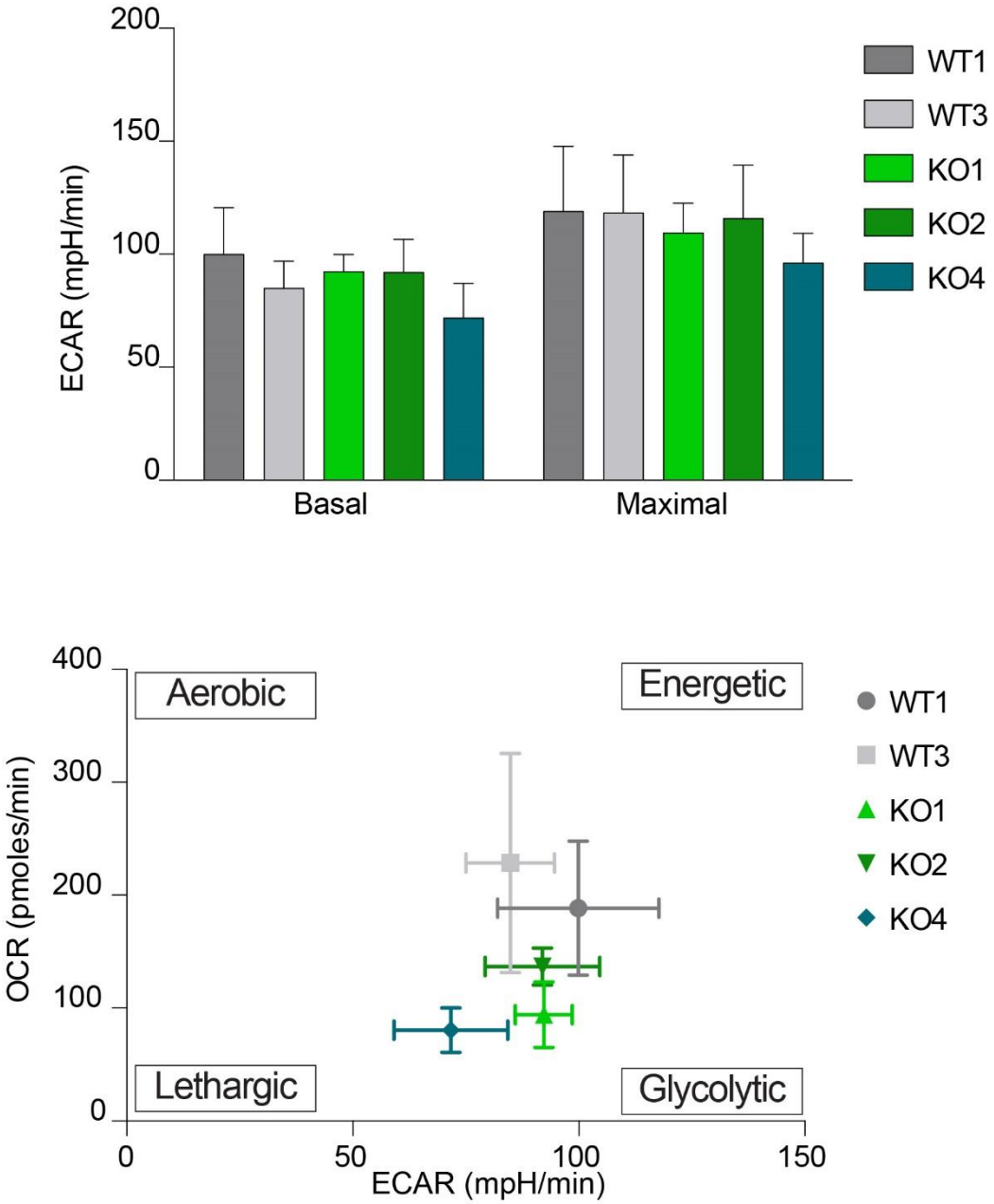

Figure 5.20: ECAR measurements and ECAR vs OCR overlay in HCT116 FlpIn TRex USP30KO cells

(Top) Extracellular acidification rate (ECAR) measurements from **Figure 5.18**. Basal ECAR is derived from the mean of measurements 1, 2 and 3. Maximal ECAR is derived after the oligomycin A injection, measurements 4, 5 and 6. (Bottom) Basal ECAR vs Basal OCR data overlay.

I then plotted the OCR against the ECAR to determine whether there were any shifts in the metabolic profiles of these cells (**Figure 5.20**, lower). The USP30KO cells appeared to be lower along the OCR axis, which was reflecting their behaviour in the basal respiration (**Figure 5.18** and **Figure 5.19**). On the other hand, the cells were not significantly shifting along the ECAR axis, except for USP30KO4 that was lower. Overall, there was no clear and consistent segregation in the behaviours between USP30KO and USP30WT cells.

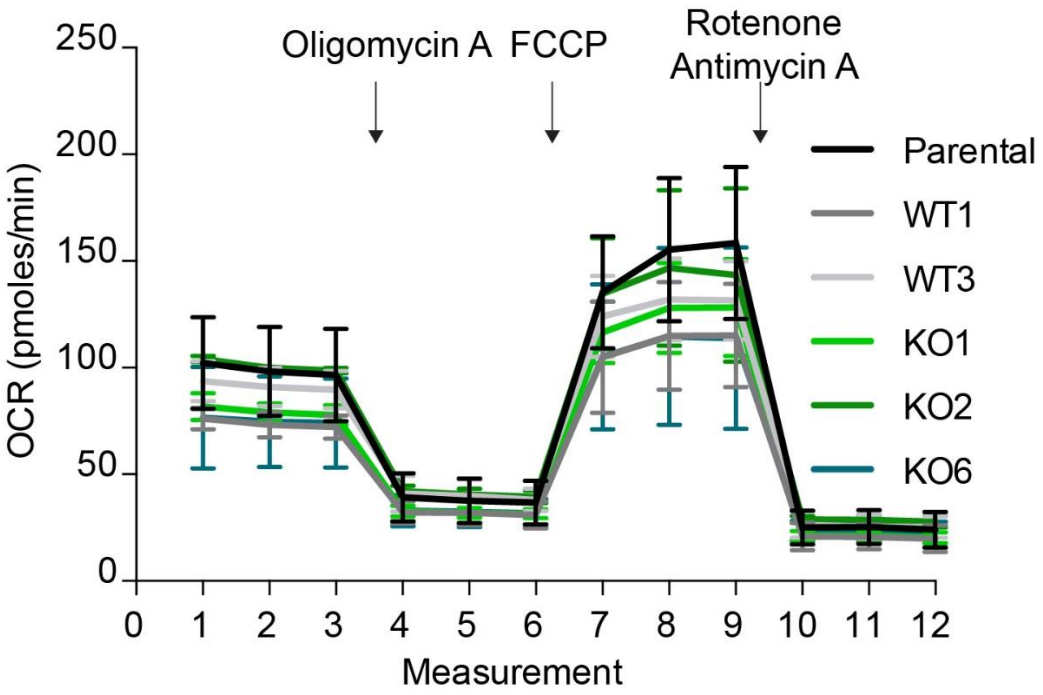

Figure 5.21: Mito Stress test in hTERT-RPE1 FpIn TRex USP30KO cells
hTERT-RPE1 FlpIn TRex USP30KO clones (1, 2 and 6), USP30WT clones (1 and 3) and the parental cell line were seeded in a 96-well Seahorse cell culture microplates. Cells were treated with 1.5 µM oligomycin A, 2.5 µM FCCP and 1 µM antimycin A/rotenone after the indicated measurements. Oxygen Consumption Rate (OCR) was measured using a Seahorse XFe96 analyser instrument. The graph shows the mean values and standard deviation for three independent experiments (n=3).

I also performed the mito stress test in the hTERT-RPE1 FlpIn TRex USP30KO cells that my colleague, Elena Marcassa generated. All three injections of the mitochondrial poisons were successful in achieving the expected responses in terms of OCR. The OCR traces showed no consistent differences in the behaviours of USP30KO and USP30WT cells (**Figure 5.21**). One USP30KO clone (KO2) behaved very similarly to parental cells, whilst one USP30WT clone (WT1) segregated with the other two USP30KO clones.

Having a closer look at the specific metabolic parameters of these cells revealed that there were no statistically significant differences either (**Figure 5.22**).

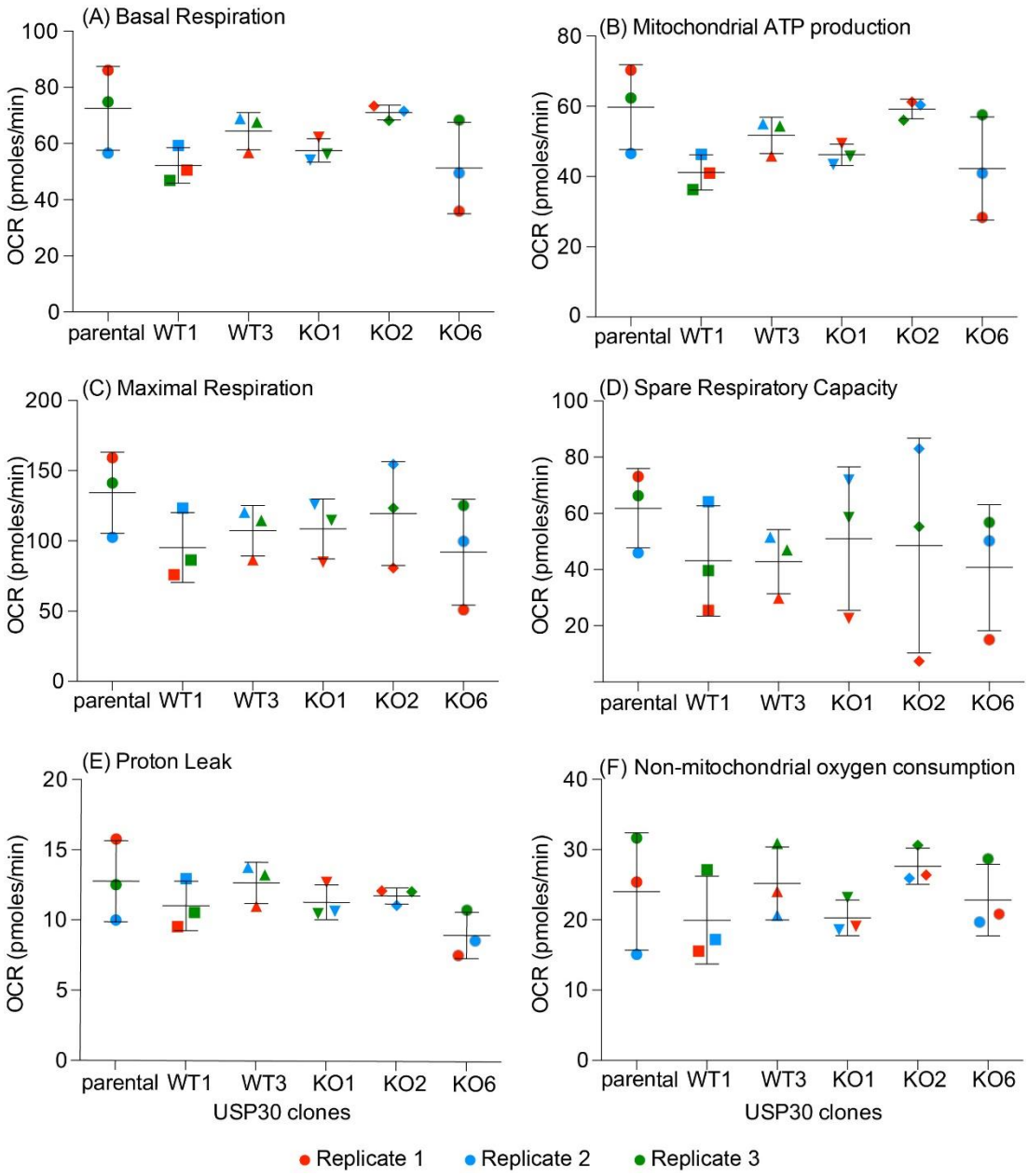

Figure 5.22: Specific metabolic parameters from Seahorse Mito Stress test in hTERT-RPE1 FlpIn TRex USP30KO cells

Data from **Figure 5.21** for (A) Basal respiration, (B) Mitochondrial ATP production, (C) Maximal Respiration, (D) Spare Respiratory Capacity, (E) Proton Leak and (F) non-mitochondrial oxygen consumption. Graphs show the mean and standard deviation over three independent experiments (n=3). Data is coloured to show the spread of data amongst independent experiments. One-way ANOVA with Sidak multiple comparisons correction. *; p> 0.05.

Similarly, both the basal and maximal glycolytic capacity of these cells were unaffected by USP30KO (**Figure 5.23**, upper). Overall, the knock-out of USP30 did not seem to change the metabolic profiles of hTERT-RPE1 FlpIn TRex cells (**Figure 5.23**, lower).

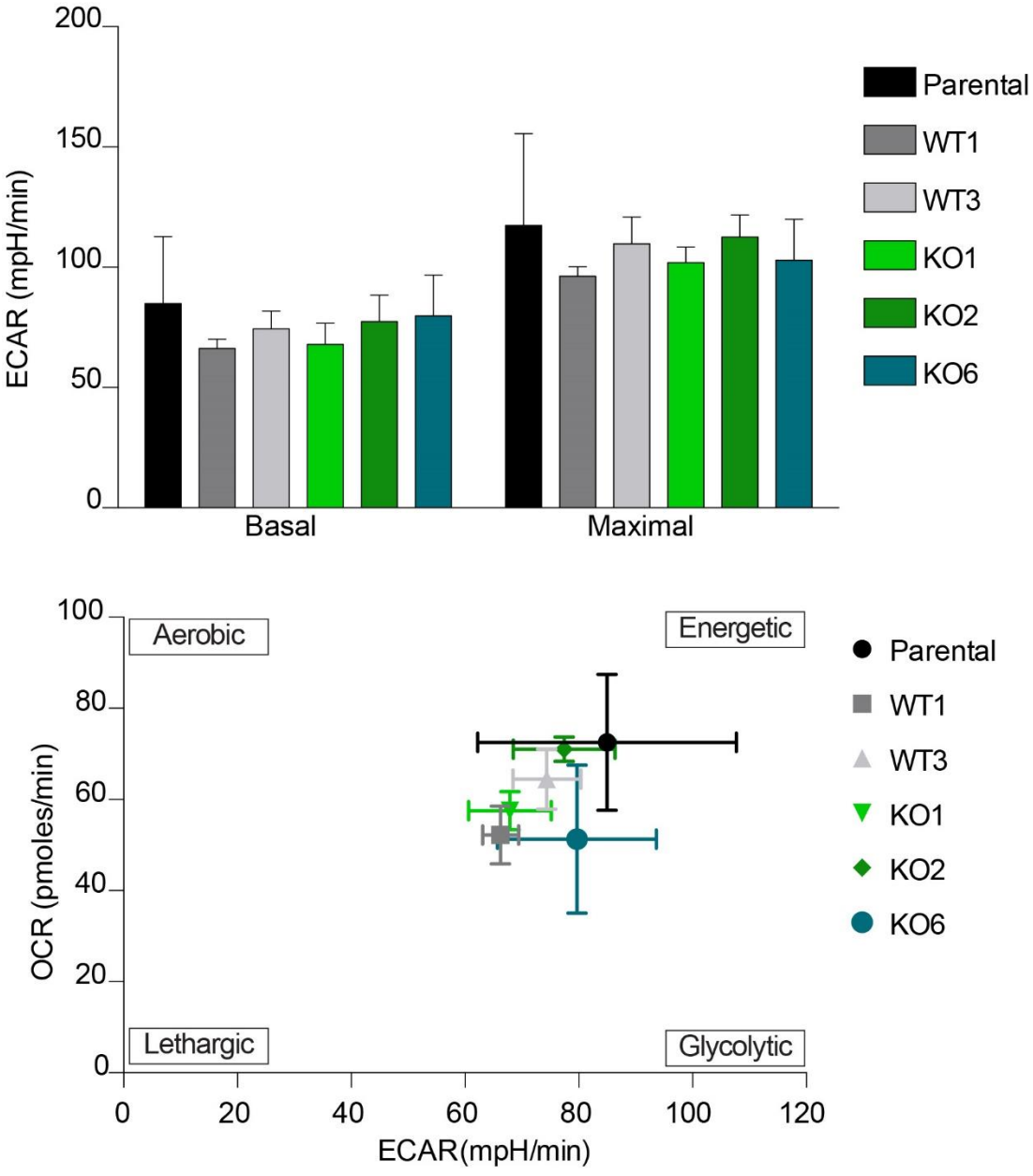

Figure 5.23: **ECAR measurements and ECAR vs OCR overlay in hTERT-RPE1 FlpIn TRex USP30KO cells**

(Top) Extracellular acidification rate (ECAR) measurements from **Figure 5.21**. Basal ECAR is derived from the mean of measurements 1, 2 and 3. Maximal ECAR is derived after the oligomycin A injection, measurements 4, 5 and 6. (Bottom) Basal ECAR vs Basal OCR data overlay. Graphs show the mean and standard deviation over three independent experiments (n=3).

5.4.2 Direct ATP measurements in USP30KO cells

I wanted to characterise the metabolic capabilities of the USP30KO cells by measuring the levels of ATP in a direct fashion. I made use of CellTiter Glo® (Promega) that is marketed as a cell viability kit and measures ATP levels, a proportional measurement of live cells. The kit employs beetle luciferin and recombinant luciferase that in the presence of ATP generates luminescence that is measured by a luminometer (**Figure 5.24**A).

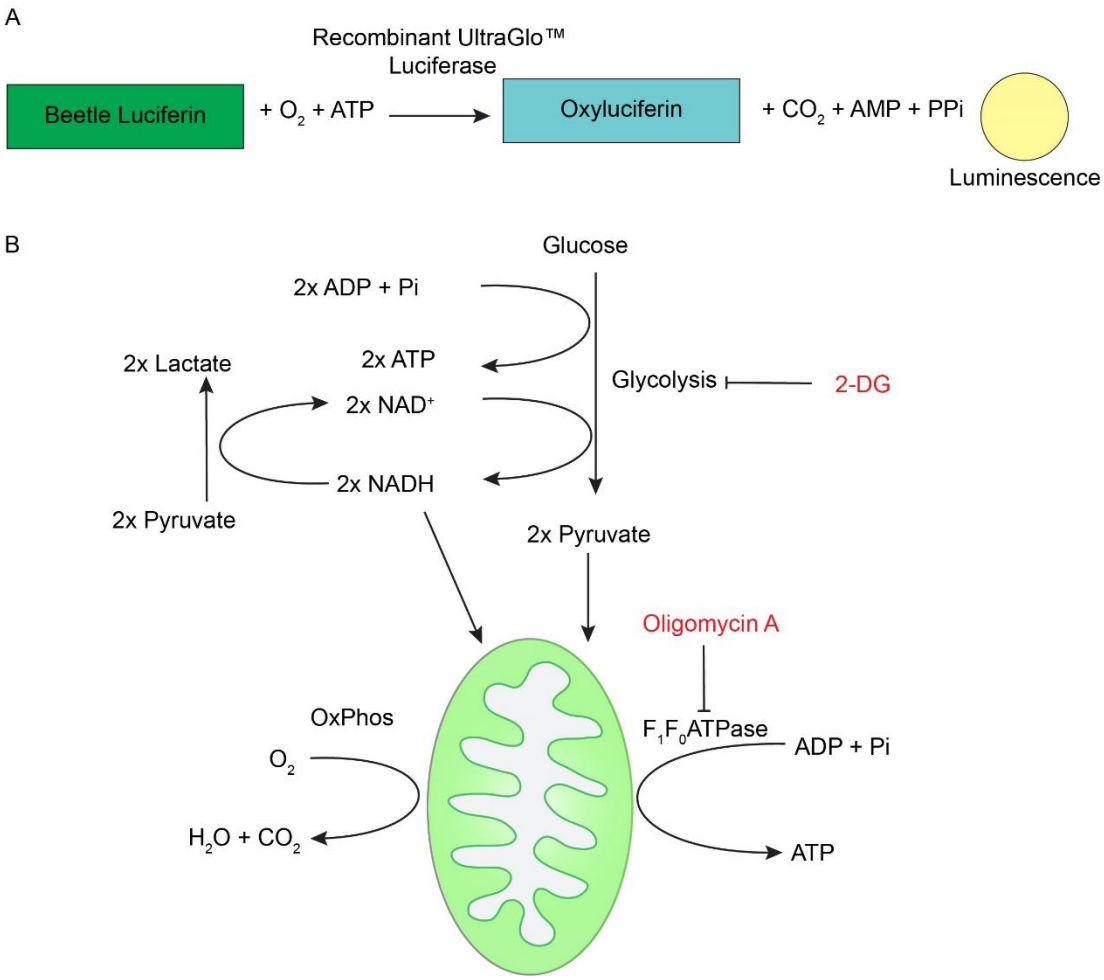

Figure 5.24: Measuring intracellular levels and sources of ATP

(A) Schematic representation of the enzymatic reaction that detects ATP levels. (B) Schematic representation of the use of Oligomycin A and 2-deoxyglucose to detect sources of ATP generated by the cell. ATP; adenosine triphosphate, AMP; adenosine monophosphate, PPi; pyrophosphate, Pi; inorganic phosphate, NAD^+; oxidised Nicotinamide adenine dinucleotide, NADH; reduced Nicotinamide adenine dinucleotide, OxPhos; oxidative phosphorylation, 2-DG; 2-deoxyglucose.

I have modified the protocol in order to determine the sources of cellular ATP as well. I seeded the same number of cells and the following day I incubated the cells with oligomycin A, which inhibits F_1F_0ATPase and therefore blocks mitochondrial ATP production. In parallel I incubated a set of cells with 2-deoxyglucose (2-DG) that blocks flux through the glycolytic pathway. The above experimental setup would allow me to determine which is the main metabolic pathway and the relative contributions to the total cellular ATP levels (**Figure 5.24**B). I first performed the experiment in the HCT116 FlpIn TRex USP30KO cells by incubating the cells with 1 µM oligomycin A or 50 mM 2-DG or both inhibitors together for 30 minutes before adding the CellTiter Glo™ reagent (**Figure 5.25**).

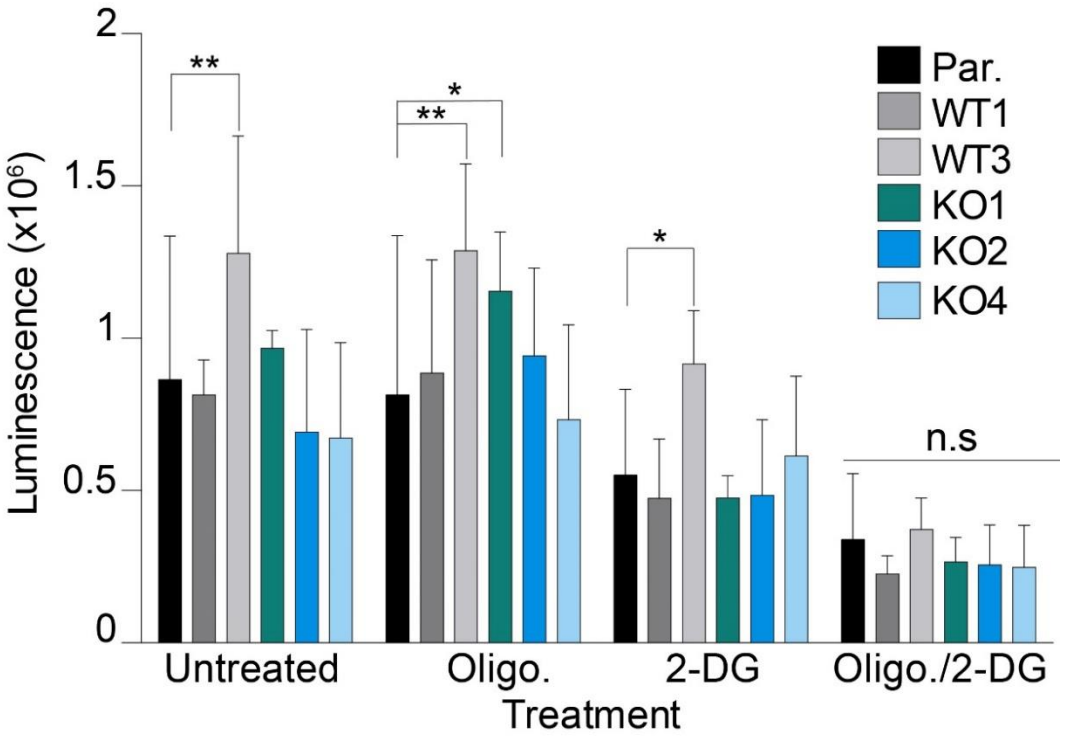

Figure 5.25: Intracellular levels and sources of ATP in HCT116 FlpIn TRex USP30KO cells

HCT116 FlpIn TRex USP30KO cells were treated with 1 µM Oligomycin A (Oligo) or 50 mM 2-deoxyglucose (2-DG) or both or left untreated. Luminescence signal indicates the levels of ATP in each condition. The bar charts represent the mean and error bars the range of three independent experiments (n=3). Two-way ANOVA with Bonferroni correction to allow for multiple comparisons to the parental cell line *; $p<0.05$, **; $p<0.01$, ***; $p<0.001$, ns; non-significant.

The basal ATP levels did not appear to be significantly different between wild-type and USP30KO cells. USP30WT3, but not any other clones, showed a statistically significant difference compared to the parental cell line, however this was most likely reflecting clonal variation as both cell lines were wild-type for USP30. Treatment with oligomycin A produced no measurable differences compared to untreated, indicating that Oxidative Phosphorylation (OxPhos) is dispensable for ATP production in these cells. The above observation was consistent regardless of USP30 status. On the contrary, treatment with 2-DG caused a decrease of about 50% in luminescence output across all clones. The above indicated that these cells utilised glycolytic metabolism and were unable to sufficiently upregulate OxPhos to cover their ATP demands, when glycolysis was inhibited. When I co-treated cells with both 2-DG and oligomycin A, there was a further decrease in luminescence compared to 2-DG treatment alone. The difference between dual inhibition and 2-DG inhibition alone is reflecting the small contribution of OxPhos in these cells. Overall, it appeared that these cells were highly glycolytic while mitochondrial function was dispensable under these conditions, and USP30 status was not affecting this phenotype. I therefore considered making these cells dependent on mitochondria for their ATP requirements and assessing whether USP30 was important in this setting, by growing the cells in media containing galactose instead of glucose (Rossignol et al., 2004; MacVicar and Lane, 2014; Shiratori et al., 2019). The standard DMEM medium I have been using to grow the HCT116 FlpIn TRex cells contains 25 mM glucose. I therefore used DMEM without any glucose, which I supplemented with 25 mM galactose instead and grew the cells in the presence of galactose for a period of two weeks to acclimatise them to the new substrate.

I then incubated the HCT116 FlpIn TRex USP30KO cells with oligomycin A and 2-DG in the galactose-containing media (**Figure 5.26**). In the untreated condition, there were no major changes in the levels of ATP across cell lines suggesting galactose was not differentially affecting ATP levels in USP30KO and USP30WT cells. Treating the cells with oligomycin A reduced the levels of ATP across all cell lines to approximately 50% of the untreated, suggesting OxPhos was required for ATP generation in these cells.

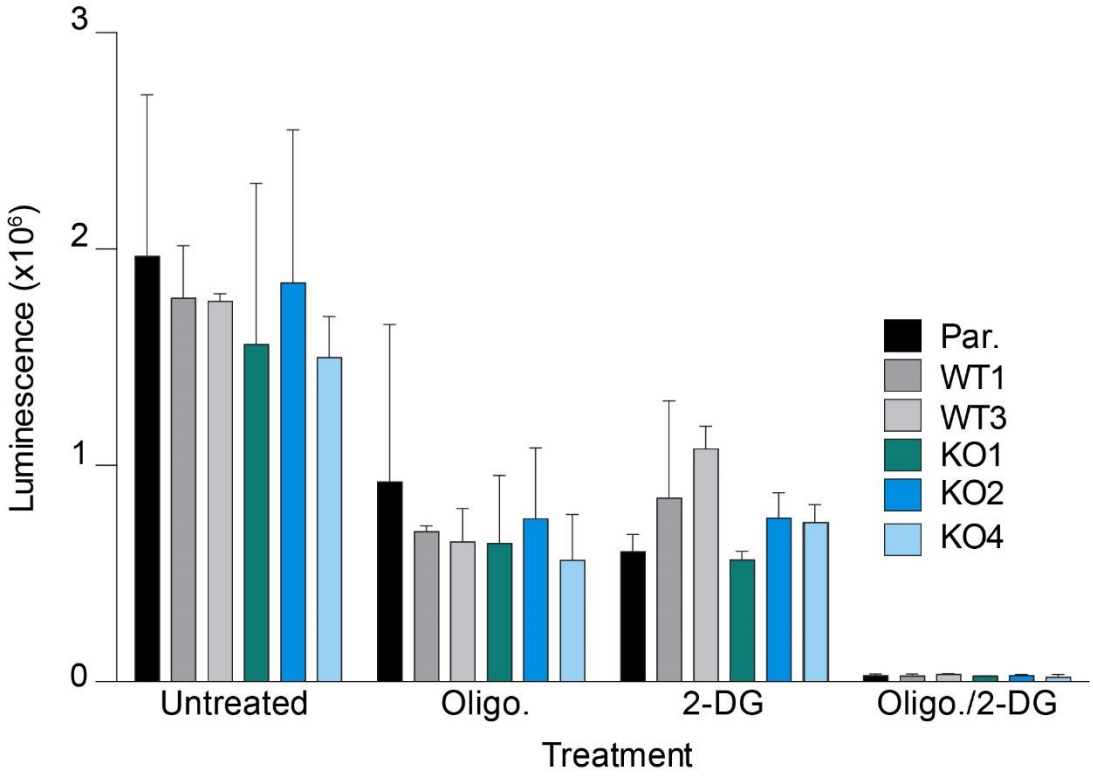

Figure 5.26: Intracellular levels and sources of ATP in galactose pre-conditioned HCT116 FlpIn TRex USP30KO cells

Galactose pre-conditioned HCT116 FlpIn TRex USP30KO cells were treated with 1 µM Oligomycin A (Oligo) or 50 mM 2-deoxyglucose (2-DG) or both or left untreated. Luminescence signal indicates the levels of ATP in each condition. Bar charts represent the mean and error bars the range between two independent experiments (n=2).

Similarly, treating the cells with 2-DG reduced the levels of ATP to about 50% of untreated, suggesting glycolysis was still required for the metabolism of galactose and ATP generation. Dually inhibiting both pathways resulted in a dramatic decrease in the ATP levels, suggesting both pathways are required to generate ATP in cells grown in galactose. Importantly, there were no differences in the behaviours of USP30KO and USP30WT cells. The HCT116 cells are an immortalised cancer cell line and similarly to most cancer cell line is highly glycolytic (Rossignol et al., 2004). HCT116 FlpIn TRex cells harbor activating mutations in the *KRAS* oncogene and I hypothesized that an immortalised non-cancer cell line may behave differently.

I employed the same approach for the hTERT-RPE1 FlpIn TRex USP30KO cells grown in their regular DMEM/F-12 medium, which contains 16 mM glucose (**Figure 5.27**). Interestingly, WT3, KO2 and KO6 exhibited

elevated levels of ATP under basal conditions compared to the parental and WT1 clones. It is difficult however, to evaluate whether the differences were related to USP30 or clonal variation. A further complication was that WT3 and KO6 were generated using the sgRNA and therefore their consistent behaviour may reflect non-specific effects of the same sgRNA (sgUSP30-2) during the CRISPR editing process. Treatment with Oligomycin A did not significantly change the levels of ATP detected in each cell line and neither did I observe any changes between USP30KO and USP30WT cells. Inhibition of glycolysis using 2-DG reduced the levels of ATP across all clones indicating that hTERT-RPE1 FlpIn TRex cells were glycolytic and USP30 status did not alter their metabolic state under these conditions. Simultaneous inhibition of both pathways reduced the levels of ATP further compared to the single 2-DG treatment, indicating that OxPhos still operated in the 2-DG inhibited cells. It appeared that the hTERT-RPE1 FlpIn TRex cells, just like the HCT116 FlpIn TRex cells, were primarily glycolytic as well.

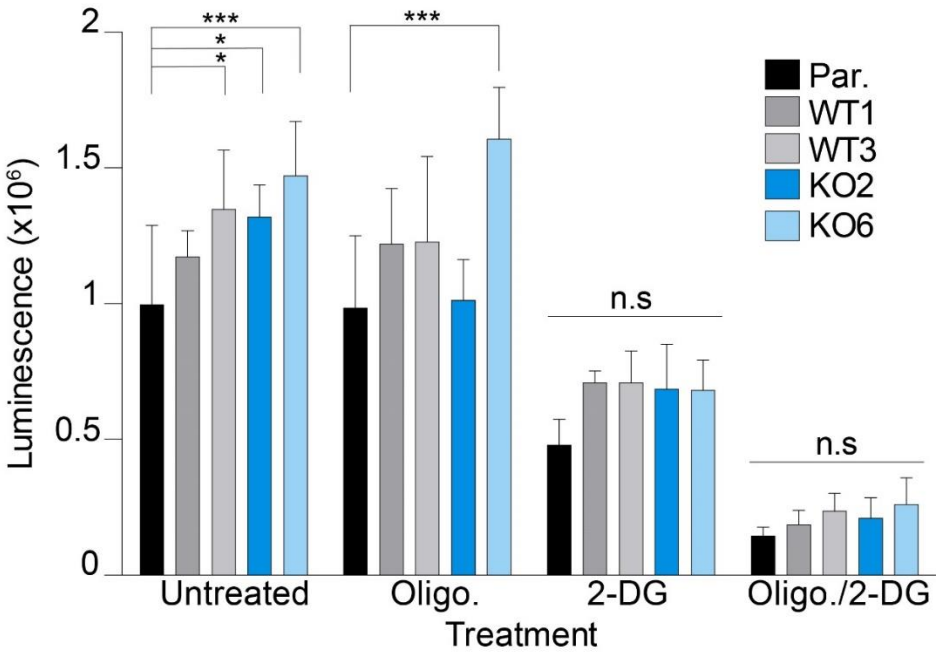

Figure 5.27: Intracellular levels and sources of ATP in hTERT-RPE1 FlpIn cells

Cells were treated with 1.5 µM Oligomycin A (Oligo) or 50 mM 2-deoxyglucose (2-DG) or both or left untreated. Luminescence signal indicates the levels of ATP in each condition. Bar charts represent the mean and error bars the range between three independent experiments (n=3). Two-way ANOVA with Bonferroni correction to allow for multiple comparisons to the parental cell line *; $p<0.05$, **; $p<0.01$, ***; $p<0.001$, ns; non-significant.

5.4.3 Investigating the proliferation of USP30KO cells

I next investigated the effect of USP30KO on the ability of cells to grow and proliferate. I seeded an equal number of the HCT116 FlpIn TRex USP30KO cells (KO1, KO2 and KO4), the USP30WT clones (WT1 and WT3) and the parental line in four 6-well plates and used one plate per day to count the number of cells over 4 days. I then used the cell numbers to generate growth curves to measure their proliferation over a 4-day period (**Figure 5.28**). Already by day 3 and more clearly by day 4, the USP30KOs 2 and 4 began to diverge from USP30WT1 and the parental in terms of growth. USP30KO clones 2 and 4 grew the slowest over the four-day period, while USP30WT1 and the parental line grew at the fastest. On average, USP30KO2 and KO4 exhibited nearly half the growth rate of their wild-type counterparts. USP30WT3 and USP30KO1 on the other hand grew in a nearly identical pattern to each other in the middle of these two extremes. Overall, two USP30KO clones proliferated at a slower rate compared to two of the wild-type controls and all three USP30KO clones grew at a slower rate compared to the parental line.

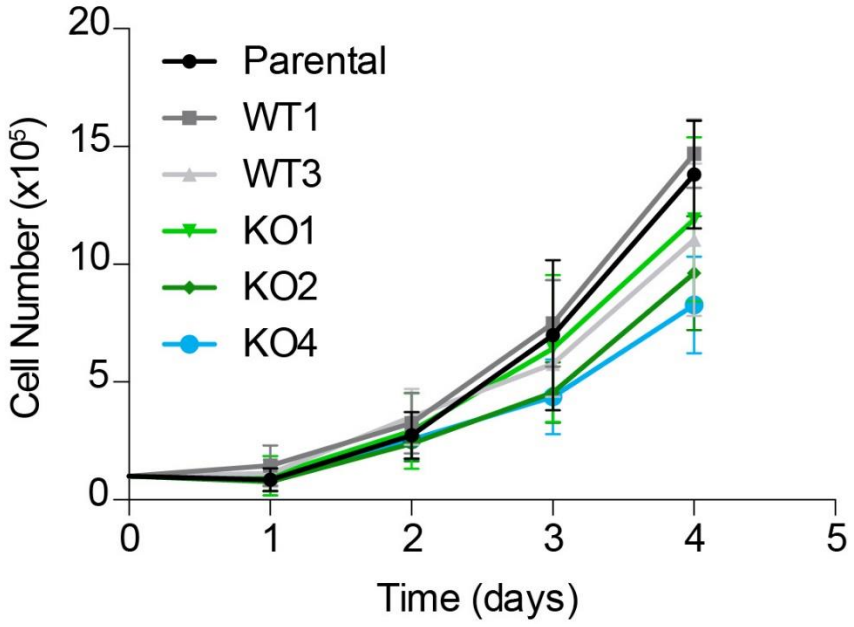

Figure 5.28: Growth curves of HCT116 FlpIn TRex USP30KO cells
HCT116 FlpIn TRex cells were counted at the indicated time points and total cell number was calculated. The graph shows the mean and error bars the range between three independent experiments (n=3).

I sought to investigate the differences in growth between USP30KO and USP30WT cells over a more considerable length of time. The CFA is a more versatile assay since it allowed simultaneous evaluation of the number of colony formation units and the colony surface area in a population of cells.

I seeded the HCT116 FlpIn TRex USP30KO cells in 12-well plates in the presence of high glucose (25 mM), which is the standard formulation of the media of these cells, or the equivalent concentration of galactose over a period of 10 days. I then fixed and stained the colonies formed using crystal violet. The number and surface area of the colonies were quantitated using a GelCount colony analyser (Oxford Optronics, Oxford, UK), courtesy of Dr. Jason Parsons (University of Liverpool, UK). There was a striking difference between wild-type and USP30KO cells in the presence of glucose (**Figure 5.29**A). The USP30KO cells consistently grew visibly smaller colonies compared to their USP30WT counterparts. However, the number of colonies across clones was very similar (**Figure 5.29**B) indicating that the number of colony-initiating cells was not affected by USP30 deletion. Instead, the difference lay in the surface area occupied by the colonies (**Figure 5.29**C). To some degree, the results of the CFA in glucose recapitulated the differences in growth rates seen in **Figure 5.28**.

However, the CFA revealed a much clearer differential between wild-type and USP30KO cells and importantly, WT3 and KO1, which previously (**Figure 5.28**) did not exhibit a similar behaviour to their respective counterparts, were segregating consistently in this assay. Importantly, the differential in growth between wild-type and USP30KO cells was lost when cells were made dependent on OxPhos by growing them in galactose. My data suggest that USP30 is relevant for proliferation under conditions where glycolysis is favoured. In contexts where glycolysis is suppressed, proliferation is similarly suppressed regardless of USP30 status in the cells.

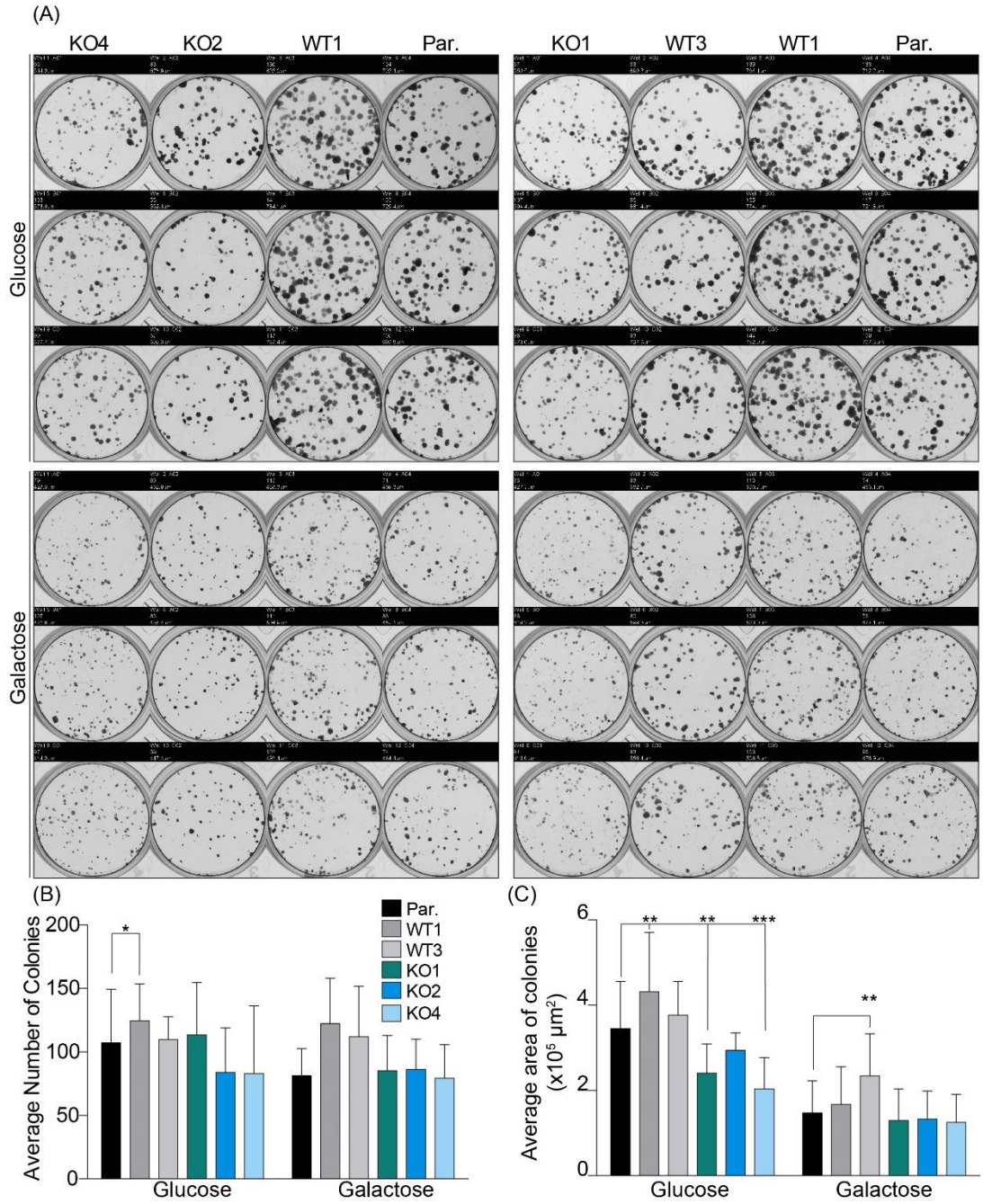

Figure 5.29: CFA in HCT116 FlpIn TRex USP30KO cells

(A) Representative images of crystal violet-stained colonies of HCT116 FlpIn TRex cells grown in glucose or galactose for 10 days. Quantitation of (B) number of colonies and (C) Average Area of Colonies per condition per cell line per well. Bar charts represent the mean and error bars the range between three independent experiments (n=3). Two-way ANOVA with Bonferroni correction to allow for multiple comparisons to the parental cell line *; $p<0.05$, **; $p<0.01$, ***; $p<0.001$, ns; non-significant.

I sought to perform the analogous experiment in the hTERT-RPE1 FlpIn TRex USP30KO cells. Performing a CFA in the hTERT-RPE1 FlpIn cells proved challenging since the cells did not appear to form colonies and rather grew as a “lawn”. I therefore evaluated their proliferation in glucose and galactose using simple growth curves as I had done for the HCT116 FlpIn TRex USP30KO cells (**Figure 5.28**). The hTERT-RPE1 FlpIn TRex USP30KO2 proliferated at a very similar rate to USP30WT3 and the parental cells in glucose, whilst USP30KO6 and USP30WT1 proliferated slower (**Figure 5.30**A). USP30KO clones (2 and 6) and USP30WT3 were growing at an accelerated rate compared to USP30WT1 and the parental cell line when the cells were grown in galactose (**Figure 5.30**B). The overall proliferation of the cells grown in galactose was reduced compared to the cells in glucose. However, it appeared that the USP30KO cells were affected to a lesser extent when forced to use their mitochondria for generating ATP.

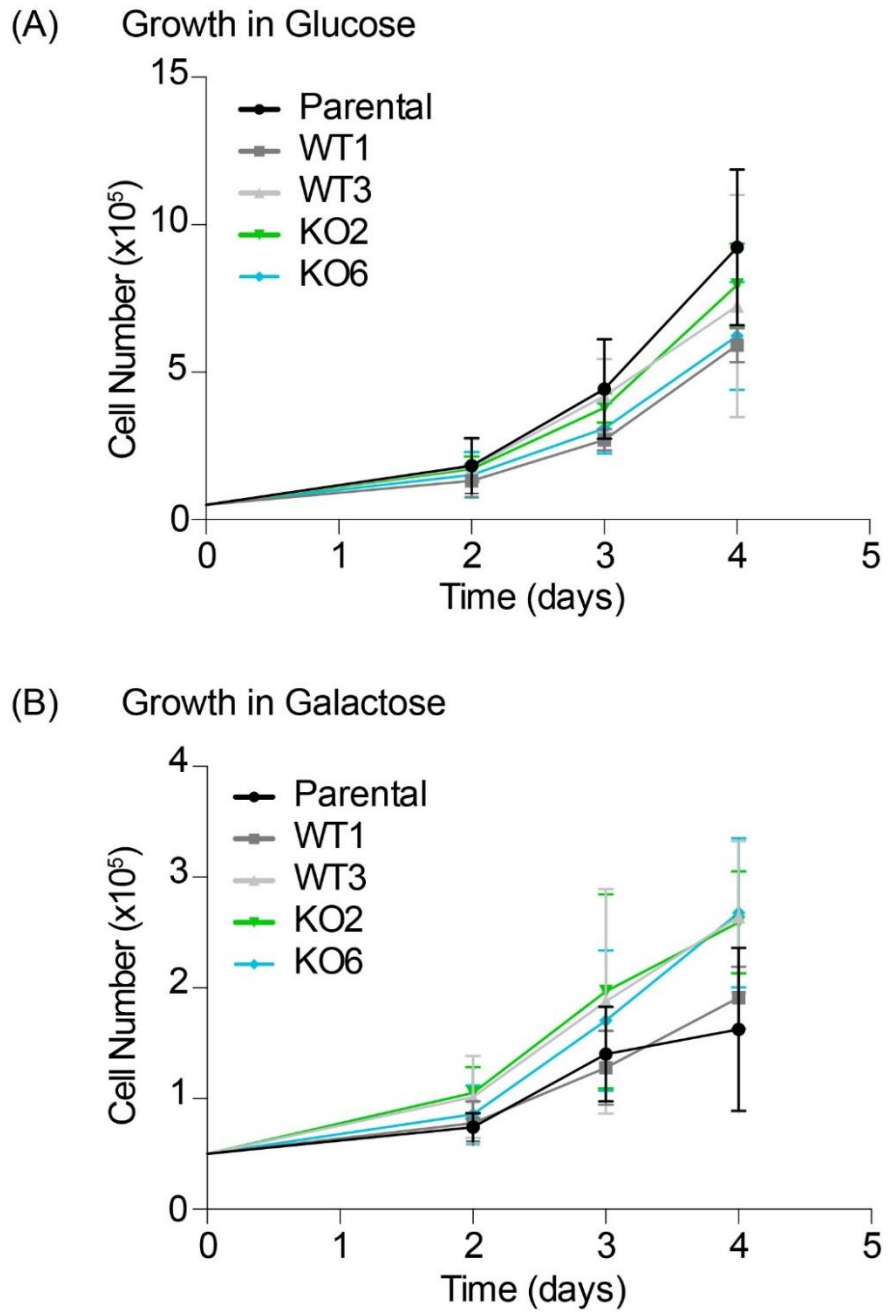

Figure 5.30: Growth curves of hTERT-RPE1 FlpIn TRex USP30KO cells in glucose and galactose

hTERT-RPE1 FlpIn TRex USP30KO cells were counted at the indicated time points and total cell number was calculated. The graph shows the mean and error bars the range between three independent experiments (n=3).

5.5 RNA-seq and proteomics in HCT116 FlpIn TRex USP30KO cells

5.5.1 Introduction to RNA-seq

RNA-sequencing (RNA-seq) and proteomics are a part of the -omics technologies routinely used to gain in-depth biologically meaningful information in an unbiased fashion. They can be particularly helpful in opening novel biology for previously uncharacterised genes or proteins, as they can be used to generate new hypotheses and shed light into the molecular and cellular mechanism of action of a gene or protein. RNA-seq is a very useful methodology because it can provide crucial information on changes to the transcriptional programme of a cell in a diseased state, at a particular developmental stage, or in response to a drug treatment or genome alterations such as a CRISPR/Cas-mediated modification. The purpose of this type of experiment is to characterise the transcriptome, which is the total RNA transcripts of cells, in a qualitative and quantitative manner using high-throughput sequencing technology.

The first step in the procedure is to isolate total RNA from the desired samples using an RNA extraction methodology. The quality and integrity of the sample is then assessed before proceeding farther. The target RNA of interest is enriched or alternatively non-desired RNAs, such as ribosomal RNA, are de-enriched. An oligo dT enrichment can be performed, to enrich the samples for mRNA transcripts. The next step is to convert the single-stranded RNA into a cDNA sequencing library that consists of short strands of double-stranded DNA between 50 and 200 nucleotides in length ligated to adaptors. The cDNA library is then subjected to high through-put sequencing. The sequence library generated is then aligned to a reference genome to identify the transcripts or may even be assembled *de novo* without any prior knowledge. The data can then be used to generate a transcription profile and a differential gene expression (DGE) profile for multiple samples that are to be compared.

Through our collaboration with Forma Therapeutics (Boston, MA, USA), I had the opportunity to perform RNA-sequencing (RNA-seq) on the HCT116 FlpIn TRex USP30KO cells that I generated and get an overview of the impact the knock-out of USP30 was having on the transcriptome.

5.5.2 RNA-seq procedure in the HCT116 FlpIn TRex USP30KO cells

I chose to compare two USP30KO clones (KO2 and KO4), that were generated using sgUSP30-1 and -2 respectively, and behaved consistently to each other in the assays that I performed (**Figure 5.18**, **Figure 5.28** and **Figure 5.29**). As my reference cell line, I used the WT1 generated using sgUSP30-1 as well as the parental cell line, which served as complimentary wild-type cells.

I prepared total RNA from the four cell lines in two independent RNA extractions. I quantitated the concentration of the RNA using a Nanodrop instrument and sent the samples to Rory Coffey at Forma Therapeutics (Boston, MA, USA) for further processing. Rory performed a number of quality control steps before proceeding including re-quantifying the concentration of the RNA samples and assessing their quality using a Bioanalyzer. Samples were required to have an RNA integrity number (RIN) of 7 or higher (Schroeder et al., 2006). The samples I had sent were all determined to be of high quality with RIN ~ 10. An oligo dT enrichment was performed on each sample and they were multiplexed together in the same run for paired-end sequencing. Plotting fragments per kilobase million (FPKM) for each transcript of one technical replicate vs the second replicate, showed the replicates were highly consistent. (**Figure 5.31**).

The above allowed Rory to bioinformatically pool the data together when performing the analyses for greater statistical power. Data with FPKM <5 was excluded as it could not be reliably quantitated based on the external RNA controls consortium (ERCC) standard spike-in used (Jiang et al., 2011). The pooled sequencing data was aligned to the reference genome GRCh38 using TopHat (version 2.1.1.) and CUFFLINKS (version 2.1.1.) was used to normalise and quantitate the data across samples to produce the differential expression profiles. CUFFLINKS was used to perform outlier analysis on the data to determine the hits that were significant.

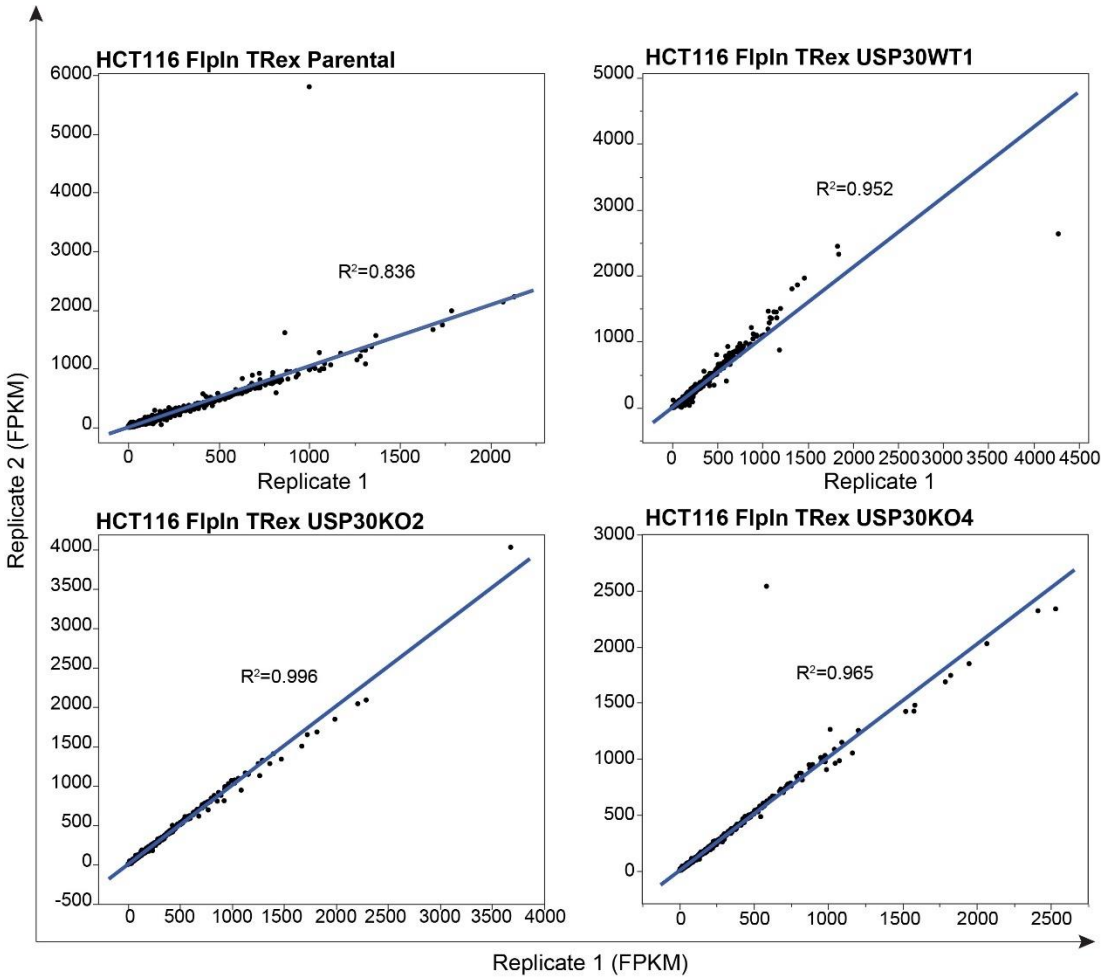

Figure 5.31: Correlation between technical replicates in the RNA-seq of HCT116 FlpIn TRex USP30KO cells

The fragments per kilobase million (FPKM) for each of the transcripts of the two technical replicates per sample were plotted against each other. The best fit line is shown and the linear regression term (R^2) was calculated as a measure of the correlation between the two replicates.

5.5.3 RNA-seq hits in HCT116 FlpIn TRex USP30KO cells

I compared both USP30KO clones to the parental and USP30WT1 clone, as the former was the starting population of cells used for the generation of USP30KO cells and the latter was one of the clones that was subjected to the same procedure as the USP30KOs, (using sgUSP30-1) but retained USP30 expression. I plotted the fold change (FC) of USP30KO2 and USP30KO4 over the parental and USP30WT1 against each other as $\log_2$ transformed values in order to determine which of the transcripts were consistently changing in the same direction between the two USP30KO clones (**Figure 5.32**). I limited the range of the graphs to only include entries with $\log_2$ FC ±6, since none of the outliers lay outside that range. Outliers were the transcripts with $\log_2$ FC ±1 as long as it met the cut-off of FPKM > 5.

Overall, it seemed that most transcripts were unaffected by the USP30KO as the cloud of grey dots remained in the centre of the graph. Most of the transcripts that were changing appeared to do so in the same direction for both USP30KO clones. Those that were consistently changing in both USP30KO (red dots) were mostly confined to the outer parts of the cloud, in contrast to the majority from those that were changing in only one USP30KO clone (blue dots).

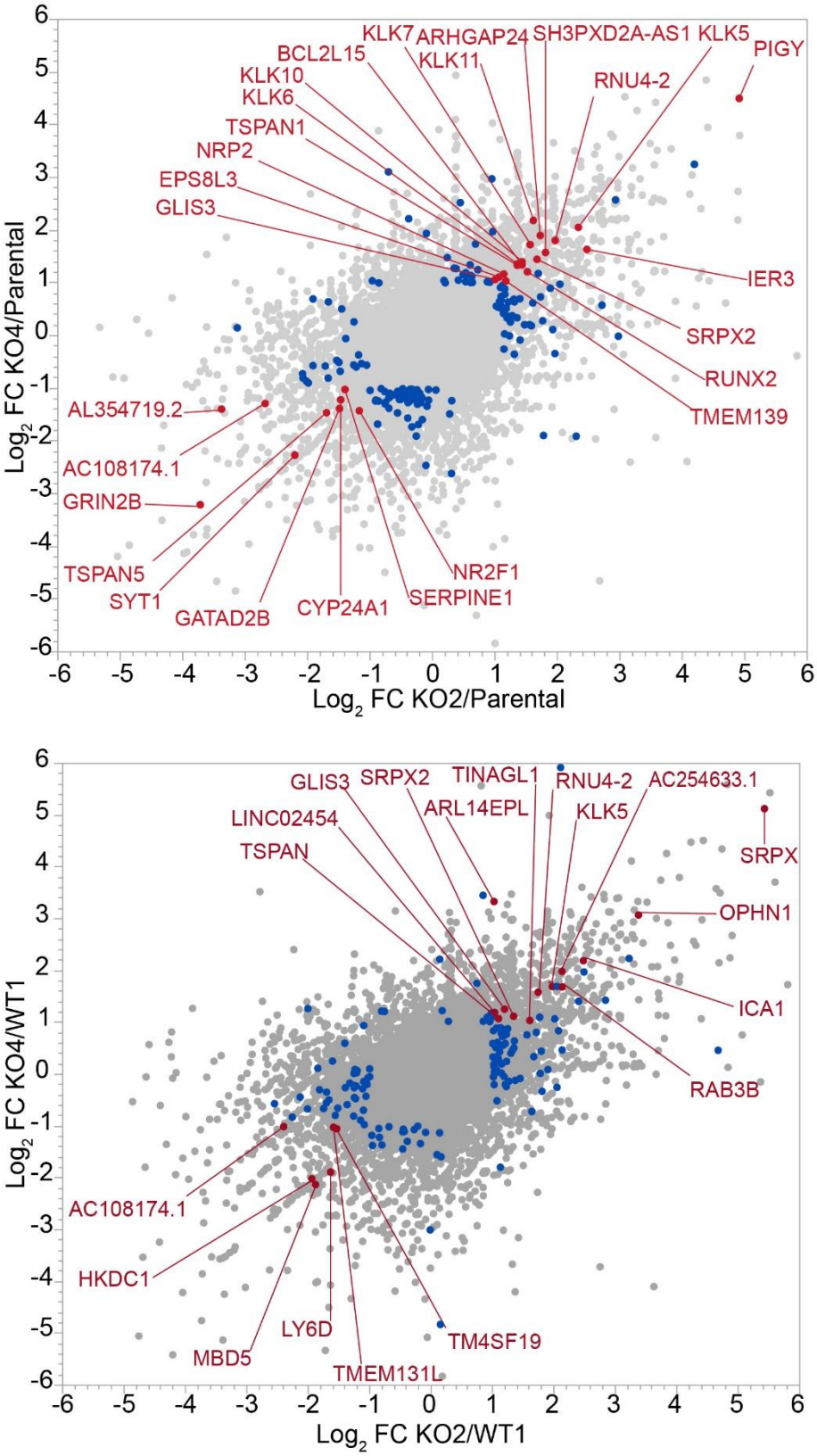

Figure 5.32: RNA-seq in HCT116 FlpIn TRex USP30KO cells

The fold change (FC) of transcripts in USP30KO2 and USP30KO4 compared to parental (upper) and USP30WT1 (lower) are plotted as log_2 transformed values. Each dot represents a transcript. Outliers for one of the USP30KO clones are shown in blue or for both USP30KO clones in red.

I compared the transcripts that were in the RNA-seq dataset to the 1157 genes defined as mitochondrial according to MitoCarta 2.0 (Calvo et al., 2016). In my dataset, 1055 transcripts were identified as mitochondrial transcripts according to this classification (**Figure 5.33**). Most of these were found in the very centre of the cloud, suggesting that transcription of mitochondrial proteins was largely unaffected by USP30KO. Only one mitochondrial protein was considered an outlier and that was CYP24A1, a mitochondrial cytochrome P450 family member. The function of CYP24A1 is to perform mono-oxygenation reactions in drug metabolism and synthesis of cholesterols and lipids. The transcript of CYP24A1 was de-enriched in USP30KO clones 2 and 4 compared to the parental with $\log_2$ fold change of -1.47 and -1.21 respectively. It was not considered an outlier when the datasets of USP30KO2 and 4 were compared to USP30WT1 with $\log_2$ fold changes of 0.66 and 0.91 respectively.

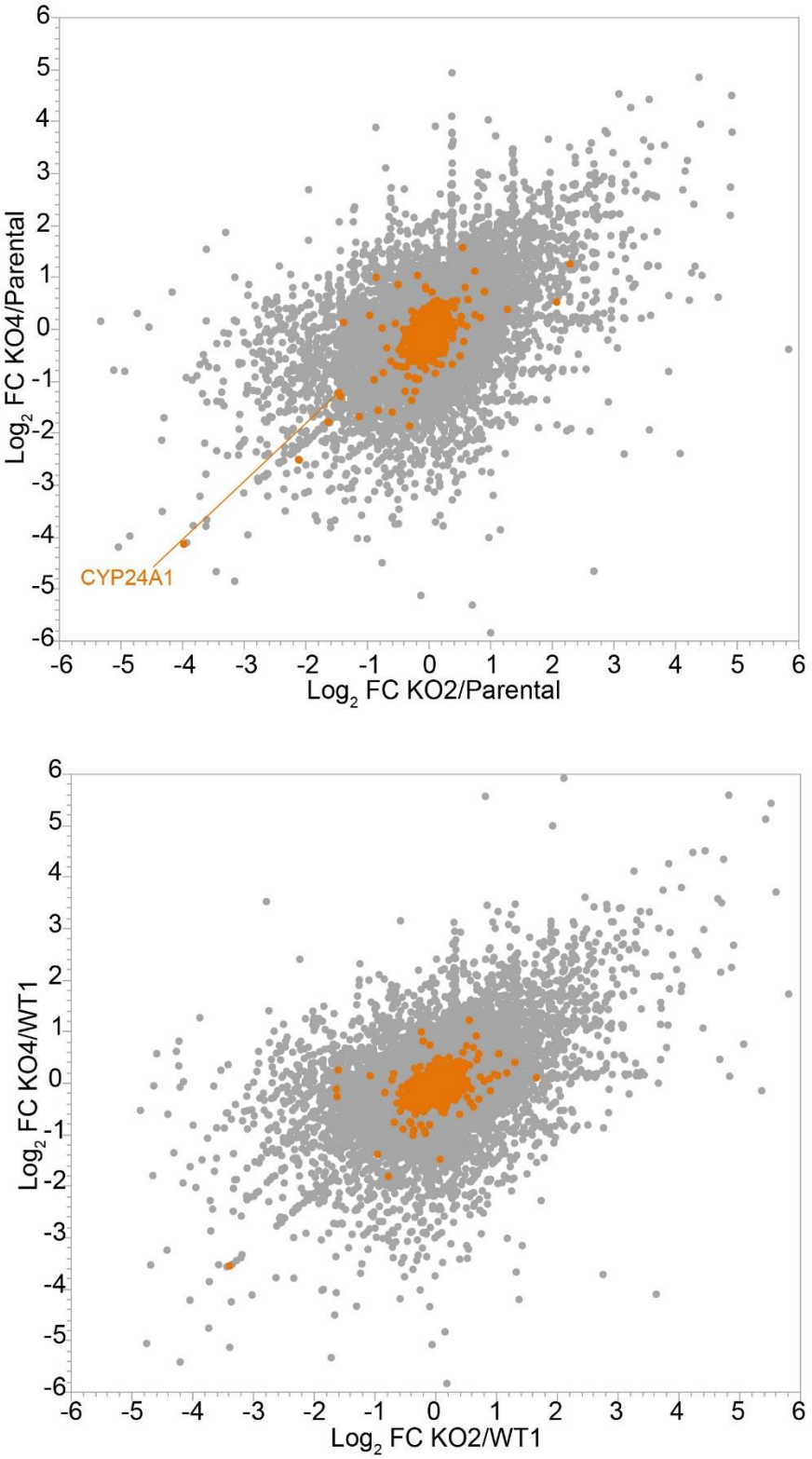

Figure 5.33: RNA-seq in HCT116 FlpIn TRex USP30KO cells annotated as mitochondrial proteins according to MitoCarda 2.0

The fold change of transcripts in USP30KO2 and USP30KO4 compared to parental (upper) and USP30WT1 (lower) are plotted as log_2 transformed values against each other on the same set of axes. Each orange dot represents a transcript that is coding for a mitochondrial protein according to MitoCarta 2.0.

I compiled the RNA-seq data hits where I compared the outlier transcripts consistently changing in both USP30KO clones in a Venn diagram (**Figure 5.34**). The number of transcripts upregulated and downregulated are shown in green and red respectively.

Five transcripts were consistently upregulated in the USP30KO clones compared to both controls (USP30WT1 and parental), whilst 2 were downregulated. The transcripts that were in the other overlapping regions could be an indication of clonal variation between clones. For instance, the region overlapping between KO2/parental and KO4/parental but excluded KO2 and KO4 compared to WT1 is likely to reflect changes in the transcriptome between clones USP30KO2 and KO4 and are therefore unrelated to the USP30 status of the cells. Similarly, the region overlapping KO2/parental and KO2/WT1 and excludes KO4 to compared to either WT1 and parental cells, is more likely to reflect the clonal nature of WT1.

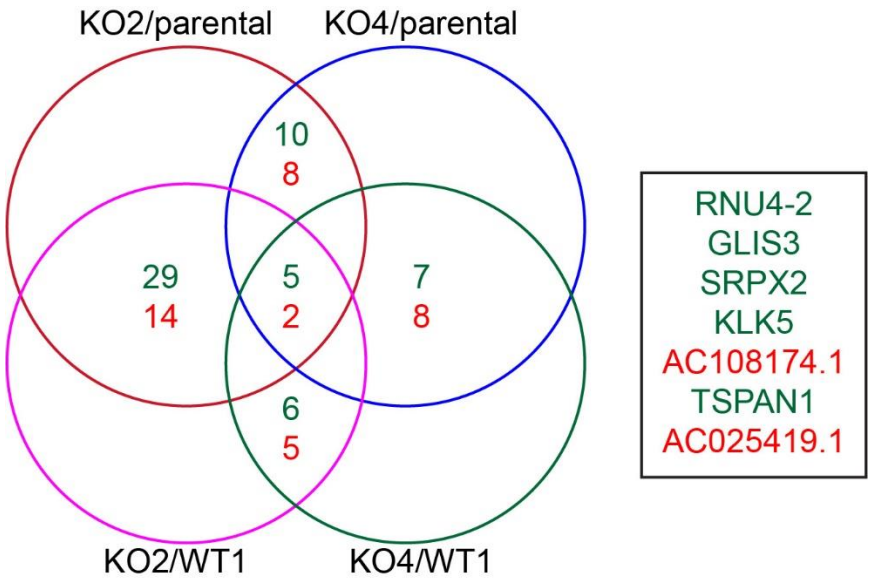

Figure 5.34: Overlap between changes in USP30KO clone transcriptome
The transcripts that were outliers in both USP30KO clones (2 and 4) compared to the parental and USP30WT1 are shown on the Venn diagram. The numbers indicate the number of hits in each section of the Venn diagram. Numbers and transcript names coloured in green and red correspond to upregulated and downregulated transcripts. The box lists the transcripts that are outliers across both USP30KO compared to USP30WT1 and the parental cells.

The 5 transcripts which were found to be consistently upregulated in the USP30KO clones were: RNU4-2 belongs to the family of small nuclear RNAs involved in the assembly and regulation of the spliceosome during transcription (Wan et al., 2020). GLIS3 is a Zinc finger transcription factor that functions in the development of pancreatic β-cells. GLIS3 has been implicated in the development of diabetes in patients who harbour rare variants of this gene (Amin et al., 2018; Sun et al., 2019). TSPAN1 is a transmembrane protein whilst KLK5 and SRPX2 are secreted proteins, all of which are involved in processes such as cell adhesion, migration and cancer cell metastasis (Caubet et al., 2004; Hou et al., 2015; Li et al., 2020). The two transcripts that are downregulated, AC108174.1 and AC025419.1, are long non-coding (lnc)RNAs located on chromosomes 5 and 12 respectively. For the latter lncRNA, it is interesting that the USP30 locus is found on the same chromosome arm, 12q14.3 for AC025419.1 and 12q24.11 for USP30.

5.6 Small-scale proteome in HCT116 FlpIn TRex USP30KO cells

USP30 is a DUB and one of its potential functions could be to rescue proteins from proteasomal degradation. The loss of USP30 may therefore induce the destabilisation of its substrates. In order to capture such potential USP30 substrates in an unbiased manner, I performed an initial small scale proteomic experiment in a stable isotopic labelling of amino acids in culture (SILAC) configuration on our in-house Orbitrap LTQ (Ong et al., 2002), with the intention of performing a more comprehensive experiment later to be analysed on a more powerful Orbitrap in the lab of Matthias Trost (Newcastle, UK).

I wanted to compare two of the USP30KO clones to two of the USP30WT clones. I labelled the two USP30WT clones (1 and 3) with heavy isotopes and USP30KO2 and USP30KO4 with light and medium isotopes respectively. A SILAC-based proteomic experiment allows for multiplexing of up to three samples. Differentially expressed proteins can be identified and quantitated based on the shift in mass-to-charge ratio (m/z) introduced by the heavier isotopes in the proteins (**Figure 5.35**). I cultured the cells for a minimum of 6 passages over 2 weeks, until over 95% of the proteins had incorporated the isotopically-labelled amino acids.

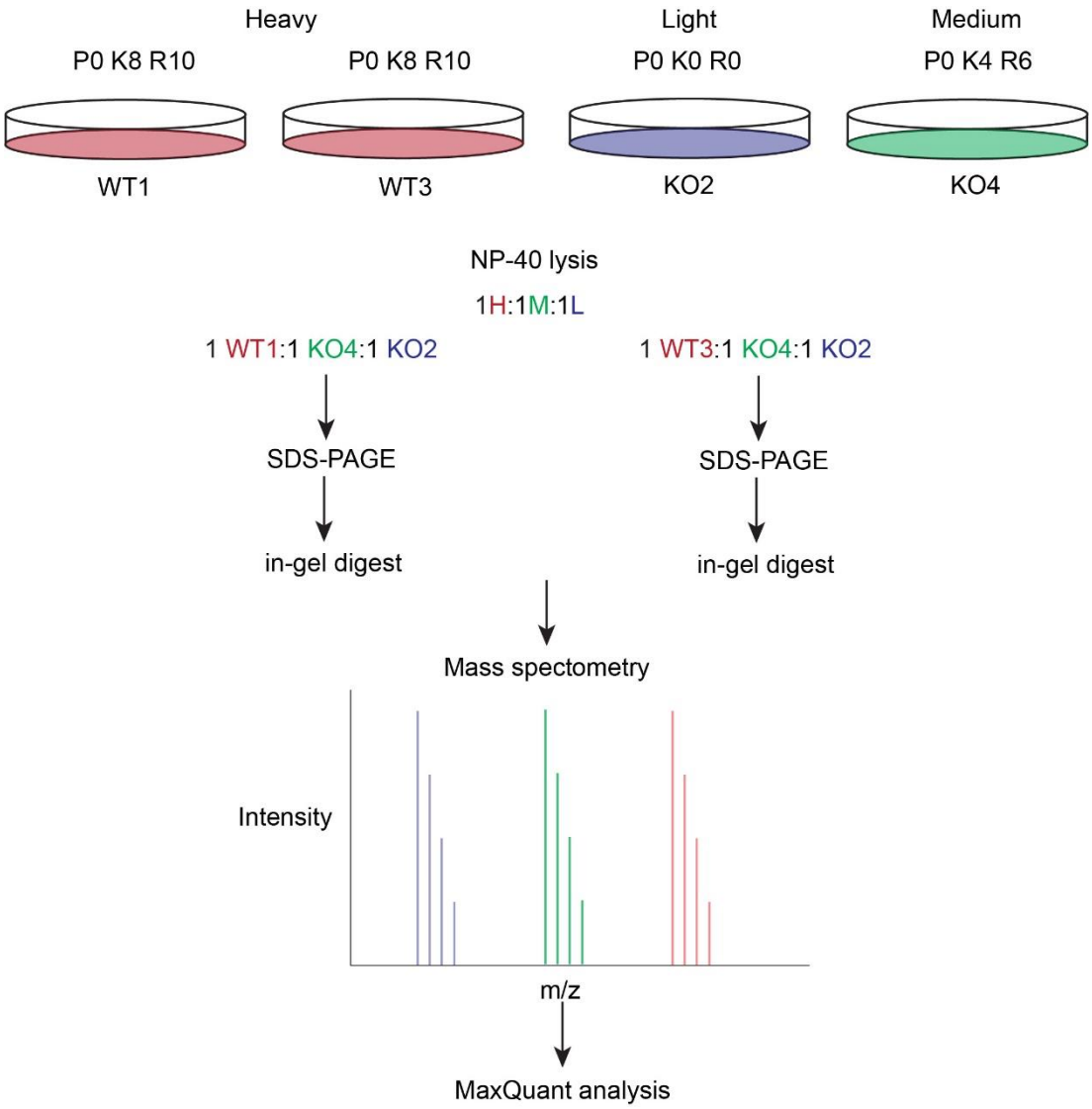

Figure 5.35: SILAC experiment work-flow

HCT116 FlpIn TRex USP30WT1 and USP30WT3 cells were labelled with medium supplemented with Heavy amino acids (P0K8R10), USP30KO4 with Medium amino acids (P0K4R6) and USP30KO2 with Light amino acids (P0K0R0). Cells were lysed in NP-40 lysis buffer supplemented with MPIs (1:250) and the protein concentration was determined using a BCA assay. The samples were mixed in a 1:1:1 ratio before being resolved on as SDS-PAGE gel followed by in-gel digestion and peptide extraction. The peptides were analyzed on an Orbitrap LTQ time-of-flight instrument (ThermoFisher), identified and quantitated using MaxQuant software.

The ratio of the intensities between medium and light to heavy were indicative of the levels of protein expression in USP30KO4 and USP30KO2 respectively, compared to either USP30WT1 and USP30WT3. The above allowed me to compare the levels of expression of protein in two of the USP30KO clones to two wild-type cell lines, in a quantitative manner. The significance b was calculated using Perseus as a statistical test for determining proteins whose expression was significantly changed between USP30KO and USP30WT cells (Cox and Mann, 2008; Tyanova et al., 2016).

I plotted the $\log_2$ transformed fold change of USP30KO2 and USP30KO4 to USP30WT1 and USP30WT3 separately and annotated the proteins that are considered mitochondrial according to MitoCarta 2.0 (**Figure 5.36**). The coverage was 2086 proteins in USP30KO2 and USP30KO4 compared to USP30WT1 and 1952 proteins in USP30KO2 and USP30KO4 compared USP30WT3. The majority of proteins annotated as mitochondrial laid in the middle of the cloud, suggesting that most mitochondrial proteins were not changing in the USP30KO clones.

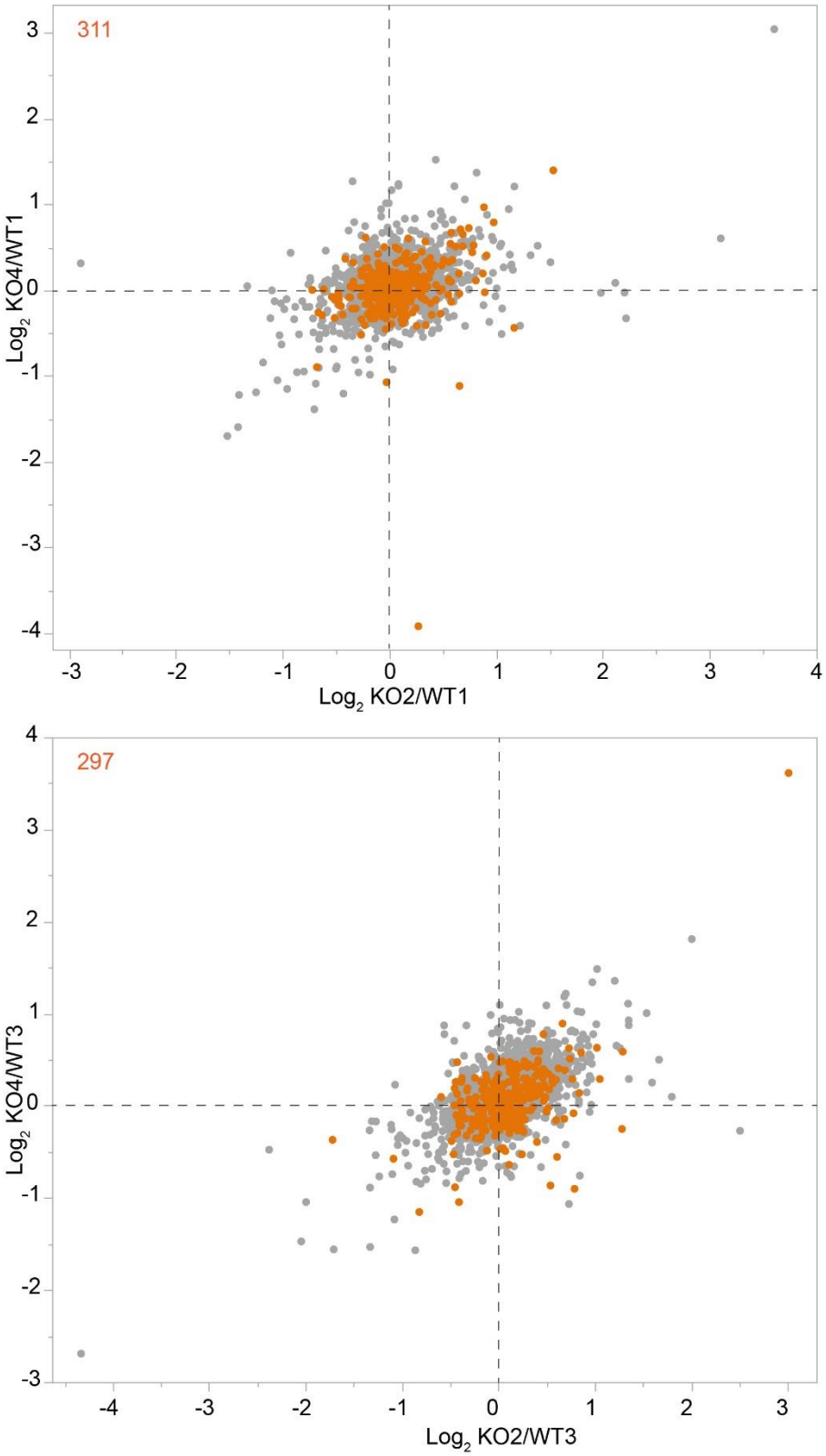

Figure 5.36: Mitochondrial proteins in the small-scale USP30KO cell proteome

The logarithms of the fold change between USP30KO2 and USP30KO4 proteomes normalised to USP30WT1 (upper) and USP30WT3 (lower) to base 2 (log_2 FC) are plotted against each other. Mitochondrial proteins according to MitoCarta 2.0 are shown in orange with the number of proteins identified as mitochondrial shown in the upper-left corner of each graph.

There were outliers in both comparisons, but none overlapped between the two sets. There were some interesting hits such as the SLC25A3 and 5 that were both increased in the USP30KO clones compared to USP30WT1. These are mitochondrial inner membrane proteins that import phosphate from the cytosol and exchange cytosolic ADP for mitochondrial ATP respectively. In unison, these two proteins provide ADP/phosphate for the mitochondrial F_1F_0ATPase to generate ATP and export mitochondrial ATP into the cytosol for consumption. Other mitochondrial proteins include UQCRC2, a subunit of ubiquinol-cytochrome c oxidoreductase (complex III of the ETC) that was increased in the USP30KO clones compared to USP30WT1. Furthermore, proteins involved in metabolic pathways were seen changing. FASN (fatty acid synthase) a cytosolic enzyme involved in fatty acid synthesis that was elevated in the USP30KO cells compared to USP30WT1. Higher levels of FASN may allow for enhanced levels of fatty acid synthesis and promote biosynthetic capacity and proliferation. PFKP (6-phosphofructokinase) that functions in glycolysis were also increased in USP30KO cells compared to USP30WT3, which may suggest enhanced glycolytic capacity in these cells. SLC2A1 (GLUT1) a glucose transporter of the cell surface membrane that was decreased in the USP30KO cells compared to USP30WT3. The decrease in the levels of a ubiquitously-expressed glucose transporter such as SLC2A1 (GLUT1) could in principle account for the slower growth of the HCT116 FlpIn TRex USP30KO cells that I observed (**Figure 5.28** and **Figure 5.29**).

The levels of ALDH1A3 (aldehyde dehydrogenase 1 family, A3) expression were increased the USP30KO clones. ALDH1A3 is involved in the processing of aldehydes into carboxylic acids and this enzyme is crucial in the detoxification of endogenous and exogenous aldehydes. High expression levels of ALDH1A3 correlated with poor prognosis in patients suffering with glioma and considered a stem cell marker for this type of cancers (Gan et al., 2020; Ni et al., 2020).

LYPLA1 or APT-1 was the outlier annotated as a mitochondrial protein increasing in the USP30KO clones when compared to USP30WT3. LYPLA1 (Lysophospholipase 1) is a hydrolase that depalmitoylates G proteins such as RAS, which can affect their localisation and function as peripheral membrane proteins (Dekker et al., 2010).

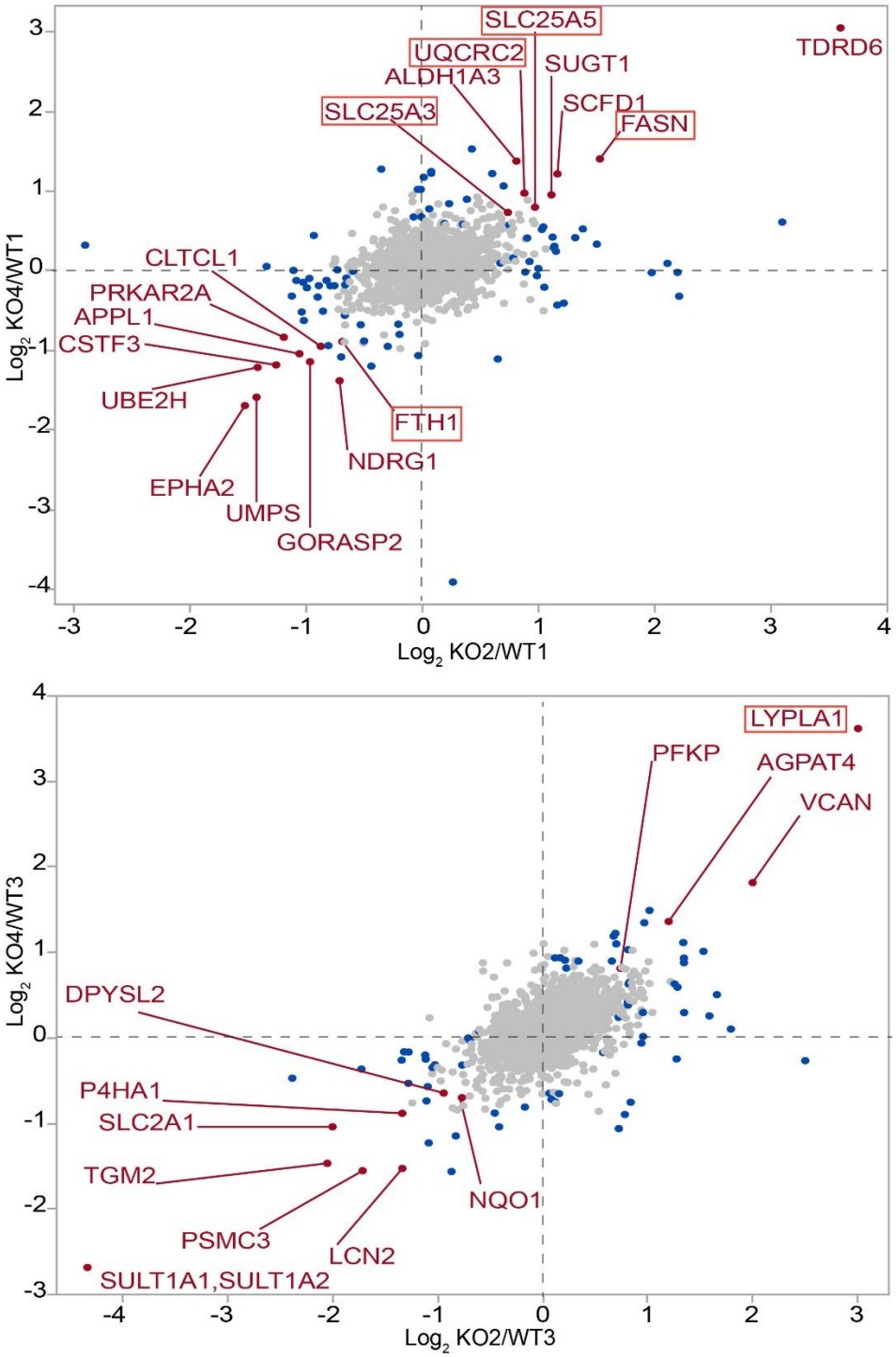

Figure 5.37: Small-scale proteome of HCT116 FlpIn TRex USP30KO cells

The logarithms of the fold change (FC) between USP30KO2 and USP30KO4 proteomes normalised to USP30WT1 (upper) and USP30WT3 (lower) to base 2 (log_2 FC) are plotted against each other. The blue dots are proteins which were deemed significant in one of the USP30KO clones, red dots were deemed significant in both USP30KO clones and grey for neither USP30KO clone based on the significance b calculated by Perseus. Only proteome hits that were significant in both USP30KO clones are annotated. Proteins in orange boxes are classified as mitochondrial proteins according to MitoCarta 2.0.

Another notable hit was NQO1 whose levels were reduced in the USP30KO clones compared to the USP30WT3 (**Figure 5.37**). NQO1 (NAD(P)H quinone dehydrogenase 1) is a cytosolic enzyme that reduces quinones using NADH or NADPH as a source of electrons and it has been implicated in the management of free radicals in cells (Pey et al., 2019). NQO1 is often upregulated in response to cellular stress and a reduction in its activity is linked to a higher risk in developing cancer (Lajin and Alachkar, 2013).

5.7 Conclusions

5.7.1 Generation and characterisation of HCT116 FlpIn TRex USP30KO cells

I made use of CRISPR/Cas9 editing technology to generate USP30KO cells in the HCT116 FlpIn TRex cell line. This endeavour yielded three USP30KO clones and two USP30WT clones that I carried forward for further characterisation (**Table 5.2**). There were no consistent changes in the levels of major BH3 family proteins BAK, BAX, MCL-1, BCL-2 and BCL-X_L in these KO cells (**Figure 5.3**).

The loss of USP30 did not appear to affect the steady state levels of TOMM complex components TOMM20 and TOMM22 in USP30KO cells, whilst depolarisation of mitochondria did not induce detectable ubiquitylation of these two components either. The transcriptome and small-scale proteome I performed in the HCT116 FlpIn TRex USP30KO cells suggested that the majority of transcripts and proteins, which are annotated as mitochondrial remain unchanged in USP30 null cells (**Figure 5.33** and **Figure 5.36**). The above results were consistent with the data obtained by my colleague, Elena Marcassa in the full proteome experiment performed in the hTERT-RPE1 FlpIn TRex USP30KO cells. Elena saw no changes in the levels of core mitochondrial proteins nor in the mitochondrial footprint of the cells (Marcassa *et al*, unpublished). Furthermore, we observed no significant changes to most mitochondrial and peroxisomal proteins in the proteomic experiments we performed in the SH-SY5Y USP30KO and USP30 inhibitor-treated cells in the presence of A/O (Rusilowicz-Jones et al., 2020). Ubiquitylome analysis revealed that only a subset of OMM proteins were displaying enhanced levels of ubiquitylation in response to A/O, notably the VDACs and TOMM complex

components TOMM20, 40 and 70. However, these proteins remained unchanged at the level of the proteome. Taken together, these results suggest that USP30 loss does not affect mitochondrial mass.

5.7.2 The response of HCT116 FlpIn TRex USP30KO cells to BH3 mimetics

I wanted to address the question of whether USP30KO cells like USP30-depleted cells were sensitized to BH3 mimetics. I made use of several complimentary approaches to tackle that question including TMRE uptake to look at loss of mitochondrial membrane potential, PS externalisation and immunoblotting to look at PARP cleavage and caspase 3 cleavage. I also combined the above approaches in the same experiments where possible in order to gain more insight into the molecular mechanism of how USP30 affected apoptotic cell death i.e. at what stage was cell death accelerated and/or enhanced. I encountered some difficulties when assessing the response of these cells to BH3 mimetics, partly to the different HCT116 FlpIn TRex USP30 clones not clearly segregating between KOs and WTs. In general, two out of three KOs appeared to be more sensitive to BH3 mimetics than the parental cells. However, the WT clones also appeared to be similarly sensitized. This indicated that the increased sensitivity was reflecting the clonal nature of the cells and/or off-target effects of the sgRNAs used to generate the cells. I concluded that the long-term loss of USP30 may be compensated for by an adaptation mechanism or the variability between clones was larger than the effect of USP30 loss.

One of the time-course experiments I performed showed some evidence that apoptosis in response to BH3 mimetics may be accelerated in USP30KO cells (**Figure 5.11**). The above may suggest that USP30 normally suppresses the initiation of BH3 mimetic-induced apoptosis. More data in the USP30KO cells is required to support this model but it would be consistent with previous published data from our lab (Liang et al., 2015a) and my own data in the USP30-depleted cells.

Dynamin-related protein 1 (DRP-1) is a GTPase that regulates mitochondrial fission. DRP-1 was shown to be required for BH3 mimetic-induced cell death and efficient cytochrome c release following MOMP (Milani et al., 2017). DRP-1 is thought to promote fragmentation of mitochondria

during apoptosis, which facilitates the release of cytochrome c from the inter-membrane space through the pores on the outer membrane formed by BAK/BAX. USP30 may prevent DRP-1 association or activity at the OMM, thus reducing the efficiency by which cytochrome c is released into the cytosol. Alternatively, the loss of USP30 creates more entry sites for DRP-1 to associate on mitochondria and therefore accelerates the release of cytochrome c during apoptosis.

The data in the hTERT-RPE1 FlpIn TRex USP30KO cells did not provide any strong evidence of sensitisation to BH3 mimetics this far. One possibility may be that the assay was reaching saturation at the time-points that I chose to investigate. For this reason, a more refined approach may be needed such as attempting a time-course in order to evaluate whether it is the kinetics of the process that are affected.

5.7.3 Metabolic characterisation of USP30KO cells by Seahorse technology

When performing the Mito stress assay in the HCT116 FlpIn TRex USP30 clones I noticed a rather high variation in responses between biological replicates as shown by the large error bars (**Figure 5.18**). The USP30KO cells appeared to have lower basal and lower levels of ATP generated through the ETC, which may indicate downregulation of mitochondrial metabolism (**Figure 5.19**). Furthermore, maximal respiration was lower, albeit to a small degree, in the USP30KO clones, which further supports the ETC was operating at a lower capacity in the USP30KO cells. Lastly, USP30KO cells displayed lower levels of proton leak in the Seahorse assay, which suggests a healthier mitochondrial network that experiences less proton leak and is more efficient at producing ATP. This model would also fit with the role of USP30 in regulating basal mitophagy. In the absence of USP30 the threshold of mitochondrial damage required to trigger mitophagy could be lower. Therefore, the quality control system operating on mitochondria is more stringent resulting in overall healthier, better-coupled and more efficient mitochondria. The lower non-mitochondrial oxygen consumption may be interpreted as reduced ROS production in relation to the known role of USP30 in mitophagy and also pexophagy, since both organelles are known to produce ROS. By analogy to

mitophagy, pexophagy might be used to clear peroxisomes that produce higher ROS or are less able to handle ROS.

Hepatocellular carcinoma (HCC) cells isolated from USP30KO mice revealed reduced OCR and ECAR, both basal and maximal, compared to HCC cells from wild-type mice, suggesting that USP30 enhanced mitochondrial and glycolytic metabolism (Gu et al., 2020). The above was partly in agreement with my data in the HCT116 FlpIn TRex USP30KO where USP30KO lowered the OCR but did not seem to alter ECAR (**Figure 5.20**B).

The Seahorse data from the hTERT-RPE1 FlpIn TRex USP30KO was overall less variable between independent experiments (**Figure 5.21**). However, there were no significant differences between USP30KO and USP30WT cells when cells were grown in their standard medium (**Figure 5.22**). Retro-respectively looking at the hTERT-RPE1 FlpIn TRex USP30KO Seahorse data in conjunction with the cell proliferation data of these cells in galactose (**Figure 5.30**), it would be interesting to repeat the Seahorse experiments with the same cells pre-conditioned to galactose.

5.7.4 Transcriptome and proteome in the HCT116 FlpIn TRex USP30KO cells

During the writing of this thesis, the comprehensive proteomes of HCT116 FlpIn TRex USP30KO and hTERT-RPE1 FlpIn TRex USP30KO cells were completed in Newcastle, which allowed me to cross-reference the data between these data sets and my RNA-seq and small-scale proteome.

HKDC1 (hexokinase domain containing protein 1) is a low activity hexokinase that was shown to associate with the OMM and whose overexpression led to reduced glycolytic and mitochondrial metabolism (Pusec et al., 2019). HKDC1 transcripts were reduced in USP30KO cells, which may contribute to reduced metabolic capacity, which in turn reduced proliferation of USP30KO cells. However, the comprehensive proteome analysis of HCT116 FlpIn TRex USP30 and hTERT-RPE1 FlpIn TRex USP30KO did not cover HKDC1 itself. Hexokinases (HK) 1 and 2 remained constant in the HCT116 FlpIn TRex USP30KO cell proteome, whilst HK2 protein levels were reduced in hTERT-RPE1 FlpIn TRex USP30KO2 compared to the parental, with USP30KO6 compared to parental similarly showing a smaller decrease (Marcassa *et al*, unpublished).

Furthermore, BCL2L15 (BFK) is a BH3-only protein that is a weak inducer of apoptosis (Coultas et al., 2003). BFK has been described to be cytosolic and able to inhibit BCL-X_L and BCL-w but not BCL-2. Upregulation of BCL2L15 transcript in the USP30KO cells may weakly promote apoptosis as seen in certain instances in the cell death experiments I performed (**Figure 5.9** and **Figure 5.11**). However, the data from the more comprehensive proteome in the HCT116 FlpIn TRex USP30KO cells suggested the expression levels of BCL2L15 were unaffected. it is not known whether the changes in the levels of a transcript directly translate to analogous or equivalent changes of the respective protein. The interpretation of RNA-seq data presents an additional conundrum especially in the context of a DUB whose function often is to rescue proteins from degradation and enhance their stability. The levels of a transcript may be elevated in the USP30KO cells as a compensatory mechanism due to its protein product being destabilised and reduced in the absence of USP30.

SLC2A1 (GLUT1) was shown to be reduced in my small-scale proteome in the USP30KO cells to USP30WT3 comparison (**Figure 5.37**). GLUT1 protein levels were similarly reduced in USP30KO2 compared to parental in the more comprehensive proteome in the HCT116 FlpIn TRex cells, whilst remained unchanged in the hTERT-RPE1 FlpIn TRex USP30KO cell.

FASN protein levels appeared higher in the USP30KO clones in my small-scale proteome experiment (**Figure 5.37**). However, the more comprehensive proteome performed in the same cells revealed that USP30KO1 had lower levels of FASN than the parental cells in one of the experiments and remained unchanged in the other two preparations. In fact, FASN was consistently lower in USP30KO2 compared to the parental cells in the proteome of hTERT-RPE1 FlpIn TRex cells. Interestingly, FASN has been shown to interact with and be positively regulated by USP30 (Gu et al., 2020). The authors showed that the levels of FASN were lower in HCC tumours derived from USP30KO mice. The same study showed that overexpression of FLAG-USP30 in USP30-depleted HepG2 cells restored the levels of FASN back to the control. In the same experiment, the catalytically inactive mutant (C77S) failed to rescue FASN protein levels, demonstrating that USP30 catalytic activity was mediating the stabilisation of FASN in liver cells.

5.7.5 Model of USP30 promoting mitochondrial metabolism and enhancing cell proliferation

Overexpression and activating mutations in KRAS were shown to drive the transcriptional expression of key glycolytic enzymes such as hexokinases (HK), phosphofructokinase (PFK), lactate dehydrogenase (LDH) as well as the glucose transporter GLUT1 (Ying et al., 2012). This KRAS-driven transcriptional programming promotes glycolytic metabolism and, more importantly, promotes flux through the biosynthetic non-oxidative arm of the pentose phosphate pathway (Ying et al., 2012; Pupo et al., 2019). Our lab showed that USP30 is required for HGF-dependent cell scattering of A549 cells, placing USP30 downstream of RTK and KRAS signalling (Buus et al., 2009). The reduced OCR and proliferation of USP30KO cells in glucose may relate to the mutant KRAS status (G13D) of HCT116 FlpIn TRex cells. The above may also explain why the hTERT-RPE1 FlpIn TRex cells did not follow the same pattern where there was no clear segregation of USP30KO and USP30WT cells in terms of OCR and proliferation in glucose (**Figure 5.23** and **Figure 5.30**). USP30 is downstream of KRAS signalling and might be required for the KRAS-mediated transcriptional reprogramming that drives proliferation through upregulation of glycolytic and other biosynthetic genes.

Cells derive the majority of their ATP through the metabolism of glutamine through the TCA cycle (Reitzer et al., 1979). Glutamine is converted into glutamate, which then is converted into α-ketoglutarate and enters the TCA cycle, which feeds the ETC (**Figure 5.38**).

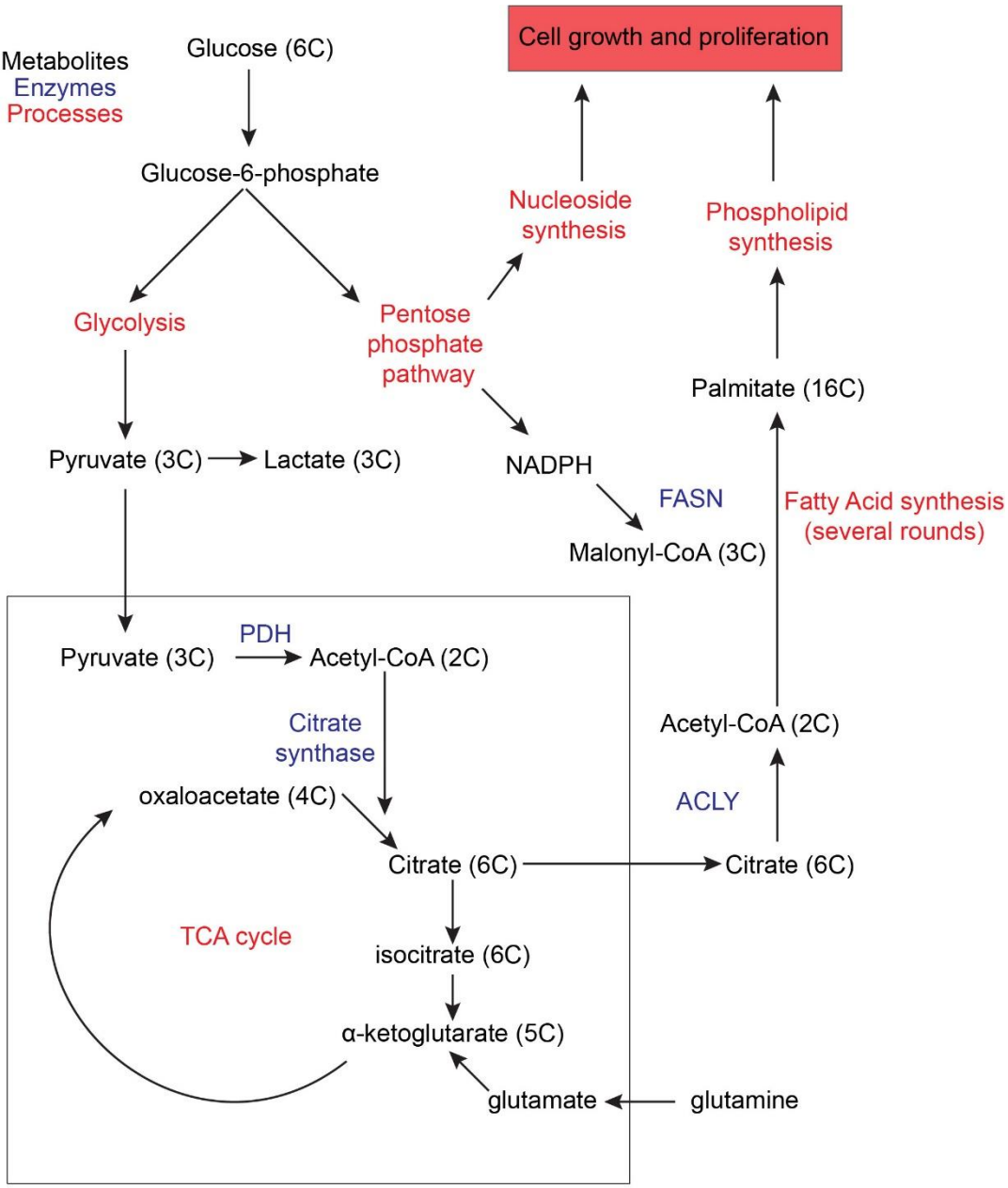

Figure 5.38: Overview of cell metabolism in glucose

The diagram shows the different key intermediates of the pathways, the enzymes that catalysed the reactions and the compartmentalisation of the processes between cytosolic and mitochondrial processes. Metabolites are shown in black, key enzymes are shown in blue and metabolic processes are shown in red. The number of carbon atoms is shown in brackets next to the name of key metabolites. TCA, tricarboxylic acid cycle; PDH, pyruvate dehydrogenase; ACLY, ATP citrate lyase; FASN, fatty acid synthase; CoA, coenzyme A; ATP, adenosine triphosphate; NAD(P)H; reduced nicotinamide adenine dinucleotide (phosphate).

In fact, only a minor percentage of glucose-derived carbon enters the TCA cycle and the majority of glucose is channelled into the oxidative part of the pentose phosphate pathway that is destined for the synthesis of macromolecules. The remaining glucose is metabolised through glycolysis to generate ATP with the final product being lactate (**Figure 5.38**).

An estimated 50% of the ATP is derived from the oxidative catabolism of glutamine even in the presence of glucose (**Figure 5.38**). The percentage of cellular ATP that is derived from the metabolism of glutamine jumps up to 98% when the cells are given galactose instead (**Figure 5.39**). It appears that in galactose, a larger portion of glutamine is used for ATP generation and a lesser amount can be used for biosynthesis, which results in the cells becoming more dependent on their mitochondria for ATP generation (Reitzer et al., 1979).

Collectively, the above postulate that the HCT116 FlpIn TRex USP30KO cells fail to drive high expression of glycolytic genes presumably mediated by their KRAS mutant status (Alves et al., 2015). In turn, the reduced ability of the USP30KO cells to metabolise glucose and channel it into biosynthetic pathway retards their proliferation, as seen in my proliferation and colony formation assays (**Figure 5.28** and **Figure 5.29**). In galactose, the biosynthetic capacity of cells is already reduced since the cells have lower flux through their biosynthetic pentose phosphate pathway. Therefore, any enhancement offered by USP30 becomes negligible in galactose.

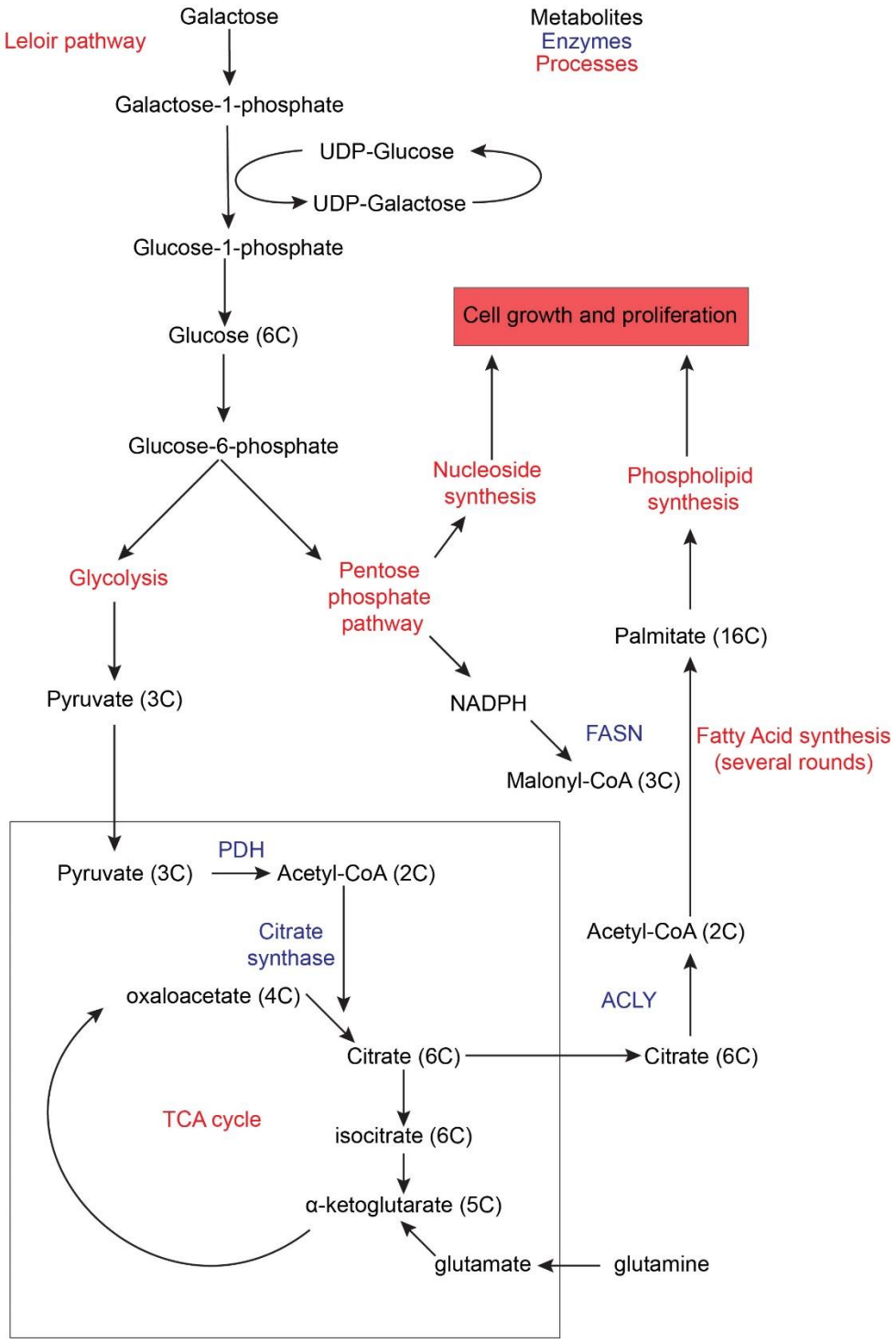

Figure 5.39: Overview of cell metabolism in galactose

The diagram shows the different key intermediates of the pathways, the enzymes that catalysed the reactions and the compartmentalisation of the processes between cytosolic and mitochondrial processes. Metabolites are shown in black, key enzymes are shown in blue and metabolic processes are shown in red. The number of carbon atoms is shown in brackets next to the name of key metabolites. TCA, tricarboxylic acid cycle; PDH, pyruvate dehydrogenase; ACLY, ATP citrate lyase; FASN, fatty acid synthase; CoA, coenzyme A; ATP, adenosine triphosphate; UDP, uridine diphosphate; NAD(P)H; reduced nicotinamide adenine dinucleotide (phosphate).

Lipogenesis is the synthesis of fatty acids from excess glucose in the body and requires a “fed-state”. The above implies that the metabolic requirements of the cells are met through the metabolism of glucose and there is an excess of glucose that can be used to synthesise fatty acids (FA) as long-term storage molecules. For that reason, lipogenesis and FA β-oxidation are tightly regulated by hormonal and allosteric mechanisms on key enzymes. The building blocks for fatty acid synthesis is acetyl coenzyme A (Acetyl-CoA) that is generated in the mitochondrion through the action of pyruvate dehydrogenase (PDH) on pyruvate. Acetyl-CoA is then conjugated with oxaloacetate into citrate by citrate synthase. Citrate can either be metabolised in the tricarboxylic acid cycle (TCA) to generate ATP through the ETC or may be exported into the cytosol as a building block for fatty acids. Exported citrate is converted back to oxaloacetate and Acetyl-CoA by ATP-citrate lyase (ACLY), and Acetyl-CoA undergoes several rounds of further processing into fatty acids, typically in the form of palmitate. Fatty acid synthase (FASN) therefore requires Acetyl-CoA but also reducing power in the form of cytosolic NADPH. NADPH is generated in the cytoplasm through the metabolism of glucose in the oxidative arm of the pentose phosphate pathway.

For the cell to synthesize fatty acids from glucose it must meet two important requirements. Firstly, it must generate enough ATP from glucose metabolism alone and have excess glucose to shuttle a portion of, in the form of citrate, away from the TCA cycle and into the cytoplasm to generate Acetyl-CoA. Secondly, there must be sufficient glucose to meet the energetic requirements of the cells through glycolysis and the TCA cycle in order to shuttle glucose through the pentose phosphate pathway to generate NADPH. The balance between how much ATP can be generated through glycolysis of glucose and how much glucose can be funnelled into the biosynthetic pathways is critical. In galactose, the cells are forced to shuttle more carbon subunits into the TCA cycle to generate sufficient ATP, resulting in a tighter coupling between glycolysis and TCA cycle. The tighter coupling between glycolysis and TCA cycle is reflected in the sensitivity of galactose-grown cells to both glycolytic and mitochondrial poisons (**Figure 5.26**). Therefore, a lower percentage of glucose can be salvaged for shuttling into fatty acid synthesis in the galactose-grown cells.

As mentioned above, USP30 has been proposed to promote lipogenesis through stabilisation of the key enzymes FASN and ACLY (Gu et al., 2020). My data on the growth of HCT116 FlpIn TRex USP30KO cells has shown that USP30 enhances proliferation of cells grown in glucose but the enhancement is lost when the cells were placed in galactose (**Figure 5.28** and **Figure 5.29**). The above may be explained in terms of reduced levels of ACLY and FASN and thus reduced lipogenesis, which in turn results in reduced phospholipid synthesis and reduced proliferation. The growth benefit of USP30 expressing cells compared to USP30KO cells disappears in cells grown in galactose, as under these conditions, lipogenesis is disfavoured.

Chapter 6: The role of USP30 in opposing the PINK1/Parkin axis in neurodegeneration

6.1 Introduction

6.1.1 USP30 opposes PINK1 and Parkin during mitophagy

USP30 opposes Parkin activity during mitophagy by deubiquitylating a subset of Parkin substrates (Bingol et al., 2014; Cunningham et al., 2015; Liang et al., 2015a). Furthermore, the work of Elena Marcassa in our lab demonstrated that depleting or knocking out USP30 in cells enhanced the basal rate of mitophagy (Marcassa et al., 2018). Most importantly, Elena showed that co-depleting cells of PINK1 abolished the enhancement achieved through USP30 depletion or loss. The above observation places USP30 upstream of PINK1 in the pathway and provided the first evidence that USP30 restricts the threshold for basal mitophagy (Marcassa et al., 2018).

The current model suggests that USP30 opposes mitophagy both upstream and downstream of PINK1 and Parkin activities (**Figure 6.1**). Most of the work that has been performed in the field of PINK1/Parkin-dependent mitophagy uses cells that overexpress Parkin (Bingol et al., 2014; Cunningham et al., 2015; Liang et al., 2015a). Such studies have the limitation that once Parkin becomes activated, USP30 has very limited capacity to restrict its activity. The E3 ligase activity is so high that USP30 is not able to efficiently antagonise it. Furthermore, PINK1 and Parkin engage in a strong positive feed-forward mechanism. PINK1 phosphorylates ubiquitin on Ser65, which recruits and activates Parkin to mitochondria. PINK1 also phosphorylates Parkin on an analogous position (Ser65) in the ubiquitin-like domain (UBL) of Parkin further enhancing its activity (Shiba-Fukushima et al., 2012, 2014; McWilliams et al., 2018a). Parkin ubiquitylates OMM proteins, generating more ubiquitin substrate for PINK1 to phosphorylate. Interestingly, phospho-Ser65 ubiquitin (pS65-Ub) was shown to be a poor substrate for USP30 (Wauer et al., 2015; Huguenin-Dezot et al., 2016; Gersch et al., 2017). Collectively, the high levels of Parkin that synergise with PINK1 to generate pS65-Ub and the inability of USP30 to cleave phosphorylated ubiquitin chains, prevent us from

looking at the early events of mitophagy around pS65-Ub generation. The system becomes saturated and irreversible early on and USP30 has little opportunity to act. It was necessary to simplify the experimental model by using cells that lacked detectable Parkin expression in order to better capture the events leading up to pS65-Ub generation on mitochondria, where the amplification of Parkin was not a complicating factor.

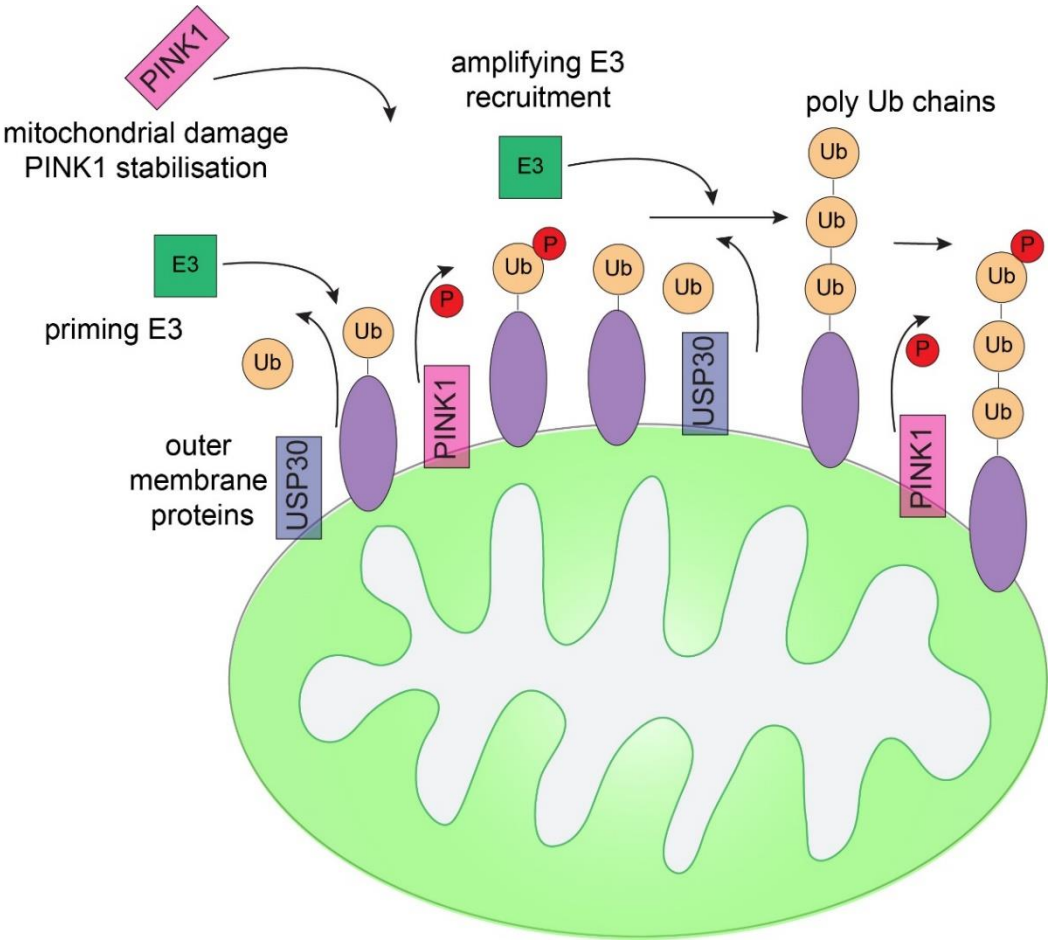

Figure 6.1: USP30 opposes PINK1 and Parkin during mitophagy

A priming E3 ligase ubiquitylates outer mitochondrial membrane proteins. USP30 removes the ubiquitin while PINK1 may use these ubiquitylated proteins as a substrate once PINK1 becomes stabilised on damaged mitochondria. The accumulation of phosphorylated-S65 Ub on outer mitochondria recruits an amplifying E3 ligase, that is Parkin in cells that express it. The E3 ligase further ubiquitylates OMM proteins, of which some are deubiquitylated by USP30. The E3 ligase activity results in further PINK1 substrate being deposited onto mitochondria outer membrane. E3, E3 ubiquitin ligase, Ub, ubiquitin; PINK1, PTEN-induced kinase; USP30, ubiquitin specific peptidase 30; P; phosphate.

6.2 Characterisation of phospho-Ser65 Ubiquitin-specific antibodies

I initially sought to characterise pS65-Ub-specific antibodies in terms of their suitability and specificity in detecting pS65-Ub by immunoblot and by immunofluorescence. I wanted to validate that generation of pS65-Ub as detected by the available antibodies was indeed PINK1-dependent as previously described and establish which of the bands and staining were due to pS65-Ub (Kane et al., 2014; Kazlauskaite et al., 2014; Koyano et al., 2014).

I depleted PINK1 and USP30 (siRNA oligo D1) in hTERT-RPE1 YFP-Parkin cells and then induced mitophagy by treating with 1 μM oligomycin A and 1 μM antimycin A (A/O) for 1 hour. With this experiment I also wanted to optimise the use of these antibodies for immunoblotting and as such tested whether using 5% fat-free milk (Marvel) of 5% fat-free BSA worked best as a blocking reagent (**Figure 6.2**).

I aligned the blots as closely as possible based on the molecular weight markers as such that it would be possible to compare the two antibodies in the same blocking buffer. YFP-Parkin is expressed at high levels in these cells (data not shown) and 1 hour of A/O was sufficient to generate a strong pS65-Ub signal with both antibodies in both blocking reagents. The first interesting observation was that pS65-Ub signal evolved across the entire lane, suggesting that both small and large proteins become decorated with pS65-Ub during mitophagy. Furthermore, the evolution of signal in the lower molecular weight range may indicate proteins that are mono-ubiquitylated proteins becoming phosphorylated by PINK1 in response to depolarisation. The above may suggest that certain proteins can be decorated with single pS65-Ub moieties and not necessarily long chains. The signal was however stronger towards the higher molecular weight range, which may represent poly-ubiquitylated proteins becoming phosphorylated. There were also certain bands that were changing consistently between the two antibodies, irrespective of blocking reagent (**Figure 6.2**, red arrows).

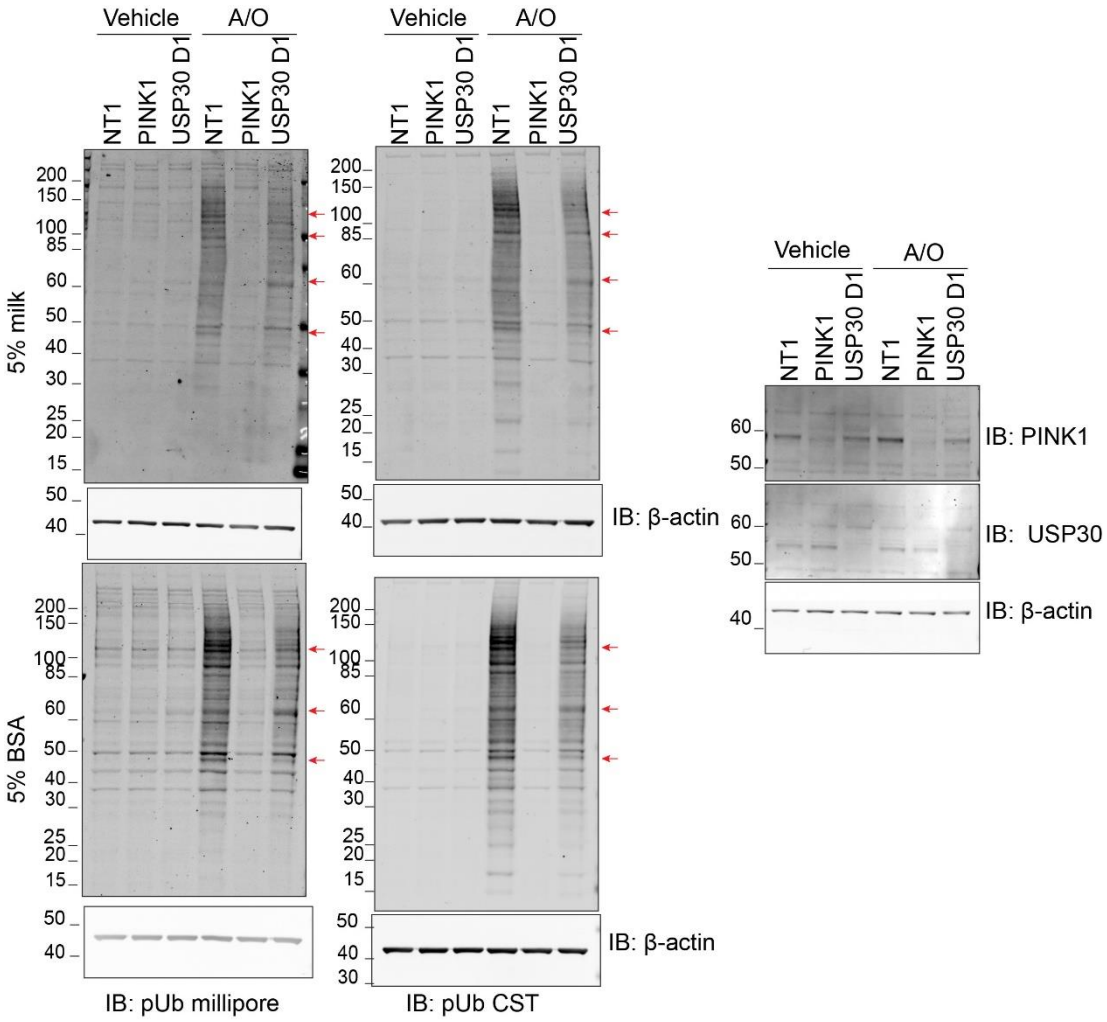

Figure 6.2: pS65-Ubiquitin signal by immunoblot is PINK1 dependent in hTERT-RPE1 YFP-Parkin cells

hTERT-RPE1 YFP-Parkin cells were transfected with siRNA against PINK1 or USP30 (D1) or non-targeting oligo (NT1) for 72 hours. Cells were treated with 1 μM antimycin A and 1 μM oligomycin A (A/O) for 1 hour before being lysed in NP-40 lysis buffer supplemented with PhosSTOP and MPIs (1:250). Immunoblot analysis was performed to optimise the blocking and incubation conditions between 5% fat-free milk (Marvel) or 5% fat-free BSA in TBST for two pS65-Ub (pUb) specific antibodies from Millipore or Cell Signalling Technologies (CST). Red arrows indicate bands that respond to A/O treatment and are detected by both antibodies.

These bands appear to be PINK1 dependent as well as sensitive to USP30 depletion as they are weaker in that condition. The antibody from Cell Signalling Technologies (CST) overall produced a cleaner signal and with lower background compared to the Millipore antibody in both incubation buffers. Using BSA as a blocking reagent produced a cleaner blot with lower background using both antibodies as well. It was re-assuring that the PINK1-depleted cells treated with A/O produced no higher signal than in the control oligo vehicle-treated cells. The above suggested that the signal was entirely PINK1 dependent and required the addition of A/O. Interestingly, USP30-depleted cells had lower levels of pS65-Ub across all antibodies and blocking buffers. The above observation may suggest that pS65-Ub accumulation may have different dynamics in USP30-depleted cells, hinting at either altered generation or decay through enhanced pS65-Ub dephosphorylation and/or deubiquitylation. Alternatively, it may suggest accelerated degradation of phospho-ubiquitylated proteins in the absence of USP30.

I also wanted to validate the antibodies for use in immunofluorescence microscopy. I conducted a similar experiment where I depleted PINK1 in hTERT-RPE1 YFP-Parkin cells and treated with A/O (1 μM each) as above. I then fixed the cells and stained with for pS65-Ub using the CST antibody in the red channel and for TOMM20 in the blue channel (**Figure 6.3**). YFP-Parkin was recruited to TOMM20 stained puncta in response to depolarisation. The pS65-Ub signal co-localised with YFP-Parkin and TOMM20 stain in response to A/O and PINK1 depletion prevented YFP-Parkin translocation and pS65-Ub signal generation. The experiment demonstrated that the CST antibody was suitable for IF experiments to visualise pS65-Ub on mitochondria and that the signal was specific as it was PINK1 dependent.

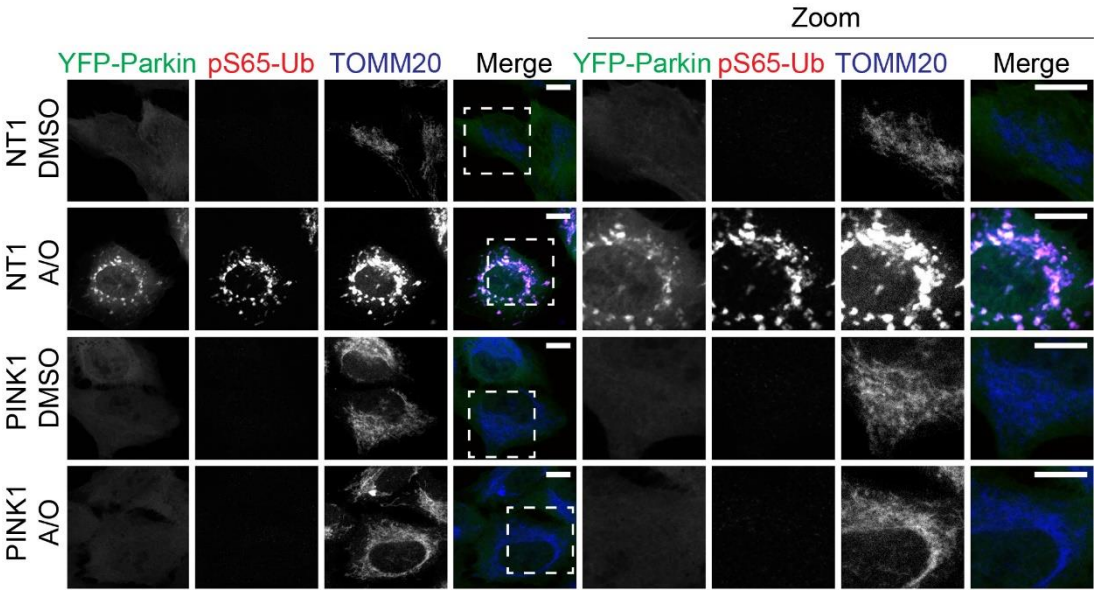

Figure 6.3: pS65-Ub is dependent on PINK1 in hTERT-RPE1 YFP-Parkin by immunofluorescence

hTERT-RPE1 YFP-Parkin cells were transfected with siRNA against PINK1 or non-targeting oligo (NT1) for 72 hours. Cells were treated with antimycin A and oligomycin A (A/O 1 μM each) for 1 hour before being fixed with 4% PFA/PBS, blocked in 3% BSA/PBS, and stained for pS65-Ub using the Cell Signalling Technologies (CST) and for TOMM20. Images were acquired with a 63x oil immersion objective on a Zeiss 3i spinning disk confocal microscope. Scale bars are 10 μm.

My colleague, Elena Marcassa, validated the pS65-Ub antibody from Millipore in a similar experiment, which showed the same pattern as my experiment: pS65-Ub generated on mitochondria accompanied by YFP-Parkin recruitment in a PINK1-dependent manner. We also acquired a directly conjugated version of the same Millipore antibody coupled to AlexaFluor488 (AF488), which may produce less background staining in IF. I investigated the directly conjugated antibody, however the hTERT-RPE1 YFP-Parkin cells were unsuitable for this experiment since YFP-Parkin and AF488 fluorescence emission spectra overlap. I therefore used the SH-SY5Y cells instead, which express Parkin endogenously. Treating the SH-SY5Y cells with A/O (1 μM each) for four hours produced a strong pS65-Ub signal (**Figure 6.4**).

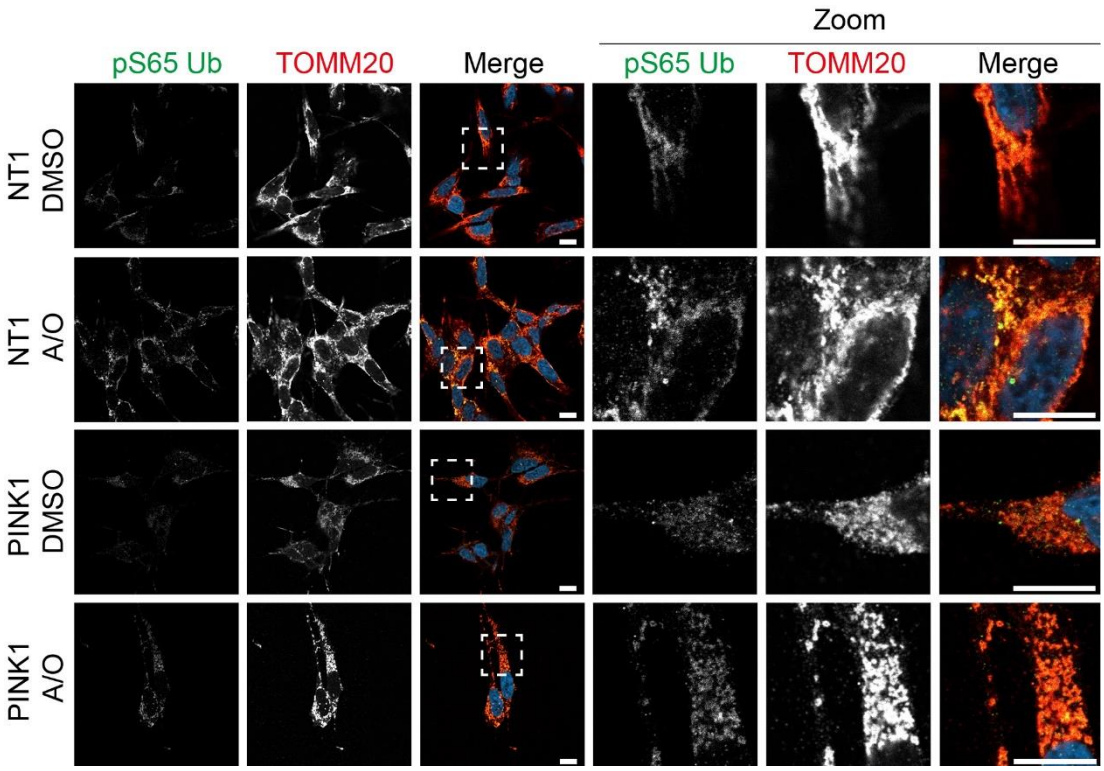

Figure 6.4: pS65-Ub is PINK1 dependent in SH-SY5Y cells

SH-SY5Y cells were transfected with 40 nM siRNA oligos against PINK1 or non-targeting oligo (NT1) for 72 hours. Cells were treated with 1 μM antimycin A and 1 μM oligomycin A (A/O) for four hours, before fixation in 4% PFA/PBS and stained with for pS65-Ub AF488 (Millipore) and for TOMM20. Images were acquired using a 60x oil-immersion objective on a Zeiss LSM800 scanning confocal microscope. Scale bars are 10 μm.

In the vehicle treatment, a weak pS65-Ub signal evolved, which was lower in the PINK1-depleted cells, suggesting that some pS65-Ub may evolve constitutively in the absence of a depolarisation trigger, potentially reflecting some low level steady state mitochondrial damage. It is important to emphasise however that PINK1 depletion was not 100% efficient as shown by the accompanying immunoblot (**Figure 6.5**). The blot revealed that even basally (vehicle), some full length (FL) PINK1 was accumulating, as well as in the PINK1-depleted cells (**Figure 6.5**, high exposure blot). Furthermore, in the presence of A/O, the pS65-Ub signal was dramatically reduced, but not absent in the PINK1 depleted cells. In the DMSO treated cells, all the signal evolved is insensitive to PINK1 depletion, suggesting it is was background.

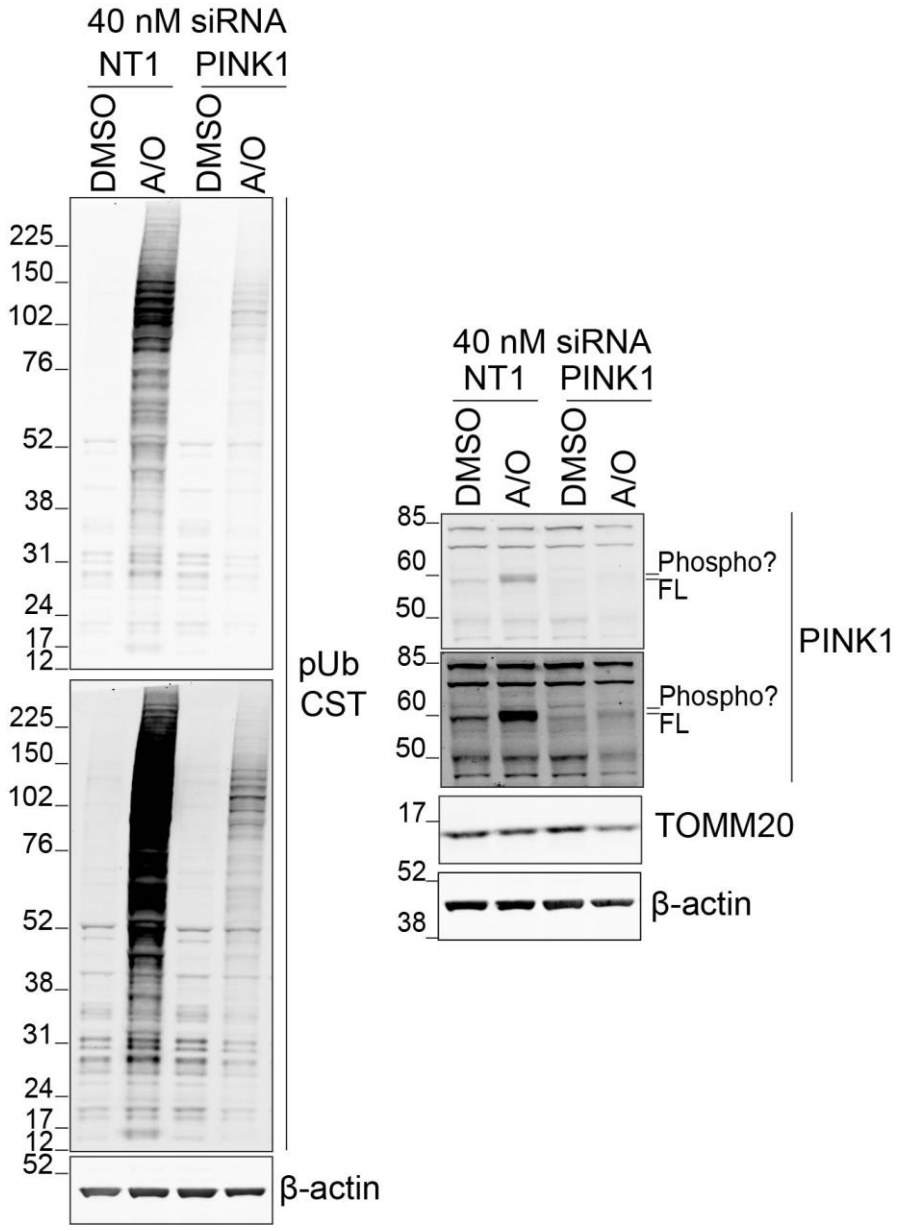

Figure 6.5: PINK1 is not entirely depleted in SH-SY5Y cells

SH-SY5Y cells were transfected with 40 nM siRNA oligos against PINK1 or non-targeting oligo (NT1) for 72 hours. Cells were treated with 1 µM antimycin A and 1 µM oligomycin A (A/O) for four hours, before being lysed in NP-40 lysis buffer supplemented with PhosSTOP and MPIs (1:250). FL, full length; Phospho?, suspected band for the phosphorylated PINK1.

6.3 Phospho-S65 Ubiquitin generation in cells lacking detectable endogenous Parkin

6.3.1 Uncoupling PINK1 phosphorylation from ubiquitylation during mitophagy

I wanted to dwell deeper into the mechanism by which PINK1 generates pS65-Ub on mitochondria. One question that arose was what the ubiquitin substrate for PINK1 on mitochondria was and where it was coming from. In the model that I described above a priming E3 is constantly ubiquitylating OMM proteins, which PINK1 can phosphorylate once PINK1 is stabilised in response to mitochondrial damage (**Figure 6.1**). This ubiquitin substrate may be removed by USP30 and other DUBs. The above creates a small steady state pool of ubiquitin constantly on mitochondria. However, one cannot exclude the possibility that there is no ubiquitin substrate for PINK1 on mitochondria prior to mitochondrial damage. i.e. the priming E3 does not act at steady state and instead becomes activated upon mitochondrial damage, and this is when USP30 may act to counteract its activity.

I was interested in differentiating between the two possible models by directly looking at the ability of PINK1 to generate pS65-Ub on mitochondria on the ubiquitin substrate already available. The challenge however was that upon incidence of mitochondrial damage and PINK1 stabilisation, it is possible that even in the absence of Parkin, there are consecutive waves of ubiquitylation that follow PINK1 phosphorylation of ubiquitin due to the activity of alternative E3 ligases. FBXO7(*PARK15*), one of the adaptors of the SCF complex (Skowyra et al., 1997), was shown to be an E3 ligase involved in promoting mitophagy through interactions with PINK1 and Parkin (Burchell et al., 2013; Vincow et al., 2013). Furthermore, TOMM20 was shown to be a direct substrate of SCF^{FBXO7} (Teixeira et al., 2016).

ARIH1 was also a candidate E3 ligase in the context of mitophagy. Overexpressed ARIH1 was shown to behave similarly to overexpressed Parkin by responding to a depolarisation trigger in a PINK1-dependent manner on mitochondria (Villa et al., 2017). In this context, ARIH1 acted as an amplifying E3 ligase, however it cannot be ruled out that it may in addition act as a priming E3 ligase in mitophagy, especially considering ARIH1 is the priming E3 ligase for all Cullin E3 ligases (Scott et al., 2016).

The fundamental question I sought to investigate was whether there was any ubiquitin PINK1 substate on mitochondrial at steady state. I therefore needed a way to uncouple the two processes of ubiquitylation and phosphorylation and only allow for PINK1 phosphorylation to occur. I achieved this by blocking global ubiquitylation in cells with the use of a ubiquitin E1 activating enzyme inhibitor, MLN-7243/TAK-243 (McGrath et al., 1991; Best et al., 2018; Hyer et al., 2018). Therefore, any pS65-Ub signal generated would be a result of PINK1 activity on already available ubiquitin substrate on mitochondria. TAK-243 is able to fit in the ATP-binding pocket of UBE1, resulting in a ubiquitin-TAK-243 adduct instead (Misra et al., 2017). UBE1 is the major UAE in mammalian cells thus inhibiting it blocks the majority of ubiquitylation in the cells (Hyer et al., 2018). In parallel I sought to investigate the potential contributions of the Cullins as priming and amplifying E3 ligases, by specifically blocking Cullin E3 ligase activity with MLN-4924 (Brownell et al., 2010). MLN-4924 is a highly selective compound that targets the NEDD8 activating enzyme, UBA3 (Gong and Yeh, 1999; Bohnsack and Haas, 2003). Neddylation, the addition of NEDD8 on Cullins, is required for ubiquitin E3 ligase activity (Kawakami, 2001; Sakata et al., 2007; Duda et al., 2008). Both SCF^{FBXO7} and ARIH1 require neddylation for activity, due to Cullin 1 in SCF requiring neddylation itself and ARIH1 needing to interact with neddylated Cullin 1 to switch to an open conformation (Kelsall et al., 2013, 1; Scott et al., 2016).

I performed an experiment where I pre-treated hTERT-RPE1 FlpIn TRex cells that do not express detectable Parkin with 1 μM TAK-243 or 1 μM MLN-7243 for 15 min prior to treating with A/O (1 μM) for 4 hours (**Figure 6.6**). The ubiquitin (VU1) blot revealed that the TAK-243 inhibitor was blocking global ubiquitylation as ubiquitylated proteins were lost through degradation and deubiquitylation at steady state. Furthermore, the Cullin 5 (CUL5) blot demonstrated that Cullin 5 neddylation was lost in the presence of MLN-4924, suggesting inhibition of neddylation. However, generation of pS65-Ub in the presence of MLN-4924 was unaffected, suggesting the Cullins were not involved as E3 ubiquitin ligases in this context. The generation of pS65-Ub in response to depolarisation was largely suppressed but not entirely abolished in the presence of TAK-243.

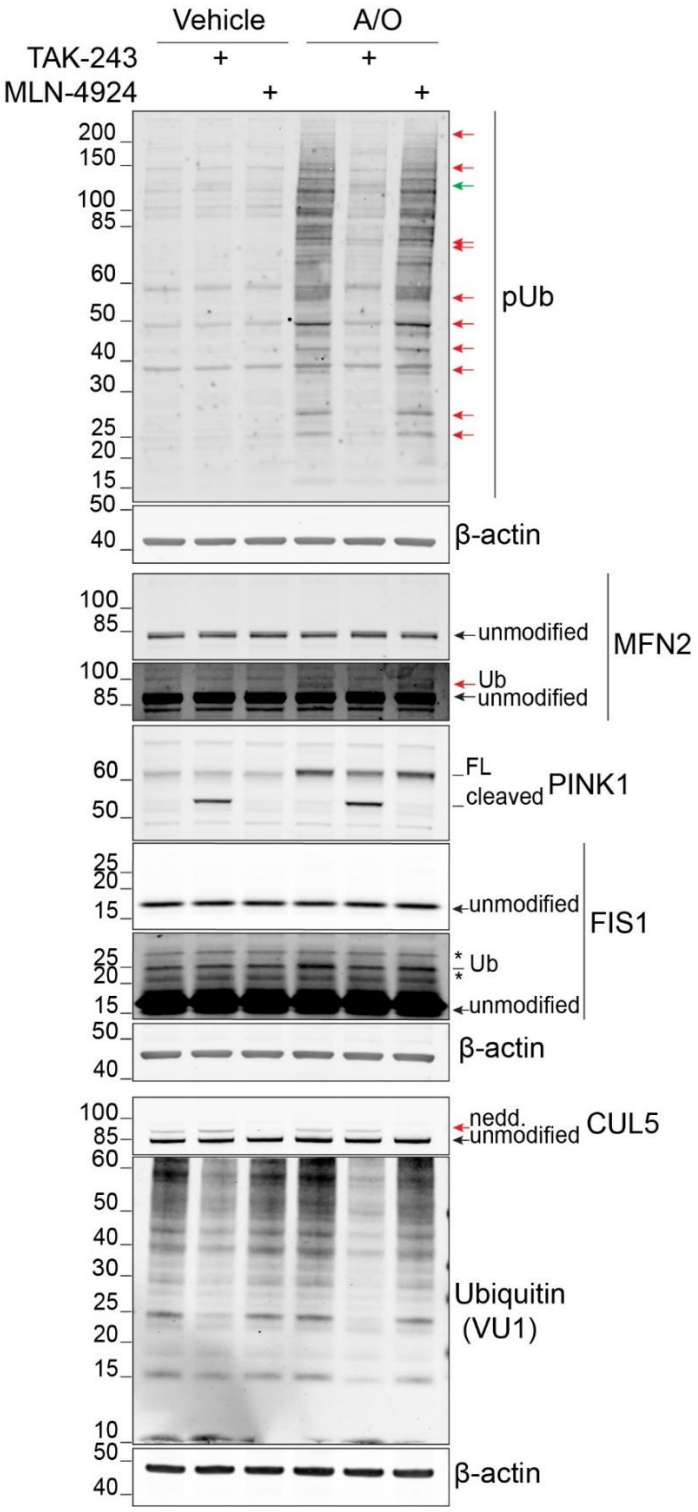

Figure 6.6: Pre-treatment with TAK-243 largely suppresses but does not completely abolish pS65-Ub generation

hTERT-RPE1 FlpIn TRex cells were pre-treated with 1 μM TAK-243 or 1 μM MLN-4924 and treated with 1 μM antimycin A and 1 μM oligomycin A (A/O) for 4 hours. Cells were lysed in NP-40 lysis buffer supplemented with PhosSTOP and MPIs (1:250). In the pS65-Ub (pUb) blot the red arrows points to bands that are sensitive to TAK-243 and green arrows to bands that are only visible in the presence of TAK-243. FL, full-length; Ub, ubiquitylated; nedd., neddylated; * non-specific bands.

It was apparent that certain bands in the pS65-Ub blot were dependent on global ubiquitylation (**Figure 6.6**). The bands marked with a red arrow are those that disappear in the presence of TAK-243. Such proteins are those that are not ubiquitylated at steady state and only become ubiquitylated and subsequently phosphorylated after the mitophagy trigger is introduced. Bands that are less sensitive to the presence of TAK-243 reflect proteins of which only a small fraction is ubiquitylated at steady state and upon mitophagy trigger the fraction that is ubiquitylated increases. The last category of bands that were differentially changing in response to TAK-243 were those indicated by green arrows. These bands were only becoming detectable when TAK-243 was included and in fact, were independent of A/O. The latter category may reflect proteins whose ubiquitylation is very long-lived but insufficient to target them for degradation. The fact that the band was visible even in the absence of A/O may suggest that PINK1 may act on these proteins at steady state or reflecting low levels of mitochondrial damage resulting in local stabilisation of PINK1. Given that most of the bands in the pS65-Ub blot are PINK1 dependent and triggered by A/O, the most likely explanation for the bands highlighted by green arrows is that they are non-specific. The block in ubiquitylation allows for a protein to accumulate which then non-specifically cross-reacts with the pS65-Ub antibody.

Another interesting part of this experiment was the behaviour of PINK1. Pre-treating the cells with TAK-243 produced significant levels of cleaved PINK1. PINK1 is constantly being made and imported in healthy mitochondria through the TOMM complex and cleaved by PARL that resides on the inner mitochondrial membrane. The cleaved fragment is then exported back into the cytosol and ubiquitylated and degraded through the proteasome. However due to the absence of ubiquitylation the cleaved product could not be ubiquitylated and targeted for proteasomal degradation. Cleaved levels of PINK1 in the presence of A/O and TAK-243 reached the same levels as with the pre-treatment with TAK-243 alone. This suggested that the majority of PINK1 was still getting cleaved even in the presence of a mitophagy trigger. This may reflect that not the entire cell population has depolarised mitochondria or not the entirety of the mitochondrial network was depolarised across the cells. Alternatively, there are two distinct pools of PINK1, only one of which could be

stabilised by depolarisation and the other pool kept getting cleaved even in depolarised mitochondria.

6.3.2 pS65-Ub time course in the presence or absence of TAK-243 in hTERT-RPE1 FlpIn TREx cells

I wanted to investigate the kinetics of the process of pS65-Ub generation in response to depolarisation, in the presence or absence of TAK-243. I treated the hTERT-RPE1 FlpIn TRex cells with A/O for 30', 1, 2, 3 or 4 hours with and without a 15 min pre-treatment of TAK-243 (**Figure 6.7**A). In the absence of TAK-243, pS65-Ub could already be detected at the earliest timepoint (30 min) and the signal increased up to the final 4 hour timepoint in response to A/O (**Figure 6.7**B). Interestingly, there were two big step-wise increases in pS65-Ub signal, between the 1 to 2 hours timepoints and between the 3 and 4 hours timepoints (**Figure 6.8**C). As expected, the total ubiquitin blot did not show any changes in the total ubiquitin profile of the cells (**Figure 6.7**C). I quantitated how the pS65-Ub signal changed across the entire molecular weight range in response to increasing lengths of A/O treatment (**Figure 6.8**B, left panel). It appeared that over time the high molecular weight bands were increasing in intensity the most. This may reflect increasing poly-ubiquitylation of OMM proteins and subsequent phosphorylation by PINK1.

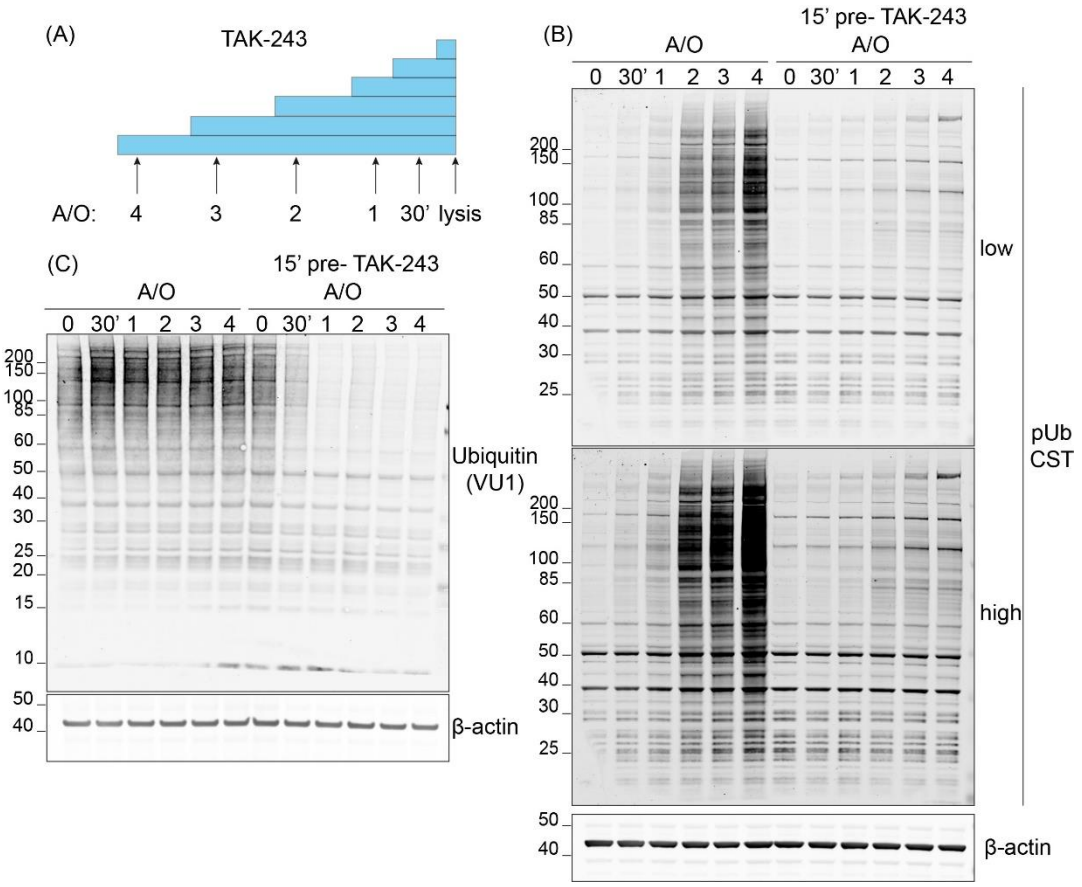

Figure 6.7: pS65-Ub time course in hTERT-RPE1 FlpIn TRex cells

(A) Schematic diagram illustrating the experimental setup. hTERT-RPE1 FlpIn TRex cells were pre-treated with 1 μM TAK-243 and treated with 1 μM antimycin A and 1 μM oligomycin A (A/O) for 30', 1, 2, 3 or 4 hours. All pre-treatments were performed 15 min before the respective A/O treatment. Cells were lysed in NP-40 lysis buffer supplemented with PhosSTOP and MPIs (1:250). The blue bars indicate the duration of the TAK-243 treatment and the arrows the addition of A/O. The (B) pS65-Ub blot (low and high exposures) and (C) total ubiquitin (VU1) blots. Low and high indicate low and high exposures for the pS65-Ub blots.

When TAK-243 was included as a 15 min pre-treatment, there was a small increase in the pS65-Ub signal that reached a plateau already at the early timepoints. The above suggested that there was very limited ubiquitin PINK1 substrate already present on mitochondria and that most of the ubiquitin that was acting as PINK1 substrate was being added after depolarisation by an amplifying E3 ubiquitin ligase. When global ubiquitylation was inhibited by the use of the TAK-243 inhibitor, there was very small increase in the intensity and distribution of bands, mostly confined to the high molecular weight range (**Figure 6.8**B, right panel).

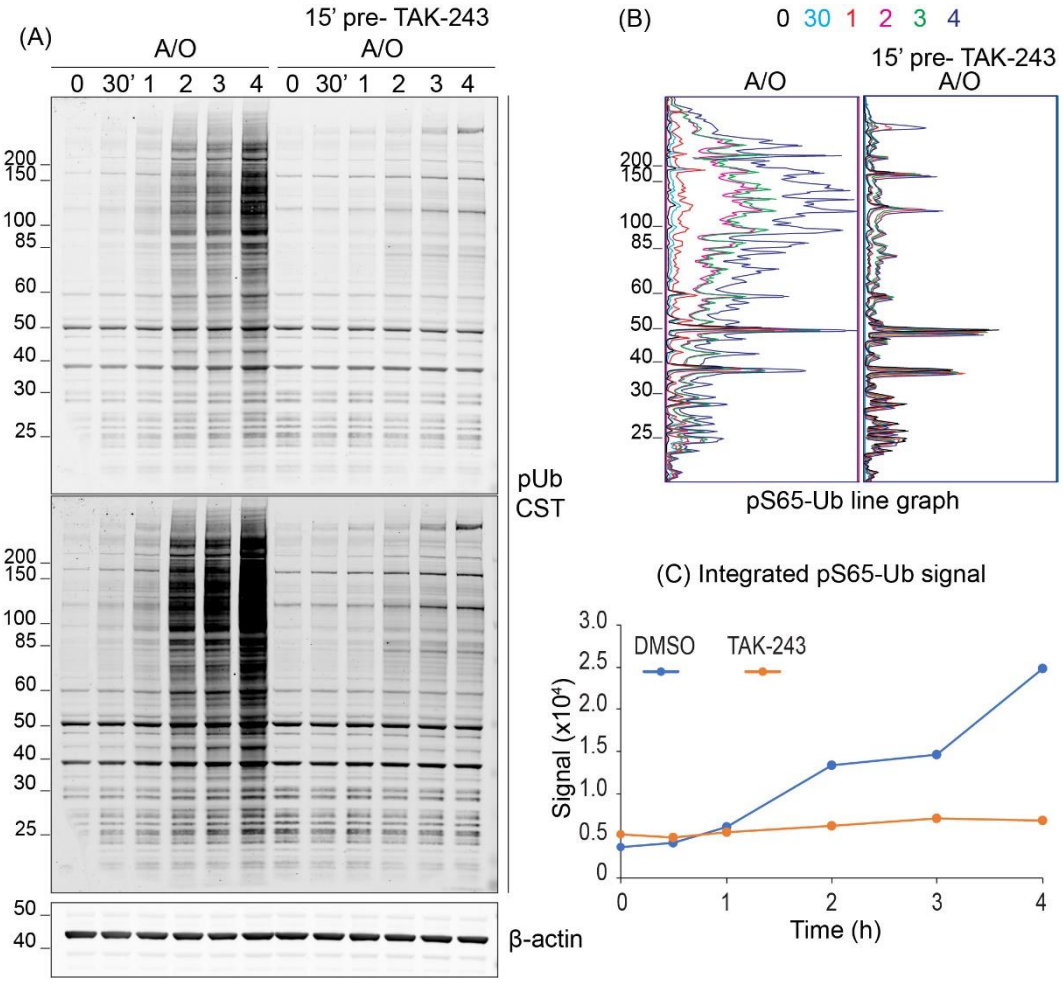

Figure 6.8: pS65-Ub signal quantitation in hTERT-RPE1 FlpIn TRex cells
(A) pS65-Ub Immunoblot from Figure 6.7 and the resulting quantitation of (B) integrated pS65-Ub signal and (C) line graph of pS65-Ub evolving over time.

Depolarising mitochondria in the presence of TAK-243 showed a marginal increase in pS65-Ub, which reached a plateau at the 2-hour timepoint (**Figure 6.8**C). During the first hour of depolarisation, the integrated pS65-Ub signal was the same in the presence or absence of TAK-243, which reflects the total ubiquitin that acts as PINK1 substrate. The data suggests that there is very limited ubiquitin PINK1 substrate on mitochondria at steady state and that the majority of the ubiquitin that is used as PINK1 substrate is added following depolarisation and PINK1 stabilisation.

The behaviours of the different PINK1 species were also very interesting (**Figure 6.9**). Quantitating the band intensity of the full length (FL) and cleaved PINK1 across all the conditions showed a very drastic change in their behaviours (**Figure 6.9**B). The full length species of PINK1 accumulated in a bi-phasic fashion in response to A/O. There was an increase in the levels of PINK1 at the 2-hour time point, which may also explain the behaviour of the pS65-Ub signal that was following a bi-phasic pattern as well (**Figure 6.8**C). The levels of full length PINK1 appeared to reach a plateau by the 2-hour time point and showed a minor increase from the 3rd and 4th hour time points. This may suggest that there is a maximum amount of full length of PINK1 that may accumulate in cells in response to A/O, perhaps a maximum number of TOMM complexes that are PINK1-competent in terms of stabilising the full length species. A longer time-course may be needed to determine this however.

The full length species of PINK1 was unaffected by the addition of TAK-243 (**Figure 6.9**B, blue and orange traces). Full length PINK1 was stabilised with the same kinetics and to the same extent both in the presence or absence of TAK-243, suggesting ubiquitylation was not required for PINK1 stabilisation in response to depolarisation. On the contrary, the cleaved fragment remained essentially undetectable in the absence of TAK-243 and yet accumulated very rapidly in its presence (**Figure 6.9**B, grey and yellow traces respectively). The cleaved fragment of PINK1 in the presence of TAK-243 appeared to be slowing down in terms of its accumulation. Initially, the cleaved species accumulated very rapidly. However, by the 3rd hour timepoint, the curve became less steep, which may suggest a negative feedback loop of the cleaved fragment not being degraded and suppressing PINK1 expression in the cells. The high levels of cleaved PINK1 fragment in the presence of TAK-243, were also indicative of the high turnover of PINK1 in cells.

These findings further support the data from the previous experiment (**Figure 6.6**), reinforcing the concept of two PINK1 pools, only one of which responded to A/O leading to its stabilisation. This experiment also gave some information on the kinetics, suggesting that the accumulation of cleaved PINK1 was indeed very rapid.

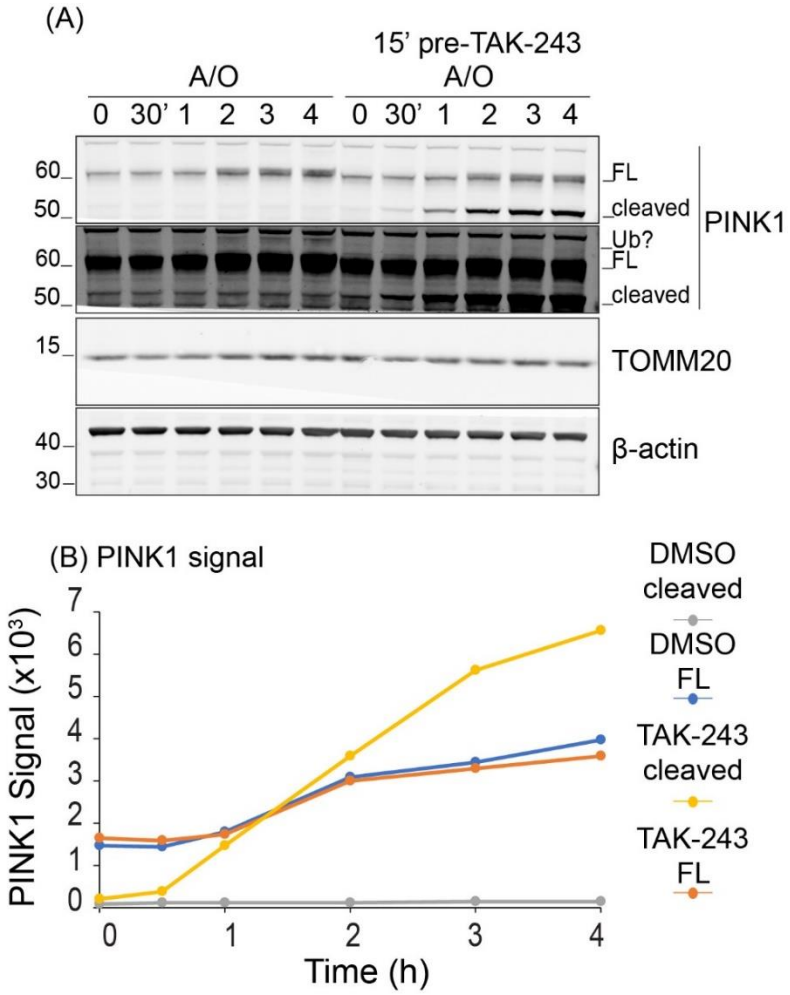

Figure 6.9: The behaviour of the different PINK1 species during the time-course of A/O in the presence or absence of TAK-243

(A) The PINK1 and TOMM20 immunoblots for the experiment in **Figure 6.7**. (B) The quantitation of the different PINK1 species (full length and cleaved) in the presence of absence of TAK-243. FL, full length; Ub?, suspected ubiquitylation band for PINK1.

The observations were very reproducible, as a second experiment I performed showed a very similar pattern for pS65-Ub generation (**Figure 6.10**) and the different PINK1 species (**Figure 6.11**) in the presence or absence of TAK-243. The signal of pS65-Ub generated in the absence of TAK-243 followed the same two-step pattern and this was suppressed by inclusion of TAK-243.

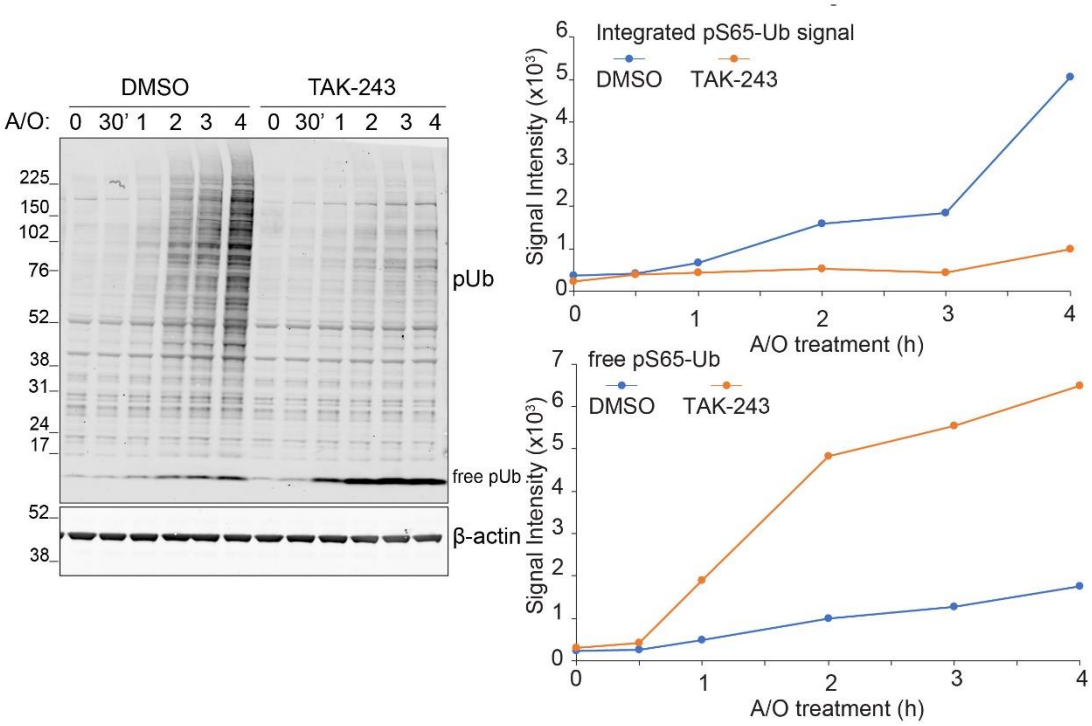

Figure 6.10: Time course repetition with a focus on free pS65-Ub
hTERT-RPE1 FlpIn TRex cells were pre-treated with 1 μM TAK-243 and treated with 1 μM antimycin A and 1 μM oligomycin A (A/O) for 30', 1, 2, 3 or 4 hours. All pre-treatments were performed 15 min before the respective A/O treatment. Cells were lysed in NP-40 lysis buffer supplemented with PhosSTOP and MPIs (1:250). Free pUb, free unconjugated monomeric pS65-Ub. The graph (above) shows the quantitation of the total (integrated) pS65-Ub signal with the free pS65-Ub signal omitted and the graph (below) shows the free pS65-Ub across in the presence or absence (DMSO) of TAK-243.

This experiment gave me the opportunity to also look at free (unconjugated) pS65-Ub that I had previously not managed to capture (**Figure 6.10**). Free (unconjugated) monomeric pS65-Ub followed similar kinetics pattern in increasing intensity as the total pS65-Ub. However, in the presence of TAK-243 the signal of free pS65-Ub increased at higher rate. A mechanism may operate whereby phospho-ubiquitylated proteins are extracted from the OMM and the ubiquitin chains removed *en bloc* and then cleaved into monomeric ubiquitin moieties, some of which remain phosphorylated. The above hypothesis is challenged however by data showing that many DUBs process phospho-ubiquitin chains less efficiently than their non-phosphorylated counterparts (Wauer et al., 2015; Huguenin-Dezot et al., 2016; Gersch et al., 2017).

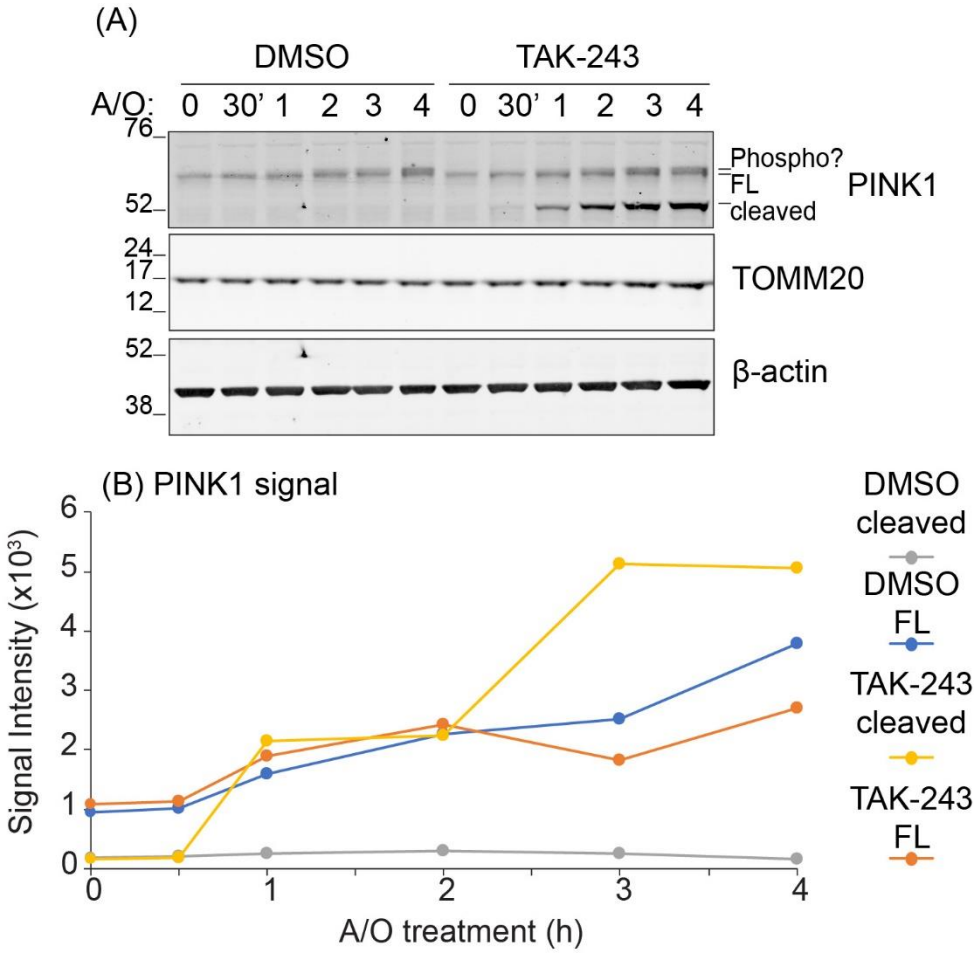

Figure 6.11: The behaviours of the different PINK1 species are reproducible

(A) The PINK1 and TOMM20 immunoblots for the experiment in **Figure 6.10**. (B) The quantitation of the different PINK1 species (full length and cleaved) in the presence of absence of TAK-243. FL, full length; Phospho?, suspected phosphorylated band for PINK1.

A more probable explanation may be that PINK1 was still able to efficiently phosphorylate unconjugated free ubiquitin in the proximity of mitochondria and its activity was not limited to ubiquitin incorporated onto OMM proteins.

The behaviour of PINK1 was also reproducible in this experiment (**Figure 6.11**). The full length species accumulated with nearly identical kinetics in response to A/O and were unaffected by the presence of the TAK-243 inhibitor. The cleaved fragment of PINK1 was barely detectable in the absence of TAK-243. The cleaved fragment however accumulated rapidly in the presence of TAK-243 and the signal appeared to plateau by the 3rd hour of treatment.

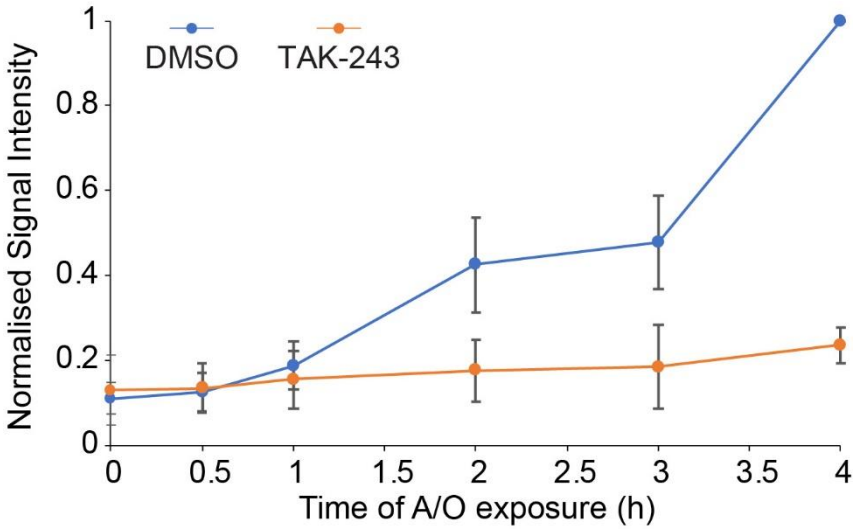

Figure 6.12: pS65-Ub signal evolution in the presence or absence of TAK-243

The integrated pS65-Ub signal in the presence or absence of TAK-243 from Figure 6.7 and Figure 6.10 were normalised to the maximum signal of each experiment and were plotted as a time-course graph. The time-points show the mean between two independent experiments (n=2) and the error bars are the range.

I normalised the pS65-Ub signal to the maximum signal achieved within each experiment and plotted it to generate time-course graphs (**Figure 6.12**). The time-course experiment with A/O in the presence or absence of TAK-243 pre-treatment showed a very clear and consistent pattern (**Figure 6.12**); The two-step accumulation of pS65-Ub in the absence of TAK-243. In the presence of TAK-243, the increase only appeared to reach approximately 20% of the maximum that was possible, and it seemed to have occurred during the fourth and last hour of A/O treatment. The above meant that approximately 80% of all pS65-Ub signal required *de novo* ubiquitylation.

6.3.3 Kinetics of pS65-Ub signal decay over time

I next set out to investigate the persistence of the pS65-Ub signal and inquire how disabling the ubiquitylation machinery affects the stability and decay of pS65-Ub over time. Following depolarisation with A/O there are consecutive waves of phosphorylation performed by PINK1 and ubiquitylation performed by E3 ligases. Given how different the signal intensity of pS65-Ub in response to A/O between in the presence or in the absence of TAK-243 in my set of experiments, I thought that TAK-243 may be used as an acute trigger

to remove ubiquitylation from the cascade once it has been initiated. In this situation, only PINK1 phosphorylation would be allowed to proceed farther upon addition of TAK-243. This experiment would allow me to see whether PINK1 phosphorylation alone would be sufficient to maintain the levels of pS65-Ub or the signal would start to decay, suggesting that ubiquitylation was still needed for maintenance.

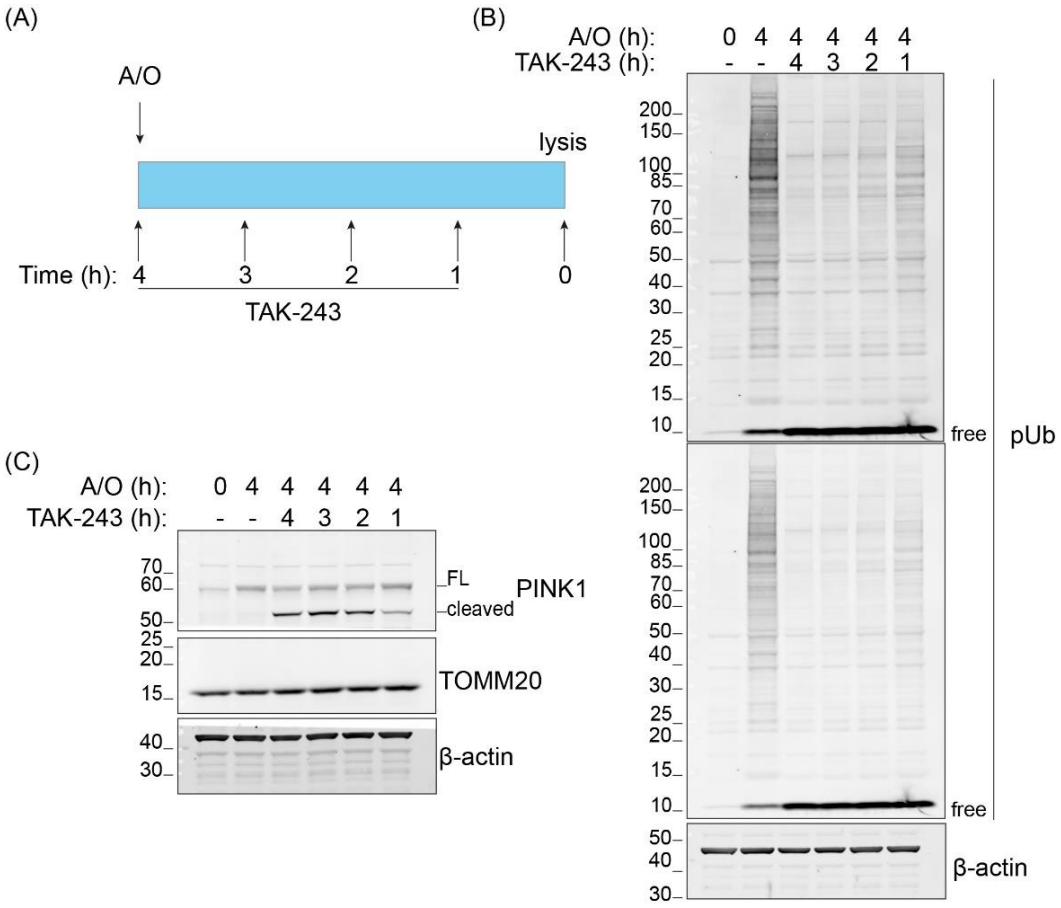

Figure 6.13: Blocking pS65-Ub signal generation with TAK-243

hTERT-RPE1 FlpIn TRex cells were treated with 1 μM antimycin A and 1 μM oligomycin A (A/O) for a total of four hours. The cells were treated with 1 μM TAK-243 at one-hour intervals to block ubiquitylation prior to lysis (A). Cells were lysed in NP-40 lysis buffer supplemented with PhosSTOP and MPIs (1:250). (B) pS65-Ub blot and (C) PINK1 and TOMM20 blots. free, unconjugated monomeric pS65-Ub.

I treated the hTERT-RPE1 FlpIn TRex cells with 1 μM A/O for a total of four hours and added TAK-243 to the cells at one-hour intervals prior to lysis, as to block ubiquitylation without removing the A/O (**Figure 6.13**A). The total pS65-Ub signal achieved without impediments after four hours of A/O can be seen in lane 2 (**Figure 6.13**B). There was only a small quantity of signal when both A/O and TAK-243 were added simultaneously (**Figure 6.13**B, lane 3). When TAK-243 inhibitor was included in the last hour before lysis there was significantly less pS65-Ub signal compared to leaving the TAK-243 inhibitor out (**Figure 6.13**B, lane 6). The above observation suggested that disabling ubiquitylation only for the last hour during the four-hour mitophagy trigger was sufficient to lose a significant pS65-Ub signal. The pS65-Ub signal appeared to be highly unstable in the absence of intact ubiquitylation machinery, which could be a result of extraction of pS65-Ub-decorated proteins for proteasomal degradation or a result of enhanced dephosphorylation/deubiquitylation over phosphorylation/ubiquitylation.

I revisited the time-course experiments with A/O in the presence or absence of TAK-243 in order to compare the growth and decay of pS65-Ub signal between the two sets of experiments. In the signal decay experiment using TAK-243 the pS65-Ub was lost with increasing exposure to TAK-243, suggesting that PINK1 phosphorylation operating alone was not sufficient to maintain pS65-Ub levels (**Figure 6.14**A). This experiment warranted further refining because it failed to capture true pS65-Ub signal decay in response to TAK-243. As it was set up, the experiment resembled the time-course experiments in response to A/O in the presence of TAK-243. The lower pS65-Ub signal when TAK-243 was added was a combined effect of halting ubiquitylation, and thus preventing the system from reaching its theoretical maximum, and true pS65-Ub decay due to dephosphorylation, deubiquitylation and degradation of pS65-Ub-decorated proteins.

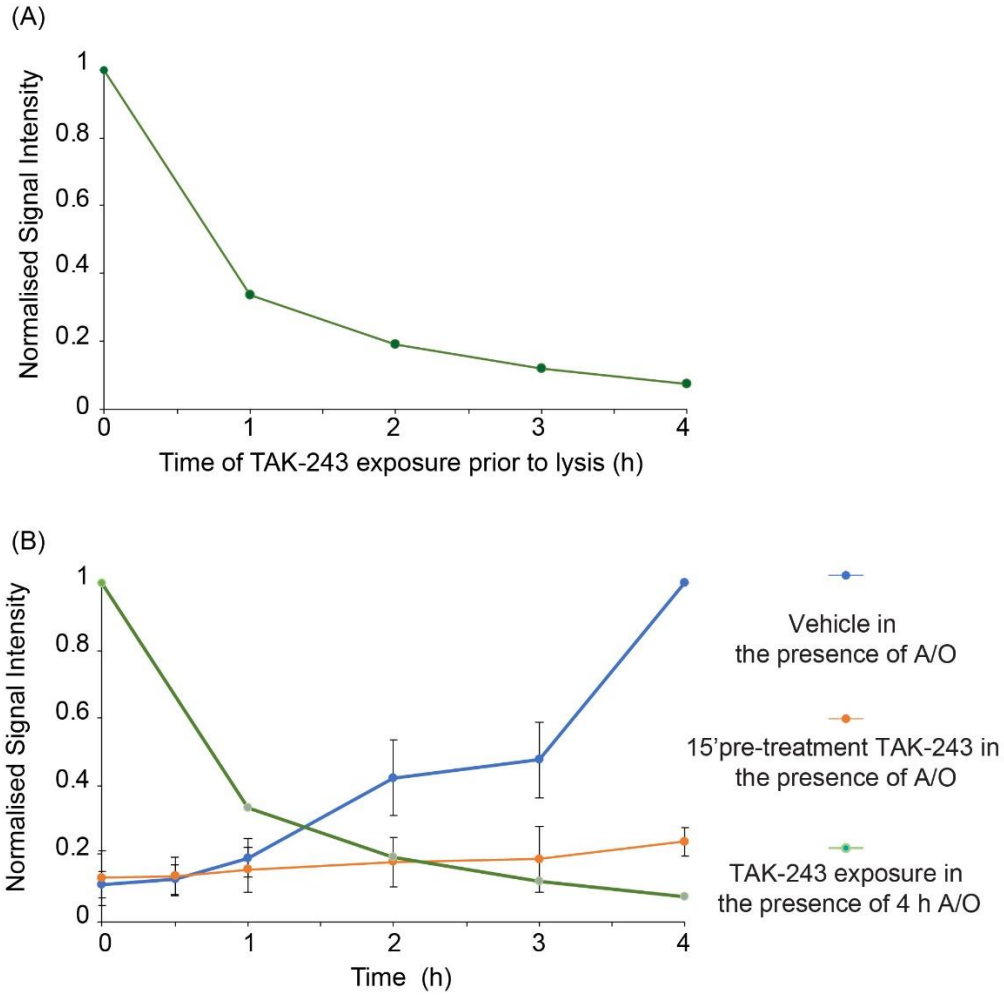

Figure 6.14: Comparison of pS65-Ub signal generation and decay using TAK-243 in hTERT-RPE1 FlpIn TRex cells

(A) The graph shows the decay of pS65-Ub signal normalised to the maximum signal over the course of 4 hours of A/O upon addition of TAK-243 prior to lysis from **Figure 6.13**.

(B) The graphs from **Figure 6.12** and (A) above superimposed on the same set of axes to directly compare pS65-Ub generation and decay.

I therefore combined the data from both experiments on the same set of axes in order to circumvent this limitation, recognising however that performing another set of experiments where pS65-Ub generation was completely unhindered for each of the time-points tested in parallel would have been superior (**Figure 6.14** B). I might have plotted the two datasets on the same axes, but it must be acknowledged that the x-axis of time is actually showing different parametres. The x-axis for the first set of experiments (**Figure 6.12**) shows the time the cells were exposed to A/O with their respective 15' pre-treatment with TAK-243. The x-axis in the second set (**Figure 6.14** A) shows at which time point prior to lysis the cells were exposed to TAK-243 over the

same four-hour treatment with A/O. Having the data normalised to the maximum signal achieved at four hours of A/O within each experiment allowed for some comparisons to be made. At the four-hour time point, there was a difference between having the TAK-243 as a 15' pre-treatment (**Figure 6.14**B, orange) and added simultaneously with the A/O (**Figure 6.14**B, green). The difference was rather small but may have a biological significance. The expected result would be that pre-treating the cells with TAK-243 would generate lower pS65-Ub signal due to the ubiquitylation machinery having more time to discharge the already loaded ubiquitin prior to engagement with PINK1. However, in my quantitation I saw the opposite: the simultaneous treatment with A/O and TAK-243 generated lower pS65-Ub. Having the ubiquitylation machinery disabled only for the last hour of the four-hour A/O treatment reduced the pS65-Ub signal down to ~33% (0.33) of the theoretical maximum. Interestingly, the pS65-Ub signal at the 3-hour timepoint in the absence of TAK-243 was higher (0.47). The difference of 0.14 in signal therefore accounted for pS65-Ub lost during that last one hour where ubiquitylation was inhibited. At the 2-hour timepoint where cells had experienced A/O for 2 hours already before TAK-243 was added for a further 2 hours, the pS65-Ub signal was even lower (0.19) while the theoretical maximum signal with 2 hours of A/O was 0.42. At this timepoint, the difference between theoretical and achieved pS65-Ub signal is a lot higher and most definitely accounted for pS65-Ub loss.

The PINK1 blot (**Figure 6.13**C) showed that full length PINK1 was only dependent on the duration of the A/O treatment. The most peculiar was the behaviour of the cleaved fragment that rapidly accumulated in the presence of TAK-243, even when the TAK-243 inhibitor was included only in the shortest time points. The above reinforced the idea that there were two pools of PINK1 in the cells, only of which was responding to A/O and the other one was not and instead was revealing itself in the absence of ubiquitylation. Most importantly, the cleaved PINK1 fragment was stabilised in the presence of TAK-243 when it was added both before (**Figure 6.7**) and after (**Figure 6.13**) the A/O treatment, suggesting the two pools of PINK1 are independent of each other.

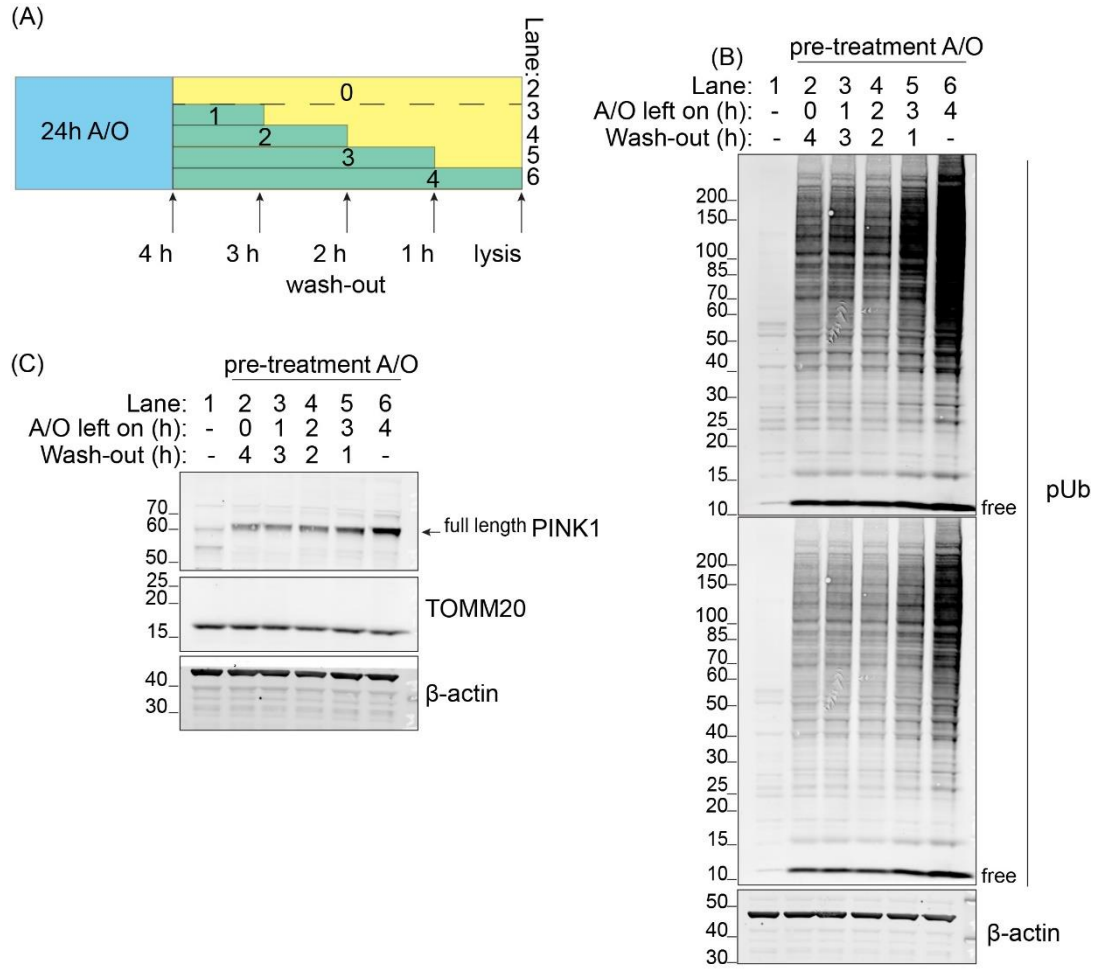

Figure 6.15: pS65-Ub loss with A/O wash-out

hTERT-RPE1 FlpIn TREx cells were treated with 1 μM antimycin A and 1 μM oligomycin A (A/O) for a total of 24 hours. The A/O trigger was either maintained or washed out at one-hour intervals for a further four hours prior to lysis. Cells were lysed in NP-40 lysis buffer supplemented with PhosSTOP and MPIs (1:250).

Having investigated the loss of pS65-Ub in the absence of global ubiquitylation whilst the mitophagy trigger was still in place, I wanted to investigate the stability of pS65-Ub when the mitophagy trigger was removed instead. I therefore treated the hTERT-RPE1 FlpIn TRex cells with A/O for 24 hours in order to get a strong pS65-Ub signal and then performed a washout to remove the A/O at one-hour timepoints over the next four hours and allowed the cells to recover from the trigger (**Figure 6.15**A). There was loss of pS65-Ub signal upon A/O washout even for 1 hour (lanes 5 and 6). The reduction of pS65-Ub signal was a lot slower for the longer washouts (lanes 2-4) and appeared to plateau and did not return to basal levels over the longest timepoint that I used (**Figure 6.15**B). A similar pattern was observed for PINK

(full length), whereby there was a small reduction in the levels of PINK1, suggesting that full length PINK1 was quite stable even after withdrawal of A/O and did not decrease immediately (**Figure 6.15**C).

6.4 pS65-Ub dynamics in hTERT-RPE1 FlpIn TRex USP30KO cells

6.4.1 USP30 suppresses the PINK1-dependent component of basal mitophagy

Elena Marcassa in our lab showed that depleting or knocking-out USP30 in U2OS and hTERT-RPE1 cells increased the basal rate of mitophagy measured with pH-sensitive fluorescently tagged mitochondrially-targeted probes such as mito-mKeima (Katayama et al., 2011) and mCherry-GFP-Fis1$_{101-152}$ (Mito-QC) (Allen et al., 2013; McWilliams et al., 2016). Furthermore, Elena showed that co-depleting cells of PINK1 restored the basal levels of mitophagy, suggesting that USP30 acted upstream of PINK1 in limiting PINK1's ability to initiate mitophagy (Marcassa et al., 2018). This would position USP30 epistatically upstream of PINK1 activity. Our lab proposed a model in which depletion or deletion of USP30 allows more ubiquitin to be deposited onto OMM proteins, which in turn creates a greater amount of ubiquitin that acts as substrate for PINK1 upon mitophagy initiation. The above would explain why USP30 depletion or knock-out was allowing for the enhanced turnover of mitochondria and why PINK1 depletion on its own had no apparent effect on the rate of mitophagy. However, we have been unable to detect measurable changes in total ubiquitin on mitochondrial fractions or in the ubiquitylation status of key OMM proteins such as TOMM20 simply by knocking-out USP30. The changes might be too low to measure directly in the absence of the amplification mediated by the global depolarisation of mitochondria. I was presented with an opportunity to test our model by measuring pS65-Ub generation instead of ubiquitin in USP30KO cells by disabling global ubiquitylation with TAK-243. In the presence of TAK-243, PINK1 would only act on ubiquitin already available on mitochondria without addition of new ubiquitin. Since the pS65-Ub signal is very low in the absence of mitochondria damage, measuring pS65-Ub was expected to give a better

signal to noise ratio over total ubiquitin and reveal even small differences between USP30KO and wild-type cells.

6.4.2 pS65-Ub signal evolution in the presence or absence of TAK-243 in USP30KO cells

I performed a short time-course experiment in hTERT-RPE1 FlpIn TRex USP30KO (USP30KO6) cells and the parental line in the presence or absence of TAK-243 (**Figure 6.16**). In the absence of TAK-243, there was a similar increase in pS65-Ub across USP30KO and parental cells with the exception of certain bands that appeared to be enriched in USP30KO6. I highlighted a few of those bands on the blot using black arrows. The trace of the pS65-Ub signal across the entire lane did not show major changes in signal between USP30KO and parental cells. The magenta trace that corresponds to USP30KO6 at the two-hour time-point was uniformly higher than its respective wildtype (green trace). Certain bands (black arrows) were more intense in the USP30KO cells, suggesting these might be USP30-regulated proteins that were preferentially decorated with pS65-Ub during A/O treatment. Interestingly, there were bands (red arrows) that appeared to be of higher intensity in the USP30KO6 even in the absence of A/O, suggesting a small subset of proteins being decorated with pS65-Ub in the absence of an acute mitophagy trigger.

The generation of pS65-Ub was overall suppressed in both USP30KO and parental cells in the presence of TAK-243. However, there was less pS65-Ub generated in USP30KO6. More specifically, bands indicated by cyan arrows that in the absence of TAK-243 were of higher intensity in the USP30KO6 cells, were now of lower intensity in USP30KO6 in the presence of TAK-243. Bands indicated by black arrows were not changing between USP30KO cells and the parental cell line in the absence of TAK-243 and yet were lower in USP30KO6 in the presence of TAK-243. The above may suggest that USP30KO6 was subject to higher pS65-Ub phosphatase activity throughout (black arrows).

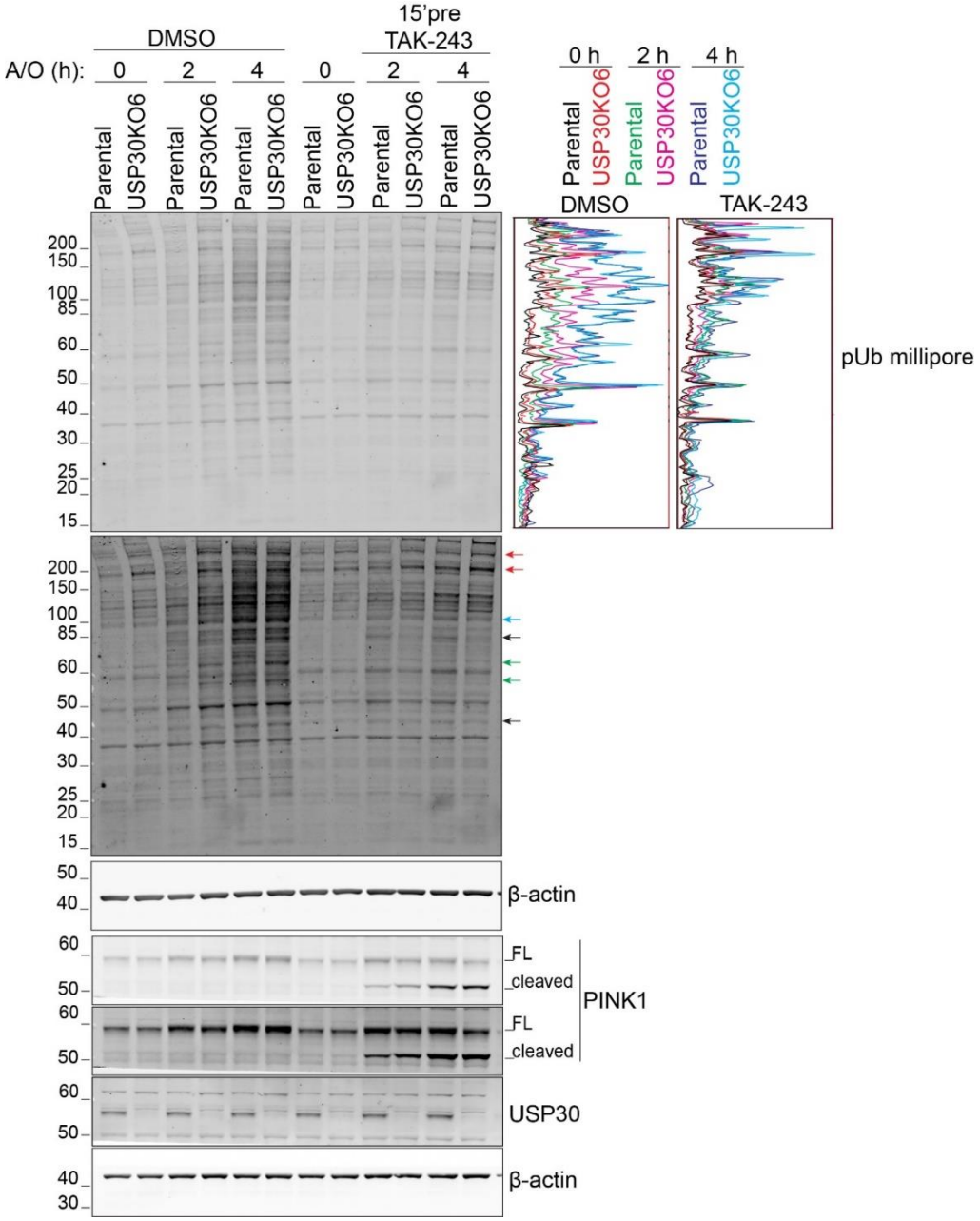

Figure 6.16: pS65-Ub signal evolution in USP30KO cells

hTERT-RPE1 FlpIn TRex cells and USP30KO cells (USP30KO6) were pre-treated with 1 µM TAK-243 and treated with 1 µM antimycin A and 1 µM oligomycin A (A/O) for 2 or 4 hours. All pre-treatments were performed 15 min before the respective A/O treatment. Cells were lysed in NP-40 lysis buffer supplemented with PhosSTOP and MPIs (1:250). Quantitation of pS65-Ub signal across the entire lane. Arrows indicate bands that differentially change in USP30KO cells compared to the parental cell line. Red arrows indicate bands that are stronger in USP30KO in the presence or absence of TAK-243. Cyan arrows indicate bands that are stronger in USP30KO6 in the absence of TAK-243 and weaker in the presence of TAK-243. Green arrows indicate bands that are stronger in USP30KO6 in the absence of TAK-243 and not changing in the presence of TAK-243.Black arrows indicate bands that are not differentially changing in USP30KO6 in the absence of TAK-243 and are higher in USP30KO6 in the presence of TAK-243.

Alternatively, USP30KO cells had lower ubiquitin that was suitable substrate for PINK1 during treatment with A/O. The above directly contradicted the model that was proposed above (6.4.1) whereby USP30KO cells had more ubiquitin PINK1 substrate. Interestingly, the bands indicated by red arrows remained at higher intensity in USP30KO cells throughout, both in the presence or absence of TAK-243.

The accumulation of the full length PINK1 species appeared to be slightly lower in USP30KO than parental cells. Despite full length PINK1 being lower in USP30KO cells, pS65-Ub accumulation was fairly even. The behaviour of the cleaved fragment of PINK1 in the presence of TAK-243 was interesting as well. At the 2-hour timepoint, the cleaved PINK1 fragment was higher in USP30KO6 compared to parental. The difference appeared to even out by the 4-hour timepoint. The above may suggest that the two distinct pools of PINK1 may be affected in USP30KO cells. More specifically the pool of PINK1 that was unresponsive to A/O was increased and in turn the pool that was stabilised by A/O was lower, which may also explain the behaviour of full length PINK1. The above observation warranted further investigation by performing a more extended time course experiment in the presence or absence of TAK-243 in USP30KO6 and wild-type cells.

I also looked at how the total ubiquitin signal behaved in the same cells (**Figure 6.17**). The total ubiquitin signal and pattern were not different in USP30KO and wild-type cells even in the presence of A/O. In the presence of TAK-243 however, there was a decrease in total ubiquitylation of proteins as was expected with inhibition of global ubiquitylation with TAK-243. I made an interesting observation that USP30KO6 appeared to have lower total ubiquitin stain in the high molecular weight range. The above may reflect loss of ubiquitylated proteins, in that molecular weight range, that is accelerated in USP30KO, which was unexpected. The expectation was that the loss of a DUB would increase the ubiquitylation of proteins instead of decreasing it. Alternatively, the loss of a DUB was destabilising those proteins altogether thus the ubiquitylated species were also reduced.

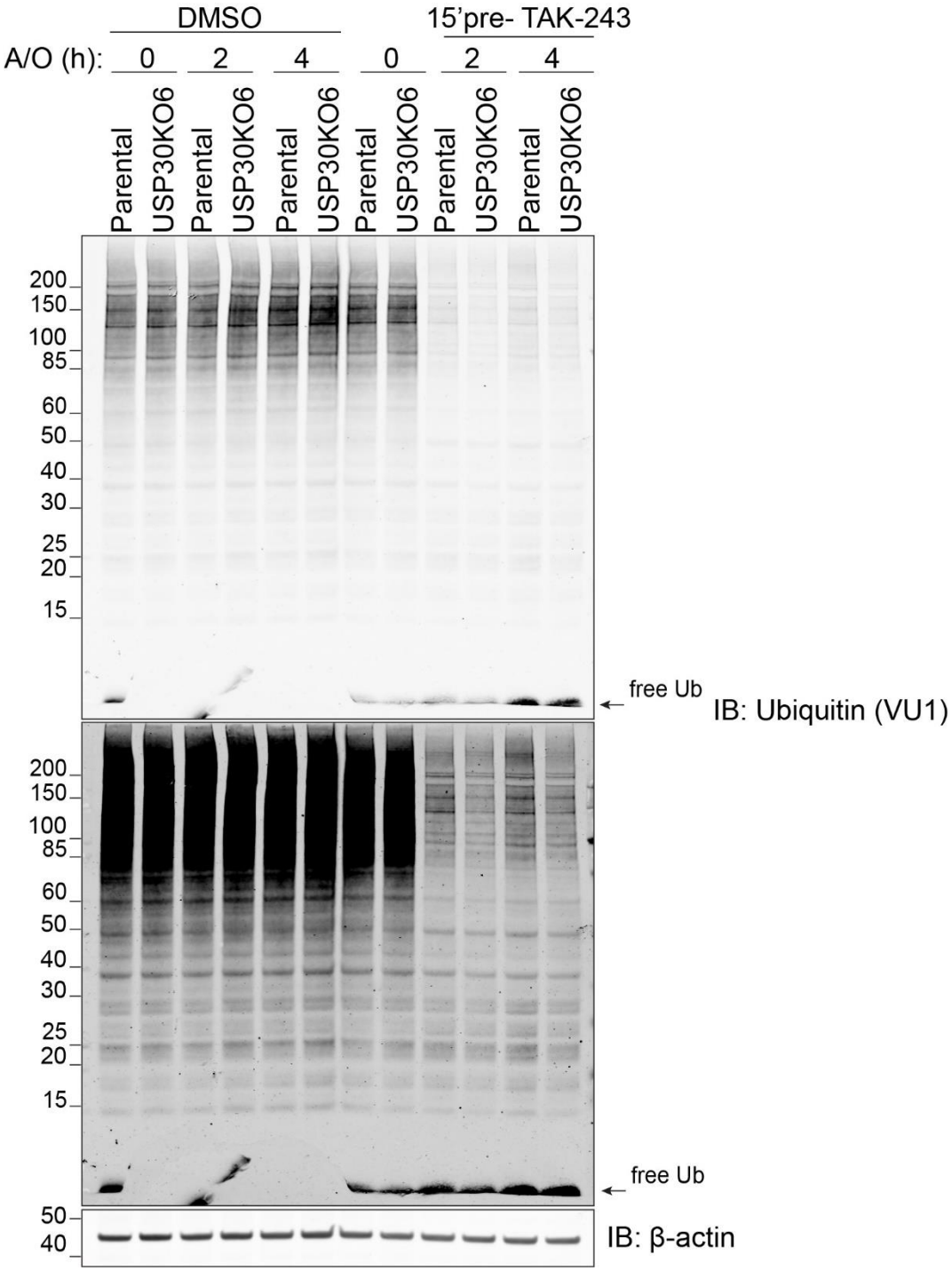

Figure 6.17: Total ubiquitin signal in hTERT-RPE1 FlpIn TRex USP30KO cells in response to A/O in the presence or absence of TAK-243

hTERT-RPE1 FlpIn TRex cells and USP30KO cells (USP30KO6) were pre-treated with 1 µM TAK-243 and treated with 1 µM antimycin A and 1 µM oligomycin A (A/O) for 2 or 4 hours. All pre-treatments were performed 15 min before the respective A/O treatment. Cells were lysed in NP-40 lysis buffer supplemented with PhosSTOP and MPIs (1:250). Free Ub, unconjugated monomeric ubiquitin.

The blots of pS65-Ub and total ubiquitin in the presence of TAK-243 appeared to have that pattern in common: pS65-Ub and total ubiquitin were both reduced in the USP30KO6 cells.

6.5 Comparison of USP30 inhibition with genetic loss of USP30 in cells with endogenous Parkin expression

6.5.1 Validating FT385 as an USP30 inhibitor

The lab's collaboration with Forma Therapeutics/Celgene gave me the opportunity to be involved in the development and characterisation of lead compounds as USP30 inhibitors. One such compound that has been developed was FT3967385 (FT385) (Rusilowicz-Jones et al., 2020). The most well-established method to phenotypically evaluate USP30 loss is by monitoring TOMM20 loss and ubiquitylation in the presence of depolarisation, most commonly in Parkin overexpressing cells (Bingol et al., 2014; Cunningham et al., 2015; Liang et al., 2015a; Gersch et al., 2017).

I performed a small-scale titration experiment by treating the hTERT-RPE1 YFP-Parkin cells with increasing concentrations of FT385 (200 nM, 500 nM and 1 μM) and treated with A/O for one hour to evaluate TOMM20 ubiquitylation by immunoblot. I also included the highest concentration of FT385 in the absence of A/O as an additional condition (**Figure 6.18**). Treating cells with FT385 in presence of A/O induced higher levels of TOMM20 ubiquitylation compared to A/O alone, suggesting that FT385 was effective as a USP30 inhibitor. Several bands were visible that corresponded to multiple ubiquitin moieties conjugated to TOMM20, all of which were showing enhanced ubiquitylation in the presence of FT385. MFN2 loss was unaffected by the addition of FT385 indicative that the effects of the compound were not on the global ubiquitylation of all OMM proteins. I also looked at PINK1 protein levels that remained unchanged by USP30 inhibition. Interestingly, pS65-Ub accumulation remained largely unchanged, except for a minority of bands marked with red arrows that appeared to be of higher intensity in the presence of FT385. The bands that were changing in this experiment appeared to be fewer than in the experiments in the previous section where I was comparing USP30KO and wild-type cells (**Figure 6.16**).

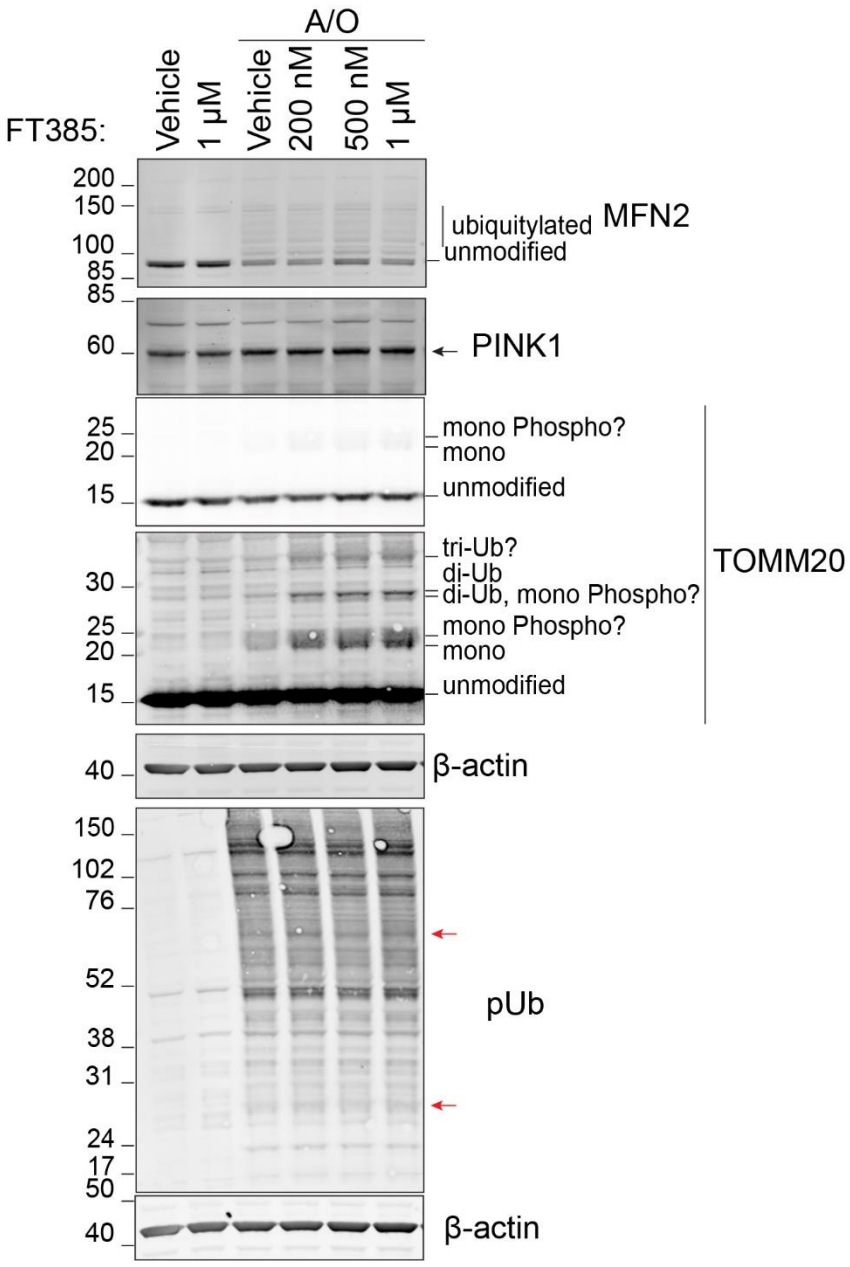

Figure 6.18: Treatment with FT385 enhanced TOMM20 ubiquitylation in hTERT-RPE1 YFP-Parkin cells

hTERT-RPE1 YFP-Parkin were treated with 200 nM, 500 nM and 1 µM FT385 or vehicle (DMSO) in the presence or absence of 1 µM antimycin A and 1 µM oligomycin A (1 µM A/O) for 1 hour. The cells were lysed in NP-40 lysis supplemented with PhosSTOP and MPIs. Mono, di and tri correspond to mono-, di-, and tri-ubiquitylated species. Phospho?, suspected phosphorylated species. Red arrows indicate pS65-Ub bands that are differentially changing between FT385-treated and control cells.

This may be due to the high levels of Parkin expression in these cells that were already very much limiting the opportunity of USP30 to act in reversing the ubiquitylation. Overall, this experiment suggests that FT385 acts as a USP30 inhibitor in this Parkin overexpressing cell line model.

I sought to investigate whether the effect of FT385 in terms of TOMM20 ubiquitylation in the presence of A/O was specific to USP30. To accomplish the above, I made use of a USP30KO cell line in the hTERT-RPE1 YFP-Parkin cells (USP30KO1E) generated by Emma Rusilowicz-Jones in our lab. I treated USP30KO1E and the parental line with 200 nM FT385 or with DMSO in the presence or absence of A/O (**Figure 6.19**). The inhibitor-treated parental cells displayed higher levels of TOMM20 ubiquitylation compared to A/O alone. Furthermore, the USP30KO1E cells had the same levels of ubiquitylated TOMM20 as the inhibitor treated parental cells in the presence of A/O, suggesting that USP30KO and USP30-inhibited cells were behaving the same. The levels of MFN2 and the ubiquitylation pattern of MFN2 and FIS1 were unaffected by USP30 inhibition or USP30 deletion in the presence of A/O. Most importantly however, treating the USP30KO cells with FT385 did not further increase TOMM20 ubiquitylation in the presence of A/O, suggesting the effect of FT385 was through USP30.

In conclusion, FT385 behaved as a USP30 inhibitor in cells overexpressing Parkin by way of TOMM20 ubiquitylation. Furthermore, FT385 phenocopied the genetic loss of USP30 through CRISPR KO. Lastly, there was no additional effect of FT385 in USP30KO cells in this assay, suggesting the effects of FT385 were through USP30 inhibition (Rusilowicz-Jones et al., 2020).

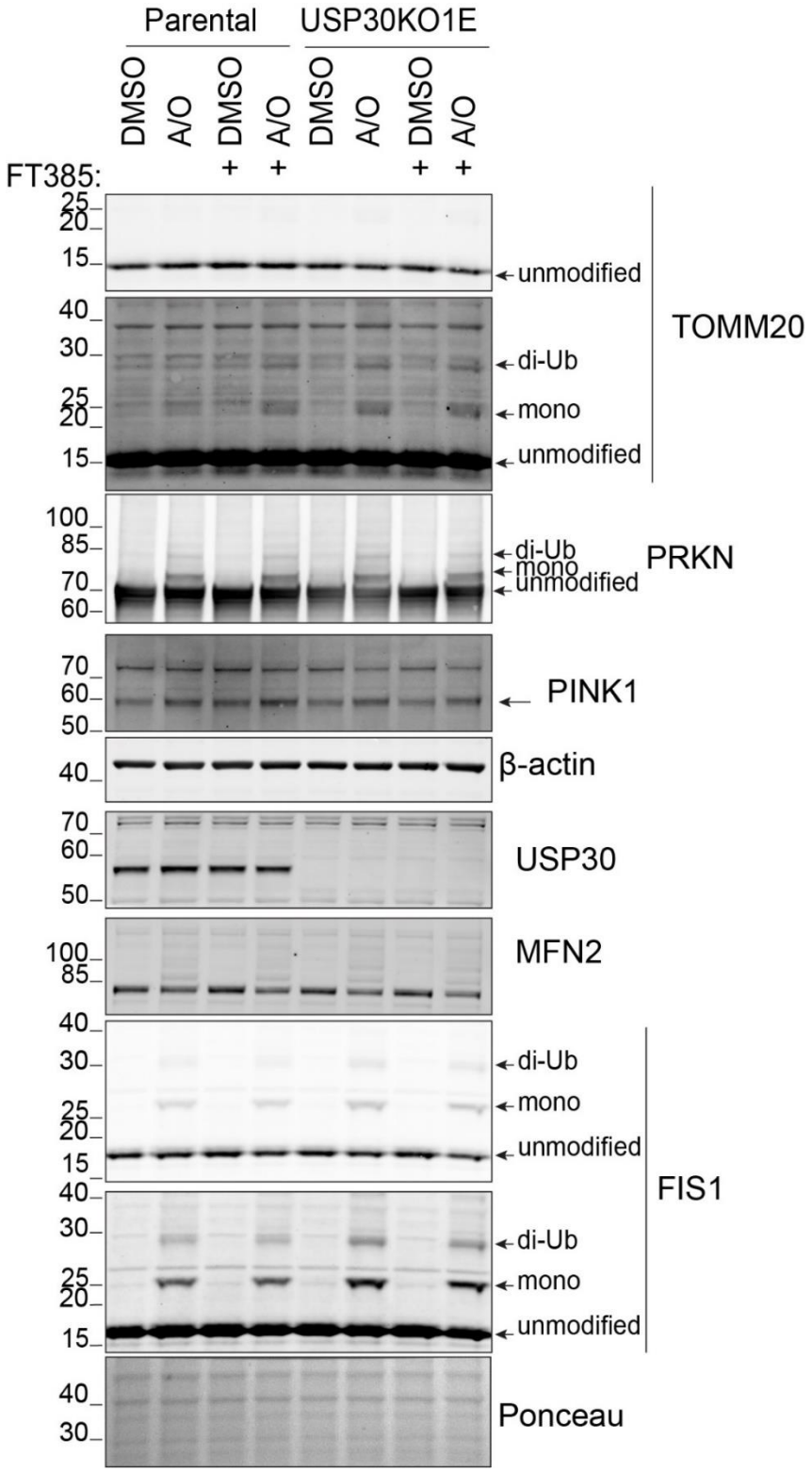

Figure 6.19: The effect of FT385 in hTERT-RPE1 YFP-Parkin USP30KO cells

hTERT-RPE1 YFP-Parkin USP30KO (USP30KO1E) and parental cells were treated with 200 nM FT385 or DMSO (vehicle) in the absence or presence of 1 μM antimycin A and 1 μM oligomycin A (A/O) for 1 hour. Cells were lysed in NP-40 lysis buffer supplemented with PhosSTOP and MPIs and samples were analysed by immunoblot.

I sought to investigate the effects of the inhibitor in cells without any detectable Parkin, before proceeding to cells that express Parkin. I treated the hTERT-RPE1 FlpIn TRex cells with A/O for 2 and 4 hours in the presence or absence of 200 nM FT385 for the same duration (**Figure 6.20**). The evolution of pS65-Ub was higher in the FT385-treated cells in response to A/O at both 2- and 4-hour time-points. The differences between inhibitor-treated and control cells were more striking at the discrete bands indicated by the red arrows, which was indicative that a subset of proteins were exhibiting altered phospho-ubiquitylation status by USP30 inhibition. This effect phenocopied the data in the USP30KO cells above and suggested USP30 inhibition and genetic KO were very similar (**Figure 6.16**). In the same experiment I also assessed whether having the FT385 compound for longer than the exposure to A/O alone. I therefore included conditions whereby I treated the cells with FT385 for 24 hours while inducing mitophagy with A/O in the last 2 or 4 hours. In these instances of having the inhibitor on the cells for longer periods, the pS65-Ub signal appeared to be weaker compared to A/O alone for the same duration. It may therefore suggest that prolonged inhibition of USP30 in these cells may reduce pS65-Ub by reducing PINK1 levels, which was seen in some instances.

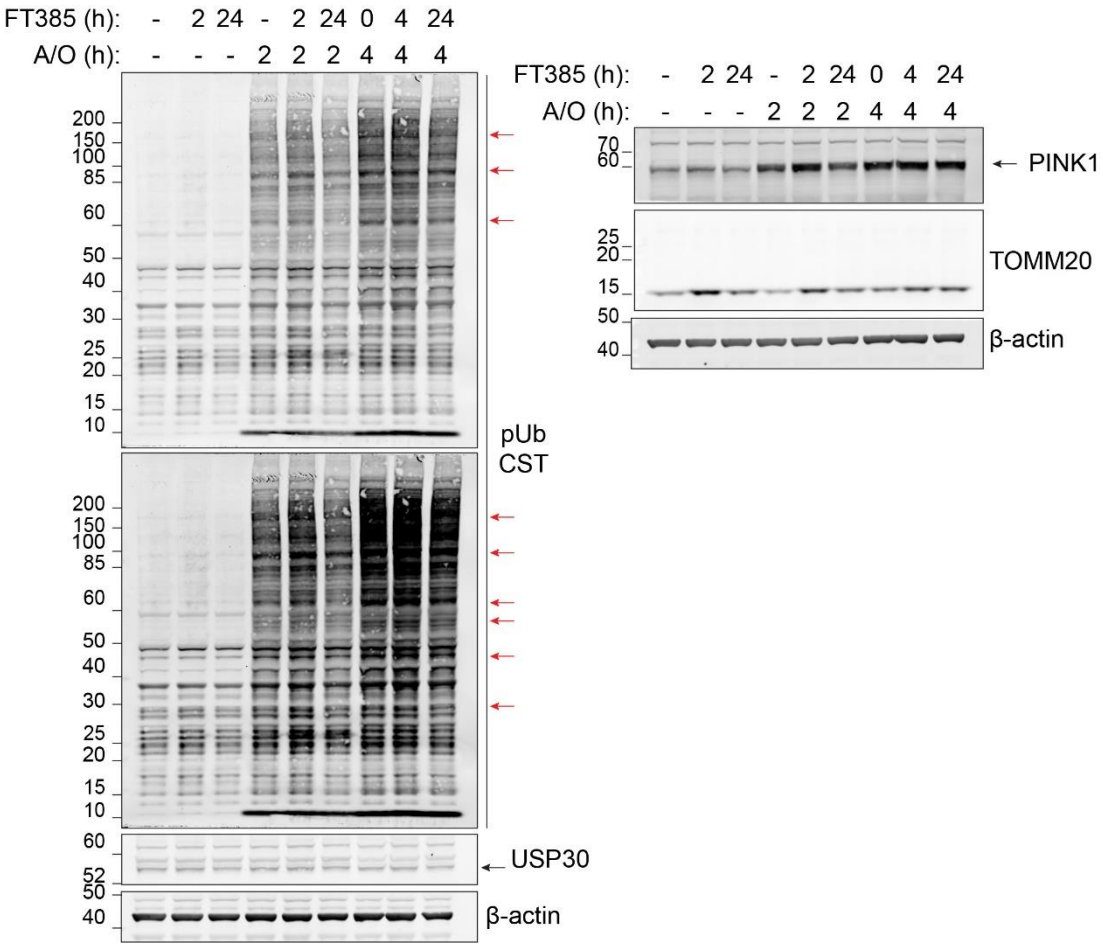

Figure 6.20: The effect of FT385 in hTERT-RPE1 FlpIn TRex cells

hTERT-RPE1 FlpIn TRex cells were treated with 200 nM FT385 for 2 or 24 hours in the presence of absence of 1 μM antimycin A and 1 μM oligomycin A (A/O) for 2 or 24 hours as indicated. Cells were lysed in NP-40 lysis buffer supplemented with PhosSTOP and MPIs and samples were analysed by immunoblot. Horizontal red arrows point to bands differentially changing in the FT385 treated cells and horizontal black arrows point to the specific bands in the USP30 and PINK1 immunoblots.

I then sought to investigate the effect of FT385 as a USP30 inhibitor in SH-SY5Y cells that express detectable levels of endogenous Parkin. I wanted to directly compare the effect of the inhibitor in wild-type and USP30KO cells that my colleague Jane Jardine generated. I treated the SH-SY5Y cells with 200 nM FT385 in the presence or absence of A/O for 4 hours and in parallel treated the USP30KO clone (USP30KO11) with A/O for 4 hours (**Figure 6.21**).

The inhibitor-treated and USP30KO cells displayed the same levels of ubiquitylated TOMM20 in response to A/O, whereas the wild-type control cells exhibited no detectable TOMM20 ubiquitylation. Furthermore, inhibitor-treated and USP30KO cells showed elevated levels of pS65-Ub compared to control wild-type cells. More specifically, certain pS65-Ub bands appeared to be of higher intensity in the inhibitor treated and USP30KO cells. The molecular weight range between 30 and 85 kDa appeared to be most affected by USP30 loss or inhibition as shown in the pS65-Ub traces (**Figure 6.21**, cyan and magenta traces). The ubiquitin blot revealed that there were no measurable changes in the pattern of ubiquitylated proteins in the total cell lysate and the changes that were USP30-dependent were only at the level of pS65-Ub.

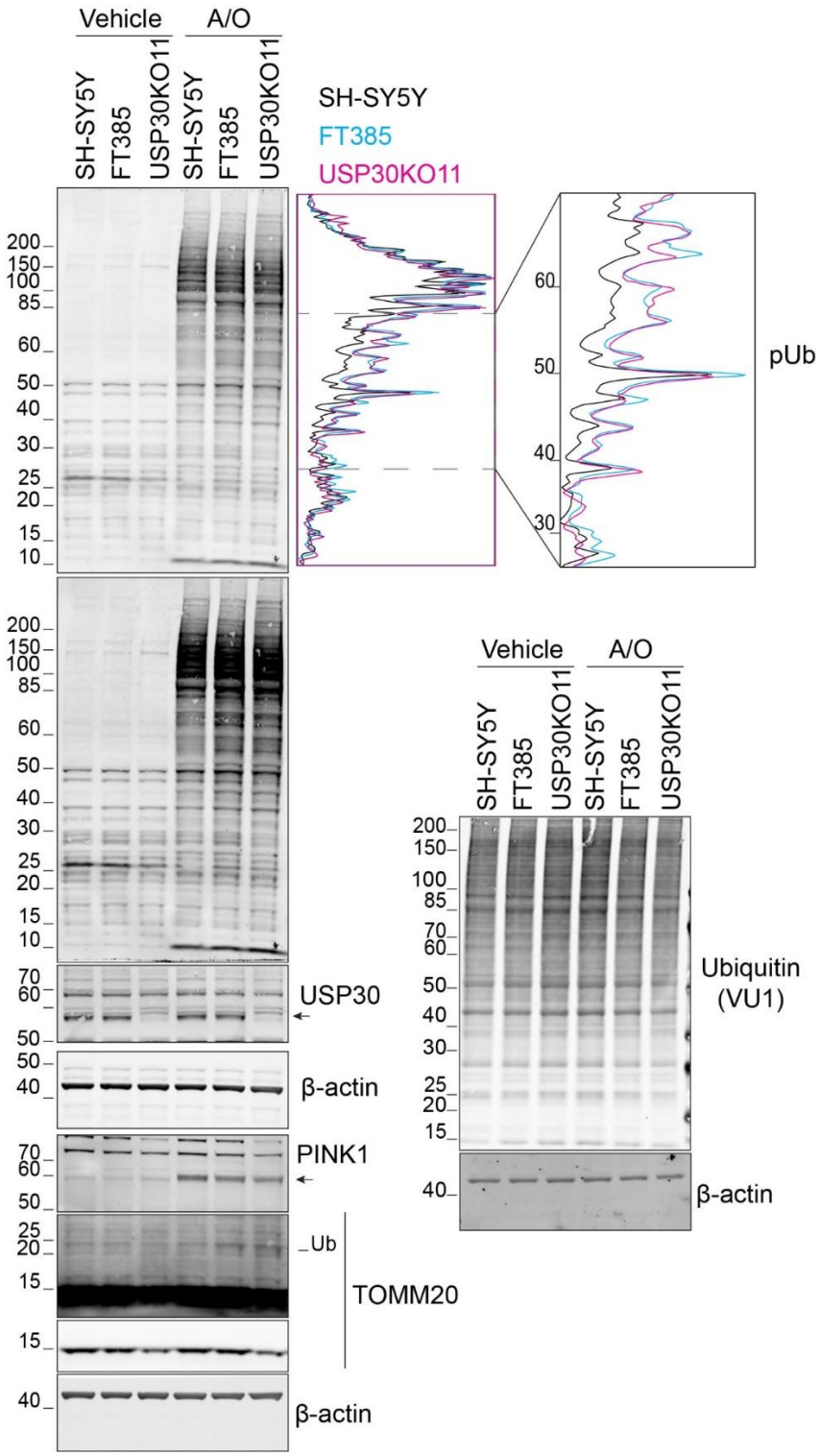

Figure 6.21: USP30-inhibitor treated and USP30KO SH-SY5Y cells in the presence of A/O

SH-SY5Y cells, FT385 (200 nM)-treated SH-SY5Y cells and USP30KO SH-SY5Y (USP30KO11) cells were treated with 1 μM antimycin A and 1 μM oligomycin A (A/O) for 4 hours. Cells were lysed in NP-40 lysis buffer supplemented with PhosSTOP and MPIs and samples analysed by immunoblot. The traces of pS65-Ub signal in the presence of A/O is shown next to the blot. Arrows show the specific bands for the relevant blots. Ub, ubiquitylated species

I repeated the above experiment and included another USP30KO clone (USP30KO-D) as an additional comparison to the inhibitor treated wild-type cells (**Figure 6.22**). I found that both the wild type control cells showed no detectable TOMM20 ubiquitylation while the USP30KO clones and the inhibitor-treated cells displayed similar levels of the ubiquitylated form. Furthermore, pS65-Ub was elevated in the USP30KOs and inhibitor treated cells. Similar to the previous experiment, the differences were not evenly distributed across all the molecular weight ranges but most apparent between 30 and 85 kDa.

In conclusion FT385 is a potent USP30 inhibitor that recapitulates the genetic loss of USP30 in terms of TOMM20 ubiquitylation in cells with Parkin overexpression and with endogenous. FT385 may be a promising compound to study USP30 biology in contexts where USP30 genetic manipulation by CRISPR or siRNA-mediated depletion is difficult.

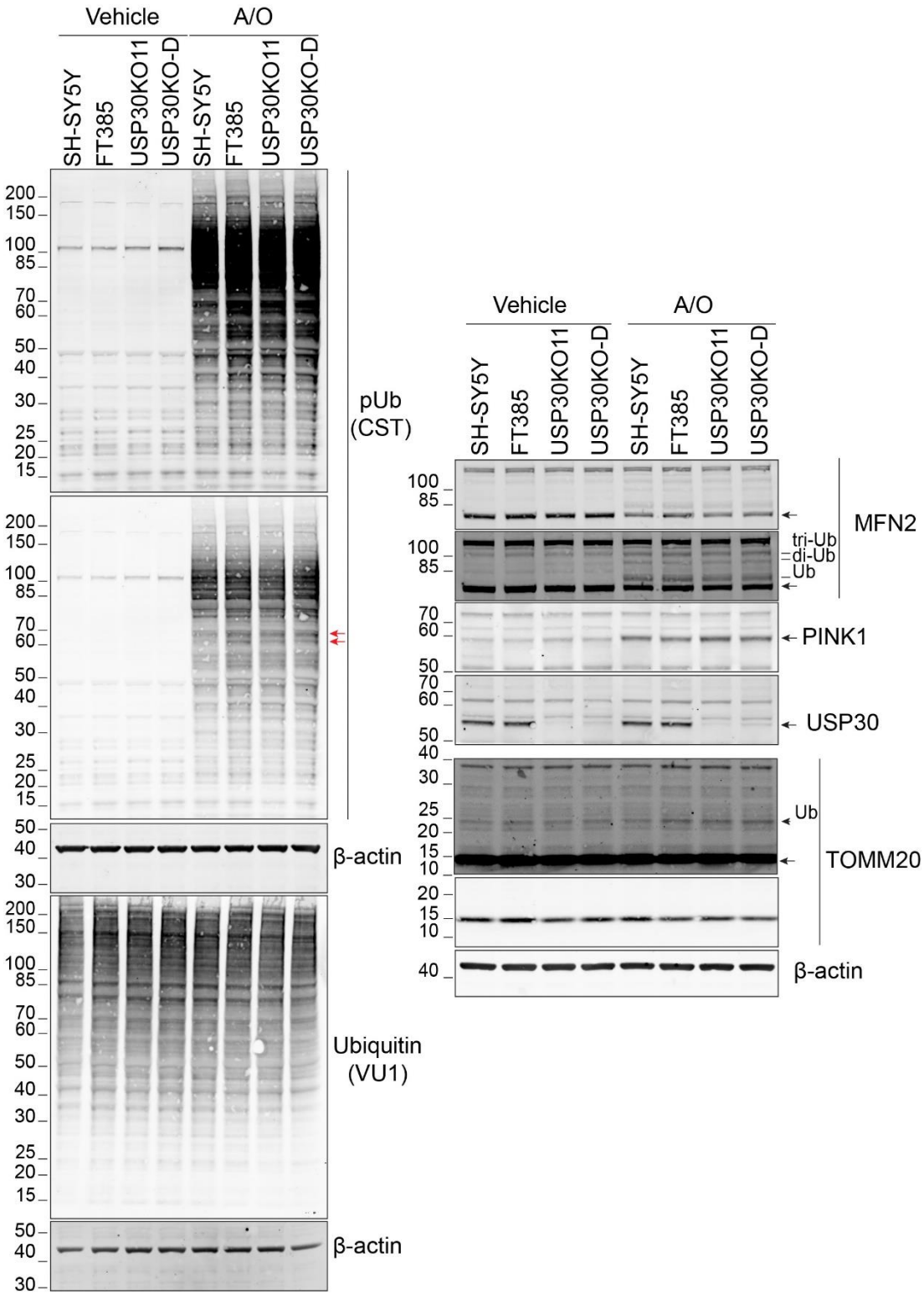

Figure 6.22: FT385-treated and USP30KO SH-SY5Y in the presence of A/O

SH-SY5Y cells, FT385 (200 nM)-treated SH-SY5Y cells and USP30KO SH-SY5Y (USP30KO11 and USP30KO-D) cells were treated with 1 μM antimycin A and 1 μM oligomycin A (A/O) for 4 hours. Cells were lysed in NP-40 lysis buffer supplemented with PhosSTOP and MPIs. Arrows show the specific bands for the relevant blots. Ub, ubiquitylated species. Red arrowheads show the unmodified band for TOMM20, red arrows show the ubiquitylated species of TOMM20.

6.6 Conclusions

6.6.1 Phospho-S65 Ubiquitin dynamics in a Parkin-independent manner

I have performed PINK1-depletion experiments to determine the PINK1 requirement for pS65-Ub generation in response to A/O using pS65-Ub specific antibodies. The antibodies proved to be suitable for use in immunoblot and immunofluorescence microscopy to detect pS65-Ub in cells that overexpress Parkin and cells that express endogenous levels of Parkin. I also investigated the accumulation of pS65-Ub in response to A/O in cells without detectable endogenous Parkin and found it to exhibit a bi-phasic pattern. This bi-phasic phosphorylation of ubiquitin chains by PINK1 has been observed in *in vitro* phosphorylation experiments of di- and tetra-ubiquitin chains incubated with recombinant PINK1 from the human body louse (Pediculus humanus corporis) (PhPINK1) (Gersch et al., 2017). The authors have shown that recombinant PhPINK1 preferentially phosphorylated the distal ubiquitin first when provided with K6-linked di-ubiquitin substrate, followed by the proximal ubiquitin. The authors noted that the second phosphorylation was considerably slower than the first phosphorylation event. The differences in the rates between the first and the second phosphorylation event by PhPINK1 were less pronounced when di- and tetra-ubiquitin chains of other linkages were provided as substrate, with K63-linked ubiquitin chains exhibiting preference for internal ubiquitin phosphorylation first. Overexpressed Parkin has been shown to generate poly-ubiquitin chains on mitochondria with K6, K11, K48 and K63 linkages (Ordureau et al., 2014; Cunningham et al., 2015). Recombinant USP30 preferentially removed K6 and K11 ubiquitin chains from intact mitochondria isolated from CCCP-treated cells, suggesting the role of USP30 in regulating mitophagy through these two ubiquitin chains (Cunningham et al., 2015). The question arises on how the ubiquitin landscape is shaped on mitochondria in terms of chain linkage after depolarisation in cells without detectable Parkin. The bi-phasic accumulation of pS65-Ub that I observed may hint towards K6-linked ubiquitin chain acting as PINK1 substrate. It is possible to visualise changes in the levels of specific ubiquitin linked chains using chain specific antibodies or ubiquitin linkage-specific affimers (Michel et al., 2017). However, without a mitochondrial enrichment

method it remains technically difficult to assess whether ubiquitin chains of specific linkage are preferentially added during depolarisation and how efficiently these chains can be used as a PINK1 substrate.

6.6.2 Phospho-S65 Ubiquitin signal stability and decay

I made use of TAK-243 to induce an acute block of ubiquitylation during depolarisation with A/O. Blocking ubiquitylation while the ubiquitylation/phosphorylation cascade has already been initiated resulted in the cessation of further pS65-Ub generation. Furthermore, the pS65-Ub signal decreased, suggesting it is unstable in the presence of PINK1 phosphorylation alone. The possible explanations for the reduction in pS65-Ub during the course of the experiments can be a result of different activities. One possible explanation is that proteins which are sufficiently decorated with ubiquitin or pS65-Ub are extracted and targeted for proteasomal degradation. It is not yet known whether the fate of pS65-Ub decorated OMM proteins differs from that of their non-phosphorylated counterparts. Therefore a portion of the pS65-Ub signal may be lost through proteasomal degradation of OMM proteins. Alternatively, the activity of DUBs on pS65-Ub-decorated proteins results in cleavage of pS65-Ub chains from proteins. The activity of many DUBs was shown to be reduced against pS65-Ub and therefore seems an unlikely scenario (Huguenin-Dezot et al., 2016; Gersch et al., 2017). The third possible explanation lays in the activity of protein phosphatases towards pS65-Ub. Two phosphatases have been described to dephosphorylate pS65-Ub, PTEN-L and PPEF2. PTEN-L is the long isoform of the most commonly known PTEN tumour suppressor and a fraction of which was shown to associate with mitochondria (Wang et al., 2018). Overexpression of PTEN-L prevented the translocation of Parkin to mitochondria and prevented loss of mitochondrial membrane proteins in response to depolarisation. Furthermore, PTEN-L was shown to reverse the phosphorylation on pS65-Ub chains following CCCP treatment. PPEF2 was the second phosphatase to be identified for pS65-Ub (Wall et al., 2019). The authors conducted a CCCP washout experiment in cells overexpressing Parkin and quantitated how the poly-ubiquitin and pS65-Ub decayed over time in mitochondria fractions. They found that pS65-Ub was lost very soon after CCCP washout while poly-ubiquitin persisted. The authors

determined that pS65-Ub-conjugated on proteins had nearly half the half-life of poly-ubiquitin in their experimental system, which suggested dephosphorylation was proceeding deubiquitylation in this context. Depleting cells of PPEF2 resulted in the persistence of the pS65-Ub signal on proteins after CCCP washout, suggesting PPEF2 dephosphorylated pS65-Ub-decorated proteins on mitochondria. Collectively, the major mechanism of pS65-Ub signal decay after TAK-243 treatment or A/O washout is likely to be dephosphorylation.

6.6.3 Ubiquitin PINK1 substrate is limiting at the outer mitochondrial membrane

The experiments included in this chapter were aimed at unravelling how much ubiquitin is available to serve as PINK1 substrate when mitophagy is acutely induced. To achieve this, I made use of TAK-243 to inhibit global ubiquitylation in cells, trigger mitophagy using A/O and then monitor the ability of PINK1 to generate pS65-Ub in the absence of *de novo* ubiquitylation. The data showed that PINK1 was able to generate some pS65-Ub under those conditions, which suggested there is a very limited amount of ubiquitin that acted as a PINK1 substrate and that the majority of ubiquitin PINK1 substrate was incorporated following PINK1 stabilisation on the OMM. The data supports the model whereby there are two types of E3 ubiquitin ligases during mitophagy, one for priming and another for amplification of the signal (**Figure 6.1**). The priming E3 ligase maintains a basal level of ubiquitylation on OMM proteins for PINK1 to phosphorylate and the amplifying E3 that is activated in a PINK1-dependent mechanism. The most well-characterised example of an amplifying E3 that fits the above description is Parkin (Narendra et al., 2008, 2010). Parkin recruitment and activation is highly dependent on PINK1 activation in both cells that overexpress it and at the endogenous level. Parkin activation and recruitment to mitochondria (Phu et al., 2020) is regulated by direct PINK1 phosphorylation on the UBL domain of Parkin (Shiba-Fukushima et al., 2012) and binding of Parkin onto pS65-Ub (Kazlauskaite et al., 2014; Koyano et al., 2014; Kane et al., 2014). ARIH1 has also been shown to be recruited to mitochondria in response to depolarisation in a PINK1-dependent manner and mediate mitophagy in lieu of Parkin (Villa et al., 2017). ARIH1 is

of particular interest because, similarly to Parkin, is a RING-between-RING E3 ubiquitin ligase (Wenzel et al., 2011) that functions in association with Cullin RING ligases (CRLs) by conjugating the first ubiquitin onto protein substrates that are then elongated by CRLs (Scott et al., 2016). However, ARIH1 has not been shown to be directly phosphorylated by PINK1 nor bind pS65-Ub and therefore the PINK1 requirement for ARIH1 recruitment to mitochondria remains unknown. Furthermore, my work suggested that Neddylation was dispensable for pS65-Ub generation in these cells, suggesting against the involvement of ARIH1 in this context as a priming or amplifying E3 ligase (**Figure 6.6**).

6.6.4 There are two distinct pools of PINK1 in cells and the role of USP30

The experiments that I performed were designed to address questions around ubiquitin as a PINK1 substrate and the dynamics of pS65-Ub generation by PINK1. The turnover of PINK1 is high in healthy cells, which makes it very challenging to detect. The full length PINK1 is constantly being cleaved and only accumulates in instances where mitochondria are damaged or PINK1 import is blocked (Narendra et al., 2010). The cleaved fragment is rapidly targeted for proteasomal degradation and can be detected with the use of proteasome inhibitors that prevent its degradation (Yamano and Youle, 2013). The use of TAK-243, which inhibits ubiquitylation, was expected to stabilise the cleaved form as shown by the accumulation of the cleaved form in the absence of depolarisation (**Figure 6.6**). In the presence of both A/O and TAK-243 however, the expectation would be that no cleaved PINK1 would accumulate since the mitochondrial damage would prevent its import and cleavage. Surprisingly, I found that a portion of PINK1 did indeed accumulate as the full length protein but so did the cleaved form and to similar levels as in the absence of TAK-243. The expectation was that A/O would be acting upstream of TAK-243 in the context of PINK1 cleavage. The data suggested that only a fraction of PINK1 responded to A/O and the majority of PINK1 was still being cleaved and targeted for degradation. The data therefore suggests that there might be two pools of PINK1 that engage into the import, cleavage and degradation cycle. The first pool of PINK1 can be stabilised by A/O and the other pool continues to be imported and cleaved even in the presence of

A/O. A published study reported a similar finding whereby simultaneously treating HeLa cells with CCCP and the proteasome inhibitor MG132 revealed accumulation of both full length and cleaved species of PINK1 (Sekine et al., 2019). The difference between my data and the study was that in the study the major species was the full length PINK1 when treated with CCCP and MG132. My data showed that the cleaved fragment of PINK1 was the major species when cells were treated with A/O and TAK-243 (**Figure 6.9**B and **Figure 6.11**B). The discrepancy between my data and the study by Sekine *at al* (2019) in terms whether the full length or the cleaved fragment of PINK1 in the major species could be due to differences in the rates of synthesis and turnover between these two pools in the different cell lines. The same study demonstrated that TOMM7 knock-out was preventing full length PINK1 accumulation in the presence of depolarisation, suggesting that TOMM7 is required for stabilising the depolarisation-sensitive pool of PINK1. TOMM7 may in fact be facilitating the lateral translocation of stabilised PINK1 on the OMM (Sekine, 2019). Co-depletion of TIMM23 in TOMM7KO cells completely abolished full length PINK1 stabilisation upon depolarisation, suggesting TIMM23 is required for PINK1 stabilisation during mitochondrial damage. I have not investigated the involvement of TOMM7 and TIMM23 in my experiments. However, there are analogies between my data and the data from the Sekine *et al* (2019) study that implicates TOMM7 in the regulation of PINK1. The common theme is the existence of two pools of cycling PINK1 of which one responds as a sensor of mitochondrial damage.

The experiments performed in USP30KO cells (USP30KO6) in the presence of TAK-243 revealed that the ratio of pools of PINK1 may be affected by USP30. In one experiment, USP30KO accumulated lower full length PINK1 and higher cleaved PINK1 in the presence of TAK-243 (**Figure 6.16**). The above warrants further investigation before drawing further conclusions but it may suggest that USP30 was promoting interactions between TOMM7 and PINK1. In this model, USP30 activity may be affecting the two pools of PINK1 and the ratio of PINK1 that may be stabilised by mitochondrial damage. The above hypothesis may be part of the mechanism by which USP30 loss promotes mitophagy.

6.6.5 USP30KO cells have certain proteins preferentially enriched with pS65-Ub in the presence of A/O, yet have lower ubiquitin PINK1 substrate at steady state

I investigated how pS65-Ub behaved in USP30KO cells and I saw there was an upward trend in pS65-Ub in USP30KO cells in response to A/O. One limitation in the hTERT-RPE1 FlpIn TREx cells was the uneven accumulation of PINK1. USP30KO6 accumulated lower levels of full length PINK1 and arguably resulted in overall lower pS65-Ub. However, the work in SH-SY5Y cells produced more consistent results. Two USP30KO clones (KO11 and KO-D) and the cells treated with the USP30 inhibitor (FT385) consistently resulted in higher pS65-Ub compared to the control SH-SY5Y cells. Overall, PINK1 accumulation was unaffected by USP30 deletion or inhibition in the SH-SY5Y cells and therefore the data is more convincing and reliable. More specifically, there was only a subset of proteins that appeared to be enriched with pS65-Ub in USP30KO cells and the next important question to address was to identify these differentially enriched proteins. Given the poor processivity of USP30 against pS65-Ub chains, it is unlikely that USP30 removes pS65-Ub from proteins. The enhanced levels of pS65-Ub in USP30KO and USP30 inhibitor-treated cells may be explained by USP30 regulating the ubiquitylation of key OMM proteins, which may act as a priming ubiquitin substrate for PINK1 activity (Rusilowicz-Jones et al., 2020). Candidate proteins include existing USP30 substrates such as TOMM20 (Liang et al., 2015a; Gersch et al., 2017) and novel substrates recently identified in our lab such as more components of the TOMM complex, TOMM5, 40 and 70 (Rusilowicz-Jones et al., 2020).

The loss of a DUB was expected to induce an increase in ubiquitin and in this case the loss of USP30 was expected to increase the levels of ubiquitin on mitochondria. My data however suggests that USP30KO cells exhibited reduced pS65-Ub in the presence of TAK-243, suggesting lower ubiquitin PINK1 substrate in these cells. This was further complicated by the observations of overall higher pS65-Ub in USP30KO and USP30 inhibitor-treated cells discussed above. The discrepancy may be attributed to USP30KO having only a small effect in the global levels of ubiquitylation on mitochondria. In other words, the ubiquitin on USP30 substrates may indeed increase when USP30 is lost, however that increase is below the detection

limit of the assays used. Furthermore, the loss of USP30 may promote the destabilisation of an E3 ligase which in turn globally regulates ubiquitin levels on mitochondria, resulting in overall lower ubiquitin. MUL-1 is a mitochondria E3 ligase that is a known USP30 substrate itself (Cunningham et al., 2015) whose activity has been shown to be overlapping with USP30 when it comes to mitochondrial substrates (Phu et al., 2020).

Chapter 7: Conclusions

7.1 USP30 localises on mitochondria and peroxisomes

Our lab has shown that USP30 localises on peroxisomes as well as mitochondria (Marcassa et al., 2018). Together with Emma Rusilowicz-Jones, I have shown that peroxisomal USP30 is an integral membrane protein orientated such that the catalytic domain faces the cytosol.

My work has shown that the three basic residues N-terminal to the TM domain mediate USP30 localisation to peroxisomes, a feature that is not required for mitochondrial localisation (Nakamura and Hirose, 2008). USP30 localises on peroxisomes using distinct targeting sequences than those for mitochondria and it can reach peroxisomes independently of mitochondria altogether (Marcassa et al., 2018; Riccio et al., 2019a).

7.2 USP30 localises to the TOMM complex where it restricts ubiquitin accumulation

Ubiquitin deposited on TOMM complex subunits as well as other OMM proteins by the activity of E3 ligases, serves as substrate for PINK1. Once ubiquitin is phosphorylated, it subsequently recruits and activates Parkin (Marcassa et al., 2018; Rusilowicz-Jones et al., 2020). Phosphorylated ubiquitin on the distal end of ubiquitin chains serves as a poor substrate for USP30 (Gersch et al., 2017). Furthermore, USP30 is thought to act on proteins that are proximal to the TOMM complexes where it localises. More specifically, it is thought to preferentially deubiquitylate lysine residues on OMM proteins that are proximal to the OMM bilayer (~35 Å) (Gersch et al., 2017; Ordureau et al., 2020). USP30 may also be able to act downstream of Parkin, deubiquitylating some of the same Parkin substrates and limiting the accumulation of ubiquitin on mitochondria (Bingol et al., 2014; Liang et al., 2015a; Ordureau et al., 2020; Rusilowicz-Jones et al., 2020). More specifically, my work and our lab has collectively shown that USP30 acts on a subset of ubiquitylated substrates on the OMM such as TOMM complex subunits, most notably TOMM20, and SYNJ2BP (Liang et al., 2015a; Rusilowicz-Jones et al., 2020, 2021). In turn, the reduced ubiquitylation of key OMM proteins prevents

accumulation of pS65-Ub on mitochondria that limits Parkin activity and recruitment to mitochondria (Ordureau et al., 2020; Rusilowicz-Jones et al., 2020, 2021). In conclusion, USP30 is associated with the TOMM complexes, denying the PINK1/Parkin pathway an initial burst in mitophagic flux by restricting the accumulation of ubiquitin on TOMM complex components (**Figure 7.1**).

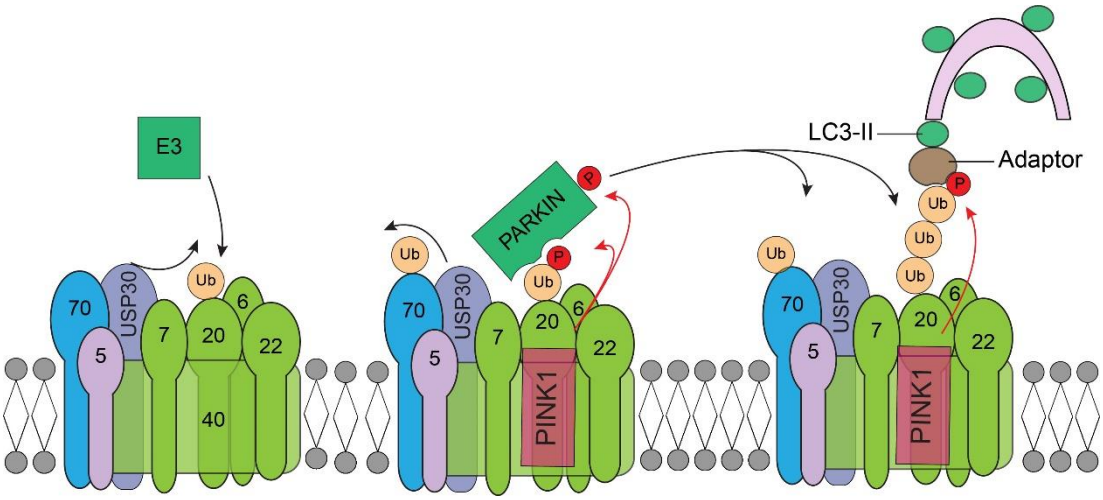

Figure 7.1: USP30 operates at the TOMM complex where it regulates mitophagy

USP30 localises at TOMM complexes on the OMM where it opposes the ubiquitylation of TOMM complex subunits by E3 ligases. Upon induction of mitochondrial damage, PINK1 becomes stabilised at the TOMM complexes and phosphorylates ubiquitin on TOMM complex components. The generation of pS65-Ub on TOMM complexes recruits and activates Parkin. PINK1 phosphorylates Parkin on the UBL domain leading to full activation. Parkin ubiquitylates OMM proteins, generating more substrate for PINK1. The poor processivity of USP30 against phosphorylated ubiquitin and ubiquitylation of OMM proteins on sites far from its reach leave USP30 with limited capacity to act at this stage. The decoration of OMM proteins with ubiquitin leads to the recruitment of the LC3-II decorated autophagosome membrane through autophagy receptors, leading to the engulfment and degradation of the damaged mitochondrion. Black arrows indicate ubiquitylation and deubiquitylation. Red arrows indicate phosphorylation by PINK1.

7.3 USP30 regulates basal and stress-induced pexophagy

Luminal or peroxisomal matrix proteins are post-translationally imported into peroxisomes by shuttle proteins such as PEX5. PEX5 is a peroxin (peroxisome biogenesis factor) that mediates the import of proteins containing the peroxisomal target signal type 1 (PTS1) sequence (Brocard and Hartig, 2006). The C-terminus of Catalase and ACOX1 contain the -SKL sequence, the PTS1 consensus recognised by PEX5 in the cytosol. PEX5 shuttles its protein cargo into the lumen of the peroxisome by interacting with PEX13/14 and the RING complex comprising of PEX2/10/12 in the peroxisomal membrane (Azevedo and Schliebs, 2006; Oeljeklaus et al., 2012). The cargo is released into the lumen and PEX5 becomes subsequently mono-ubiquitylated by the PEX2 RING complex (Williams et al., 2007). Mono-ubiquitylated PEX5 is then exported back into the cytosol in an ATP-dependent manner through the PEX1/6/26 complex. USP9x has been proposed to deubiquitylate PEX5 in order to begin another shuttle cycle (Grou et al., 2012). Peroxisomes that fail to deubiquitylate PEX5 and complete the import cycle, accumulate ubiquitylated PEX5 that results in their autophagosomal engulfment and degradation (Nuttall et al., 2014; Law et al., 2017; Riccio et al., 2019a).

Accumulation of ubiquitylated proteins on peroxisomes results in pexophagy (**Figure 7.2**) (Kim et al., 2008a; Deosaran et al., 2013; Sargent et al., 2016). PEX2 has been identified as the E3 ligase that mediates pexophagy by ubiquitylating PEX5, as part of its import cycle, as well as PMP70 under conditions of starvation or oxidative stress (Sargent et al., 2016). USP30 was shown to deubiquitylate PEX5 and PMP70 and maintain the levels of ubiquitin on peroxisomes low, thus preventing pexophagy (Riccio et al., 2019a; b). My work placed USP30 as a transmembrane protein on peroxisomes with the catalytic domain facing into the cytosol. The localisation and membrane topology of USP30 allow it to act on ubiquitylated proteins on the cytosolic side of the peroxisomal membrane.

In summary, USP30 opposes both basal and starvation-induced pexophagy by preventing the accumulation of ubiquitin on peroxisomes imposed by the PEX2 RING complex (Marcassa et al., 2018, 2019; Riccio et al., 2019a; b).

.

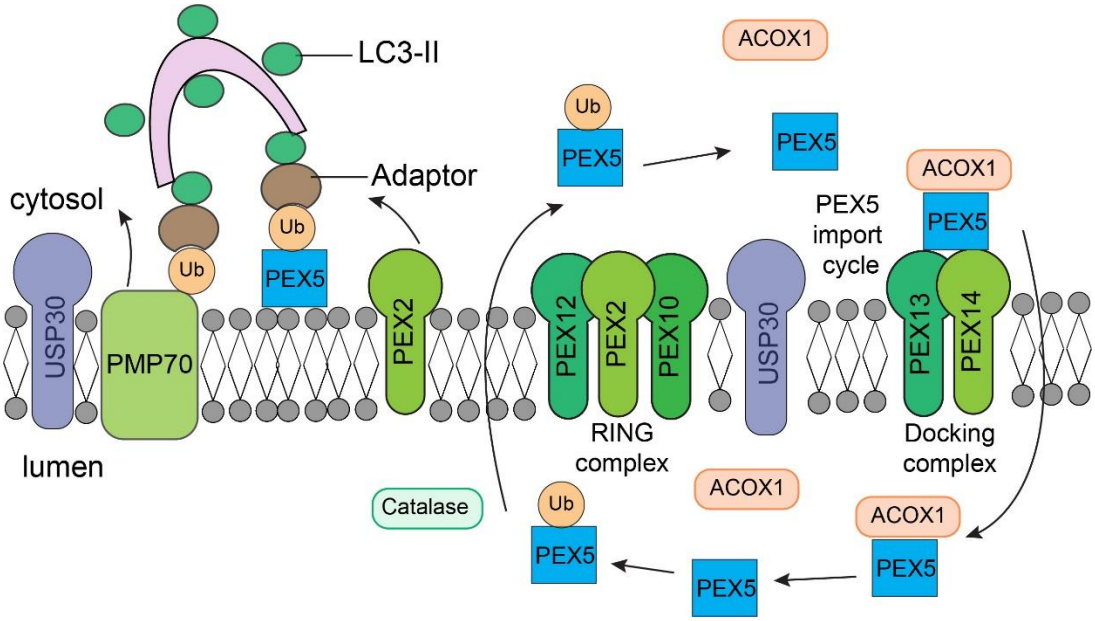

Figure 7.2: USP30 function on peroxisomes

The diagram depicts the PEX5 import cycle of proteins such as ACOX1 and Catalase that are imported into the peroxisome lumen (matrix). PEX5 recognises the cargo and binds to the PEX13/14 docking complex. Once PEX5 shuttles the cargo into the lumen, they dissociate and PEX5 is ubiquitinated by the PEX2 RING complex to facilitate the export of PEX5 back into the cytosol. PEX5 can be deubiquitylated by USP30 to complete the import cycle. Accumulation of ubiquitylated PEX5 on the peroxisome membrane results in the recruitment of autophagy receptors to the peroxisome and results in the autophagic uptake of the organelle. Conditions of starvation or oxidative stress may also induce the ubiquitylation of PMP70, a modification which USP30 also reverses. Deposition of ubiquitin on peroxisomal proteins PMP70 and PEX5 collectively induce pexophagy.

7.4 USP30 is a promising target in the treatment of Parkinson's disease

Parkinson's disease (PD) is currently the second most common neurodegenerative disease with approximately 10% of all cases having an inherited genetic component to their aetiology (Balestrino and Schapira, 2020). PD is characterised by the progressive loss of the dopamine-producing neurons in the *substantia nigra* region of the brain. Defects in complex I of the mitochondrial electron transport chain were detected in the brains of patients with PD (Schapira et al., 1989; Bindoff et al., 1989; Chen et al., 2019). Furthermore, farmers exposed to pesticides, many of which are thought to target the electron transport chain, have higher incidences of PD than the general population (Kab et al., 2017; Pouchieu et al., 2018). Mutations in Parkin (*PARK2*) and PINK1 (*PARK6*) combined are the most prevalent mutations encountered in hereditary forms of early onset juvenile parkinsonism. The above collectively suggests that mitochondrial dysfunction as well as failure to execute mitophagy properly contribute to the aetiology and pathophysiology of PD (Park et al., 2018).

PINK1 and Parkin synergise in the same mitochondrial pathway of mitophagy to ensure proper mitochondrial health and their identification as genes associated with PD sparked a surge in the research around their biology and function. Furthermore, there is a vested interest in the development of compounds that act as PINK1 and Parkin activators in an attempt to correct some of these mitochondrial defects (Miller and Muqit, 2019; Ge et al., 2020). Efforts are underway to develop small molecules that promote kinase activity or dimerization or autophosphorylation of PINK1 to enhance its activity, either directly or indirectly (Lambourne and Mehellou, 2018). Kinetin triphosphate, an ATP analogue, is a suitable neo-substrate for PINK1 and promotes PINK1 kinase activity *in vitro* and in cells (Hertz et al., 2013). Indirect activators of PINK1 include agents that induce mitochondrial depolarisation that leads to PINK1 activation. Niclosamide is one such compound that has been shown to be safe *in vivo* and used to treat tapeworm infestations. Niclosamide activates PINK1 and promotes Parkin translocation and activity at mitochondria (Barini et al., 2018). Parkin undergoes a number of conformational changes from its auto-inhibited closed conformation to its extended and active conformation (Gundogdu et al., 2021). Molecules are being developed to act as allosteric

activators for Parkin that promote the switch from the auto-inhibited form to the active conformation (Miller and Muqit, 2019). However, activating molecules may not benefit patients who harbour the respective catalytically inactive mutants in these genes.

USP30 was identified as a suppressor of the PINK1/Parkin pathway in the regulation of mitophagy (Bingol et al., 2014; Liang et al., 2015a; Marcassa et al., 2018). More importantly, USP30 silencing was found to correct the defects associated with the loss of PINK1 and Parkin in Drosophila (Bingol et al., 2014). Since these early observations, USP30 has emerged as a valid target for therapeutic intervention in the treatment of Parkinson's disease. Our data suggests USP30 silencing requires PINK1 in order to enhance basal mitophagy and therefore the expectation would be that USP30 inhibitors would not benefit patients with loss-of-function mutations in PINK1 (Marcassa et al., 2018). The above is further supported by data from our lab showing USP30 loss and inhibition elevate the levels of pS65-Ub in depolarised cells, which also requires PINK1 activity (Rusilowicz-Jones et al., 2020).

A number of small molecule inhibitors against USP30 have been developed over the last few years, most of which are based on N-cyano pyrrolidines or racemic mixtures of phenylalanine derivatives (Kluge et al., 2018; Rusilowicz-Jones et al., 2020, 2021; Luo et al., 2021; Tsefou et al., 2021). Our lab has been involved in the development and characterisation of one such compound that was discussed in the previous chapter, FT3967385 (Rusilowicz-Jones et al., 2020). Our work has shown that FT385 is a specific DUB inhibitor against USP30 whose inhibitory effect closely resembles the genetic KO of USP30. I have shown that TOMM20 ubiquitylation is sensitive to USP30 status in the cells, whether by genetic KO or through inhibition by FT385. Furthermore, the generation of pS65-Ub was elevated in cells lacking USP30.

Inhibition of USP30 *in vivo* is expected to increase the rate of basal mitophagy thus maintaining a healthier mitochondrial network in patients (Marcassa et al., 2018). The inhibition of USP30 is expected to benefit patients with mutations in Parkin (Bingol et al., 2014; Rusilowicz-Jones et al., 2021). However, the therapeutic benefits of USP30 inhibition need to be investigated in sporadic cases of PD as well. While PINK1 and Parkin mutations are rare

and most PD cases are sporadic, mitochondrial dysfunction has also been reported for the latter cases (Ryan et al., 2015). The above would suggest that USP30 inhibition may still be a good candidate for intervention, even though the concept requires further validation (Miller and Muqit, 2019; Schwartzentruber et al., 2020; Rusilowicz-Jones et al., 2021).

7.5 The molecular mechanism of how USP30 depletion enhances the effects of BH3 mimetics remains elusive

My work has shown that in the USP30-depleted cells, sensitisation can be achieved to a variety of BH3 mimetics that target distinct members of the anti-apoptotic BCL-2 family of proteins. The failure of certain BH3 mimetics, such as ABT-199 and A-1210477, to induce apoptosis when used individually, even in USP30-depleted cells, suggests that USP30 does not operate at the level of the anti-apoptotic BCL-2 family. Similarly to the control cells, USP30-depleted cells remained dependent on BCL-X_L and MCL-1 for survival. USP30 depletion did not reprogramme the cells with respect to which anti-apoptotic proteins are important for their survival but rather enhanced their existing apoptotic responses.

One of the main reasons for the generation of USP30KO cells was to gain an insight in the mechanism by which USP30 loss was sensitizing cells to BH3 mimetics. More specifically, the aims were to discover novel USP30 substrates that were relevant in the context of apoptotic cell death and the ubiquitin E3 ligases that USP30 was opposing in this context. My data showed a weak sensitisation for some but not all of the USP30KO clones in the HCT116 FlpIn TRex cell line and the hTERT-RPE1 FlpIn TRex cells. The clonal nature of these cells could be masking the effects of USP30 loss in response to BH3 mimetics. Alternatively, the long term loss of USP30 may induce a compensatory mechanism in these cells and restore their response back to near baseline. I was therefore reluctant to take the project further since more work was needed to build this project on more robust data before dwelling into more detail.

Changes to key components of the apoptotic cascade such as BAK/BAX and MCL-1 would be the obvious starting point when investigating the mechanism of sensitized cell death. Both the small-scale and more

comprehensive proteomes in the HCT116 FlpIn TRex USP30KO cells as well as our proteomic datasets from hTERT-RPE1 and SH-SY5Y cells revealed no significant changes in the levels of expression of members of the broader BCL-2 family (Rusilowicz-Jones et al., 2020, Marcassa et al.,unpublished). We have recently employed unbiased approaches looking at the proteome and ubiquitylome of USP30 null and USP30 inhibitor-treated cells in order to identify USP30 substrates (Rusilowicz-Jones et al., 2020). Adding a stressor such as depolarisation in the form of A/O treatment, allowed us to amplify the effects of USP30 loss at the levels of proteome and ubiquitylome. A similar approach may be beneficial in the discovery of USP30 substrates in the context of apoptotic cell death. The question would be which proteins are differentially affected (proteome analysis) and/or differentially ubiquitylated (ubiquitylome analysis) in USP30 null cells in response to BH3 mimetics.

7.6 USP30 as a target in malignancies and metabolic disorders

One of the very first pieces of evidence implicating USP30 in the contexts of cancer was the observation that USP30-depleted cells were not scattering in response to HGF thus phenocopying the effects of c-Met receptor depletion (Buus et al., 2009). The above implicated USP30 in receptor tyrosine kinase and KRAS signalling as well as in the mechanism of epithelial to mesenchymal transition (EMT), a process required for cancer cell invasion and metastasis (Xiang et al., 2017).

Mitochondrial dysfunction is a common occurrence and often a driver in cancer (Moro, 2019). Accumulation of mutations in mitochondrial (mt) DNA have been reported in a variety of cancers, a mechanism that often leads to excessive generation of ROS, accumulation of more somatic mutations in nuclear genes and inflammation (Guaragnella et al., 2014; Guerra et al., 2017). Furthermore, the deletion of genes involved in mitochondrial quality control, such as PINK1 and Parkin, is associated with increased risk and accelerated disease progression in pancreatic ductal adenocarcinoma (Li et al., 2018). Targeting USP30 may benefit patients with cancer by relieving mitochondrial dysfunction and improve disease outcome.

KRAS mutations are common in many of the most prevalent cancers, including lung, pancreatic and colorectal (Timar and Kashofer, 2020; Prior et

al., 2020). Approaches to inhibit or modulate mutant KRAS-driven cancers exist by targeting downstream effectors such as ERK or PI3K/mTOR (Smalley and Smalley, 2018; Yang et al., 2019). Small molecule inhibitors have recently been developed and tested to specifically target mutant KRAS (Nagasaka et al., 2021; Huang et al., 2021). Alternative approaches to target KRAS-driven tumours include targeting lipogenesis. In fact, lipogenesis was shown to be upregulated and driven by mutations in KRAS (Gouw et al., 2017). KRAS mutant cancers are associated with higher expression levels of FASN, ACLY and acetyl Coenzyme A carboxylase (ACC), which in turn increase *de novo* lipogenesis (Bartolacci et al., 2017; Singh et al., 2018). KRAS-driven cancers were shown to be sensitive to FASN inhibition, suggesting they are dependent on lipogenesis and targeting lipogenesis presents a therapeutic opportunity against these. USP30 was recently shown to support lipogenesis and hepatic carcinogenesis by stabilising the protein levels of key proteins FASN and ACLY (Gu et al., 2020). My data supports the notion that USP30 enhances oxidative metabolism and accelerates the growth of cancer cells. The exact mechanism by which the above is achieved remains unknown. USP30 inhibition may serve as a potential alternative mean to target the FASN/ACLY lipogenesis axis as well as proliferation, in the contexts of malignancies.

The association of USP30 with lipogenesis may also make it an attractive target in metabolic diseases and disorders, such as obesity and type II diabetes. Metabolic disorders that include obesity and diabetes are often accompanied by mitochondrial dysfunction. Mitochondria isolated from obese people or individuals with type II diabetes exhibited reduced mtDNA content and an even more significant reduction in the operational capacity of the electron transport chain compared to leaner volunteers (Ritov et al., 2005). Impaired mitophagy has been linked to developing diabetes-related vascular dysfunction, atherosclerosis and cardiomyopathy (Tang et al., 2014). Strategies that increase mitophagy and improve mitochondrial performance, such as USP30 inhibition, may therefore benefit patients suffering from certain metabolic disorders (Rusilowicz-Jones et al., 2020, 2021).

7.7 Concluding Remarks

My work has expanded aspects of USP30 biology spanning from apoptotic cell death, metabolism, cell proliferation and the role of USP30 in the PINK1/Parkin pathways. The potential of USP30 as an actionable target in the treatment and management of PD is strengthened by some of the biology discussed in the thesis and the collective work of our lab (Liang et al., 2015a; Marcassa et al., 2018; Rusilowicz-Jones et al., 2020, 2021). It will be interesting to explore whether USP30 is as relevant in other disease settings, as I briefly touched upon above.

References

Aarreberg, L.D., K. Esser-Nobis, C. Driscoll, A. Shuvarikov, J.A. Roby, and M. Gale. 2019. Interleukin-1β Induces mtDNA Release to Activate Innate Immune Signaling via cGAS-STING. *Mol. Cell*. 74:801-815.e6. doi:10.1016/j.molcel.2019.02.038.

Abdul Rehman, S.A., Y.A. Kristariyanto, S.-Y. Choi, P.J. Nkosi, S. Weidlich, K. Labib, K. Hofmann, and Y. Kulathu. 2016. MINDY-1 Is a Member of an Evolutionarily Conserved and Structurally Distinct New Family of Deubiquitinating Enzymes. *Mol. Cell*. 63:146–155. doi:10.1016/j.molcel.2016.05.009.

Acehan, D., X. Jiang, D.G. Morgan, J.E. Heuser, X. Wang, and C.W. Akey. 2002. Three-dimensional structure of the apoptosome: implications for assembly, procaspase-9 binding, and activation. *Mol. Cell*. 9:423–432. doi:10.1016/s1097-2765(02)00442-2.

Allen, G.F.G., R. Toth, J. James, and I.G. Ganley. 2013. Loss of iron triggers PINK1/Parkin-independent mitophagy. *EMBO Rep.* 14:1127–1135. doi:10.1038/embor.2013.168.

Alves, S., L. Castro, M.S. Fernandes, R. Francisco, P. Castro, M. Priault, S.R. Chaves, M.P. Moyer, C. Oliveira, R. Seruca, M. Côrte-Real, M.J. Sousa, and A. Preto. 2015. Colorectal cancer-related mutant KRAS alleles function as positive regulators of autophagy. *Oncotarget*. 6:30787–30802. doi:10.18632/oncotarget.5021.

Ambroggio, X.I., D.C. Rees, and R.J. Deshaies. 2003. JAMM: A Metalloprotease-Like Zinc Site in the Proteasome and Signalosome. *PLoS Biol.* 2:e2. doi:10.1371/journal.pbio.0020002.

Amin, S., B. Cook, T. Zhou, Z. Ghazizadeh, R. Lis, T. Zhang, M. Khalaj, M. Crespo, M. Perera, J.Z. Xiang, Z. Zhu, M. Tomishima, C. Liu, A. Naji, T. Evans, D. Huangfu, and S. Chen. 2018. Discovery of a drug candidate for GLIS3-associated diabetes. *Nat. Commun.* 9:2681. doi:10.1038/s41467-018-04918-x.

Andrew, S.E., Y. Paul Goldberg, B. Kremer, H. Telenius, J. Theilmann, S. Adam, E. Starr, F. Squitieri, B. Lin, M.A. Kalchman, R.K. Graham, and M.R. Hayden. 1993. The relationship between trinucleotide (CAG) repeat length and clinical features of Huntington's disease. *Nat. Genet.* 4:398–403. doi:10.1038/ng0893-398.

Auger, K.R., C.L. Carpenter, L.C. Cantley, and L. Varticovski. 1989. Phosphatidylinositol 3-kinase and its novel product, phosphatidylinositol 3-phosphate, are present in Saccharomyces cerevisiae. *J. Biol. Chem.* 264:20181–20184.

Avruch, J., X. Long, S. Ortiz-Vega, J. Rapley, A. Papageorgiou, and N. Dai. 2009. Amino acid regulation of TOR complex 1. *Am. J. Physiol. Endocrinol. Metab.* 296:E592-602. doi:10.1152/ajpendo.90645.2008.

Axe, E.L., S.A. Walker, M. Manifava, P. Chandra, H.L. Roderick, A. Habermann, G. Griffiths, and N.T. Ktistakis. 2008. Autophagosome formation from membrane compartments enriched in phosphatidylinositol 3-phosphate and dynamically connected to the endoplasmic reticulum. *J. Cell Biol.* 182:685–701. doi:10.1083/jcb.200803137.

Azevedo, J.E., and W. Schliebs. 2006. Pex14p, more than just a docking protein. *Biochim. Biophys. Acta BBA - Mol. Cell Res.* 1763:1574–1584. doi:10.1016/j.bbamcr.2006.09.002.

Bagchi, A., and A.A. Mills. 2008. The Quest for the 1p36 Tumor Suppressor. *Cancer Res.* 68:2551–2556. doi:10.1158/0008-5472.CAN-07-2095.

Baker, R.T., and P.G. Board. 1991. The human ubiquitin-52 amino acid fusion protein gene shares several structural features with mammalian ribosomal protein genes. *Nucleic Acids Res.* 19:1035–1040. doi:10.1093/nar/19.5.1035.

Baker, R.T., and P.G. Board. Nucleotide sequence of a human ubiquitin Ub B processed pseudogene. 1.

Balestrino, R., and A.H.V. Schapira. 2020. Parkinson disease. *Eur. J. Neurol.* 27:27–42. doi:10.1111/ene.14108.

Barini, E., A. Miccoli, F. Tinarelli, K. Mulholland, H. Kadri, F. Khanim, L. Stojanovski, K.D. Read, K. Burness, J.J. Blow, Y. Mehellou, and M.M.K. Muqit. 2018. The Anthelmintic Drug Niclosamide and Its Analogues Activate the Parkinson's Disease Associated Protein Kinase PINK1. *Chembiochem Eur. J. Chem. Biol.* 19:425–429. doi:10.1002/cbic.201700500.

Bartolacci, C., M. Padanad, C. Andreani, M. Melegari, S. Rindhe, K. George, A. Frankel, J. McDonald, and P.P. Scaglioni. 2017. Fatty Acid Synthase Is a Therapeutic Target in Mutant KRAS Lung Cancer. *J. Thorac. Oncol.* 12:S1538. doi:10.1016/j.jtho.2017.06.030.

Bassik, M.C., L. Scorrano, S.A. Oakes, T. Pozzan, and S.J. Korsmeyer. 2004. Phosphorylation of BCL-2 regulates ER Ca2+ homeostasis and apoptosis. *EMBO J.* 23:1207–1216. doi:10.1038/sj.emboj.7600104.

Benard, G., A. Neutzner, G. Peng, C. Wang, F. Livak, R.J. Youle, and M. Karbowski. 2010. IBRDC2, an IBR-type E3 ubiquitin ligase, is a regulatory factor for Bax and apoptosis activation. *EMBO J.* 29:1458–1471. doi:10.1038/emboj.2010.39.

Bernardini, J.P., J.M. Brouwer, I.K. Tan, J.J. Sandow, S. Huang, C.A. Stafford, A. Bankovacki, C.D. Riffkin, A.Z. Wardak, P.E. Czabotar, M. Lazarou,

and G. Dewson. 2019. Parkin inhibits BAK and BAX apoptotic function by distinct mechanisms during mitophagy. *EMBO J.* 38:e99916. doi:10.15252/embj.201899916.

Bernardini, J.P., M. Lazarou, and G. Dewson. 2017. Parkin and mitophagy in cancer. *Oncogene*. 36:1315–1327. doi:10.1038/onc.2016.302.

Berry, B.J., A.J. Trewin, A.M. Amitrano, M. Kim, and A.P. Wojtovich. 2018. Use the Protonmotive Force: Mitochondrial Uncoupling and Reactive Oxygen Species. *J. Mol. Biol.* 430:3873–3891. doi:10.1016/j.jmb.2018.03.025.

Bertrand, M.J.M., S. Milutinovic, K.M. Dickson, W.C. Ho, A. Boudreault, J. Durkin, J.W. Gillard, J.B. Jaquith, S.J. Morris, and P.A. Barker. 2008. cIAP1 and cIAP2 Facilitate Cancer Cell Survival by Functioning as E3 Ligases that Promote RIP1 Ubiquitination. *Mol. Cell*. 30:689–700. doi:10.1016/j.molcel.2008.05.014.

Besche, H.C., Z. Sha, N.V. Kukushkin, A. Peth, E. Hock, W. Kim, S. Gygi, J.A. Gutierrez, H. Liao, L. Dick, and A.L. Goldberg. 2014. Autoubiquitination of the 26S Proteasome on Rpn13 Regulates Breakdown of Ubiquitin Conjugates. *EMBO J.* 33:1159–1176. doi:10.1002/embj.201386906.

Best, S.R., T. Rowland, C. Paiva, N. Bruss, S.E. Spurgeon, A. Berger, and A.V. Danilov. 2018. TAK-243, a Small Molecule Inhibitor of Ubiquitin-Activating Enzyme (UAE), Induces ER Stress and Apoptosis in CLL Cells. *Blood*. 132:1867–1867. doi:10.1182/blood-2018-99-114964.

Bett, J.S., M.S. Ritorto, R. Ewan, E.G. Jaffray, S. Virdee, J.W. Chin, A. Knebel, T. Kurz, M. Trost, M.H. Tatham, and R.T. Hay. 2015. Ubiquitin C-terminal hydrolases cleave isopeptide- and peptide-linked ubiquitin from structured proteins but do not edit ubiquitin homopolymers. *Biochem. J.* 466:489–498. doi:10.1042/BJ20141349.

Bhogaraju, S., S. Kalayil, Y. Liu, F. Bonn, T. Colby, I. Matic, and I. Dikic. 2016. Phosphoribosylation of Ubiquitin Promotes Serine Ubiquitination and Impairs Conventional Ubiquitination. *Cell*. 167:1636-1649.e13. doi:10.1016/j.cell.2016.11.019.

Bhujabal, Z., Å.B. Birgisdottir, E. Sjøttem, H.B. Brenne, A. Øvervatn, S. Habisov, V. Kirkin, T. Lamark, and T. Johansen. 2017. FKBP8 recruits LC3A to mediate Parkin-independent mitophagy. *EMBO Rep.* 18:947–961. doi:10.15252/embr.201643147.

Bienko, M. 2005. Ubiquitin-Binding Domains in Y-Family Polymerases Regulate Translesion Synthesis. *Science*. 310:1821–1824. doi:10.1126/science.1120615.

Billen, L.P., C.L. Kokoski, J.F. Lovell, B. Leber, and D.W. Andrews. 2008. Bcl-XL Inhibits Membrane Permeabilization by Competing with Bax. *PLoS Biol.* 6:e147. doi:10.1371/journal.pbio.0060147.

Bindoff, L.A., M. Birch-Machin, N.E. Cartlidge, W.D. Parker, and D.M. Turnbull. 1989. Mitochondrial function in Parkinson's disease. *Lancet Lond. Engl.* 2:49. doi:10.1016/s0140-6736(89)90291-2.

Bingol, B., J.S. Tea, L. Phu, M. Reichelt, C.E. Bakalarski, Q. Song, O. Foreman, D.S. Kirkpatrick, and M. Sheng. 2014. The mitochondrial deubiquitinase USP30 opposes parkin-mediated mitophagy. *Nature*. 510:370–375. doi:10.1038/nature13418.

Birgisdottir, Å.B., T. Lamark, and T. Johansen. 2013. The LIR motif – crucial for selective autophagy. *J. Cell Sci.* 126:3237–3247. doi:10.1242/jcs.126128.

Bock, F.J., and S.W.G. Tait. 2020. Mitochondria as multifaceted regulators of cell death. *Nat. Rev. Mol. Cell Biol.* 21:85–100. doi:10.1038/s41580-019-0173-8.

Bohnsack, R.N., and A.L. Haas. 2003. Conservation in the Mechanism of Nedd8 Activation by the Human AppBp1-Uba3 Heterodimer. *J. Biol. Chem.* 278:26823–26830. doi:10.1074/jbc.M303177200.

Bolotin, A., B. Quinquis, A. Sorokin, and S.D. Ehrlich. 2005. Clustered regularly interspaced short palindrome repeats (CRISPRs) have spacers of extrachromosomal origin. *Microbiology*. 151:2551–2561. doi:10.1099/mic.0.28048-0.

Borodovsky, A., B.M. Kessler, R. Casagrande, H.S. Overkleeft, K.D. Wilkinson, and H.L. Ploegh. 2001. A novel active site-directed probe specific for deubiquitylating enzymes reveals proteasome association of USP14. *EMBO J.* 20:5187–5196. doi:10.1093/emboj/20.18.5187.

Bortner, C.D., N.B.E. Oldenburg, and J.A. Cidlowski. 1995. The role of DNA fragmentation in apoptosis. *Trends Cell Biol.* 5:21–26. doi:10.1016/S0962-8924(00)88932-1.

Boutet, S.C., M.-H. Disatnik, L.S. Chan, K. Iori, and T.A. Rando. 2007. Regulation of Pax3 by proteasomal degradation of monoubiquitinated protein in skeletal muscle progenitors. *Cell*. 130:349–362. doi:10.1016/j.cell.2007.05.044.

Branigan, E., J. Carlos Penedo, and R.T. Hay. 2020. Ubiquitin transfer by a RING E3 ligase occurs from a closed E2~ubiquitin conformation. *Nat. Commun.* 11. doi:10.1038/s41467-020-16666-y.

Breitschopf, K. 1998. A novel site for ubiquitination: the N-terminal residue, and not internal lysines of MyoD, is essential for conjugation and degradation of the protein. *EMBO J.* 17:5964–5973. doi:10.1093/emboj/17.20.5964.

Bremm, A., S.M.V. Freund, and D. Komander. 2010. Lys11-linked ubiquitin chains adopt compact conformations and are preferentially hydrolyzed

by the deubiquitinase Cezanne. *Nat. Struct. Mol. Biol.* 17:939–947. doi:10.1038/nsmb.1873.

Bremm, A., and D. Komander. 2011. Emerging roles for Lys11-linked polyubiquitin in cellular regulation. *Trends Biochem. Sci.* doi:10.1016/j.tibs.2011.04.004.

Breslow, D.K., D.M. Cameron, S.R. Collins, M. Schuldiner, J. Stewart-Ornstein, H.W. Newman, S. Braun, H.D. Madhani, N.J. Krogan, and J.S. Weissman. 2008. A comprehensive strategy enabling high-resolution functional analysis of the yeast genome. *Nat. Methods*. 5:711–718. doi:10.1038/nmeth.1234.

Briceño, E., A. Calderon, and J. Sotelo. 2007. Institutional experience with chloroquine as an adjuvant to the therapy for glioblastoma multiforme. *Surg. Neurol.* 67:388–391. doi:10.1016/j.surneu.2006.08.080.

Brocard, C., and A. Hartig. 2006. Peroxisome targeting signal 1: Is it really a simple tripeptide? *Biochim. Biophys. Acta BBA - Mol. Cell Res.* 1763:1565–1573. doi:10.1016/j.bbamcr.2006.08.022.

Brouns, S.J.J., M.M. Jore, M. Lundgren, E.R. Westra, R.J.H. Slijkhuis, A.P.L. Snijders, M.J. Dickman, K.S. Makarova, E.V. Koonin, and J. van der Oost. 2008. Small CRISPR RNAs Guide Antiviral Defense in Prokaryotes. *Science*. 321:960–964. doi:10.1126/science.1159689.

Brownell, J.E., M.D. Sintchak, J.M. Gavin, H. Liao, F.J. Bruzzese, N.J. Bump, T.A. Soucy, M.A. Milhollen, X. Yang, A.L. Burkhardt, J. Ma, H.-K. Loke, T. Lingaraj, D. Wu, K.B. Hamman, J.J. Spelman, C.A. Cullis, S.P. Langston, S. Vyskocil, T.B. Sells, W.D. Mallender, I. Visiers, P. Li, C.F. Claiborne, M. Rolfe, J.B. Bolen, and L.R. Dick. 2010. Substrate-Assisted Inhibition of Ubiquitin-like Protein-Activating Enzymes: The NEDD8 E1 Inhibitor MLN4924 Forms a NEDD8-AMP Mimetic In Situ. *Mol. Cell*. 37:102–111. doi:10.1016/j.molcel.2009.12.024.

Brunner, T. 2003. Fas (CD95/Apo-1) ligand regulation in T cell homeostasis, cell-mediated cytotoxicity and immune pathology. *Semin. Immunol.* 15:167–176. doi:10.1016/S1044-5323(03)00035-6.

Bulatov, E., and A. Ciulli. 2015. Targeting Cullin–RING E3 ubiquitin ligases for drug discovery: structure, assembly and small-molecule modulation. *Biochem. J.* 467:365–386. doi:10.1042/BJ20141450.

Burchell, V.S., D.E. Nelson, A. Sanchez-Martinez, M. Delgado-Camprubi, R.M. Ivatt, J.H. Pogson, S.J. Randle, S. Wray, P.A. Lewis, H. Houlden, A.Y. Abramov, J. Hardy, N.W. Wood, A.J. Whitworth, H. Laman, and H. Plun-Favreau. 2013. The Parkinson's disease–linked proteins Fbxo7 and Parkin interact to mediate mitophagy. *Nat. Neurosci.* 16:1257–1265. doi:10.1038/nn.3489.

Busiello, R.A., S. Savarese, and A. Lombardi. 2015. Mitochondrial uncoupling proteins and energy metabolism. *Front. Physiol.* 6. doi:10.3389/fphys.2015.00036.

Buus, R., M. Faronato, D.E. Hammond, S. Urbé, and M.J. Clague. 2009. Deubiquitinase Activities Required for Hepatocyte Growth Factor-Induced Scattering of Epithelial Cells. *Curr. Biol.* 19:1463–1466. doi:10.1016/j.cub.2009.07.040.

Cakir, Z., K. Funk, J. Lauterwasser, F. Todt, R.M. Zerbes, A. Oelgeklaus, A. Tanaka, M. van der Laan, and F. Edlich. 2017. Parkin promotes proteasomal degradation of misregulated BAX. *J. Cell Sci.* 130:2903–2913. doi:10.1242/jcs.200162.

Calvo, S.E., K.R. Clauser, and V.K. Mootha. 2016. MitoCarta2.0: an updated inventory of mammalian mitochondrial proteins. *Nucleic Acids Res.* 44:D1251–D1257. doi:10.1093/nar/gkv1003.

Campagne, A., M.-K. Lee, D. Zielinski, A. Michaud, S. Le Corre, F. Dingli, H. Chen, L.Z. Shahidian, I. Vassilev, N. Servant, D. Loew, E. Pasmant, S. Postel-Vinay, M. Wassef, and R. Margueron. 2019. BAP1 complex promotes transcription by opposing PRC1-mediated H2A ubiquitylation. *Nat. Commun.* 10. doi:10.1038/s41467-018-08255-x.

Campbell, K.J., and S.W.G. Tait. 2018. Targeting BCL-2 regulated apoptosis in cancer. *Open Biol.* 8:1–11. doi:10.1098/rsob.180002.

Cao, X., X. Deng, and W.S. May. 2003. Cleavage of Bax to p18 Bax accelerates stress-induced apoptosis, and a cathepsin-like protease may rapidly degrade p18 Bax. *Blood*. 102:2605–2614. doi:10.1182/blood-2003-01-0211.

Cardozo, T., and M. Pagano. 2004. The SCF ubiquitin ligase: insights into a molecular machine. *Nat. Rev. Mol. Cell Biol.* 5:739–751. doi:10.1038/nrm1471.

Carpio, M.A., R.E. Means, A.L. Brill, A. Sainz, B.E. Ehrlich, and S.G. Katz. 2021. BOK controls apoptosis by Ca2+ transfer through ER-mitochondrial contact sites. *Cell Rep.* 34:108827. doi:10.1016/j.celrep.2021.108827.

Carpio, M.A., M. Michaud, W. Zhou, J.K. Fisher, L.D. Walensky, and S.G. Katz. 2015. BCL-2 family member BOK promotes apoptosis in response to endoplasmic reticulum stress. *Proc. Natl. Acad. Sci.* 112:7201–7206. doi:10.1073/pnas.1421063112.

Carroll, R.G., E. Hollville, and S.J. Martin. 2014. Parkin sensitizes toward apoptosis induced by mitochondrial depolarization through promoting degradation of Mcl-1. *Cell Rep.* 9:1538–1553. doi:10.1016/j.celrep.2014.10.046.

Castañeda, C.A., E.K. Dixon, O. Walker, A. Chaturvedi, M.A. Nakasone, J.E. Curtis, M.R. Reed, S. Krueger, T.A. Cropp, and D. Fushman. 2016. Linkage via K27 Bestows Ubiquitin Chains with Unique Properties among Polyubiquitins. *Structure*. 24:423–436. doi:10.1016/j.str.2016.01.007.

Caubet, C., N. Jonca, M. Brattsand, M. Guerrin, D. Bernard, R. Schmidt, T. Egelrud, M. Simon, and G. Serre. 2004. Degradation of corneodesmosome proteins by two serine proteases of the kallikrein family, SCTE/KLK5/hK5 and SCCE/KLK7/hK7. *J. Invest. Dermatol.* 122:1235–1244. doi:10.1111/j.0022-202X.2004.22512.x.

Cebollero, E., F. Reggiori, and C. Kraft. 2012. Reticulophagy and Ribophagy: Regulated Degradation of Protein Production Factories. *Int. J. Cell Biol.* 2012:1–9. doi:10.1155/2012/182834.

Chadchankar, J., V. Korboukh, L.C. Conway, H.J. Wobst, C.A. Walker, P. Doig, S.J. Jacobsen, N.J. Brandon, S.J. Moss, and Q. Wang. 2019. Inactive USP14 and inactive UCHL5 cause accumulation of distinct ubiquitinated proteins in mammalian cells. *PLOS ONE*. 14:e0225145. doi:10.1371/journal.pone.0225145.

Challis, C., A. Hori, T.R. Sampson, B.B. Yoo, R.C. Challis, A.M. Hamilton, S.K. Mazmanian, L.A. Volpicelli-Daley, and V. Gradinaru. 2020. Gut-seeded α-synuclein fibrils promote gut dysfunction and brain pathology specifically in aged mice. *Nat. Neurosci.* 23:327–336. doi:10.1038/s41593-020-0589-7.

Chan, N.C., A.M. Salazar, A.H. Pham, M.J. Sweredoski, N.J. Kolawa, R.L.J. Graham, S. Hess, and D.C. Chan. 2011. Broad activation of the ubiquitin-proteasome system by Parkin is critical for mitophagy. *Hum. Mol. Genet.* 20:1726–1737. doi:10.1093/hmg/ddr048.

Chang, H.Y., and X. Yang. 2000. Proteases for Cell Suicide: Functions and Regulation of Caspases. *Microbiol. Mol. Biol. Rev.* 64:821–846. doi:10.1128/MMBR.64.4.821-846.2000.

Chang, L., and D. Barford. 2014. Insights into the anaphase-promoting complex: a molecular machine that regulates mitosis. *Curr. Opin. Struct. Biol.* 29:1–9. doi:10.1016/j.sbi.2014.08.003.

Chau, V., J. Tobias, A. Bachmair, D. Marriott, D. Ecker, D. Gonda, and A. Varshavsky. 1989. A multiubiquitin chain is confined to specific lysine in a targeted short-lived protein. *Science*. 243:1576–1583. doi:10.1126/science.2538923.

Chen, C., D.M. Turnbull, and A.K. Reeve. 2019. Mitochondrial Dysfunction in Parkinson's Disease-Cause or Consequence? *Biology*. 8. doi:10.3390/biology8020038.

Chen, G., Z. Han, D. Feng, Y. Chen, L. Chen, H. Wu, L. Huang, C. Zhou, X. Cai, C. Fu, L. Duan, X. Wang, L. Liu, X. Liu, Y. Shen, Y. Zhu, and Q.

Chen. 2014. A regulatory signaling loop comprising the PGAM5 phosphatase and CK2 controls receptor-mediated mitophagy. *Mol. Cell*. 54:362–377. doi:10.1016/j.molcel.2014.02.034.

Chen, Q., L. Sun, and Z.J. Chen. 2016. Regulation and function of the cGAS–STING pathway of cytosolic DNA sensing. *Nat. Immunol.* 17:1142–1149. doi:10.1038/ni.3558.

Chen, Y., Y. Lu, C. Lu, and L. Zhang. 2009. Beclin-1 Expression is a Predictor of Clinical Outcome in Patients with Esophageal Squamous Cell Carcinoma and Correlated to Hypoxia-Inducible Factor (HIF)-1α Expression. *Pathol. Oncol. Res.* 15:487–493. doi:10.1007/s12253-008-9143-8.

Chen, Z., J. Hagler, V.J. Palombella, F. Melandri, D. Scherer, D. Ballard, and T. Maniatis. 1995. Signal-induced site-specific phosphorylation targets I kappa B alpha to the ubiquitin-proteasome pathway. *Genes Dev.* 9:1586–1597. doi:10.1101/gad.9.13.1586.

Chen, Z., L. Liu, Q. Cheng, Y. Li, H. Wu, W. Zhang, Y. Wang, S.A. Sehgal, S. Siraj, X. Wang, J. Wang, Y. Zhu, and Q. Chen. 2017. Mitochondrial E3 ligase MARCH5 regulates FUNDC1 to fine-tune hypoxic mitophagy. *EMBO Rep.* 18:495–509. doi:10.15252/embr.201643309.

Chen, Z.J., and L.J. Sun. 2009. Nonproteolytic Functions of Ubiquitin in Cell Signaling. *Mol. Cell*. 33:275–286. doi:10.1016/j.molcel.2009.01.014.

Chinnaiyan, A.M. 1999. The Apoptosome: Heart and Soul of the Cell Death Machine. *Neoplasia*. 1:5–15. doi:10.1038/sj.neo.7900003.

Chipuk, J.E. 2004. Direct Activation of Bax by p53 Mediates Mitochondrial Membrane Permeabilization and Apoptosis. *Science*. 303:1010–1014. doi:10.1126/science.1092734.

Chiu, Y.-H., Q. Sun, and Z.J. Chen. 2007. E1-L2 Activates Both Ubiquitin and FAT10. *Mol. Cell*. 27:1014–1023. doi:10.1016/j.molcel.2007.08.020.

Choudhary, C., C. Kumar, F. Gnad, M.L. Nielsen, M. Rehman, T.C. Walther, J.V. Olsen, and M. Mann. 2009. Lysine Acetylation Targets Protein Complexes and Co-Regulates Major Cellular Functions. *Science*. 325:834–840. doi:10.1126/science.1175371.

Christensen, D.E., P.S. Brzovic, and R.E. Klevit. 2007. E2–BRCA1 RING interactions dictate synthesis of mono- or specific polyubiquitin chain linkages. *Nat. Struct. Mol. Biol.* 14:941–948. doi:10.1038/nsmb1295.

Christoforidis, S., M. Miaczynska, K. Ashman, M. Wilm, L. Zhao, S.C. Yip, M.D. Waterfield, J.M. Backer, and M. Zerial. 1999. Phosphatidylinositol-3-OH kinases are Rab5 effectors. *Nat. Cell Biol.* 1:249–252. doi:10.1038/12075.

Ciechanover, A., H. Heller, S. Elias, A.L. Haas, and A. Hershko. 1980. ATP-dependent conjugation of reticulocyte proteins with the polypeptide required for protein degradation. *Proc. Natl. Acad. Sci.* 77:1365–1368. doi:10.1073/pnas.77.3.1365.

Ciechanover, A., H. Heller, R. Katz-Etzion, and A. Hershko. 1981. Activation of the heat-stable polypeptide of the ATP-dependent proteolytic system. *Proc. Natl. Acad. Sci.* 78:761–765. doi:10.1073/pnas.78.2.761.

Ciechanover, A., Y. Hod, and A. Hershko. 1978. A heat-stable polypeptide component of an ATP-dependent proteolytic system from reticulocytes. *Biochem. Biophys. Res. Commun.* 81:1100–1105. doi:10.1016/0006-291X(78)91249-4.

Clague, M.J., I. Barsukov, J.M. Coulson, H. Liu, D.J. Rigden, and S. Urbe. 2013. Deubiquitylases From Genes to Organism. *Physiol. Rev.* 93:1289–1315. doi:10.1152/physrev.00002.2013.

Clague, M.J., and S. Urbé. 2017. Integration of cellular ubiquitin and membrane traffic systems: focus on deubiquitylases. *FEBS J.* 284:1753–1766. doi:10.1111/febs.14007.

Clague, M.J., S. Urbé, and D. Komander. 2019. Breaking the chains: deubiquitylating enzyme specificity begets function. *Nat. Rev. Mol. Cell Biol.* doi:10.1038/s41580-019-0099-1.

Clerici, M., M.P.A. Luna-Vargas, A.C. Faesen, and T.K. Sixma. 2014. The DUSP–Ubl domain of USP4 enhances its catalytic efficiency by promoting ubiquitin exchange. *Nat. Commun.* 5. doi:10.1038/ncomms6399.

Cohen, G.M. 1997. Caspases: the executioners of apoptosis. *Biochem. J.* 326:1–16. doi:10.1042/bj3260001.

Cope, G.A. 2002. Role of Predicted Metalloprotease Motif of Jab1/Csn5 in Cleavage of Nedd8 from Cul1. *Science*. 298:608–611. doi:10.1126/science.1075901.

Cornelissen, T., D. Haddad, F. Wauters, C. Van Humbeeck, W. Mandemakers, B. Koentjoro, C. Sue, K. Gevaert, B. De Strooper, P. Verstreken, and W. Vandenberghe. 2014. The deubiquitinase USP15 antagonizes Parkin-mediated mitochondrial ubiquitination and mitophagy. *Hum. Mol. Genet.* 23:5227–5242. doi:10.1093/hmg/ddu244.

Costello, J.L., I.G. Castro, F. Camões, T.A. Schrader, D. McNeall, J. Yang, E.-A. Giannopoulou, S. Gomes, V. Pogenberg, N.A. Bonekamp, D. Ribeiro, M. Wilmanns, G. Jedd, M. Islinger, and M. Schrader. 2017. Predicting the targeting of tail-anchored proteins to subcellular compartments in mammalian cells. *J. Cell Sci.* 130:1675–1687. doi:10.1242/jcs.200204.

Coultas, L., M. Pellegrini, J.E. Visvader, G.J. Lindeman, L. Chen, J.M. Adams, D.C.S. Huang, and A. Strasser. 2003. Bfk: a novel weakly proapoptotic member of the Bcl-2 protein family with a BH3 and a BH2 region. *Cell Death Differ.* 10:185–192. doi:10.1038/sj.cdd.4401204.

Coux, O., K. Tanaka, and A.L. Goldberg. 1996. Structure and Functions of the 20S and 26S Proteasomes. *Annu. Rev. Biochem.* 65:801–847. doi:10.1146/annurev.bi.65.070196.004101.

Covill-Cooke, C., V.S. Toncheva, J. Drew, N. Birsa, G. López-Doménech, and J.T. Kittler. 2020. Peroxisomal fission is modulated by the mitochondrial Rho-GTPases, Miro1 and Miro2. *EMBO Rep.* 21. doi:10.15252/embr.201949865.

Cox, J., and M. Mann. 2008. MaxQuant enables high peptide identification rates, individualized p.p.b.-range mass accuracies and proteome-wide protein quantification. *Nat. Biotechnol.* 26:1367–1372. doi:10.1038/nbt.1511.

Crighton, D., S. Wilkinson, J. O'Prey, N. Syed, P. Smith, P.R. Harrison, M. Gasco, O. Garrone, T. Crook, and K.M. Ryan. 2006. DRAM, a p53-Induced Modulator of Autophagy, Is Critical for Apoptosis. *Cell*. 126:121–134. doi:10.1016/j.cell.2006.05.034.

Crighton, D., S. Wilkinson, and K.M. Ryan. 2007. DRAM links autophagy to p53 and programmed cell death. *Autophagy*. 3:72–74. doi:10.4161/auto.3438.

Cunningham, C.N., J.M. Baughman, L. Phu, J.S. Tea, C. Yu, M. Coons, D.S. Kirkpatrick, B. Bingol, and J.E. Corn. 2015. USP30 and parkin homeostatically regulate atypical ubiquitin chains on mitochondria. *Nat. Cell Biol.* 17:160–169. doi:10.1038/ncb3097.

Czabotar, P.E., E.F. Lee, M.F. van Delft, C.L. Day, B.J. Smith, D.C.S. Huang, W.D. Fairlie, M.G. Hinds, and P.M. Colman. 2007. Structural insights into the degradation of Mcl-1 induced by BH3 domains. *Proc. Natl. Acad. Sci. U. S. A.* 104:6217–6222. doi:10.1073/pnas.0701297104.

Dadakhujaev, S., E.J. Jung, H.S. Noh, Y.-S. Hah, C.J. Kim, and D.R. Kim. 2009. Interplay between autophagy and apoptosis in TrkA-induced cell death. *Autophagy*. 5:103–105. doi:10.4161/auto.5.1.7276.

Daou, S., I. Hammond-Martel, N. Mashtalir, H. Barbour, J. Gagnon, N.V.G. Iannantuono, N.S. Nkwe, A. Motorina, H. Pak, H. Yu, H. Wurtele, E. Milot, F.A. Mallette, M. Carbone, and E.B. Affar. 2015. The BAP1/ASXL2 Histone H2A Deubiquitinase Complex Regulates Cell Proliferation and Is Disrupted in Cancer. *J. Biol. Chem.* 290:28643–28663. doi:10.1074/jbc.M115.661553.

D'Arcy, M.S. 2019. Cell death: a review of the major forms of apoptosis, necrosis and autophagy. *Cell Biol. Int.* 43:582–592. doi:10.1002/cbin.11137.

Daskalaki, I., I. Gkikas, and N. Tavernarakis. 2018. Hypoxia and Selective Autophagy in Cancer Development and Therapy. *Front. Cell Dev. Biol.* 6. doi:10.3389/fcell.2018.00104.

Datta, S.R., H. Dudek, X. Tao, S. Masters, H. Fu, Y. Gotoh, and M.E. Greenberg. 1997. Akt Phosphorylation of BAD Couples Survival Signals to the Cell-Intrinsic Death Machinery. *Cell*. 91:231–241. doi:10.1016/S0092-8674(00)80405-5.

Davids, M.S., and A. Letai. 2013. ABT-199: Taking Dead Aim at BCL-2. *Cancer Cell*. 23:139–141. doi:10.1016/j.ccr.2013.01.018.

De Cesare, V., D. Carbajo Lopez, P.D. Mabbitt, A.J. Fletcher, M. Soetens, O. Antico, N.T. Wood, and S. Virdee. 2021. Deubiquitinating enzyme amino acid profiling reveals a class of ubiquitin esterases. *Proc. Natl. Acad. Sci.* 118:e2006947118. doi:10.1073/pnas.2006947118.

Deas, E., H. Plun-Favreau, S. Gandhi, H. Desmond, S. Kjaer, S.H.Y. Loh, A.E.M. Renton, R.J. Harvey, A.J. Whitworth, L.M. Martins, A.Y. Abramov, and N.W. Wood. 2011. PINK1 cleavage at position A103 by the mitochondrial protease PARL. *Hum. Mol. Genet.* 20:867–879. doi:10.1093/hmg/ddq526.

Debrincat, M.A., I. Pleines, M. Lebois, R.M. Lane, M.L. Holmes, J. Corbin, C.J. Vandenberg, W.S. Alexander, A.P. Ng, A. Strasser, P. Bouillet, M. Sola-Visner, B.T. Kile, and E.C. Josefsson. 2015. BCL-2 is dispensable for thrombopoiesis and platelet survival. *Cell Death Dis.* 6:e1721–e1721. doi:10.1038/cddis.2015.97.

Decout, A., J.D. Katz, S. Venkatraman, and A. Ablasser. 2021. The cGAS–STING pathway as a therapeutic target in inflammatory diseases. *Nat. Rev. Immunol.* doi:10.1038/s41577-021-00524-z.

Decuypere, J.-P., J.B. Parys, and G. Bultynck. 2012. Regulation of the Autophagic Bcl-2/Beclin 1 Interaction. *Cells*. 1:284–312. doi:10.3390/cells1030284.

Dehan, E., F. Bassermann, D. Guardavaccaro, G. Vasiliver-Shamis, M. Cohen, K.N. Lowes, M. Dustin, D.C.S. Huang, J. Taunton, and M. Pagano. 2009. betaTrCP- and Rsk1/2-mediated degradation of BimEL inhibits apoptosis. *Mol. Cell*. 33:109–116. doi:10.1016/j.molcel.2008.12.020.

Dekker, F.J., O. Rocks, N. Vartak, S. Menninger, C. Hedberg, R. Balamurugan, S. Wetzel, S. Renner, M. Gerauer, B. Schölermann, M. Rusch, J.W. Kramer, D. Rauh, G.W. Coates, L. Brunsveld, P.I.H. Bastiaens, and H. Waldmann. 2010. Small-molecule inhibition of APT1 affects Ras localization and signaling. *Nat. Chem. Biol.* 6:449–456. doi:10.1038/nchembio.362.

Delbridge, A.R.D., and A. Strasser. 2015. The BCL-2 protein family, BH3-mimetics and cancer therapy. *Cell Death Differ.* 22:1071–1080. doi:10.1038/cdd.2015.50.

Deosaran, E., K.B. Larsen, R. Hua, G. Sargent, Y. Wang, S. Kim, T. Lamark, M. Jauregui, K. Law, J. Lippincott-Schwartz, A. Brech, T. Johansen, and P.K. Kim. 2013. NBR1 acts as an autophagy receptor for peroxisomes. *J. Cell Sci.* 126:939–952. doi:10.1242/jcs.114819.

Desagher, S., A. Osen-Sand, A. Nichols, R. Eskes, S. Montessuit, S. Lauper, K. Maundrell, B. Antonsson, and J.C. Martinou. 1999. Bid-induced conformational change of Bax is responsible for mitochondrial cytochrome c release during apoptosis. *J. Cell Biol.* 144:891–901. doi:10.1083/jcb.144.5.891.

Deshaies, R.J., and C.A.P. Joazeiro. 2009. RING Domain E3 Ubiquitin Ligases. *Annu. Rev. Biochem.* 78:399–434. doi:10.1146/annurev.biochem.78.101807.093809.

Deter, R.L., and C. de Duve. 1967. INFLUENCE OF GLUCAGON, AN INDUCER OF CELLULAR AUTOPHAGY, ON SOME PHYSICAL PROPERTIES OF RAT LIVER LYSOSOMES. *J. Cell Biol.* 33:437–449. doi:10.1083/jcb.33.2.437.

Dewson, G. 2001. Bax to the wall: Bax- and Bak-induced mitochondrial dysfunction in apoptosis. *Trends Biochem. Sci.* 26:353. doi:10.1016/S0968-0004(01)01889-8.

Dewson, G., T. Kratina, H.W. Sim, H. Puthalakath, J.M. Adams, P.M. Colman, and R.M. Kluck. 2008. To Trigger Apoptosis, Bak Exposes Its BH3 Domain and Homodimerizes via BH3:Groove Interactions. *Mol. Cell*. 30:369–380. doi:10.1016/j.molcel.2008.04.005.

Dikic, I., and Z. Elazar. 2018. Mechanism and medical implications of mammalian autophagy. *Nat. Rev. Mol. Cell Biol.* 19:349–364. doi:10.1038/s41580-018-0003-4.

Dimova, N.V., N.A. Hathaway, B.-H. Lee, D.S. Kirkpatrick, M.L. Berkowitz, S.P. Gygi, D. Finley, and R.W. King. 2012. APC/C-mediated multiple monoubiquitylation provides an alternative degradation signal for cyclin B1. *Nat. Cell Biol.* 14:168–176. doi:10.1038/ncb2425.

Ding, Q., X. He, J.-M. Hsu, W. Xia, C.-T. Chen, L.-Y. Li, D.-F. Lee, J.-C. Liu, Q. Zhong, X. Wang, and M.-C. Hung. 2007. Degradation of Mcl-1 by β-TrCP Mediates Glycogen Synthase Kinase 3-Induced Tumor Suppression and Chemosensitization. *Mol. Cell. Biol.* 27:4006–4017. doi:10.1128/MCB.00620-06.

Ding, W.-X., and X.-M. Yin. 2012. Mitophagy: mechanisms, pathophysiological roles, and analysis. *Biol. Chem.* 393:547–564. doi:10.1515/hsz-2012-0119.

Dittmar, G., and K.F. Winklhofer. 2020. Linear Ubiquitin Chains: Cellular Functions and Strategies for Detection and Quantification. *Front. Chem.* 7. doi:10.3389/fchem.2019.00915.

Doménech, E., C. Maestre, L. Esteban-Martínez, D. Partida, R. Pascual, G. Fernández-Miranda, E. Seco, R. Campos-Olivas, M. Pérez, D. Megias, K. Allen, M. López, A.K. Saha, G. Velasco, E. Rial, R. Méndez, P. Boya, M. Salazar-Roa, and M. Malumbres. 2015. AMPK and PFKFB3 mediate glycolysis and survival in response to mitophagy during mitotic arrest. *Nat. Cell Biol.* 17:1304–1316. doi:10.1038/ncb3231.

Dooley, H.C., M.I. Wilson, and S.A. Tooze. 2015. WIPI2B links PtdIns3P to LC3 lipidation through binding ATG16L1. *Autophagy*. 11:190–191. doi:10.1080/15548627.2014.996029.

Draber, P., S. Kupka, M. Reichert, H. Draberova, E. Lafont, D. de Miguel, L. Spilgies, S. Surinova, L. Taraborrelli, T. Hartwig, E. Rieser, L. Martino, K. Rittinger, and H. Walczak. 2015. LUBAC-Recruited CYLD and A20 Regulate Gene Activation and Cell Death by Exerting Opposing Effects on Linear Ubiquitin in Signaling Complexes. *Cell Rep.* 13:2258–2272. doi:10.1016/j.celrep.2015.11.009.

Duda, D.M., L.A. Borg, D.C. Scott, H.W. Hunt, M. Hammel, and B.A. Schulman. 2008. Structural Insights into NEDD8 Activation of Cullin-RING Ligases: Conformational Control of Conjugation. *Cell*. 134:995–1006. doi:10.1016/j.cell.2008.07.022.

Durcan, T.M., M.Y. Tang, J.R. Pérusse, E.A. Dashti, M.A. Aguileta, G.-L. McLelland, P. Gros, T.A. Shaler, D. Faubert, B. Coulombe, and E.A. Fon. 2014. USP8 regulates mitophagy by removing K6-linked ubiquitin conjugates from parkin. *EMBO J.* 33:2473–2491. doi:10.15252/embj.201489729.

Dynek, J.N., T. Goncharov, E.C. Dueber, A.V. Fedorova, A. Izrael-Tomasevic, L. Phu, E. Helgason, W.J. Fairbrother, K. Deshayes, D.S. Kirkpatrick, and D. Vucic. 2010. c-IAP1 and UbcH5 promote K11-linked polyubiquitination of RIP1 in TNF signalling. *EMBO J.* 29:4198–4209. doi:10.1038/emboj.2010.300.

Ebato, C., T. Uchida, M. Arakawa, M. Komatsu, T. Ueno, K. Komiya, K. Azuma, T. Hirose, K. Tanaka, E. Kominami, R. Kawamori, Y. Fujitani, and H. Watada. 2008. Autophagy Is Important in Islet Homeostasis and Compensatory Increase of Beta Cell Mass in Response to High-Fat Diet. *Cell Metab.* 8:325–332. doi:10.1016/j.cmet.2008.08.009.

Eccles, R.L., M.T. Czajkowski, C. Barth, P.M. Müller, E. McShane, S. Grunwald, P. Beaudette, N. Mecklenburg, R. Volkmer, K. Zühlke, G. Dittmar, M. Selbach, A. Hammes, O. Daumke, E. Klussmann, S. Urbé, and O. Rocks. 2016. Bimodal antagonism of PKA signalling by ARHGAP36. *Nat. Commun.* 7:12963. doi:10.1038/ncomms12963.

Eddins, M.J., C.M. Carlile, K.M. Gomez, C.M. Pickart, and C. Wolberger. 2006. Mms2–Ubc13 covalently bound to ubiquitin reveals the structural basis of linkage-specific polyubiquitin chain formation. *Nat. Struct. Mol. Biol.* 13:915–920. doi:10.1038/nsmb1148.

Eddins, M.J., R. Varadan, D. Fushman, C.M. Pickart, and C. Wolberger. 2007. Crystal Structure and Solution NMR Studies of Lys48-linked Tetraubiquitin at Neutral pH. *J. Mol. Biol.* 367:204–211. doi:10.1016/j.jmb.2006.12.065.

Edlich, F., S. Banerjee, M. Suzuki, M.M. Cleland, D. Arnoult, C. Wang, A. Neutzner, N. Tjandra, and R.J. Youle. 2011. Bcl-xLretrotranslocates Bax from the mitochondria into the cytosol. *Cell*. 145:104–116. doi:10.1016/j.cell.2011.02.034.

Edmonson, A.M., D.K. Mayfield, V. Vervoort, B.R. DuPont, and G. Argyropoulos. 2002. Characterization of a Human Import Component of the Mitochondrial Outer Membrane, TOMM70A. *Cell Commun. Adhes.* 9:15–27. doi:10.1080/15419060212186.

Eisner, V., M. Picard, and G. Hajnóczky. 2018. Mitochondrial dynamics in adaptive and maladaptive cellular stress responses. *Nat. Cell Biol.* 20:755–765. doi:10.1038/s41556-018-0133-0.

Elia, A.E.H., A.P. Boardman, D.C. Wang, E.L. Huttlin, R.A. Everley, N. Dephoure, C. Zhou, I. Koren, S.P. Gygi, and S.J. Elledge. 2015. Quantitative Proteomic Atlas of Ubiquitination and Acetylation in the DNA Damage Response. *Mol. Cell*. 59:867–881. doi:10.1016/j.molcel.2015.05.006.

Elliott, P.R., and D. Komander. 2016. Regulation of Met1-linked polyubiquitin signalling by the deubiquitinase OTULIN. *FEBS J.* 283:39–53. doi:10.1111/febs.13547.

Elliott, P.R., D. Leske, M. Hrdinka, K. Bagola, B.K. Fiil, S.H. McLaughlin, J. Wagstaff, N. Volkmar, J.C. Christianson, B.M. Kessler, S.M.V. Freund, D. Komander, and M. Gyrd-Hansen. 2016. SPATA2 Links CYLD to LUBAC, Activates CYLD, and Controls LUBAC Signaling. *Mol. Cell*. 63:990–1005. doi:10.1016/j.molcel.2016.08.001.

Elliott, P.R., S.V. Nielsen, P. Marco-Casanova, B.K. Fiil, K. Keusekotten, N. Mailand, S.M.V. Freund, M. Gyrd-Hansen, and D. Komander. 2014. Molecular basis and regulation of OTULIN-LUBAC interaction. *Mol. Cell*. 54:335–348. doi:10.1016/j.molcel.2014.03.018.

Ellis, H. 1986. Genetic control of programmed cell death in the nematode C. elegans. *Cell*. 44:817–829. doi:10.1016/0092-8674(86)90004-8.

Elmore, S. 2007. Apoptosis: A Review of Programmed Cell Death. *Toxicol. Pathol.* 35:495–516. doi:10.1080/01926230701320337.

Emmerich, C.H., A. Ordureau, S. Strickson, J.S.C. Arthur, P.G.A. Pedrioli, D. Komander, and P. Cohen. 2013. Activation of the canonical IKK complex by K63/M1-linked hybrid ubiquitin chains. *Proc. Natl. Acad. Sci.* 110:15247–15252. doi:10.1073/pnas.1314715110.

Esteban-Martínez, L., E. Sierra-Filardi, R.S. McGreal, M. Salazar-Roa, G. Mariño, E. Seco, S. Durand, D. Enot, O. Graña, M. Malumbres, A. Cvekl, A.M. Cuervo, G. Kroemer, and P. Boya. 2017. Programmed mitophagy is essential for the glycolytic switch during cell differentiation. *EMBO J.* 36:1688–1706. doi:10.15252/embj.201695916.

Etlinger, J.D., and A.L. Goldberg. 1977. A soluble ATP-dependent proteolytic system responsible for the degradation of abnormal proteins in reticulocytes. *Proc. Natl. Acad. Sci.* 74:54–58. doi:10.1073/pnas.74.1.54.

Fang, X., S. Yu, A. Eder, M. Mao, R.C. Bast, D. Boyd, and G.B. Mills. 1999. Regulation of BAD phosphorylation at serine 112 by the Ras-mitogen-activated protein kinase pathway. *Oncogene*. 18:6635–6640. doi:10.1038/sj.onc.1203076.

Fiesel, F.C., E.D. James, R. Hudec, and W. Springer. 2017. Mitochondrial targeted HSP90 inhibitor Gamitrinib-TPP (G-TPP) induces PINK1/Parkin-dependent mitophagy. *Oncotarget*. 8:106233–106248. doi:10.18632/oncotarget.22287.

Finley, D., S. Sadis, B.P. Monia, P. Boucher, D.J. Ecker, S.T. Crooke, and V. Chau. 1994. Inhibition of proteolysis and cell cycle progression in a multiubiquitination-deficient yeast mutant. *Mol. Cell. Biol.* 14:5501–5509. doi:10.1128/MCB.14.8.5501.

Fortin, A., S.P. Cregan, J.G. MacLaurin, N. Kushwaha, E.S. Hickman, C.S. Thompson, A. Hakim, P.R. Albert, F. Cecconi, K. Helin, D.S. Park, and R.S. Slack. 2001. APAF1 is a key transcriptional target for p53 in the regulation of neuronal cell death. *J. Cell Biol.* 155:207–216. doi:10.1083/jcb.200105137.

Fouad, S., O.S. Wells, M.A. Hill, and V. D'Angiolella. 2019. Cullin Ring Ubiquitin Ligases (CRLs) in Cancer: Responses to Ionizing Radiation (IR) Treatment. *Front. Physiol.* 10. doi:10.3389/fphys.2019.01144.

Francisco, T., T.A. Rodrigues, M.O. Freitas, C.P. Grou, A.F. Carvalho, C. Sá-Miranda, M.P. Pinto, and J.E. Azevedo. 2013. A Cargo-centered Perspective on the PEX5 Receptor-mediated Peroxisomal Protein Import Pathway. *J. Biol. Chem.* 288:29151–29159. doi:10.1074/jbc.M113.487140.

Freemont, P.S., I.M. Hanson, and J. Trowsdale. 1991. A novel gysteine-rich sequence motif. *Cell*. 64:483–484. doi:10.1016/0092-8674(91)90229-R.

Fu, M., P. St-Pierre, J. Shankar, P.T.C. Wang, B. Joshi, and I.R. Nabi. 2013. Regulation of mitophagy by the Gp78 E3 ubiquitin ligase. *Mol. Biol. Cell*. 24:1153–1162. doi:10.1091/mbc.E12-08-0607.

Gan, C., D. Pierscianek, N. El Hindy, Y. Ahmadipour, K. Keyvani, U. Sure, and Y. Zhu. 2020. The predominant expression of cancer stem cell marker ALDH1A3 in tumor infiltrative area is associated with shorter overall survival of human glioblastoma. *BMC Cancer*. 20:672. doi:10.1186/s12885-020-07153-0.

Ganley, I.G., D.H. Lam, J. Wang, X. Ding, S. Chen, and X. Jiang. 2009. ULK1·ATG13·FIP200 Complex Mediates mTOR Signaling and Is Essential for Autophagy. *J. Biol. Chem.* 284:12297–12305. doi:10.1074/jbc.M900573200.

Gao, H.-M., P.T. Kotzbauer, K. Uryu, S. Leight, J.Q. Trojanowski, and V.M.-Y. Lee. 2008. Neuroinflammation and oxidation/nitration of alpha-synuclein linked to dopaminergic neurodegeneration. *J. Neurosci. Off. J. Soc. Neurosci.* 28:7687–7698. doi:10.1523/JNEUROSCI.0143-07.2008.

Garcia-Ratés, S., and S. Greenfield. 2017. Cancer and neurodegeneration: two sides, same coin? *Oncotarget*. 8:22307–22308. doi:10.18632/oncotarget.16190.

Garneau, J.E., M.-È. Dupuis, M. Villion, D.A. Romero, R. Barrangou, P. Boyaval, C. Fremaux, P. Horvath, A.H. Magadán, and S. Moineau. 2010. The CRISPR/Cas bacterial immune system cleaves bacteriophage and plasmid DNA. *Nature*. 468:67–71. doi:10.1038/nature09523.

Gatti, M., S. Pinato, A. Maiolica, F. Rocchio, M.G. Prato, R. Aebersold, and L. Penengo. 2015. RNF168 Promotes Noncanonical K27 Ubiquitination to Signal DNA Damage. *Cell Rep.* 10:226–238. doi:10.1016/j.celrep.2014.12.021.

Gaullier, J.-M., D. Gillooly, A. Simonsen, and H. Stenmark. 1999. Regulation of endocytic membrane traffic by phosphatidylinositol 3-phosphate. *Biochem. Soc. Trans.* 27:666–670. doi:10.1042/bst0270666.

Ge, P., V.L. Dawson, and T.M. Dawson. 2020. PINK1 and Parkin mitochondrial quality control: a source of regional vulnerability in Parkinson's disease. *Mol. Neurodegener.* 15:20. doi:10.1186/s13024-020-00367-7.

George, S., and P. Brundin. 2015. Immunotherapy in Parkinson's Disease: Micromanaging Alpha-Synuclein Aggregation. *J. Park. Dis.* 5:413–424. doi:10.3233/JPD-150630.

Gerlach, B., S.M. Cordier, A.C. Schmukle, C.H. Emmerich, E. Rieser, T.L. Haas, A.I. Webb, J.A. Rickard, H. Anderton, W.W.-L. Wong, U. Nachbur, L. Gangoda, U. Warnken, A.W. Purcell, J. Silke, and H. Walczak. 2011. Linear ubiquitination prevents inflammation and

regulates immune signalling. *Nature*. 471:591–596. doi:10.1038/nature09816.

Gersch, M., C. Gladkova, A.F. Schubert, M.A. Michel, S. Maslen, and D. Komander. 2017. Mechanism and regulation of the Lys6-selective deubiquitinase USP30. *Mol. Biol.* 24:16.

Giam, M., D.C.S. Huang, and P. Bouillet. 2008. BH3-only proteins and their roles in programmed cell death. *Oncogene*. 27:S128–S136. doi:10.1038/onc.2009.50.

Goedert, M., M.G. Spillantini, R. Jakes, D. Rutherford, and R.A. Crowther. 1989. Multiple isoforms of human microtubule-associated protein tau: sequences and localization in neurofibrillary tangles of Alzheimer's disease. *Neuron*. 3:519–526. doi:10.1016/0896-6273(89)90210-9.

Goedert, M., C.M. Wischik, R.A. Crowther, J.E. Walker, and A. Klug. 1988. Cloning and sequencing of the cDNA encoding a core protein of the paired helical filament of Alzheimer disease: identification as the microtubule-associated protein tau. *Proc. Natl. Acad. Sci.* 85:4051–4055. doi:10.1073/pnas.85.11.4051.

Goldknopf, I.L., and H. Busch. 1977. Isopeptide linkage between nonhistone and histone 2A polypeptides of chromosomal conjugate-protein A24. *Proc. Natl. Acad. Sci.* 74:864–868. doi:10.1073/pnas.74.3.864.

Goldstein, G., M. Scheid, U. Hammerling, D.H. Schlesinger, H.D. Niall, and E.A. Boyse. 1975. Isolation of a polypeptide that has lymphocyte-differentiating properties and is probably represented universally in living cells. *Proc. Natl. Acad. Sci.* 72:11–15. doi:10.1073/pnas.72.1.11.

Gomez-Bougie, P., E. Ménoret, P. Juin, C. Dousset, C. Pellat-Deceunynck, and M. Amiot. 2011. Noxa controls Mule-dependent Mcl-1 ubiquitination through the regulation of the Mcl-1/USP9X interaction. *Biochem. Biophys. Res. Commun.* 413:460–464. doi:10.1016/j.bbrc.2011.08.118.

Gong, L., and E.T.H. Yeh. 1999. Identification of the Activating and Conjugating Enzymes of the NEDD8 Conjugation Pathway. *J. Biol. Chem.* 274:12036–12042. doi:10.1074/jbc.274.17.12036.

Gong, Y., T.I. Zack, L.G.T. Morris, K. Lin, E. Hukkelhoven, R. Raheja, I.L. Tan, S. Turcan, S. Veeriah, S. Meng, A. Viale, S.E. Schumacher, P. Palmedo, R. Beroukhim, and T.A. Chan. 2014. Pan-cancer genetic analysis identifies PARK2 as a master regulator of G1/S cyclins. *Nat. Genet.* 46:588–594. doi:10.1038/ng.2981.

Goodrich, J.S. 2004. Hrb27C, Sqd and Otu cooperatively regulate gurken RNA localization and mediate nurse cell chromosome dispersion in Drosophila oogenesis. *Development*. 131:1949–1958. doi:10.1242/dev.01078.

Gouw, A.M., L.S. Eberlin, K. Margulis, D.K. Sullivan, G.G. Toal, L. Tong, R.N. Zare, and D.W. Felsher. 2017. Oncogene KRAS activates fatty acid synthase, resulting in specific ERK and lipid signatures associated with lung adenocarcinoma. *Proc. Natl. Acad. Sci. U. S. A.* 114:4300–4305. doi:10.1073/pnas.1617709114.

Greaves, G., M. Milani, M. Butterworth, R.J. Carter, D.P. Byrne, P.A. Eyers, X. Luo, G.M. Cohen, and S. Varadarajan. 2019. BH3-only proteins are dispensable for apoptosis induced by pharmacological inhibition of both MCL-1 and BCL-XL. *Cell Death Differ.* 26:1037–1047. doi:10.1038/s41418-018-0183-7.

Grenfell, S.J., J.S. Trausch-Azar, P.M. Handley-Gearhart, A. Ciechanover, and A.L. Schwartz. 1994. Nuclear localization of the ubiquitin-activating enzyme, E1, is cell-cycle-dependent. *Biochem. J.* 300:701–708. doi:10.1042/bj3000701.

Grice, G.L., I.T. Lobb, M.P. Weekes, S.P. Gygi, R. Antrobus, and J.A. Nathan. 2015. The Proteasome Distinguishes between Heterotypic and Homotypic Lysine-11-Linked Polyubiquitin Chains. *Cell Rep.* 12:545–553. doi:10.1016/j.celrep.2015.06.061.

Griewahn, L., A. Köser, and U. Maurer. 2019. Keeping Cell Death in Check: Ubiquitylation-Dependent Control of TNFR1 and TLR Signaling. *Front. Cell Dev. Biol.* 7:117. doi:10.3389/fcell.2019.00117.

Grotegut, S., D. von Schweinitz, G. Christofori, and F. Lehembre. 2006. Hepatocyte growth factor induces cell scattering through MAPK/Egr-1-mediated upregulation of Snail. *EMBO J.* 25:3534–3545. doi:10.1038/sj.emboj.7601213.

Grou, C.P., T. Francisco, T.A. Rodrigues, M.O. Freitas, M.P. Pinto, A.F. Carvalho, P. Domingues, S.A. Wood, J.E. Rodríguez-Borges, C. Sá-Miranda, M. Fransen, and J.E. Azevedo. 2012. Identification of Ubiquitin-specific Protease 9X (USP9X) as a Deubiquitinase Acting on Ubiquitin-Peroxin 5 (PEX5) Thioester Conjugate*. *J. Biol. Chem.* 287:12815–12827. doi:10.1074/jbc.M112.340158.

Gu, L., Y. Zhu, X. Lin, B. Lu, X. Zhou, F. Zhou, Q. Zhao, E.V. Prochownik, and Y. Li. 2020. The IKKβ-USP30-ACLY Axis Controls Lipogenesis and Tumorigenesis. *Hepatology*. doi:10.1002/hep.31249.

Guang, M.H.Z., E.L. Kavanagh, L.P. Dunne, P. Dowling, L. Zhang, S. Lindsay, D. Bazou, C.Y. Goh, C. Hanley, G. Bianchi, K.C. Anderson, P. O'Gorman, and A. McCann. 2019. Targeting Proteotoxic Stress in Cancer: A Review of the Role that Protein Quality Control Pathways Play in Oncogenesis. *Cancers*. 11. doi:10.3390/cancers11010066.

Guaragnella, N., S. Giannattasio, and L. Moro. 2014. Mitochondrial dysfunction in cancer chemoresistance. *Biochem. Pharmacol.* 92:62–72. doi:10.1016/j.bcp.2014.07.027.

Guerra, F., N. Guaragnella, A.A. Arbini, C. Bucci, S. Giannattasio, and L. Moro. 2017. Mitochondrial Dysfunction: A Novel Potential Driver of Epithelial-to-Mesenchymal Transition in Cancer. *Front. Oncol.* 7:295. doi:10.3389/fonc.2017.00295.

Gundogdu, M., R. Tadayon, G. Salzano, G.S. Shaw, and H. Walden. 2021. A mechanistic review of Parkin activation. *Biochim. Biophys. Acta BBA - Gen. Subj.* 1865:129894. doi:10.1016/j.bbagen.2021.129894.

Gupta, A., S. Anjomani-Virmouni, N. Koundouros, M. Dimitriadi, R. Choo-Wing, A. Valle, Y. Zheng, Y.-H. Chiu, S. Agnihotri, G. Zadeh, J.M. Asara, D. Anastasiou, M.J. Arends, L.C. Cantley, and G. Poulogiannis. 2017a. PARK2 Depletion Connects Energy and Oxidative Stress to PI3K/Akt Activation via PTEN S-Nitrosylation. *Mol. Cell*. 65:999-1013.e7. doi:10.1016/j.molcel.2017.02.019.

Gupta, A., S. Anjomani-Virmouni, N. Koundouros, and G. Poulogiannis. 2017b. *PARK2* loss promotes cancer progression via redox-mediated inactivation of PTEN. *Mol. Cell. Oncol.* 4:e1329692. doi:10.1080/23723556.2017.1329692.

Gupta, I., K. Singh, N.K. Varshney, and S. Khan. 2018. Delineating Crosstalk Mechanisms of the Ubiquitin Proteasome System That Regulate Apoptosis. *Front. Cell Dev. Biol.* 6:11. doi:10.3389/fcell.2018.00011.

Gutierrez, M.G., D.B. Munafó, W. Berón, and M.I. Colombo. 2004. Rab7 is required for the normal progression of the autophagic pathway in mammalian cells. *J. Cell Sci.* 117:2687–2697. doi:10.1242/jcs.01114.

Haahr, P., N. Borgermann, X. Guo, D. Typas, D. Achuthankutty, S. Hoffmann, R. Shearer, T.K. Sixma, and N. Mailand. 2018. ZUFSP Deubiquitylates K63-Linked Polyubiquitin Chains to Promote Genome Stability. *Mol. Cell*. 70:165-174.e6. doi:10.1016/j.molcel.2018.02.024.

Haas, A.L., J.V. Warms, A. Hershko, and I.A. Rose. 1982. Ubiquitin-activating enzyme. Mechanism and role in protein-ubiquitin conjugation. *J. Biol. Chem.* 257:2543–2548.

Haas, T.L., C.H. Emmerich, B. Gerlach, A.C. Schmukle, S.M. Cordier, E. Rieser, R. Feltham, J. Vince, U. Warnken, T. Wenger, R. Koschny, D. Komander, J. Silke, and H. Walczak. 2009. Recruitment of the Linear Ubiquitin Chain Assembly Complex Stabilizes the TNF-R1 Signaling Complex and Is Required for TNF-Mediated Gene Induction. *Mol. Cell*. 36:831–844. doi:10.1016/j.molcel.2009.10.013.

Hafner, A., M.L. Bulyk, A. Jambhekar, and G. Lahav. 2019. The multiple mechanisms that regulate p53 activity and cell fate. *Nat. Rev. Mol. Cell Biol.* 20:199–210. doi:10.1038/s41580-019-0110-x.

Hamazaki, J., S. Iemura, T. Natsume, H. Yashiroda, K. Tanaka, and S. Murata. 2006. A novel proteasome interacting protein recruits the

deubiquitinating enzyme UCH37 to 26S proteasomes. *EMBO J.* 25:4524–4536. doi:10.1038/sj.emboj.7601338.

Han, J., L.A. Goldstein, W. Hou, and H. Rabinowich. 2007. Functional Linkage between NOXA and Bim in Mitochondrial Apoptotic Events. *J. Biol. Chem.* 282:16223–16231. doi:10.1074/jbc.M611186200.

Han, W., H. Pan, Y. Chen, J. Sun, Y. Wang, J. Li, W. Ge, L. Feng, X. Lin, X. Wang, X. Wang, and H. Jin. 2011. EGFR Tyrosine Kinase Inhibitors Activate Autophagy as a Cytoprotective Response in Human Lung Cancer Cells. *PLoS ONE*. 6:e18691. doi:10.1371/journal.pone.0018691.

Hanahan, D., and R.A. Weinberg. 2011. Hallmarks of cancer: The next generation. *Cell*. 144:646–674. doi:10.1016/j.cell.2011.02.013.

Hanahan, D., R.A. Weinberg, and S. Francisco. 2000. The Hallmarks of Cancer Review University of California at San Francisco. 100:57–70.

Hara, T., K. Nakamura, M. Matsui, A. Yamamoto, Y. Nakahara, R. Suzuki-Migishima, M. Yokoyama, K. Mishima, I. Saito, H. Okano, and N. Mizushima. 2006. Suppression of basal autophagy in neural cells causes neurodegenerative disease in mice. *Nature*. 441:885–889. doi:10.1038/nature04724.

Hara, T., A. Takamura, C. Kishi, S.-I. Iemura, T. Natsume, J.-L. Guan, and N. Mizushima. 2008. FIP200, a ULK-interacting protein, is required for autophagosome formation in mammalian cells. *J. Cell Biol.* 181:497–510. doi:10.1083/jcb.200712064.

Harbour, J.W., M.D. Onken, E.D.O. Roberson, S. Duan, L. Cao, L.A. Worley, M.L. Council, K.A. Matatall, C. Helms, and A.M. Bowcock. 2010. Frequent Mutation of BAP1 in Metastasizing Uveal Melanomas. *Science*. 330:1410–1413. doi:10.1126/science.1194472.

Harrigan, J.A., X. Jacq, N.M. Martin, and S.P. Jackson. 2018. Deubiquitylating enzymes and drug discovery: emerging opportunities. *Nat. Rev. Drug Discov.* 17:57–78. doi:10.1038/nrd.2017.152.

Hart, L.S., J.T. Cunningham, T. Datta, S. Dey, F. Tameire, S.L. Lehman, B. Qiu, H. Zhang, G. Cerniglia, M. Bi, Y. Li, Y. Gao, H. Liu, C. Li, A. Maity, A. Thomas-Tikhonenko, A.E. Perl, A. Koong, S.Y. Fuchs, J.A. Diehl, I.G. Mills, D. Ruggero, and C. Koumenis. 2012. ER stress-mediated autophagy promotes Myc-dependent transformation and tumor growth. *J. Clin. Invest.* 122:4621–4634. doi:10.1172/JCI62973.

Hassink, G.C., B. Zhao, R. Sompallae, M. Altun, S. Gastaldello, N.V. Zinin, M.G. Masucci, and K. Lindsten. 2009. The ER-resident ubiquitin-specific protease 19 participates in the UPR and rescues ERAD substrates. *EMBO Rep.* 10:755–761. doi:10.1038/embor.2009.69.

He, W., L. Zhang, O.D. Villarreal, R. Fu, E. Bedford, J. Dou, A.Y. Patel, M.T. Bedford, X. Shi, T. Chen, B. Bartholomew, and H. Xu. 2019. De novo identification of essential protein domains from CRISPR-Cas9 tiling-sgRNA knockout screens. *Nat. Commun.* 10:4541. doi:10.1038/s41467-019-12489-8.

Hengartner, M.O., R. Ellis, and R. Horvitz. 1992. Caenorhabditis elegans gene ced-9 protects cells from programmed cell death. *Nature*. 356:494–499. doi:10.1038/356494a0.

Herman, P.K., and S.D. Emr. 1990. Characterization of VPS34, a gene required for vacuolar protein sorting and vacuole segregation in Saccharomyces cerevisiae. *Mol. Cell. Biol.* 10:6742–6754. doi:10.1128/MCB.10.12.6742.

Hermanns, T., C. Pichlo, I. Woiwode, K. Klopffleisch, K.F. Witting, H. Ovaa, U. Baumann, and K. Hofmann. 2018. A family of unconventional deubiquitinases with modular chain specificity determinants. *Nat. Commun.* 9. doi:10.1038/s41467-018-03148-5.

Hershko, A., A. Ciechanover, A.L. Haas, and I.A. Rose. 1980. Proposed role of ATP in protein breakdown: Conjugation of proteins with multiple chains of the polypeptide of ATP-dependent proteolysis. *Proc Natl Acad Sci USA*. 4.

Hershko, A., A. Ciechanover, and I.A. Rose. 1979. Resolution of the ATP-dependent proteolytic system from reticulocytes: a component that interacts with ATP. *Proc. Natl. Acad. Sci.* 76:3107–3110. doi:10.1073/pnas.76.7.3107.

Hershko, A., and H. Heller. 1985. Occurrence of a polyubiquitin structure in ubiquitin-protein conjugates. *Biochem. Biophys. Res. Commun.* 128:1079–1086. doi:10.1016/0006-291X(85)91050-2.

Hershko, A., H. Heller, S. Elias, and A. Ciechanover. 1983. Components of ubiquitin-protein ligase system. Resolution, affinity purification, and role in protein breakdown. *J. Biol. Chem.* 258:8206–8214.

Hertz, N.T., A. Berthet, M.L. Sos, K.S. Thorn, A.L. Burlingame, K. Nakamura, and K.M. Shokat. 2013. A neo-substrate that amplifies catalytic activity of parkinson's-disease-related kinase PINK1. *Cell*. 154:737–747. doi:10.1016/j.cell.2013.07.030.

Hill, B.G., G.A. Benavides, J.R. Lancaster, S. Ballinger, L. Dell'Italia, J. Zhang, and V.M. Darley-Usmar. 2012. Integration of cellular bioenergetics with mitochondrial quality control and autophagy. *Biol. Chem.* 393:1485–1512. doi:10.1515/hsz-2012-0198.

Hill, S., K. Reichermeier, D.C. Scott, L. Samentar, J. Coulombe-Huntington, L. Izzi, X. Tang, R. Ibarra, T. Bertomeu, A. Moradian, M.J. Sweredoski, N. Caberoy, B.A. Schulman, F. Sicheri, M. Tyers, and G. Kleiger. 2019.

Robust cullin-RING ligase function is established by a multiplicity of poly-ubiquitylation pathways. *eLife*. 8. doi:10.7554/eLife.51163.

Hillen, W., K. Schollmeier, and C. Gatz. 1984. Control of expression of the Tn10-encoded tetracycline resistance operon. II. Interaction of RNA polymerase and TET repressor with the tet operon regulatory region. *J. Mol. Biol.* 172:185–201. doi:10.1016/s0022-2836(84)80037-6.

Hilt, W., and D.H. Wolf. 1995. Proteasomes of the yeastS. cerevisiae: genes, structure and functions. *Mol. Biol. Rep.* 21:3–10. doi:10.1007/BF00990964.

Hjerpe, R., Y. Thomas, J. Chen, A. Zemla, S. Curran, N. Shpiro, L.R. Dick, and T. Kurz. 2012a. Changes in the ratio of free NEDD8 to ubiquitin triggers NEDDylation by ubiquitin enzymes. *Biochem. J.* 441:927–939. doi:10.1042/BJ20111671.

Hjerpe, R., Y. Thomas, and T. Kurz. 2012b. NEDD8 Overexpression Results in Neddylation of Ubiquitin Substrates by the Ubiquitin Pathway. *J. Mol. Biol.* 421:27–29. doi:10.1016/j.jmb.2012.05.013.

Hoege, C., B. Pfander, G.-L. Moldovan, G. Pyrowolakis, and S. Jentsch. 2002. RAD6-dependent DNA repair is linked to modification of PCNA by ubiquitin and SUMO. *Nature*. 419:135–141. doi:10.1038/nature00991.

Holloway, A., M. Simmonds, A. Azad, J.L. Fox, and A. Storey. 2015. Resistance to UV-induced apoptosis by β-HPV5 E6 involves targeting of activated BAK for proteolysis by recruitment of the HERC1 ubiquitin ligase. *Int. J. Cancer*. 136:2831–2843. doi:10.1002/ijc.29350.

Homma, T., D. Ishibashi, T. Nakagaki, T. Fuse, T. Mori, K. Satoh, R. Atarashi, and N. Nishida. 2015. Ubiquitin-specific protease 14 modulates degradation of cellular prion protein. *Sci. Rep.* 5. doi:10.1038/srep11028.

Hosokawa, N., T. Sasaki, S. Iemura, T. Natsume, T. Hara, and N. Mizushima. 2009. Atg101, a novel mammalian autophagy protein interacting with Atg13. *Autophagy*. 5:973–979. doi:10.4161/auto.5.7.9296.

Hospenthal, M.K., S.M.V. Freund, and D. Komander. 2013. Assembly, analysis and architecture of atypical ubiquitin chains. *Nat. Struct. Mol. Biol.* 20:555–565. doi:10.1038/nsmb.2547.

Hospenthal, M.K., T.E.T. Mevissen, and D. Komander. 2015. Deubiquitinase-based analysis of ubiquitin chain architecture using Ubiquitin Chain Restriction (UbiCRest). *Nat. Protoc.* 10:349–361. doi:10.1038/nprot.2015.018.

Hou, F.-Q., X.-F. Lei, J.-L. Yao, Y.-J. Wang, and W. Zhang. 2015. Tetraspanin 1 is involved in survival, proliferation and carcinogenesis of pancreatic cancer. *Oncol. Rep.* 34:3068–3076. doi:10.3892/or.2015.4272.

Hu, M., P. Li, L. Song, P.D. Jeffrey, T.A. Chenova, K.D. Wilkinson, R.E. Cohen, and Y. Shi. 2005. Structure and mechanisms of the proteasome-associated deubiquitinating enzyme USP14. *EMBO J.* 24:3747–3756. doi:10.1038/sj.emboj.7600832.

Hua, R., S.K. Gidda, A. Aranovich, R.T. Mullen, and P.K. Kim. 2015. Multiple Domains in PEX16 Mediate Its Trafficking and Recruitment of Peroxisomal Proteins to the ER: Analysis of PEX16 Functional Domains. *Traffic*. 16:832–852. doi:10.1111/tra.12292.

Huang, L. 1999. Structure of an E6AP-UbcH7 Complex: Insights into Ubiquitination by the E2-E3 Enzyme Cascade. *Science*. 286:1321–1326. doi:10.1126/science.286.5443.1321.

Huang, L., Z. Guo, F. Wang, and L. Fu. 2021. KRAS mutation: from undruggable to druggable in cancer. *Signal Transduct. Target. Ther.* 6:386. doi:10.1038/s41392-021-00780-4.

Huang, S.Y., M.B. Barnard, M. Xu, S. Matsui, S.M. Rose, and W.T. Garrard. 1986. The active immunoglobulin kappa chain gene is packaged by non-ubiquitin-conjugated nucleosomes. *Proc. Natl. Acad. Sci.* 83:3738–3742. doi:10.1073/pnas.83.11.3738.

Huang, T., J. Li, and R.A. Byrd. 2014. Solution structure of lysine-free (K0) ubiquitin: Solution Structure of K0-Ub. *Protein Sci.* 23:662–667. doi:10.1002/pro.2450.

Huguenin-Dezot, N., V. De Cesare, J. Peltier, A. Knebel, Y.A. Kristaryianto, D.T. Rogerson, Y. Kulathu, M. Trost, and J.W. Chin. 2016. Synthesis of Isomeric Phosphoubiquitin Chains Reveals that Phosphorylation Controls Deubiquitinase Activity and Specificity. *Cell Rep.* 16:1180–1193. doi:10.1016/j.celrep.2016.06.064.

Huibregtse, J.M., M. Scheffner, S. Beaudenon, and P.M. Howley. 1995. A family of proteins structurally and functionally related to the E6-AP ubiquitin-protein ligase. *Proc. Natl. Acad. Sci. U. S. A.* 92:2563–2567. doi:10.1073/pnas.92.7.2563.

Huseinovic, A., M. van Dijk, N.P.E. Vermeulen, F. van Leeuwen, J.M. Kooter, and J.C. Vos. 2018. Drug toxicity profiling of a Saccharomyces cerevisiae deubiquitinase deletion panel shows that acetaminophen mimics tyrosine. *Toxicol. In Vitro*. 47:259–268. doi:10.1016/j.tiv.2017.12.007.

Hyer, M.L., M.A. Milhollen, J. Ciavarri, P. Fleming, T. Traore, D. Sappal, J. Huck, J. Shi, J. Gavin, J. Brownell, Y. Yang, B. Stringer, R. Griffin, F. Bruzzese, T. Soucy, J. Duffy, C. Rabino, J. Riceberg, K. Hoar, A. Lublinsky, S. Menon, M. Sintchak, N. Bump, S.M. Pulukuri, S. Langston, S. Tirrell, M. Kuranda, P. Veiby, J. Newcomb, P. Li, J.T. Wu, J. Powe, L.R. Dick, P. Greenspan, K. Galvin, M. Manfredi, C. Claiborne, B.S. Amidon, and N.F. Bence. 2018. A small-molecule inhibitor of the

ubiquitin activating enzyme for cancer treatment. *Nat. Med.* 24:186–193. doi:10.1038/nm.4474.

Ichimura, Y., T. Kirisako, T. Takao, Y. Satomi, Y. Shimonishi, N. Ishihara, N. Mizushima, I. Tanida, E. Kominami, M. Ohsumi, T. Noda, and Y. Ohsumi. 2000. A ubiquitin-like system mediates protein lipidation. *Nature*. 408:488–492. doi:10.1038/35044114.

Inuzuka, H., S. Shaik, I. Onoyama, D. Gao, A. Tseng, R.S. Maser, B. Zhai, L. Wan, A. Gutierrez, A.W. Lau, Y. Xiao, A.L. Christie, J. Aster, J. Settleman, S.P. Gygi, A.L. Kung, T. Look, K.I. Nakayama, R.A. DePinho, and W. Wei. 2011. SCFFBW7 regulates cellular apoptosis by targeting MCL1 for ubiquitylation and destruction. *Nature*. 471:104–109. doi:10.1038/nature09732.

Ishino, Y., H. Shinagawa, K. Makino, M. Amemura, and A. Nakata. 1987. Nucleotide sequence of the iap gene, responsible for alkaline phosphatase isozyme conversion in Escherichia coli, and identification of the gene product. *J. Bacteriol.* 169:5429–5433. doi:10.1128/JB.169.12.5429-5433.1987.

Itakura, E., C. Kishi, K. Inoue, and N. Mizushima. 2008. Beclin 1 Forms Two Distinct Phosphatidylinositol 3-Kinase Complexes with Mammalian Atg14 and UVRAG. *Mol. Biol. Cell*. 19:5360–5372. doi:10.1091/mbc.e08-01-0080.

Itakura, E., C. Kishi-Itakura, and N. Mizushima. 2012. The Hairpin-type Tail-Anchored SNARE Syntaxin 17 Targets to Autophagosomes for Fusion with Endosomes/Lysosomes. *Cell*. 151:1256–1269. doi:10.1016/j.cell.2012.11.001.

Iwashita, S., M. Tsuchida, M. Tsukuda, Y. Yamashita, Y. Emi, Y. Kida, M. Komori, Y. Kashiwayama, T. Imanaka, and M. Sakaguchi. 2010. Multiple organelle-targeting signals in the N-terminal portion of peroxisomal membrane protein PMP70. *J. Biochem. (Tokyo)*. 147:581–590. doi:10.1093/jb/mvp205.

Jacomin, A.-C., A. Bescond, E. Soleilhac, B. Gallet, G. Schoehn, M.-O. Fauvarque, and E. Taillebourg. 2015. The Deubiquitinating Enzyme UBPY Is Required for Lysosomal Biogenesis and Productive Autophagy in Drosophila. *PloS One*. 10:e0143078. doi:10.1371/journal.pone.0143078.

Jäger, S., C. Bucci, I. Tanida, T. Ueno, E. Kominami, P. Saftig, and E.-L. Eskelinen. 2004. Role for Rab7 in maturation of late autophagic vacuoles. *J. Cell Sci.* 117:4837–4848. doi:10.1242/jcs.01370.

Jensen, D.E., M. Proctor, S.T. Marquis, H.P. Gardner, S.I. Ha, L.A. Chodosh, A.M. Ishov, N. Tommerup, H. Vissing, Y. Sekido, J. Minna, A. Borodovsky, D.C. Schultz, K.D. Wilkinson, G.G. Maul, N. Barlev, S.L. Berger, G.C. Prendergast, and F.J. Rauscher. 1998. BAP1: a novel

ubiquitin hydrolase which binds to the BRCA1 RING finger and enhances BRCA1-mediated cell growth suppression. *Oncogene*. 16:1097–1112. doi:10.1038/sj.onc.1201861.

Jiang, G.-M., Y. Tan, H. Wang, L. Peng, H.-T. Chen, X.-J. Meng, L.-L. Li, Y. Liu, W.-F. Li, and H. Shan. 2019. The relationship between autophagy and the immune system and its applications for tumor immunotherapy. *Mol. Cancer*. 18:17. doi:10.1186/s12943-019-0944-z.

Jiang, L., F. Schlesinger, C.A. Davis, Y. Zhang, R. Li, M. Salit, T.R. Gingeras, and B. Oliver. 2011. Synthetic spike-in standards for RNA-seq experiments. *Genome Res.* 21:1543–1551. doi:10.1101/gr.121095.111.

Jiao, L., S. Ouyang, N. Shaw, G. Song, Y. Feng, F. Niu, W. Qiu, H. Zhu, L.-W. Hung, X. Zuo, V. Eleonora Shtykova, P. Zhu, Y.-H. Dong, R. Xu, and Z.-J. Liu. 2014. Mechanism of the Rpn13-induced activation of Uch37. *Protein Cell*. 5:616–630. doi:10.1007/s13238-014-0046-z.

Jin, J., X. Li, S.P. Gygi, and J.W. Harper. 2007. Dual E1 activation systems for ubiquitin differentially regulate E2 enzyme charging. *Nature*. 447:1135–1138. doi:10.1038/nature05902.

Jin, S.M., and R.J. Youle. 2013. The accumulation of misfolded proteins in the mitochondrial matrix is sensed by PINK1 to induce PARK2/Parkin-mediated mitophagy of polarized mitochondria. *Autophagy*. 9:1750–1757. doi:10.4161/auto.26122.

Joazeiro, C.A. 1999. The Tyrosine Kinase Negative Regulator c-Cbl as a RING-Type, E2-Dependent Ubiquitin-Protein Ligase. *Science*. 286:309–312. doi:10.1126/science.286.5438.309.

Josephs, S.F., T.E. Ichim, S.M. Prince, S. Kesari, F.M. Marincola, A.R. Escobedo, and A. Jafri. 2018. Unleashing endogenous TNF-alpha as a cancer immunotherapeutic. *J. Transl. Med.* 16. doi:10.1186/s12967-018-1611-7.

Jung, C.H., C.B. Jun, S.-H. Ro, Y.-M. Kim, N.M. Otto, J. Cao, M. Kundu, and D.-H. Kim. 2009. ULK-Atg13-FIP200 complexes mediate mTOR signaling to the autophagy machinery. *Mol. Biol. Cell*. 20:1992–2003. doi:10.1091/mbc.e08-12-1249.

Jung, E.J., and D.R. Kim. 2008. Apoptotic cell death in TrkA-overexpressing cells: kinetic regulation of ERK phosphorylation and caspase-7 activation. *Mol. Cells*. 26:12–17.

Kab, S., J. Spinosi, L. Chaperon, A. Dugravot, A. Singh-Manoux, F. Moisan, and A. Elbaz. 2017. Agricultural activities and the incidence of Parkinson's disease in the general French population. *Eur. J. Epidemiol.* 32:203–216. doi:10.1007/s10654-017-0229-z.

Kale, J., E.J. Osterlund, and D.W. Andrews. 2018. BCL-2 family proteins: changing partners in the dance towards death. *Cell Death Differ.* 25:65–80. doi:10.1038/cdd.2017.186.

Kamadurai, H.B., J. Souphron, D.C. Scott, D.M. Duda, D.J. Miller, D. Stringer, R.C. Piper, and B.A. Schulman. 2009. Insights into ubiquitin transfer cascades from a structure of a UbcH5B approximately ubiquitin-HECT(NEDD4L) complex. *Mol. Cell*. 36:1095–1102. doi:10.1016/j.molcel.2009.11.010.

Kanaji, S., J. Iwahashi, Y. Kida, M. Sakaguchi, and K. Mihara. 2000. Characterization of the Signal That Directs Tom20 to the Mitochondrial Outer Membrane. *J. Cell Biol.* 151:277–288. doi:10.1083/jcb.151.2.277.

Kanayama, A., R.B. Seth, L. Sun, C.-K. Ea, M. Hong, A. Shaito, Y.-H. Chiu, L. Deng, and Z.J. Chen. 2004. TAB2 and TAB3 Activate the NF-κB Pathway through Binding to Polyubiquitin Chains. *Mol. Cell*. 15:535–548. doi:10.1016/j.molcel.2004.08.008.

Kane, L.A., M. Lazarou, A.I. Fogel, Y. Li, K. Yamano, S.A. Sarraf, S. Banerjee, and R.J. Youle. 2014. PINK1 phosphorylates ubiquitin to activate Parkin E3 ubiquitin ligase activity. *J. Cell Biol.* 205:143–153. doi:10.1083/jcb.201402104.

Kashiwayama, Y., K. Asahina, H. Shibata, M. Morita, A.C. Muntau, A.A. Roscher, R.J.A. Wanders, N. Shimozawa, M. Sakaguchi, H. Kato, and T. Imanaka. 2005. Role of Pex19p in the targeting of PMP70 to peroxisome. *Biochim. Biophys. Acta BBA - Mol. Cell Res.* 1746:116–128. doi:10.1016/j.bbamcr.2005.10.006.

Kataoka, T., N. Holler, O. Micheau, F. Martinon, A. Tinel, K. Hofmann, and J. Tschopp. 2001. Bcl-rambo, a Novel Bcl-2 Homologue That Induces Apoptosis via Its Unique C-terminal Extension. *J. Biol. Chem.* 276:19548–19554. doi:10.1074/jbc.M010520200.

Katayama, H., T. Kogure, N. Mizushima, T. Yoshimori, and A. Miyawaki. 2011. A Sensitive and Quantitative Technique for Detecting Autophagic Events Based on Lysosomal Delivery. *Chem. Biol.* 18:1042–1052. doi:10.1016/j.chembiol.2011.05.013.

Kawakami, T. 2001. NEDD8 recruits E2-ubiquitin to SCF E3 ligase. *EMBO J.* 20:4003–4012. doi:10.1093/emboj/20.15.4003.

Kazlauskaite, A., C. Kondapalli, R. Gourlay, D.G. Campbell, M.S. Ritorto, K. Hofmann, D.R. Alessi, A. Knebel, M. Trost, and M.M.K. Muqit. 2014. Parkin is activated by PINK1-dependent phosphorylation of ubiquitin at Ser65. *Biochem. J.* 460:127–141. doi:10.1042/BJ20140334.

Kelsall, I.R., D.M. Duda, J.L. Olszewski, K. Hofmann, A. Knebel, F. Langevin, N. Wood, M. Wightman, B.A. Schulman, and A.F. Alpi. 2013. TRIAD1 and HHARI bind to and are activated by distinct neddylated Cullin-RING

ligase complexes. *EMBO J.* 32:2848–2860. doi:10.1038/emboj.2013.209.

Kelsall, I.R., J. Zhang, A. Knebel, J.S.C. Arthur, and P. Cohen. 2019. The E3 ligase HOIL-1 catalyses ester bond formation between ubiquitin and components of the Myddosome in mammalian cells. *Proc. Natl. Acad. Sci.* 116:13293–13298. doi:10.1073/pnas.1905873116.

Kerr, J.F., A.H. Wyllie, and A.R. Currie. 1972. Apoptosis: a basic biological phenomenon with wide-ranging implications in tissue kinetics. *Br. J. Cancer*. 26:239–257. doi:10.1038/bjc.1972.33.

Keusekotten, K., P.R. Elliott, L. Glockner, B.K. Fiil, R.B. Damgaard, Y. Kulathu, T. Wauer, M.K. Hospenthal, M. Gyrd-Hansen, D. Krappmann, K. Hofmann, and D. Komander. 2013. OTULIN Antagonizes LUBAC Signaling by Specifically Hydrolyzing Met1-Linked Polyubiquitin. *Cell*. 153:1312–1326. doi:10.1016/j.cell.2013.05.014.

Kihara, A., Y. Kabeya, Y. Ohsumi, and T. Yoshimori. 2001. Beclin-phosphatidylinositol 3-kinase complex functions at the trans-Golgi network. *EMBO Rep.* 2:330–335. doi:10.1093/embo-reports/kve061.

Kim, H., S.C. Botelho, K. Park, and H. Kim. 2015. Use of carbonate extraction in analyzing moderately hydrophobic transmembrane proteins in the mitochondrial inner membrane: Carbonate Extraction of Mitochondrial MPs. *Protein Sci.* 24:2063–2069. doi:10.1002/pro.2817.

Kim, H.T., and A.L. Goldberg. 2018. UBL domain of Usp14 and other proteins stimulates proteasome activities and protein degradation in cells. *Proc. Natl. Acad. Sci.* 115:E11642–E11650. doi:10.1073/pnas.1808731115.

Kim, P.K., D.W. Hailey, R.T. Mullen, and J. Lippincott-Schwartz. 2008a. Ubiquitin signals autophagic degradation of cytosolic proteins and peroxisomes. *Proc. Natl. Acad. Sci. U. S. A.* 105:20567–20574. doi:10.1073/pnas.0810611105.

Kim, R.Q., W.J. van Dijk, and T.K. Sixma. 2016. Structure of USP7 catalytic domain and three Ubl-domains reveals a connector α-helix with regulatory role. *J. Struct. Biol.* 195:11–18. doi:10.1016/j.jsb.2016.05.005.

Kim, W., E.J. Bennett, E.L. Huttlin, A. Guo, J. Li, A. Possemato, M.E. Sowa, R. Rad, J. Rush, M.J. Comb, J.W. Harper, and S.P. Gygi. 2011. Systematic and Quantitative Assessment of the Ubiquitin-Modified Proteome. *Mol. Cell*. 44:325–340. doi:10.1016/j.molcel.2011.08.025.

Kim, Y., J. Park, S. Kim, S. Song, S.-K. Kwon, S.-H. Lee, T. Kitada, J.-M. Kim, and J. Chung. 2008b. PINK1 controls mitochondrial localization of Parkin through direct phosphorylation. *Biochem. Biophys. Res. Commun.* 377:975–980. doi:10.1016/j.bbrc.2008.10.104.

Kinner, A., and R. Kölling. 2003. The yeast deubiquitinating enzyme Ubp16 is anchored to the outer mitochondrial membrane. *FEBS Lett.* 549:135–140. doi:10.1016/S0014-5793(03)00801-9.

Kipps, T.J., H. Eradat, S. Grosicki, J. Catalano, W. Cosolo, I.S. Dyagil, S. Yalamanchili, A. Chai, S. Sahasranaman, E. Punnoose, D. Hurst, and H. Pylypenko. 2015. A phase 2 study of the BH3 mimetic BCL2 inhibitor navitoclax (ABT-263) with or without rituximab, in previously untreated B-cell chronic lymphocytic leukemia. *Leuk. Lymphoma*. 56:2826–2833. doi:10.3109/10428194.2015.1030638.

Kirisako, T., K. Kamei, S. Murata, M. Kato, H. Fukumoto, M. Kanie, S. Sano, F. Tokunaga, K. Tanaka, and K. Iwai. 2006. A ubiquitin ligase complex assembles linear polyubiquitin chains. *EMBO J.* 25:4877–4887. doi:10.1038/sj.emboj.7601360.

Kirkpatrick, D.S., S.A. Gerber, and S.P. Gygi. 2005. The absolute quantification strategy: a general procedure for the quantification of proteins and post-translational modifications. *Methods*. 35:265–273. doi:10.1016/j.ymeth.2004.08.018.

Kitada, T., S. Asakawa, N. Hattori, H. Matsumine, Y. Yamamura, S. Minoshima, M. Yokochi, Y. Mizuno, and N. Shimizu. 1998. Mutations in the parkin gene cause autosomal recessive juvenile parkinsonism. *Nature*. 392:605–608. doi:10.1038/33416.

Kizilboga, T., E.A. Baskale, J. Yildiz, I.M. Akcay, E. Zemheri, N.D. Can, C. Ozden, S. Demir, F. Ezberci, and G. Dinler-Doganay. 2019. Bag-1 stimulates Bad phosphorylation through activation of Akt and Raf kinases to mediate cell survival in breast cancer. *BMC Cancer*. 19. doi:10.1186/s12885-019-6477-4.

Klein, C., and A. Westenberger. 2012. Genetics of Parkinson's Disease. *Cold Spring Harb. Perspect. Med.* 2:a008888–a008888. doi:10.1101/cshperspect.a008888.

Klinkenberg, M., N. Thurow, S. Gispert, F. Ricciardi, F. Eich, J.H.M. Prehn, G. Auburger, and D. Kögel. 2010. Enhanced vulnerability of PARK6 patient skin fibroblasts to apoptosis induced by proteasomal stress. *Neuroscience*. 166:422–434. doi:10.1016/j.neuroscience.2009.12.068.

Kluge, A.F., B.R. Lagu, P. Maiti, M. Jaleel, M. Webb, J. Malhotra, A. Mallat, P.A. Srinivas, and J.E. Thompson. 2018. Novel highly selective inhibitors of ubiquitin specific protease 30 (USP30) accelerate mitophagy. *Bioorg. Med. Chem. Lett.* 28:2655–2659. doi:10.1016/j.bmcl.2018.05.013.

Komander, D., M.J. Clague, and S. Urbé. 2009a. Breaking the chains: Structure and function of the deubiquitinases. *Nat. Rev. Mol. Cell Biol.* 10:550–563. doi:10.1038/nrm2731.

Komander, D., C.J. Lord, H. Scheel, S. Swift, K. Hofmann, A. Ashworth, and D. Barford. 2008. The Structure of the CYLD USP Domain Explains Its Specificity for Lys63-Linked Polyubiquitin and Reveals a B Box Module. *Mol. Cell*. 29:451–464. doi:10.1016/j.molcel.2007.12.018.

Komander, D., and M. Rape. 2012. The Ubiquitin Code. *Annu. Rev. Biochem.* 81:203–229. doi:10.1146/annurev-biochem-060310-170328.

Komander, D., F. Reyes-Turcu, J.D.F. Licchesi, P. Odenwaelder, K.D. Wilkinson, and D. Barford. 2009b. Molecular discrimination of structurally equivalent Lys 63-linked and linear polyubiquitin chains. *EMBO Rep.* 10:466–473. doi:10.1038/embor.2009.55.

Kotschy, A., Z. Szlavik, J. Murray, J. Davidson, A.L. Maragno, G. Le Toumelin-Braizat, M. Chanrion, G.L. Kelly, J.-N. Gong, D.M. Moujalled, A. Bruno, M. Csekei, A. Paczal, Z.B. Szabo, S. Sipos, G. Radics, A. Proszenyak, B. Balint, L. Ondi, G. Blasko, A. Robertson, A. Surgenor, P. Dokurno, I. Chen, N. Matassova, J. Smith, C. Pedder, C. Graham, A. Studeny, G. Lysiak-Auvity, A.-M. Girard, F. Gravé, D. Segal, C.D. Riffkin, G. Pomilio, L.C.A. Galbraith, B.J. Aubrey, M.S. Brennan, M.J. Herold, C. Chang, G. Guasconi, N. Cauquil, F. Melchiore, N. Guigal-Stephan, B. Lockhart, F. Colland, J.A. Hickman, A.W. Roberts, D.C.S. Huang, A.H. Wei, A. Strasser, G. Lessene, and O. Geneste. 2016. The MCL1 inhibitor S63845 is tolerable and effective in diverse cancer models. *Nature*. 538:477–482. doi:10.1038/nature19830.

Koulich, E., X. Li, and G.N. DeMartino. 2008. Relative structural and functional roles of multiple deubiquitylating proteins associated with mammalian 26S proteasome. *Mol. Biol. Cell*. 19:1072–1082. doi:10.1091/mbc.e07-10-1040.

Koyano, F., K. Okatsu, H. Kosako, Y. Tamura, E. Go, M. Kimura, Y. Kimura, H. Tsuchiya, H. Yoshihara, T. Hirokawa, T. Endo, E.A. Fon, J.-F. Trempe, Y. Saeki, K. Tanaka, and N. Matsuda. 2014. Ubiquitin is phosphorylated by PINK1 to activate parkin. *Nature*. 510:162–166. doi:10.1038/nature13392.

Kravtsova-Ivantsiv, Y., S. Cohen, and A. Ciechanover. 2009. Modification by Single Ubiquitin Moieties Rather Than Polyubiquitination Is Sufficient for Proteasomal Processing of the p105 NF-κB Precursor. *Mol. Cell*. 33:496–504. doi:10.1016/j.molcel.2009.01.023.

Kristariyanto, Y.A., S.A. Abdul Rehman, S. Weidlich, A. Knebel, and Y. Kulathu. 2017. A single MIU motif of MINDY -1 recognizes K48-linked polyubiquitin chains. *EMBO Rep.* 18:392–402. doi:10.15252/embr.201643205.

Kristariyanto, Y.A., S.A. Abdul Rehman, D.G. Campbell, N.A. Morrice, C. Johnson, R. Toth, and Y. Kulathu. 2015a. K29-Selective Ubiquitin Binding Domain Reveals Structural Basis of Specificity and Heterotypic

Nature of K29 Polyubiquitin. *Mol. Cell*. 58:83–94. doi:10.1016/j.molcel.2015.01.041.

Kristariyanto, Y.A., S.-Y. Choi, S.A.A. Rehman, M.S. Ritorto, D.G. Campbell, N.A. Morrice, R. Toth, and Y. Kulathu. 2015b. Assembly and structure of Lys33-linked polyubiquitin reveals distinct conformations. *Biochem. J.* 467:345–352. doi:10.1042/BJ20141502.

Kulak, N.A., G. Pichler, I. Paron, N. Nagaraj, and M. Mann. 2014. Minimal, encapsulated proteomic-sample processing applied to copy-number estimation in eukaryotic cells. *Nat. Methods*. 11:319–324. doi:10.1038/nmeth.2834.

Kulathu, Y., F.J. Garcia, T.E.T. Mevissen, M. Busch, N. Arnaudo, K.S. Carroll, D. Barford, and D. Komander. 2013. Regulation of A20 and other OTU deubiquitinases by reversible oxidation. *Nat. Commun.* 4. doi:10.1038/ncomms2567.

Kuma, A., M. Komatsu, and N. Mizushima. 2017. Autophagy-monitoring and autophagy-deficient mice. *Autophagy*. 13:1619–1628. doi:10.1080/15548627.2017.1343770.

Kupka, S., M. Reichert, P. Draber, and H. Walczak. 2016. Formation and removal of poly-ubiquitin chains in the regulation of tumor necrosis factor-induced gene activation and cell death. *FEBS J.* 283:2626–2639. doi:10.1111/febs.13644.

Kwasna, D., S.A. Abdul Rehman, J. Natarajan, S. Matthews, R. Madden, V. De Cesare, S. Weidlich, S. Virdee, I. Ahel, I. Gibbs-Seymour, and Y. Kulathu. 2018. Discovery and Characterization of ZUFSP/ZUP1, a Distinct Deubiquitinase Class Important for Genome Stability. *Mol. Cell*. 70:150-164.e6. doi:10.1016/j.molcel.2018.02.023.

Lafont, E., T. Hartwig, and H. Walczak. 2018. Paving TRAIL's Path with Ubiquitin. *Trends Biochem. Sci.* 43:44–60. doi:10.1016/j.tibs.2017.11.002.

Lajin, B., and A. Alachkar. 2013. The NQO1 polymorphism C609T (Pro187Ser) and cancer susceptibility: a comprehensive meta-analysis. *Br. J. Cancer*. 109:1325–1337. doi:10.1038/bjc.2013.357.

Lambourne, O.A., and Y. Mehellou. 2018. Chemical Strategies for Activating PINK1, a Protein Kinase Mutated in Parkinson's Disease. *Chembiochem Eur. J. Chem. Biol.* 19:2433–2437. doi:10.1002/cbic.201800497.

Lamoliatte, F., E. Bonneil, C. Durette, O. Caron-Lizotte, D. Wildemann, J. Zerweck, H. Wenshuk, and P. Thibault. 2013. Targeted Identification of SUMOylation Sites in Human Proteins Using Affinity Enrichment and Paralog-specific Reporter Ions. *Mol. Cell. Proteomics*. 12:2536–2550. doi:10.1074/mcp.M112.025569.

Larsen, C.N., B.A. Krantz, and K.D. Wilkinson. 1998. Substrate Specificity of Deubiquitinating Enzymes: Ubiquitin C-Terminal Hydrolases †. *Biochemistry*. 37:3358–3368. doi:10.1021/bi972274d.

Larsen, C.N., J.S. Price, and K.D. Wilkinson. 1996. Substrate Binding and Catalysis by Ubiquitin C-Terminal Hydrolases: Identification of Two Active Site Residues †. *Biochemistry*. 35:6735–6744. doi:10.1021/bi960099f.

Lauterwasser, J., F. Todt, R.M. Zerbes, T.N. Nguyen, W. Craigen, M. Lazarou, M. van der Laan, and F. Edlich. 2016. The porin VDAC2 is the mitochondrial platform for Bax retrotranslocation. *Sci. Rep.* 6:32994. doi:10.1038/srep32994.

Law, K.B., D. Bronte-Tinkew, E. Di Pietro, A. Snowden, R.O. Jones, A. Moser, J.H. Brumell, N. Braverman, and P.K. Kim. 2017. The peroxisomal AAA ATPase complex prevents pexophagy and development of peroxisome biogenesis disorders. *Autophagy*. 13:868–884. doi:10.1080/15548627.2017.1291470.

Lazarou, M., D.A. Sliter, L.A. Kane, S.A. Sarraf, C. Wang, J.L. Burman, D.P. Sideris, A.I. Fogel, and R.J. Youle. 2015. The ubiquitin kinase PINK1 recruits autophagy receptors to induce mitophagy. *Nature*. 524:309–314. doi:10.1038/nature14893.

Leber, B., J. Lin, and D.W. Andrews. 2007. Embedded together: the life and death consequences of interaction of the Bcl-2 family with membranes. *Apoptosis Int. J. Program. Cell Death*. 12:897–911. doi:10.1007/s10495-007-0746-4.

Lee, B.-H., Y. Lu, M.A. Prado, Y. Shi, G. Tian, S. Sun, S. Elsasser, S.P. Gygi, R.W. King, and D. Finley. 2016. USP14 deubiquitinates proteasome-bound substrates that are ubiquitinated at multiple sites. *Nature*. 532:398–401. doi:10.1038/nature17433.

Lee, E.F., T.J. Harris, S. Tran, M. Evangelista, S. Arulananda, T. John, C. Ramnac, C. Hobbs, H. Zhu, G. Gunasingh, D. Segal, A. Behren, J. Cebon, A. Dobrovic, J.M. Mariadason, A. Strasser, L. Rohrbeck, N.K. Haass, M.J. Herold, and W.D. Fairlie. 2019. BCL-XL and MCL-1 are the key BCL-2 family proteins in melanoma cell survival. *Cell Death Dis.* 10. doi:10.1038/s41419-019-1568-3.

Lee, H.-J., K. Na, M.-S. Kwon, H. Kim, K.S. Kim, and Y.-K. Paik. 2009. Quantitative analysis of phosphopeptides in search of the disease biomarker from the hepatocellular carcinoma specimen. *PROTEOMICS*. 9:3395–3408. doi:10.1002/pmic.200800943.

Lee, J.J., A. Sanchez-Martinez, A.M. Zarate, C. Benincá, U. Mayor, M.J. Clague, and A.J. Whitworth. 2018. Basal mitophagy is widespread in Drosophila but minimally affected by loss of Pink1 or parkin. *J. Cell Biol.* 217:1613–1622. doi:10.1083/jcb.201801044.

Lee, K.-S., Z. Wu, Y. Song, S.S. Mitra, A.H. Feroze, S.H. Cheshier, and B. Lu. 2013. Roles of PINK1, mTORC2, and mitochondria in preserving brain tumor-forming stem cells in a noncanonical Notch signaling pathway. *Genes Dev.* 27:2642–2647. doi:10.1101/gad.225169.113.

Lee, S.B., J.J. Kim, H.-J. Nam, B. Gao, P. Yin, B. Qin, S.-Y. Yi, H. Ham, D. Evans, S.-H. Kim, J. Zhang, M. Deng, T. Liu, H. Zhang, D.D. Billadeau, L. Wang, E. Giaime, J. Shen, Y.-P. Pang, J. Jen, J.M. van Deursen, and Z. Lou. 2015. Parkin Regulates Mitosis and Genomic Stability through Cdc20/Cdh1. *Mol. Cell*. 60:21–34. doi:10.1016/j.molcel.2015.08.011.

Lee, Y.-K., and J.-A. Lee. 2016. Role of the mammalian ATG8/LC3 family in autophagy: differential and compensatory roles in the spatiotemporal regulation of autophagy. *BMB Rep.* 49:424–430. doi:10.5483/bmbrep.2016.49.8.081.

Lenkinski, R.E., D.M. Chen, J.D. Glickson, and G. Goldstein. 1977. Nuclear magnetic resonance studies of the denaturation of ubiquitin. *Biochim. Biophys. Acta BBA - Protein Struct.* 494:126–130. doi:10.1016/0005-2795(77)90140-4.

Letai, A., M.C. Bassik, L.D. Walensky, M.D. Sorcinelli, S. Weiler, and S.J. Korsmeyer. 2002. Distinct BH3 domains either sensitize or activate mitochondrial apoptosis, serving as prototype cancer therapeutics. *Cancer Cell*. 2:183–192. doi:10.1016/s1535-6108(02)00127-7.

Leverson, J.D., D.C. Phillips, M.J. Mitten, E.R. Boghaert, D. Diaz, S.K. Tahir, L.D. Belmont, P. Nimmer, Y. Xiao, X.M. Ma, K.N. Lowes, P. Kovar, J. Chen, S. Jin, M. Smith, J. Xue, H. Zhang, A. Oleksijew, T.J. Magoc, K.S. Vaidya, D.H. Albert, J.M. Tarrant, N. La, L. Wang, Z.-F. Tao, M.D. Wendt, D. Sampath, S.H. Rosenberg, C. Tse, D.C.S. Huang, W.J. Fairbrother, S.W. Elmore, and A.J. Souers. 2015a. Exploiting selective BCL-2 family inhibitors to dissect cell survival dependencies and define improved strategies for cancer therapy. *Sci. Transl. Med.* 7:279ra40. doi:10.1126/scitranslmed.aaa4642.

Leverson, J.D., H. Zhang, J. Chen, S.K. Tahir, D.C. Phillips, J. Xue, P. Nimmer, S. Jin, M. Smith, Y. Xiao, P. Kovar, A. Tanaka, M. Bruncko, G.S. Sheppard, L. Wang, S. Gierke, L. Kategaya, D.J. Anderson, C. Wong, J. Eastham-Anderson, M.J.C. Ludlam, D. Sampath, W.J. Fairbrother, I. Wertz, S.H. Rosenberg, C. Tse, S.W. Elmore, and A.J. Souers. 2015b. Potent and selective small-molecule MCL-1 inhibitors demonstrate on-target cancer cell killing activity as single agents and in combination with ABT-263 (navitoclax). *Cell Death Dis.* 6:e1590–e1590. doi:10.1038/cddis.2014.561.

Levinger, L., and A. Varshavsky. 1982. Selective arrangement of ubiquitinated and D1 protein-containing nucleosomes within the drosophila genome. *Cell*. 28:375–385. doi:10.1016/0092-8674(82)90355-5.

Lewy, F. 1912. Paralysis agitans. I. *Pathol. Anat. Handb. Neurol.*

Li, C., Y. Zhang, X. Cheng, H. Yuan, S. Zhu, J. Liu, Q. Wen, Y. Xie, J. Liu, G. Kroemer, D.J. Klionsky, M.T. Lotze, H.J. Zeh, R. Kang, and D. Tang. 2018. PINK1 and PARK2 Suppress Pancreatic Tumorigenesis through Control of Mitochondrial Iron-Mediated Immunometabolism. *Dev. Cell*. 46:441-455.e8. doi:10.1016/j.devcel.2018.07.012.

Li, J., W. Qi, G. Chen, D. Feng, J. Liu, B. Ma, C. Zhou, C. Mu, W. Zhang, Q. Chen, and Y. Zhu. 2015. Mitochondrial outer-membrane E3 ligase MUL1 ubiquitinates ULK1 and regulates selenite-induced mitophagy. *Autophagy*. 11:1216–1229. doi:10.1080/15548627.2015.1017180.

Li, X., J. Liu, H. Sun, Y. Zou, J. Chen, Y. Chen, C. Chen, and X. Wu. 2020. SRPX2 promotes cell proliferation and invasion via activating FAK/SRC/ERK pathway in non-small cell lung cancer. *Acta Biochim. Pol.* 67:165–172. doi:10.18388/abp.2020_5158.

Li, Y., T. Hahn, K. Garrison, Z.-H. Cui, A. Thorburn, J. Thorburn, H.-M. Hu, and E.T. Akporiaye. 2012. The vitamin E analogue α-TEA stimulates tumor autophagy and enhances antigen cross-presentation. *Cancer Res.* 72:3535–3545. doi:10.1158/0008-5472.CAN-11-3103.

Lian, B.S.X., A.E.H. Yek, H. Shuvas, S.F. Abdul Rahman, K. Muniandy, and N. Mohana-Kumaran. 2018. Synergistic anti-proliferative effects of combination of ABT-263 and MCL-1 selective inhibitor A-1210477 on cervical cancer cell lines. *BMC Res. Notes*. 11. doi:10.1186/s13104-018-3302-0.

Liang, J.-R., A. Martinez, J.D. Lane, U. Mayor, M.J. Clague, and S. Urbe. 2015a. USP30 deubiquitylates mitochondrial Parkin substrates and restricts apoptotic cell death. *EMBO Rep.* 16:618–627. doi:10.15252/embr.201439820.

Liang, P., Y. Xu, X. Zhang, C. Ding, R. Huang, Z. Zhang, J. Lv, X. Xie, Y. Chen, Y. Li, Y. Sun, Y. Bai, Z. Songyang, W. Ma, C. Zhou, and J. Huang. 2015b. CRISPR/Cas9-mediated gene editing in human tripronuclear zygotes. *Protein Cell*. 6:363–372. doi:10.1007/s13238-015-0153-5.

Liang, X., M.E. De Vera, W.J. Buchser, A.R. de Vivar Chavez, P. Loughran, D.B. Stolz, P. Basse, T. Wang, B. Van Houten, H.J. Zeh, and M.T. Lotze. 2012. Inhibiting Systemic Autophagy during Interleukin 2 Immunotherapy Promotes Long-term Tumor Regression. *Cancer Res.* 72:2791–2801. doi:10.1158/0008-5472.CAN-12-0320.

Liang, X.H., S. Jackson, M. Seaman, K. Brown, B. Kempkes, H. Hibshoosh, and B. Levine. 1999. Induction of autophagy and inhibition of tumorigenesis by beclin 1. *Nature*. 402:672–676. doi:10.1038/45257.

Liang, X.H., L.K. Kleeman, H.H. Jiang, G. Gordon, J.E. Goldman, G. Berry, B. Herman, and B. Levine. 1998. Protection against fatal Sindbis virus encephalitis by beclin, a novel Bcl-2-interacting protein. *J. Virol.* 72:8586–8596. doi:10.1128/JVI.72.11.8586-8596.1998.

Lim, G.G., and K. Lim. 2017. Parkin-independent mitophagy—FKBP8 takes the stage. *EMBO Rep.* 18:864–865. doi:10.15252/embr.201744313.

Lin, S., B.T. Staahl, R.K. Alla, and J.A. Doudna. 2014. Enhanced homology-directed human genome engineering by controlled timing of CRISPR/Cas9 delivery. *eLife*. 3:e04766. doi:10.7554/eLife.04766.

Lindqvist, L.M., M. Heinlein, D.C.S. Huang, and D.L. Vaux. 2014. Prosurvival Bcl-2 family members affect autophagy only indirectly, by inhibiting Bax and Bak. *Proc. Natl. Acad. Sci. U. S. A.* 111:8512–8517. doi:10.1073/pnas.1406425111.

Lindqvist, L.M., and D.L. Vaux. 2014. BCL2 and related prosurvival proteins require BAK1 and BAX to affect autophagy. *Autophagy*. 10:1474–1475. doi:10.4161/auto.29639.

Liu, C.-W., X. Li, D. Thompson, K. Wooding, T. Chang, Z. Tang, H. Yu, P.J. Thomas, and G.N. DeMartino. 2006. ATP Binding and ATP Hydrolysis Play Distinct Roles in the Function of 26S Proteasome. *Mol. Cell*. 24:39–50. doi:10.1016/j.molcel.2006.08.025.

Liu, J., C. Zhang, W. Hu, and Z. Feng. 2018a. Parkinson's disease-associated protein Parkin: an unusual player in cancer. *Cancer Commun.* 38:40. doi:10.1186/s40880-018-0314-z.

Liu, L., D. Feng, G. Chen, M. Chen, Q. Zheng, P. Song, Q. Ma, C. Zhu, R. Wang, W. Qi, L. Huang, P. Xue, B. Li, X. Wang, H. Jin, J. Wang, F. Yang, P. Liu, Y. Zhu, S. Sui, and Q. Chen. 2012. Mitochondrial outer-membrane protein FUNDC1 mediates hypoxia-induced mitophagy in mammalian cells. *Nat. Cell Biol.* 14:177–185. doi:10.1038/ncb2422.

Liu, X., J.M. Reitsma, J.L. Mamrosh, Y. Zhang, R. Straube, and R.J. Deshaies. 2018b. Cand1-Mediated Adaptive Exchange Mechanism Enables Variation in F-Box Protein Expression. *Mol. Cell*. 69:773-786.e6. doi:10.1016/j.molcel.2018.01.038.

Liu, Y., and W.F. Bodmer. 2006. Analysis of P53 mutations and their expression in 56 colorectal cancer cell lines. *Proc. Natl. Acad. Sci. U. S. A.* 103:976–81. doi:10.1073/pnas.0510146103.

Liu, Y., L. Fallon, H.A. Lashuel, Z. Liu, and P.T. Lansbury. 2002. The UCH-L1 Gene Encodes Two Opposing Enzymatic Activities that Affect α-Synuclein Degradation and Parkinson's Disease Susceptibility. *Cell*. 111:209–218. doi:10.1016/S0092-8674(02)01012-7.

Liu, Y.-C., J. Pan, C. Zhang, W. Fan, M. Collinge, J.R. Bender, and S.M. Weissman. 1999. A MHC-encoded ubiquitin-like protein (FAT10) binds noncovalently to the spindle assembly checkpoint protein MAD2. *Proc. Natl. Acad. Sci.* 96:4313–4318. doi:10.1073/pnas.96.8.4313.

Liu, Z., P. Chen, H. Gao, Y. Gu, J. Yang, H. Peng, X. Xu, H. Wang, M. Yang, X. Liu, L. Fan, S. Chen, J. Zhou, Y. Sun, K. Ruan, S. Cheng, M.

Komatsu, E. White, L. Li, H. Ji, D. Finley, and R. Hu. 2014. Ubiquitylation of Autophagy Receptor Optineurin by HACE1 Activates Selective Autophagy for Tumor Suppression. *Cancer Cell*. 26:106–120. doi:10.1016/j.ccr.2014.05.015.

Llambi, F., T. Moldoveanu, S.W.G. Tait, L. Bouchier-Hayes, J. Temirov, L.L. McCormick, C.P. Dillon, and D.R. Green. 2011. A Unified Model of Mammalian BCL-2 Protein Family Interactions at the Mitochondria. *Mol. Cell*. 44:517–531. doi:10.1016/j.molcel.2011.10.001.

Llambi, F., Y.-M. Wang, B. Victor, M. Yang, D.M. Schneider, S. Gingras, M.J. Parsons, J.H. Zheng, S.A. Brown, S. Pelletier, T. Moldoveanu, T. Chen, and D.R. Green. 2016. BOK Is a Non-canonical BCL-2 Family Effector of Apoptosis Regulated by ER-Associated Degradation. *Cell*. 165:421–433. doi:10.1016/j.cell.2016.02.026.

Lomonosova, E., and G. Chinnadurai. 2008. BH3-only proteins in apoptosis and beyond: an overview. *Oncogene*. 27:S2–S19. doi:10.1038/onc.2009.39.

Luo, H., B. Jing, Y. Xia, Y. Zhang, M. Hu, H. Cai, Y. Tong, L. Zhou, L. Yang, J. Yang, H. Lei, H. Xu, C. Liu, and Y. Wu. 2019. WP1130 reveals USP24 as a novel target in T-cell acute lymphoblastic leukemia. *Cancer Cell Int.* 19:56. doi:10.1186/s12935-019-0773-6.

Luo, H., J. Krigman, R. Zhang, M. Yang, and N. Sun. 2021. Pharmacological inhibition of USP30 activates tissue-specific mitophagy. *Acta Physiol.* doi:10.1111/apha.13666.

Luo, X., K.L. O'Neill, and K. Huang. 2020. The third model of Bax/Bak activation: a Bcl-2 family feud finally resolved? *F1000Research*. 9:935. doi:10.12688/f1000research.25607.1.

MacVicar, T.D.B., and J.D. Lane. 2014. Impaired OMA1-dependent cleavage of OPA1 and reduced DRP1 fission activity combine to prevent mitophagy in cells that are dependent on oxidative phosphorylation. *J. Cell Sci.* 127:2313–2325. doi:10.1242/jcs.144337.

Madden, E., S.E. Logue, S.J. Healy, S. Manie, and A. Samali. 2019. The role of the unfolded protein response in cancer progression: From oncogenesis to chemoresistance. *Biol. Cell*. 111:1–17. doi:10.1111/boc.201800050.

Madeira, F., Y. mi Park, J. Lee, N. Buso, T. Gur, N. Madhusoodanan, P. Basutkar, A.R.N. Tivey, S.C. Potter, R.D. Finn, and R. Lopez. 2019. The EMBL-EBI search and sequence analysis tools APIs in 2019. *Nucleic Acids Res.* 47:W636–W641. doi:10.1093/nar/gkz268.

Maiti, T.K., M. Permaul, D.A. Boudreaux, C. Mahanic, S. Mauney, and C. Das. 2011. Crystal structure of the catalytic domain of UCHL5, a proteasome-associated human deubiquitinating enzyme, reveals an unproductive form of the enzyme: Unproductive form of the catalytic site

in UCHL5. *FEBS J.* 278:4917–4926. doi:10.1111/j.1742-4658.2011.08393.x.

Maiuri, M.C., G. Le Toumelin, A. Criollo, J.C. Rain, F. Gautier, P. Juin, E. Tasdemir, G. Pierron, K. Troulinaki, N. Tavernarakis, J.A. Hickman, O. Geneste, and G. Kroemer. 2007. Functional and physical interaction between Bcl-XL and a BH3-like domain in Beclin-1. *EMBO J.* 26:2527–2539. doi:10.1038/sj.emboj.7601689.

Makarova, K.S., L. Aravind, and E.V. Koonin. 2000. A novel superfamily of predicted cysteine proteases from eukaryotes, viruses and Chlamydia pneumoniae. *Trends Biochem. Sci.* 25:50–52. doi:10.1016/S0968-0004(99)01530-3.

Malakhov, M.P., O.A. Malakhova, K.I. Kim, K.J. Ritchie, and D.-E. Zhang. 2002. UBP43 (USP18) Specifically Removes ISG15 from Conjugated Proteins. *J. Biol. Chem.* 277:9976–9981. doi:10.1074/jbc.M109078200.

Malik, R., R. Lenobel, A. Santamaria, A. Ries, E.A. Nigg, and R. Körner. 2009. Quantitative Analysis of the Human Spindle Phosphoproteome at Distinct Mitotic Stages. *J. Proteome Res.* 8:4553–4563. doi:10.1021/pr9003773.

Mallick, D.J., R.S. Soderquist, D. Bates, and A. Eastman. 2019. Confounding off-target effects of BH3 mimetics at commonly used concentrations: MIM1, UMI-77, and A-1210477. *Cell Death Dis.* 10:185. doi:10.1038/s41419-019-1426-3.

Mandemaker, I.K., L. van Cuijk, R.C. Janssens, H. Lans, K. Bezstarosti, J.H. Hoeijmakers, J.A. Demmers, W. Vermeulen, and J.A. Marteijn. 2017. DNA damage-induced histone H1 ubiquitylation is mediated by HUWE1 and stimulates the RNF8-RNF168 pathway. *Sci. Rep.* 7:15353. doi:10.1038/s41598-017-15194-y.

Marani, M., T. Tenev, D. Hancock, J. Downward, and N.R. Lemoine. 2002. Identification of Novel Isoforms of the BH3 Domain Protein Bim Which Directly Activate Bax To Trigger Apoptosis. *Mol. Cell. Biol.* 22:3577–3589. doi:10.1128/MCB.22.11.3577-3589.2002.

Marcassa, E., A. Kallinos, J. Jardine, E.V. Rusilowicz-Jones, M.J. Clague, and S. Urbé. 2019. New aspects of USP30 biology in the regulation of pexophagy. *Autophagy*. 15:1634–1637. doi:10.1080/15548627.2019.1615304.

Marcassa, E., A. Kallinos, J. Jardine, E.V. Rusilowicz-jones, A. Martinez, S. Kuehl, M. Islinger, M.J. Clague, and S. Urbé. 2018. Dual role of USP 30 in controlling basal pexophagy and mitophagy. 1–14. doi:10.15252/embr.201745595.

Maria Fimia, G., A. Stoykova, A. Romagnoli, L. Giunta, S. Di Bartolomeo, R. Nardacci, M. Corazzari, C. Fuoco, A. Ucar, P. Schwartz, P. Gruss, M. Piacentini, K. Chowdhury, and F. Cecconi. 2007. Ambra1 regulates

autophagy and development of the nervous system. *Nature*. 447:1121–1125. doi:10.1038/nature05925.

Marraffini, L.A., and E.J. Sontheimer. 2008. CRISPR Interference Limits Horizontal Gene Transfer in Staphylococci by Targeting DNA. *Science*. 322:1843–1845. doi:10.1126/science.1165771.

Marshall, R.S., and R.D. Vierstra. 2019. Dynamic Regulation of the 26S Proteasome: From Synthesis to Degradation. *Front. Mol. Biosci.* 6:40. doi:10.3389/fmolb.2019.00040.

Matheoud, D., T. Cannon, A. Voisin, A.-M. Penttinen, L. Ramet, A.M. Fahmy, C. Ducrot, A. Laplante, M.-J. Bourque, L. Zhu, R. Cayrol, A. Le Campion, H.M. McBride, S. Gruenheid, L.-E. Trudeau, and M. Desjardins. 2019. Intestinal infection triggers Parkinson's disease-like symptoms in Pink1-/- mice. *Nature*. 571:565–569. doi:10.1038/s41586-019-1405-y.

Mathieu, A.-L., O. Sperandio, V. Pottiez, S. Balzarin, A. Herlédan, J.O. Elkaïm, M.-L. Fogeron, C. Piveteau, S. Dassonneville, B. Deprez, B.O. Villoutreix, N. Bonnefoy, and F. Leroux. 2014. Identification of Small Inhibitory Molecules Targeting the Bfl-1 Anti-Apoptotic Protein That Alleviates Resistance to ABT-737. *J. Biomol. Screen.* 19:1035–1046. doi:10.1177/1087057114534070.

Matlashewski, G., L. Banks, D. Pim, and L. Crawford. 1986. Analysis of human p53 proteins and mRNA levels in normal and transformed cells. *Eur. J. Biochem.* 154:665–672. doi:10.1111/j.1432-1033.1986.tb09449.x.

Maytal-Kivity, V., N. Reis, K. Hofmann, and M.H. Glickman. 2002. MPN+, a putative catalytic motif found in a subset of MPN domain proteins from eukaryotes and prokaryotes, is critical for Rpn11 function. *BMC Biochem.* 3:28. doi:10.1186/1471-2091-3-28.

McCoy, M.K., A. Kaganovich, I.N. Rudenko, J. Ding, and M.R. Cookson. 2014. Hexokinase activity is required for recruitment of parkin to depolarized mitochondria. *Hum. Mol. Genet.* 23:145–156. doi:10.1093/hmg/ddt407.

McCullough, J., M.J. Clague, and S. Urbé. 2004. AMSH is an endosome-associated ubiquitin isopeptidase. *J. Cell Biol.* 166:487–492. doi:10.1083/jcb.200401141.

McGrath, J.P., S. Jentsch, and A. Varshavsky. 1991. UBA 1: an essential yeast gene encoding ubiquitin-activating enzyme. *EMBO J.* 10:227–236. doi:10.1002/j.1460-2075.1991.tb07940.x.

McWilliams, T.G., E. Barini, R. Pohjolan-Pirhonen, S.P. Brooks, F. Singh, S. Burel, K. Balk, A. Kumar, L. Montava-Garriga, A.R. Prescott, S.M. Hassoun, F. Mouton-Liger, G. Ball, R. Hills, A. Knebel, A. Ulusoy, D.A. Di Monte, J. Tamjar, O. Antico, K. Fears, L. Smith, R. Brambilla, E. Palin, M. Valori, J. Eerola-Rautio, P. Tienari, O. Corti, S.B. Dunnett, I.G. Ganley, A. Suomalainen, and M.M.K. Muqit. 2018a. Phosphorylation of

Parkin at serine 65 is essential for its activation *in vivo*. *Open Biol.* 8:180108. doi:10.1098/rsob.180108.

McWilliams, T.G., A.R. Prescott, G.F.G. Allen, J. Tamjar, M.J. Munson, C. Thomson, M.M.K. Muqit, and I.G. Ganley. 2016. mito-QC illuminates mitophagy and mitochondrial architecture in vivo. *J. Cell Biol.* 214:333–345. doi:10.1083/jcb.201603039.

McWilliams, T.G., A.R. Prescott, L. Montava-Garriga, G. Ball, F. Singh, E. Barini, M.M.K. Muqit, S.P. Brooks, and I.G. Ganley. 2018b. Basal Mitophagy Occurs Independently of PINK1 in Mouse Tissues of High Metabolic Demand. *Cell Metab.* 27:439-449.e5. doi:10.1016/j.cmet.2017.12.008.

Meas, R., and P. Mao. 2015. Histone ubiquitylation and its roles in transcription and DNA damage response. *DNA Repair*. 36:36–42. doi:10.1016/j.dnarep.2015.09.016.

Mérino, D., M. Giam, P.D. Hughes, O.M. Siggs, K. Heger, L.A. O'Reilly, J.M. Adams, A. Strasser, E.F. Lee, W.D. Fairlie, and P. Bouillet. 2009. The role of BH3-only protein Bim extends beyond inhibiting Bcl-2–like prosurvival proteins. *J. Cell Biol.* 186:355–362. doi:10.1083/jcb.200905153.

Mevissen, T.E.T., M.K. Hospenthal, P.P. Geurink, P.R. Elliott, M. Akutsu, N. Arnaudo, R. Ekkebus, Y. Kulathu, T. Wauer, F. El Oualid, S.M.V. Freund, H. Ovaa, and D. Komander. 2013. OTU deubiquitinases reveal mechanisms of linkage specificity and enable ubiquitin chain restriction analysis. *Cell*. 154:169–184. doi:10.1016/j.cell.2013.05.046.

Michaud, M., X. Xie, J.M. Bravo-San Pedro, L. Zitvogel, E. White, and G. Kroemer. 2014. An autophagy-dependent anticancer immune response determines the efficacy of melanoma chemotherapy. *Oncoimmunology*. 3:e944047. doi:10.4161/21624011.2014.944047.

Michel, M.A., P.R. Elliott, K.N. Swatek, M. Simicek, J.N. Pruneda, J.L. Wagstaff, S.M.V. Freund, and D. Komander. 2015. Assembly and Specific Recognition of K29- and K33-Linked Polyubiquitin. *Mol. Cell*. 58:95–109. doi:10.1016/j.molcel.2015.01.042.

Michel, M.A., K.N. Swatek, M.K. Hospenthal, and D. Komander. 2017. Ubiquitin Linkage-Specific Affimers Reveal Insights into K6-Linked Ubiquitin Signaling. *Mol. Cell*. 68:233-246.e5. doi:10.1016/j.molcel.2017.08.020.

Michelle, C., P. Vourc'h, L. Mignon, and C.R. Andres. 2009. What Was the Set of Ubiquitin and Ubiquitin-Like Conjugating Enzymes in the Eukaryote Common Ancestor? *J. Mol. Evol.* 68:616–628. doi:10.1007/s00239-009-9225-6.

Mihara, M., S. Erster, A. Zaika, O. Petrenko, T. Chittenden, P. Pancoska, and U.M. Moll. 2003. p53 Has a Direct Apoptogenic Role at the

Mitochondria. *Mol. Cell*. 11:577–590. doi:10.1016/S1097-2765(03)00050-9.

Milani, M., D.P. Byrne, G. Greaves, M. Butterworth, G.M. Cohen, P.A. Eyers, and S. Varadarajan. 2017. DRP-1 is required for BH3 mimetic-mediated mitochondrial fragmentation and apoptosis. *Cell Death Dis.* 8:e2552. doi:10.1038/cddis.2016.485.

Miller, S., and M.M.K. Muqit. 2019. Therapeutic approaches to enhance PINK1/Parkin mediated mitophagy for the treatment of Parkinson's disease. *Neurosci. Lett.* 705:7–13. doi:10.1016/j.neulet.2019.04.029.

Misra, M., M. Kuhn, M. Löbel, H. An, A.V. Statsyuk, C. Sotriffer, and H. Schindelin. 2017. Dissecting the Specificity of Adenosyl Sulfamate Inhibitors Targeting the Ubiquitin-Activating Enzyme. *Structure*. 25:1120-1129.e3. doi:10.1016/j.str.2017.05.001.

Mitchell, P. 1961. Coupling of Phosphorylation to Electron and Hydrogen Transfer by a Chemi-Osmotic type of Mechanism. *Nature*. 191:144–148. doi:10.1038/191144a0.

Miyamoto, S., A.N. Murphy, and J.H. Brown. 2008. Akt mediates mitochondrial protection in cardiomyocytes through phosphorylation of mitochondrial hexokinase-II. *Cell Death Differ.* 15:521–529. doi:10.1038/sj.cdd.4402285.

Mizushima, N., and M. Komatsu. 2011. Autophagy: Renovation of Cells and Tissues. *Cell*. 147:728–741. doi:10.1016/j.cell.2011.10.026.

Mizushima, N., and B. Levine. 2010. Autophagy in mammalian development and differentiation. *Nat. Cell Biol.* 12:823–830. doi:10.1038/ncb0910-823.

Mizushima, N., B. Levine, A.M. Cuervo, and D.J. Klionsky. 2008. Autophagy fights disease through cellular self-digestion. *Nature*. 451:1069–1075. doi:10.1038/nature06639.

Mizushima, N., T. Noda, T. Yoshimori, Y. Tanaka, T. Ishii, M.D. George, D.J. Klionsky, M. Ohsumi, and Y. Ohsumi. 1998. A protein conjugation system essential for autophagy. *Nature*. 395:395–398. doi:10.1038/26506.

Moehle, M.S., and A.B. West. 2015. M1 and M2 immune activation in Parkinson's Disease: Foe and ally? *Neuroscience*. 302:59–73. doi:10.1016/j.neuroscience.2014.11.018.

Mojica, F.J.M., G. Juez, and F. Rodriguez-Valera. 1993. Transcription at different salinities of Haloferax mediterranei sequences adjacent to partially modified PstI sites. *Mol. Microbiol.* 9:613–621. doi:10.1111/j.1365-2958.1993.tb01721.x.

Momeni, H.R. 2011. Role of calpain in apoptosis. *Cell J.* 13:65–72.

Morett, E., and P. Bork. 1999. A novel transactivation domain in parkin. *Trends Biochem. Sci.* 24:229–231. doi:https://doi.org/10.1016/S0968-0004(99)01381-X.

Moritz, A., Y. Li, A. Guo, J. Villen, Y. Wang, J. MacNeill, J. Kornhauser, K. Sprott, J. Zhou, A. Possemato, J.M. Ren, P. Hornbeck, L.C. Cantley, S.P. Gygi, J. Rush, and M.J. Comb. 2010. Akt-RSK-S6 Kinase Signaling Networks Activated by Oncogenic Receptor Tyrosine Kinases. *Sci. Signal.* 3:ra64–ra64. doi:10.1126/scisignal.2000998.

Moro, L. 2019. Mitochondrial Dysfunction in Aging and Cancer. *J. Clin. Med.* 8. doi:10.3390/jcm8111983.

Mulcahy Levy, J.M., and A. Thorburn. 2020. Autophagy in cancer: moving from understanding mechanism to improving therapy responses in patients. *Cell Death Differ.* 27:843–857. doi:10.1038/s41418-019-0474-7.

Muqit, M.M.K., P.M. Abou-Sleiman, A.T. Saurin, K. Harvey, S. Gandhi, E. Deas, S. Eaton, M.D. Payne Smith, K. Venner, A. Matilla, D.G. Healy, W.P. Gilks, A.J. Lees, J. Holton, T. Revesz, P.J. Parker, R.J. Harvey, N.W. Wood, and D.S. Latchman. 2006. Altered cleavage and localization of PINK1 to aggresomes in the presence of proteasomal stress. *J. Neurochem.* 98:156–169. doi:10.1111/j.1471-4159.2006.03845.x.

Murakawa, T., O. Yamaguchi, A. Hashimoto, S. Hikoso, T. Takeda, T. Oka, H. Yasui, H. Ueda, Y. Akazawa, H. Nakayama, M. Taneike, T. Misaka, S. Omiya, A.M. Shah, A. Yamamoto, K. Nishida, Y. Ohsumi, K. Okamoto, Y. Sakata, and K. Otsu. 2015. Bcl-2-like protein 13 is a mammalian Atg32 homologue that mediates mitophagy and mitochondrial fragmentation. *Nat. Commun.* 6. doi:10.1038/ncomms8527.

Murata, H., M. Sakaguchi, Y. Jin, Y. Sakaguchi, J. Futami, H. Yamada, K. Kataoka, and N. Huh. 2011. A New Cytosolic Pathway from a Parkinson Disease-associated Kinase, BRPK/PINK1: ACTIVATION OF AKT VIA MTORC2. *J. Biol. Chem.* 286:7182–7189. doi:10.1074/jbc.M110.179390.

Murray, J.T., C. Panaretou, H. Stenmark, M. Miaczynska, and J.M. Backer. 2002. Role of Rab5 in the Recruitment of hVps34/p150 to the Early Endosome: **Rab5 Regulation of p150/hVps34**. *Traffic*. 3:416–427. doi:10.1034/j.1600-0854.2002.30605.x.

Nagasaka, M., B. Potugari, A. Nguyen, A. Sukari, A.S. Azmi, and S.-H.I. Ou. 2021. KRAS Inhibitors– yes but what next? Direct targeting of KRAS–vaccines, adoptive T cell therapy and beyond. *Cancer Treat. Rev.* 101:102309. doi:10.1016/j.ctrv.2021.102309.

Nakajima, A., K. Kataoka, M. Hong, M. Sakaguchi, and N. Huh. 2003. BRPK, a novel protein kinase showing increased expression in mouse cancer

cell lines with higher metastatic potential. *Cancer Lett.* 201:195–201. doi:10.1016/S0304-3835(03)00443-9.

Nakamura, M., N. Tanaka, N. Kitamura, and M. Komada. 2006. Clathrin anchors deubiquitinating enzymes, AMSH and AMSH-like protein, on early endosomes. *Genes Cells*. 11:593–606. doi:10.1111/j.1365-2443.2006.00963.x.

Nakamura, N., and S. Hirose. 2008. Regulation of Mitochondrial Morphology by USP30, a Deubiquitinating Enzyme Present in the Mitochondrial Outer Membrane. *Mol. Biol. Cell*. 19:1903–1911. doi:10.1091/mbc.e07-11-1103.

Nakano, K., and K.H. Vousden. 2001. PUMA, a Novel Proapoptotic Gene, Is Induced by p53. *Mol. Cell*. 7:683–694. doi:10.1016/S1097-2765(01)00214-3.

Nakatogawa, H., and K. Mochida. 2015. Reticulophagy and nucleophagy: New findings and unsolved issues. *Autophagy*. 11:2377–2378. doi:10.1080/15548627.2015.1106665.

Narendra, D., A. Tanaka, D.-F. Suen, and R.J. Youle. 2008. Parkin is recruited selectively to impaired mitochondria and promotes their autophagy. *J. Cell Biol.* 183:795–803. doi:10.1083/jcb.200809125.

Narendra, D.P., S.M. Jin, A. Tanaka, D.-F. Suen, C.A. Gautier, J. Shen, M.R. Cookson, and R.J. Youle. 2010. PINK1 Is Selectively Stabilized on Impaired Mitochondria to Activate Parkin. *PLoS Biol.* 8:e1000298. doi:10.1371/journal.pbio.1000298.

Ni, W., Y. Xia, L. Luo, F. Wen, D. Hu, Y. Bi, and J. Qi. 2020. High expression of ALDH1A3 might independently influence poor progression-free and overall survival in patients with glioma via maintaining glucose uptake and lactate production. *Cell Biol. Int.* 44:569–582. doi:10.1002/cbin.11257.

Nijman, S.M.B., M.P.A. Luna-Vargas, A. Velds, T.R. Brummelkamp, A.M.G. Dirac, T.K. Sixma, and R. Bernards. 2005. A Genomic and Functional Inventory of Deubiquitinating Enzymes. *Cell*. 123:773–786. doi:10.1016/j.cell.2005.11.007.

Novak, I., V. Kirkin, D.G. McEwan, J. Zhang, P. Wild, A. Rozenknop, V. Rogov, F. Löhr, D. Popovic, A. Occhipinti, A.S. Reichert, J. Terzic, V. Dötsch, P.A. Ney, and I. Dikic. 2010. Nix is a selective autophagy receptor for mitochondrial clearance. *EMBO Rep.* 11:45–51. doi:10.1038/embor.2009.256.

Nucifora, F.C., L.G. Nucifora, C.-H. Ng, N. Arbez, Y. Guo, E. Roby, V. Shani, S. Engelender, D. Wei, X.-F. Wang, T. Li, D.J. Moore, O. Pletnikova, J.C. Troncoso, A. Sawa, T.M. Dawson, W. Smith, K.-L. Lim, and C.A. Ross. 2016. Ubiqutination via K27 and K29 chains signals aggregation

and neuronal protection of LRRK2 by WSB1. *Nat. Commun.* 7. doi:10.1038/ncomms11792.

Nuttall, J.M., A.M. Motley, and E.H. Hettema. 2014. Deficiency of the exportomer components Pex1, Pex6, and Pex15 causes enhanced pexophagy in *Saccharomyces cerevisiae*. *Autophagy*. 10:835–845. doi:10.4161/auto.28259.

Oeljeklaus, S., B.S. Reinartz, J. Wolf, S. Wiese, J. Tonillo, K. Podwojski, K. Kuhlmann, C. Stephan, H.E. Meyer, W. Schliebs, C. Brocard, R. Erdmann, and B. Warscheid. 2012. Identification of Core Components and Transient Interactors of the Peroxisomal Importomer by Dual-Track Stable Isotope Labeling with Amino Acids in Cell Culture Analysis. *J. Proteome Res.* 11:2567–2580. doi:10.1021/pr3000333.

O'Flanagan, C.H., and C. O'Neill. 2014. PINK1 signalling in cancer biology. *Biochim. Biophys. Acta BBA - Rev. Cancer*. 1846:590–598. doi:10.1016/j.bbcan.2014.10.006.

Oh, E., D. Akopian, and M. Rape. 2018. Principles of Ubiquitin-Dependent Signaling. *Annu. Rev. Cell Dev. Biol.* 34:137–162. doi:10.1146/annurev-cellbio-100617-062802.

Ohashi, Y., S. Tremel, G.R. Masson, L. McGinney, J. Boulanger, K. Rostislavleva, C.M. Johnson, I. Niewczas, J. Clark, and R.L. Williams. 2020. Membrane characteristics tune activities of endosomal and autophagic human VPS34 complexes. *eLife*. 9. doi:10.7554/eLife.58281.

Okatsu, K., M. Kimura, T. Oka, K. Tanaka, and N. Matsuda. 2015. Unconventional PINK1 localization to the outer membrane of depolarized mitochondria drives Parkin recruitment. *J. Cell Sci.* 128:964–978. doi:10.1242/jcs.161000.

Okatsu, K., T. Oka, M. Iguchi, K. Imamura, H. Kosako, N. Tani, M. Kimura, E. Go, F. Koyano, M. Funayama, K. Shiba-Fukushima, S. Sato, H. Shimizu, Y. Fukunaga, H. Taniguchi, M. Komatsu, N. Hattori, K. Mihara, K. Tanaka, and N. Matsuda. 2012. PINK1 autophosphorylation upon membrane potential dissipation is essential for Parkin recruitment to damaged mitochondria. *Nat. Commun.* 3. doi:10.1038/ncomms2016.

Okatsu, K., M. Uno, F. Koyano, E. Go, M. Kimura, T. Oka, K. Tanaka, and N. Matsuda. 2013. A Dimeric PINK1-containing Complex on Depolarized Mitochondria Stimulates Parkin Recruitment. *J. Biol. Chem.* 288:36372–36384. doi:10.1074/jbc.M113.509653.

Okumura, K., S. Huang, and F.A. Sinicrope. 2008. Induction of Noxa sensitizes human colorectal cancer cells expressing Mcl-1 to the small-molecule Bcl-2/Bcl-xL inhibitor, ABT-737. *Clin. Cancer Res. Off. J. Am. Assoc. Cancer Res.* 14:8132–8142. doi:10.1158/1078-0432.CCR-08-1665.

Oltersdorf, T., S.W. Elmore, A.R. Shoemaker, R.C. Armstrong, D.J. Augeri, B.A. Belli, M. Bruncko, T.L. Deckwerth, J. Dinges, P.J. Hajduk, M.K. Joseph, S. Kitada, S.J. Korsmeyer, A.R. Kunzer, A. Letai, C. Li, M.J. Mitten, D.G. Nettesheim, S. Ng, P.M. Nimmer, J.M. O'Connor, A. Oleksijew, A.M. Petros, J.C. Reed, W. Shen, S.K. Tahir, C.B. Thompson, K.J. Tomaselli, B. Wang, M.D. Wendt, H. Zhang, S.W. Fesik, and S.H. Rosenberg. 2005. An inhibitor of Bcl-2 family proteins induces regression of solid tumours. *Nature*. 435:677–681. doi:10.1038/nature03579.

O'Neill, K.L., K. Huang, J. Zhang, Y. Chen, and X. Luo. 2016. Inactivation of prosurvival Bcl-2 proteins activates Bax/Bak through the outer mitochondrial membrane. *Genes Dev.* 30:973–988. doi:10.1101/gad.276725.115.

Ong, S.-E., B. Blagoev, I. Kratchmarova, D.B. Kristensen, H. Steen, A. Pandey, and M. Mann. 2002. Stable Isotope Labeling by Amino Acids in Cell Culture, SILAC, as a Simple and Accurate Approach to Expression Proteomics. *Mol. Cell. Proteomics*. 1:376–386. doi:10.1074/mcp.M200025-MCP200.

Ordureau, A., J.-M. Heo, D.M. Duda, J.A. Paulo, J.L. Olszewski, D. Yanishevski, J. Rinehart, B.A. Schulman, and J.W. Harper. 2015. Defining roles of PARKIN and ubiquitin phosphorylation by PINK1 in mitochondrial quality control using a ubiquitin replacement strategy. *Proc. Natl. Acad. Sci.* 112:6637–6642. doi:10.1073/pnas.1506593112.

Ordureau, A., J.A. Paulo, J. Zhang, H. An, K.N. Swatek, J.R. Cannon, Q. Wan, D. Komander, and J.W. Harper. 2020. Global Landscape and Dynamics of Parkin and USP30-Dependent Ubiquitylomes in iNeurons during Mitophagic Signaling. *Mol. Cell*. 77:1124-1142.e10. doi:10.1016/j.molcel.2019.11.013.

Ordureau, A., S.A. Sarraf, D.M. Duda, J.-M. Heo, M.P. Jedrychowski, V.O. Sviderskiy, J.L. Olszewski, J.T. Koerber, T. Xie, S.A. Beausoleil, J.A. Wells, S.P. Gygi, B.A. Schulman, and J.W. Harper. 2014. Quantitative Proteomics Reveal a Feedforward Mechanism for Mitochondrial PARKIN Translocation and Ubiquitin Chain Synthesis. *Mol. Cell*. 56:360–375. doi:10.1016/j.molcel.2014.09.007.

Orian, A., H. Gonen, B. Bercovich, I. Fajerman, E. Eytan, A. Israël, F. Mercurio, K. Iwai, A.L. Schwartz, and A. Ciechanover. 2000. SCF(beta)(-TrCP) ubiquitin ligase-mediated processing of NF-kappaB p105 requires phosphorylation of its C-terminus by IkappaB kinase. *EMBO J.* 19:2580–2591. doi:10.1093/emboj/19.11.2580.

Osellame, L.D., T.S. Blacker, and M.R. Duchen. 2012. Cellular and molecular mechanisms of mitochondrial function. *Best Pract. Res. Clin. Endocrinol. Metab.* 26:711–723. doi:10.1016/j.beem.2012.05.003.

Ott, M., J.D. Robertson, V. Gogvadze, B. Zhivotovsky, and S. Orrenius. 2002. Cytochrome c release from mitochondria proceeds by a two-step process. *Proc. Natl. Acad. Sci. U. S. A.* 99:1259–1263. doi:10.1073/pnas.241655498.

Özkaynak, E., D. Finley, and A. Varshavsky. 1984. The yeast ubiquitin gene: head-to-tail repeats encoding a polyubiquitin precursor protein. *Nature*. 312:663–666. doi:10.1038/312663a0.

Park, J., S.B. Lee, S. Lee, Y. Kim, S. Song, S. Kim, E. Bae, J. Kim, M. Shong, J.-M. Kim, and J. Chung. 2006. Mitochondrial dysfunction in Drosophila PINK1 mutants is complemented by parkin. *Nature*. 441:1157–1161. doi:10.1038/nature04788.

Park, J.-S., R.L. Davis, and C.M. Sue. 2018. Mitochondrial Dysfunction in Parkinson's Disease: New Mechanistic Insights and Therapeutic Perspectives. *Curr. Neurol. Neurosci. Rep.* 18:21. doi:10.1007/s11910-018-0829-3.

Park, S.-M., J.-B. Yoon, and T.H. Lee. 2004. Receptor interacting protein is ubiquitinated by cellular inhibitor of apoptosis proteins (c-IAP1 and c-IAP2) in vitro. *FEBS Lett.* 566:151–156. doi:10.1016/j.febslet.2004.04.021.

Parkinson, J. 2002. An Essay on the Shaking Palsy. *J. Neuropsychiatry Clin. Neurosci.* 14:223–236. doi:10.1176/jnp.14.2.223.

Pastorino, J.G., and J.B. Hoek. 2008. Regulation of hexokinase binding to VDAC. *J. Bioenerg. Biomembr.* 40:171–182. doi:10.1007/s10863-008-9148-8.

Patel, K., Z.S. Ahmed, X. Huang, Q. Yang, E. Ekinci, C.M. Neslund-Dudas, B. Mitra, F.A. Elnady, Y.-H. Ahn, H. Yang, J. Liu, and Q.P. Dou. 2018. Discovering proteasomal deubiquitinating enzyme inhibitors for cancer therapy: lessons from rational design, nature and old drug reposition. *Future Med. Chem.* 10:2087–2108. doi:10.4155/fmc-2018-0091.

Pathare, G.R., I. Nagy, P. Sledz, D.J. Anderson, H.-J. Zhou, E. Pardon, J. Steyaert, F. Forster, A. Bracher, and W. Baumeister. 2014. Crystal structure of the proteasomal deubiquitylation module Rpn8-Rpn11. *Proc. Natl. Acad. Sci.* 111:2984–2989. doi:10.1073/pnas.1400546111.

Pattingre, S., and B. Levine. 2006. Bcl-2 Inhibition of Autophagy: A New Route to Cancer?: Figure 1. *Cancer Res.* 66:2885–2888. doi:10.1158/0008-5472.CAN-05-4412.

Pattingre, S., A. Tassa, X. Qu, R. Garuti, X.H. Liang, N. Mizushima, M. Packer, M.D. Schneider, and B. Levine. 2005. Bcl-2 Antiapoptotic Proteins Inhibit Beclin 1-Dependent Autophagy. *Cell*. 122:927–939. doi:10.1016/j.cell.2005.07.002.

Peng, J., D. Schwartz, J.E. Elias, C.C. Thoreen, D. Cheng, G. Marsischky, J. Roelofs, D. Finley, and S.P. Gygi. 2003. A proteomics approach to understanding protein ubiquitination. *Nat. Biotechnol.* 21:921–926. doi:10.1038/nbt849.

Pentimalli, F. 2018. BCL2: a 30-year tale of life, death and much more to come. *Cell Death Differ.* 25:7–9. doi:10.1038/cdd.2017.189.

Pereira, L., P. Soares, V. Máximo, and D.C. Samuels. 2012. Somatic mitochondrial DNA mutations in cancer escape purifying selection and high pathogenicity mutations lead to the oncocytic phenotype: pathogenicity analysis of reported somatic mtDNA mutations in tumors. *BMC Cancer*. 12. doi:10.1186/1471-2407-12-53.

Peterson, L.F., H. Sun, Y. Liu, H. Potu, M. Kandarpa, M. Ermann, S.M. Courtney, M. Young, H.D. Showalter, D. Sun, A. Jakubowiak, S.N. Malek, M. Talpaz, and N.J. Donato. 2015. Targeting deubiquitinase activity with a novel small-molecule inhibitor as therapy for B-cell malignancies. *Blood*. 125:3588–3597. doi:10.1182/blood-2014-10-605584.

Pey, A.L., C.F. Megarity, and D.J. Timson. 2019. NAD(P)H quinone oxidoreductase (NQO1): an enzyme which needs just enough mobility, in just the right places. *Biosci. Rep.* 39. doi:10.1042/BSR20180459.

Phu, L., C.M. Rose, J.S. Tea, C.E. Wall, E. Verschueren, T.K. Cheung, D.S. Kirkpatrick, and B. Bingol. 2020. Dynamic Regulation of Mitochondrial Import by the Ubiquitin System. *Mol. Cell*. 77:1107-1123.e10. doi:10.1016/j.molcel.2020.02.012.

Pietrocola, F., J. Pol, E. Vacchelli, S. Rao, D.P. Enot, E.E. Baracco, S. Levesque, F. Castoldi, N. Jacquelot, T. Yamazaki, L. Senovilla, G. Marino, F. Aranda, S. Durand, V. Sica, A. Chery, S. Lachkar, V. Sigl, N. Bloy, A. Buque, S. Falzoni, B. Ryffel, L. Apetoh, F. Di Virgilio, F. Madeo, M.C. Maiuri, L. Zitvogel, B. Levine, J.M. Penninger, and G. Kroemer. 2016. Caloric Restriction Mimetics Enhance Anticancer Immunosurveillance. *Cancer Cell*. 30:147–160. doi:10.1016/j.ccell.2016.05.016.

Piotrowski, J., R. Beal, L. Hoffman, K.D. Wilkinson, R.E. Cohen, and C.M. Pickart. 1997. Inhibition of the 26 S Proteasome by Polyubiquitin Chains Synthesized to Have Defined Lengths. *J. Biol. Chem.* 272:23712–23721. doi:10.1074/jbc.272.38.23712.

Plechanovová, A., E.G. Jaffray, M.H. Tatham, J.H. Naismith, and R.T. Hay. 2012. Structure of a RING E3 ligase and ubiquitin-loaded E2 primed for catalysis. *Nature*. 489:115–120. doi:10.1038/nature11376.

Poewe, W., K. Seppi, C.M. Tanner, G.M. Halliday, P. Brundin, J. Volkmann, A.-E. Schrag, and A.E. Lang. 2017. Parkinson disease. *Nat. Rev. Dis. Primer*. 3. doi:10.1038/nrdp.2017.13.

Polson, H.E.J., J. de Lartigue, D.J. Rigden, M. Reedijk, S. Urbé, M.J. Clague, and S.A. Tooze. 2010. Mammalian Atg18 (WIPI2) localizes to omegasome-anchored phagophores and positively regulates LC3 lipidation. *Autophagy*. 6:506–522. doi:10.4161/auto.6.4.11863.

Ponder, K.G., and L.H. Boise. 2019. The prodomain of caspase-3 regulates its own removal and caspase activation. *Cell Death Discov.* 5. doi:10.1038/s41420-019-0142-1.

Pouchieu, C., C. Piel, C. Carles, A. Gruber, C. Helmer, S. Tual, E. Marcotullio, P. Lebailly, and I. Baldi. 2018. Pesticide use in agriculture and Parkinson's disease in the AGRICAN cohort study. *Int. J. Epidemiol.* 47:299–310. doi:10.1093/ije/dyx225.

Poulogiannis, G., R.E. McIntyre, M. Dimitriadi, J.R. Apps, C.H. Wilson, K. Ichimura, F. Luo, L.C. Cantley, A.H. Wyllie, D.J. Adams, and M.J. Arends. 2010. PARK2 deletions occur frequently in sporadic colorectal cancer and accelerate adenoma development in Apc mutant mice. *Proc. Natl. Acad. Sci.* 107:15145–15150. doi:10.1073/pnas.1009941107.

Pourcel, C., G. Salvignol, and G. Vergnaud. 2005. CRISPR elements in Yersinia pestis acquire new repeats by preferential uptake of bacteriophage DNA, and provide additional tools for evolutionary studies. *Microbiology*. 151:653–663. doi:10.1099/mic.0.27437-0.

Powers, E.T., R.I. Morimoto, A. Dillin, J.W. Kelly, and W.E. Balch. 2009. Biological and Chemical Approaches to Diseases of Proteostasis Deficiency. *Annu. Rev. Biochem.* 78:959–991. doi:10.1146/annurev.biochem.052308.114844.

Prior, I.A., F.E. Hood, and J.L. Hartley. 2020. The Frequency of Ras Mutations in Cancer. *Cancer Res.* 80:2969–2974. doi:10.1158/0008-5472.CAN-19-3682.

Pupo, E., D. Avanzato, E. Middonti, F. Bussolino, and L. Lanzetti. 2019. KRAS-Driven Metabolic Rewiring Reveals Novel Actionable Targets in Cancer. *Front. Oncol.* 9:848. doi:10.3389/fonc.2019.00848.

Pusec, C.M., A. De Jesus, M.W. Khan, A.R. Terry, A.E. Ludvik, K. Xu, N. Giancola, H. Pervaiz, E. Daviau Smith, X. Ding, S. Harrison, N.S. Chandel, T.C. Becker, N. Hay, H. Ardehali, J. Cordoba-Chacon, and B.T. Layden. 2019. Hepatic HKDC1 Expression Contributes to Liver Metabolism. *Endocrinology*. 160:313–330. doi:10.1210/en.2018-00887.

Qiu, X., and D.S. Fay. 2006. ARI-1, an RBR family ubiquitin-ligase, functions with UBC-18 to regulate pharyngeal development in C. elegans. *Dev. Biol.* 291:239–252. doi:10.1016/j.ydbio.2005.11.045.

Qu, X., J. Yu, G. Bhagat, N. Furuya, H. Hibshoosh, A. Troxel, J. Rosen, E.-L. Eskelinen, N. Mizushima, Y. Ohsumi, G. Cattoretti, and B. Levine. 2003.

Promotion of tumorigenesis by heterozygous disruption of the beclin 1 autophagy gene. *J. Clin. Invest.* 112:1809–1820. doi:10.1172/JCI20039.

Quesada, V., A. Díaz-Perales, A. Gutiérrez-Fernández, C. Garabaya, S. Cal, and C. López-Otín. 2004. Cloning and enzymatic analysis of 22 novel human ubiquitin-specific proteases. *Biochem. Biophys. Res. Commun.* 314:54–62. doi:10.1016/j.bbrc.2003.12.050.

Rahighi, S., F. Ikeda, M. Kawasaki, M. Akutsu, N. Suzuki, R. Kato, T. Kensche, T. Uejima, S. Bloor, D. Komander, F. Randow, S. Wakatsuki, and I. Dikic. 2009. Specific recognition of linear ubiquitin chains by NEMO is important for NF-kappaB activation. *Cell*. 136:1098–1109. doi:10.1016/j.cell.2009.03.007.

Rape, M. 2018. Ubiquitylation at the crossroads of development and disease. *Nat. Rev. Mol. Cell Biol.* 19:59–70. doi:10.1038/nrm.2017.83.

Reiter, K.H., and R.E. Klevit. 2018. Characterization of RING-Between-RING E3 Ubiquitin Transfer Mechanisms. *In* The Ubiquitin Proteasome System. T. Mayor and G. Kleiger, editors. Springer New York, New York, NY. 3–17.

Reitzer, L.J., B.M. Wice, and D. Kennell. 1979. Evidence that glutamine, not sugar, is the major energy source for cultured HeLa cells. *J. Biol. Chem.* 254:2669–2676. doi:10.1016/S0021-9258(17)30124-2.

Renehan, A.G. 2001. What is apoptosis, and why is it important? *BMJ*. 322:1536–1538. doi:10.1136/bmj.322.7301.1536.

Riccio, V., N. Demers, R. Hua, M. Vissa, D.T. Cheng, A.W. Strilchuk, Y. Wang, G.A. McQuibban, and P.K. Kim. 2019a. Deubiquitinating enzyme USP30 maintains basal peroxisome abundance by regulating pexophagy. *J Cell Biol*. jcb.201804172. doi:10.1083/jcb.201804172.

Riccio, V., G.A. McQuibban, and P.K. Kim. 2019b. USP30: protector of peroxisomes and mitochondria. *Mol. Cell. Oncol.* 6:1600350. doi:10.1080/23723556.2019.1600350.

Rieder, R.F., D.J. Wolf, J.B. Clegg, and S.L. Lee. 1975. Rapid postsynthetic destruction of unstable haemoglobin Bushwick. *Nature*. 254:725–727. doi:10.1038/254725a0.

Riley, J.S., G. Quarato, C. Cloix, J. Lopez, J. O'Prey, M. Pearson, J. Chapman, H. Sesaki, L.M. Carlin, J.F. Passos, A.P. Wheeler, A. Oberst, K.M. Ryan, and S.W. Tait. 2018. Mitochondrial inner membrane permeabilisation enables mtDNA release during apoptosis. *EMBO J.* 37:e99238. doi:https://doi.org/10.15252/embj.201899238.

Riley, J.S., and S.W. Tait. 2020. Mitochondrial DNA in inflammation and immunity. *EMBO Rep.* 21:e49799. doi:10.15252/embr.201949799.

Ritov, V.B., E.V. Menshikova, J. He, R.E. Ferrell, B.H. Goodpaster, and D.E. Kelley. 2005. Deficiency of subsarcolemmal mitochondria in obesity and type 2 diabetes. *Diabetes*. 54:8–14. doi:10.2337/diabetes.54.1.8.

Rivett, A.J., G.G.F. Mason, R.Z. Murray, and J. Reidlinger. 1997. [No title found]. *Mol. Biol. Rep.* 24:99–102. doi:10.1023/A:1006814306401.

Robey, R.B., and N. Hay. 2006. Mitochondrial hexokinases, novel mediators of the antiapoptotic effects of growth factors and Akt. *Oncogene*. 25:4683–4696. doi:10.1038/sj.onc.1209595.

Robinson, J.S., D.J. Klionsky, L.M. Banta, and S.D. Emr. 1988. Protein sorting in Saccharomyces cerevisiae: isolation of mutants defective in the delivery and processing of multiple vacuolar hydrolases. *Mol. Cell. Biol.* 8:4936–4948. doi:10.1128/mcb.8.11.4936.

Rose, I.A., and J.V.B. Warms. 1983. An enzyme with ubiquitin carboxy-terminal esterase activity from reticulocytes. *Biochemistry*. 22:4234–4237. doi:10.1021/bi00287a012.

Rosenfeldt, M.T., and K.M. Ryan. 2011. The multiple roles of autophagy in cancer. *Carcinogenesis*. 32:955–963. doi:10.1093/carcin/bgr031.

Rossignol, R., R. Gilkerson, R. Aggeler, K. Yamagata, S.J. Remington, and R.A. Capaldi. 2004. Energy Substrate Modulates Mitochondrial Structure and Oxidative Capacity in Cancer Cells. *Cancer Res.* 64:985–993. doi:10.1158/0008-5472.CAN-03-1101.

Rothe, M., M.G. Pan, W.J. Henzel, T.M. Ayres, and D.V. Goeddel. 1995. The TNFR2-TRAF signaling complex contains two novel proteins related to baculoviral inhibitor of apoptosis proteins. *Cell*. 83:1243–1252. doi:10.1016/0092-8674(95)90149-3.

Rothman, J.H., I. Howald, and T.H. Stevens. 1989. Characterization of genes required for protein sorting and vacuolar function in the yeast Saccharomyces cerevisiae. *EMBO J.* 8:2057–2065.

Rubinstein, A.D., M. Eisenstein, Y. Ber, S. Bialik, and A. Kimchi. 2011. The Autophagy Protein Atg12 Associates with Antiapoptotic Bcl-2 Family Members to Promote Mitochondrial Apoptosis. *Mol. Cell*. 44:698–709. doi:10.1016/j.molcel.2011.10.014.

Rugbjerg, K., S. Friis, C.F. Lassen, B. Ritz, and J.H. Olsen. 2012. Malignant melanoma, breast cancer and other cancers in patients with Parkinson's disease. *Int. J. Cancer*. 131:1904–1911. doi:10.1002/ijc.27443.

Rusilowicz-Jones, E.V., F.G. Barone, F.M. Lopes, E. Stephen, H. Mortiboys, S. Urbé, and M.J. Clague. 2021. Benchmarking a highly selective USP30 inhibitor for enhancement of mitophagy and pexophagy. Cell Biology.

Rusilowicz-Jones, E.V., J. Jardine, A. Kallinos, A. Pinto-Fernandez, F. Guenther, M. Giurrandino, F.G. Barone, K. McCarron, C.J. Burke, A. Murad, A. Martinez, E. Marcassa, M. Gersch, A.J. Buckmelter, K.J. Kayser-Bricker, F. Lamoliatte, A. Gajbhiye, S. Davis, H.C. Scott, E. Murphy, K. England, H. Mortiboys, D. Komander, M. Trost, B.M. Kessler, S. Ioannidis, M.K. Ahlijanian, S. Urbé, and M.J. Clague. 2020. USP30 sets a trigger threshold for PINK1–PARKIN amplification of mitochondrial ubiquitylation. *Life Sci. Alliance*. 3:e202000768. doi:10.26508/lsa.202000768.

Ryan, B.J., S. Hoek, E.A. Fon, and R. Wade-Martins. 2015. Mitochondrial dysfunction and mitophagy in Parkinson's: from familial to sporadic disease. *Trends Biochem. Sci.* 40:200–210. doi:10.1016/j.tibs.2015.02.003.

Sahtoe, D.D., W.J. van Dijk, R. Ekkebus, H. Ovaa, and T.K. Sixma. 2016. BAP1/ASXL1 recruitment and activation for H2A deubiquitination. *Nat. Commun.* 7. doi:10.1038/ncomms10292.

Sahtoe, D.D., W.J. van Dijk, F. El Oualid, R. Ekkebus, H. Ovaa, and T.K. Sixma. 2015. Mechanism of UCH-L5 activation and inhibition by DEUBAD domains in RPN13 and INO80G. *Mol. Cell*. 57:887–900. doi:10.1016/j.molcel.2014.12.039.

Sakata, E., Y. Yamaguchi, Y. Miyauchi, K. Iwai, T. Chiba, Y. Saeki, N. Matsuda, K. Tanaka, and K. Kato. 2007. Direct interactions between NEDD8 and ubiquitin E2 conjugating enzymes upregulate cullin-based E3 ligase activity. *Nat. Struct. Mol. Biol.* 14:167–168. doi:10.1038/nsmb1191.

Saleeb, R.S., D.M. Kavanagh, A.R. Dun, P.A. Dalgarno, and R.R. Duncan. 2019. A VPS33A-binding motif on syntaxin 17 controls autophagy completion in mammalian cells. *J. Biol. Chem.* 294:4188–4201. doi:10.1074/jbc.RA118.005947.

Santana-Codina, N., J.D. Mancias, and A.C. Kimmelman. 2017. The Role of Autophagy in Cancer. *Annu. Rev. Cancer Biol.* 1:19–39. doi:10.1146/annurev-cancerbio-041816-122338.

Sargent, G., T. van Zutphen, T. Shatseva, L. Zhang, V. Di Giovanni, R. Bandsma, and P.K. Kim. 2016. PEX2 is the E3 ubiquitin ligase required for pexophagy during starvation. *J. Cell Biol.* 214:677–690. doi:10.1083/jcb.201511034.

Sarkar, S., B. Ravikumar, and D.C. Rubinsztein. 2009. Chapter 5 Autophagic Clearance of Aggregate-Prone Proteins Associated with Neurodegeneration. *In* Methods in Enzymology. Elsevier. 83–110.

Sarraf, S.A., M. Raman, V. Guarani-Pereira, M.E. Sowa, E.L. Huttlin, S.P. Gygi, and J.W. Harper. 2013. Landscape of the PARKIN-dependent

ubiquitylome in response to mitochondrial depolarization. *Nature*. 496:372–376. doi:10.1038/nature12043.

Sato, Y., E. Goto, Y. Shibata, Y. Kubota, A. Yamagata, S. Goto-Ito, K. Kubota, J. Inoue, M. Takekawa, F. Tokunaga, and S. Fukai. 2015. Structures of CYLD USP with Met1- or Lys63-linked diubiquitin reveal mechanisms for dual specificity. *Nat. Struct. Mol. Biol.* 22:222–229. doi:10.1038/nsmb.2970.

Sawa-Makarska, J., V. Baumann, N. Coudevylle, S. von Bülow, V. Nogellova, C. Abert, M. Schuschnig, M. Graef, G. Hummer, and S. Martens. 2020. Reconstitution of autophagosome nucleation defines Atg9 vesicles as seeds for membrane formation. *Science*. 369:eaaz7714. doi:10.1126/science.aaz7714.

Schapira, A.H., J.M. Cooper, D. Dexter, P. Jenner, J.B. Clark, and C.D. Marsden. 1989. Mitochondrial complex I deficiency in Parkinson's disease. *Lancet Lond. Engl.* 1:1269. doi:10.1016/s0140-6736(89)92366-0.

Schlesinger, D.H., G. Goldstein, and H.D. Niall. 1975. Complete amino acid sequence of ubiquitin, an adenylate cyclase stimulating polypeptide probably universal in living cells. *Biochemistry*. 14:2214–2218. doi:10.1021/bi00681a026.

Schrader, M. ed. . 2017. Peroxisomes: Methods and Protocols. 1595. Springer New York, New York, NY.

Schroeder, A., O. Mueller, S. Stocker, R. Salowsky, M. Leiber, M. Gassmann, S. Lightfoot, W. Menzel, M. Granzow, and T. Ragg. 2006. The RIN: an RNA integrity number for assigning integrity values to RNA measurements. *BMC Mol. Biol.* 7:3. doi:10.1186/1471-2199-7-3.

Schu, P.V., K. Takegawa, M.J. Fry, J.H. Stack, M.D. Waterfield, and S.D. Emr. 1993. Phosphatidylinositol 3-kinase encoded by yeast VPS34 gene essential for protein sorting. *Science*. 260:88–91. doi:10.1126/science.8385367.

Schubert, A.F., C. Gladkova, E. Pardon, J.L. Wagstaff, S.M.V. Freund, J. Steyaert, S.L. Maslen, and D. Komander. 2017. Structure of PINK1 in complex with its substrate ubiquitin. *Nature*. 552:51–56. doi:10.1038/nature24645.

Schug, Z.T., F. Gonzalvez, R.H. Houtkooper, F.M. Vaz, and E. Gottlieb. 2011. BID is cleaved by caspase-8 within a native complex on the mitochondrial membrane. *Cell Death Differ.* 18:538–548. doi:10.1038/cdd.2010.135.

Schulman, B.A., and J. Wade Harper. 2009. Ubiquitin-like protein activation by E1 enzymes: the apex for downstream signalling pathways. *Nat. Rev. Mol. Cell Biol.* 10:319–331. doi:10.1038/nrm2673.

Schwanhäusser, B., D. Busse, N. Li, G. Dittmar, J. Schuchhardt, J. Wolf, W. Chen, and M. Selbach. 2011. Global quantification of mammalian gene expression control. *Nature*. 473:337–342. doi:10.1038/nature10098.

Schwartzentruber, A., C. Boschian, F.M. Lopes, M.A. Myszczynska, E.J. New, J. Beyrath, J. Smeitink, L. Ferraiuolo, and H. Mortiboys. 2020. Oxidative switch drives mitophagy defects in dopaminergic parkin mutant patient neurons. *Sci. Rep.* 10. doi:10.1038/s41598-020-72345-4.

Schweitzer, A., A. Aufderheide, T. Rudack, F. Beck, G. Pfeifer, J.M. Plitzko, E. Sakata, K. Schulten, F. Förster, and W. Baumeister. 2016. Structure of the human 26S proteasome at a resolution of 3.9 Å. *Proc. Natl. Acad. Sci.* 113:7816–7821. doi:10.1073/pnas.1608050113.

Schwickart, M., X. Huang, J.R. Lill, J. Liu, R. Ferrando, D.M. French, H. Maecker, K. O'Rourke, F. Bazan, J. Eastham-Anderson, P. Yue, D. Dornan, D.C.S. Huang, and V.M. Dixit. 2010. Deubiquitinase USP9X stabilizes MCL1 and promotes tumour cell survival. *Nature*. 463:103–107. doi:10.1038/nature08646.

Scott, D.C., D.Y. Rhee, D.M. Duda, I.R. Kelsall, J.L. Olszewski, J.A. Paulo, A. de Jong, H. Ovaa, A.F. Alpi, J.W. Harper, and B.A. Schulman. 2016. Two Distinct Types of E3 Ligases Work in Unison to Regulate Substrate Ubiquitylation. *Cell*. 166:1198-1214.e24. doi:10.1016/j.cell.2016.07.027.

Scriven, P., S. Coulson, R. Haines, S. Balasubramanian, S. Cross, and L. Wyld. 2009. Activation and clinical significance of the unfolded protein response in breast cancer. *Br. J. Cancer*. 101:1692–1698. doi:10.1038/sj.bjc.6605365.

Sekine, S. 2019. PINK1 import regulation at a crossroad of mitochondrial fate: the molecular mechanisms of PINK1 import. *J. Biochem. (Tokyo)*. mvz069. doi:10.1093/jb/mvz069.

Sekine, S., C. Wang, D.P. Sideris, E. Bunker, Z. Zhang, and R.J. Youle. 2019. Reciprocal Roles of Tom7 and OMA1 during Mitochondrial Import and Activation of PINK1. *Mol. Cell*. doi:10.1016/j.molcel.2019.01.002.

Sequeiros, J., and P. Coutinho. 1993. Epidemiology and clinical aspects of Machado-Joseph disease. *Adv. Neurol.* 61:139–153.

Seshagiri, S., and L.K. Miller. 1997. Caenorhabditis elegans CED-4 stimulates CED-3 processing and CED-3-induced. *Curr. Biol.* 7:455–460. doi:10.1016/S0960-9822(06)00216-8.

Seymour, J.F., M.S. Davids, J.M. Pagel, B.S. Kahl, W.G. Wierda, S. Puvvada, J.F. Gerecitano, T.J. Kipps, M.A. Anderson, D.C.S. Huang, N. Rudersdorf, L.A. Gressick, N.P. Montalvo, J. Yang, M. Zhu, M. Dunbar, E. Cerri, S.H. Enschede, R. Humerickhouse, and A.W. Roberts. 2014. ABT-199 (GDC-0199) in relapsed/refractory (R/R) chronic lymphocytic leukemia (CLL) and small lymphocytic lymphoma (SLL): High complete-

response rate and durable disease control. *J. Clin. Oncol.* 32:7015–7015. doi:10.1200/jco.2014.32.15_suppl.7015.

Shi, Y., X. Chen, S. Elsasser, B.B. Stocks, G. Tian, B.-H. Lee, Y. Shi, N. Zhang, S.A.H. de Poot, F. Tuebing, S. Sun, J. Vannoy, S.G. Tarasov, J.R. Engen, D. Finley, and K.J. Walters. 2016. Rpn1 provides adjacent receptor sites for substrate binding and deubiquitination by the proteasome. *Science*. 351. doi:10.1126/science.aad9421.

Shiba-Fukushima, K., Y. Imai, S. Yoshida, Y. Ishihama, T. Kanao, S. Sato, and N. Hattori. 2012. PINK1-mediated phosphorylation of the Parkin ubiquitin-like domain primes mitochondrial translocation of Parkin and regulates mitophagy. *Sci. Rep.* 2. doi:10.1038/srep01002.

Shiba-Fukushima, K., T. Inoshita, N. Hattori, and Y. Imai. 2014. PINK1-Mediated Phosphorylation of Parkin Boosts Parkin Activity in Drosophila. *PLoS Genet.* 10:e1004391. doi:10.1371/journal.pgen.1004391.

Shibue, T., K. Takeda, E. Oda, H. Tanaka, H. Murasawa, A. Takaoka, Y. Morishita, S. Akira, T. Taniguchi, and N. Tanaka. 2003. Integral role of Noxa in p53-mediated apoptotic response. *Genes Dev.* 17:2233–2238. doi:10.1101/gad.1103603.

Shiratori, R., K. Furuichi, M. Yamaguchi, N. Miyazaki, H. Aoki, H. Chibana, K. Ito, and S. Aoki. 2019. Glycolytic suppression dramatically changes the intracellular metabolic profile of multiple cancer cell lines in a mitochondrial metabolism-dependent manner. *Sci. Rep.* 9:18699. doi:10.1038/s41598-019-55296-3.

Shoemaker, A.R., M.J. Mitten, J. Adickes, A. Oleksijew, H. Zhang, J. Bauch, K. Marsh, D.J. Frost, D. Madar, C. Tse, S.W. Fesik, S.H. Rosenberg, and S.W. Elmore. 2006. The Bcl-2 Family Inhibitor ABT-263 Shows Significant but Reversible Thrombocytopenia in Mice. *Blood*. 108:1107–1107. doi:10.1182/blood.V108.11.1107.1107.

Shu, H.B., M. Takeuchi, and D.V. Goeddel. 1996. The tumor necrosis factor receptor 2 signal transducers TRAF2 and c-IAP1 are components of the tumor necrosis factor receptor 1 signaling complex. *Proc. Natl. Acad. Sci. U. S. A.* 93:13973–13978. doi:10.1073/pnas.93.24.13973.

Sim, C.H., K. Gabriel, R.D. Mills, J.G. Culvenor, and H.-C. Cheng. 2012. Analysis of the regulatory and catalytic domains of PTEN-induced kinase-1 (PINK1). *Hum. Mutat.* 33:1408–1422. doi:10.1002/humu.22127.

Simonsen, A., and S.A. Tooze. 2009. Coordination of membrane events during autophagy by multiple class III PI3-kinase complexes. *J. Cell Biol.* 186:773–782. doi:10.1083/jcb.200907014.

Simpson, M.V. 1953. The release of labeled amino acids from the proteins of rat liver slices. *J. Biol. Chem.* 201:143–154.

Singh, A., C. Ruiz, K. Bhalla, J.A. Haley, Q.K. Li, G. Acquaah-Mensah, E. Montal, K.R. Sudini, F. Skoulidis, I.I. Wistuba, V. Papadimitrakopoulou, J.V. Heymach, L.G. Boros, E. Gabrielson, J. Carretero, K.-K. Wong, J.D. Haley, S. Biswal, and G.D. Girnun. 2018. De novo lipogenesis represents a therapeutic target in mutant Kras non-small cell lung cancer. *FASEB J. Off. Publ. Fed. Am. Soc. Exp. Biol.* fj201800204. doi:10.1096/fj.201800204.

Singh, R., and A.M. Cuervo. 2011. Autophagy in the Cellular Energetic Balance. *Cell Metab.* 13:495–504. doi:10.1016/j.cmet.2011.04.004.

Singh, R., A. Letai, and K. Sarosiek. 2019. Regulation of apoptosis in health and disease: the balancing act of BCL-2 family proteins. *Nat. Rev. Mol. Cell Biol.* 20:175–193. doi:10.1038/s41580-018-0089-8.

Sinha, S., and B. Levine. 2008. The autophagy effector Beclin 1: a novel BH3-only protein. *Oncogene*. 27 Suppl 1:S137-148. doi:10.1038/onc.2009.51.

Skowyra, D., K.L. Craig, M. Tyers, S.J. Elledge, and J.W. Harper. 1997. F-Box Proteins Are Receptors that Recruit Phosphorylated Substrates to the SCF Ubiquitin-Ligase Complex. *Cell*. 91:209–219. doi:10.1016/S0092-8674(00)80403-1.

Sliter, D.A., J. Martinez, L. Hao, X. Chen, N. Sun, T.D. Fischer, J.L. Burman, Y. Li, Z. Zhang, D.P. Narendra, H. Cai, M. Borsche, C. Klein, and R.J. Youle. 2018. Parkin and PINK1 mitigate STING-induced inflammation. *Nature*. 561:258–262. doi:10.1038/s41586-018-0448-9.

Smalley, I., and K.S.M. Smalley. 2018. ERK Inhibition: A New Front in the War against MAPK Pathway–Driven Cancers? *Cancer Discov.* 8:140–142. doi:10.1158/2159-8290.CD-17-1355.

Smit, J.J., D. Monteferrario, S.M. Noordermeer, W.J. van Dijk, B.A. van der Reijden, and T.K. Sixma. 2012. The E3 ligase HOIP specifies linear ubiquitin chain assembly through its RING-IBR-RING domain and the unique LDD extension: HOIP RBR-LDD module specifies linear ubiquitin chains. *EMBO J.* 31:3833–3844. doi:10.1038/emboj.2012.217.

Sotelo, J., E. Briceño, and M.A. López-González. 2006. Adding Chloroquine to Conventional Treatment for Glioblastoma Multiforme: A Randomized, Double-Blind, Placebo-Controlled Trial. *Ann. Intern. Med.* 144:337. doi:10.7326/0003-4819-144-5-200603070-00008.

Soucy, T.A., P.G. Smith, M.A. Milhollen, A.J. Berger, J.M. Gavin, S. Adhikari, J.E. Brownell, K.E. Burke, D.P. Cardin, S. Critchley, C.A. Cullis, A. Doucette, J.J. Garnsey, J.L. Gaulin, R.E. Gershman, A.R. Lublinsky, A. McDonald, H. Mizutani, U. Narayanan, E.J. Olhava, S. Peluso, M. Rezaei, M.D. Sintchak, T. Talreja, M.P. Thomas, T. Traore, S. Vyskocil, G.S. Weatherhead, J. Yu, J. Zhang, L.R. Dick, C.F. Claiborne, M. Rolfe,

J.B. Bolen, and S.P. Langston. 2009. An inhibitor of NEDD8-activating enzyme as a new approach to treat cancer. *Nature*. 458:732–736. doi:10.1038/nature07884.

Spence, J., S. Sadis, A.L. Haas, and D. Finley. 1995. A ubiquitin mutant with specific defects in DNA repair and multiubiquitination. *Mol. Cell. Biol.* 15:1265–1273. doi:10.1128/MCB.15.3.1265.

Stamatakou, E., L. Wróbel, S.M. Hill, C. Puri, S.M. Son, M. Fujimaki, Y. Zhu, F. Siddiqi, M. Fernandez-Estevez, M.M. Manni, S.J. Park, J. Villeneuve, and D.C. Rubinsztein. 2020. Mendelian neurodegenerative disease genes involved in autophagy. *Cell Discov.* 6. doi:10.1038/s41421-020-0158-y.

Staropoli, J.F., C. McDermott, C. Martinat, B. Schulman, E. Demireva, and A. Abeliovich. 2003. Parkin Is a Component of an SCF-like Ubiquitin Ligase Complex and Protects Postmitotic Neurons from Kainate Excitotoxicity. *Neuron*. 37:735–749. doi:10.1016/S0896-6273(03)00084-9.

Steinhauer, W.R., R.C. Walsh, and L.J. Kalfayan. 1989. Sequence and structure of the Drosophila melanogaster ovarian tumor gene and generation of an antibody specific for the ovarian tumor protein. *Mol. Cell. Biol.* 9:5726–5732. doi:10.1128/MCB.9.12.5726.

Stella, M. 1999. HGF: a multifunctional growth factor controlling cell scattering. *Int. J. Biochem. Cell Biol.* 31:1357–1362. doi:10.1016/S1357-2725(99)00089-8.

von Stockum, S., A. Sanchez-Martinez, S. Corrà, J. Chakraborty, E. Marchesan, L. Locatello, C. Da Rè, P. Cusumano, F. Caicci, V. Ferrari, R. Costa, L. Bubacco, M.B. Rasotto, I. Szabo, A.J. Whitworth, L. Scorrano, and E. Ziviani. 2019. Inhibition of the deubiquitinase USP8 corrects a Drosophila PINK1 model of mitochondria dysfunction. *Life Sci. Alliance*. 2. doi:10.26508/lsa.201900392.

Strappazzon, F., F. Nazio, M. Corrado, V. Cianfanelli, A. Romagnoli, G.M. Fimia, S. Campello, R. Nardacci, M. Piacentini, M. Campanella, and F. Cecconi. 2015. AMBRA1 is able to induce mitophagy via LC3 binding, regardless of PARKIN and p62/SQSTM1. *Cell Death Differ.* 22:419–432. doi:10.1038/cdd.2014.139.

Su, M., Y. Mei, and S. Sinha. 2013. Role of the Crosstalk between Autophagy and Apoptosis in Cancer. *J. Oncol.* 2013:102735. doi:10.1155/2013/102735.

Sun, J., C.T. Have, M. Hollensted, N. Grarup, A. Linneberg, O. Pedersen, J.S. Nielsen, J. Rungby, C. Christensen, I. Brandslund, K. Kristiansen, W. Jun, T. Hansen, and A.P. Gjesing. 2019. Sequencing reveals protective and pathogenic effects on development of diabetes of rare GLIS3 variants. *PloS One*. 14:e0220805. doi:10.1371/journal.pone.0220805.

Sun, Y., and D.W. Leaman. 2005. Involvement of Noxa in Cellular Apoptotic Responses to Interferon, Double-stranded RNA, and Virus Infection. *J. Biol. Chem.* 280:15561–15568. doi:10.1074/jbc.M412630200.

Suzuki, H., M. Maeda, and K. Mihara. 2002. Characterization of rat TOM70 as a receptor of the preprotein translocase of the mitochondrial outer membrane. *J. Cell Sci.* 115:1895–1905.

Swatek, K.N., and D. Komander. 2016. Ubiquitin modifications. *Cell Res.* 26:399–422. doi:10.1038/cr.2016.39.

Swerdlow, P.S., D. Finley, and A. Varshavsky. 1986. Enhancement of immunoblot sensitivity by heating of hydrated filters. *Anal. Biochem.* 156:147–153. doi:10.1016/0003-2697(86)90166-1.

Szargel, R., V. Shani, F. Abd Elghani, L.N. Mekies, E. Liani, R. Rott, and S. Engelender. 2016. The PINK1, synphilin-1 and SIAH-1 complex constitutes a novel mitophagy pathway. *Hum. Mol. Genet.* 25:3476–3490. doi:10.1093/hmg/ddw189.

Tabarés-Seisdedos, R., and J.L. Rubenstein. 2013. Inverse cancer comorbidity: a serendipitous opportunity to gain insight into CNS disorders. *Nat. Rev. Neurosci.* 14:293–304. doi:10.1038/nrn3464.

Takahashi, Y., H. He, Z. Tang, T. Hattori, Y. Liu, M.M. Young, J.M. Serfass, L. Chen, M. Gebru, C. Chen, C.A. Wills, J.M. Atkinson, H. Chen, T. Abraham, and H.-G. Wang. 2018. An autophagy assay reveals the ESCRT-III component CHMP2A as a regulator of phagophore closure. *Nat. Commun.* 9. doi:10.1038/s41467-018-05254-w.

Takamura, A., M. Komatsu, T. Hara, A. Sakamoto, C. Kishi, S. Waguri, Y. Eishi, O. Hino, K. Tanaka, and N. Mizushima. 2011. Autophagy-deficient mice develop multiple liver tumors. *Genes Dev.* 25:795–800. doi:10.1101/gad.2016211.

Takatori, S., G. Ito, and T. Iwatsubo. 2008. Cytoplasmic localization and proteasomal degradation of N-terminally cleaved form of PINK1. *Neurosci. Lett.* 430:13–17. doi:10.1016/j.neulet.2007.10.019.

Takeshige, K., M. Baba, S. Tsuboi, T. Noda, and Y. Ohsumi. 1992. Autophagy in yeast demonstrated with proteinase-deficient mutants and conditions for its induction. *J. Cell Biol.* 119:301–311. doi:10.1083/jcb.119.2.301.

Takiyama, Y., M. Nishizawa, H. Tanaka, S. Kawashima, H. Sakamoto, Y. Karube, H. Shimazaki, M. Soutome, K. Endo, S. Ohta, Y. Kagawa, I. Kanazawa, Y. Mizuno, M. Yoshida, T. Yuasa, Y. Horikawa, K. Oyanagi, H. Nagai, T. Kondo, T. Inuzuka, O. Onodera, and S. Tsuji. 1993. The gene for Machado–Joseph disease maps to human chromosome 14q. *Nat. Genet.* 4:300–304. doi:10.1038/ng0793-300.

Tanaka, A., M.M. Cleland, S. Xu, D.P. Narendra, D.-F. Suen, M. Karbowski, and R.J. Youle. 2010. Proteasome and p97 mediate mitophagy and

degradation of mitofusins induced by Parkin. *J. Cell Biol.* 191:1367–1380. doi:10.1083/jcb.201007013.

Tanaka, K. 2009. The proteasome: Overview of structure and functions. *Proc. Jpn. Acad. Ser. B*. 85:12–36. doi:10.2183/pjab.85.12.

Tang, X., Y.-X. Luo, H.-Z. Chen, and D.-P. Liu. 2014. Mitochondria, endothelial cell function, and vascular diseases. *Front. Physiol.* 5:175. doi:10.3389/fphys.2014.00175.

Tasaki, T., L.C.F. Mulder, A. Iwamatsu, M.J. Lee, I.V. Davydov, A. Varshavsky, M. Muesing, and Y.T. Kwon. 2005. A Family of Mammalian E3 Ubiquitin Ligases That Contain the UBR Box Motif and Recognize N-Degrons. *Mol. Cell. Biol.* 25:7120–7136. doi:10.1128/MCB.25.16.7120-7136.2005.

Teixeira, F.R., S.J. Randle, S.P. Patel, T.E.T. Mevissen, G. Zenkeviciute, T. Koide, D. Komander, and H. Laman. 2016. Gsk3β and Tomm20 are substrates of the SCFFbxo7/PARK15 ubiquitin ligase associated with Parkinson's disease. *Biochem. J.* 473:3563–3580. doi:10.1042/BCJ20160387.

Tenno, T., K. Fujiwara, H. Tochio, K. Iwai, E.H. Morita, H. Hayashi, S. Murata, H. Hiroaki, M. Sato, K. Tanaka, and M. Shirakawa. 2004. Structural basis for distinct roles of Lys63- and Lys48-linked polyubiquitin chains: Linkage-specific conformations of polyubiquitin chains. *Genes Cells*. 9:865–875. doi:10.1111/j.1365-2443.2004.00780.x.

Testa, J.R., M. Cheung, J. Pei, J.E. Below, Y. Tan, E. Sementino, N.J. Cox, A.U. Dogan, H.I. Pass, S. Trusa, M. Hesdorffer, M. Nasu, A. Powers, Z. Rivera, S. Comertpay, M. Tanji, G. Gaudino, H. Yang, and M. Carbone. 2011. Germline BAP1 mutations predispose to malignant mesothelioma. *Nat. Genet.* 43:1022–1025. doi:10.1038/ng.912.

Thomas, A., T. Giesler, and E. White. 2000. p53 mediates Bcl-2 phosphorylation and apoptosis via activation of the Cdc42/JNK1 pathway. *Oncogene*. 19:5259–5269. doi:10.1038/sj.onc.1203895.

Thomas, M., and L. Banks. 1998. Inhibition of Bak-induced apoptosis by HPV-18 E6. *Oncogene*. 17:2943–2954. doi:10.1038/sj.onc.1202223.

Thomas, M., and L. Banks. 1999. Human papillomavirus (HPV) E6 interactions with Bak are conserved amongst E6 proteins from high and low risk HPV types. *J. Gen. Virol.* 80 (Pt 6):1513–1517. doi:10.1099/0022-1317-80-6-1513.

Thorslund, T., A. Ripplinger, S. Hoffmann, T. Wild, M. Uckelmann, B. Villumsen, T. Narita, T.K. Sixma, C. Choudhary, S. Bekker-Jensen, and N. Mailand. 2015. Histone H1 couples initiation and amplification of ubiquitin signalling after DNA damage. *Nature*. 527:389–393. doi:10.1038/nature15401.

Timar, J., and K. Kashofer. 2020. Molecular epidemiology and diagnostics of KRAS mutations in human cancer. *Cancer Metastasis Rev.* 39:1029–1038. doi:10.1007/s10555-020-09915-5.

Todt, F., Z. Cakir, F. Reichenbach, F. Emschermann, J. Lauterwasser, A. Kaiser, G. Ichim, S.W. Tait, S. Frank, H.F. Langer, and F. Edlich. 2015. Differential retrotranslocation of mitochondrial Bax and Bak. *EMBO J.* 34:67–80. doi:10.15252/embj.201488806.

Tokunaga, F., H. Nishimasu, R. Ishitani, E. Goto, T. Noguchi, K. Mio, K. Kamei, A. Ma, K. Iwai, and O. Nureki. 2012. Specific recognition of linear polyubiquitin by A20 zinc finger 7 is involved in NF-κB regulation. *EMBO J.* 31:3856–3870. doi:10.1038/emboj.2012.241.

Tong, J., S. Tan, F. Zou, J. Yu, and L. Zhang. 2017. FBW7 mutations mediate resistance of colorectal cancer to targeted therapies by blocking Mcl-1 degradation. *Oncogene*. 36:787–796. doi:10.1038/onc.2016.247.

Toshiyuki, M., and J.C. Reed. 1995. Tumor suppressor p53 is a direct transcriptional activator of the human bax gene. *Cell*. 80:293–299. doi:10.1016/0092-8674(95)90412-3.

Tse, C., A.R. Shoemaker, J. Adickes, M.G. Anderson, J. Chen, S. Jin, E.F. Johnson, K.C. Marsh, M.J. Mitten, P. Nimmer, L. Roberts, S.K. Tahir, Y. Xiao, X. Yang, H. Zhang, S. Fesik, S.H. Rosenberg, and S.W. Elmore. 2008. ABT-263: a potent and orally bioavailable Bcl-2 family inhibitor. *Cancer Res.* 68:3421–3428. doi:10.1158/0008-5472.CAN-07-5836.

Tsefou, E., A.S. Walker, E.H. Clark, A.R. Hicks, C. Luft, K. Takeda, T. Watanabe, B. Ramazio, J.M. Staddon, T. Briston, and R. Ketteler. 2021. Investigation of USP30 inhibition to enhance Parkin-mediated mitophagy: tools and approaches. Neuroscience.

Tsujimoto, Y., L. Finger, J. Yunis, P. Nowell, and C. Croce. 1984. Cloning of the chromosome breakpoint of neoplastic B cells with the t(14;18) chromosome translocation. *Science*. 226:1097–1099. doi:10.1126/science.6093263.

Tsukada, M., and Y. Ohsumi. 1993. Isolation and characterization of autophagy-defective mutants of *Saccharomyces cerevisiae*. *FEBS Lett.* 333:169–174. doi:10.1016/0014-5793(93)80398-E.

Turnbull, A.P., S. Ioannidis, W.W. Krajewski, A. Pinto-Fernandez, C. Heride, A.C.L. Martin, L.M. Tonkin, E.C. Townsend, S.M. Buker, D.R. Lancia, J.A. Caravella, A.V. Toms, T.M. Charlton, J. Lahdenranta, E. Wilker, B.C. Follows, N.J. Evans, L. Stead, C. Alli, V.V. Zarayskiy, A.C. Talbot, A.J. Buckmelter, M. Wang, C.L. McKinnon, F. Saab, J.F. McGouran, H. Century, M. Gersch, M.S. Pittman, C.G. Marshall, T.M. Raynham, M. Simcox, L.M.D. Stewart, S.B. McLoughlin, J.A. Escobedo, K.W. Bair, C.J. Dinsmore, T.R. Hammonds, S. Kim, S. Urbé, M.J. Clague, B.M.

Kessler, and D. Komander. 2017. Molecular basis of USP7 inhibition by selective small-molecule inhibitors. *Nature*. 550:481–486. doi:10.1038/nature24451.

Tyanova, S., T. Temu, P. Sinitcyn, A. Carlson, M.Y. Hein, T. Geiger, M. Mann, and J. Cox. 2016. The Perseus computational platform for comprehensive analysis of (prote)omics data. *Nat. Methods*. 13:731–740. doi:10.1038/nmeth.3901.

Tzvetkov, N., and P. Breuer. 2007. Josephin domain-containing proteins from a variety of species are active de-ubiquitination enzymes. *Biol. Chem.* 388:973–978. doi:10.1515/BC.2007.107.

Unoki, M., and Y. Nakamura. 2001. Growth-suppressive effects of BPOZ and EGR2, two genes involved in the PTEN signaling pathway. *Oncogene*. 20:4457–4465. doi:10.1038/sj.onc.1204608.

Urbé, S., H. Liu, S.D. Hayes, C. Heride, D.J. Rigden, and M.J. Clague. 2012. Systematic survey of deubiquitinase localization identifies USP21 as a regulator of centrosome- and microtubule-associated functions. *Mol. Biol. Cell*. 23:1095–1103. doi:10.1091/mbc.e11-08-0668.

Valente, E.M., P.M. Abou-Sleiman, V. Caputo, M.M.K. Muqit, K. Harvey, S. Gispert, Z. Ali, D. Del Turco, A.R. Bentivoglio, D.G. Healy, A. Albanese, R. Nussbaum, R. González-Maldonado, T. Deller, S. Salvi, P. Cortelli, W.P. Gilks, D.S. Latchman, R.J. Harvey, B. Dallapiccola, G. Auburger, and N.W. Wood. 2004. Hereditary early-onset Parkinson's disease caused by mutations in PINK1. *Science*. 304:1158–1160. doi:10.1126/science.1096284.

Valente, E.M., A.R. Bentivoglio, P.H. Dixon, A. Ferraris, T. Ialongo, M. Frontali, A. Albanese, and N.W. Wood. 2001. Localization of a Novel Locus for Autosomal Recessive Early-Onset Parkinsonism, PARK6, on Human Chromosome 1p35-p36. *Am. J. Hum. Genet.* 68:895–900. doi:10.1086/319522.

Van Humbeeck, C., T. Cornelissen, H. Hofkens, W. Mandemakers, K. Gevaert, B. De Strooper, and W. Vandenberghe. 2011. Parkin interacts with Ambra1 to induce mitophagy. *J. Neurosci. Off. J. Soc. Neurosci.* 31:10249–10261. doi:10.1523/JNEUROSCI.1917-11.2011.

VanderLinden, R.T., C.W. Hemmis, B. Schmitt, A. Ndoja, F.G. Whitby, H. Robinson, R.E. Cohen, T. Yao, and C.P. Hill. 2015. Structural Basis for the Activation and Inhibition of the UCH37 Deubiquitylase. *Mol. Cell*. 57:901–911. doi:10.1016/j.molcel.2015.01.016.

Vann, K.R., and T.G. Kutateladze. 2017. Histone H3 Dual Ubiquitylation Mediates Maintenance DNA Methylation. *Mol. Cell*. 68:261–262. doi:10.1016/j.molcel.2017.10.007.

Varadan, R., M. Assfalg, A. Haririnia, S. Raasi, C. Pickart, and D. Fushman. 2004. Solution Conformation of Lys ^{63} -linked Di-ubiquitin Chain

Provides Clues to Functional Diversity of Polyubiquitin Signaling. *J. Biol. Chem.* 279:7055–7063. doi:10.1074/jbc.M309184200.

Varadan, R., O. Walker, C. Pickart, and D. Fushman. 2002. Structural Properties of Polyubiquitin Chains in Solution. *J. Mol. Biol.* 324:637–647. doi:10.1016/S0022-2836(02)01198-1.

Varadarajan, S., M. Butterworth, J. Wei, M. Pellecchia, D. Dinsdale, and G.M. Cohen. 2013. Sabutoclax (BI97C1) and BI112D1, putative inhibitors of MCL-1, induce mitochondrial fragmentation either upstream of or independent of apoptosis. *Neoplasia N. Y. N*. 15:568–578. doi:10.1593/neo.13230.

Varfolomeev, E., T. Goncharov, A.V. Fedorova, J.N. Dynek, K. Zobel, K. Deshayes, W.J. Fairbrother, and D. Vucic. 2008. c-IAP1 and c-IAP2 Are Critical Mediators of Tumor Necrosis Factor α (TNFα)-induced NF-κB Activation. *J. Biol. Chem.* 283:24295–24299. doi:10.1074/jbc.C800128200.

Vaux, D.L., S. Cory, and J.M. Adams. 1988. Bcl-2 gene promotes haemopoietic cell survival and cooperates with c-myc to immortalize pre-B cells. *Nature*. 335:440–442. doi:10.1038/335440a0.

Veeriah, S., B.S. Taylor, S. Meng, F. Fang, E. Yilmaz, I. Vivanco, M. Janakiraman, N. Schultz, A.J. Hanrahan, W. Pao, M. Ladanyi, C. Sander, A. Heguy, E.C. Holland, P.B. Paty, P.S. Mischel, L. Liau, T.F. Cloughesy, I.K. Mellinghoff, D.B. Solit, and T.A. Chan. 2010. Somatic mutations of the Parkinson's disease–associated gene PARK2 in glioblastoma and other human malignancies. *Nat. Genet.* 42:77–82. doi:10.1038/ng.491.

Verhagen, A.M., P.G. Ekert, M. Pakusch, J. Silke, L.M. Connolly, G.E. Reid, R.L. Moritz, R.J. Simpson, and D.L. Vaux. 2000. Identification of DIABLO, a Mammalian Protein that Promotes Apoptosis by Binding to and Antagonizing IAP Proteins. *Cell*. 102:43–53. doi:10.1016/S0092-8674(00)00009-X.

Verhelst, K., I. Carpentier, M. Kreike, L. Meloni, L. Verstrepen, T. Kensche, I. Dikic, and R. Beyaert. 2012. A20 inhibits LUBAC-mediated NF-κB activation by binding linear polyubiquitin chains via its zinc finger 7. *EMBO J.* 31:3845–3855. doi:10.1038/emboj.2012.240.

Vijay-kumar, S., C.E. Bugg, and W.J. Cook. 1987. Structure of ubiquitin refined at 1.8 Å resolution. *J. Mol. Biol.* 194:531–544. doi:10.1016/0022-2836(87)90679-6.

Vijay-Kumar, S., C.E. Bugg, K.D. Wilkinson, and W.J. Cook. 1985. Three-dimensional structure of ubiquitin at 2.8 A resolution. *Proc. Natl. Acad. Sci.* 82:3582–3585. doi:10.1073/pnas.82.11.3582.

Villa, E., E. Proïcs, C. Rubio-Patiño, S. Obba, B. Zunino, J.P. Bossowski, R.M. Rozier, J. Chiche, L. Mondragón, J.S. Riley, S. Marchetti, E. Verhoeyen,

S.W.G. Tait, and J.E. Ricci. 2017. Parkin-Independent Mitophagy Controls Chemotherapeutic Response in Cancer Cells. *Cell Rep.* 20:2846–2859. doi:10.1016/j.celrep.2017.08.087.

Villumsen, M., S. Aznar, B. Pakkenberg, T. Jess, and T. Brudek. 2019. Inflammatory bowel disease increases the risk of Parkinson's disease: a Danish nationwide cohort study 1977–2014. *Gut*. 68:18–24. doi:10.1136/gutjnl-2017-315666.

Villunger, A., E.M. Michalak, L. Coultas, F. Müllauer, G. Böck, M.J. Ausserlechner, J.M. Adams, and A. Strasser. 2003. p53- and Drug-Induced Apoptotic Responses Mediated by BH3-Only Proteins Puma and Noxa. *Science*. 302:1036–1038. doi:10.1126/science.1090072.

Vincow, E.S., G. Merrihew, R.E. Thomas, N.J. Shulman, R.P. Beyer, M.J. MacCoss, and L.J. Pallanck. 2013. The PINK1-Parkin pathway promotes both mitophagy and selective respiratory chain turnover in vivo. *Proc. Natl. Acad. Sci.* 110:6400–6405. doi:10.1073/pnas.1221132110.

Vingill, S., D. Brockelt, C. Lancelin, L. Tatenhorst, G. Dontcheva, C. Preisinger, N. Schwedhelm-Domeyer, S. Joseph, M. Mitkovski, S. Goebbels, K.-A. Nave, J.B. Schulz, T. Marquardt, P. Lingor, and J. Stegmüller. 2016. Loss of FBXO7 (PARK15) results in reduced proteasome activity and models a parkinsonism-like phenotype in mice. *EMBO J.* 35:2008–2025. doi:10.15252/embj.201593585.

Virdee, S., Y. Ye, D.P. Nguyen, D. Komander, and J.W. Chin. 2010. Engineered diubiquitin synthesis reveals Lys29-isopeptide specificity of an OTU deubiquitinase. *Nat. Chem. Biol.* 6:750–757. doi:10.1038/nchembio.426.

Vogler, M., D. Dinsdale, X.-M. Sun, K.W. Young, M. Butterworth, P. Nicotera, M.J.S. Dyer, and G.M. Cohen. 2008. A novel paradigm for rapid ABT-737-induced apoptosis involving outer mitochondrial membrane rupture in primary leukemia and lymphoma cells. *Cell Death Differ.* 15:820–830. doi:10.1038/cdd.2008.25.

Volinia, S., R. Dhand, B. Vanhaesebroeck, L.K. MacDougall, R. Stein, M.J. Zvelebil, J. Domin, C. Panaretou, and M.D. Waterfield. 1995. A human phosphatidylinositol 3-kinase complex related to the yeast Vps34p-Vps15p protein sorting system. *EMBO J.* 14:3339–3348.

Volpe, E., M. Sambucci, L. Battistini, and G. Borsellino. 2016. Fas–Fas Ligand: Checkpoint of T Cell Functions in Multiple Sclerosis. *Front. Immunol.* 7. doi:10.3389/fimmu.2016.00382.

Walczak, H. 2011. TNF and ubiquitin at the crossroads of gene activation, cell death, inflammation, and cancer. - marie.dueppe@gmail.com - Gmail. 9–28.

Walden, M., S.K. Masandi, K. Pawłowski, and E. Zeqiraj. 2018. Pseudo-DUBs as allosteric activators and molecular scaffolds of protein complexes. *Biochem. Soc. Trans.* 46:453–466. doi:10.1042/BST20160268.

Wall, C.E., C.M. Rose, M. Adrian, Y.J. Zeng, D.S. Kirkpatrick, and B. Bingol. 2019. PPEF2 Opposes PINK1-Mediated Mitochondrial Quality Control by Dephosphorylating Ubiquitin. *Cell Rep.* 29:3280-3292.e7. doi:10.1016/j.celrep.2019.10.130.

Wan, R., R. Bai, X. Zhan, and Y. Shi. 2020. How Is Precursor Messenger RNA Spliced by the Spliceosome? *Annu. Rev. Biochem.* 89:333–358. doi:10.1146/annurev-biochem-013118-111024.

Wang, C., and R.J. Youle. 2012. Predominant requirement of Bax for apoptosis in HCT116 cells is determined by Mcl-1's inhibitory effect on Bak. *Oncogene*. 31:3177–3189. doi:10.1038/onc.2011.497.

Wang, G., Z.-Q. Yang, and K. Zhang. 2010. Endoplasmic reticulum stress response in cancer: molecular mechanism and therapeutic potential. *Am. J. Transl. Res.* 2:65–74.

Wang, H., L. Wang, H. Erdjument-Bromage, M. Vidal, P. Tempst, R.S. Jones, and Y. Zhang. 2004. Role of histone H2A ubiquitination in Polycomb silencing. *Nature*. 431:873–878. doi:10.1038/nature02985.

Wang, H., L. Zhai, J. Xu, H.-Y. Joo, S. Jackson, H. Erdjument-Bromage, P. Tempst, Y. Xiong, and Y. Zhang. 2006. Histone H3 and H4 Ubiquitylation by the CUL4-DDB-ROC1 Ubiquitin Ligase Facilitates Cellular Response to DNA Damage. *Mol. Cell*. 22:383–394. doi:10.1016/j.molcel.2006.03.035.

Wang, K., X.M. Yin, D.T. Chao, C.L. Milliman, and S.J. Korsmeyer. 1996. BID: a novel BH3 domain-only death agonist. *Genes Dev.* 10:2859–2869. doi:10.1101/gad.10.22.2859.

Wang, L., Y.-L. Cho, Y. Tang, J. Wang, J.-E. Park, Y. Wu, C. Wang, Y. Tong, R. Chawla, J. Zhang, Y. Shi, S. Deng, G. Lu, Y. Wu, H.W.-S. Tan, P. Pawijit, G.G.-Y. Lim, H.-Y. Chan, J. Zhang, L. Fang, H. Yu, Y.-C. Liou, M. Karthik, B.-H. Bay, K.-L. Lim, S.-K. Sze, C.T. Yap, and H.-M. Shen. 2018. PTEN-L is a novel protein phosphatase for ubiquitin dephosphorylation to inhibit PINK1–Parkin-mediated mitophagy. *Cell Res.* 28:787–802. doi:10.1038/s41422-018-0056-0.

Wang, L., G.A. Doherty, A.S. Judd, Z.-F. Tao, T.M. Hansen, R.R. Frey, X. Song, M. Bruncko, A.R. Kunzer, X. Wang, M.D. Wendt, J.A. Flygare, N.D. Catron, R.A. Judge, C.H. Park, S. Shekhar, D.C. Phillips, P. Nimmer, M.L. Smith, S.K. Tahir, Y. Xiao, J. Xue, H. Zhang, P.N. Le, M.J. Mitten, E.R. Boghaert, W. Gao, P. Kovar, E.F. Choo, D. Diaz, W.J. Fairbrother, S.W. Elmore, D. Sampath, J.D. Leverson, and A.J. Souers. 2020. Discovery of A-1331852, a First-in-Class, Potent, and Orally-

Bioavailable BCL-XL Inhibitor. *ACS Med. Chem. Lett.* 11:1829–1836. doi:10.1021/acsmedchemlett.9b00568.

Wang, Y., N. Liu, and B. Lu. 2019. Mechanisms and roles of mitophagy in neurodegenerative diseases. *CNS Neurosci. Ther.* 25:859–875. doi:10.1111/cns.13140.

Wang, Y., M. Serricchio, M. Jauregui, R. Shanbhag, T. Stoltz, C.T. Di Paolo, P.K. Kim, and G. Angus McQuibban. 2015. Deubiquitinating enzymes regulate PARK2-mediated mitophagy. *Autophagy*. 11:595–606. doi:10.1080/15548627.2015.1034408.

Waterhouse, A.M., J.B. Procter, D.M.A. Martin, M. Clamp, and G.J. Barton. 2009. Jalview Version 2--a multiple sequence alignment editor and analysis workbench. *Bioinformatics*. 25:1189–1191. doi:10.1093/bioinformatics/btp033.

Wauer, T., K.N. Swatek, J.L. Wagstaff, C. Gladkova, J.N. Pruneda, M.A. Michel, M. Gersch, C.M. Johnson, S.M. Freund, and D. Komander. 2015. Ubiquitin Ser65 phosphorylation affects ubiquitin structure, chain assembly and hydrolysis. *EMBO J.* 34:307–325. doi:10.15252/embj.201489847.

Wawrzynow, A., D. Wojtkowiak, J. Marszalek, B. Banecki, M. Jonsen, B. Graves, C. Georgopoulos, and M. Zylicz. 1995. The ClpX heat-shock protein of Escherichia coli, the ATP-dependent substrate specificity component of the ClpP-ClpX protease, is a novel molecular chaperone. *EMBO J.* 14:1867–1877. doi:10.1002/j.1460-2075.1995.tb07179.x.

Weber, A., M. Heinlein, J. Dengjel, C. Alber, P.K. Singh, and G. Häcker. 2016. The deubiquitinase Usp27x stabilizes the BH3-only protein Bim and enhances apoptosis. *EMBO Rep.* 17:724–738. doi:10.15252/embr.201541392.

Weeks, S.D., K.C. Grasty, L. Hernandez-Cuebas, and P.J. Loll. 2011. Crystal Structure of a Josephin-Ubiquitin Complex: EVOLUTIONARY RESTRAINTS ON ATAXIN-3 DEUBIQUITINATING ACTIVITY. *J. Biol. Chem.* 286:4555–4565. doi:10.1074/jbc.M110.177360.

Wei, M.C., T. Lindsten, V.K. Mootha, S. Weiler, A. Gross, M. Ashiya, C.B. Thompson, and S.J. Korsmeyer. 2000. tBID, a membrane-targeted death ligand, oligomerizes BAK to release cytochrome c. *Genes Dev.* 14:2060–2071.

Wei, Y., S. Pattingre, S. Sinha, M. Bassik, and B. Levine. 2008a. JNK1-mediated phosphorylation of Bcl-2 regulates starvation-induced autophagy. *Mol. Cell*. 30:678–688. doi:10.1016/j.molcel.2008.06.001.

Wei, Y., S. Sinha, and B. Levine. 2008b. Dual role of JNK1-mediated phosphorylation of Bcl-2 in autophagy and apoptosis regulation. *Autophagy*. 4:949–951. doi:10.4161/auto.6788.

Weir, H.J.M., J.D. Lane, and N. Balthasar. 2013. SIRT3: A Central Regulator of Mitochondrial Adaptation in Health and Disease. *Genes Cancer*. 4:118–124. doi:10.1177/1947601913476949.

Welcker, M., A. Orian, J. Jin, J.E. Grim, J. a Grim, J.W. Harper, R.N. Eisenman, and B.E. Clurman. 2004. The Fbw7 tumor suppressor regulates glycogen synthase kinase 3 phosphorylation-dependent c-Myc protein degradation. *Proc. Natl. Acad. Sci. U. S. A.* 101:9085–90. doi:10.1073/pnas.0402770101.

Wenzel, D.M., A. Lissounov, P.S. Brzovic, and R.E. Klevit. 2011. UBCH7 reactivity profile reveals parkin and HHARI to be RING/HECT hybrids. *Nature*. 474:105–108. doi:10.1038/nature09966.

Wertz, I.E., S. Kusam, C. Lam, T. Okamoto, W. Sandoval, D.J. Anderson, E. Helgason, J.A. Ernst, M. Eby, J. Liu, L.D. Belmont, J.S. Kaminker, K.M. O'Rourke, K. Pujara, P.B. Kohli, A.R. Johnson, M.L. Chiu, J.R. Lill, P.K. Jackson, W.J. Fairbrother, S. Seshagiri, M.J.C. Ludlam, K.G. Leong, E.C. Dueber, H. Maecker, D.C.S. Huang, and V.M. Dixit. 2011. Sensitivity to antitubulin chemotherapeutics is regulated by MCL1 and FBW7. *Nature*. 471:110–114. doi:10.1038/nature09779.

Wertz, I.E., K. Newton, D. Seshasayee, S. Kusam, C. Lam, J. Zhang, N. Popovych, E. Helgason, A. Schoeffler, S. Jeet, N. Ramamoorthi, L. Kategaya, R.J. Newman, K. Horikawa, D. Dugger, W. Sandoval, S. Mukund, A. Zindal, F. Martin, C. Quan, J. Tom, W.J. Fairbrother, M. Townsend, S. Warming, J. DeVoss, J. Liu, E. Dueber, P. Caplazi, W.P. Lee, C.C. Goodnow, M. Balazs, K. Yu, G. Kolumam, and V.M. Dixit. 2015. Phosphorylation and linear ubiquitin direct A20 inhibition of inflammation. *Nature*. 528:370–375. doi:10.1038/nature16165.

Wiborg, O., M.S. Pedersen, A. Wind, L.E. Berglund, K.A. Marcker, and J. Vuust. 1985. The human ubiquitin multigene family: some genes contain multiple directly repeated ubiquitin coding sequences. *EMBO J.* 4:755–759. doi:10.1002/j.1460-2075.1985.tb03693.x.

Wickliffe, K.E., S. Lorenz, D.E. Wemmer, J. Kuriyan, and M. Rape. 2011a. The Mechanism of Linkage-Specific Ubiquitin Chain Elongation by a Single-Subunit E2. *Cell*. 144:769–781. doi:10.1016/j.cell.2011.01.035.

Wickliffe, K.E., A. Williamson, H.-J. Meyer, A. Kelly, and M. Rape. 2011b. K11-linked ubiquitin chains as novel regulators of cell division. *Trends Cell Biol.* 21:656–663. doi:10.1016/j.tcb.2011.08.008.

Wiesner, T., A.C. Obenauf, R. Murali, I. Fried, K.G. Griewank, P. Ulz, C. Windpassinger, W. Wackernagel, S. Loy, I. Wolf, A. Viale, A.E. Lash, M. Pirun, N.D. Socci, A. Rütten, G. Palmedo, D. Abramson, K. Offit, A. Ott, J.C. Becker, L. Cerroni, H. Kutzner, B.C. Bastian, and M.R. Speicher. 2011. Germline mutations in BAP1 predispose to melanocytic tumors. *Nat. Genet.* 43:1018–1021. doi:10.1038/ng.910.

Wilkinson, K., K. Lee, S. Deshpande, P. Duerksen-Hughes, J. Boss, and J. Pohl. 1989. The neuron-specific protein PGP 9.5 is a ubiquitin carboxyl-terminal hydrolase. *Science*. 246:670–673. doi:10.1126/science.2530630.

Wilkinson, K.D. 2005. The discovery of ubiquitin-dependent proteolysis. *Proc. Natl. Acad. Sci.* 102:15280–15282. doi:10.1073/pnas.0504842102.

Williams, C., M. van den Berg, R.R. Sprenger, and B. Distel. 2007. A Conserved Cysteine Is Essential for Pex4p-dependent Ubiquitination of the Peroxisomal Import Receptor Pex5p. *J. Biol. Chem.* 282:22534–22543. doi:10.1074/jbc.M702038200.

Willis, S.N., L. Chen, G. Dewson, A. Wei, E. Naik, J.I. Fletcher, J.M. Adams, and D.C.S. Huang. 2005. Proapoptotic Bak is sequestered by Mcl-1 and Bcl-xL, but not Bcl-2, until displaced by BH3-only proteins. *Genes Dev.* 19:1294–1305. doi:10.1101/gad.1304105.

Winborn, B.J., S.M. Travis, S.V. Todi, K.M. Scaglione, P. Xu, A.J. Williams, R.E. Cohen, J. Peng, and H.L. Paulson. 2008. The deubiquitinating enzyme ataxin-3, a polyglutamine disease protein, edits Lys63 linkages in mixed linkage ubiquitin chains. *J. Biol. Chem.* 283:26436–26443. doi:10.1074/jbc.M803692200.

Winston, J.T., P. Strack, P. Beer-Romero, C.Y. Chu, S.J. Elledge, and J.W. Harper. 1999. The SCFbeta-TRCP-ubiquitin ligase complex associates specifically with phosphorylated destruction motifs in IkappaBalpha and beta-catenin and stimulates IkappaBalpha ubiquitination in vitro. *Genes Dev.* 13:270–283. doi:10.1101/gad.13.3.270.

Wirawan, E., L. Vande Walle, K. Kersse, S. Cornelis, S. Claerhout, I. Vanoverberghe, R. Roelandt, R. De Rycke, J. Verspurten, W. Declercq, P. Agostinis, T. Vanden Berghe, S. Lippens, and P. Vandenabeele. 2010. Caspase-mediated cleavage of Beclin-1 inactivates Beclin-1-induced autophagy and enhances apoptosis by promoting the release of proapoptotic factors from mitochondria. *Cell Death Dis.* 1:e18–e18. doi:10.1038/cddis.2009.16.

Wolter, K.G., Y.-T. Hsu, C.L. Smith, A. Nechushtan, X.-G. Xi, and R.J. Youle. 1997. Movement of Bax from the Cytosol to Mitochondria during Apoptosis. *J. Cell Biol.* 139:1281–1292. doi:10.1083/jcb.139.5.1281.

Wood, D.E., and E.W. Newcomb. 2000. Cleavage of Bax enhances its cell death function. *Exp. Cell Res.* 256:375–382. doi:10.1006/excr.2000.4859.

Wood, D.E., A. Thomas, L.A. Devi, Y. Berman, R.C. Beavis, J.C. Reed, and E.W. Newcomb. 1998. Bax cleavage is mediated by calpain during drug-induced apoptosis. *Oncogene*. 17:1069–1078. doi:10.1038/sj.onc.1202034.

Worden, E.J., K.C. Dong, and A. Martin. 2017. An AAA Motor-Driven Mechanical Switch in Rpn11 Controls Deubiquitination at the 26S Proteasome. *Mol. Cell*. 67:799-811.e8. doi:10.1016/j.molcel.2017.07.023.

Wu, H., D. Xue, G. Chen, Z. Han, L. Huang, C. Zhu, X. Wang, H. Jin, J. Wang, Y. Zhu, L. Liu, and Q. Chen. 2014. The BCL2L1 and PGAM5 axis defines hypoxia-induced receptor-mediated mitophagy. *Autophagy*. 10:1712–1725. doi:10.4161/auto.29568.

Xiang, C., J. Chen, and P. Fu. 2017. HGF/Met Signaling in Cancer Invasion: The Impact on Cytoskeleton Remodeling. *Cancers*. 9. doi:10.3390/cancers9050044.

Xiang, W., C.-Y. Yang, and L. Bai. 2018. MCL-1 inhibition in cancer treatment. *OncoTargets Ther.* 11:7301–7314. doi:10.2147/OTT.S146228.

Xiao, X., C. Liu, Y. Pei, Y.-Z. Wang, J. Kong, K. Lu, L. Ma, S.-X. Dou, P.-Y. Wang, G. Li, P. Chen, and W. Li. 2020. Histone H2A Ubiquitination Reinforces Mechanical Stability and Asymmetry at the Single-Nucleosome Level. *J. Am. Chem. Soc.* 142:3340–3345. doi:10.1021/jacs.9b12448.

Xu, G., J.S. Paige, and S.R. Jaffrey. 2010. Global analysis of lysine ubiquitination by ubiquitin remnant immunoaffinity profiling. *Nat. Biotechnol.* 28:868–873. doi:10.1038/nbt.1654.

Xu, Y., H. Hortsman, L. Seet, S.H. Wong, and W. Hong. 2001. SNX3 regulates endosomal function through its PX-domain-mediated interaction with PtdIns(3)P. *Nat. Cell Biol.* 3:658–666. doi:10.1038/35083051.

Yada, M., S. Hatakeyama, T. Kamura, M. Nishiyama, R. Tsunematsu, H. Imaki, N. Ishida, F. Okumura, K. Nakayama, and K.I. Nakayama. 2004. Phosphorylation-dependent degradation of c-Myc is mediated by the F-box protein Fbw7. *EMBO J.* 23:2116–25. doi:10.1038/sj.emboj.7600217.

Yamano, K., and R.J. Youle. 2013. PINK1 is degraded through the N-end rule pathway. *Autophagy*. 9:1758–1769. doi:10.4161/auto.24633.

Yang, J. 1997. Prevention of Apoptosis by Bcl-2: Release of Cytochrome c from Mitochondria Blocked. *Science*. 275:1129–1132. doi:10.1126/science.275.5303.1129.

Yang, J., J. Nie, X. Ma, Y. Wei, Y. Peng, and X. Wei. 2019. Targeting PI3K in cancer: mechanisms and advances in clinical trials. *Mol. Cancer*. 18:26. doi:10.1186/s12943-019-0954-x.

Yang, S., J. Wang, D.D. Brand, and S.G. Zheng. 2018. Role of TNF–TNF Receptor 2 Signal in Regulatory T Cells and Its Therapeutic Implications. *Front. Immunol.* 9:784. doi:10.3389/fimmu.2018.00784.

Yang, S., X. Wang, G. Contino, M. Liesa, E. Sahin, H. Ying, A. Bause, Y. Li, J.M. Stommel, G. Dell'antonio, J. Mautner, G. Tonon, M. Haigis, O.S. Shirihai, C. Doglioni, N. Bardeesy, and A.C. Kimmelman. 2011. Pancreatic cancers require autophagy for tumor growth. *Genes Dev.* 25:717–729. doi:10.1101/gad.2016111.

Yang, X., J.E. Brownell, Q. Xu, F. Zhu, J. Ma, H.-K. Loke, N. Rollins, T.A. Soucy, J.J. Minissale, M.P. Thomas, W.D. Mallender, L.R. Dick, P. Li, and H. Liao. 2013. Absolute Quantification of E1, Ubiquitin-Like Proteins and Nedd8–MLN4924 Adduct by Mass Spectrometry. *Cell Biochem. Biophys.* 67:139–147. doi:10.1007/s12013-013-9625-5.

Yao, T., and R.E. Cohen. 2002. A cryptic protease couples deubiquitination and degradation by the proteasome. *Nature*. 419:403–407. doi:10.1038/nature01071.

Yao, T., L. Song, W. Xu, G.N. DeMartino, L. Florens, S.K. Swanson, M.P. Washburn, R.C. Conaway, J.W. Conaway, and R.E. Cohen. 2006. Proteasome recruitment and activation of the Uch37 deubiquitinating enzyme by Adrm1. *Nat. Cell Biol.* 8:994–1002. doi:10.1038/ncb1460.

Ye, Y., M. Akutsu, F. Reyes-Turcu, R.I. Enchev, K.D. Wilkinson, and D. Komander. 2011. Polyubiquitin binding and cross-reactivity in the USP domain deubiquitinase USP21. *EMBO Rep.* 12:350–357. doi:10.1038/embor.2011.17.

Ye, Y., and M. Rape. 2009. Building ubiquitin chains: E2 enzymes at work. *Nat. Rev. Mol. Cell Biol.* 10:755–764. doi:10.1038/nrm2780.

Yecies, D., N.E. Carlson, J. Deng, and A. Letai. 2010. Acquired resistance to ABT-737 in lymphoma cells that up-regulate MCL-1 and BFL-1. *Blood*. 115:3304–3313. doi:10.1182/blood-2009-07-233304.

Yin, X., L. Cao, R. Kang, M. Yang, Z. Wang, Y. Peng, Y. Tan, L. Liu, M. Xie, Y. Zhao, K.M. Livesey, and D. Tang. 2011a. UV irradiation resistance-associated gene suppresses apoptosis by interfering with BAX activation. *EMBO Rep.* 12:727–734. doi:10.1038/embor.2011.79.

Yin, X., L. Cao, Y. Peng, Y. Tan, M. Xie, R. Kang, K.M. Livesey, and D. Tang. 2011b. A critical role for UVRAG in apoptosis. *Autophagy*. 7:1242–1244. doi:10.4161/auto.7.10.16507.

Ying, H., A.C. Kimmelman, C.A. Lyssiotis, S. Hua, G.C. Chu, E. Fletcher-Sananikone, J.W. Locasale, J. Son, H. Zhang, J.L. Coloff, H. Yan, W. Wang, S. Chen, A. Viale, H. Zheng, J. Paik, C. Lim, A.R. Guimaraes, E.S. Martin, J. Chang, A.F. Hezel, S.R. Perry, J. Hu, B. Gan, Y. Xiao, J.M. Asara, R. Weissleder, Y.A. Wang, L. Chin, L.C. Cantley, and R.A. DePinho. 2012. Oncogenic Kras Maintains Pancreatic Tumors through Regulation of Anabolic Glucose Metabolism. *Cell*. 149:656–670. doi:10.1016/j.cell.2012.01.058.

Yousefi, S., R. Perozzo, I. Schmid, A. Ziemiecki, T. Schaffner, L. Scapozza, T. Brunner, and H.-U. Simon. 2006. Calpain-mediated cleavage of Atg5 switches autophagy to apoptosis. *Nat. Cell Biol.* 8:1124–1132. doi:10.1038/ncb1482.

Yuan, W.-C., Y.-R. Lee, S.-Y. Lin, L.-Y. Chang, Y.P. Tan, C.-C. Hung, J.-C. Kuo, C.-H. Liu, M.-Y. Lin, M. Xu, Z.J. Chen, and R.-H. Chen. 2014. K33-Linked Polyubiquitination of Coronin 7 by Cul3-KLHL20 Ubiquitin E3 Ligase Regulates Protein Trafficking. *Mol. Cell*. 54:586–600. doi:10.1016/j.molcel.2014.03.035.

Yue, W., Z. Chen, H. Liu, C. Yan, M. Chen, D. Feng, C. Yan, H. Wu, L. Du, Y. Wang, J. Liu, X. Huang, L. Xia, L. Liu, X. Wang, H. Jin, J. Wang, Z. Song, X. Hao, and Q. Chen. 2014. A small natural molecule promotes mitochondrial fusion through inhibition of the deubiquitinase USP30. *Cell Res.* 24:482–496. doi:10.1038/cr.2014.20.

Yue, Z., S. Jin, C. Yang, A.J. Levine, and N. Heintz. 2003. Beclin 1, an autophagy gene essential for early embryonic development, is a haploinsufficient tumor suppressor. *Proc. Natl. Acad. Sci.* 100:15077–15082. doi:10.1073/pnas.2436255100.

Yun, J., R. Puri, H. Yang, M.A. Lizzio, C. Wu, Z.-H. Sheng, and M. Guo. 2014. MUL1 acts in parallel to the PINK1/parkin pathway in regulating mitofusin and compensates for loss of PINK1/parkin. *eLife*. 3:e01958. doi:10.7554/eLife.01958.

Zasadil, L.M., E.M.C. Britigan, and B.A. Weaver. 2013. 2n or not 2n: Aneuploidy, polyploidy and chromosomal instability in primary and tumor cells. *Semin. Cell Dev. Biol.* 24:370–379. doi:10.1016/j.semcdb.2013.02.001.

Zhang, C., S. Lee, Y. Peng, E. Bunker, E. Giaime, J. Shen, Z. Zhou, and X. Liu. 2014. PINK1 triggers autocatalytic activation of Parkin to specify cell fate decisions. *Curr. Biol. CB*. 24:1854–1865. doi:10.1016/j.cub.2014.07.014.

Zhang, J., and P.A. Ney. 2009. Role of BNIP3 and NIX in cell death, autophagy, and mitophagy. *Cell Death Differ.* 16:939–946. doi:10.1038/cdd.2009.16.

Zhang, S., M. Zhang, Y. Jing, X. Yin, P. Ma, Z. Zhang, X. Wang, W. Di, and G. Zhuang. 2018. Deubiquitinase USP13 dictates MCL1 stability and sensitivity to BH3 mimetic inhibitors. *Nat. Commun.* 9:1–12. doi:10.1038/s41467-017-02693-9.

Zhang, W., H. Ren, C. Xu, C. Zhu, H. Wu, D. Liu, J. Wang, L. Liu, W. Li, Q. Ma, L. Du, M. Zheng, C. Zhang, J. Liu, and Q. Chen. 2016. Hypoxic mitophagy regulates mitochondrial quality and platelet activation and determines severity of I/R heart injury. *eLife*. 5. doi:10.7554/eLife.21407.

Zhang, Y. 2003. Transcriptional regulation by histone ubiquitination and deubiquitination. *Genes Dev.* 17:2733–2740. doi:10.1101/gad.1156403.

Zhao, Y., M.C. Mudge, J.M. Soll, R.B. Rodrigues, A.K. Byrum, E.A. Schwarzkopf, T.R. Bradstreet, S.P. Gygi, B.T. Edelson, and N. Mosammaparast. 2018. OTUD4 Is a Phospho-Activated K63 Deubiquitinase that Regulates MyD88-Dependent Signaling. *Mol. Cell*. 69:505-516.e5. doi:10.1016/j.molcel.2018.01.009.

Zheng, N., and N. Shabek. 2017. Ubiquitin Ligases: Structure, Function, and Regulation. *Annu. Rev. Biochem.* 86:129–157. doi:10.1146/annurev-biochem-060815-014922.

Zhong, Q., W. Gao, F. Du, and X. Wang. 2005. Mule/ARF-BP1, a BH3-only E3 ubiquitin ligase, catalyzes the polyubiquitination of Mcl-1 and regulates apoptosis. *Cell*. 121:1085–1095. doi:10.1016/j.cell.2005.06.009.

Zhou, B.-B., H. Li, J. Yuan, and M.W. Kirschner. 1998. Caspase-dependent activation of cyclin-dependent kinases during Fas-induced apoptosis in Jurkat cells. *Proc. Natl. Acad. Sci.* 95:6785–6790. doi:10.1073/pnas.95.12.6785.

Zhou, C., Y. Huang, Y. Shao, J. May, D. Prou, C. Perier, W. Dauer, E.A. Schon, and S. Przedborski. 2008. The kinase domain of mitochondrial PINK1 faces the cytoplasm. *Proc. Natl. Acad. Sci. U. S. A.* 105:12022–12027. doi:10.1073/pnas.0802814105.

Zhou, F., Z. Wu, M. Zhao, R. Murtazina, J. Cai, A. Zhang, R. Li, D. Sun, W. Li, L. Zhao, Q. Li, J. Zhu, X. Cong, Y. Zhou, Z. Xie, V. Gyurkovska, L. Li, X. Huang, Y. Xue, L. Chen, H. Xu, H. Xu, Y. Liang, and N. Segev. 2019. Rab5-dependent autophagosome closure by ESCRT. *J. Cell Biol.* 218:1908–1927. doi:10.1083/jcb.201811173.

Zhu, B., K. Yan, L. Li, M. Lin, S. Zhang, Q. He, D. Zheng, H. Yang, and G. Shao. 2015. K63-linked ubiquitination of FANCG is required for its association with the Rap80-BRCA1 complex to modulate homologous recombination repair of DNA interstand crosslinks. *Oncogene*. 34:2867–2878. doi:10.1038/onc.2014.229.

Zhu, Y., S. Massen, M. Terenzio, V. Lang, S. Chen-Lindner, R. Eils, I. Novak, I. Dikic, A. Hamacher-Brady, and N.R. Brady. 2013. Modulation of serines 17 and 24 in the LC3-interacting region of Bnip3 determines pro-survival mitophagy versus apoptosis. *J. Biol. Chem.* 288:1099–1113. doi:10.1074/jbc.M112.399345.

Zhuang, N., L. Li, S. Chen, and T. Wang. 2016. PINK1-dependent phosphorylation of PINK1 and Parkin is essential for mitochondrial quality control. *Cell Death Dis.* 7:e2501–e2501. doi:10.1038/cddis.2016.396.

Zinchuk, V., O. Zinchuk, and T. Okada. 2007. Quantitative colocalization analysis of multicolor confocal immunofluorescence microscopy images: pushing pixels to explore biological phenomena. *Acta Histochem. Cytochem.* 40:101–111. doi:10.1267/ahc.07002.

Ziviani, E., R.N. Tao, and A.J. Whitworth. 2010. Drosophila Parkin requires PINK1 for mitochondrial translocation and ubiquitinates Mitofusin. *Proc. Natl. Acad. Sci.* 107:5018–5023. doi:10.1073/pnas.0913485107.

Zou, H., W.J. Henzel, X. Liu, A. Lutschg, and X. Wang. 1997. Apaf-1, a Human Protein Homologous to C. elegans CED-4, Participates in Cytochrome c–Dependent Activation of Caspase-3. *Cell*. 90:405–413. doi:10.1016/S0092-8674(00)80501-2.

Zuin, A., M. Isasa, and B. Crosas. 2014. Ubiquitin Signaling: Extreme Conservation as a Source of Diversity. *Cells*. 3:690–701. doi:10.3390/cells3030690.